ROLLING CONTACT FATIGUE TESTING OF BEARING STEELS

J.J.C. Hoo, *editor*

ROLLING CONTACT FATIGUE TESTING OF BEARING STEELS

A symposium
sponsored by
ASTM Committee A-1
on Steel, Stainless Steel,
and Related Alloys
Phoenix, Ariz., 12–14 May 1981

ASTM SPECIAL TECHNICAL PUBLICATION 771
J. J. C. Hoo, Acciaierie e Ferriere Lombarde
Falck and Acciaierie di Bolzano
editor

Foreword

The symposium on Rolling Contact Fatigue Testing of Bearing Steels was held on 12–14 May 1981 in Phoenix, Ariz. Sponsoring the event was ASTM Committee A-1 on Steel, Stainless Steel, and Related Alloys and its Subcommittee A01.28 on Bearing Steels. The chairman of the symposium was J. J. C. Hoo, Acciaierie e Ferriere Lombarde Falck and Acciaierie di Bolzano, who also served as editor of this publication.

Related
ASTM Publications

Bearing Steels: The Rating of Nonmetallic Inclusion, STP 575 (1975), 04-575000-02

Toughness of Ferritic Stainless Steels, STP 706 (1980), 04-706000-02

Methods and Models for Predicting Fatigue Crack Growth Under Random Loading, STP 748 (1981), 04-748000-30

Statistical Analysis of Fatigue Data, STP 744 (1981), 04-744000-30

Properties of Austenitic Stainless Steels and Their Weld Metals (Influence of Slight Chemistry Variations), STP 679 (1979), 04-679000-02

A Note of Appreciation
to Reviewers

Editorial Staff

Contents

Introduction

The life of a rolling bearing is calculated from the rolling contact fatigue durability of bearing steels. The ultimate life of a rolling bearing is reached when fatigue spalling develops. The empirical formula for rolling bearing life calculation used by bearing manufacturers as well as bearing users throughout the world has not been standardized. Several factors for material and application conditions must be introduced for each calculation. These factors are determined by rolling bearing manufacturers and users after many years of field experience or through extensive simulated tests, or both. Since the life of a rolling bearing is a major determining factor for the service life of any moving machine, the determination of the factors used for the bearing life formula is of the utmost importance. The rolling contact fatigue test of bearing steels is the most important test from which these factors are derived.

In building any moving machine, it is of primary concern to obtain a long endurance life of the rolling bearing. In designing a bearing life test, on the other hand, a long testing time should be avoided. The test must be accelerated so that results can be obtained within a reasonably short period of time and yet be correlative to the real application. Unfortunately, the shorter the test becomes, the farther the simulation departs from real conditions of application. An optimum compromise between these two contradictory considerations is essential. Each researcher emphasizes one or the other according to his preference. Over decades many test methods have been developed and their results published. Since the test results are not always comparable because of the different testing methods employed, it is desirable to standardize rolling contact fatigue tests.

ASTM Subcommittee A01.28 on Bearing Steels, a subcommittee of ASTM Committee A-1 on Steel, Stainless Steel, and Related Alloys, has attempted for many years to tackle the difficult problem of rolling contact fatigue testing of bearing steels. On 22-24 May 1974 an international symposium on the rating of nonmetallic inclusions in bearing steels was presented in Boston, Mass. Papers accepted by that symposium were published by ASTM under the title *Bearing Steels: The Rating of Nonmetallic Inclusion, ASTM STP 575*. The main theme of that symposium was chosen because it was universally recognized that nonmetallic inclusion is probably one of the most important factors affecting the rolling contact fatigue life of bearing steels. In the Boston symposium, in addition to discussions of various methods for

rating nonmetallic inclusions, the relationships of these inclusions to the fatigue properties of bearing steel were extensively discussed. The Boston symposium received very encouraging responses from bearing steel producers and users all over the world. It was felt by members of Subcommittee A01.28 that these efforts should be continued.

The main theme chosen for the symposium held on 12-14 May 1981 in Phoenix, Ariz., was broader than that of the previous Boston symposium. This symposium was conceived for the purpose of discussing the problem of rolling contact fatigue testing of bearing steels. Although standardization of testing is still many years away, if it can be achieved at all, it was felt that, as a first step, all the tests developed over the past decades should be thoroughly discussed and understood. Developers and designers of the most widely recognized test machines were invited to present the thinking behind their designs, the goals of their tests, the tests' merits and demerits, and the significant results obtained from the tests. Details of many testing methods were revealed for the first time. Many papers discussing effects of material and structural variations on rolling contact fatigue of bearing steels were included to show the accomplishments of these tests.

This volume is a collection of the papers presented at the Phoenix symposium. As the first book published anywhere devoted entirely to the problems of rolling contact fatigue testing of bearing steels, it is a good reference for all engineers and metallurgists working with rolling bearings and bearing steels. The results obtained by past researchers and a review of the most up-to-date state of the art are contained herein. Furthermore, this volume should stimulate innovative thinking for the future. Unselfish contributions from members of the industrial and academic communities of Italy, Japan, West Germany, the Netherlands, the United Kingdom, and the United States form the base of this book. Several papers included here report results of research contracts sponsored by governmental agencies of both the United Kingdom and the United States. Their permission for the first publication of these results is highly appreciated.

J. J. C. Hoo

Acciaierie e Ferriere Lombarde Falck, S.p.A. of Milano, Italy; Acciaierie di Bolzano, S.p.A. of Bolzano, Italy; symposium chairman and editor.

Element Testing Machines of a Given Design with Collaborative Testing Results

E. V. Zaretsky,[1] *R. J. Parker,*[1] *and W. J. Anderson*[1]

NASA Five-Ball Fatigue Tester—Over 20 Years of Research

ABSTRACT: This paper reviews, from both a technical and a historical perspective, the results of research conducted using the National Aeronautics and Space Administration five-ball fatigue tester. The test rig was conceived by W. J. Anderson in late 1958. The first data were generated in March 1959. Since then a total of approximately 500 000 test hours have been accumulated on a group of eight test rigs which are capable of running 24 h a day, 7 days a week. Studies have been conducted to determine the effect on rolling element fatigue life of contact angle, material hardness, chemistry, heat treatment and processing, lubricant type and chemistry, elastohydrodynamic film thickness, deformation and wear, vacuum, and temperature, as well as hertzian and residual stresses. A correlation was established between the results obtained using the five-ball tester and those obtained with full-scale rolling element bearings.

KEY WORDS: rolling element fatigue, bearings, ball bearings, bearing steels, fatigue testing

The determination of the rolling element fatigue life of a bearing made from a particular steel or of the effect of a specific lubricant on fatigue is an expensive undertaking. The very high scatter or dispersion in fatigue lives makes it necessary to test a large number of specimens. The cost in both money and time is high. High-quality aircraft engine bearings can cost several hundred dollars each, and the test duration can run from several hundred to several thousands of hours, depending on the load conditions and speed. Bearing companies and various research laboratories throughout the world have pioneered the use of bench-type rolling element fatigue testers which can simulate to various degrees the conditions found under full-scale bearing operation.

[1]Head of the Bearing, Gearing and Transmission Section, research manager of Bearings and Materials, and chief of the Mechanical Technologies Branch, respectively, National Aeronautics and Space Administration, Lewis Research Center, Cleveland, Ohio 44135.

These bench-type testers accelerate the generation of rolling element fatigue data because testing is done at higher stresses, thus resulting in reduced cost. The results obtained with the bench-type testers have been used to indicate trends and to rank materials and lubricants. In achieving this objective, bench-type rigs have been very successful.

Early rolling element fatigue testing was performed with what might be termed a two-disk machine [1].[2] However, up until 1956 most rolling element fatigue testing was performed on full-scale bearings. In 1957, the National Advisory Committee for Aeronautics [now the National Aeronautics and Space Administration (NASA)] published their first results [2] with what was termed the NASA spin rig [3]. About the same time that work was being performed with the spin rig, Pratt and Whitney Aircraft began utilizing what they termed a one-ball rig [4] and the General Electric Co. devised what they termed the R-C (rolling-contact) rig [5].

In 1958 it became apparent to W. J. Anderson, who then headed the rolling bearing research at the NASA Lewis Research Center, that the number of parameters that could be studied in the spin rig was limited. The reason for this was that the test load was a function of the orbital velocity of the balls in this rig. Hence, specimen loading could not be varied without varying other parameters. About this time, F. Barwell in Great Britian modified a sliding four-ball wear tester by allowing the three lower balls, which previously were fixed, to rotate in their cylindrical cup [6]. Maintaining very high contact stresses, such as > 6.9 GPa (1 000 000 psi), Barwell was able to induce a pit or spall in the upper ball running track which resembled those obtained in full-scale bearings. Anderson, capitalizing on the idea of a ball loaded against lower rotating balls, conceived of the five-ball fatigue tester. Anderson's concept incorporated an upper test ball pyramided upon four lower test balls which are positioned by a separator and are free to rotate in an angular contact raceway (see Fig. 1). The implementation of this concept was left to T. L. Carter and E. V. Zaretsky, who in January 1959 designed and fabricated the first five-ball fatigue tester at the NASA Lewis Research Center. The tester produced its first data in March 1959. Since then a total of approximately 500 000 test hours have been accumulated on a group of eight test rigs which are capable of running 24 h a day, 7 days a week. The objective of the work reported herein is to summarize over 20 years of test results obtained from the five-ball (rolling element) fatigue tester and to assess the correlation of these data with full-scale bearing data and, thus, the influence on current bearing design and operation.

Five-Ball Fatigue Tester

The NASA five-ball fatigue tester simulates very closely the kinematics of a thrust-loaded, full-scale bearing. The tester, which was first described in

---

[2] The italic numbers in brackets refer to the list of references appended to this paper.

DRIVE SPINDLE

OIL TUBE

THERMOCOUPLE

TEST SPECIMEN ASSEMBLY

SUPPORT ROD

RUBBER MOUNT

DRAIN

BASE PLATE

HEATER

REVOLUTION COUNTER

COVER PLATE

VIBRATION PICKUP

LOAD ARM

LOAD RELEASE

INSULATION

WEIGHT

(a) CUTAWAY VIEW OF FIVE-BALL FATIGUE TESTER.

LOAD

LOWER BALL

SEPARATOR

ω

CONTACT ANGLE, β

β

CONTACT AXIS

RACEWAY

UPPER TEST BALL

(b) FIVE-BALL ASSEMBLY.
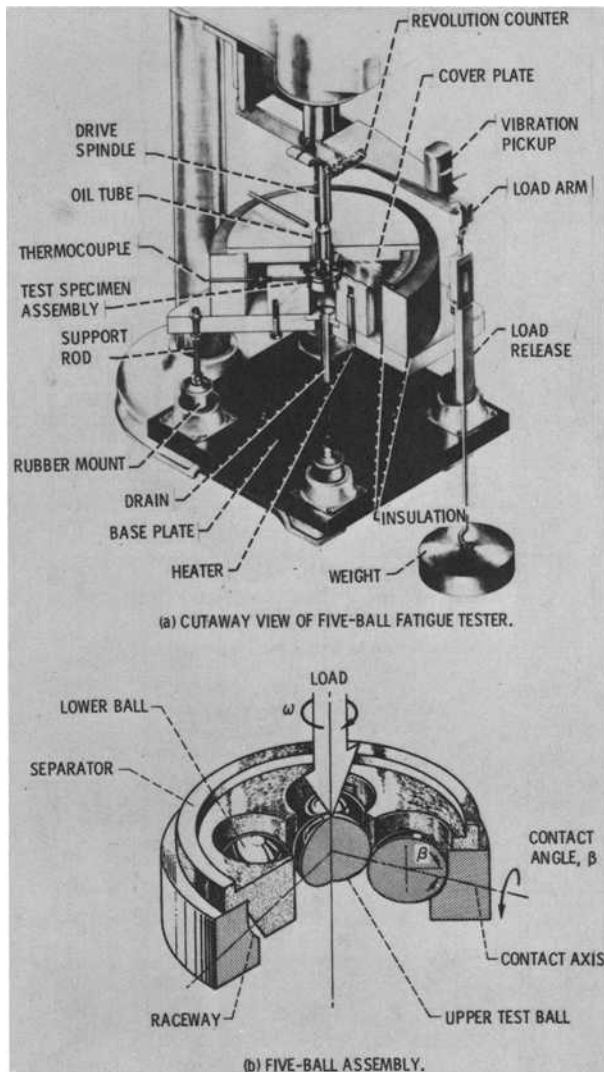
FIG. 1—*Five-ball fatigue tester.*

[7,8], essentially comprises an upper test ball pyramided upon four lower test balls which are positioned by a separator and are free to rotate in an angular contact raceway. Loading and drive are supplied through a vertical shaft, as illustrated in Fig. 1a. By varying the pitch diameter of the four lower test balls, the contact angle, β (Fig. 1b), may be varied. The angular spin velocity in the upper ball–lower ball contact, ω_2, approximately equals $\omega_1 \sin \beta$ [7,8]. By utilization of a vibration type of failure-detection and shutdown system, long-term unmonitored tests are made possible.

(c) Modification for tests at reduced pressures.

(d) Modification for low temperature and cyrogenic testing.

FIG. 1—*Continued.*

THERMOCOUPLE WIRES TO SLIPRING-BRUSH ASSEMBLY

TAPER SHAFT INSERTED INTO DRIVE SPINDLE

INSULATING TERMINAL BLOCK

MODIFIED TEST SPECIMEN WITH TONGUE

THERMOCOUPLE

RUNNING TRACK

(e) Operating-temperature measuring device.

LOAD

SHAFT COOLING WATER

THERMOCOUPLE

TEST ASSEMBLY (SEE FIG. 1(b))

DRIVE SPINDLE

INSULATION

INDUCTION HEATING COILS

HOUSING

FLEXIBLE MOUNT

LUBRICANT AND COVER GAS

(f) Modification for tests at 1366 K (2000° F).

FIG. 1—*Concluded.*

Lubrication in this rig is accomplished by introducing droplets of a fluid into a gas stream directed at the test balls. The lubricant flow rate can be controlled by adjusting the pressure upstream of a long capillary tube; the pressure drop through the capillary tube is sufficient to give excellent control for the small flow rates required. The test ball assembly is loaded by a dead weight acting on the drive shaft through a load arm. The contact load is a function of the drive shaft load and the contact angle, β. For every revolution of the drive shaft, a point on the running track of the upper test ball is stressed three times [7,8].

The system housing assembly is supported by rods held in flexible rubber mounts, as shown in Fig. 1a. Positioning of the rods and rubber mounts provides for alignment of the raceway and the four lower test balls with respect to the upper test ball and the drive shaft. Minor misalignments are absorbed by the flexible rubber mounts, as are vertical oscillations of the drive shaft created by motor and drive belt vibration. Such vibrations, if not absorbed, will increase the stress level of the ball specimens, thus influencing fatigue results. Modifications of this rig have been used for operation in a vacuum (low-pressure) environment and at temperatures from 89 to 1366 K (-300 to 2000°F) (Fig. 1c, d, and f).

Discussion of Results

The results of the various research programs conducted in the five-ball fatigue tester are discussed in terms of the effect on fatigue life of the particular parameter or variable being investigated. These include material effects (hardness, component hardnesses, residu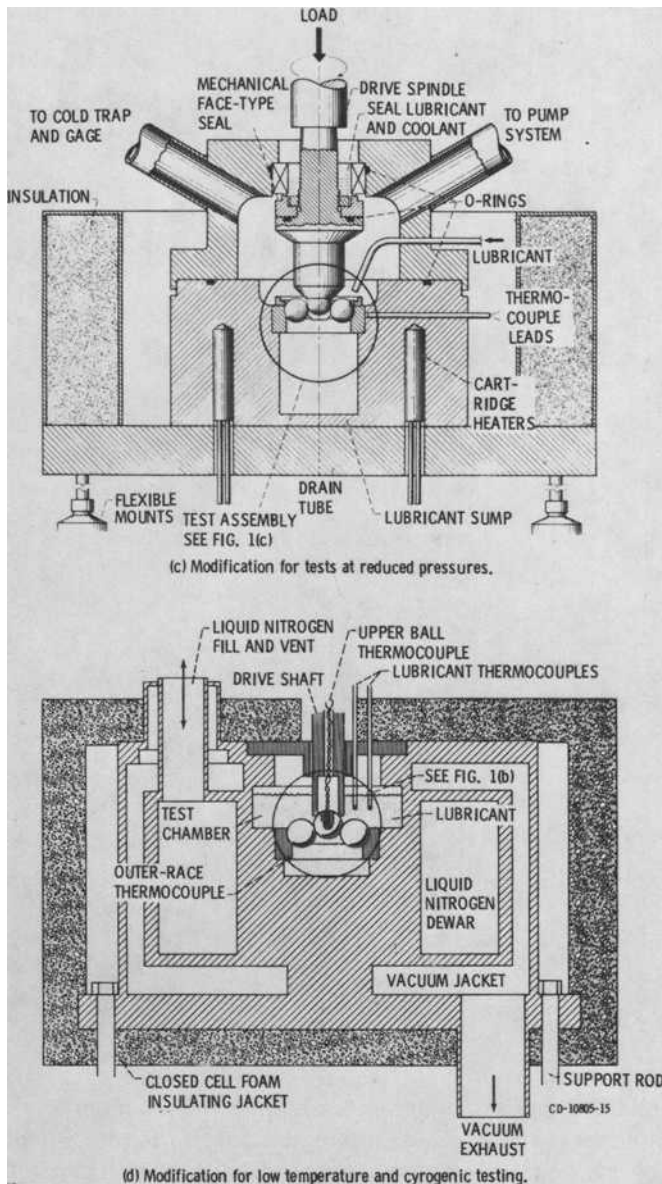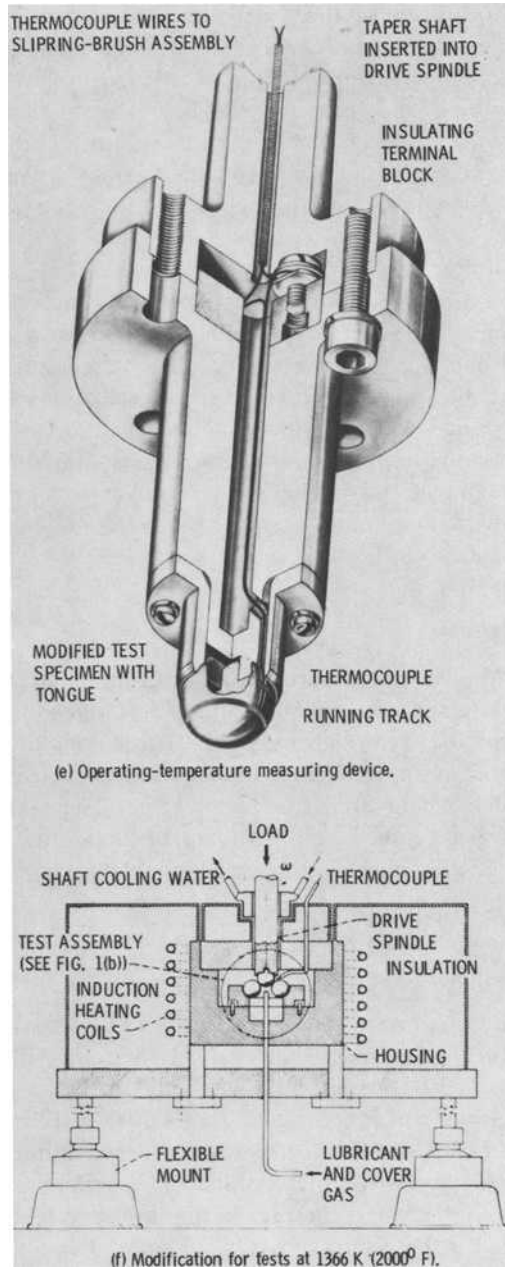al stresses, alloying element, processing, and nonferrous materials), lubricant effects (type, viscosity, temperature, and additives), geometry effects (contact angle and ball hollowness), stress effects, and wear debris analysis. Finally, there is a comparison with full-scale bearing data.

Effect of Material Hardness

The fatigue spin rig and the five-ball tester were used to determine the rolling contact fatigue life at room temperature of groups of AISI M-1, AISI M-50, Halmo, and WB-49 steel balls tempered to various hardness levels. Nominal test conditions included 5.52 GPa (800 000 psi) maximum theoretical (hertz) compressive stress and a synthetic diester lubricant. The fatigue life results were compared with material hardness, resistance to plastic deformation in rolling contact, and the previously published tensile and compressive strength data for these same heats of material. The results of these tests were reported in Refs 8 through 11.

A summary of the data from these tests is shown in Fig. 2. The rolling element fatigue life or, analogously, the load-carrying capacity of each of the
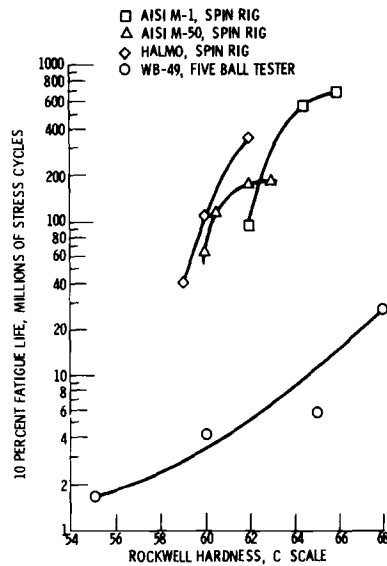
FIG. 2—*Ten percent fatigue life as a function of hardness for four tool steels [9].*

four alloy compositions studied, increased continuously as the material hardness increased. The improvement in load capacity was about 30 to 100 percent over the hardness range tested. No maximum fatigue life or load capacity at intermediate hardness values was observed. In contrast, elastic-limit and yield strength measurements [8] made on bar specimens from the same heats of materials showed optimum values at an intermediate hardness level and did not correlate with fatigue life. Resistance to plastic deformation, measured with ball specimens in rolling contact, however, did correlate with fatigue life.

These results were substantiated with bearings made of AISI 52100 steel having hardnesses of up to 63 HRC; for these bearings, the fatigue life increased with increasing hardness [12]. These findings, however, were contrary to the conclusions reached in Ref 13, wherein a maximum fatigue life was predicted at an intermediate hardness level for AISI M-50 steel.

Differential Hardness

It was reported in Refs 14 and 15 that plastic deformation can reduce the contact stress by as much as 10 percent at theoretical maximum hertz stress levels between 4.10 and 5.52 GPa (600 000 and 800 000 psi) in the five-ball fatigue tester. Therefore, where plastic deformation does occur under rolling contact, the calculated hertz stress may only be approximate [14,16]. Material hardness or resistance to plastic deformation has a twofold effect on fa-

tigue life: as the hardness is decreased, the fatigue life decreases because of an inherent decrease in material strength, but at the same time the plastic deformation increases and the contact stress decreases. This latter effect would increase the fatigue life. The two effects are, therefore, acting in opposition to each other. Based upon this premise and the apparent contradiction between the results obtained in both the spin rig and five-ball fatigue tester and those reported in Ref *13*, a program was undertaken to determine the effect of hardness differences between upper and lower test balls on rolling element fatigue life.

AISI 52100 steel balls from one heat of material were tempered to a range of hardnesses from 59.7 to 66.4 HRC. Groups of balls having averages of 60.5, 63.2, and 65.2 HRC were used as upper test balls and run with lower test balls of nominal HRC values of 60, 62, 63, 65, and 66. Nominal test conditions included an average race temperature of 339 K (150°F), 5.52 GPa (800 000 psi) maximum (hertz) compressive stress, and a highly purified naphthenic mineral oil lubricant. The fatigue life results were compared with component hardness combinations, plastic deformation of the upper test ball, retained austenite, grain size, and contact temperature. The results of these tests are reported in Refs *17* and *18* and summarized in Fig. 3.

In general, for a specific upper test ball hardness, the rolling element fatigue life and the load-carrying capacity of the test system (considering both upper and lower ball failures) increased with increasing lower test ball hardness to an intermediate hardness, where a peak life was attained. With further increases in the hardness of the lower balls, the system life and capacity decreased. The peak life hardness combination occurred for each of three lots of upper test balls, where the hardness of the lower test balls was approx-
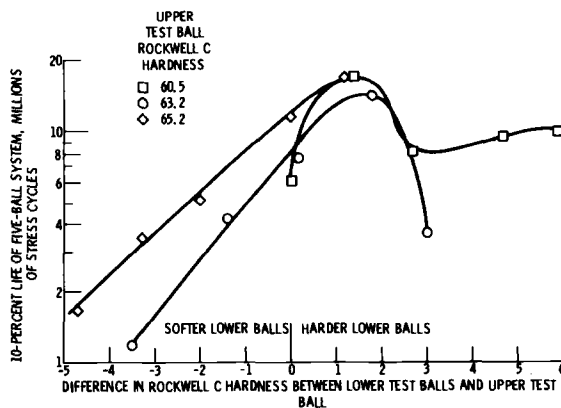
FIG. 3—*Ten percent life of the five-ball system as a function of the difference in hardness between the lower test balls and upper test ball with lower and upper balls of AISI 52100 steel [17].*

imately 1 to 2 HRC points greater than that of the upper test ball. The improvement in load capacity at the intermediate hardness, where a peak life was observed, was as much as 130 percent over the capacity at the lowest hardness.

There was no apparent correlation between fatigue life and material properties such as retained austenite and grain size. Additionally, no correlation existed between the resistance to plastic deformation between elements of different hardnesses and fatigue life. Further, no correlation existed between the rolling element fatigue life and the temperatures measured at the edge of the contact zone (Fig. 1e) for each hardness combination.

To illustrate the effect of the hardness differential, ΔH, on the bearing fatigue and load capacity, four lots of AISI 52100, 207-size, deep-groove ball bearings, each with balls of a specific hardness and races of 63 HRC, were fatigue tested at a radial load of 5870 N (1320 lb) and a speed of 2750 rpm, with a mineral oil lubricant and with no heat added [18,19]. The relative bearing load capacity is shown as a function of ΔH in Fig. 4. For comparison purposes, the range of predicted relative capacity based on the five-ball fatigue data is also presented. The correlation with the five-ball data is excellent. It can be concluded that maximum bearing fatigue life and load capacity can be achieved where the hardness of the rolling elements of the bearing is 1 to 2 HRC points greater than that of the races.

Based upon these results, the data of Ref 12, which were among the earliest data to show an effect of hardness on life, were reanalyzed considering the hardness differences between the balls and race [18]. The reanalyzed data not only indicated the optimum ΔH relationship but also exhibited relative life values of approximately the same magnitude with varying ΔH as those shown for the 207-size bearings in Ref 18.
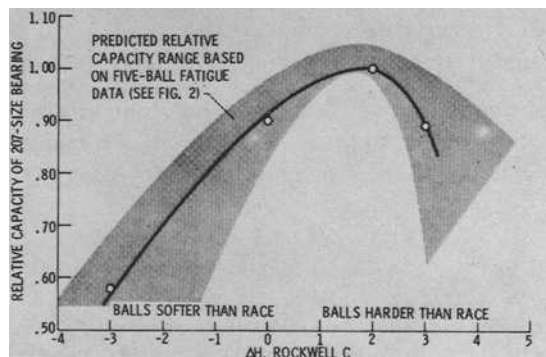
FIG. 4—The relative radial load-carrying capacity of 207-size deep-groove ball bearings as a function of the difference in hardness between the balls and races [18].

From the data of Ref *17* a relationship which approximates the effect of bearing hardness on fatigue life was obtained, where

$$\frac{L_2}{L_1} = e^{0.1(HRC_2 - HRC_1)}$$

L_1 and L_2 are the bearing 10 percent fatigue lives at bearing hardnesses HRC_1 and HRC_2, respectively, at a ΔH of 0.

Residual Stress

It was shown in Refs *20* and *21* that residual compressive stresses are developed in bodies in rolling contact, the magnitude of which appeared to be a function of time. Additionally, residual compressive stresses induced by mechanical processing operations were found to increase the fatigue life of balls and complete bearings [22]. A unit volume on the upper test ball running track in the five-ball system is stressed many more times than a point on any of the lower test balls, so that the upper test ball would be likely to absorb more energy and build up a proportionally greater amount of subsurface residual stress than would each of the lower test balls.

Induced residual stress can either increase or decrease the maximum shear stress [23], according to the following equation

$$(\tau_{max})_r = -4.67 \times 10^6 \left(\frac{P_n}{R^2 S_{max}} \right)^{1/2} - \frac{1}{2} (\pm S_{ry})$$

where

P_n = normal load;
R = radius of curvature of sphere;
S_{max} = maximum hertz stress; and
S_{ry} = residual stress in the y (rolling direction).

The positive or negative sign of S_{ry} indicates a tensile or a compressive residual stress, respectively. A compressive residual stress would reduce the maximum shear stress and increase fatigue life [23] according to the expression

$$L \propto \left(\frac{1}{(\tau_{max})_r} \right)^9$$

Five upper test balls of 63.2 HRC that were run in the five-ball tester [17] for approximately the same number of stress cycles against lower balls of 59.7, 61.8, 63.4, 65.0, and 66.2 HRC were selected for residual stress measurements. Standard X-ray diffraction techniques were used to measure residual stresses at a depth of 0.13 mm (0.005 in.) beneath the running track,

which was the calculated depth of the maximum shear stress. The residual stresses below the track were found to be compressive and varied between 1.23 and 2.03 GPa (178 000 and 294 000 psi).

The measured compressive residual stresses are plotted as a function of ΔH in Fig. 5. From this figure, note that the measured stress increases with increasing lower test ball hardness to an intermediate hardness where a peak was obtained. On the basis of these limited data, the apparent maximum residual stress occurs at a value of ΔH slightly greater than zero.

The measured values of compressive residual stress were used to calculate theoretical 10 percent lives of the upper test ball using the aforementioned relationships. These calculated 10 percent lives predict a peak life at the maximum compressive residual stress, which occurs at a ΔH slightly greater than zero. Although these results, which are based on limited residual stress measurements, do not show the predicted peak life at a ΔH of 1 to 2 HRC points, such as was experimentally determined, it is apparent that an interrelationship exists among the differences in component hardness, the induced compressive residual stress, and the fatigue life.

Based upon the results obtained with the five-ball tests, subsurface residual stress measurements were made on AISI 52100 steel inner races from the 207-size, deep-groove ball bearings in which ΔH ranged from -1.1 to 3.5 HRC points [24]. These bearings had been run at an inner-race speed of 2750 rpm and a radial load of 5870 N (1320 lb), producing maximum hertz stresses of 2.43 and 2.32 GPa (352 000 and 336 000 psi) at the inner and outer races, respectively. The residual stress measurements were made in a circumferential direction at various depths below the inner-race running track surface
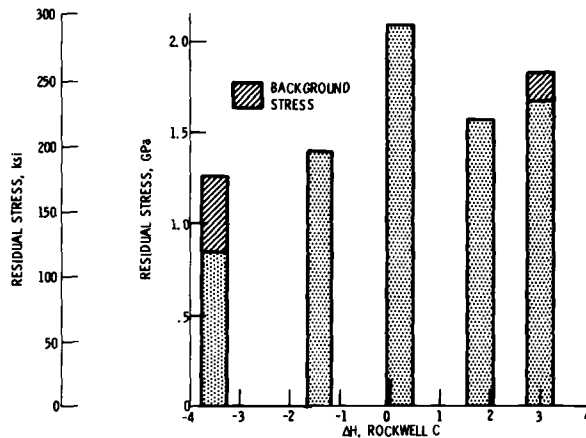
FIG. 5—*Measured compressive residual stress in the track of upper test balls having a hardness of 63.2 HRC as a function of the difference in hardness between the lower test balls and upper test ball [18].*

on a total of 19 of the bearings that had been run for nominally 200, 600, and 1600 h. The measurements indicated that the maximum compressive residual stresses occur in approximately the same ΔH range for which the maximum fatigue lives were observed. Again, good correlation with five-ball tester results was indicated. In addition, no relationship between running time and residual stress could be determined from these measurements.

Lubricant Effects

Bearing failure by fatigue is affected by the physical and chemical properties of the lubricant. Knowledge of how these chemical and physical properties affect rolling element fatigue is a useful guide both in selecting existing lubricants for bearing applications and in developing new lubricant formulations. Specifically, for aircraft engine bearing applications, it is important to know the effect these lubricants have on the bearing life and reliability.

Effect of Lubricant Type—The NASA fatigue spin rig and five-ball fatigue tester were used to determine the rolling element fatigue lives at room temperature and at 422 K (300°F) of groups of AISI M-2 and AISI M-1 steel balls run with nine lubricants having varied chemical and physical characteristics [16]. These lubricants were classified as three basic types: esters, mineral oils, and silicones. Longer fatigue lives were obtained at room temperature with the silicone and the dioctyl sebacates than with other lubricants; at 422 K (300°F), however, the silicone and the mineral oils gave the longer lives. The relative order of fatigue results obtained in the five-ball fatigue tester compared favorably with that obtained with 7208-size bearings tested with the same lubricants (Fig. 6).
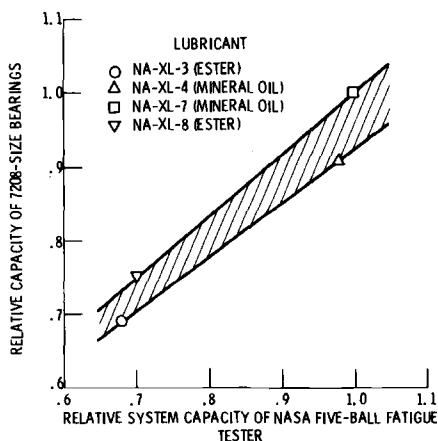
FIG. 6—*The relative load-carrying capacity of 7208-size bearings as a function of the relative capacity of a five-ball fatigue tester for various lubricants at 422 K (300°F) [16].*

A correlation is suggested between the plastically deformed profile radius of the upper test ball running track at ambient temperature after 30 000 stress cycles of operation and rolling element fatigue life. The fatigue results obtained did not correlate with the temperatures measured at the edge of the contact zone of the test specimens (Fig. 1e) during rolling contact in the five-ball fatigue tester at 422 K (300°F) outer-race temperature. The measured contact temperature differences among the lubricants were insignificant.

Elastohydrodynamic (EHD) film thickness measurements using X-ray techniques were made with a rolling-contact disk machine under simulated five-ball test conditions [15] with several of the lubricants used in Ref 16. Under certain conditions [15], elastohydrodynamic lubrication was found to exist at initial maximum hertz stress levels up to 5.52 GPa (800 000 psi).

Polyphenyl Ethers—In the early 1960s the polyphenyl ethers were among the lubricants most often considered for bearings, gears, and hydraulic systems in applications where high thermal and oxidative stability and resistance to nuclear radiation were necessary. Because the polyphenyl ethers have these desirable properties, along with relatively low vapor pressures, they were being considered as lubricants for a closed organic lubrication loop in space power generation systems such as SNAP-8. In such a system, the lubricant would be exposed to pressures less than atmospheric.

A modified five-ball fatigue tester (Fig. 1c) was used to determine the relative lubricating characteristics in rolling contact of polyphenyl ethers and mineral oils [25]. The test conditions were a race temperature of 422 K (300°F), a shaft speed of 4900 rpm, and a test duration of 6 h with AISI M-50 balls. Measurements on the upper ball were made to determine the effects on wear of reduced pressure, lubricant degassing, contact angle, and contact stress.

Use of a four-ring polyphenyl ether (4P3E) resulted in several times more wear than a naphthenic mineral oil when the fluids were tested at pressures near their vapor pressures at 422 K (300°F). In tests at atmospheric pressure in an argon atmosphere, the 4P3E polyphenyl ether exhibited more wear than a paraffinic oil. Greater wear occurred when the 4P3E polyphenyl ether was tested at a pressure near its vapor pressure than when it was tested at atmospheric pressure in argon with all other conditions being equal. Increased wear at higher contact angles and higher contact stresses was accompanied by increased darkening of the 4P3E polyphenyl ether. The polyphenyl ethers appear to be inferior to the mineral oils in their ability to provide elastohydrodynamic lubrication. However, rolling contact fatigue tests in the five-ball fatigue tester indicated that the fatigue life with a 5P4E polyphenyl ether at 422K (300°F) and atmospheric pressure may be expected to be comparable to that with the mineral oils.

Reduced Pressure Environment—Rolling element fatigue life is affected by lubricant viscosity. In general, as lubricant viscosity increases, so does the fatigue life of a rolling element bearing [26]. Decreases in apparent bulk vis-

cosity of a superrefined mineral oil and an ester-based oil were obtained by saturating the lubricating fluid with nitrogen gas [27]. Conversely, exposing the lubricating fluid to a reduced-pressure environment can increase the bulk viscosity be degassing the lubricant.

A modified five-ball fatigue tester (Fig. 1c) was used to investigate the effect of a reduced-pressure environment on rolling element fatigue life, deformation, and wear of AISI 52100 steel balls with a superrefined naphthenic mineral oil used as the lubricant. Tests were conducted at atmospheric pressure, at a 20 deg contact angle, with a thrust load of 267 N (60 lb) to produce an initial maximum hertz stress of 5.52 GPa (800 000 psi) at a shaft speed of 4 900 rpm with no heat added [28, 29]. The atmospheric pressure tests served as reference data for tests conducted at a reduced pressure, approximately the vapor pressure of the lubricant. For these reduced-pressure tests, the ball specimens were lubricated either by a quasi-mist method or by immersion in the lubricant. In both cases, all other test conditions were the same as those in the atmospheric pressure tests.

No significant difference in the fatigue lives was observed between tests conducted at atmospheric pressure and those conducted at reduced ambient pressure. The amounts of deformation and wear for the two pressure conditions differed little, regardless of the lubrication mode employed. This was an indication that a sufficient EHD lubricating film existed at the reduced-pressure levels.

Cryogenic Environment—In the late 1960s interest focused on the possible use of liquid lubrication in place of a dry lubricant film for bearings operating in a cryogenic environment. A lubricant capable of forming an EHD film in cryogenic applications must be liquid in the cryogenic temperature range. It must also be able to operate at the maximum system temperature without evaporating. The fluid should be chemically inert and not be susceptible to water absorption, which may cause corrosion of the bearing components. In addition, good heat-transfer properties are desirable.

A class of fluids that exhibits many of the properties required for cryogenic applications is the fluorinated polyethers. While some of their fluid properties such as viscosity and heat-transfer characteristics are clearly defined, the ability of these fluids to provide adequate lubrication and life needed to be determined.

Rolling element lubrication tests were conducted with 12.7-mm (½-in.)-diameter AISI 52100 steel balls in a five-ball fatigue tester modified for cryogenic temperature testing (Fig. 1d) [30]. Test conditions included a drive shaft speed of 4 750 rpm, a maximum hertz stress range of 3.45 to 5.52 GPa (500 000 to 800 000 psi), outer-race temperatures of 89 to 227 K (160 to 410°R), and contact angles of 10, 20, 30, and 40 deg. Four fluorinated polyether fluids with different viscosities were used as the lubricants.

The deformation and wear of the test specimens lubricated with the fluo-

rinated polyether fluids compared favorably with those of test specimens run at room temperature with conventional lubricants. This result indicates that the fluorinated polyether fluids have the ability to form adequate EHD films at outer-race temperatures from 89 to 227 K (160 to 410°R).

The fatigue lives with the four fluorinated polyether fluids in the cryogenic temperature range were compared with that obtained with a superrefined mineral oil at room temperature [31]. There was no statistical difference between the fatigue lives obtained with the fluorinated polyether fluid and those obtained with the superrefined mineral oil at 169 K (305°R) and 328 K (590°R), respectively. This result indicates that at lower temperatures with the polyether no fatigue life derating of AISI 52100 is necessary. The operating characteristics of the fluorinated polyether fluids at cryogenic temperatures compared favorably with those of the superrefined mineral oil at room temperature.

Traction Fluids—In recent years there has been renewed interest in mechanical transmissions which use the principle of traction for power transfer. In these devices, torque is transmitted between rolling elements across a thin elastohydrodynamic lubricant film under high contact pressure. Consequently, the magnitude of the contact pressure required to transmit a given amount of torque is principally dependent on the tractive properties of the lubricant. Lubricants formulated for traction-drive applications typically have high coefficients of traction. The generic term for these oils is traction fluids.

Rolling element fatigue tests were run in the five-ball fatigue tester with two traction fluids, a tetraester with and without additives, a synthetic paraffinic oil, and a paraffinic mineral oil [32,33]. Standard test conditions for all tests consisted of a maximum hertz stress of 5.52 GPa (800 000 psi), a contact angle of 30 deg, and an upper-ball speed of 10 700 rpm. All tests were run at room temperature (that is, no heat was added). Outer-race temperatures varied from 339 to 353 K (150 to 175°F) for the synthetic lubricants and averaged approximately 336 K (146°F) for the mineral oil.

The results of the rolling element fatigue tests are summarized in Table 1. The paraffinic mineral oil gave longer lives than any of the synthetic lubricants tested. The 10 percent life with the mineral oil was 34.8 million stress cycles, whereas the lives with the synthetic lubricants ranged from 9.5 million to 17.9 million cycles. The statistical significance of the differences between these lives and that of the mineral oil is reflected by the confidence numbers given in Table 1. They indicate the percentage of time that components lubricated with the mineral oil would show fatigue lives superior to the fatigue lives of identical components lubricated with each of the synthetic lubricants. A confidence number greater than 95 percent, which is equivalent to a 2-σ confidence level, indicates a high degree of certainty. Although all of the synthetic lubricants show lives less than the mineral oil, only the lives with the tetraester base and the synthetic paraffinic oil approach statistically signifi-

TABLE 1—Rolling element fatigue life of AISI 52100 balls lubricated with one of several synthetic lubricants or a paraffinic mineral oil in the five-ball fatigue tester [33].[a]

Lubricant	Rolling Element Fatigue Life, Millions of Upper-Ball Stress Cycles		Weibull Slope	Failure Index[b]	Confidence Number,[c] percent	
	10 Percent Life	50 Percent Life			10 Percent Life	50 Percent Life
Paraffinic mineral oil	34.8	214	1.04	15 out of 37	...	...
Formulated tetraester	14.3	71.1	1.17	35 out of 39	83	>99
Tetraester base	10.5	46.2	1.27	38 out of 40	92	>99
Traction fluid 1	17.9	115.9	1.01	21 out of 32	69	94
Traction fluid 2	17.3	72.7	1.31	15 out of 28	72	>99
Synthetic paraffinic oil	9.5	91.9	0.83	26 out of 36	87	>99

[a]Maximum hertz stress, 5.52 GPa (800 000 psi); shaft speed, 10 700 rpm; contact angle, 30 deg.
[b]Number of failures out of the total number of tests.
[c]Percentage of time that the fatigue life with the mineral oil will be greater than that with the specific synthetic lubricant.

cant differences at the 10 percent life level. At the 50 percent life level, all ex-perimental lives with the synthetic lubricants are significantly less than those with the mineral oil.

The rolling element fatigue lives obtained with the traction fluids were not significantly different on a statistical basis from those obtained with the tetra-ester oil or the paraffinic mineral oil.

Erratic test behavior was observed in those tests using the traction fluid that contained an antiwear additive. Rolling element surface distress and overheat-ing occasionally caused premature termination of tests with this lubricant.

Lubricant Additive Effects

Lubricant additives can prevent or minimize wear and surface damage to bearings and gears whose components are in contact under very thin film or boundary lubrication conditions. These antiwear or extreme pressure (EP) additives either adsorb onto the surfaces or react with the surfaces to form protective coatings or surface films. The value of additives for this protection is well known, and their use is commonplace.

To determine the effects of antiwear and EP additives on rolling element fatigue life, it is necessary to run fatigue tests at EHD film conditions where classic subsurface rolling element fatigue is the sole mode of failure. This ob-jective was accomplished by testing in the NASA five-ball fatigue tester at test conditions where classic subsurface rolling element fatigue could be ex-pected [34] with three different steel ball materials.

Rolling element fatigue tests were conducted in the five-ball fatigue tester using a base oil with and without surface active additives. The 12.7-mm (0.500-in.)-diameter test balls were either AISI 52100, AISI M-50, or AISI 1018 steel. The test lubricant was an acid-treated white oil containing either 2.5 percent sulfurized terpene, 1 percent didodecyl phosphite, or 5 percent chlorinated wax. Nine combinations of materials and lubricants (six contain-ing additives) were tested at conditions including a maximum hertz stress of 5.52 GPa (800 000 psi), a shaft speed of 10 700 rpm, and a race temperature of 339 K (150°F). The results of these tests are summarized in Table 2.

Base Oil Plus 2.5 Percent Sulfurized Terpene—For both the AISI 52100 and AISI 1018 steels the 2.5 percent sulfurized terpene additive apparently reduced fatigue life by approximately 50 percent. For the AISI M-50 steel, however, the fatigue life was essentially unchanged from that obtained with the base oil. The combined confidence number for the three successive tests is 92 percent. In combining the data for the three materials it is assumed that the reduction in life is unrelated to the bearing steel chemistry. With this assumption, it can be concluded that the 2.5 percent sulfurized terpene can reduce rolling element fatigue life by as much as 50 percent under the test conditions reported.

TABLE 2—*Rolling element fatigue life of steel balls with an acid-treated white oil with and without surface-active additives [34].*[a]

Material	Lubricant	Rolling Element Fatigue Life, Millions of Upper-Ball Stress Cycles		Weibull Slope	Failure Index[b]	Confidence Number,[c] percent
		L_{10}	L_{50}			
AISI 52100	base oil	37.0	202	1.11	10 out of 30	...
	base oil plus 2.5 percent sulfurized terpene	17.8	39.2	2.39	24 out of 30	81
	base oil plus 1 percent didodecyl phosphite	33.9	92.8	1.87	25 out of 30	54
	base oil plus 5 percent chlorinated wax	4.8	15.1	1.63	30 out of 30	99
AISI M-50	base oil	14.6	44.5	1.69	28 out of 30	...
	base oil plus 2.5 percent sulfurized terpene	15.9	34.1	2.47	30 out of 31	59
AISI 1018	base oil	7.8	25.0	1.16	30 out of 30	...
	base oil plus 2.5 percent sulfurized terpene	4.2	26.7	1.02	29 out of 30	83
	base oil plus 1 percent didodecyl phosphite	6.4	24.4	1.40	30 out of 30	65

[a]Maximum hertz stress, 5.52 GPa (800 000 psi); shaft speed, 10 700 rpm; contact angle, 30 deg; race temperature, 339 K (150°F).
[b]Indicates the number of failures out of the total number of tests.
[c]Percentage of time that the 10 percent life with the base oil will be greater than (or less than, as the case may be) the 10 percent life with the additive.

Base Oil Plus 1 Percent Didodecyl Phosphite—The 1 percent didodecyl phosphite additive was run with the AISI 52100 and AISI 1018 steels. The combined confidence number for these two series of tests was 68 percent, or approximately equivalent to a 1-sigma confidence, and was not considered statistically significant. The results with this additive showed essentially no statistical difference between the lives using the base oil with the additive and those without the additive.

Base Oil Plus 5 Percent Chlorinated Wax—Only in the tests with the chlorinated-wax additive with AISI 52100 balls was surface distress observed. In this case, eight tests were not included in the analysis because of multiple spalling and considerable surface distress in the running track. Even with these early failures deleted from the analysis, the life with this additive was significantly less than that without the additive.

It was evident that with this lubricant–additive–material–test condition, the EHD film was marginal. This result suggests the possibility that the lubricant rheology of the base oil (viscosity or pressure–viscosity effects, or both) has been altered by the chlorinated-wax additive. Further, the influence of this additive can be detrimental to rolling element fatigue life.

The additives used with the base oil did not change the life ranking of bearing steels in these tests where rolling element fatigue was of subsurface origin. That is, regardless of the additive content of the lubricant, the lives with the three materials ranked in descending order as follows: AISI 52100, AISI M-50, AISI 1018.

Effect of Contact Angle

Aside from the material and lubricant criteria required for improving bearing life and reliability, design considerations are also important. The bearing contact angle is one of these design factors. Bearing contact angle can be defined as the angle made by a line passing through the points of contact of the ball and both raceways with a plane perpendicular to the axis of the bearing when both races are centered with respect to each other and one race is axially displaced with respect to the other without the application of measurable force. The actual bearing contact angle depends on various operating variables, including bearing load and speed, and may be different at both races.

As the contact angle is increased, the spin velocity, ω_s, (and therefore relative sliding between the ball and race) is increased. The sliding is a function of the angular speed of the bearing inner race, the geometry of the bearing, and the applied thrust load. The ball spin affects the surface traction forces and heat generation. These, in turn, affect the elastohydrodynamic film thickness and, possibly, the subsurface shear stress. All of these factors, in turn, can affect the rolling element fatigue life.

An experimental program was initiated to determine the effect on bearing

fatigue and load capacity of the changes in various factors caused by a change in the contact angle. The five-ball fatigue tester was used to determine the rolling element fatigue lives of 12.7-mm ($\frac{1}{2}$-in.)-diameter M-1 steel balls at four contact angles: 10, 20, 30, and 40 deg. These tests were run at an initial maximum hertz stress of 5.52 GPa (800 000 psi) using a synthetic diester lubricant meeting the MIL-L-7808C specification [14]. The contact angle for the five-ball fatigue test assembly is shown in Fig. 1b.

Figure 7 shows the fatigue results for these test conditions. These results indicate that the fatigue life decreases as the contact angle increases. The data are in agreement with other data obtained in a Pratt and Whitney modified one-ball fatigue tester [14] for 30, 45, and 55 deg contact angles. These data are also shown in Fig. 7. (Since both sets of data had a common contact angle of 30 deg, the fatigue lives were compared with the fatigue lives at this angle.)

To obtain an estimate of the variation of contact temperature with contact angle, β, temperature measurements were made in a modified five-ball fatigue tester (Fig. 1e). Each upper ball had a thermocouple attached, the tip of which was approximately 0.25 mm (0.01 in.) away from the edge of the running track. Several measurements were made at running conditions of 5.52 GPa (800 000 psi), a shaft speed of 10 000 rpm, and contact angles of 10, 20, 30, and 40 deg. The data obtained with these balls are summarized in Fig. 8. These temperatures are believed to represent a much better approximation of actual contact temperatures than the temperatures measured at the outside diameter of the race. A linear increase in temperature is observed
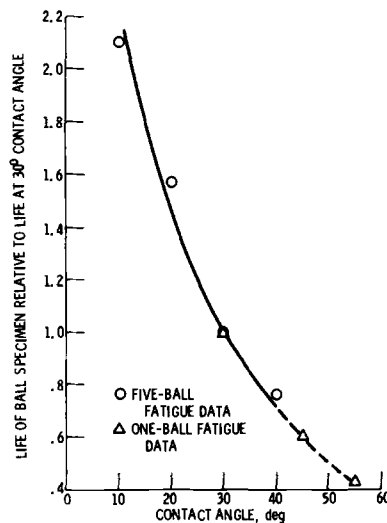

FIG. 7—*The effect of the contact angle on rolling element fatigue for a constant hertz stress* [14].
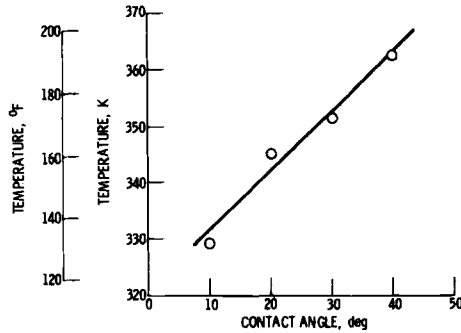
FIG. 8—*Temperature at the edge of a contact area as a function of the contact angle. Maximum hertz stress, 5.52 GPa (800 000 psi); 10 000 rpm; five-ball fatigue tester [14].*

with increasing contact angle. The near-contact temperature at the 40 deg contact angle is approximately 33 K (60°F) higher than that at the 10 deg contact angle.

Rolling element fatigue tests were conducted with 12.7-mm (½-in.)-diameter AISI 52100 steel balls in the five-ball fatigue tester modified for cryogenic temperature testing [35]. The test conditions included a drive shaft speed of 4 750 rpm; a maximum hertz stress of 5.52 GPa (800 000 psi); an outer-race temperature of 130 K (235°R); a lubricant temperature of 170 K (305°R); and contact angles of 20, 30, and 40 deg. A fluorinated ether fluid was used as the lubricant.

There was a decrease in the fatigue life as the contact angle increased. However, the differences among the fatigue lives obtained at 20, 30, and 40-deg contact angles were not statistically significant. This trend of a decreasing fatigue life with an increasing contact angle in fluorinated ether fluid at 170 K (305°R) is identical to the trend with the diester fluid at contact angles of 20, 30, and 40 deg at 328 K (590°R). Analysis indicates that the decrease in fatigue life is caused by a decreased EHD film thickness and decreased ball hardness caused, in turn, by an increased contact temperature.

Effect of Bearing Steel

Alloying Elements—A considerable number of studies have been performed to determine the rolling element fatigue lives of various bearing materials. (A list of references related to these studies can be found in Ref 36.) However, none of these previous studies maintained the required close control of operating and processing variables, such as material hardness, melting technique, and lubricant type and batch, for a completely unbiased material comparison. It was necessary to compare these materials in rolling element fatigue tests or actual bearing tests. The more standard mechanical tests such as ten-

sion and compression tests or rotating beam tests could not be correlated with rolling element fatigue results [8].

Eight steels (AISI 52100, M-1, M-2, M-10, M-50, M-42, T-1, and Halmo) were tested in the five-ball fatigue tester [36–38]. Groups of 12.7-mm (½-in.)-diameter balls of each of these materials were tested at a maximum hertz stress of 5.52 GPa (800 000 psi), a contact angle of 30 deg, and a shaft speed of 10 000 rpm. The tests were run at a race temperature of 339 K (150°F) with a superrefined naphthenic mineral oil as the lubricant.

In each of the tests, all five balls of the five-ball system were from the particular material lot being tested. From 25 to 30 five-ball tests were run for each material lot. Each test was suspended when either an upper or a lower ball failed or when a cutoff time of 100 h was reached.

The 10 percent lives for each material lot are shown in Table 3. A 2 to 1 ratio in the 10 percent lives of two lots of the same material is observed with both AISI 52100 and AISI M-10 steels. The only difference between lots of the same material is that they were heat treated separately. The different values of fatigue life among the material lots cannot be attributed to the slight variations in the material properties, such as hardness, grain size, retained austenite, and cleanliness, since no clear trends were apparent. These slight material property differences may be a result of slight variations in the execution of the heat treatment. The variation in the 10 percent fatigue lives between material lots may also be normal scatter in rolling element fatigue data. Based upon previous experience, a 2 to 1 ratio in fatigue lives among lots of the same material is not unusual.

The tests with all three heat treatment lots of each material were grouped together to compare the fatigue lives of the various materials. A Weibull analysis was performed on the combined results for each material.

The materials containing the greatest weight percentage of alloying elements were those with the lowest fatigue lives. This effect is shown in Fig. 9, where the relative 10 percent lives are plotted against the total weight percent of the alloying elements tungsten, chromium, vanadium, molybdenum, and cobalt. Individually, each element shows no consistent effect on fatigue life. The possible exception is tungsten, which is present in significant quantities in the four lowest-lived materials, AISI M-1, AISI M-2, AISI T-1, and AISI M-42. The effect, therefore, seems to be a cumulative one. When present in high percentages, these alloying elements appear to be detrimental to rolling element fatigue life.

There was a strong indication that a relationship existed among these alloying elements and the size and distribution of the metal carbides, which vary with alloy content and heat treatment. In Ref 39 a carbide parameter was derived based upon a statistical analysis which related the rolling element fatigue life to the total number of residual carbide particles per unit area, the median residual carbide size, and the percentage of residual carbide area. A

comparison of the data contained in Table 3 and the carbide parameter, C', is shown in Fig. 10.

Processing Variables—Rolling element bearings for main shaft applications in aircraft turbine engines are made primarily of either AISI M-50 or Type 18-4-1 steels. AISI M-50 steel has been used in such applications since about 1957 and is today the standard material used by American jet engine manufacturers [40]. Type 18-4-1 steels are used for these applications primarily by the European jet engine manufacturers. Both materials contain alloying elements to promote high hardness values and good hardness retention at the high temperatures experienced by main shaft bearings. Both contain significant chromium and vanadium, but AISI M-50 contains molybdenum, whereas Type 18-4-1 steel contains tungsten.

Current aircraft turbine engine manufacturers' material specifications demand a double vacuum melted (VIMVAR, for vacuum induction melted–vacuum arc remelted) AISI M-50 steel for main shaft bearings. With this material, ball bearing fatigue lives of nearly 100 times the Anti-Friction Bearing Manufacturers Association (AFBMA)-predicted life have been obtained [40]. Reduction in the inclusion content, trace elements, and interstitial gas content due to double vacuum melting is considered responsible for a major portion of this life advancement.

Rolling element fatigue tests were conducted in the five-ball fatigue tester with VIMVAR AISI M-50, electroflux remelt (EFR) Type 18-4-1, and VAR Type 18-4-1 materials [41]. Two groups of each material were subjected to slightly different heat treatments. The results and test conditions are shown in Fig. 11. Individual data points for each Weibull plot are given in Ref 41.

A statistical comparison of the test results indicates that the rolling element fatigue life of VIMVAR AISI M-50 is not significantly different from that of EFR or VAR Type 18-4-1 steel. The slight variations in heat-treatment procedures for each material resulted in statistically insignificant differences in rolling element fatigue life. These results are contrary to what would have been predicted based on the total percentage of alloying elements, as previously discussed. Since the Type 18-4-1 material had a higher alloy content, it would have been expected to have a lower fatigue life. These data suggest that the melting process may have a far stronger influence on rolling element fatigue life than the material chemistry.

AMS 5749 steel combines the tempering, hot hardness, and hardness retention characteristics of AISI M-50 steel with the corrosion and oxidation resistance of AISI 440C stainless steel. The effects of double vacuum melting and retained austenite on the rolling element fatigue life of AMS 5749 steel were determined in tests run in the five-ball fatigue tester [42,43]. The results and test conditions are shown in Fig. 12.

Double vacuum melting (VIMVAR) produced an AMS 5749 material with a rolling element fatigue life of at least 14 times that for the same material

TABLE 3—*Fatigue results with groups of 1/2-in. diameter^a balls run in five-ball fatigue testers.^{b}*

Material	Heat Treatment Lot	Average Hardness, HRC	Retained Austenite, Volume Percent^c	Austenitic Grain Size^d	Cleanliness Rating^e		Life, Millions of Upper-Ball Stress Cycles		Slope	Failure Index^g	Carbide parameter, C'^{h}
					Class^f	Type	B$_{10}$	B$_{50}$			
52100	A	62.5	4.90	13	B1	heavy	18.5	114	1.04	22 out of 29	1.22
	B	62.0	4.10	13	D1	thin	30.1	130	1.29	22 out of 29	1.17
	C	62.5	0.80	13	D1	thin	12.9	84	1.00	19 out of 25	0.76
	combined	...	...	...	...	...	21.2	109	1.15	63 out of 83	1.00
Halmo	A	60.8	0.60	8	D2	heavy	22.0	74	1.56	25 out of 30	0.58
	B	60.8	1.00	8	D1	heavy	12.9	57	1.26	28 out of 30	0.64
	C	61.1	1.70	8	D2	heavy	12.9	68	1.14	26 out of 30	0.69
	combined	...	...	...	...	...	16.4	66	1.35	79 out of 90	0.63
M-50	A	62.6	1.90	10	B1	heavy	15.3	35	2.29	29 out of 29	0.60
	B	62.2	2.90	9	D2	heavy	12.3	36	1.73	24 out of 30	0.54
	C	62.3	1.50	10	D1	heavy	14.2	48	1.55	26 out of 29	0.50
	combined	...	...	...	...	...	14.4	39	1.89	79 out of 88	0.56
M-10	A	62.2	1.10	9	D3	heavy	19.4	65	1.56	26 out of 30	0.36
	B	62.0	2.40	6	D2	heavy	8.3	46	1.11	30 out of 30	0.39
	C	61.8	1.60	6	D1	thin	13.1	42	1.62	29 out of 30	0.35
	combined	...	...	...	...	...	13.2	50	1.40	85 out of 90	0.37

Material	Class									
T-1	A	61.4	7.30	11	B1	heavy	6.6	50	0.92	26 out of 30	0.26
	B	61.4	5.20	9	D1	thin	8.4	59	0.97	26 out of 30	0.33
	C	61.0	9.50	10	D1	heavy	8.5	74	0.87	23 out of 30	0.30
	combined	...	...	...	...	...	8.6	59	0.98	75 out of 90	0.29
M-1	A	63.3	2.90	10	B2	heavy	8.2	43	1.13	29 out of 30	0.32
	B	63.4	3.30	9	A1	heavy	5.9	37	1.02	29 out of 30	0.34
	C	63.5	1.00	8	A2	heavy	6.7	33	1.18	29 out of 29	0.38
	combined	...	...	...	...	...	7.6	38	1.18	87 out of 89	0.33
M-2	A	63.4	1.70	6	B1	heavy	5.8	35	1.05	28 out of 30	0.36
	B	63.4	2.40	10	D1	thin	5.5	26	1.23	28 out of 29	0.36
	C	63.4	2.30	9	D1	heavy	4.2	31	0.95	29 out of 30	0.35
	combined	...	...	...	...	...	5.7	30	1.13	85 out of 89	0.36
M-42	A	61.8	1.00	9	A1	thin	1.0	6.6	0.97	30 out of 30	0.07
	B	61.3	4.40	10	D1	heavy	1.7	8.9	1.12	27 out of 30	0.07
	C	61.3	4.90	8	D1	heavy	1.4	5.8	1.33	30 out of 30	0.07
	combined	...	...	...	...	...	1.4	7.0	1.18	87 out of 90	0.07

[a] 1/2 in. = 12.7 mm.

[b] Maximum hertz stress, 5.52 GPa (800 000 psi); contact angle, 30 deg, shaft speed, 10 300 rpm; race temperature, 339 K (150°F) [39].

[c] Determined from the integrated peak intensities of (220) γ and (200) α planes.

[d] Methods of Estimating the Average Grain Size of Metals (ASTM E 112-80).

[e] Recommended Practice for Determining the Inclusion Content of Steel (ASTM E 45-76), Method A (table shows predominate inclusion class and type).

[f] Inclusion classes: A = sulfides, B = alumina, C = silicates, D = globular oxides.

[g] Indicates number of failures out of total number of tests.
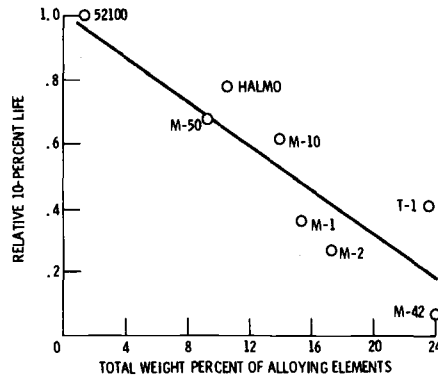
[h] Defined in Ref 39.

FIG. 9—*The effect of the total weight percent of alloying elements tungsten, chromium, vanadium, molybdenum, and cobalt on rolling element fatigue life at 339 K (150°F) [36].*
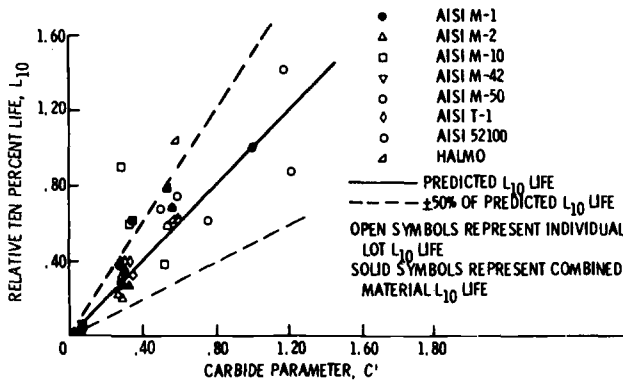

FIG. 10—*The individual and average 10 percent life, L_{10}, for eight bearing materials as a function of the carbide parameter [39].*

with vacuum induction melting alone. The VIMVAR AMS 5749 steel balls gave lives from 6 to 12 times greater than VIMVAR AISI M-50 steel balls. Similar tests in the rolling contact (RC) fatigue tester [43] showed no significant difference in the lives of the two materials. The difference between the five-ball results and the RC rig results are not yet understood.

A material processing method commonly called ausforming has been studied in the five-ball fatigue tester. The ausforming process consists of an isothermal "warm working" operation performed while the material is in a metastable austenitic condition. The austenite is subsequently transformed in either the lower bainite or the martensite transformation region of the time–temperature–transformation (TTT) curve. If the ausforming method is to be applied, the steel must have a sluggish transformation behavior in the tem-
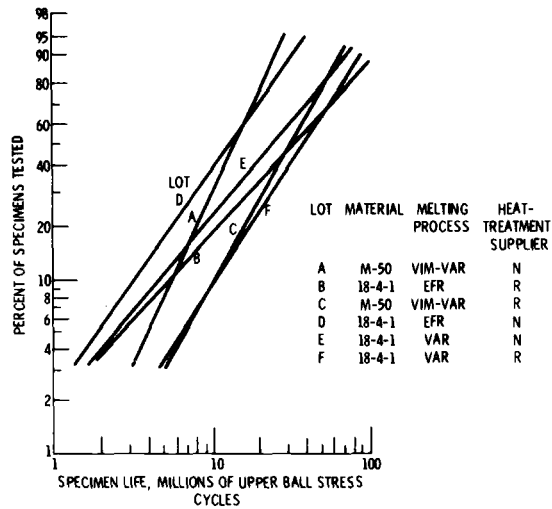
FIG. 11—*Rolling element fatigue life of VIMVAR AISI M-50, EFR Type 18-4-1, and VAR Type 18-4-1 steel balls in the five-ball fatigue tester. Maximum hertz stress, 5520 MPa (800 000 psi); shaft speed, 10 700 rpm; contact angle, 30 deg; temperature, 339 K (150°F); Type II ester (MIL-L-23699) lubricant [41].*
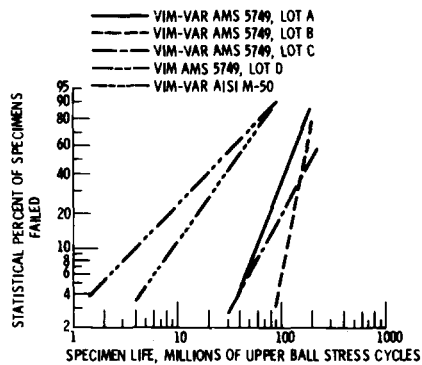
FIG. 12—*Summary of rolling-element fatigue data with AMS 5749 and AISI M-50 balls in the five-ball fatigue tester. Maximum hertz stress, 5.52 GPa (800 000 psi); shaft speed, 10 700 rpm; contact angle, 30 deg; temperature, 339 K (150°F); lubricant, superrefined naphthenic mineral oil [42].*

perature range where "warm working" is to take place. AISI M-50 is such a steel.

The five-ball fatigue tester was used to determine the effect of ausforming on the rolling element fatigue life of 11.1-mm (7/16-in.)-diameter consumable-electrode vacuum melted (CVM) AISI M-50 steel balls [44]. One group of ausformed balls and two groups of CVM processed AISI M-50 steel balls were tested at a maximum hertz stress of 5.52 GPa (800 000 psi), a shaft

speed of 10 000 rpm, and a contact angle of 23 deg with no heat added. A paraffinic mineral oil was used as the lubricant.

The ausformed balls were fabricated from AISI M-50 bar material, which was extruded to a cross-sectional area 20 percent of the original area (80 percent reduction in cross-sectional area), while the material was in a metastable austenitic condition. The 10 percent fatigue life of this group of ausformed balls was three and four times that of two groups of CVM-processed AISI M-50 balls.

Ausforming results in a reduction in size and a more uniform distribution of carbide particles than with conventionally processed AISI M-50 steel. Thus, the smaller, more uniformly distributed carbide particles could have accounted for the longer fatigue life by lessening the severity of dislocation pileups which cause stress concentrations and accelerate crack initiation and propagation. It is believed that the "warm work" imparted to the material during the ausforming process provided more numerous nucleation sites, which accounts for the relatively uniform carbide precipitation. The added strain energy also speeded up the time-dependent precipitation process which was apparently completed before the material cooled to room temperature.

Unpublished data from NASA tests performed with VIMVAR AISI M-50 120-mm-bore angular-contact ball bearings made by ausforming showed that forging laps were induced in the raceways of the bearing because of the relatively low forging temperature. These forging laps acted as nuclei for fatigue spalls in a rather short period of time. The conclusion reached is that ausforming can result in improved rolling element fatigue life, but problems with forging, particularly the large, massive parts and the costs thereof, far exceeded its benefits.

Nonferrous Materials

In the late 1950s and early 1960s it was anticipated that aerospace technology would require bearings to operate reliably at temperatures between 644 and 1366 K (700 and 2000°F). Since this temperature range is beyond the range in which ferrous bearing materials are capable of operating for any significant length of time, refractory materials such as ceramics and cermets were considered.

The first nonferrous material studied in the five-ball fatigue tester was a crystallized glass ceramic (Pyroceram 9608) [7,10]. Rolling element fatigue spalls similar to those observed for bearing steel balls were produced, but the room-temperature load-carrying capacity was found to be approximately $\frac{1}{15}$ that of a group of previously tested AISI M-1 bearing steel balls. Tests at maximum hertz stresses of 1.83, 2.03, and 2.28 GPa (265 000, 295 000, and 330 000 psi) and a speed of 2 430 rpm showed that the fatigue life of the ceramic varied inversely with approximately the 11th to 13th power of stress.

The rate of fatigue spall development was much slower than that which is normal for steel balls. An intentional overrun for a period several times that which produced the initial fatigue spalling did not produce a general breakdown of the test surface. The scatter between shortlived and long-lived specimens was much lower for the crystallized glass ceramic than is normal for bearing steels (higher Weibull slope). Since the ceramic does not have appreciable foreign matter comparable to the nonmetallic inclusions in steel, this low scatter indicates that the degree of structural homogeneity may be an important factor in the life scatter of bearing materials.

Variation in the contact angle, which produces variations in the relative sliding of the contacting surfaces, did not produce any significant differences in the fatigue life of specimens run at the same contact load (hertz stress). The fatigue life at 644 K (700°F) was approximately one third of that observed at room temperature. This may not indicate a thermal effect in the material itself, since variation in lubricant viscosity over this temperature range could produce this difference in life. These tests indicated that the crystallized glass ceramic may be useful in low-load, short-duration applications where an operating temperature above the limits of steels is the paramount design consideration.

Subsequent to the tests with the crystallized glass ceramic, tests were conducted in the five-ball fatigue tester with four other refractory materials: hot-pressed alumina, cold-pressed-and-sintered alumina, self-bonded silicon carbide, and nickel-bonded titanium carbide cermet [45–47]. The results and test conditions are shown in Fig. 13. The support balls were of AISI 52100 and AISI M-50 steel in the 300 and 644 K (80 and the 700°F) tests, respectively. Preliminary tests were also performed with each of the four refractory materials at higher temperatures from 866 to 1366 K (1100 to 2000°F). For these tests, hot-pressed alumina support balls were used with molybdenum disulfide lubrication in a modified five-ball tester (Fig. 1f).

The failure pits in all four materials were shallow, eroded areas, apparently of surface origin, and were unlike the fatigue pits found in bearing steels. The progression of an incipient failure for all four materials was a slow process that frequently consumed one half of the total running time of the specimen.

The lives of hot-pressed alumina and nickel-bonded titanium carbide cermet varied inversely with stress to an average power of approximately 10. However, the cold-pressed-and-sintered alumina and the self-bonded silicon carbide were less sensitive and exhibited an average stress-life exponent ranging from 7 to 8.

The capacity at 300 K (80°F) of hot-pressed alumina was about 7 percent that of a typical bearing steel but was the highest of the four materials studied. Preliminary tests at elevated temperatures indicated that hot-pressed alumina is capable of rolling contact operation at temperatures up to 1366 K (2000°F) without gross wear or plastic deformation.
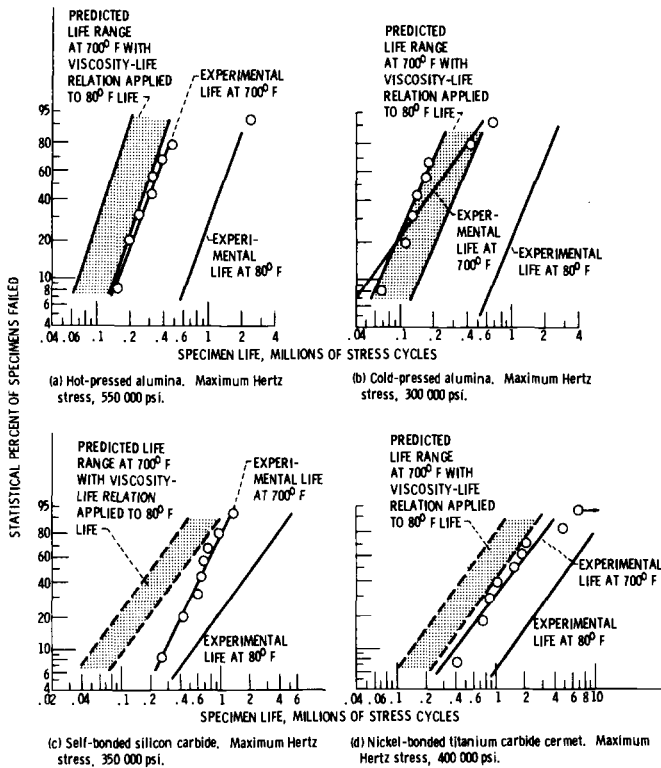
FIG. 13—*The effect of a 644 K (700°F) race temperature on the life of 12.7-mm (1/2-in.) diameter ball specimens of four refractory materials in the five-ball fatigue tester. Shaft speed, 9 500 rpm; contact angle, 20 deg; lubricant, highly refined naphthenic mineral oil; viscosity at 300 K (80°F), 150 cSt; viscosity at 644 K (700°F), 0.6 cSt; maximum hertz stress, 1.72 to 4.48 GPa (250 000 to 650 000 psi) [47].*

It was concluded in Ref *47* that the ability of a ceramic or cermet material to be functional in rolling contact applications appears to be related to its physical properties and surface condition. Consequently, surface finish appears to be an important criterion for long life. Since the surface finish was related to the amount of porosity or to the presence of a weak second phase, such conditions should be avoided for proposed high-temperature bearing materials.

Hot-pressed silicon nitride has a low specific gravity (41 percent that of bearing steel) and has a potential application as low-mass balls for very high-speed ball bearings. Hot-pressed silicon nitride balls were tested under rolling contact conditions in the five-ball fatigue tester [*48–50*]. The test conditions were maximum hertz stresses of 4.27 and 5.52 GPa (620 000 and 800 000 psi), a race temperature of 328 K (130°F), a speed of 9 400 rpm, and a super-refined naphthenic mineral oil as the lubricant. The fatigue lives were com-

pared with those for typical bearing steels AISI 52100 and AISI M-50. An analytical program was used to predict the dynamic performance character- istics and fatigue life of high-speed ball bearings with silicon nitride balls in relation to that of bearings containing steel balls.

Extrapolation of the experimental results to contact loads which result in stress levels typical of those in rolling element bearing applications indicated that hot-pressed silicon nitride running against steel may be expected to yield fatigue lives comparable to or greater than those of bearing-quality steel run- ning against steel. The fatigue spalls on the silicon nitride balls were similar in appearance to those observed in tests with typical bearing steels. The fatigue life with the hot-pressed silicon nitride is considerably greater than that of any other ceramic or cermet tested.

A digital computer analysis indicates that there is no improvement in the lives of 120-mm-bore angular-contact ball bearings of the same geometry operating at DN values from 2 to 4 million where hot-pressed silicon nitride balls are used in place of steel balls. DN is defined as the bearing bore in millimetres times shaft speed in revolutions per minute. The higher modulus of elasticity of silicon nitride tends to offset the benefits of its lower density. The principal value of silicon nitride may lie in bearings in marginally lubri- cated corrosive environments rather than in extensive speed applications.

Hollow Rolling Elements

In the mid-1960s analyses indicated that bearings operating at DN values above 1.5 million would experience reduced life because of high centrifugal forces and increased hertz stresses at the outer race and ball contacts. At that time engine designers anticipated turbine bearing speeds increasing to the range of 2.5 to 3 million DN after 1980, with consequent significant decreases in fatigue life.

A possible solution to the problem caused by ball centrifugal force was the use of hollow balls in the bearing. Obviously, removal of a large percentage of the mass from the ball will reduce the centrifugal force.

The five-ball fatigue tester was used to determine the rolling element fa- tigue lives of solid 12.7-mm (½-in.)-diameter balls [51,52] and hollow balls with 2.54-mm (0.100-in.) wall thickness (weight reduction of 21.7 percent from that of a solid ball) [51,52]. The upper test balls fabricated from CVM AISI 52100 steel were run against solid AISI 52100 steel lower support balls. The results and test conditions are shown in Fig. 14.

The hollow balls were fabricated by a technique that included rough-form- ing hemispherical shells, joining them together by electron-beam welding, heat treating, and finishing to an AFBMA 10 specification, comparable to that of the solid balls. Both the hollow balls and the solid balls were fatigue tested to obtain comparative data. The results shown in Fig. 14 indicate that
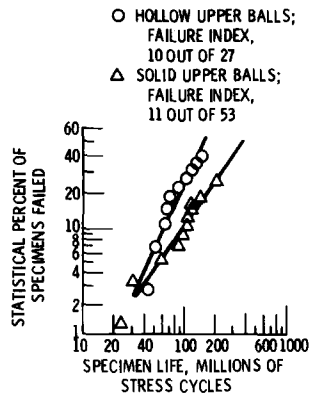
FIG. 14—*The rolling element fatigue life of CVM AISI 52100 steel hollow and solid balls in the five-ball fatigue tester. Maximum hertz stress, 5.52 GPa (800 000 psi), speed 10 600 rpm; no heat added; lubricant, superrefined naphthenic mineral oil; contact angle, 20 deg.*

the differences in fatigue life between the two groups of balls are not statistically significant.

The probability of a fatigue spall occurring in the weld area was calculated as 6.5 percent for those tests in which the running track crossed the weld. One of the ten fatigue spalls that occurred on the hollow balls was in the weld. This spall was a classic subsurface type, similar in appearance to those occurring in the area outside of the weld and in the conventional solid balls.

Only minor differences in hardness were measured on a section of the hollow ball wall cut through a diameter normal to the weld. Similar metallographic structures were observed on the weld zone and the parent material. These results indicated that there was extremely good control during the manufacturing process and that the presence of a weld zone should not be detrimental to the rolling element fatigue life of the balls.

To explore the effects of higher percentages of weight reduction, additional testing was conducted with CVM AISI M-50 balls of 17.5-mm ($^{11}/_{16}$-in.) diameter and a wall thickness of 1.52 mm (0.060 in.) [52,53]. This represents a weight reduction of 56.5 percent from that of a solid ball. These results are shown in Fig. 15. The 10 percent life obtained with these hollow balls was approximately one fifth that for a comparable solid ball.

Seven of these hollow balls were electropolished to determine the orientation of the weld. On each of six failed balls, the running track crossed the weld. The fatigue spall on five of these six balls was adjacent to or directly on the weld. The spall on the other ball was clearly away from the weld area. The running track on the seventh ball did not cross the weld. This ball had no fatigue spall after 300 h (530 million stress cycles) of running time.

Four of the failed balls with the spall adjacent to the weld were sectioned parallel to and through the running track. In each ball, a crack was found
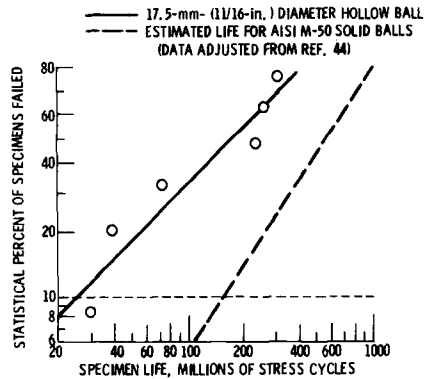
FIG. 15—*The rolling element fatigue life of CVM AISI M-50 steel balls in the five-ball fatigue tester. Maximum hertz stress, 4.83 GPa (700 000 psi); speed, 10 600 rpm; no heat added; lubricant, superrefined naphthenic mineral oil; contact angle, 34.5 deg.*

that passed through the weld area and connected the outside surface spall to the inside surface.

From the width, shape, and pattern of these cracks, it was concluded that they initiated at the inner surface of the ball and propagated to the outer surface, resulting in a spall that resembles those of classic subsurface rolling element fatigue. It was also concluded that these hollow balls from the fatigue tests had probably failed in flexure because of a stress concentration in the region of the weld. The stress concentration appeared to be at the notch formed at the edge of the weld.

The ball with the spall away from the weld area was also sectioned through the spall parallel to the running track. No cracks could be seen connecting the spall and the inner surface of the ball. This failure was apparently not a result of flexure of the wall and probably was classic subsurface fatigue.

The 12.7-mm (½-in.)-diameter AISI 52100 steel hollow balls, with a 21.7 percent weight reduction, compared satisfactorily with solid balls in fatigue tests. However, the 17.5-mm (¹¹/₁₆-in.)-diameter AISI M-50 steel hollow balls with a 56.5 percent weight reduction did not compare very well with solid balls in fatigue tests. The fact that the balls were of different material and size should not have made any significant difference in the fatigue comparisons. It is probable that a weight reduction of 56.5 percent results in a wall that is simply too thin for use in a bearing ball.

Additional experiments were conducted [54] to compare the rolling element fatigue life of electron-beam-welded hollow balls with wall thicknesses of 1.78 mm (0.070 in.) with previously run solid balls and hollow balls of 1.52-mm (0.060-in.) wall thickness. These balls, also made from AISI M-50 steel, had a weight reduction of 50 percent.

The fatigue life of these hollow balls, determined in the five-ball fatigue

tester at a maximum hertz stress of 4.83 GPa (700 000 psi) was not signifi-
cantly less than that of the previously run solid balls of the same material.
The ball failures on the hollow balls with the 50 percent weight reduction
resulted from classic subsurface fatigue and did not occur in the weld area.
However, subsequent tests [53,54] with 215-series bearings with hollow balls
with both the 56.5 and the 50 percent weight reductions had ball failures at-
tributed to flexure fatigue. These bearings were not heavily loaded [thrust
load of 2240 N (500 lb)], but the normal ball load was more than twice that of
the five-ball test. The authors have concluded that hollow balls with a weight
reduction of 50 percent or greater have a wall that is too thin for use in bear-
ings for aircraft turbine engines.

A number of additional problems exist with the use of hollow balls in bear-
ings, which are inherent in the manufacture of the ball. Two significant prob-
lems are difficulty in (a) maintaining a uniform wall thickness and (b) con-
trolling the weld penetration around the periphery of the ball. Unless these
problems are overcome, hollow balls will have an unbalance or a slightly dif-
ferent stiffness at the weld, or both. Under dynamic conditions, these factors
could adversely affect the life of the ball.

Stress–Life Relationship

Four groups of 12.7-mm (½-in.)-diameter balls were tested, each at a level
of maximum hertz stress in the range of 4.48 to 6.03 GPa (650 000 to 875 000
psi) [55,56]. Tests were run in the five-ball fatigue tester at a contact angle of
30 deg and a shaft speed of 10 000 rpm with a paraffinic mineral oil as the
lubricant. All the balls were from one heat of vacuum-degassed AISI 52100
material. The results of these tests are shown in Fig. 16. At the four stress
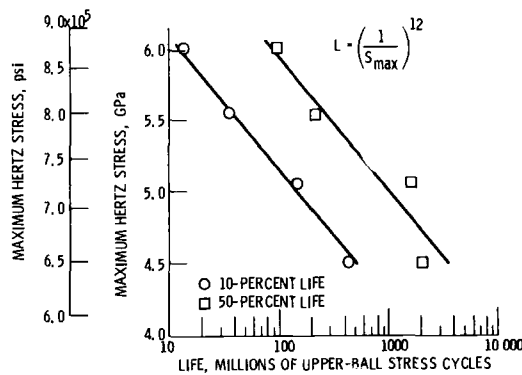levels tested, the fatigue lives were inversely proportional to the maximum

FIG. 16—*The effect of the maximum hertz stress on the life of vacuum-degassed AISI 52100
balls tested in the five-ball fatigue tester* [55].

hertz stress raised to the power of 12. This result agrees with a survey of the literature [55,56], which suggests that a stress–life exponent of approximately 12 is typical of vacuum-processed bearing steels. The exponent of 9, which was initially determined and verified with air-melted materials, has been generally accepted by the bearing industry. Results of this investigation indicate that the load–life relationship for vacuum-processed bearing steels may be a fourth power relationship rather than the third power relationship that has been generally accepted. However, tests run with consumable-electrode vacuum melted AISI M-50 steel angular-contact ball bearings at 533 K (500°F) at three thrust loads did not show a significant deviation from the accepted ninth power stress–life relationship [56].

Ferrographic Analysis

A ferrographic analysis was used to determine the types and quantities of wear debris generated during accelerated rolling element fatigue tests in the five-ball fatigue tester [57,58]. Lubricant samples were taken from tests previously reported [42,43]. The ball specimens were made of AMS 5749, a corrosion-resistant, high-temperature bearing steel. The lubricant was a super-refined naphthenic mineral oil. The conditions included a maximum hertz stress of 5.52 GPa (800 000 psi) and a shaft speed of 10 000 rpm. Four types of debris were observed: normal rubbing wear particles, fatigue microspall particles, spheres, and friction polymer deposits. For about half of the tests, the fatigue spall particle rating and the number of spherical particles reached a maximum during the last third of the test duration. The number of spheres observed in these accelerated fatigue tests was much lower than others have reported during long-duration testing under lower loads. Laminar particles, sometimes associated with rolling contact fatigue, were not observed in this study. The characterization of wear debris as a function of time was of limited use in predicting fatigue failures in these accelerated tests.

Correlation with Full-Scale Bearings

A prime purpose of accelerated rolling element fatigue testing is to study phenomena which occur in rolling element bearings and in a relatively short time period at reduced cost. Ultimately, however, the various trends and discoveries which are recognized from these tests must be incorporated in and validated with full-scale bearing tests.

While it may be difficult, although not impossible, to predict actual bearing life [59] from them, or based on them, bench-type fatigue tests, such as those run in the NASA five-ball fatigue tester, can rank material, lubricant, or operating variables on a relative life basis [5,14–18,36]. This is illustrated in Fig. 6, which is a comparison of the relative load capacity in the five-ball

tester to that obtained with 7208-size bearings where the lubricant type is the variable [16]. Figure 17 compares the relative load capacity obtained in the five-ball system to that obtained with the 207-size bearings where ball hardness is the variable [18]. As can be seen for both the material hardness and the lubricant variables, the correlation of the five-ball tester results with those of full-scale bearing tests on a relative basis is excellent. For both sizes of bearings, the maximum stress level was approximately 2.41 GPa (350 000 psi) at the inner race-ball contact in comparison with 5.52 GPa (800 000 psi) for the five-ball tester.

Additional work was performed with 120-mm-bore ball bearings made from AISI M-1, AISI M-50, and WB-49 steels [36,60]. The bearings were tested at an outer-race temperature of 589 K (600°F). The 10 percent lives of the AISI M-50 and AISI M-1 bearings exceeded the calculated AFBMA life by factors of 13 and 6, respectively. The bearings with WB-49 races showed lives less than the AFBMA life.

The magnitudes of the life differences seen in these bearing tests at 589 K (600°F) correlate well with the five-ball fatigue test results. Relative 10 percent fatigue lives are shown in Fig. 18. Using the AISI M-50 10 percent life as a comparison, the AISI M-1 data for the five-ball fatigue tests and the bearing tests agree remarkably well. WB-49 and AISI M-42, both of which are alloys containing relatively high percentages of cobalt and with similar microstructures, show reasonably good agreement between the five-ball fatigue tests and the bearing tests.

These examples of excellent correlation of five-ball fatigue tester data with full-scale bearing fatigue data show that this tester can reliably identify qualitative effects of many variables on rolling element fatigue life. As an accelerated test, it does so in a timely and relatively inexpensive manner. As such it has had a broad and significant effect on full-scale bearing research and, thus, on the present state of the art of bearings.
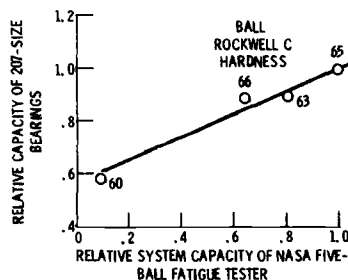

FIG. 17—*The relative capacity of 207-size bearings as a function of the relative capacity of the five-ball fatigue tester for various ball hardnesses. The nominal hardness of upper ball (for five-ball tests) and inner race (for bearings) is 63 HRC [18].*
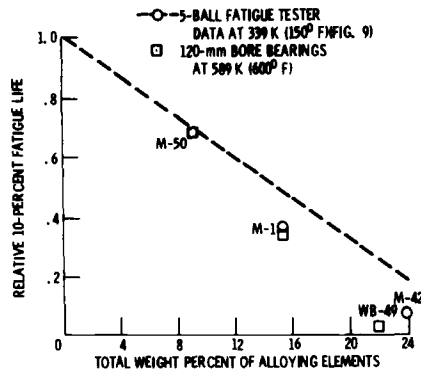
FIG. 18—*The effect of the total weight percent of alloying elements on the fatigue life of 120-mm-bore bearings at 589 K (600°F) [36].*

Summary of Results

The NASA five-ball fatigue tester was conceived by W. J. Anderson in late 1958. The first data were generated in March 1959. Since then a total of approximately 500 000 test hours have been accumulated on a group of eight test rigs which are capable of running 24 h a day, 7 days a week. Studies have been conducted on the effect on rolling element fatigue life of the contact angle, material hardness, chemistry, heat treatment and processing, lubricant type and chemistry, elastohydrodynamic film thickness, deformation and wear, vacuum, and temperature, as well as hertzian and residual stresses. From a survey of all the reports of tests using the five-ball fatigue tester, the following results were obtained:

1. A relationship was established between component hardness and fatigue life. The maximum bearing fatigue life can be achieved where the rolling elements of the bearing are 1 to 2 HRC points (ΔH) greater than the races.

2. A relationship was established between subsurface compressive residual stress and rolling element fatigue life. The value of the maximum shear stress was effectively reduced by the presence of the compressive residual stress, thus increasing the life.

3. An interrelationship was established between lubricant type, elasto-hydrodynamic film thickness, and rolling element fatigue life.

4. There was no apparent effect of a reduced pressure environment on rolling element fatigue.

5. The operating characteristics and rolling element fatigue life of fluorinated polyether fluids at cryogenic temperatures compared favorably with those of a superrefined mineral oil at room temperature.

6. The rolling element fatigue lives obtained with traction fluids were not significantly different on a statistical basis from those obtained with a tetra-ester oil or a paraffinic mineral oil.

7. Lubricant additives can reduce rolling element fatigue life below that obtained with the lubricant base stock without additives. However, the additives used with the base oil did not change the life ranking of bearing steels in those tests where the rolling element fatigue was of subsurface origin.

8. There was a decrease in the fatigue life with increased contact angle (ball spin). The decrease in fatigue life was attributed primarily to decreased elastohydrodynamic film thickness caused by increased contact temperature.

9. A relationship was established between the material alloying elements and the rolling element fatigue life. This related to a statistically derived carbide factor, which, in turn, related the rolling element fatigue life to the total number of residual carbide particles per unit area, the median residual carbide size, and the percentage of residual carbide area.

10. Double vacuum melting had a far greater effect on improving rolling element fatigue life than material chemistry.

11. Ausforming improved the fatigue life of AISI M-50 steel balls over that of conventionally forged balls of the same heat of material. However, for full-scale bearings, the cost of ausforming exceeded its benefits.

12. The use of nonferrous materials at temperatures to 1366 K (2000°F) was established. However, the lives obtained were significantly less than those obtained at room temperature with conventional bearing steels.

13. The rolling element fatigue life of hot-pressed silicon nitride material was found to be considerably greater than that of any other ceramic or cermet material tested.

14. The primary mode of failure for hollow rolling elements was by flexure fatigue. Where failure was by classic subsurface rolling element fatigue, there was no statistical difference in life between the hollow and solid balls.

15. At four stress levels the fatigue lives were in inverse proportion to the maximum hertz stress to the power of 12. This would suggest that the load–life relationship for vacuum-processed bearing steels may be a fourth power relationship rather than the third power relationship that has been generally accepted.

16. The characterization of wear debris as a function of time using ferrographic analysis was of limited use in predicting fatigue failures in accelerated rolling element fatigue tests.

17. A qualitative correlation was established between the rolling element fatigue results in the five-ball fatigue tester and those in full-scale bearing tests.

18. The use of the five-ball fatigue tester has been established as a reliable, relatively inexpensive, and timely method of determining qualitative effects on rolling element fatigue life.

References

[1] Way, S., *Journal of Applied Mechanics*, Vol. 2, No. 2, June 1935, pp. A49–A58, A110–A114.

[2] Bear, H. R. and Butler, R. H., "Preliminary Metallographic Studies of Ball Fatigue Under Rolling-Contact Conditions," NACA TN-3925, National Aeronautics and Space Administration, Washington, D.C., 1957.

[3] Macks, E. F., *Lubrication Engineering*, Vol. 9, No. 5, Oct. 1953, pp. 254–258.

[4] Shevchenko, R. P., "Lubricant Requirements for High Temperature Bearings," SAE Paper No. 660072, presented at the Automotive Engineering Congress, Detroit, Mich., Jan. 1966.

[5] Baughman, R. A., "Experimental Laboratory Studies of Bearing Fatigue," ASME Paper No. 58-A-235, American Society of Mechanical Engineers, Annual Meeting, New York, Nov. 1958.

[6] Barwell, F. T. and Scott, D., *Engineering*, Vol. 182, No. 4713, 6 July 1956, pp. 9–12.

[7] Carter, T. L. and Zaretsky, E. V., "Rolling-Contact Fatigue Life of a Crystallized Glass Ceramic," NASA TN D-259, National Aeronautics and Space Administration, Washington, D.C., 1960.

[8] Carter, T. L., Zaretsky, E. V., and Anderson, W. J., "Effect of Hardness and Other Mechanical Properties on Rolling-Contact Fatigue Life of Four High-Temperature Bearing Steels," NASA TN D-270, National Aeronautics and Space Administration, Washington, D.C., 1960.

[9] Zaretsky, E. V. and Anderson, W. J., *A.S.T.M. Proceedings*, Vol. 60, 1960, pp. 627–649.

[10] Zaretsky, E. V. and Anderson, W. J., *Journal of Basic Engineering*, Vol. 83, No. 4, Dec. 1961, pp. 603–612.

[11] Anderson, W. J. and Zaretsky, E. V. in *Proceedings of the Symposium on Aspects of Rolling Contact Phenomena*, J. B. Bidwell, Ed., Elsevier, Amsterdam, 1962, pp. 317–345.

[12] Irwin, Arthur S., "Effect of Bearing Temperatures on Capacities of Bearings of Various Materials," paper presented at Third Spring Lubrication Symposium, American Society of Mechanical Engineers, New York, 14–15 March 1960.

[13] Baughman, R. A., *Journal of Basic Engineering*, Vol. 82, No. 2, June 1960, pp. 287–294.

[14] Zaretsky, E. V., Anderson, W. J., and Parker, R. J., *Transactions of the American Society of Lubrication Engineers*, Vol. 5, No. 1, Jan. 1962, pp. 210–219.

[15] Zaretsky, E. V., Sibley, L. B., and Anderson, W. J., *Journal of Basic Engineering*, Vol. 85, No. 3, Sept. 1963, pp. 439–450.

[16] Zaretsky, E. V., Anderson, W. J., and Parker, R. J., "Effect of Nine Lubricants on Rolling-Contact Fatigue Life," NASA TN D-1404, National Aeronautics and Space Administration, Washington, D.C., 1962.

[17] Zaretsky, E. V., Parker, R. J., and Anderson, W. J., "Effect of Component Differential Hardnesses on Rolling-Contact Fatigue and Load Capacity," NASA TN D-2640, National Aeronautics and Space Administration, Washington, D.C., 1965.

[18] Zaretsky, E. V., Parker, R. J., and Anderson, W. J., *Journal of Lubrication Technology*, Vol. 89, No. 1, Jan. 1967, pp. 47–62.

[19] Zaretsky, E. V., Parker, R. J., Anderson, W. J., and Reichard, D. W., "Bearing Life and Failure Distribution as Affected by Actual Component Differential Hardness," NASA TN D-3101, National Aeronautics and Space Administration, Washington, D.C., 1965.

[20] Bush, J. J., Grube, W. L., and Robinson, G. H., *Transactions, American Society for Metals*, Vol. 54, No. 3, 1961, pp. 390–412, 818–824.

[21] Almen, J. O. in *Rolling Contact Phenomena*, J. B. Bidwell, Ed., Elsevier, New York, 1962, pp. 400–424.

[22] Scott, R. L., Kepple, R. K., and Miller, M. H. in *Rolling Contact Phenomena*, J. B. Bidwell, Ed., Elsevier, New York, 1962, pp. 301–316.

[23] Zaretsky, E. V., Parker, R. J., Anderson, W. J., and Miller, S. T., "Effect of Component Differential Hardnesses on Residual Stress and Rolling-Contact Fatigue," NASA TN D-2664, National Aeronautics and Space Administration, Washington, D.C., 1965.

[24] Zaretsky, E. V., Parker, R. J., and Anderson, W. J., *Journal of Lubrication Engineering*, Vol. 91, No. 2, April 1969, pp. 314–319.

[25] Parker, R. J., Zaretsky, E. V., and Anderson, W. J., "Rolling-Contact Lubrication Studies with Polyphenyl Ethers at Reduced Pressures," NASA TN D-3130, National Aeronautics and Space Administration, Washington, D.C., 1965.

[26] Carter, T. L., "A Study of Some Factors Affecting Rolling-Contact Fatigue Life," NASA TR-R-60, National Aeronautics and Space Administration, Washington, D.C., 1960.

[27] Klaus, E. E., Johnson, R. H., and Fresco, G. P., *Transactions of the American Society for Lubrication Engineers,* Vol. 9, No. 2, April 1966, pp. 113–120.

[28] Reichard, D. W., Parker, R. J., and Zaretsky, E. V., *Transactions of the American Society of Lubrication Engineers,* Vol. 11, No. 3, 1968, pp. 275–281.

[29] Reichard, D. W., Parker, R. J., and Zaretsky, E. V., "Reduced-Pressure Environment Effects on Rolling-Element Fatigue Life with Super-Refined Mineral Oil Lubricant," NASA TN D-4348, National Aeronautics and Space Administration, Washington, D.C., 1968.

[30] Dietrich, M. W., Townsend, D. P., and Zaretsky, E. V., "Rolling-Element Lubrication with Fluorinated Polyether at Cryogenic Temperatures (160° to 410°R)," NASA TN D-5566, National Aeronautics and Space Administration, Washington, D.C., 1969.

[31] Dietrich, M. W., Townsend, D. P., and Zaretsky, E. V., *Journal of Lubrication Technology,* Vol. 93, No. 3, 1971, pp. 364–370.

[32] Loewenthal, S. H. and Parker, R. J., "Rolling-Element Fatigue Life with Two Synthetic Cycloaliphatic Traction Fluids," NASA TN D-8124, National Aeronautics and Space Administration, Washington, D.C., 1976.

[33] Parker, R. J. in *Rolling-Contact Fatigue Performance Testing of Lubricants,* R. Tourret and E. P. Wright, Eds., Heyden and Son Ltd., London, 1977, pp. 281–295.

[34] Parker, R. J. and Zaretsky, E. V., "Effect of Lubricant Extreme-Pressure Additives on Rolling-Element Fatigue Life," NASA TN D-7383, National Aeronautics and Space Administration, Washington, D.C., 1973.

[35] Dietrich, M. W., Townsend, D. P., and Zaretsky, E. V., "Effect of Contact Angle on Rolling-Element Fatigue Life with a Fluorinated Ether Lubricant at a Cryogenic Temperature of 170 K (305°R)," NASA TN D-6367, National Aeronautics and Space Administration, Washington, D.C., 1971.

[36] Parker, R. J. and Zaretsky, E. V., *Journal of Lubrication Technology,* Vol. 94, No. 2, April 1972, pp. 165–173.

[37] Parker, R. J., Zaretsky, E. V., and Dietrich, M. W., "Rolling-Element Fatigue Lives of Four M-Series Steels and AISI 52100 at 150°F," NASA TN D-7033, National Aeronautics and Space Administration, Washington, D.C., 1971.

[38] Parker, R. J., Zaretsky, E. V., and Dietrich, M. W., "Rolling-Element Fatigue Lives of AISI T-1, AISI M-42, AISI 52100, and Halmo at 150°F," NASA TN D-6179, National Aeronautics and Space Administration, Washington, D.C., 1971.

[39] Chevalier, J. L., Zaretsky, E. V., and Parker, R. J., *Journal of Lubrication Technology,* Vol. 95, No. 3, July 1972, pp. 287–297.

[40] Bamberger, E. N., Zaretsky, E. V., and Signer, H., *Journal of Lubrication Technology,* Vol. 98, No. 4, Oct. 1976, pp. 580–585.

[41] Parker, R. J. and Zaretsky, E. V., "Rolling-Element Fatigue Life of AISI M-50 and 18-4-1 Balls," NASA TP-1202, National Aeronautics and Space Administration, Washington, D.C., 1978.

[42] Parker, R. J. and Hodder, R. S., "Effect of Double Vacuum Melting and Retained Austenite on Rolling-Element Fatigue Life of AMS 5749 Bearing Steel," NASA TP 1060, National Aeronautics and Space Administration, Washington, D.C., 1977.

[43] Parker, R. J. and Hodder, R. S., *Journal of Lubrication Technology,* Vol. 100, No. 2, April 1978, pp. 226–235.

[44] Parker, R. J. and Zaretsky, E. V., "Rolling-Element Fatigue Life of Ausformed M-50 Steel Balls," NASA TN D-4954, National Aeronautics and Space Administration, Washington, D.C., 1968.

[45] Parker, R. J., Grisaffe, S. J., and Zaretsky, E. V., "Surface Failure of Alumina Balls Due to Repeated Stresses Applied in Rolling Contact at Temperatures to 2000°F," NASA TN D-2274, National Aeronautics and Space Administration, Washington, D.C., 1964.

[46] Parker, R. J., Grisaffe, S. J., and Zaretsky, E. V., "Surface Failure of Titanium Carbide Cermet and Silicon Carbide Balls in Rolling Contact at Temperatures to 2000°F," NASA TN D-2459, National Aeronautics and Space Administration, Washington, D.C., 1964.

[47] Parker, R. J., Grisaffe, S. J., and Zaretsky, E. V., *Transactions of the American Society of Lubrication Engineers*, Vol. 18, No. 3, July 1965, pp. 208–216.

[48] Parker, R. J. and Zaretsky, E. V., "Rolling-Element Fatigue Life of Silicon Nitride Balls—Preliminary Test Results," NASA TM X-68174, National Aeronautics and Space Administration, Washington, D.C., 1972.

[49] Parker, R. J. and Zaretsky, E. V., "Rolling-Element Fatigue Life of Silicon Nitride Balls," NASA TN D-7794, National Aeronautics and Space Administration, Washington, D.C., 1974.

[50] Parker, R. J. and Zaretsky, E. V., *Journal of Lubrication Technology*, Vol. 97, No. 3, July 1975, pp. 350–357.

[51] Scibbe, H. W., Parker, R. J., and Zaretsky, E. V., "Rolling-Element Fatigue Life of SAE 52100 Steel Hollow Balls," NASA TN D-3832, National Aeronautics and Space Administration, Washington, D.C., 1967.

[52] Coe, H. H., Parker, R. J., and Scibbe, H. W., *Journal of Lubrication Technology*, Vol. 93, No. 1, Jan. 1971, pp. 47–59.

[53] Coe, H. H., Scibbe, H. W., and Parker, R. J., "Performance of 75-mm Bore Bearing to 1.8 Million DN Using Electron-Beam Welded Hollow Balls," NASA TN D-5800, National Aeronautics and Space Administration, Washington, D.C., 1970.

[54] Coe, H. H., Parker, R. J., and Scibbe, H. W., "Performance of 75-Millimeter-Bore Bearings Using Electron-Beam-Welded Hollow Balls with a Diameter Ratio of 1.26," NASA TN D-7869, National Aeronautics and Space Administration, Washington, D.C., 1975.

[55] Parker, R. J. and Zaretsky, E. V., "Reevaluation of the Stress–Life Relation in Rolling-Element Bearings," NASA TN D-6745, National Aeronautics and Space Administration, Washington, D.C., 1972.

[56] Parker, R. J., Zaretsky, E. V., and Bamberger, E. N., *Journal of Lubrication Technology*, Vol. 96, No. 3, July 1974, pp. 391–397.

[57] Jones, W. R., Jr., and Parker, R. J., "Characterization of Wear Debris Generated in Accelerated Rolling-Element Fatigue Tests," NASA TP-1203, National Aeronautics and Space Administration, Washington, D.C., 1978.

[58] Jones, W. R., Jr. and Parker, R. J., *Transactions of the American Society of Lubrication Engineers*, Vol. 22, No. 1, Jan. 1979, pp. 37–45.

[59] Morrow, J., "Correlation of the Pitting Fatigue Life of Bearings with Rolling Contact Rig Data," ASME Paper No. 65-WA/CF-5, American Society of Mechanical Engineers, Winter Annual Meeting, Chicago, Ill., Nov. 1965.

[60] Bamberger, E. N. and Zaretsky, E. V., "Fatigue Lives at 600°F of 120-Millimeter-Bore Ball Bearings of AISI M-50, AISI M-1, and WB-49 Steels," NASA TN D-6156, National Aeronautics and Space Administration, Washington, D.C., 1971.

J. M. Hampshire,[1] J. V. Nash,[1] and G. E. Hollox[1]

Materials Evaluation by Flat Washer Testing

ABSTRACT: A flat washer test for assessing the rolling contact fatigue performance of bearing materials is described in detail. Measurements of the life of commercial bearing quality SAE 52100 steel has established the baseline against which the relative performance of different steels or developments in heat treatment and bearing manufacturing can be judged. The life of carburized SAE 8720 steel has been shown to be inferior to that of SAE 52100 because of the lower level of cleanness of carburizing steels. Electroslag remelting of SAE 52100 produces an improvement in life. Heat treatment to produce lower bainite in SAE 52100 is advantageous, particularly under conditions of water-contaminated lubrication or where the use of fire-resistant fluids is required. Sinter forging is a viable production route for SAE 52100 bearings when the powder oxygen content is controlled.

KEY WORDS: bearings, fatigue, martensite, bainite, hydrogen embrittlement, fire-resistant fluids, SAE 52100 steel, SAE 8720 steel, electroslag remelting, sinter forging, bearing steels

Two of the major features of a rolling bearing which affect its service life are the quality of the material from which it is made and the standard to which it is heat treated.

The standards adopted by producers around the world are based on the experience of many years of manufacturing and service combined with developments in understanding the factors controlling bearing life. No responsible producer today would introduce any change in established standards without some form of testing and results on which to base such a change. Full bearing testing is time-consuming and expensive. Accordingly, different companies

---

[1]Materials research manager, project metallurgist, and former group chief metallurgist, respectively, Bearing Research Centre, RHP Bearings Limited, Newark, Notts, England NG24 2JF.

and research institutions have developed, over the years, a number of tests based on a variety of component forms, for example, balls, washers, cones, and rods. It is not the intention of this paper to compare, contrast, and relate the different types of testing; it is hoped that will be one of the outcomes of this publication. Instead this paper will describe the flat washer test used as a research, development, and quality assurance tool by RHP Bearings Limited, to present the results of some of the programs, showing the relative performance of different types of steel, and to discuss the effects of some metallurgical variables on performance.

Bearing Life

Rolling bearings are reliable components which allow rotational motion with minimum friction and accurate location while transmitting high loads. In service, life is more often than not limited by incorrect fitting, corrosion, ingress of dirt, inadequate lubrication, and a host of other external conditions, often beyond the control of the bearing manufacturer. Most bearing companies offer advice and recommendations to avoid early failure from such features, but even under well-lubricated conditions, correctly selected, installed, and maintained bearings will fail eventually by some form of fatigue of the contacting surfaces. A generally accepted failure mode consists of subsurface crack nucleation at a preexisting defect in the region of high shear stress beneath a contact zone followed by propagation of the crack to form, eventually, a pit at the surface (Fig. 1). In service, this process usually leads to rough running, excessive vibration, or audible noise, and it is these features which are used to detect the failure of bearings in test rigs.

The main difference between test rigs and typical service conditions is in the stress level. In most service applications, failure occurs after several millions of stress repetitions, possibly spanning many years. To give convenient test times, bearing life is usually evaluated under conditions of high load and speed, where fatigue failure occurs in hours or weeks rather than years. At RHP Bearings Limited tests under such conditions are treated as "screening tests," which are relatively cheap, convenient, and quick to carry out. Their main use is in studying the effects of changes in metallurgical variables. Any worthwhile trends are confirmed in a variety of rigs which test full bearings under stress levels closer to those encountered in normal applications [1].[2] Finally, developments are evaluated in a subassembly test which recognizes that bearings in service are not subjected to a simple stress system but to a complex variety of conditions. An example of such a rig used for testing automobile wheel hub bearings has been published elsewhere [2].

---

[2]The italic numbers in brackets refer to the list of references appended to this paper.
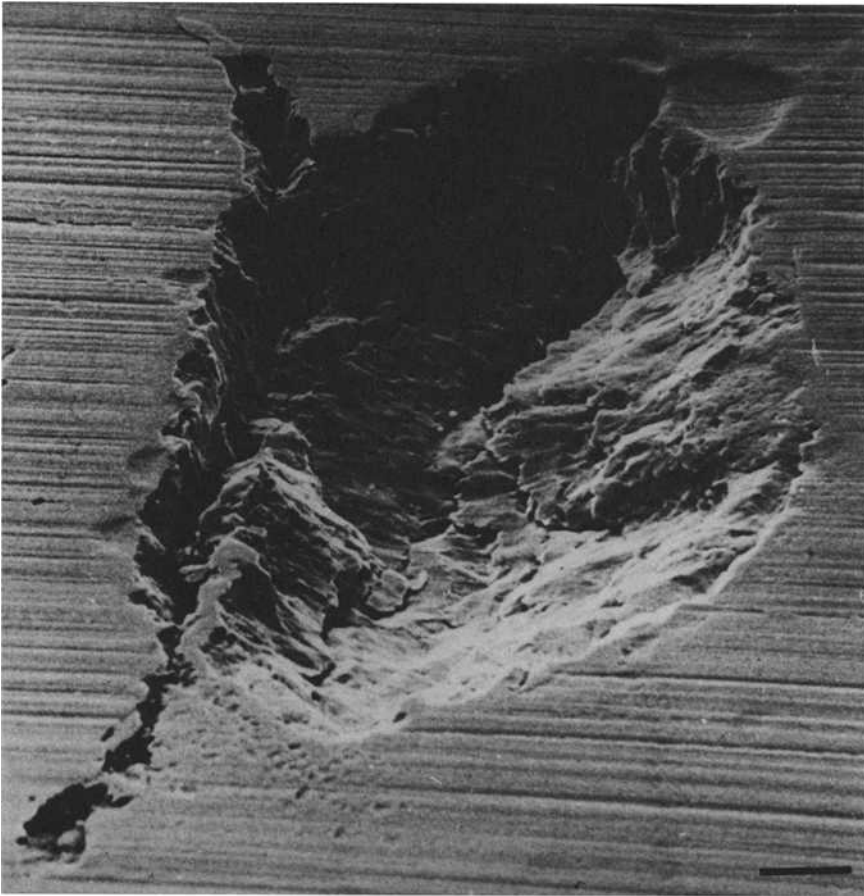
FIG. 1—*A typical rolling contact fatigue pit in the surface of a tested flat washer (marker is 20 μm).*

The Flat-Washer Screening Test

Test Sample

The component in the screening test is a flat washer, with a 74.6-mm outside diameter, 50.8-mm bore, and 6.35-mm width (Fig. 2). All the results discussed in this paper were obtained from flat washers manufactured from bars 75 to 85 mm in diameter, except where stated.

The advantages of this sample configuration are that the specimens are cheap and simple to manufacture under workshop conditions so that there are no interruptions to normal bearing production caused by development batches often of nonstandard materials or heat treatments. Raw material is

FIG. 2—*A test washer showing a ball rolling track and typical fatigue pit. The outer diameter of the washer is 74.6 mm.*
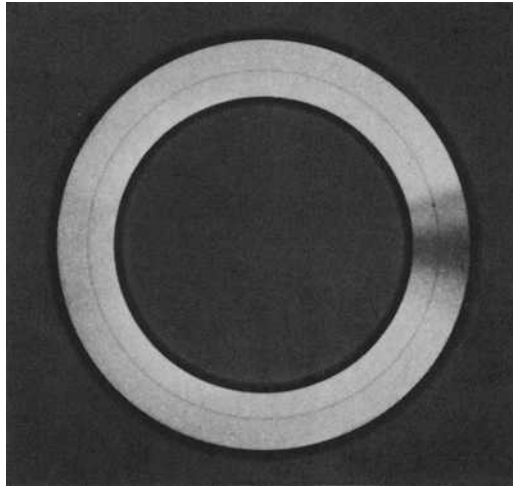
readily available from steel producers as round billet. Comparisons are thus made between different steels at a constant stage in their manufacturing route. Results are not affected by variation in the reduction in area, and grain flow is maintained normal to the test surface, thus avoiding the variation in similar components made, for example, from tube.

After appropriate heat treatment, test washers are ground on the faces and bore under full coolant flow. Finish grinding is carried out with extreme care, removing 2.5 μm of material per pass, again with full coolant flow. Interstage etch inspection is carried out to check for grinding abuse. The final surface finish is held within 0.1 to 0.2 μm roughness average (RA).

Test Configuration and Stress Level

The test washers are paired with slave washers and, after stringent cleaning, are assembled with 16 balls, 7.9375 mm (5/16 in.) in diameter, held in a nylon cage. The balls have a maximum diameter variation of 0.5 μm, and runout of the test washer and slave washer pair is held at 8 μm. Slave washers and balls are replaced after every test. Fitting is carried out with care to avoid damage that could invalidate the test results.

The test assembly is shown in Fig. 3. The upper and lower test washers are located on the central driven shaft, with their respective slave washers located on fixed upper and lower housings. The load is applied to the test bearing assembly by means of a dead weight lever system with a 30:1 mechanical ad-
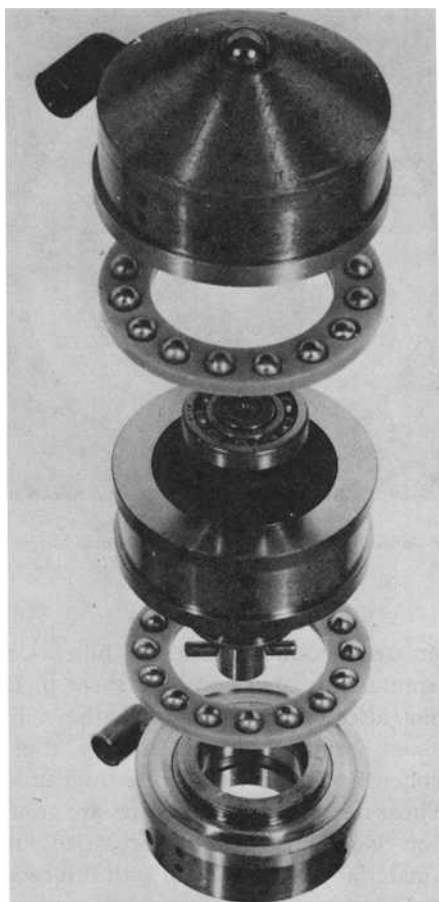
FIG. 3—*A flat washer test assembly illustrating the test washers located on the central driven shaft.*

vantage, through a ball sunk into a central hole in the upper loading housing to ensure axial application.

The fatigue test configuration is nominally one of point contact, consisting of a ball rolling on a flat rotating test washer. All the tests are conducted at the same maximum surface compression stress level of 4 170 MN·m^{-2} (600 000 psi) by applying a load of 444.8 N (100 lbf) per ball. Testing is conducted at a shaft speed of 1 500 rpm, which subjects any one point on the washer to 720 000 stress repetitions per hour.

The estimated L_{10} life for the test conditions is 13.26 $\times$ 10^6 stress repetitions (18.41 h) using the Lundberg and Palmgren theory [3].

Lubrication

The lubricant used in all the flat washer tests discussed in this paper was a mineral oil, Carnea 100, which is metered to each bearing assembly at a rate of 0.28 litre/min through a recirculating filtered pump feed system fitted to each bank of rigs. A dual filtration system consisting of a coarse filter of felt on steel gauze followed by a fine ceramic filter with a pore diameter of 15 to 20 μm ensures that minimal fatigue debris reaches the contact area. The temperature of the oil leaving the test washer contact zone is measured by means of thermocouples situated in the oil throwout path. The oil condition—viscosity, acidity, moisture content, specific gravity, and particle content—is monitored regularly and maintained within strict limits.

Several methods are available for calculating the lubricant film thickness, derived either theoretically or experimentally [4-9]. The degree of lubrication or lubricant film thickness parameter, conventionally designated λ, is defined as the ratio of the lubricant film thickness to the surface roughness. At low λ, surface asperities are in contact, and the life may be low because of the different interactions which lead to surface-initiated fatigue. At high λ, these extraneous effects, which prevent the assessment of subsurface nucleated fatigue life, are eliminated. Any λ in excess of 2 is considered generally to represent the conditions of subsurface-initiated fatigue. Since it is relatively simple and takes into account the three-dimensional factors in ball contact, the method of Archard [7] is used to calculate the lubricant film thickness and hence the λ values. Accordingly, the flat washer test conditions using an oil temperature of 40°C approximates to $\lambda = 3$. Over the tolerance range of the surface finish of the washer, λ is 2.8 to 5.6. Similar λ values, in the range 1.9 to 8.7, are given in applying the calculations associated with Dowson [5], Grubin [6], Foord [8], and Hamrock [9].

Test Procedure

A test series normally comprises 30 ostensibly identical washers which are run until either fatigue failure occurs or a suspension time of 250 h is reached. A piezoelectric accelerometer mounted on each loading arm directly above the test assembly continually monitors the vibration, and the test rig stops automatically once the vibration exceeds a preset level. A digital hour meter records the duration of each test. Fatigue test data are analyzed by Weibull statistics, the main parameter recorded being the L_{10} life, which is defined as the life within which 10 percent of the batch will fail or, alternatively, the life which 90 percent of the test components will exceed.

To validate the test data, all test washers are hardness tested and nital etched to check for grinding abuse after testing. None was found in the series reported in this paper. The three lowest life failures are metallurgically ex-

amined (*a*) to determine the nature of the fatigue pit and (*b*) its origin and cause, where possible, and (*c*) to ensure that the metallurgical condition of the material was that intended for the test series.

Full traceability of the test components is maintained through all stages of manufacturing back to the source of the steel.

Steels Tested

The wrought steels designated A to F discussed in this paper had the compositions shown in Table 1.

In any discussions of bearing life, the subject of steel inclusion content must be considered. The approach adopted in this work has been to consider the average cleanness of the different steels by examining a section through the test washers in the region of a failure rather than any general assessment of total cast steel cleanness. The test washer section and position is similar to that required in the J–K analysis, as summarized in the ASTM Recommended Practice for Determining the Inclusion Content of Steel (E 45–76) Method 3. The frequency of the different inclusion types is shown in Fig. 4. A more quantitative measure is obtained by adding the product of the different field ratings and their frequency, as shown in Table 2.

The relative cleanness of the different steels is shown by the data in Table 2 to be consistent with their method of manufacture and chemical composition. Steels A and D, that is, SAE 52100 steels, had a generally similar level of inclusions. Both steels were electric arc melted and vacuum degassed, thus meeting the requirements of the ASTM Specifications for High-Carbon Ball and Roller Bearing Steel (A 295–79). Steels E and F were quite different. Steel E was electroslag remelted SAE 52100, which is significantly cleaner, while Steel F was electric arc melted and vacuum degassed SAE 8720, which conforms to the requirements of the ASTM Specifications for Carburizing Steels for Anti-Friction Bearings (A 534–79). This latter steel had a high level of sulfides, which may be attributed to the higher sulfur content of the steel. Of greater relevance to fatigue life, the steel contained a higher proportion of oxide inclusions than SAE 52100, which was consistent with a higher retention of oxygen in the lower carbon steel during the steel-making process.

Results and Discussion

Life of SAE 52100 Steel from Different Sources

The standard steel used by RHP Bearings Limited is conventional SAE 52100 (known also by designations including 100 Cr 6, 100C6, EN31, and 534A99) to the requirements embodied in ASTM Specifications A 295–79. Flat-washer testing of different and new sources of steel is carried out for

TABLE 1—Chemical analysis of the steels used in this work, in weight percent.

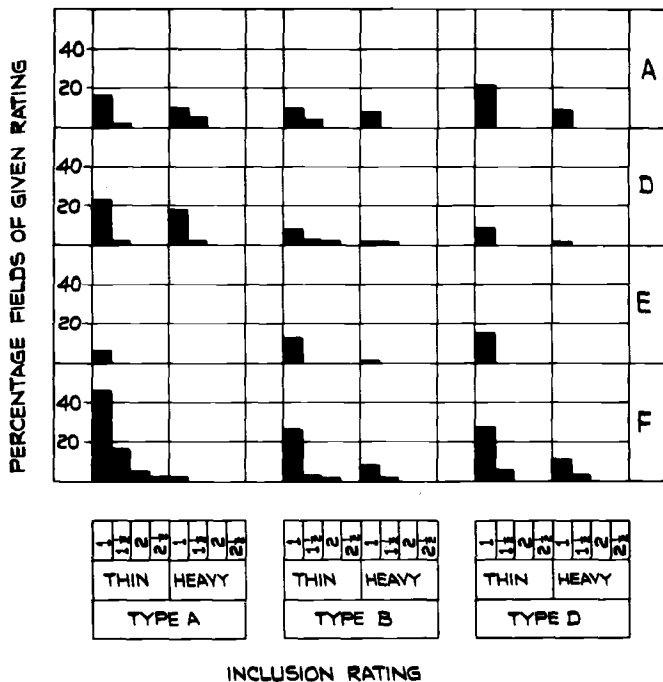| Source	C	Cr	Si	Mn	Mo	Ni	Cu	S	P	Type
A	1.02	1.36	0.30	0.35	0.04	0.11	0.15	0.010	0.017	SAE 52100
B	0.98	1.51	0.27	0.36	...	...	...	0.010	0.016	SAE 52100
C	1.08	1.61	0.31	0.67	0.03	0.09	...	0.008	0.014	SAE 52100
D	1.04	1.38	0.28	0.30	0.02	0.06	0.10	0.007	0.007	SAE 52100
E	1.04	1.41	0.21	0.35	0.04	0.14	0.25	0.006	0.015	ESR 52100
F	0.18	0.50	0.20	0.93	...	0.49	0.19	0.021	0.013	SAE 8720

FIG. 4—*The relative inclusion content of the different steels tested.*

TABLE 2—*Quantitative assessment of inclusions in the steels tested.*

Source	Type A Sulfides	Type B + Type D Oxides	Total
A	33.0	48.5	81.5
D	45.0	25.5	70.5
E	6.0	26.0	32.0
F	90.5	129.5	220.0

routine quality assurance. The results from four different suppliers labeled A to D, are given in Table 3 in units of millions of stress repetitions.

The variation in life within one cast, from Supplier A, has been examined in some detail in eleven separate investigations. Lives in millions of stress repetitions are shown in Table 4.

The L_{10} range is 27.3 to 50.5 million stress repetitions. As the L_{10} range for the three other sources of steel given in Table 3 falls within the same range, this is taken as the best estimate to date of the range of the life of several sources of standard SAE 52100 steel. Steel quality from new sources, new

TABLE 3—*Fatigue life of SAE 52100 steel from four sources.*

Source	Hardness, VHN 30	L_{10}, millions of stress repetitions	L_{50}, millions of stress repetitions
A	752 to 836	34.1	91.9
B	804 to 823	49.3	358
C	798 to 810	32.8	104
D	786 to 807	46.2	98.7

TABLE 4—*Variation in fatigue life in eleven series of flat washers from one cast of SAE 52100 steel.*

Source	Hardness, VHN 30	L_{10}, millions of stress repetitions	L_{50}, millions of stress repetitions
A1	775 to 804	48.9	124.5
A2	775 to 810	27.3	59.4
A3	752 to 775	35.3	96.9
A4	775 to 817	32.1	108.1
A5	798 to 810	31.3	113.7
A6	786 to 823	30.5	73.6
A7	792 to 836	50.5	123.0
A8	786 to 823	28.1	68.9
A9	783 to 798	28.1	93.4
A10	786 to 823	28.9	68.8
A11	786 to 823	34.5	80.0
Average		34.1	91.9

developments, or new process variables is evaluated against this "standard cast range" of fatigue life.

Comparison of this range in life with the estimated life of 13.26×10^6 stress repetitions supports the view that the life of bearing steel may be upgraded from the theoretical value on which the International Organization for Standardization (ISO) calculations are based. Indeed, the average value of 34.5×10^6 stress repetitions is a factor of 2.6 above the calculated life. Support for this order of increase in life is given in full-bearing 6208 testing by Hobbs [1].

Electroslag remelted casts of SAE 52100 compositions show a superior life to that of the vacuum degassed "standard cast range" (Fig. 5). The most recent data on a steel, designated E in Table 1, has shown an L_{10} life of 96.3 million stress repetitions, some seven times in excess of the calculated life and with an L_{50} of 230 million stress repetitions. This trend is consistent with the higher cleanness resulting from this refining process. The improvement in life is confined to the removal of lower life failures rather than a general life increase.
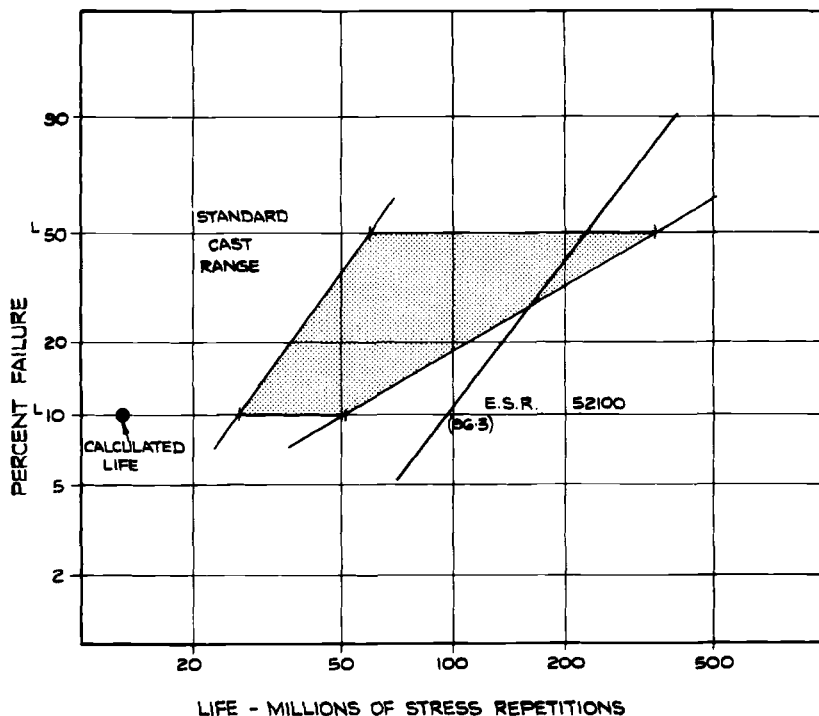
FIG. 5—*The life of electroslag remelted SAE 52100 steel compared with the standard cast range, showing the improved fatigue life associated with the better level of cleanness in the former.*

Life of Case-Hardened SAE 8720 Steel

The high surface hardness required in a bearing may be attained by using high-carbon through-hardening steels or low-carbon steels after an appropriate carburizing treatment. Both types of steel are in widespread use around the world for bearing components. The standards most commonly governing the cleanness requirements of case-hardening steels are summarized in ASTM Specifications A 534–79.

The results of testing four series of test washers from the same cast, designated F, of bearing quality SAE 8720 are given in millions of stress repetitions in Table 5. The L_{10} life is in the range 15.8 to 21.1 million stress repetitions and is virtually independent of the metallurgical condition of the case structure, since retained austenite, surface hardness, and case depth in the range used appear to have no significant effect. This life is significantly below that of the standard cast range for SAE 52100 steels (Fig. 6).

For all the low life results, the fatigue pits were shown to be associated with alumina inclusion trails, an example of which is shown in Fig. 7. These are a

TABLE 5—*Fatigue life of SAE 8720 steel for four different case depths.*

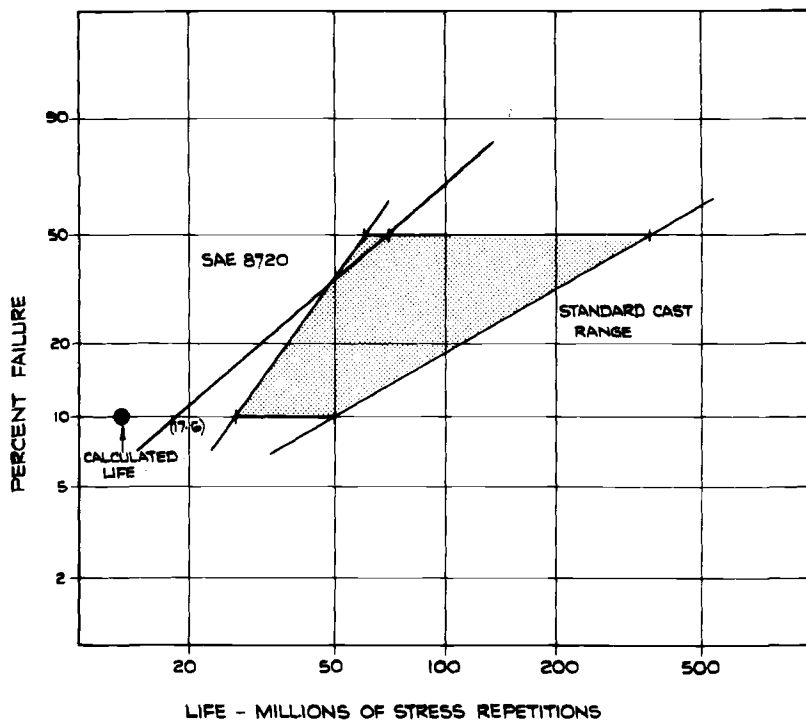|	Condition			L_{10}, millions of stress repetitions	L_{50}, millions of stress repetitions
Source	Surface Hardness, VHN 5	Case Depth, mm	Structure		
F1	758	0.75	fine martensite + 10% austenite	21.1	56.2
F2	725	0.66	fine martensite + 10% austenite	15.8	66.0
F3	753	0.93	fine martensite + 15% austenite	17.0	72.0
F4	672	1.83	coarse martensite + 30% austenite	16.6	65.6
Average				17.6	65.0

FIG. 6—*The life of SAE 8720 steel compared with the standard cast range for SAE 52100 steel, suggesting the superior performance of the latter.*
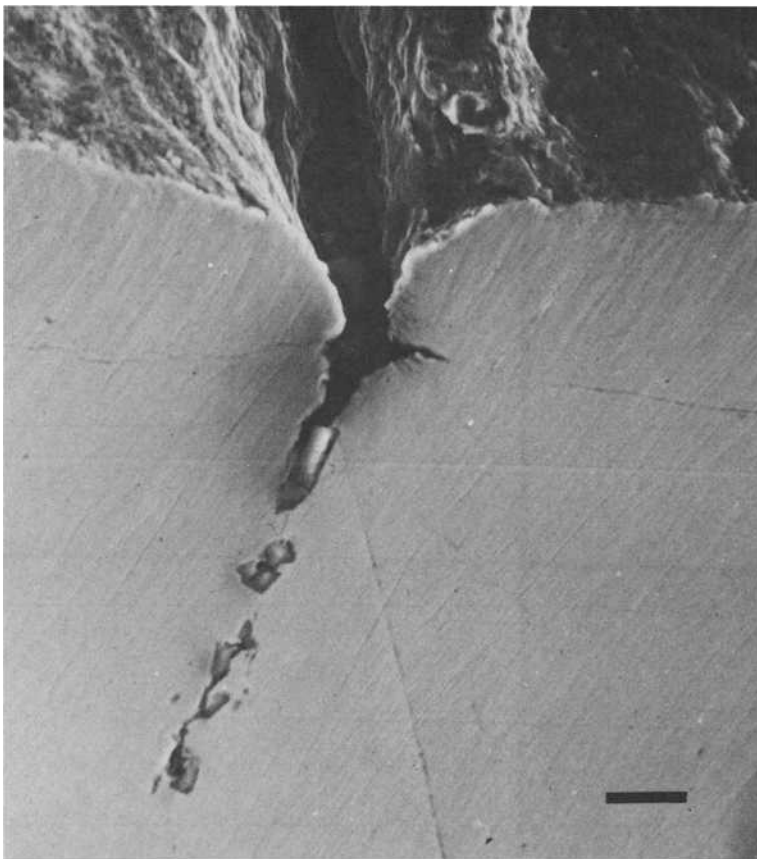
FIG. 7a—A section through the failure site of SAE 8720 washers, showing an association with B-type alumina inclusion trails (the marker is 40 μm).

characteristic feature of low-carbon steels as a result of their chemistry and the low carbon–high oxygen equilibrium in liquid steel.

Although the present data suggest that carburizing steels exceed the calculated life, they do so by a factor less than that for high-carbon steels because the latter steels can be produced to a better cleanness level. Expected advantages from residual compressive stresses in the surface layers appear to be outweighed by the detrimental effect of inclusions under the full lubrication test conditions. To attain the potential advantages of residual stress, it appears to be necessary to use carburizing steels at a greater level of cleanness, such as that from electroslag or vacuum remelting processes, with consequent cost penalties. The more extensive use of through-hardening steels is therefore endorsed, except for special applications, where, for example, bulk toughness is an overriding factor in the choice of steel for a component.
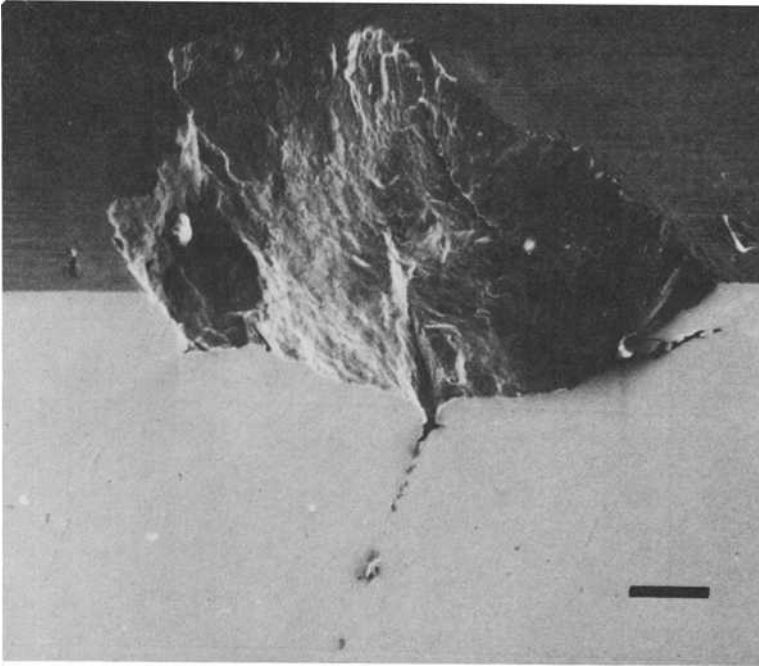
FIG. 7b—*A higher magnification of Fig. 7a (the marker is 10 μm).*

TABLE 6—*Effect of martensite and lower bainite on the fatigue life in one cast of SAE 52100 steel.*

Source	Hardness, VHN 30	Structure	L_{10}, millions of stress repetitions	L_{50}, millions of stress repetitions
C1	873	martensite	31.7	55.4
C2	847	martensite	39.1	60.5
C3	832	martensite	43.9	105.9
C4	817	martensite	36.4	100.8
C5	800	martensite	33.1	105.8
C6	781	martensite	36.5	70.6
C7	742	martensite	27.3	80.6
C8	812	martensite/ 5% lower bainite	49.3	100.8
C9	776	martensite/ 15% lower bainite	46.4	105.9
C10	724	martensite/ 30% lower bainite	41.4	121.0
C11	673	lower bainite	44.4	110.9

Lower Bainite Heat Treatment of SAE 52100 Steel

Little attention has been paid to the effects on life of lower bainite or mixed lower bainite-martensite structures in SAE 52100.

The results of testing several batches of flat washers are summarized in Table 6; the lives are given in millions of stress repetitions.

As can be seen in Fig. 8, the L_{10} life of lower bainite and duplex lower
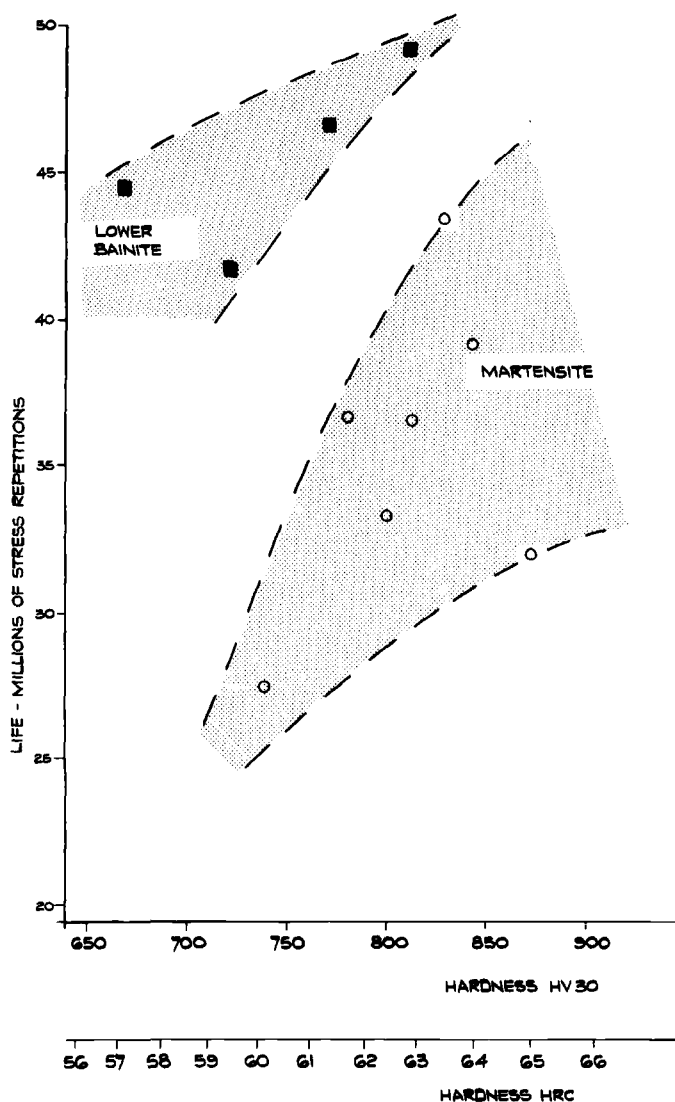

FIG. 8—*The comparative lives of lower bainite and martensite heat-treated SAE 52100 steel as a function of hardness.*

bainite–martensite bearings lies in a band above that for martensite bearings as a function of hardness. The highest fatigue life is given in mixed structures associated with the hardness of 750 to 800 VHN 30, which corresponds to a structure of 5 to 40 percent lower bainite in martensite. Moreover, the fatigue life of fully lower bainite structures at a hardness of 650 to 700 VHN 30 appears equivalent to that of martensite structures at a hardness of 750 to 850 VHN 30, the hardness range conventionally associated with bearings.

The superior properties of bainite support the earlier observations of Davenport [10], Carreka [11], and Erkuen [12] of a higher rotating bending fatigue limit in austempered high-carbon steels and also the similar observations on taper roller bearings under fully bainitic conditions. A full discussion of these effects is presented elsewhere [13]. Suffice it to say, high-carbon lower bainite appears to have higher toughness and ductility than high-carbon martensite because of its internal microstructure [14]. Lower bainite consists of ferrite laths with a high dislocation density and fine precipitation of carbides within those laths (Fig. 9); it does not exhibit the more brittle twinned structure of martensite at the high-carbon content of SAE 52100 (Fig. 10).

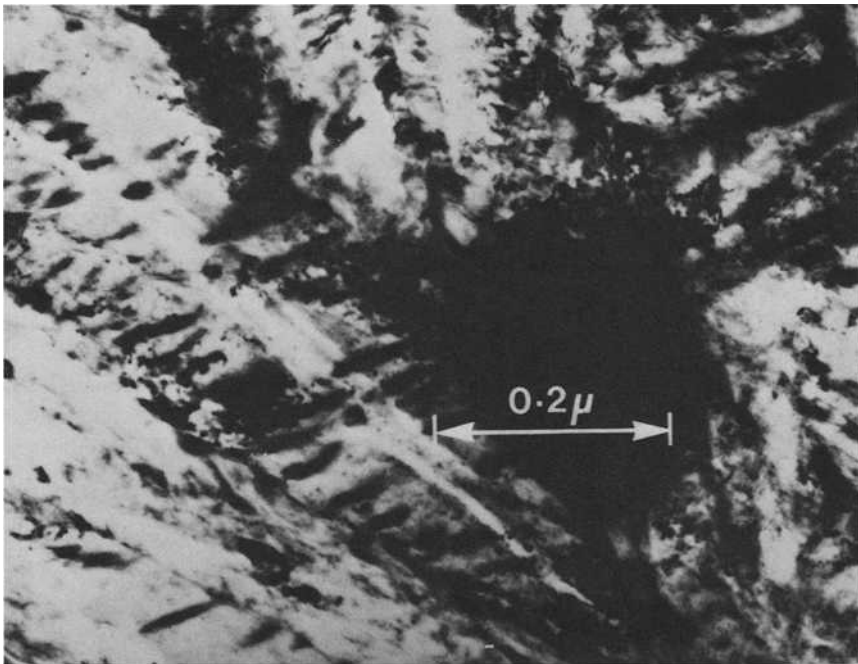Support for the advantageous effect of lower bainite has been obtained in

FIG. 9—*The lath structure of lower bainite in SAE 52100 steel (marker is 0.2 μm).*
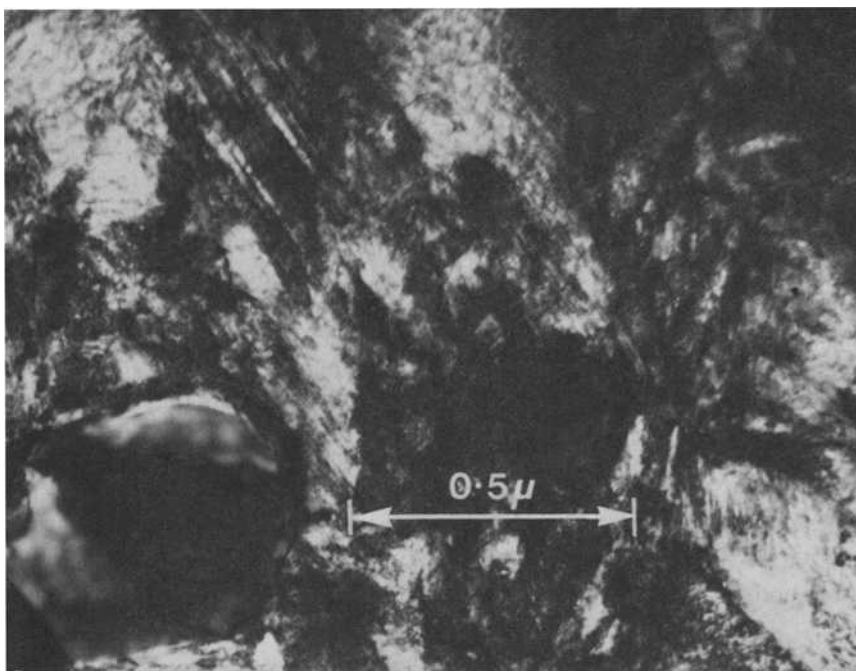
FIG. 10—*The twinned structure of tempered martensite in SAE 52100 steel (marker is 0.5 μm).*

testing bearings under conditions where conventionally heat-treated bearings fail catastrophically, such as in the presence of water or when lubricated with certain fire-resistant fluids [15]. For example, lower bainite size 6205 bearings lubricated by water show a life of 168 h in comparison with 52 h associated with martensite bearings (Fig. 11). Martensite bearings tempered to the same hardness as the lower bainite show a very minor improvement in life to 74 h under the same test conditions. In addition, in a slurry containing 10 percent coal dust (Fig. 12), lower bainite bearings show twice the life of martensite bearings. Significantly, the final failure of the martensite bearings was accompanied frequently by gross fracture of the rings, whereas this was rare with lower bainite, which indicates the importance of toughness in this application.

Similar levels of improvement in life have been shown by the use of lower bainite bearings in certain high-water base and water–glycol fire-resistant fluids using the Institute of Petroleum Test Method IP/303/74 (Unisteel flat washer test) and in size 6208 bearing testing [1]. The improved performance of such bearings in the presence of water appears to be a result of improved resistance to hydrogen-induced embrittlement and crack growth [15].

It is important to emphasize that lower bainite in high-carbon steels is pro-
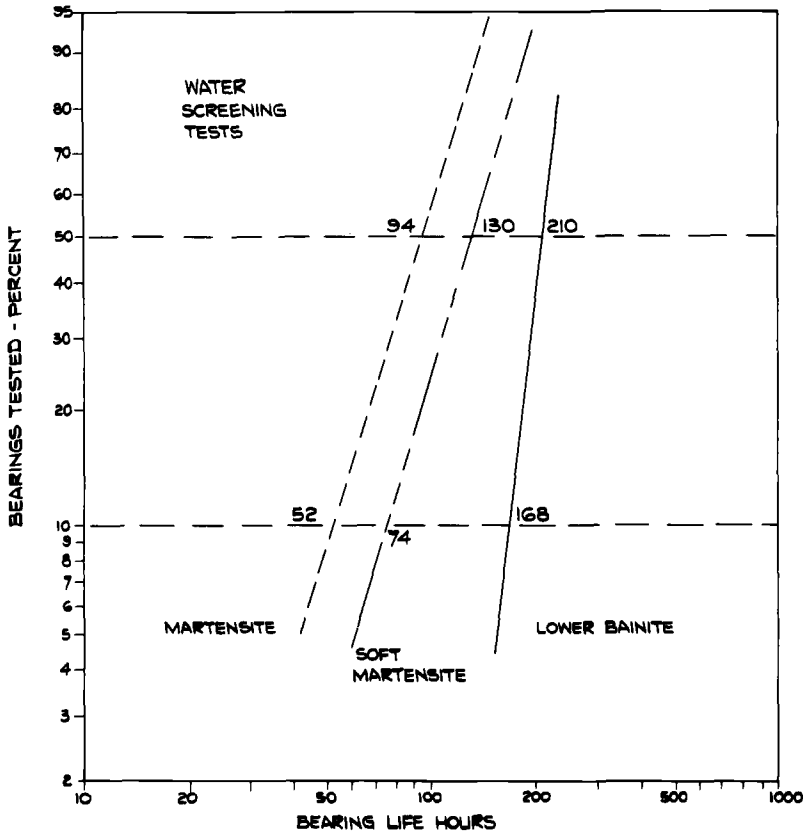
FIG. 11—*The improved life of lower bainite bearings compared with martensite under water lubrication.*

duced by quenching from the austenitizing temperature into molten salt and holding until the austenite undergoes isothermal transformation to lower bainite. This lower bainite is very different in its properties from the structures containing pearlite or upper bainite produced by continuous cooling during a slack quench; slack-quenched upper bainite appears to reduce toughness and fatigue life [*16*].

Sinter-Forged High-Carbon Steel Bearings

Powder metallurgy methods are of growing importance in the manufacture of engineering components. In critically stressed areas, such as in a bearing track, it is essential to have full densification of the material, which is usually achieved by sinter forging or other hot processing techniques. Moreover, the powder manufacturing must be controlled to minimize inclusion content.
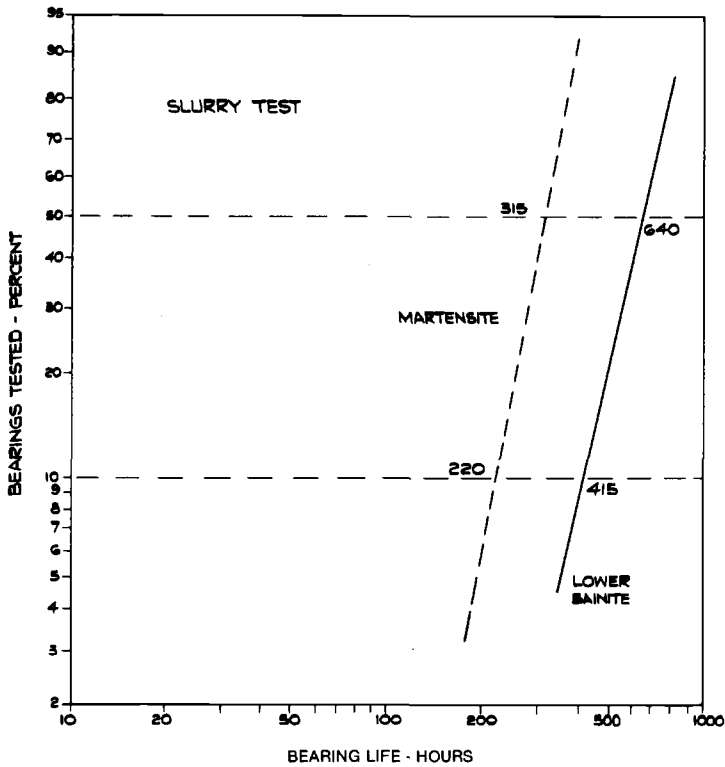
FIG. 12—*The improved life of lower bainite bearings compared with martensite in a water-coal dust slurry.*

Flat washer tests have been used to evaluate the quality of sinter-forged components produced by different methods. When the material is fully dense, through-hardened components made from steel powders based on SAE 52100 can be produced with an adequate fatigue life, as shown in Table 7; the lives, again, are registered in millions of stress repetitions.

The first three series of powders in Table 7 all gave fatigue lives within the standard casts range (Fig. 13). However, when oxygen levels were high (650

TABLE 7—*Fatigue life of four different series of high-carbon sinter-forged flat washers.*

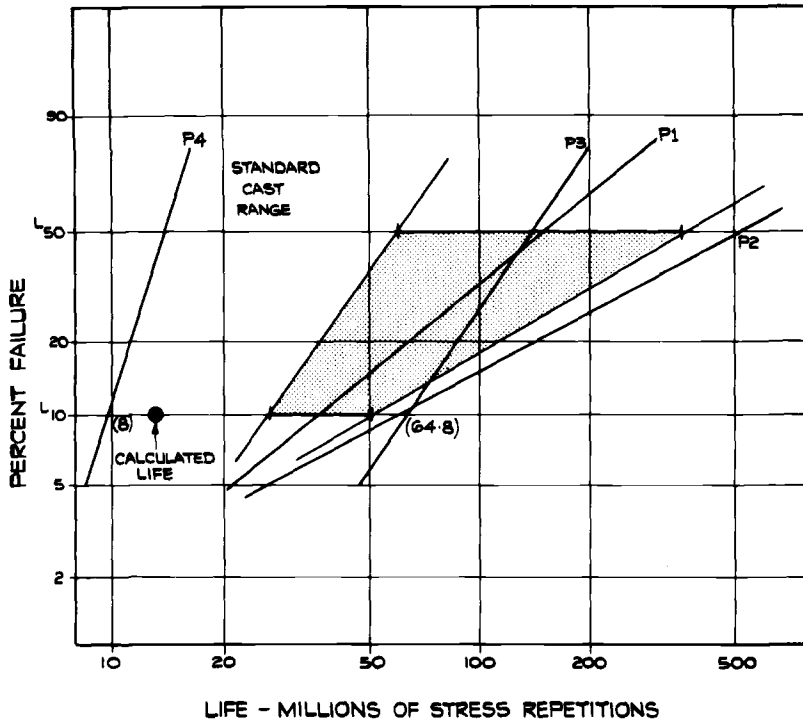| Source	Hardness, VHN 30	L_{10}, millions of stress repetitions	L_{50}, millions of stress repetitions
P1	741 to 775	37.3	151.4
P2	741 to 775	60.5	533.0
P3	767 to 782	64.8	144.0
P4	763 to 776	8.0	14.1

FIG. 13—*The life of sinter-forged high-carbon bearing steels compared with the standard cast range for SAE 52100 steel.*

ppm), as in the case of the fourth series listed in the table, the powders had a high inclusion content, and the life was substantially reduced.

Conclusions

1. The flat washer screening test provides a viable method for assessing the influence of metallurgical variables on the rolling contact fatigue life of bearings.

2. The life of the components manufactured in standard bearing quality SAE 52100 high-carbon steel exceeds that of low-carbon SAE 8720 case-hardened components because of the inferior cleanness of the latter.

3. Electroslag remelting improves life in standard bearing quality SAE 52100 because it yields better steel cleanness.

4. Lower bainite SAE 52100 bearings have a better performance than conventional martensite bearings in such environments as water and fire-resistant fluids where hydrogen embrittlement is a factor. This is due to the higher toughness and resistance to crack propagation of lower bainite.

5. High oxygen levels are deleterious to the fatigue life of sinter-forged bearing steel, but at low oxygen levels properties equivalent to or better than those of wrought products may be obtained in sinter-forged high-carbon steels.

References

[1] Hobbs, R. A., this publication, pp. 206-218.
[2] Poon, S. Y. and Williams, S. G., *Automotive Engineer*, Aug.-Sept. 1977, pp. 54-57.
[3] Lundberg, G. and Palmgren, A., *Acta Polytechnica, Mechanical Engineering Series*. Vol. 1, No. 3, 1947.
[4] Cheng, H. S., *Journal of Lubrication Technology, Transactions of the American Society of Mechanical Engineers*, Jan. 1970, pp. 155-162.
[5] Dowson, D. and Higginson, G. R., *Elastohydrodynamic Lubrication*. Pergamon Press, New York, 1977.
[6] Grubin, A. N. and Vinogradova, I. E., *DSIR Translations*. London No. 337, 1949, from *Central Scientific Research Institution for Technology and Mechanical Engineering*, Moscow 30, 1946, pp. 115-166.
[7] Archard, J. F. and Cowking, E. W., Symposium on Elastohydrodynamic Lubrication, *Proceedings of the Institution of Mechanical Engineers*. Vol. E 180, Part 3B, 1965, pp. 17-26.
[8] Foord, C. A., Harman, W. C., and Cameron A., *Transactions of the American Society of Lubrication Engineers*. Vol. 11, 1968, p. 31.
[9] Hamrock, B. J. and Dowson, D., *E.H.L. Symposium*, University of Leeds, Paper II (ii), 1978, pp. 22-27.
[10] Davenport, E. S., *Heat Treatment and Forging*. Vol. 23, 1937, pp. 170-173.
[11] Carreka, R. P., M.Sc. thesis, University of Illinois, Urbana, Ill., 1947.
[12] Erkuen, N. M., M.Sc. thesis, University of Illinois, Urbana, Ill., 1948.
[13] von Bergen, R. T. and Hollox, G. E., to be published in Proceedings of Conference on Advances in Physical Metallurgy and Applications to Steels, Liverpool, England, 21-23 Sept. 1981.
[14] Kelly, P. M. and Nutting, J., *Journal of the Iron and Steel Institute*. Vol. 177, 1961, pp. 199-211.
[15] Hollox, G. E., Hobbs, R. A., and Hampshire, J. M., *Wear*, Vol. 68, 1981, pp. 229-240.
[16] Rice, S. L., paper presented at the International Symposium on Rolling Contact Fatigue Testing of Bearing Steels, Phoenix, Ariz., 12-14 May 1981, American Society for Testing and Materials, Philadelphia.

K. L. Day[1]

Unisteel Testing of Aircraft Engine Bearing Steels

ABSTRACT: A modified form of "Unisteel" testing was adopted over 15 years ago with the basic objective of screening aircraft bearing materials and their heat treatment prior to, or as an alternative to, full-scale testing. The aim was to obtain a statistically significant quantity of data relatively quickly and relatively cheaply in comparison with full-scale rig or engine testing. The rig and its operating techniques are described with their known virtues and shortcomings as well as a description of the typical results analysis technique used. Typical comparative results obtained from a range of through-hardened materials are included to illustrate the variations obtained from different melting sources, heat treatments, and so on.

KEY WORDS: bearings, bearing alloys, failure, materials fatigue, fatigue tests, statistical analysis, bearing steels

Some 20 years ago it became apparent that material development for aircraft engine bearings which relied on full-scale testing for evaluation prior to usage in engines was not only relatively expensive and time-consuming but frequently gave way to higher-priority engineering-linked bearing problems. Frequently, after several years of testing, results would indicate that the basic concept was not valid or even that technology had already superseded the material being tested.

Aircraft engine bearings are, by the necessity of the duties involved, frequently of complex design with integral flanges for retention of races, oil cooling or lubrication, and other features which make small batch quantities very expensive to manufacture. This is particularly so if special material is involved, as was often the case for rig evaluation. There appeared to be a need for an accelerated test that was relatively simple, quick, and low in cost but

[1] Project development metallurgist—technology, Engine Support Laboratory, Rolls–Royce Ltd., Derby, England DE2 8BJ.

still valid for evaluating alternatives and thus one that would enable the still necessary full-scale testing to be channeled into the most fruitful avenues.

Certainly all of these points were true 20 years ago, but they are even more relevant today.

About 20 years ago, technical discussions with a major supplier of commercial carbon chrome steel revealed that this supplier had discussed the design of a rig to demonstrate improvements in melting practice with bearing manufacturers who used their material. This resulted in the machine described by Johnson and Sewell [1].[2] Drawings of this machine were made available and a similar rig was built in the Rolls–Royce Ltd. laboratories at Derby, England.

Initial trials were encouraging but quickly revealed that when a move was made from commercial air-melted 1 percent CCr steel to vacuum arc remelted (VAR) steel, the test times greatly increased and that with Type 18-4-1 tool steel failure was difficult to achieve in a reasonable time.

The machine, which was by now being manufactured commercially by a subsidiary of the steel company, was called the "Unisteel" rig, as the parent company was the United Steel Companies Ltd., Sheffield, England, now part of British Steel. Manufacturing rights of the rig are now held by W. H. Mayes & Son (Windsor) Ltd., Berkshire, England.

The standard load applied was 340.2 kg. Rolls–Royce Ltd. embarked on a program to raise this load to a level which could produce failure on an improved material in a reasonable amount of time. This showed that about a 60 percent increase was possible before ball failures became a problem. In practice, to suit the availability of weights already at hand, the load was rounded off to 517.1 kg (1140 lb).

Details of the Rig used by Rolls-Royce Ltd.

The basic Unisteel rig, as described by Johnson and co-workers [1,2] and shown in Fig. 1, is unaltered but for the use of the higher load of 517.1 kg [3]. This results in a nominal maximum hertzian compressive stress between 4.48 GN/m^2 and 4.65 GN/m^2, depending on the material under test. This level of stress is probably of the order of 2.5 times the maximum normally experienced in engine bearings but is not outside the worst possible transient conditions and is therefore regarded as a practicable means of accelerating testing.

When the testing started it was considered appropriate to use an aircraft synthetic ester oil instead of mineral oils, which had previously been used on these rigs. At this time, D Eng RD2487 was the most commonly used oil in Rolls-Royce engines, and experience had already been gained on other rigs using Esso EATO 35, a 7.5 cSt oil, which conforms to D Eng RD2487.

This oil still remains in use on the rig because of its consistency between

---

[2]The italic numbers in brackets refer to the list of references appended to this paper.
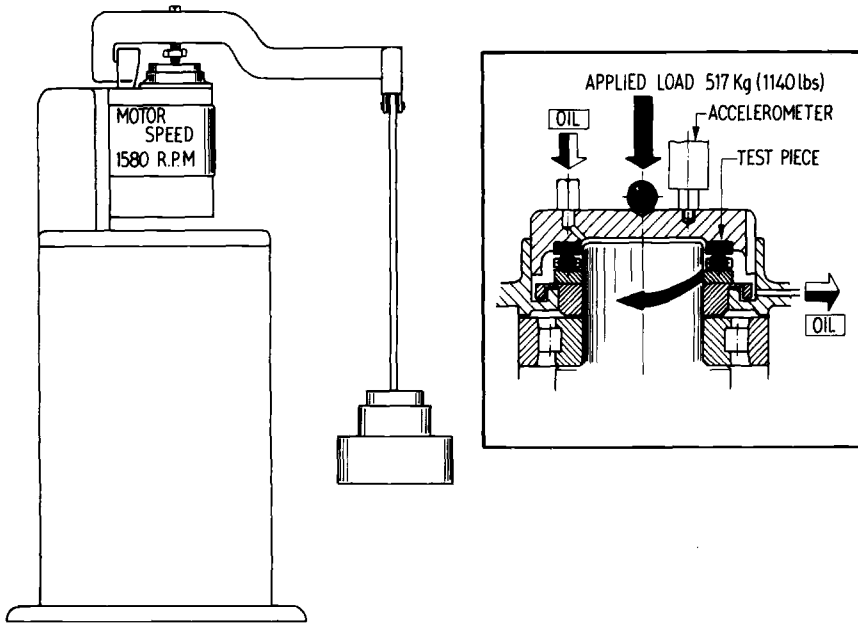
FIG. 1—*Basic Unisteel rig.*

batches and its long shelf life, which is superior to alternatives that have now superseded it in engine use. Most alternatives have been introduced to improve operation at higher temperatures, which is not necessary on a rig operating at ambient temperature. Thermocouples attached to the specimen have shown no variation outside a range of 50 to 60°C. To date, the arguments for changing to a more modern aircraft engine lubricant have been insufficient to warrant losing the baseline comparisons currently available to us. The rig is lubricated by a controlled drip feed set at 2 to 3 drops per minute.

The speed of the rigs, nominally 1500 rpm, has been checked, and adjustments have been made for each rig in assessing the revolutions achieved for each specimen.

In general, rig reliability has been excellent, which has led to confidence in letting the rig run unattended on a 24-h, 7-day-a-week basis. On isolated occasions, blockage of the drip feed oil system has led to excessive cage wear, but the vibration pickups have shut down the rig. Even in the earlier days before a transistorized vibration monitoring system, which is triggered from a dual accelerometer in the test head, was incorporated, advanced failure only necessitated changing the test assembly and cleaning out the test head.

The main replacements necessary are drive belts at periodic intervals with occasional bottom thrust bearings after an extended life usually of several years. All maintenance, mechanical and electronic, is carried out in-house.

Routine servicing is carried out daily, which involves checking and logging the running time, changing the specimens which have failed or reached a predetermined life, and topping off the oil reservoirs.

The Test Specimen Used by Rolls-Royce Ltd.

The standard specimen is shown in Fig. 2 and is normally produced from forged and rolled bar reduced to approximately an 82.5-mm diameter. This is a useful size for producing the finished test specimen, but it also produces a reduction from the original ingot that is representative of a large number of aircraft engine bearing races.

Turning and heat treatments are carried out in facilities within the company's laboratories. Finish grinding, etch inspection, and, on some materials, final lapping of the test surfaces are carried out by one of the bearing suppliers or other test houses such as steel makers who take part in cooperative programs with Rolls-Royce Ltd.

Basically, the aim has been to produce final levels of accuracy and surface finish comparable with those produced on engine bearings. Some evaluation of different forms of final lapping has been necessary because of different facilities available and the fact that the honing used on bearing tracks is not readily reproduced on the faces of the flat specimen.

Ø 75,3897 (2·9681)
75,3847 (2·9679)
LOC.

Ø51,7144 (2·036)
51,5874 (2·031)

5,5550 (0·2187)
5,4788 (0·2157)

0,2 μm
(8μ")

0,2 μm
(8μ")

BREAK SHARP EDGES 0,254 (0·010)

DIMENSIONS IN MM's (INS.)

THESE FACES TO BE FLAT
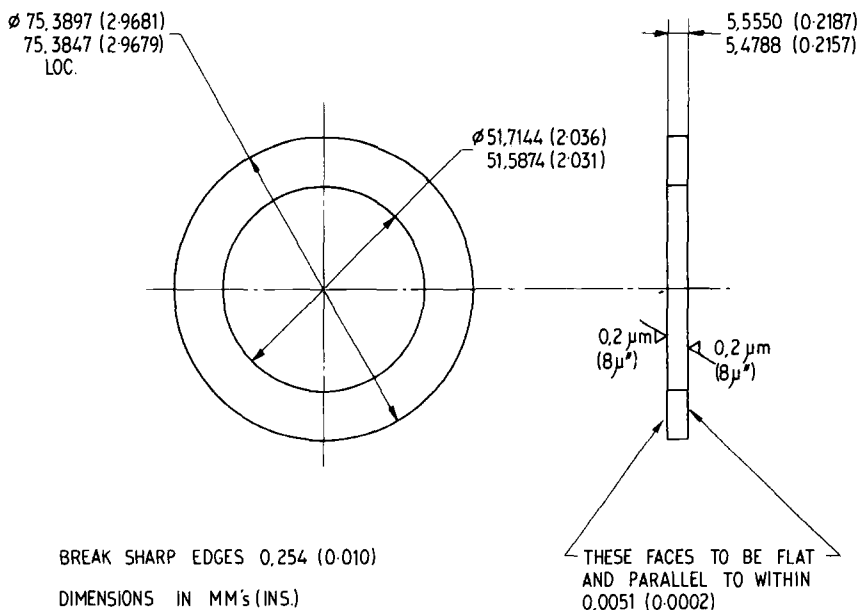AND PARALLEL TO WITHIN
0,0051 (0·0002)

FIG. 2—*Unisteel test specimen.*

All specimens are checked for surface finish on each test face and the results recorded. The normal requirements are that an 0.2-μm center line average (CLA) shall not be exceeded, but binocular examination is also carried out to ensure that random larger grit scores and other defects will not interfere with the ball path.

Slave Bearing Details

The rig was designed to take the small race from a standard catalog single-thrust bearing. With the passage of time this has become a special item but is still available to Unisteel rig users. It is manufactured in 1 percent CCr steel. With binocular inspection it has been found to be possible to reuse these pieces after inspection and they usually complete several test runs.

The same applies to the 18-pocket brass cage which is used with a complement of nine 7.9-mm balls and is usually only replaced when pocket wear becomes excessive.

The balls are replaced for each test run and are usually made of 1 percent CCr steel. With improvements in commercial balls since testing started, it is now possible to standardize on commercial balls produced from vacuum degassed material with good reliability. For the most reliable results, however, vacuum arc remelted material is used for test materials such as tool steels because of the longer test times and greater stress levels due to the difference in Young's modulus (that is, 18-4-1 tool steel has a higher Young's modulus). Normally the load is not readjusted for test materials with a different Young's modulus, although differences are not ignored in assessment of the results.

Analysis of Test Results

The standard procedure adopted is to manufacture 15 test pieces and test both sides of each, which gives a potential of 30 test results. In practice some losses are experienced in test piece manufacture, and some test results are discounted because of factors such as primary failure of slave pieces or lubrication. These latter effects are minimal, and often a result can be included in the analysis as being unfailed at a given life. In some instances these pieces can still be run on to a satisfactory life. Appropriate failure analysis is necessary to obtain maximum information from test data. Normally 24 to 28 good results are subjected to statistical analysis and represent the minimum number of results needed to be able to produce an L_5 (or B_5), that is, the 5 percent failure life value, which is regarded as more meaningful than L_{10} for aircraft engine use. It would be preferable to analyze for an L_1 value, but for confidence the test sample size would need to be increased by a factor of at least 3, which would severely restrict the amount of testing that

could be achieved in a given time at a given cost. The compromise adopted has proven an effective one.

Depending on the test objectives and previous experience on the material under test, it is now usual practice to select a running time at which testing will be suspended if failure has not occurred in order to expedite testing, but normally this practice has to be balanced against sufficient failures to enable a true Weibull analysis to be carried out.

Consideration of various analysis techniques has led to the adoption of the basic Weibull plotting of results after median ranking of the individual results. Straightening of the line by the use of a correction factor is used, and the L_5, L_{10}, and L_{50} are then determined from this line.

Review of the use of a log normal plot, which has the effect of a more profound straightening of the line plotted through individual results, was found to have an effect on L_5 values of less than 1, which is not considered significant. A log normal plot does, however, have a distinct disadvantage compared with the standard Weibull in that the latter still clearly shows family groups. It is believed that an understanding of the reasons for these families is important to subsequent engine bearing performance. Such an understanding certainly aids in planning the post-test investigation and metallography to get maximum information from a minimum of effort.

A typical table of results is shown in Table 1, and a Weibull plot from these results is illustrated in Fig. 3.

Typical Test Results

The test series completed now are well in excess of 150, with nearly 30 different materials evaluated, some of these under different temper conditions or with other heat treatment variables. Similarly, different steel melting practices have been evaluated from both a given supplier and alternative suppliers. These sources have included suppliers in the United Kingdom, France, Germany, Sweden, and the United States.

Table 2 shows results obtained on 1 percent CCr steel in a standard temper state of 150 to 165°C over a period of some 15 years and includes sources no longer available, mainly because of plant replacement or rationalization.

It has proved possible to select suppliers and assess not only improvements in materials but also their cost-effectiveness; that is, is the improvement sufficient to warrant the extra cost involved?

Broad trends indicate progressive improvement from early air-melt techniques through vacuum degassing to vacuum arc remelting. However, there is significant variation for each technique, particularly from different sources, so that the results from the different techniques overlap.

These results extend the work reported in Refs 1, 2, 4, and 5 and are mainly in broad agreement. However, we cannot confirm the beneficial claims made for the encapsulation of the harder nondeformable inclusions by

TABLE 1—*Typical table of unisteel test results.*

| Test Piece No.	Running Time, h	Rig No.	Running Time, revolutions	Test Piece Hardness, HRC	Surface Finish, µm	Remarks
1	80.2	3	7.71×10^6	61.5	0.089	
2	150.0 U/F[a]	3	14.4	61.5	0.127	
3	208.3 U/F	4	19.6	61	0.227	
4	80.1	4	7.52	61.5	0.127	
5	66.4	5	6.24	61	0.076	
6	67.0	5	6.30	61	0.089	
7	100.2	6	9.40	61	0.064	
8	27.5	6	...	...	...	not used; secondary to slave race failure
9	13.2	7	1.24	62	0.140	
10	75.9	7	7.16	61.5	0.127	
11	146.1	8	13.8	62	0.102	
12	106.0	8	10.0	62	0.076	
13	17.8	9	1.67	61.5	0.051	
14	9.4	9	0.88	61	0.076	
15	20.0 U/F	10	1.88	61.5	0.076	cut out failure; test piece OK at 20 h
16	44.1	10	4.15	62	0.076	
17	50.1	11	4.72	62	0.102	
18	48.9	11	4.6	62	0.127	
19	...	9	...	...	...	belt slip; running time unknown
20	41.6	9	3.92	62.5	0.152	
21	25.6	7	2.41	61.5	0.127	
22	45.6	7	4.30	62.5	0.089	
23	26.7	6	2.51	62	0.089	
24	23.2 U/F	6	2.18	61.5	0.114	cutout failure; test piece OK at 23.2 h
25	24.8	11	2.34	61.5	0.140	

[a] U/F = Unfailed suspended test.
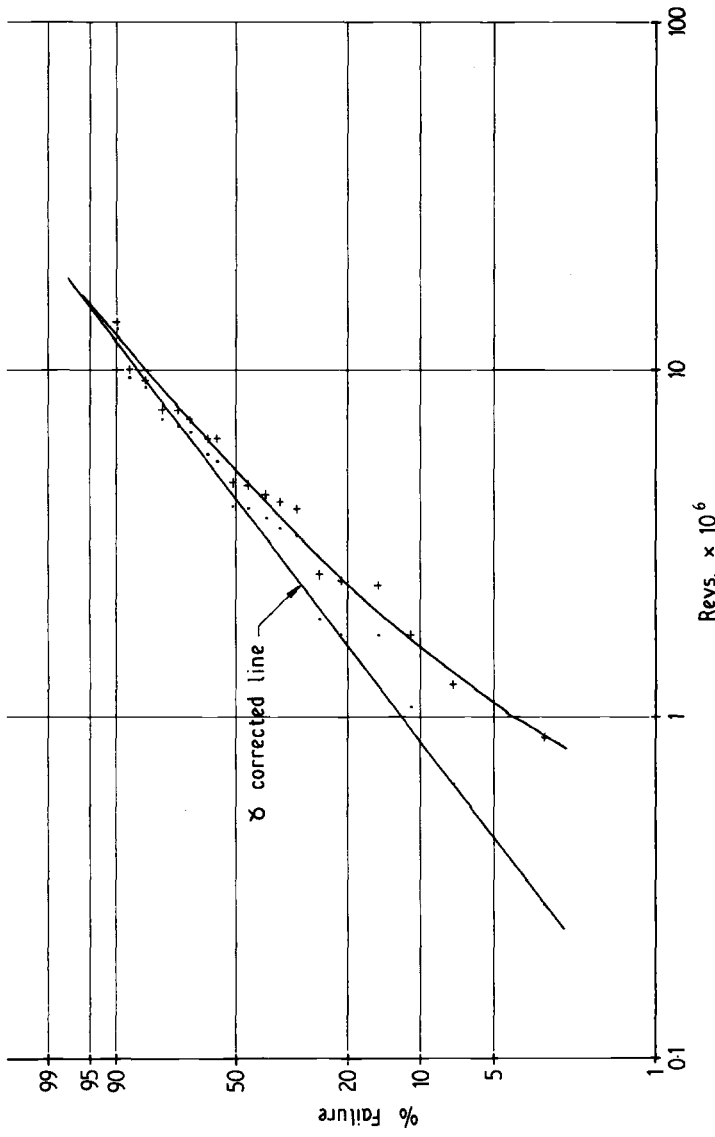
FIG. 3—*Typical Weibull plot.*

TABLE 2—*Test result analysis obtained on 1 percent CCr steel in 150 to 165°C temper condition.*[a]

Test Series No.	Source	Melting Route	Weibull Life, millions of revolutions		
			L_5	L_{10}	L_{50}
1	A	A/M (1)	0.9	1.3	3.8
2	B	VAR	4.3	5.1	8.2
3	C	VIMVAR	4.8	6.8	17.2
4	A	A/M (2)	0.8	1.2	5.3
5	B	VD (a)	1.2	1.5	4.4
6	D	VAR (Dev)	9.6	15.0	>38.0
7	E	VD	2.9	3.6	10.0
8	B	A/M	0.3	0.3	1.0
9	F	VD	0.7	1.4	7.3
10	G	VD tube	1.4	1.5	3.0
11	G	VD bar	1.1	1.5	5.0
12	G	VD as (10) + deep freeze	1.1	1.5	4.0
13	H	VD	3.5	4.9	17.5
14	I	VD (a)	1.0	1.8	8.2
15	I	VD (b)	0.9	1.4	6.2
16	I	A/M	0.9	1.4	3.7
17	B	VD (b)	1.5	2.8	>25.0
18	B	VAR	2.5	4.9	20

[a]Key:
A/M = air melt
VAR = vacuum arc remelted.
VIMVAR = vacuum induction remelted plus vacuum arc remelted.
VD = air melt plus vacuum degassing process.
(1) and (2) or (a) and (b) = different melting plant at the same source.
DEV = development cast.
10 = Test Series 10.

sulfides, either from direct test results or from metallographic examination, and we prefer freedom from all inclusions as far as possible. The general trends are presented more clearly in the bar chart in Fig. 4.

Test Series 6 (Table 2) shows what the material is potentially capable of, but these results have yet to be equalled by means of a production melting route. Table 3 shows a series of tests carried out to evaluate the effects of different test piece finishing techniques effected by different test houses. Five different finishing techniques were tested in five test houses, as indicated. The results were remarkably similar and gave increased confidence in the overall test method and ability to utilize both different sources of finishing and testing, provided proper controls were applied.

Table 4 is a selection of test results obtained on AISI M-50 steels, which shows trends similar to the carbon chrome steel in that vacuum induction melted plus vacuum arc remelted (VIMVAR) material has generally given higher results than vacuum arc remelted (VAR) material. In view of the ex-
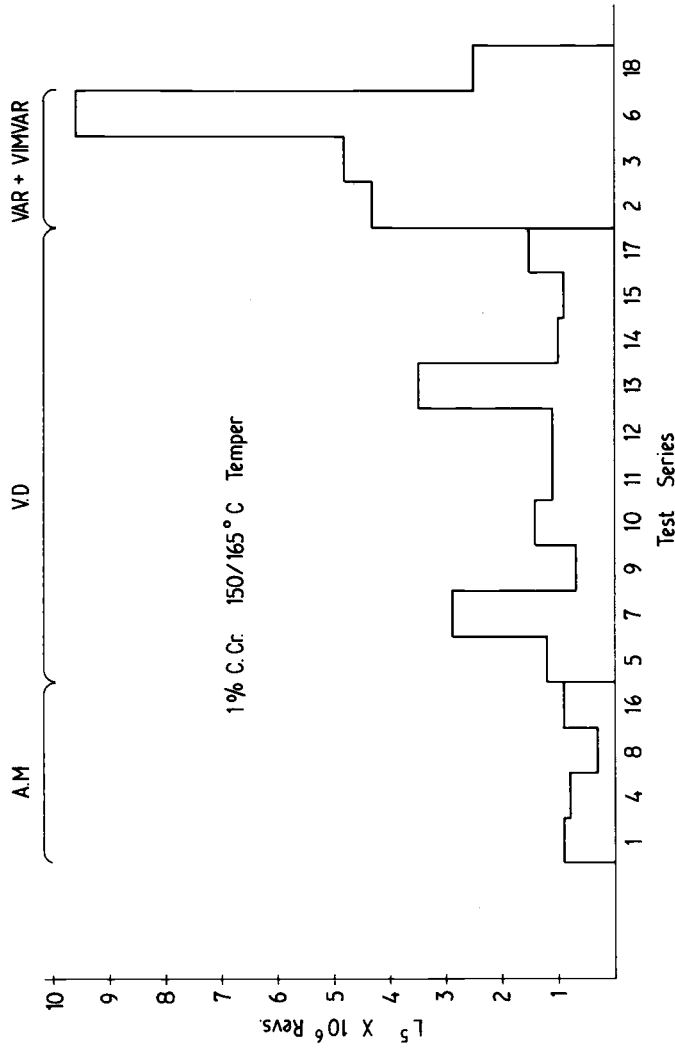
FIG. 4—*Comparison of the L5 test results of 1 percent CCr steel.*

TABLE 3—*Results comparing different specimen finishing techniques and different test houses.*

Test Piece Finish Series No.	Test Houses	Weibull Life, millions of revolutions		
		L_5	L_{10}	L_{50}
1	A B C	7.7	11.8	33.5
2	A B D	7.8	12.5	40.5
3	A	6.8	10.4	33.2
4	E	9.0	11.7	23.8
5	A	7.8	10.3	19.8

tensive background experience on this material in the United States, it is of interest to note that other sources are capable of producing comparable results. The reasons for the variations obtained have not been readily apparent but would appear to lie predominantly in the heat treatment. Our experience to date has shown that the inclusion of a deep-freeze treatment has been beneficial to fatigue performance, although nominally intended to ensure stabilization by completing austenite transformation.

Table 5 is a further selection of testing results on 18-4-1-type high-speed tool steel traditionally used in the United Kingdom, which has been the counterpart of the M-50 steel used in the United States. The same trends are apparent with progressive improvement from air melt material to vacuum arc remelt and, currently, electroslag remelt material. The latter, from selected sources, is not only capable of generally higher fatigue performance than alternative bearing steels but can achieve this performance with greater consistency. It has, however, become relatively expensive material and, therefore, now tends to be utilized only for the more demanding applications combining high duty or high operating temperature, or both.

The VAR route is no longer a preferred method for this material because of a tendency for it to segregate, which could lead to poor yields and present extra inspection requirements. The electroslag route has proven to be significantly superior in this respect once production methods have been established. The results of both the AISI M-50 and the 18-4-1 materials are presented in the form of a bar chart in Fig. 5.

The only previously published results comparing M-50 and 18-4-1 steels were carried out in conjunction with the National Aeronautics and Space Administration and are reported by Parker and Zaretsky [6]. These results show that when the materials were made into balls the differences were small.

Associated Failure Investigations and Metallography

All specimens are measured for surface finish and may be rechecked if the failure origin site indicates the need. For example, it is possible to provide an

TABLE 4—*Test result analysis values obtained on AISI M-50 steel.*

Test Series No.[a]	Supplier	Melt Route	Heat Treatment			Weibull Life, millions of revolutions		
			Harden, deg Celsius	Temper, deg Celsius	Deep Freeze	L_5	L_{10}	L_{50}
1	a	VAR	1120	550	yes	9.8	11.4	20.0
2	b	VAR	1120	550	yes	8.4	11.8	25.0
3	b	VAR	1100	540	no	2.7	3.8	14.2
4	c	VAR	1090	550	no[c]	2.6	6.6	22.0
5	d	VAR	1090	550	no[c]	0.8	1.5	7.0
6	e	EFR[b]	1110	550	yes	9.0	10.5	18.5
7	f	VIMVAR	1110	550	yes	>13.5	>40	>40
8	f	VIMVAR	1090	550	no[c]	5.0	7.1	>40
9	h	VIMVAR	1110	540	yes	11.5	26.0	>30
10	b	VIMVAR	1100	560	yes	9.4	14.0	39
11	b	VIMVAR	1100	560	yes	7.8	9.2	35.0
12	g	VIMVAR	1110	550	yes	9.0	9.5	35
13	g	VIMVAR	1110	550	yes	14.1	17.3	35
14	g	VIMVAR	1110	550	yes	9.4	12.3	35
15	g	VIMVAR	1110	550	yes	10.0	13.2	35

[a]Series 4, 5, 7, 8, and 9 had sources in the United States, and the remainder had sources in the United Kingdom and Europe.
[b]EFR = Electroflux (slag) remelted.
[c]Minimum specification hardness of 61 HRC not attained.

TABLE 5—*Test result analysis values obtained on 18-4-1 high-speed tool steel.*

Test Series No.	Source of Material	Melt Route	Weibull Life, millions of revolutions		
			L_5	L_{10}	L_{50}
1	A	A/M[a]	1.1	1.4	3.4
2	A	VAR[b]	11.8	16.0	>36.0
3	A	VAR	20.25	33.5	>38.0
4	B	VAR	9.5	12.0	37.0
5	C	VAR	2.9	3.4	7.7
6	B (a)[c]	VAR	9.2	14.0	>37.0
7	B (b)	VAR	9.2	11.6	36.0
8	A	EFR[d]	10.8	14.2	>37.0
9	A	EFR	>31.0	>46.0	>100.0
10	A	EFR	25.0	34.0	>39.0
11	B	EFR	>23.0	25.5	>30.0
12	B	EFR	20.0	17.5	>22.0
13	B	EFR	9.3	9.4	>30.0
14	B	EFR	16.2	>25.0	>30.0
15	B	EFR	22.5	>26.0	>30.0
16	A	EFR	>25.0		
17	A	EFR	>25.0		
18	A	EFR	>20.0		
19	D	EFR	>23.5	>23.5	>23.5
20	D	EFR	17.5	20.0	>25.0
21	D	EFR	16.8	36.0	>40.0

[a]A/M = air melt.
[b]VAR = vacuum arc remelted.
[c]Minor heat treatment variation occurs between (a) and (b).
[d]EFR = electroflux (slag) remelted.

acceptable CLA but still have a surface scratch which appears to nucleate the failure origin (see Fig. 6). All specimens are therefore subjected to binocular microscope examination to check their validity for inclusion in the results analysis.

Similarly, failures are normally rechecked for grinding abuse. An example of a faulty specimen is shown in Fig. 7. This problem was also found in Ref 4.

At least two specimens are subjected to microexamination, usually one with low life failure and one with long life runout. Frequently, other specimens are also examined to ensure their validity and, equally important, to determine the significant features that affect specimen life.

In earlier days inclusions were a significant factor, as indicated in their coverage in *Bearing Steels: The Rating of Nonmetallic Inclusion, ASTM STP 575*. More recently, improvements in commercial steel-making practice have been such that other factors appear to be more significant, for example, the effects of segregation (see Figs. 8 and 9) and other microstructural effects and features. The structural changes that occur show a strong association
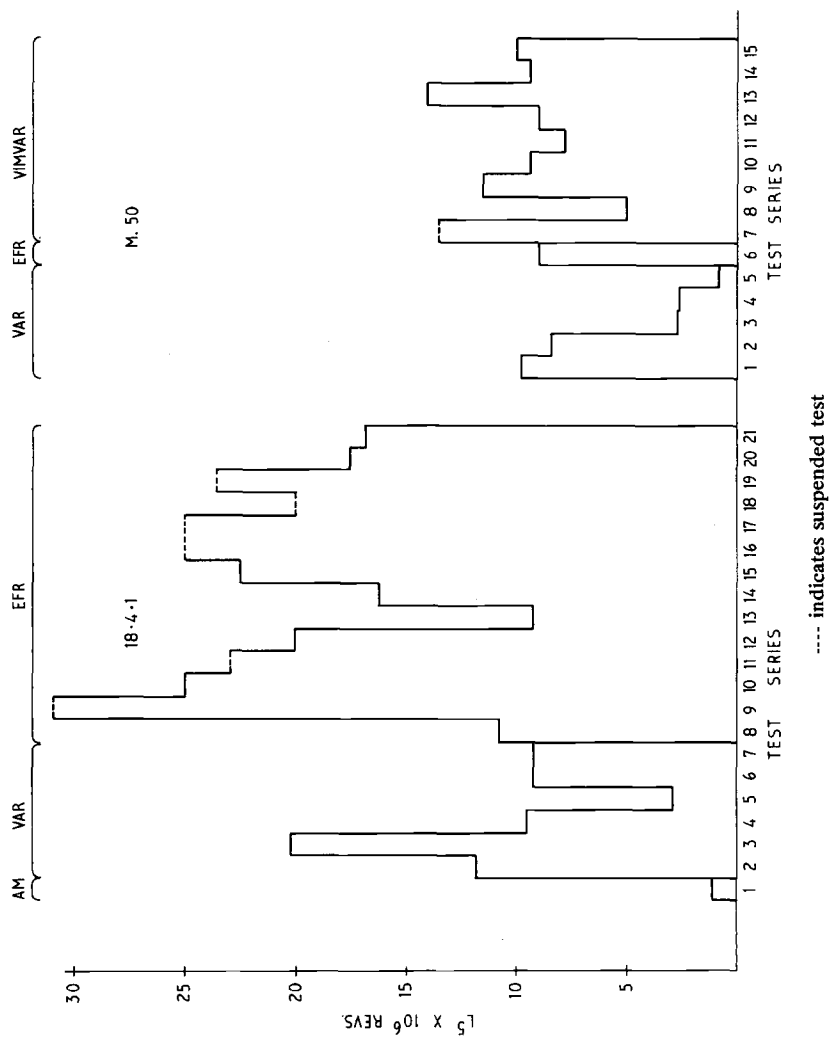
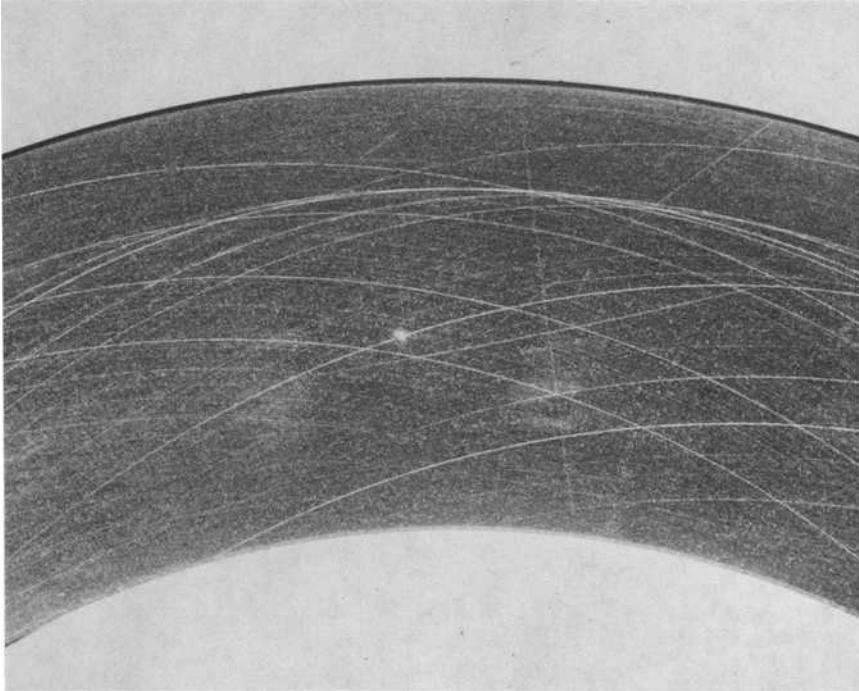FIG. 5—*Comparison of L$_5$ test results of 18-4-1 and M-50 steel.*

FIG. 6—*Failure origin induced by a surface scratch (× 5).*

with carbides in clean steels, whereas such changes concentrated around inclusions when these were present [7]. However, carbides appear to be essential for the overall properties of bearing steels, and there is currently increased interest in determining the correct path for future developments in this area.

Occasionally results are obtained in which no logical explanation for isolated low life failures can be found. In these cases X-ray crystallography has been utilized to examine structural and internal stress states. Likewise, the scanning electron microscope is now part of the standard metallographic analysis which can also utilize transmission electron microscope or microprobe equipment if required.

Discussion

The Unisteel rig adapted to run with a higher load than standard has been shown to be capable of providing reproducible results on aircraft engine bearing materials in a condition closely approximating bearing tracks, with
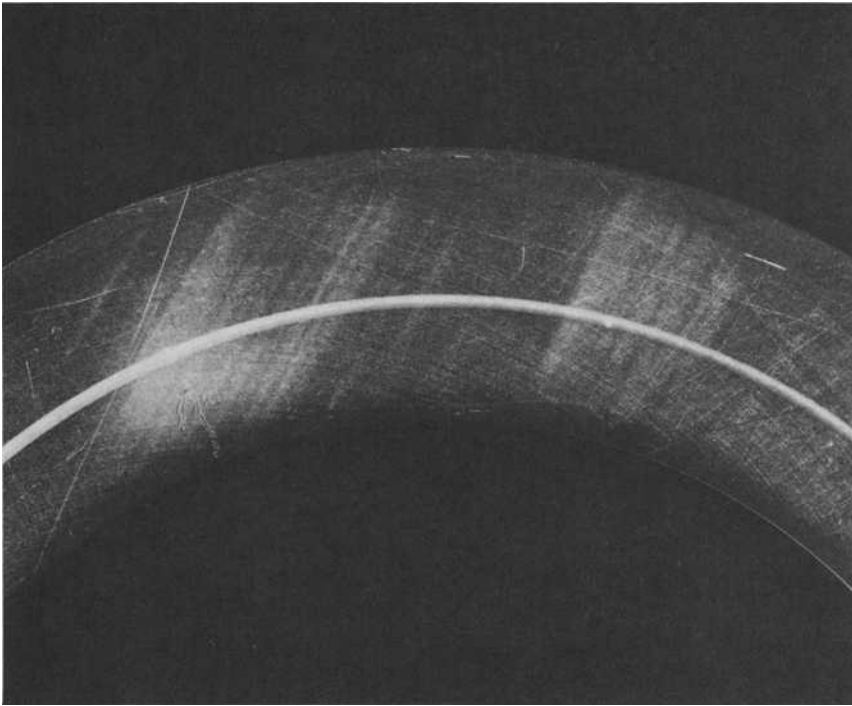
FIG. 7—*Failure origin associated with a grinding burn (×3).*

test conditions going part of the way to actual engine conditions. The rig does not claim to simulate engine bearing conditions but is a useful preliminary sorter of multivariables before resorting to time-consuming, expensive, full-scale testing. It can serve as a useful research and development tool in carrying out this initial sorting and also as a control on production sources and changes that inevitably occur in production processes. Due largely to the data bank built up over the years, there is great resistance to changing the test in any way. In fact, experiments to increase testing speed were dropped because the lives increased, presumably because of the generation of better oil films. Similarly, attempts to run the test head at elevated temperature, thereby reducing test lives, resulted in such poor utilization of the testing time, because of delays in handling, that this technique was also abandoned. Speed and temperature effects are better covered by full-scale rigs, although even they never reproduce the correct dynamics and other factors. General experience, however, has shown a good relationship between the Unisteel rig and full-scale testing.

FIG. 8—*Failure origin associated with segregation (×20).*

Conclusions

The Unisteel rig, adapted for a higher load and the use of synthetic lubricants, has been demonstrated to have filled a gap which existed between basic metallographic examination of aircraft bearing steels and full-scale rig or engine testing.

The latter testing is now so expensive that only limited capacity is available, and some prior evaluation has become even more important.

The Unisteel rig has the advantage over other alternatives, particularly where larger bearings are involved, of being capable of testing material in a metallurgical state representative of engine bearings.
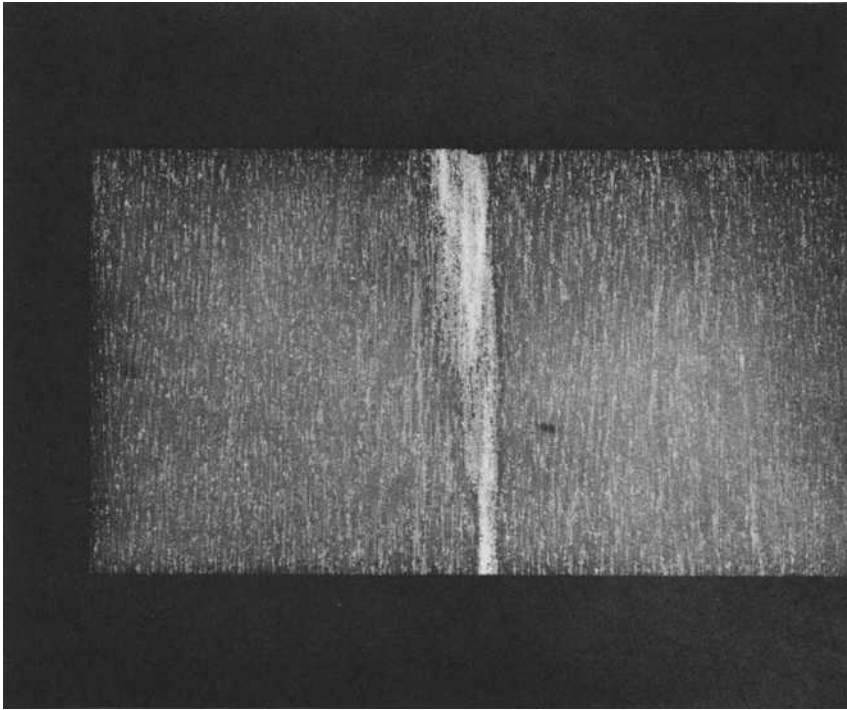
FIG. 9—*Microsection through the segregation illustrated in Fig. 8 (×10).*

Howse, head of Engine Support Laboratories. Finally, the author thanks R. G. Pickard and other colleagues for assistance with the details of preparation of the manuscript.

References

[1] Johnson, R. F., and Sewell, J. F., *Journal of Iron and Steel Institute,* 1960, pp. 414–444.
[2] Johnson, R. F., Sewell, J. F., and Robinson, J. L. in *Bearing Steels: The Rating of Nonmetallic Inclusion, ASTM STP 575,* American Society for Testing and Materials, Philadelphia, 1975, pp. 114–137.
[3] Palmgren, A., *Ball and Roller Bearing Engineering,* 3rd ed., S.K.F. Industries, Burbank, Calif., 1959.
[4] Johnson, R. F. and Blank, J. R., *Proceedings of the Symposium on Fatigue in Rolling Contact,* Institution of Mechanical Engineers, London, 1964, pp. 95–102.
[5] Meredith, J. E. and Sewell, J. F. in *Bearing Steels: The Rating of Nonmetallic Inclusion, ASTM STP, 575,* American Society for Testing and Materials, Philadelphia, 1975, pp. 66–95.
[6] Parker, R. J. and Zaretsky, E. V., "Rolling Element Fatigue Life of AISI M50 and 18/4/1 Balls," NASA TP-1202, National Aeronautics and Space Administration, Washington, D.C., April 1978.
[7] Davies, W. J. and Day, K. L., *Proceedings of the Symposium on Fatigue in Rolling Contact,* Institution of Mechanical Engineers, London, 1964, pp. 23–40.

E. N. Bamberger[1] and J. C. Clark[1]

Development and Application of the Rolling Contact Fatigue Test Rig

ABSTRACT: The rolling contact (RC) fatigue test rig was developed specifically for rapid and inexpensive evaluation of materials and processes for rolling element bearing applications. The simple geometry of the test specimen, a cylindrical bar, makes it ideal for evaluating new materials where only limited quantities of the material may initially be available and also permits precise control of the mechanical and thermal processing of the test specimen.

This paper will discuss the development of the RC rig and will detail some of the major investigatory programs which have been performed in the authors' laboratory. This includes the evaluation of metallic and nonmetallic materials for bearing operation, effects of different metallurgical structures on rolling contact fatigue, and the investigation of unique processes such as ausforming and hollow rolling elements. The results of these investigations will show the relevance of the RC rig to full-scale bearing tests and to actual bearing operation in service. Last, the initial work performed on the second-generation RC rig, a high-speed version capable of surface speeds up to 25 m/s (82 ft/s), permitting operation well into the elastohydrodynamic regime, will be briefly reviewed.

KEY WORDS: bearings, rolling element, rolling contact fatigue, steel, fatigue tests, bearing material, ausforming, bearing steels

In a recent paper by Bamberger [1][2] the development of rolling element bearing materials is traced from the beginning of the steel industry to the present. In this paper it was pointed out that the development and evolution of bearing materials was fairly static until the early to mid-1950s. At this point, the aircraft gas turbine engine was beginning to make increasing demands on structural materials, including those used for bearings. These

---

[1]Principal engineer, Advanced Bearing Technology, and manager, Bearings, Seals, and Drives Design Technology, respectively, Aircraft Engine Group, General Electric Co., Cincinnati, Ohio 45215.

[2]The italic numbers in brackets refer to the list of references appended to this paper.

ever-increasing demands required tools which could rapidly and inexpensively evaluate new and modified materials. It is interesting to note that in the 1946 Symposium on Testing of Bearings, sponsored by ASTM [2], only full-scale bearing tests were discussed. While full-scale bearing tests are perhaps even today still the optimum tool for establishing bearing life parameters, the time and cost required to perform these in sufficient numbers to achieve statistically valid data become ever more prohibitive. This coupled with the fact that some of the potential candidates for structural bearing materials are available only in small quantities, made it imperative to look toward a simplified component test to use in evaluating these materials.

Some attempts toward this goal had been made by using other types of fatigue tests, such as rotating beam fatigue tests, to establish rolling element fatigue life and behavior. These efforts were generally unsatisfactory. In the mid-1950s, Macks [3] and Barnes and Ryder [4] made notable contributions through development of test methods for studying fatigue as related to bearing applications. As the need for improved bearing materials became more urgent, studies were initiated in the authors' laboratory to develop a rolling contact (RC) fatigue test machine which could accurately simulate the stress pattern of a ball–race contact. The result was the RC rig which, for the past two decades, has been used successfully to evaluate new materials, processes, and lubricants for bearing application. This paper will describe the RC rig, present a life-calculation model, and detail some highlights of investigatory studies performed in the authors' laboratory with this instrument.

RC Rig Description

Because the RC rig was primarily developed in response to a need to evaluate new bearing materials quickly and inexpensively, the configuration of the test specimen geometry was of the utmost importance. Consequently, a simple shape, a cylindrical bar, was selected because it could be easily manufactured; it required a minimal amount of material; and all processing, including heat treatment, grinding, and surface treatments, could be performed without special tooling. The ability to do all the processing "in house" further permitted direct control of all the phases of the test specimen manufacturing cycle. Additionally, it made possible the examination of a large number of processing variables using a minimal amount of material. To achieve the hertzian contact stresses, it was decided to use two hemispherically ground toroidal rollers, individually supported and mechanically loaded against the bar. The original RC rig is shown in Fig. 1. Figure 2 presents a schematic illustration of the test bar geometry superimposed on a curve showing hertzian stress as a function of applied load for the RC rig. The load train consists of a fine-threaded turnbuckle and a variable capacity load cell designed and calibrated for maximum sensitivity in the load range most commonly used. A velocity–vibration pickup was installed to monitor
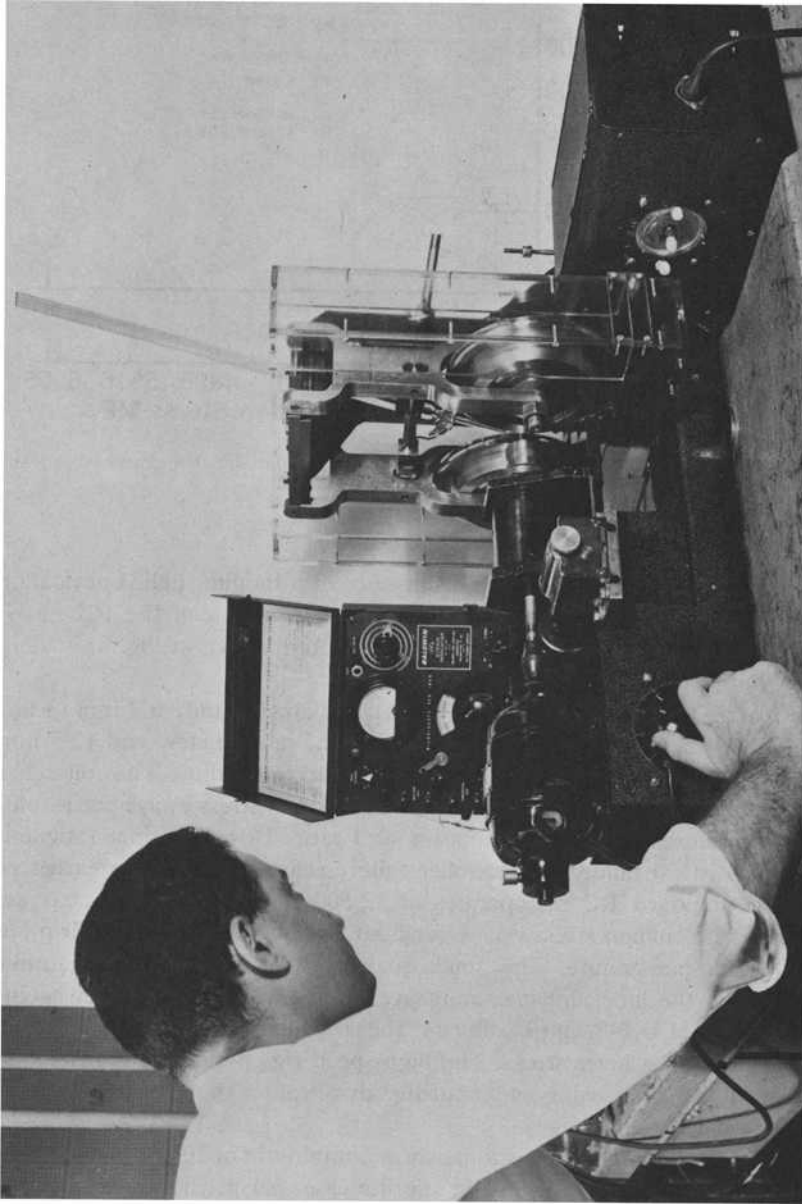
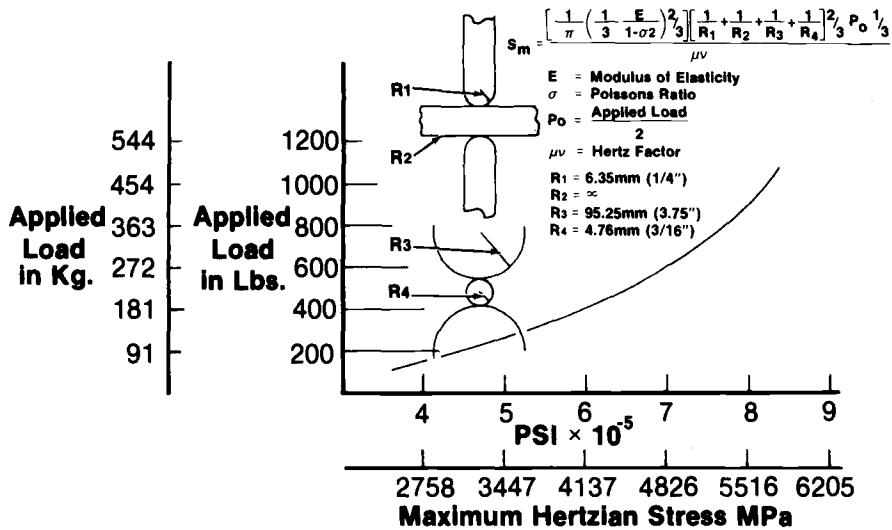FIG. 1—Original model of the rolling contact fatigue tester (RC rig).

$$S_m = \frac{\left[\frac{1}{\pi}\left(\frac{1}{3}\frac{E}{1-\sigma 2}\right)^{2/3}\right]\left[\frac{1}{R_1}+\frac{1}{R_2}+\frac{1}{R_3}+\frac{1}{R_4}\right]^{2/3}P_o^{1/3}}{\mu\nu}$$

E = Modulus of Elasticity
σ = Poissons Ratio
P_o = $\dfrac{\text{Applied Load}}{2}$
$\mu\nu$ = Hertz Factor
R_1 = 6.35mm (1/4")
R_2 = ∞
R_3 = 95.25mm (3.75")
R_4 = 4.76mm (3/16")

FIG. 2—*Schematic draws of the RC rig test specimen (maximum hertzian stress as a function of applied load).*

the test and terminate it upon the occurrence of a fatigue spall. Lubrication is drip fed. Figure 3 shows the latest high-speed version of the RC rig. It should be noted that the basic bar–roller geometry, shown in Fig. 4, is identical to that of the original model.

The RC rig test bar is 9.525 mm (⅜ in.) in diameter and 76.2 mm (3 in.) long. The rollers are a nominal 190 mm (7½ in.) in diameter, and 12.7 mm (½ in.) thick, with a 6.35-mm (¼-in.) hemispherical radius. The roller–bar diameter ratio is 20:1, and because the bar sees two stress cycles per revolution, roller failures should be at about a 40:1 ratio. However, since fatigue is a totally statistical failure mode, roller failures can and do occur earlier or later. The standard RC rig operates at 12 500 rpm with the test bar accumulating 1.5 million stress cycles per hour. Normal lubrication is drip fed at ~20 drops per minute. This small quantity is sufficient because, unlike for a bearing, the lubricant does not have to serve as a heat transfer agent. The normal load is 148 kg (326 lb) per roller, which results in a 4 826 MPa (700 ksi) maximum hertz stress. The high-speed rig operates in the range of 10 000 to 50 000 rpm, using an air turbine drive rather than the a-c motor of the standard RC rig.

The general test procedure is to perform a minimum of 10 and a maximum of 20 tests per test series. Except in specific cases, suspension is normally at 36 million stress cycles. A number of tests can be performed on one bar, which is an important benefit especially when evaluating experimental materials that may be available only in limited amounts.
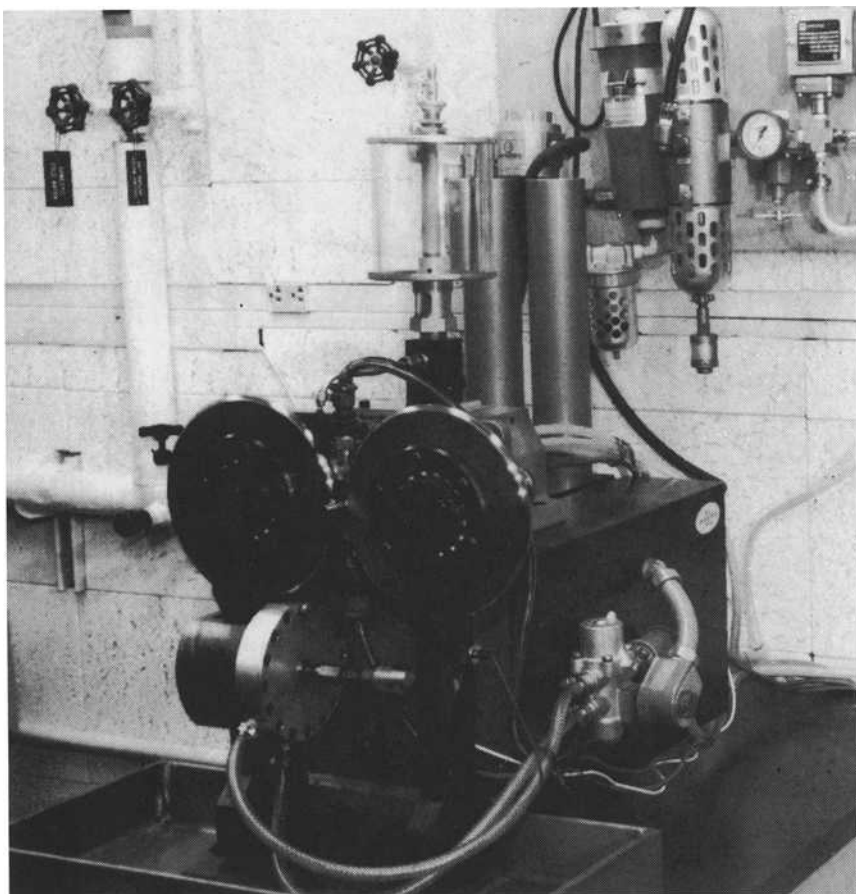
FIG. 3—*High-speed RC rig.*

The first major task after the rig had been developed was to ensure that failures produced with the rig were comparable in both macro and micro features to those experienced in full-scale bearing tests. This was accomplished by comparing the spalling failures generated on the RC rig with spalls occurring in full-scale bearing tests. Figure 5 shows this comparison on both the macro and micro scale.

The second task was to establish a rationale for relating the RC rig test results to the performance of actual bearings. It was fortuitous that in the same general time frame, Morrow and Moyar at the University of Illinois had been working on the generic problem of correlating laboratory fatigue behavior of metals with the spalling failures seen on rolling elements in concentrated contact.
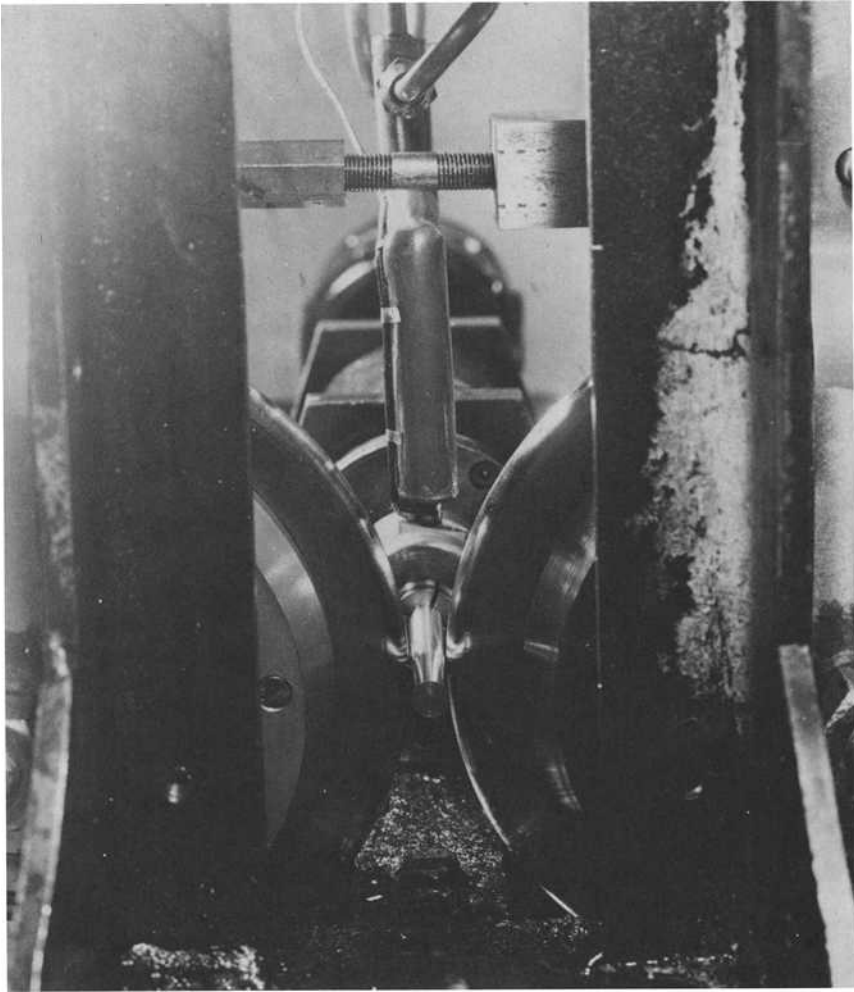
FIG. 4—*RC rig test bar-roller configuration.*

During the summer of 1959, Morrow collaborated with the authors' laboratory in a program to define the major operational parameters of the RC rig vis-à-vis actual bearing operation and to establish a sound engineering basis for using the rig as a predictive device. Much of this work has been published in Refs 5 and 6 and thus will not be repeated here. What will be discussed in the next section are considerations of the stress–life relationship in the RC rig, as well as the influence of elastohydrodynamics (EHD) on RC rig test results.
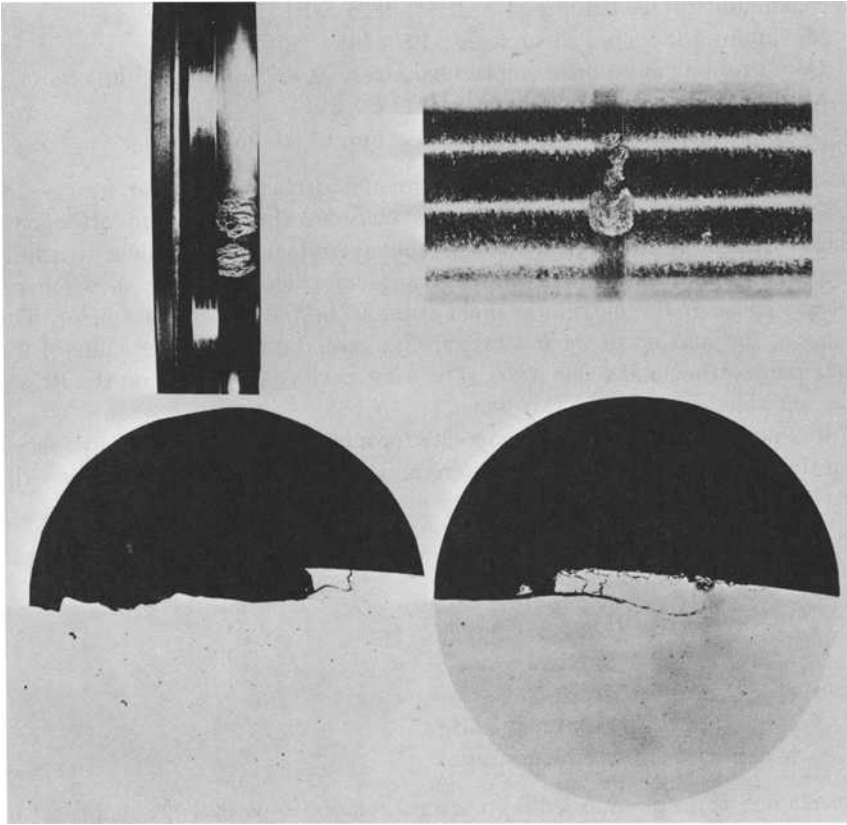
FIG. 5—*Comparison of failure modes of full-scale bearings* (left) *and RC rig* (right).

Stress-Life Relationships

Relationships for surface and subsurface stresses for point contacts are developed in Refs 7, 8, and 9. The general equations are somewhat complicated and their derivations are beyond the scope of the present paper. However, these equations have been programmed into computer routines that form the basis for a program (RCRSLE) which serves as an analysis tool for the RC rig. The program includes surface stresses, subsurface stresses, and the elastohydrodynamic aspects of the rig. For the normal test load of 148 kg (326 lb), test temperature (ambient room temperature), and M-50 steel, the data are tabulated here. The program has the capability of calculating stresses for different materials and combinations of materials.

Semiminor axis of contact ellipse: 0.34 mm (0.0134 in.)
Semimajor axis of contact ellipse: 0.42 mm (0.0167 in.)

Maximum surface compressive stress: 4826 MPa (700 ksi)
Maximum orthogonal shear stress: 1074 MPa (155.7 ksi)
Depth to maximum orthogonal shear stress: 0.127 mm (0.005 in.)
Maximum shear stress: 1535 MPa (222.6 ksi)
Depth to maximum shear stress: 0.178 mm (0.007 in.)

It should be noted that both the orthogonal and maximum shear stresses are calculated because many investigators consider the maximum orthogonal shear stress to be the critical stress in rolling contact fatigue. Since it is fully reversing, it is considered to have a range of twice the value shown here. Others consider the maximum shear stress to be the critical parameter. The value of the maximum shear stress always exceeds the absolute value of the maximum orthogonal shear stress. The work performed to date on the RC rig has not aided in resolving this issue.

It is possible to determine a capacity for a concentrated contact by following the basic formulation of Lundberg and Palmgren [7], which can be written as

$$\ln \frac{1}{\varsigma} = f(\tau, N, Z_0)$$

where

ς = probability of survival,
τ = critical shear stress,
N = number of stress cycles, and
Z_0 = depth of critical shear stress.

Developing this equation leads to several relationships that are empirical in nature and require test data for determination. In practical terms, the specific capacity of a device such as the RC rig is not a significant factor, since all test results are ultimately compared to a baseline. Therefore, it was found sufficient to define the RC rig capacity simply as the load that would give a B_{10} life (90 percent probability of survival) of 1 million cycles when testing vacuum induction melted–vacuum arc remelted (VIMVAR) M-50 material (AMS-6491). This capacity has been calculated to be 306 kg (675 lb).

This value was determined by taking extensive RC rig test data at the following conditions:

Material: VIMVAR M-50 steel
Hardness: HRC 62 to 64
Load: 148 kg (326 lb)
Oil: Type I (MIL-L-7808)
Rig speed: 12 500 rpm
Lambda ratio: 0.9
Lubrication life factor: 0.4

The value for C would then be calculated from the life equation for point contact.

$$L = F \left(\frac{C}{P} \right)^3$$

where

L = millions of stress cycles,
F = lubrication factor per American Society of Mechanical Engineers (ASME) [10],
C = capacity of bar [306 kg (675 lb)], and
P = applied load.

Using the ASME recommended design value for the lubrication factor, 0.4 for a lambda value of 0.90, the RC rig capacity has the following definition:

RC rig capacity—the load expected to give a B_{10} life of 1 million stress cycles using VIMVAR M-50 at a lambda ratio of 0.9.

All other life-modifying factors are equal to 1.0.

Most testing has been accomplished at loads of 148 kg (326 lb), which is equivalent to a maximum hertzian stress of 4826 MPa (700 ksi). However, a program was run to determine the effect of different loads (stresses). Since stress varies as the cube root of the load, from the previous equation life would be expected to vary inversely as the ninth power of the stress. The test results presented in Fig. 6 show a very good correlation with the theoretical values.

Elastohydrodynamic Considerations

The RC rig was developed in the same time period as the early investigations of the effects of EHD on bearing performance [11,12]. As a result, this variable was only introduced in later years with the development of the high-speed version of the rig, which permitted variation of the film thickness as a function of speed. However, the earlier test results remain valid, because the parameters in the film thickness and the surface finishes have been held constant.

For the RC rig EHD considerations, the formula developed by Cheng [13] is used to calculate the minimum film thickness

$$h_{min} = 1.38(R_X)^{0.27}(\mu_0 \cdot \alpha v)^{0.73} \left(\frac{P}{E^*} \right)^{-0.19}$$

h_{min} = minimum film thickness, μm (μin.),
R_x = equivalent radius of curvature of rolling direction, m (in.),

$\mu_0 =$ viscosity of contacting surfaces, Pa·s (lb/in.^{2}),
$\alpha =$ pressure viscosity coefficient, Pa^{-1} [(in.^{2}/lb)$^{-1}$],
$\nu =$ velocity,
$P =$ pressure, Pa (psi), and
$E^* =$ equivalent modulus of elasticity, Pa (psi).

Using this equation and temperatures measured by optical pyrometers, the minimum film thickness as a function of rig speed has been calculated and is shown in Fig. 7 as a ratio (lambda ratio) of the composite surface finish.

$$\lambda = \frac{h_{min}}{\sigma}$$

$$\sigma = \sqrt{\sigma_1{}^2 + \sigma_2{}^2}$$

Figure 7 shows that the rig operating at 12 500 rpm does not reach the full film lubrication range. However, with the higher speeds available using the high-speed rigs, λ ratios typical of full-scale bearing tests can be generated.

To summarize the stress–life–EHD aspects, the stresses in the RC rig are higher than those experienced in full-scale bearing tests, whereas the lambda ratio is in the same range as that of high-performance bearing tests.

The last section of this paper will cite a number of programs performed with the RC rig, illustrating its usefulness in the area of bearing materials and lubrication technology. Where possible, these examples will also be related to actual bearing performance, thus illustrating the degree of agreement attainable.

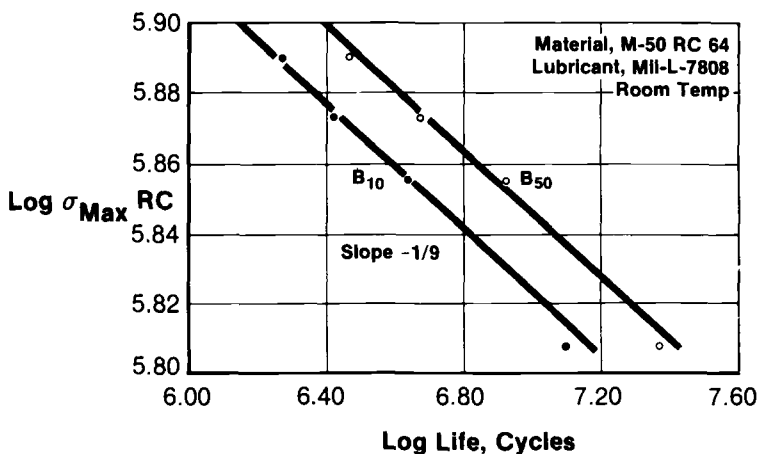It should be noted that during the initial work performed by Morrow, at

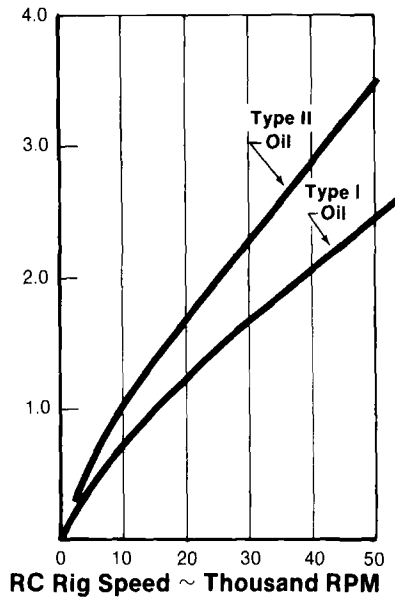FIG. 6—*Log–log plot of RC data showing the slope to be* $-\frac{1}{9}$.

FIG. 7—*Film thickness as a function of speed on the RC rig. Lambda ratio,* $\lambda = h_{min}/\sigma$.

the authors' laboratory, four specific cases were investigated where full-scale bearing test results were predicted based on RC rig tests. These results, reported in Refs 5 and 6, show a remarkably good agreement between the predicted and experimental lives of the bearings. The following examples are concerned with a generic "ranking" of RC rig versus full-scale bearing data.

Material Processing

In the early 1960s, work was initiated to apply thermomechanical working (ausforming) to bearing materials to improve rolling element fatigue life. The process of ausforming consists of severely working a material while in the metastable austenitic condition. With materials such as M-50, which have a deep bay region (stable austenite) in the time–temperature–transformation curve, this will result in strain-induced carbide precipitation as well as a highly strained martensitic structure, both of which act to improve rolling element fatigue life. All of the initial work on this process development effort was performed using the RC rig and was reported in Ref 14. Initially, the study was concerned with the amount of deformation or work needed to pro-duce the maximum increase in rolling element fatigue life. As shown in Fig. 8, this turned out to be about 80 percent. As a result of these encouraging data, a program was initiated to ausform the rings and balls for 35-mm-bore ball bearings, to test these bearings, and to establish the validity of the RC
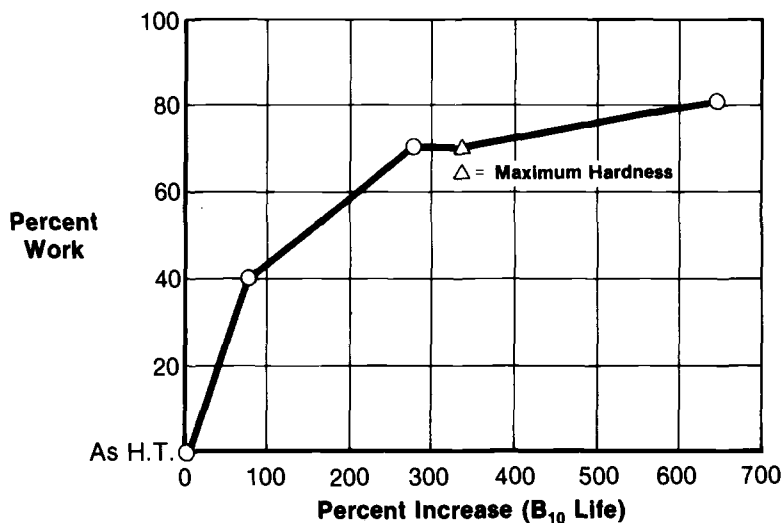
FIG. 8—*Effect of ausforming on rolling element fatigue life.*

rig findings. The results of this work, reported in Ref *15*, confirmed the RC rig data in that the ausformed M-50 bearings had nine times the life of standard heat-treated M-50. The RC rig had predicted an approximate 6.5-fold increase.

Further confirmation of this was obtained from a National Aeronautics and Space Administration (NASA) program where ausformed M-50 balls [11 mm ($\frac{7}{16}$ in.) in diameter] were compared with standard M-50 balls using a five-ball rig. The results reported in Ref *16* showed a life improvement of threefold to fourfold for the ausformed balls. It might be noted here that the NASA five-ball tester, which is described in another paper in this volume, has always shown good agreement with RC rig test results.

Last, in a more recent program [*17*] where 35-mm-bore ausformed bearings produced by a high-energy-rate extrusion process were again tested, the data showed an approximate sevenfold increase in the life of these parts compared to normally processed M-50.

Melting Practice Evaluation

In the late 1960s a number of different primary melting techniques were being used to produce M-50, and it was considered desirable to select that process which would produce the most consistent and extended rolling element fatigue life. Consequently, the author's laboratory initiated a comprehensive evaluation with the RC rig to evaluate the different melting methods. Over an approximately 3-year time span, 23 heats of material were

investigated. These included combinations of air vacuum arc remelted (AIR-VAR), double vacuum arc remelted (VARVAR), and vacuum induction melted–vacuum arc remelted (VIMVAR) materials. The results of these tests are shown in Fig. 9. Based on these results, the decision was made to standardize on the VIMVAR material, and this now has become the aircraft engine bearing standard in the United States. While back-to-back full-scale bearing tests were not performed during this evaluation, extensive bearing testing and engine experience has validated the decision to use VIMVAR material. Retrospectively, at least one specific comparison can be made, based on 120-mm full-scale bearing tests performed as part of two NASA-sponsored programs. Data reported in Refs 18 and 19 show the superiority of VIMVAR M-50 over AIRVAR M-50. The AIRVAR material was tested at 2268-kg (5000-lb) thrust load and the VIMVAR at a 2631-kg (5800-lb) thrust load. Despite this discrepancy, the VIMVAR material was still superior.

Microstructural Anomaly

During the course of a bearing evaluation program, a microstructural anomaly was uncovered in the M-50 bearing material. This consisted of a duplex grain structure such as that shown in Fig. 10. A normal M-50 microstructure is also shown in Fig. 10 for comparison. There was concern that this duplex structure might influence bearing performance and, specifically, fatigue life. A heat-treatment study performed in the authors' laboratory pinpointed the cause of the duplex structure (an excessively rapid cool-
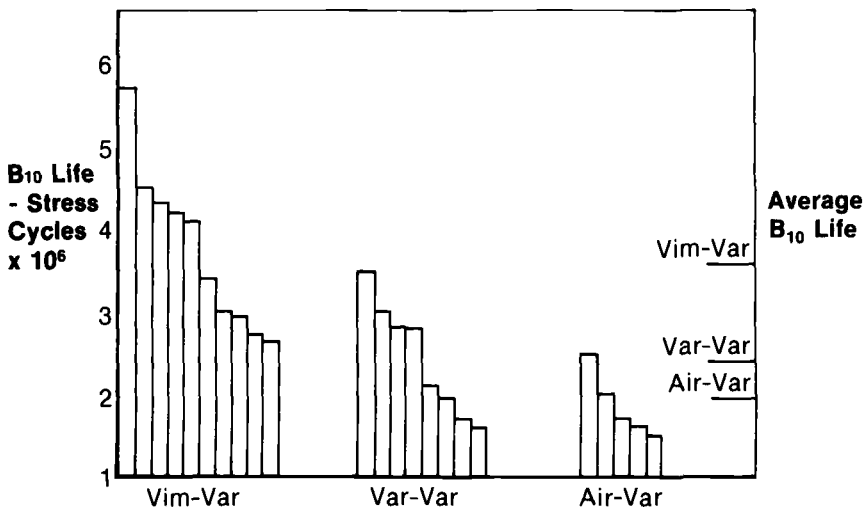

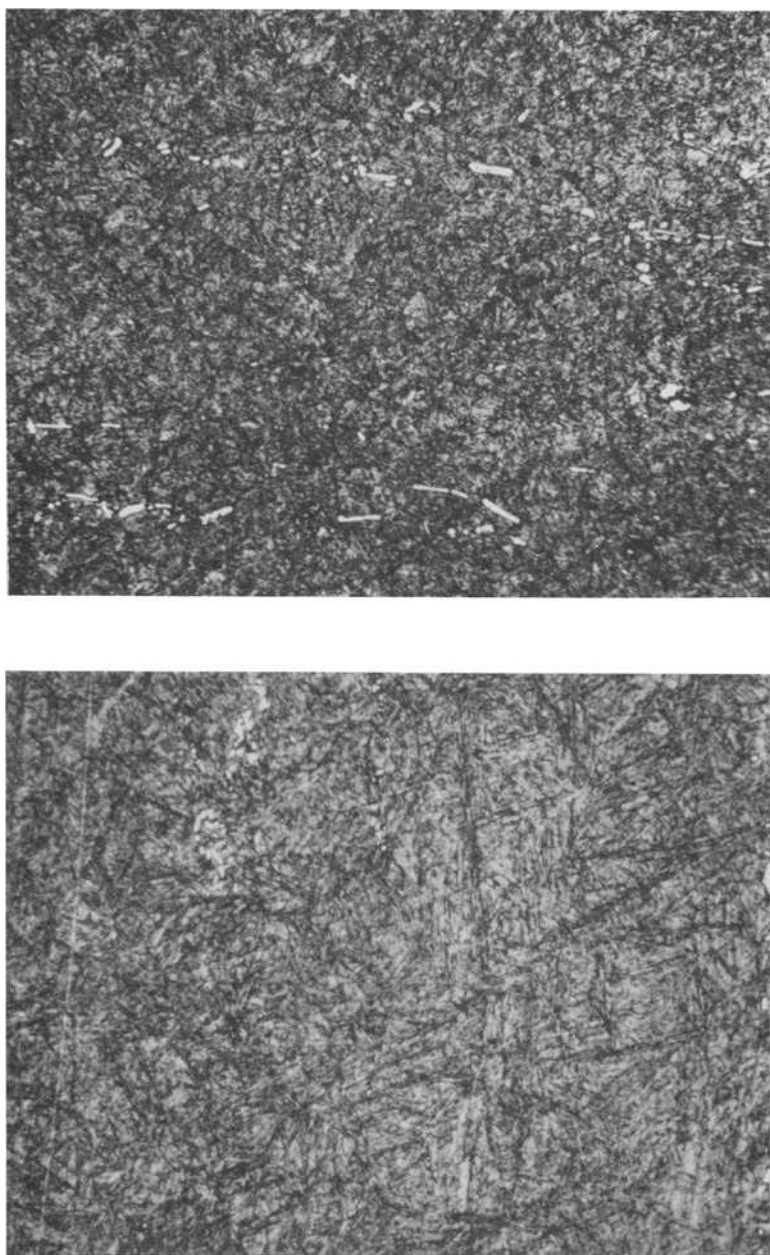FIG. 9—*RC rig evaluation of AISI M-50 melting procedures. Each bar represents 20 tests.*

FIG. 10—(Left) Duplex microstructure in M-50 bearing material; (right) normal M-50 microstructure (2 percent nital; magnification ×450).

ing rate from the annealing cycle after forging), and a number of RC rig test bars were made containing the duplex microstructure.

Subsequent testing showed that the duplex structure, while not desirable, did not have any apparent influence on the rolling element fatigue life when compared with bars made from the same heat of material but containing a homogeneous structure. The full-scale bearing tests were then continued, and the results confirmed the RC rig prediction in that the duplex structure did not deleteriously influence the fatigue life in full-scale bearing tests.

Hollow Rolling Elements

A more unique application of the RC rig was in defining the limitations and failure modes of hollow rolling elements. The impetus for the use of hollow or reduced mass rolling elements was the projected increase in bearing speeds or DN (DN = bearing bore in millimetres times the inner race revolutions per minute) for advanced aircraft gas turbines. Stress analysis had shown that the high hertzian stresses at the outer race contacts, caused by centrifugal ball or roller loading, could seriously shorten the bearing fatigue life [20]. Calculations showed that this detrimental effect could be negated [21] by reducing the mass of the rolling elements. Consequently, a considerable amount of work was devoted to developing hollow rolling elements.

Hollow balls fabricated by joining two hemispherical shells [22,23] met with problems such as stress concentrations in the weld area, which acted as stress raisers and caused early failures, or nonuniform wall thicknesses which resulted in ball unbalance. In other studies [24] where these difficulties were largely overcome, short lives were obtained in single-ball tests, and short-time destructive ball fractures were experienced in full-scale bearing tests. It was shown that significant bending stresses at the inside diameter of hollow balls were present [25], and this aided in the understanding of the experimental results.

All of these data indicated the one serious shortcoming of the hollow ball concept: in order to achieve the needed mass reduction (approximately 50 percent), the wall thickness of the ball had to be so thin that flexural fatigue became the primary mode of failure.

The reality of this shortcoming was proven in a study to determine the effect of wall thickness and material on the flexural fatigue of hollow rolling elements [26]. Using the RC rig and test bars having outside diameter/inside diameter (OD/ID) hollowness ratios ranging from 2.0 to 1.2 (Fig. 11), the tests were conducted on both Type 52100 and M-50 material. The objective was to determine the crossover point between normal spalling-fatigue failures and bending failures resulting in fracture. The data for M-50, shown in Fig. 12, clearly indicated that at an OD/ID ratio of 1.4, flexural failures began to occur, and at the OD/ID ratio of 1.2, representing a 50 percent mass reduc-
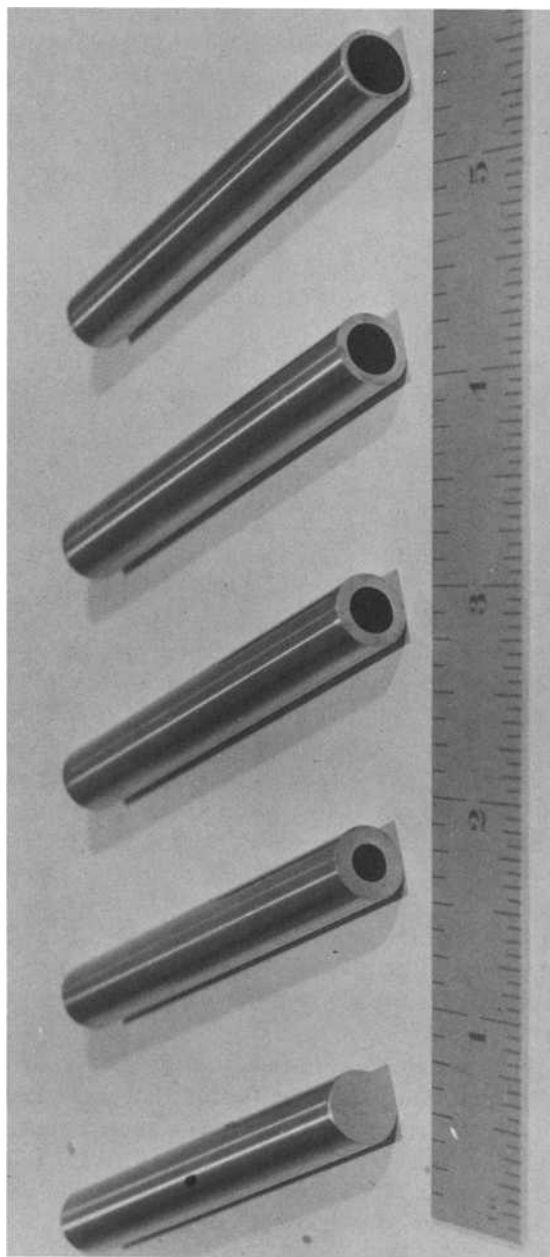
FIG. 11—Hollow rolling contact fatigue test bars. The outside diameter/inside diameter ratio is (from left to right) none, 2.0, 1.6, 1.4. and 1.2.
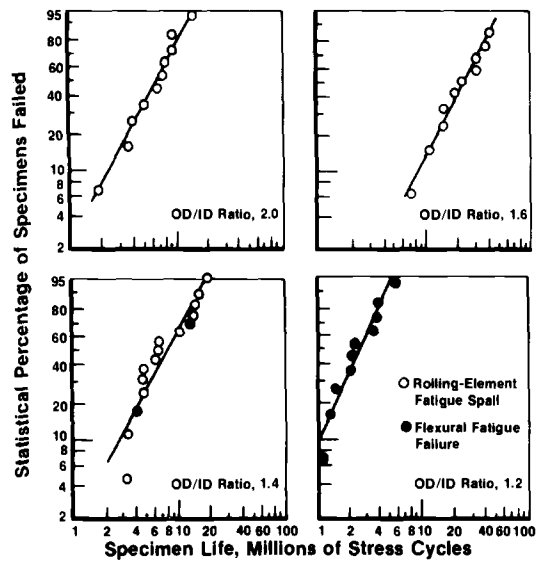
FIG. 12—*Fatigue lives of AISI M-50 hollow test bars in a rolling contact fatigue test.*

tion, fracture was the predominant failure mode. Typical failures are shown in Fig. 13. These failures were quite similar to those experienced in the full-scale bearing tests [24].

Component Life Prediction

An example of the RC rig's ability to project the performance of bearing components, as related to heat-to-heat variation in the steel used to make these components, was illustrated in work described in Ref 18. In this NASA-sponsored program, several high-temperature [589 K (600°F)] lubricants were being evaluated in full-scale (120-mm bore) ball bearing tests. Prior to the bearing tests, RC rig tests were performed as a matter of course on the two heats of M-50 being used. One heat was used for producing the rings, and the second heat was used to manufacture the balls. The RC rig data indicated that the ball heat had a significantly lower rolling contact fatigue life than the heat of material used for the rings. It was consequently noted, before the start of the bearing test series, that more ball failures might occur than would normally be expected on a statistical basis. The subsequent full-scale bearing tests results proved this to be absolutely correct. This *a priori* information can be extremely valuable, since it can eliminate the tendency to blame the test or test conditions for an unexpected event, along with much needless, time-consuming, and expensive reexamination of test procedures.

As part of this same test series, another material (WB-49) was tested along

with M-50. The RC rig data on the WB-49 showed it to be inferior to the M-50 in terms of rolling element fatigue life. The following tabulation shows the comparison between the initial RC rig test and the full-scale bearing test results:

Material	Lubricant	RC Rig B_{10} Life, stress cycles $\times$ 10^6	Bearing Test B_{10} Life, h
M-50	XRM-177[a]	3.85	252
WB-49	XRM-177	1.45	84

[a]Synthetic hydrocarbon.

Last, the three high-temperature lubricants being evaluated in this program were also tested on the RC rig prior to full-scale bearing testing. The RC rig ranked these lubricants in the same order as the full-scale bearing tests.

This brings up an issue which merits some discussion. While the RC rig has been used for lubricant evaluations, these studies must be viewed in the perspective of the EHD effects on concentrated-contact performance. As shown earlier in this paper, the standard RC rig, that is, the low-speed (12 500 rpm) version, operates in the boundary or mixed EHD regime. Consequently, caution must be used when data obtained under these conditions are extrapolated to bearings which are operating under full EHD lubrication. By the same token, all data from simulated component tests such as the RC rig as well as other similar tests must be treated cautiously, especially when attempting to directly project bearing behavior in full-scale tests.

For example, particular attention must be paid to the processing of the test bar (or ball) as against that of a ring. Normally the bar or ball will experience significantly more mechanical working than the rings of a bearing. Consequently, grain flow and carbide morphology can vary greatly and affect results. A specific case in point was in an evaluation of AMS-5749. Reference 1 cites both RC rig and five-ball rig data on this material. However, actual bearing tests (45-mm bore) resulted in lives short of those obtained with either of the two component tests. Subsequent metallurgical evaluation showed the failed bearing rings to have larger carbides and considerable carbide banding at a 45-deg angle to the raceway surface. On the other hand, the RC rig bar had smaller, more dispersed carbides, with the grain flow parallel or conforming to the running track. The balls used in the five-ball tester had even finer, uniformly dispersed carbides. This is a typical case where test specimen manufacture differs sufficiently from the actual component and thus can result in a divergence between component and full-scale bearing test results. Perhaps the lesson here is that when a specific manufacturing process produces good results in tests such as the RC rig, it becomes
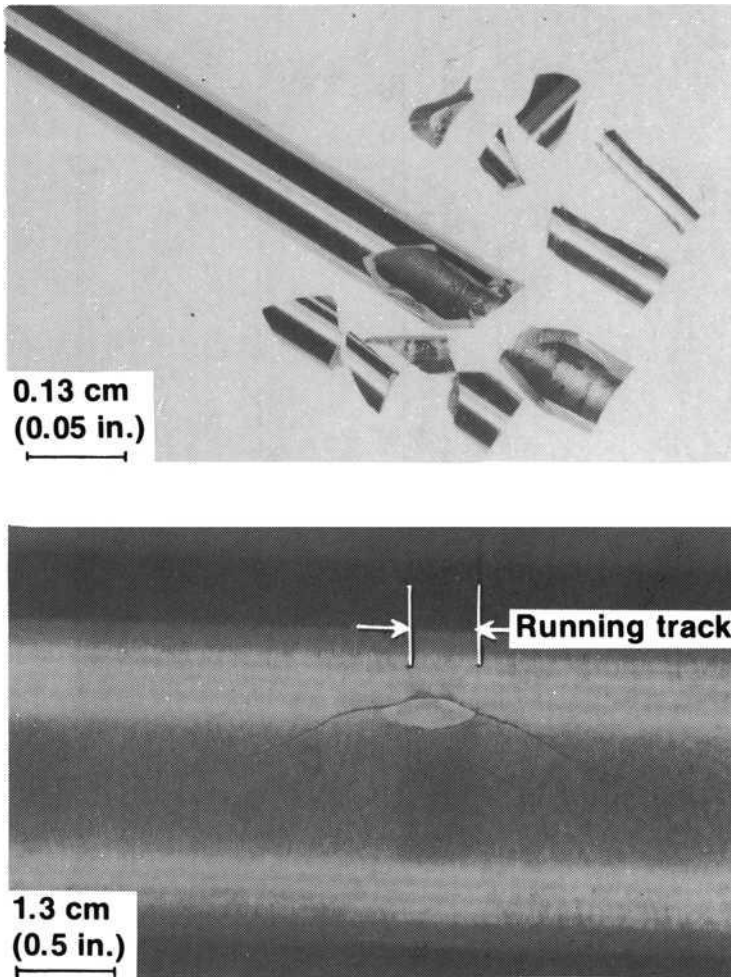
FIG. 13—*Typical flexural fatigue failures of hollow test bars.* (Top) *Fracture of hollow test bar due to flexural fatigue;* (bottom) *the failure appearance on the bar surface was sensed early, and the test was terminated before total fracture occurred.*

important to ensure that the process used to make an actual component results in equivalent material characteristics.

In conclusion, it should be mentioned that the authors' laboratory has, for the past several years, been operating a high-speed rig which can perform testing through the entire spectrum of lubrication from boundary to full EHD. Initial results with this high-speed rig were recently reported in Ref 27. The summary of test results (Table 1) shows the very dramatic effects of in-

TABLE 1—Summary of test results.

Test Series	Rolling Speed, rpm (m/s)	Lubricant Type	Film Thickness, μm (μin.)	Film[a] Thickness Ratio	B_{10} Life, $\times 10^6$ cycles	B_{50} Life, $\times 10^6$ cycles	Weibull Slope	Failure[b] Index	B_{10} Life, Ratio, L_f
A	5 000 (2.5)	1[c]	0.13 (5.00)	0.45	4.88	6.97	5.27	10/10	0.66
B	10 000 (5.0)	1	0.21 (8.30)	0.75	5.07	11.39	2.33	10/10	0.69
C	25 000 (12.5)	1	0.42 (16.35)	1.48	7.39	20.29	1.87	10/10	1.00
D	50 000 (25.0)	1	0.69 (27.30)	2.48	25.86	66.75	1.98	10/10	3.50
E	50 000 (25.0)	11[d]	0.98 (38.70)	3.52	48.12	584.50	0.75	4/10	6.51

[a]The composite surface roughness was calculated to be 2.8 μm (11 μin.).
[b]The number of failures out of the total number of tests.
[c]MIL-L-7808G.
[d]MIL-L-23699.

creasing film thickness ratio, Λ, on the rolling contact fatigue life of M-50. The high-speed RC rig opens up a vast new area for exploratory work which will make this device even more useful in the coming years.

References

[1] Bamberger, E. N., *Bearing Design—Historical Aspects, Present Technology and Future Problems*, ASME Century 2 Publication No. H00160, American Society of Mechanical Engineers, New York, 1980, pp. 1-46.

[2] Symposium on Testing of Bearings, Forty-Ninth Annual Meeting, American Society for Testing and Materials, Philadelphia, June 1946.

[3] Macks, E. F., *Lubrication Engineering*, Vol. 9, 1953, pp. 254-258.

[4] Barnes, G. C. and Ryder, E. A., "A Look at Some Turbine Engine Problems," Preprint No. 693, Society of Automotive Engineers, New York, 1956.

[5] Moyar, G. J. and Morrow, J. D., *University of Illinois Bulletin*, Vol. 62, No. 35, Nov. 1964.

[6] Morrow, J. D., *Journal of Basic Engineering, A.S.M.E. Transactions*, Vol. 88, Series D, Sept. 1966, pp. 583-588.

[7] Lundberg, G. and Palmgren, A., *Mechanical Engineering Series*, Vol. 1, No. 3, 1947.

[8] Thomas, H. R. and Hoersch, V. A., "Stresses Due to the Pressure of One Elastic Solid Upon Another," *University of Illinois Bulletin*, July 1930.

[9] Jones, A. B., *Analysis of Stresses and Deflections*, New Departure Engineering Data, New Departure Bearing Division, General Motors Corp., Bristol, Conn., 1964.

[10] Bamberger, E. N., Harris, T. A., Kacmarsky, W. M., Moyer, C. A., Parker, R. J., Sherlock, J. J., and Zaretsky, E. V., *Life Adjustment Factors for Ball and Roller Bearings—An Engineering Design Guide*, American Society of Mechanical Engineers, New York, 1971.

[11] Grubin, A. N. in *Investigation of the Contact of Machine Components*, Translation of Russian Book No. 30, Kh. F. Ketova, Ed., Central Scientific Institute for Technology and Mechanical Engineering, Moscow, 1949, Chapter 2.

[12] Dowson, D. and Higginson, G. R., *Journal of Mechanical Engineering Science*, Vol. 1, No. 1, 1959, pp. 6-15.

[13] Cheng, H. S., *Journal of Lubrication Technology*, Vol. 92, Series F, No. 1, Jan. 1970, pp. 155-162.

[14] Bamberger, E. N., *Journal of Lubrication Technology*, Vol. 89, No. 1, Jan. 1967, pp. 63-75.

[15] Bamberger, E. N., "The Production, Testing and Evaluation of Ausformed Ball Bearings, Final Engineering Report," Bu-Weps Contract NOw-65-0070-f, Department of the Navy, Washington, D.C., June 1966.

[16] Parker, R. J. and Zaretsky, E. V., "Rolling Element Fatigue Life of Ausformed M-50 Balls," NASA TN D-4954, National Aeronautics and Space Administration, Lewis Research Center, Cleveland, Ohio, Dec. 1968.

[17] Bamberger, E. N., Clark, J. C., Russell, T. E., and Smeaton, D. A., "Axial-Centrifugal Compressor Program, Evaluation of Ausformed Bearings," Report No. TR-75-55, U.S. Army Air Mobility R & D Laboratory, Fort Eustis, Va., Oct. 1975.

[18] Bamberger, E. N., "Bearing Fatigue Investigation," NASA CR 72290, National Aeronautics and Space Administration, Sept. 1967.

[19] Bamberger, E. N., "Bearing Fatigue Investigation II," NASA CR 134621, National Aeronautics and Space Administration, June 1974.

[20] Jones, A. B., *American Society of Mechanical Engineers, Transactions*, Vol. 74, No. 5, July 1952, pp. 695-703.

[21] Harris, T. A., *A.S.L.E. Transactions*, Vol. II, No. 4, Oct. 1968, pp. 290-294.

[22] Coe, H. H., Parker, R. J., and Scibbe, H. W., *Journal of Lubrication Technology*, Series F, Vol. 93, No. 1, Jan. 1971, pp. 47-59.

[23] Coe, H. H., Parker, R. J., and Scibbe, H. W., "Performance of 75-Millimeter-Bore Bearings Using Electron-Beam-Welded Hollow Balls with a Diameter Ratio of 1.26," NASA TN-D-7869, National Aeronautics and Space Administration, Cleveland, Ohio, 1975.

[24] Potts, J. R., "Manufacturing Methods for Production of Hollow-Ball Bearings for Use in Gas Turbine Engines," AFML-TR-72-170, AD 904689L, U.S. Air Force, WPAFB, Dayton, Ohio, Sept. 1972.

[25] Nypan, L. J., Coe, H. H., and Parker, R. J., *Journal of Lubrication Technology*, Series F, Vol. 98, No. 3, July 1976, pp. 472-475.

[26] Bamberger, E. N. and Parker, R. J., *Journal of Lubrication Technology*, Vol. 100, No. 1, Jan. 1978, pp. 39-46.

[27] Nahm, A. H. and Bamberger, E. N., *Journal of Lubrication Technology*, Vol. 102, No. 4, Oct. 1980, pp. 534-538.

[28] Payson, P., *The Metallurgy of Tool Steels*. Wiley, New York, 1962.

DISCUSSION

R. S. Hodder[1] *(written discussion)*—During the verbal presentation of this paper Bamberger described the RC rig test results associated with study of a duplexed microstructure in M-50 material. It was pointed out that the cause of this microstructure was too rapid a cooling from the anneal temperature, and it was further pointed out that the existence of this microstructure was not detrimental to the fatigue properties of the material. The details of results of this study will be of particular interest to others who have encountered this type of microstructure. Thus, any elaboration on the subject would be welcomed. For example, would it be possible to identify the microstructure more descriptively with regard to grain size or martensitic needle structure or both? Any embellishment would be a valuable contribution.

E. N. Bamberger and J. C. Clark (authors' closure)—The duplex microstructure to which Mr. Hodder refers is illustrated in Fig. 10 of this paper. The structure is characterized by the presence of random patches of coarse martensite needles in an otherwise homogeneous fine-grained martensitic material. The normal grain size of the material is ASTM 8 or finer, whereas the size of the duplex grains was found to be as large as ASTM 1 to 2. As mentioned in the text of our paper, the specific cause for this duplex structure was traced to an excessively rapid cooling rate from the postforge annealing cycle. Payson [28] discusses a similar microstructural anomaly and attributes the cause to a double hardening cycle.

[1]Latrobe Steel Company, Latrobe, Pa.

Douglas Glover[1]

A Ball–Rod Rolling Contact Fatigue Tester

ABSTRACT: This paper describes the development of an accelerated rolling contact fatigue tester that minimizes the testing variables through the use of simple, expendable components. The important design features of the tester and the specimen and rolling element finishing technique are described. Test results comparing two similar testers are presented for both steel and ceramic.

KEY WORDS: rolling contact, fatigue bearing, element tester, rolling bearings, bearing steels

Standard methods for measuring most engineering properties of materials have been well established by appropriate industrial or government organizations. For measuring the rolling contact fatigue life of bearing materials, however, there are no established standards. Since there are no standards to reference, it is important when reporting bearing fatigue data to define fully the parameters of the test and specimens so that others can relate the data to their experience. The purpose of this paper is to describe in detail a bearing material bench tester developed by the Ball and Roller Bearing Group of Federal–Mogul, referred to as the ball–rod rolling contact fatigue (RCF) tester. In future technical papers published by Federal–Mogul this paper will be referenced as a source of information regarding the testing detail.

Full-scale bearing tests constitute the ultimate proof of a bearing material, but full-scale bearing tests are expensive and time-consuming, because of the need to manufacture the sample bearings and because of the long test time involved. A more cost-effective and expedient way to study a large number of bearing materials is to use a bench tester, which utilizes a test specimen of

---

[1]Manager of Research, Federal–Mogul, Ann Arbor, Mich. 48104.

simple geometry. By use of the bench tester, many complex variables encountered in a full-scale bearing test are minimized. With an economical bench tester it is practical to utilize several units in order to reduce the time elapsed for material evaluation. These factors helped to shape the objectives for the design of the ball–rod RCF tester.

This paper describes the design of the ball–rod RCF tester and presents calculations for the loads and motions unique to the tester. The results of several test series of a bearing steel and a ceramic are discussed.

Design

Tester

The basic principle of the ball–rod RCF tester, as illustrated in Fig. 1, consists of a rotating cylindrical test specimen alternately stressed by rolling contact with three radially loaded balls. The three balls, separated by a retainer, are radially loaded against the test specimen by two tapered bearing cups thrust-loaded by three compression springs. From the calculations shown in Fig. 1 and Table 1, it can be seen that the radial load for each ball equals 4.27 times the individual spring load applied to the tapered cups.

A cross sectional drawing (Fig. 2) shows the design detail of the ball–rod RCF tester. The 9.5-mm (⅜-in.) diameter test specimen is held in a vertical position by a precision collet. The specimen is rotated at 3600 rpm by a direct-drive electric motor mounted in line with the specimen below the table. The three 12.7-mm (½-in.) diameter balls, equally spaced by a bronze retainer, are loaded radially against the cylindrical specimen through the thrust loading of the two tapered roller bearing cups. Thrust loading is applied to the cups by the attachment of the upper cup housing to the spring retainer plate with the load application bolts. The spring load between the spring retainer plate and the lower cup housing is preset as a subassembly by adjusting the nut on the spring calibration bolt. Proper adjustment is reached when a load applied to the springs by a calibrated dead weight will cause separation of the spring retainer plate and the lower cup housing. This system of applying the load eliminates the necessity of calibrating the spring load each time a test is performed, as would be necessary if the upper and lower cup housings were connected directly with the springs. An accelerometer coupled with a shutdown device monitors the vibration of the cup housings. When a preset vibration level is exceeded, indicating the presence of a surface crack or fatigue spall, the motor is automatically stopped. The test duration is measured by an hour meter connected electrically to the motor. Lubrication is applied by a drip feed to the end of the test specimen or by total immersion of the rotating components.

The specimen, loading mechanism, and drive motor form a compact unit (Fig. 3), which is suspended through two sets of shock mounts from the table

FIG. 1—*Tester schematic.*
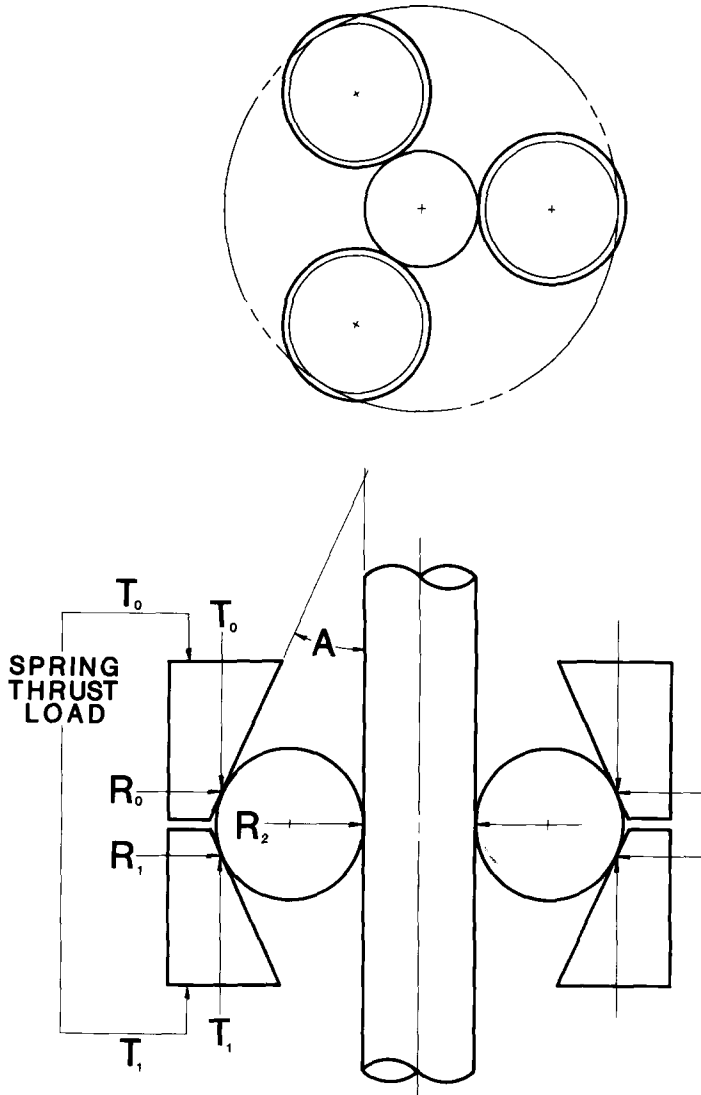
of the test bench (Fig. 4). Test benches now under construction incorporate six test units in a single test bench 1.8 m (6 ft) wide by 0.6 m (2 ft) deep. Use of the double shock mounts provides sufficient isolation so that vibrations set up by a fatigue spall in one test unit will not shut down other units in the bench.

With the unique spring-loaded design of the ball–rod RCF tester, small

TABLE 1—*Radial load calculations from Fig. 1.*

	English Units	ISO Units
A = cup angle	25.083 deg	25.083 deg
$T_0 = T_1$ = spring thrust load	57 lb	253.65 N
R_0 = radial load between upper cup and ball		
$R_0 = \dfrac{T_0}{\tan A}$	121.79 lb	541.97 N
R_1 = radial load between lower cup and ball		
$R_1 = \dfrac{T_1}{\tan A}$	121.79 lb	541.97 N
R_2 = radial load between one ball and specimen		
$R_2 = R_0 + R_1$	243.59 lb	1083.98 N

misalignments of the specimen, balls, and cups can be accommodated without imposing a significant change in the test load or ball motion.

Test Specimen

For over 10 years Federal–Mogul has used the rolling contact (RC) rig [1][2] developed by General Electric for bearing material evaluation [2,3]. The test specimen used in the RC rig is a cylindrical rod 9.5 mm (⅜ in.) in diameter and approximately 76.2 mm (3 in.) long (Fig. 5). This convenient specimen is readily produced within close dimensional and surface finish tolerances using conventional tool room equipment. Each rod is typically used to obtain several individual tests. For these reasons, and because of the favorable experience with the RC rig, the rod-type test specimen was incorporated into the new tester design.

Balls

During the early development of the ball-rod RCF tester, it was determined that the test time was excessive when using standard AISI 52100 Grade-24 balls with surface finishes under 0.013 μm (0.5 μin.) arithmetic average (AA). Also, with the standard ball finish over 50 percent of the balls failed during testing. It was found that increasing the roughness of the balls to 0.089 μm (3.5μin.) AA reduced testing to a reasonable time and reduced ball failures to less than 1 percent during testing. The reduced test time with the

---

[2]The italic numbers in brackets refer to the list of references appended to this paper.

1. Specimen
2. Ball
3. Tapered bearing cup
4. Ball retainer
5. Compression spring
6. Upper cup housing
7. Spring retainer plate
8. Lower cup housing
9. Shock mount
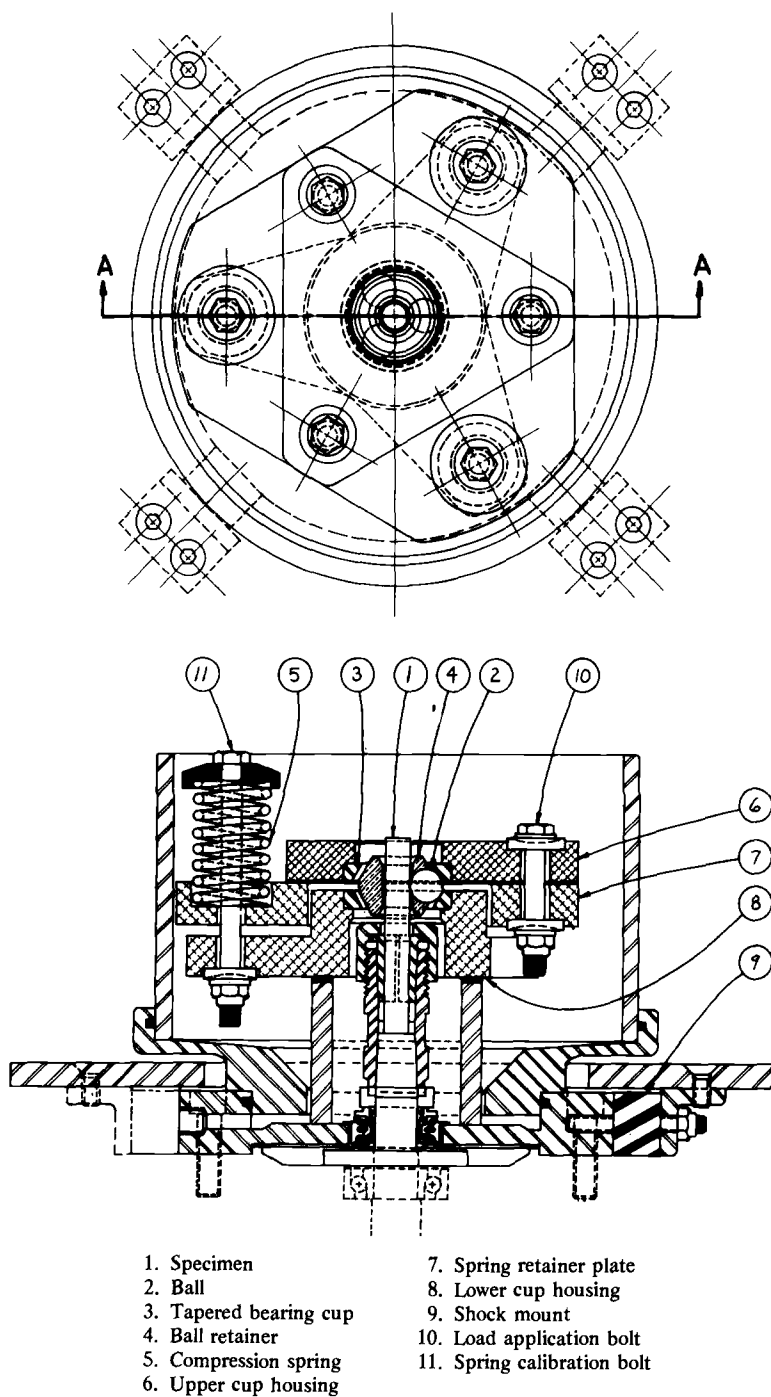10. Load application bolt
11. Spring calibration bolt

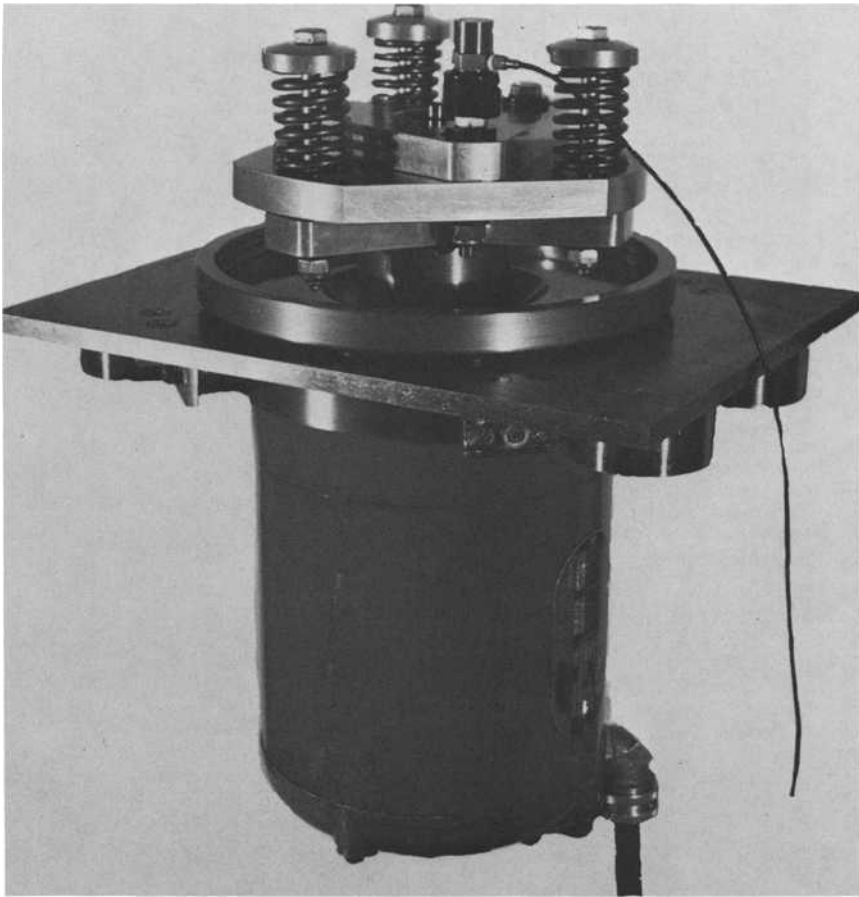FIG. 2—*Cross section of ball–rod RCF tester.*

FIG. 3—*Ball-rod RCF tester No. 6.*

rougher balls is apparently due to the reduction in the ratio of the oil film to the surface finish [4]. Roughening of the balls is accomplished by abrasive blasting in lots of 60 balls in a commercial rotating drum-type abrasive blaster. The abrasive medium, air pressure, and time are closely controlled to produce a repeatable and uniform surface finish.

After they are blasted, the balls are ultrasonically cleaned in a Freon solution to remove the imbedded abrasive.

Cups

The ball-rod RCF tester utilizes two standard bearing cups with a track angle of 25 deg. The large-end face of the cups is reground to provide clear-
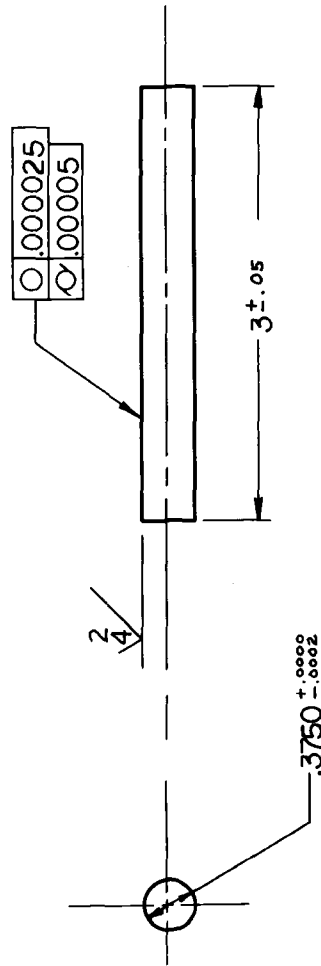
FIG. 4—*Ball-rod RCF test bench.*

FIG. 5—*Test specimen design. The measurements are in inches; 1 in. = 25.4 mm.*

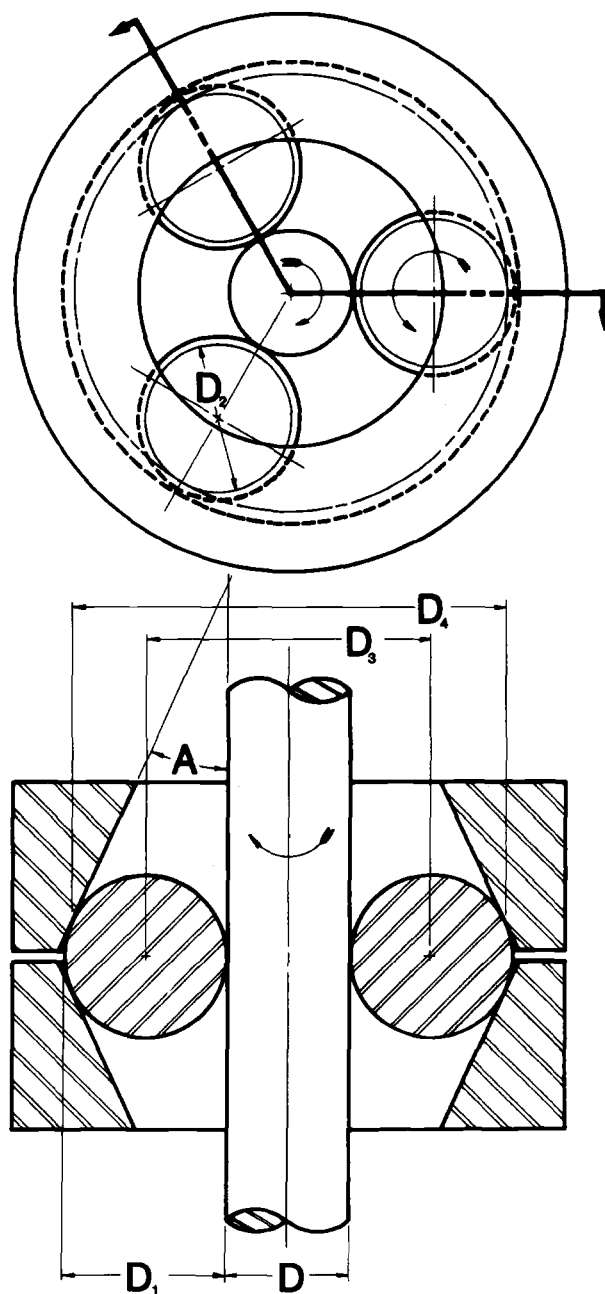FIG. 6—*Ball-rod RCF tester No. 5.*

FIG. 7—*Tester schematic for calculation of rotational speed.*

ance. Standard tapered bearing cups were selected over special angular contact ball bearing outer races because the simpler geometry of the tapered cups allows closer control of the test conditions, and the tapered cups provide economical replacement components.

Test Procedure

The four series of material evaluation tests described in the following sections were conducted to determine if specimen preparation, ball preparation, and tester conditions could be controlled sufficiently to produce consistent results between two ball-rod RCF testers. The tests were conducted with prototype testers identified as Testers 5 and 6. Both testers were built to the principles previously described but represent two stages of development. Although the test specimen, balls, and tapered cup geometry are identical, there is a considerable difference in the details of construction between the two testers, as seen in Figs. 3 and 6.

During the course of each test series an effort was made to test each specimen an equal number of times on each tester. The balls were replaced after each individual test on a specimen, or after each test suspension. This procedure ensured a uniform condition at the beginning of each test. The two tapered bearing cups were normally replaced after four tests.

The spring load calibration was checked before each test series was run. Lubrication was applied by drip feed at the rate of 10 drops per minute. Exxon's Terresic 100, an International Organization for Standardization (ISO) viscosity grade 100 mineral oil, was used in Test Series 1 and 2. A synthetic lubricant, Mil-L-23699, was used for Test Series 3 and 4. The vibration analyzer was set close to ambient vibration, so that a small fatigue crack or spall would cause a shutdown. The actual number of stress cycles to failure was calculated by multiplying the running time in minutes times the actual motor speed of 3 600 rpm times 2.389 (the number of stress cycles per revolution of the test bar, as derived in Fig. 7 and Table 2). An individual spring load of 253.65 N (57 lb) was used for the entire test series, which resulted in a ball load of 1083.98 N (243.6 lb). The calculated hertz stress for this load with AISI M-50 specimens was 5.52 GPa (786 000 psi). With the silicon nitride specimens, which have a higher modulus of elasticity, the calculated hertz stress for this load was 5.93 GPa (860 000 psi).

Test Materials

The bearing steel tests reported in this paper were performed using test specimens made from a single heat of M-50 steel produced by vacuum induction melting followed by vacuum arc remelting. All M-50 test specimens were given the following hardening heat treatment:

(*a*) preheat: 843 ± 8°C (1550 ± 15°F) for 20 to 30 min;

(*b*) high heat: 1110 ± 5.5°C (2030 ± 10°F) for 6 min at temperature;

(*c*) quench: 565.5 ± 11°C (1050 ± 20°F) in salt;

(*d*) air cool to room temperature; and

(*e*) temper three times for 2 h at 546 ± 5.5°C (1015 ± 10°F) with a −73.3°C (−100°F) deep freeze after the first temper.

For the ceramic material tests, NC132 hot-pressed silicon nitride, produced by Norton Co., was used. These test specimens were produced for a joint Federal–Mogul and Teledyne CAE program sponsored by the U.S. Navy.

Test Series Description

Each test series consisted of a minimum of eight individual tests run on each tester.

TABLE 2—*Calculations for component rotational speeds from Fig. 7.*

	English Units	ISO Units
D = specimen diameter	0.375 in.	0.952 cm
D_1 = ball diameter	0.500 in.	1.270 cm
A = cup angle	25.083 deg	25.083 deg
D_2 = ball contact diameter with cup	0.453 in.	1.151 cm
$\quad D_2 = D_1 \cos A$		
D_3 = pitch diameter of balls and retainer	0.875 in	2.223 cm
$\quad D_3 = D + D_1$		
D_4 = cup contact diameter with balls	1.328 in.	3.374 cm
$\quad D_4 = D_3 + D_2$		
E = ball revolutions for one revolution of retainer		
$\quad E = \dfrac{D_4}{D_2}$	2.932	2.932
F = shaft revolutions for one revolution of retainer		
$\quad F = 1 + \dfrac{ED_1}{D}$	4.909	4.909
H = number of stress cycles between ball and specimen for one revolution of retainer		
$\quad H = F - 1$	3.909	3.909
K = number of stress cycles between balls and specimen for one revolution of specimen		
$\quad K = \dfrac{3H}{F}$	2.389	2.389

Test Series 1

A total of six M-50 test specimens were evaluated. Eight individual tests were run on each specimen for a total of 48 tests for the series. For each specimen the eight tests were divided equally between Testers 5 and 6. The test balls used for Test Series 1 were prepared in three separate abrasive blast lots.

Test Series 2

Two M-50 specimens were included in this test series, with a total of eight individual tests run on each specimen. As in Series 1, the individual tests on each specimen were equally divided between testers. Before this test series was started, the spring load on both testers was removed and then reloaded and calibrated.

Test Series 3

This test series with M-50 specimens was conducted in the same manner as Series 2, except that lubricant was changed to Mil-L-23699.

Test Series 4

Test Series 4 evaluated the suitability of the ball–rod RCF tester for use in testing ceramic bearing material. Six specimens were utilized for this test series. Because of the time constraints for this evaluation it was not possible to run an equal number of tests on each bar or on each tester.

FIG. 8—*Typical fatigue spall in M-50.*

TABLE 3—*Summary*

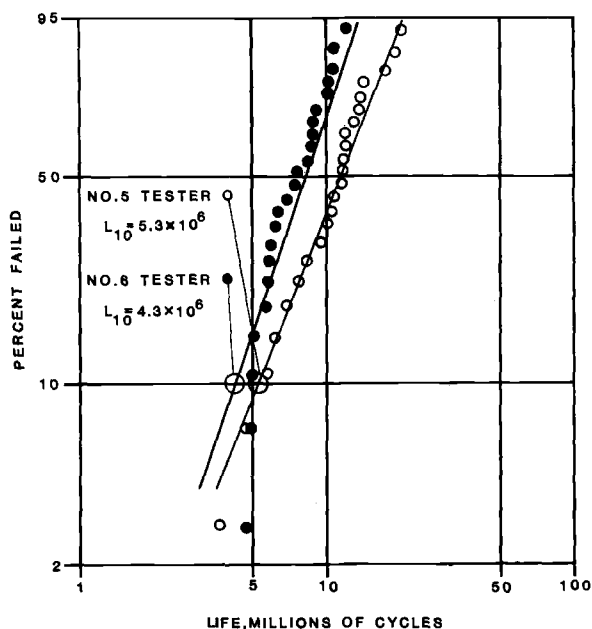| Test Series	Tester Number	Material	Lubrication	L_{10}, Million Cycles	L_{50}, Million Cycles	Slope	Correlation
1	5	M-50	Terresic 100	5.3	11.5	2.5	0.98
	6	M-50	Terresic 100	4.3	8.4	2.8	0.88
2	5	M-50	Terresic 100	5.0	9.2	3.3	0.99
	6	M-50	Terresic 100	5.1	9.6	3.1	0.95
3	5	M-50	MIL-L-23699	4.0	11.5	1.9	0.99
	6	M-50	MIL-L-23699	5.6	13.9	2.3	0.92
4	5	Si_3N_4	MIL-L-23699	27.7	59.53	2.5	0.94
	6	Si_3N_4	MIL-L-23699	31.8	62.0	3.2	0.93

FIG. 9—*Rolling contact fatigue results in M-50 steel with Terresic 100 oil.*

Test Results and Discussion

Tester Performance

During the four test series reported 101 individual tests were run, with only one incident of ball spalling. All other spalls were of classic subsurface origin on the wear track of the test specimen. With few exceptions, the three balls

of test results.

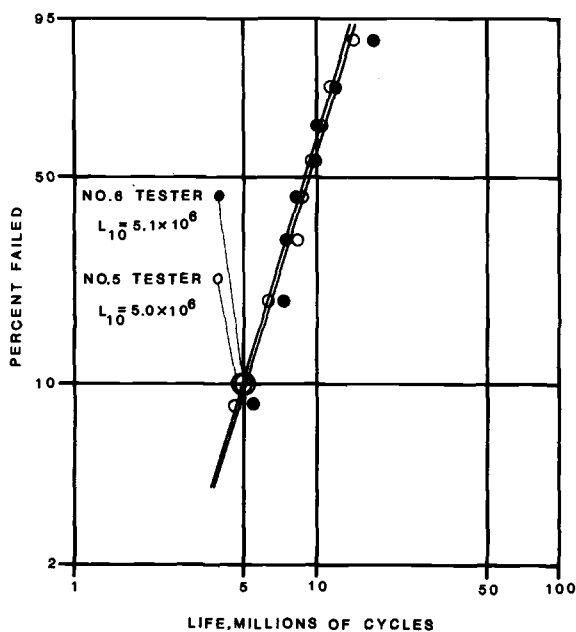| Number of Tests	L_{10} 90% Confidence Band, Million Cycles		L_{50}, 90% Confidence Band, Million Cycles	
	Low	High	Low	High
24	2.3	8.4	9.4	12.4
24	2.9	6.3	7.1	9.2
8	2.8	8.8	7.0	11.6
8	2.7	9.2	7.3	12.2
8	1.3	11.2	6.9	18.4
8	2.2	13.3	9.2	19.9
12	15.1	51.3	44.6	73.5
9	17.2	57.8	46.6	78.9

FIG. 10—*Rolling contact fatigue results in M-50 steel with Terresic 100 oil.*

rotated on a single axis throughout an individual test. Only a slight amount of wear was observed on the tapered bearing cups when they were replaced after every fourth test.

The shutdown sensitivity was sufficient to terminate the test when a fatigue crack formed across the width of the test track or when a small fatigue spall developed in the test track (Fig. 8). The spring load on both testers remained
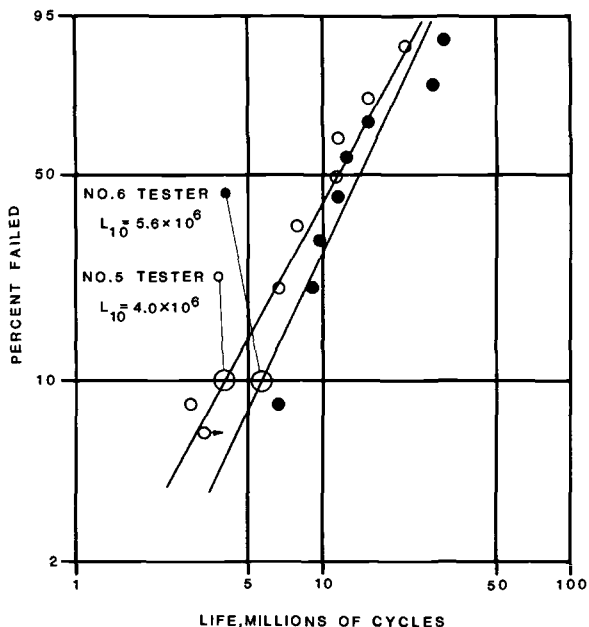
FIG. 11—*Rolling contact fatigue results in M-50 steel with MIL-L-23699 oil.*

constant throughout each of the four test series without the need for adjustment.

Test Results

The individual test lives of each test series were analyzed by Weibull statistics with the results tabulated in Table 3. Weibull plots of the test data are shown in Figs. 9 through 12.

In Test Series 2, 3, and 4, 10 and 50 percent (L_{10} and L_{50}) lives from Testers 5 and 6 were within each other's 90 percent confidence band. In Test Series 1 the results from Testers 5 and 6 were slightly outside of the other's L_{50} 90 percent confidence band.

For all the test series, the Weibull slopes ranged from 1.9 to 3.3, which is within the range experienced in full-scale bearing tests and other element tests of similar materials [5].

Spalls that developed in the silicon nitride ceramic specimens were similar in size to the M-50 spalls (Fig. 13). The exceptional fatigue life of the silicon nitride compared with that of the M-50 confirms the results reported using other types of testers [6].
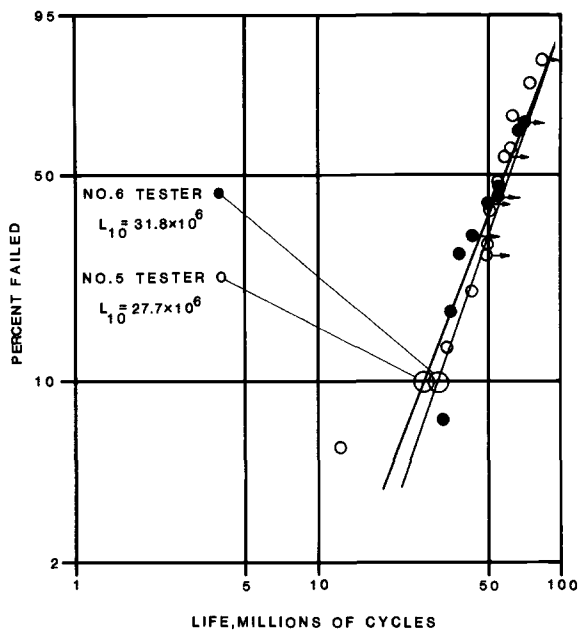
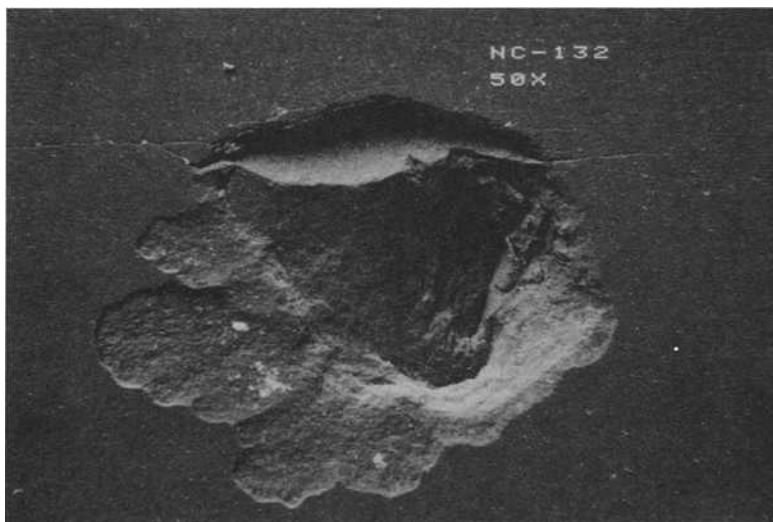FIG. 12—*Rolling contact fatigue results with silicon nitride.*

FIG. 13—*Typical fatigue spall with silicon nitride.*

Conclusions

Comparable test data were obtained from two ball–rod RCF testers utilizing the same design principles but made to different design details. One could expect even closer results from testers made to the same design detail.

The use of expendable low-cost bearing components in the ball–rod RCF tester substantially reduced the material evaluation costs in comparison with those of full-scale bearing tests and those of other element testers used by Federal–Mogul. In addition, it was determined that less operator skill was required to produce reliable results with the ball–rod RCF tester than with these other testers.

Acknowledgment

References

[1] General Electric Co. development, U.S. Patent No. 3,053,073.
[2] Sundberg, D. V., "Ceramic Roller Bearings for High Speed and High Temperature Applications," SAE Paper 740241, Society of Automotive Engineers, Feb. 1974.
[3] Adams, J. S. and Glover, D., "Hot Forged Powder Metal Rolling Bearing," SAE Paper 750856, Society of Automotive Engineers, Sept. 1975.
[4] Skurka, J., *Journal of Lubrication Technology*, Vol. 91, 1969, pp. 1–8.
[5] Coordinating Research Council, Inc., "Rolling Contact Fatigue Test Results for Various EHD Film Thickness Ratios from Selected Test Rigs," CRC Report No. 506, Coordinating Research Council, Inc., New York, April 1979.
[6] Baumbartner, H. R. and Cowley, P. E., "Silicon Nitride in Rolling Contact Bearings," Naval Air Systems Command, Washington, D.C., Contract N00019-74-C-0157, 15 March 1974 to 15 July 1975.

S. Ito,[1] *N. Tsushima,*[1] *and H. Muro*[1]

Accelerated Rolling Contact Fatigue Test by a Cylinder-to-Ball Rig

---

ABSTRACT: The cylinder-to-ball type of rolling contact fatigue rig is one of the most accelerated test rigs and is suitable for investigation of the influences of material and heat-treatment factors on rolling contact fatigue life. It has such merits as ease of manufacture, high precision, and easy replacement of the specimen and a high loading speed with high contact stress. The transition in the life levels of ball bearing steels and carburizing steels in relation to the year of production, beginning in 1964, is described. As examples of the test results, the influences of the fiber orientation and the forging ratio are described. The influence of the fiber orientation is great for ball bearing steel and not as great for carburizing steel. Bar forging greatly increases the rolling contact fatigue life whereas upset forging does not.

KEY WORDS: rolling contact fatigue, accelerated test rig, fiber orientation influence, forging ratio influence, bearing steels

Many factors influence the rolling contact fatigue life of rolling bearings. Factors concerning the bearing itself include the material used, the forging ratio, type of heat treatment used, and the bearing's dimensions, internal design, precision, surface roughness, and so forth. Factors concerning the running conditions include the loading conditions, rotating speed, errors in alignment, lubrication, and others.

Rolling contact fatigue is affected in such a complicated way by these many factors that it is desirable in the investigation of rolling contact fatigue strength to simplify the test so that these factors will interact as little as possible. Since the rolling fatigue life of high-hardness steel is greatly scattered, it is necessary to determine statistically the life value through a number of tests.

[1]Chief engineer, senior research scientist, and managing director, respectively, NTN Toyo Bearing Co. Ltd., Higashikata, (511) Kuwana, Japan.

125

Life testing is divided roughly into a test with a bearing and a test with a specimen. This paper describes an accelerated rolling contact fatigue test conducted with a cylinder-to-ball type of rig, which is the type used most frequently in our laboratory in tests using specimens (pivot, ring, cylinder, or disk).

Construction of the Rig

The appearance of the rig can be seen in Fig. 1, and the schematic construction of the essential part of the rig is shown in Fig. 2.

In this test rig a cylinder specimen is subjected to rolling contact against two balls. The load is given to the specimen through a driving roll, to which a lever is attached, thus magnifying the coil spring load. The specimen is supported by two balls, which are supported by three guide rolls, each of which has a groove. The driving roll drives the specimen, which is followed by the balls and the guide rolls. The load is applied to the specimen twice per revolution of the specimen. The contact track is shifted from the center of the specimen so that two life tests can be done by reversing the orientation of the specimen. Rolling contact of the specimen with the driving roll occurs at the end of the specimen and gives so little contact stress that it does not concern the rolling contact fatigue of the contact area between the specimen and the balls. When flaking occurs in the specimen or a ball, a sharp increase in the vibration level activates a switch to end the test.

The load and rotating speed of the rig are as follows:

Contact load between the specimen and a ball: $0.708 \, P_0$
Rotating speed of a 12-mm diameter cylinder specimen: $68/12 \, N$
   $= 5.667 \, N$
Rotating speed of a 19.05-mm (¾-in.) diameter ball: $68/19.05 \, N$
   $= 3.570 \, N$

where P_0 = total load and N = rotating speed of the driving roll.

When the rotating speed of the driving roll is 4 000 rpm, the rotating speed of the specimen is 22 677 rpm, and the loading speed is twice as fast, 45 334 cpm, which is the highest loading speed in our rolling contact fatigue life test rigs. The testing time for 1×10^7 loading cycles is about 220 min. Lubricant is supplied by splashing 56 turbine oil from the rotation of the lower guide roll, which is kept dipped in the oil.

The ease of manufacture, high precision, and easy replacement of the specimen, because of its simple shape, make this test the most suitable for investigating the influences of material and heat-treatment factors upon rolling contact fatigue life. A rolling contact fatigue test of balls can also be done, though this is not as efficient.

By changing the sizes of the balls and guide rolls, a rolling contact fatigue life of cylinders up to 38 mm in diameter can be tested.
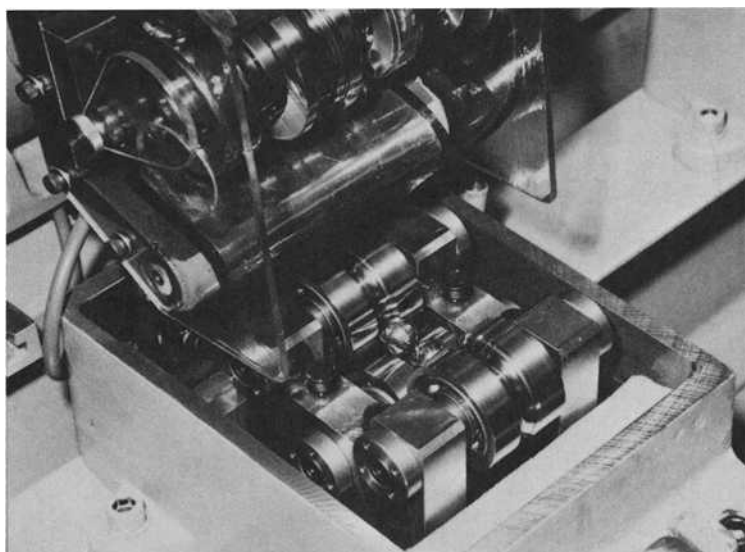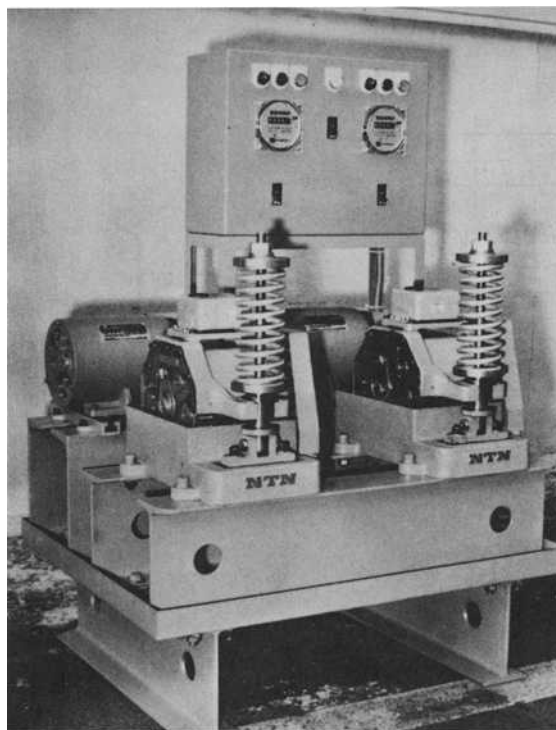
FIG. 1—(Top) *Cylinder-to-ball type of test rig:* (bottom) *inside the test rig.*
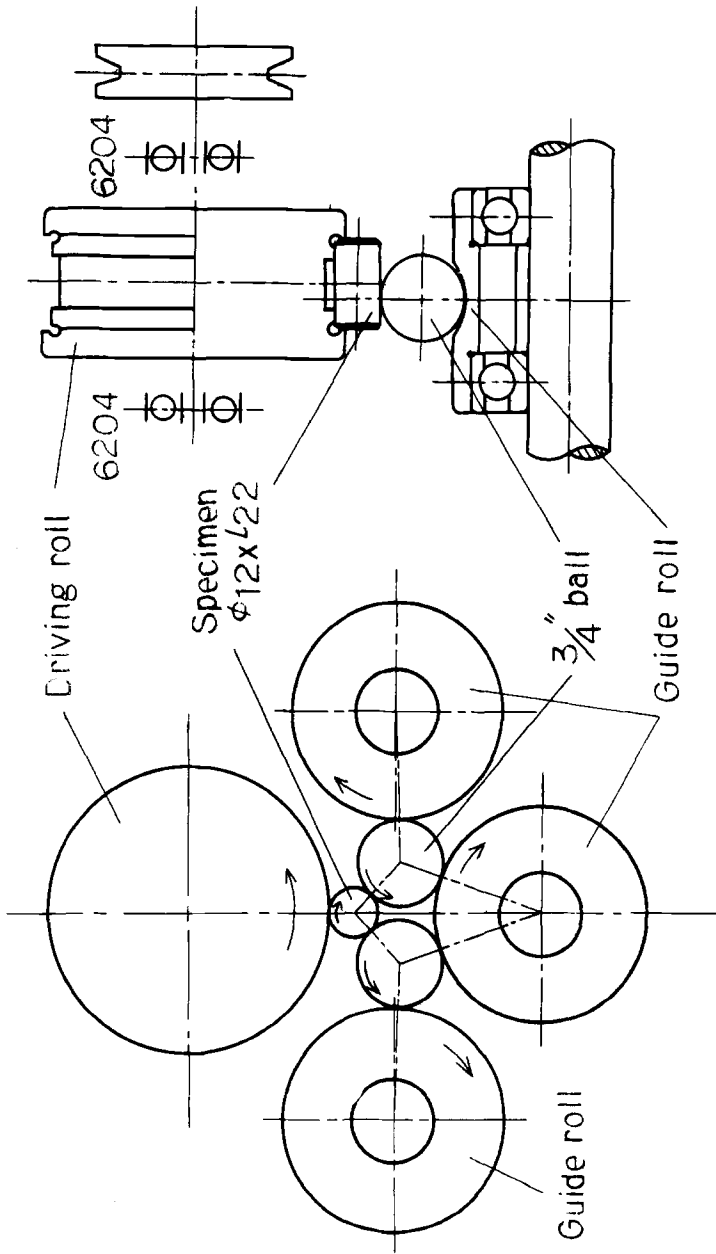
FIG. 2—Schematic drawing of the construction of the essential part of the rig illustrated in Fig. 1 (3/4 in. = 19.05 mm).

Test Conditions

The standard test conditions of this test rig are as follows:

Hertzian maximum contact stress: $P_{max} = 5\,880$ MPa (contact load 2548 N)
Loading speed: 46 240 cpm
Lubrication: 56 turbine splashing[2]
Number of specimens in one lot: 24
Life: total loading cycles till initiation of flaking on the raceway

Transition of Life Level

Every year since 1964, when this type of test rig was developed, the periodic life test of various bearing materials manufactured by various steel makers has been conducted to confirm the level of rolling contact fatigue life.

Specimens are machined from bars of the same size in the same process as that shown in Fig. 3, then heat treated and ground, and the outer surface is superfinished.

Figure 4 shows the changes in the L_{10} life of various test materials in relation to the year of manufacture. The life level increases gradually with the year of manufacture.

Figure 5 shows the Weibull distributions of lives of 14-lot and 22-lot
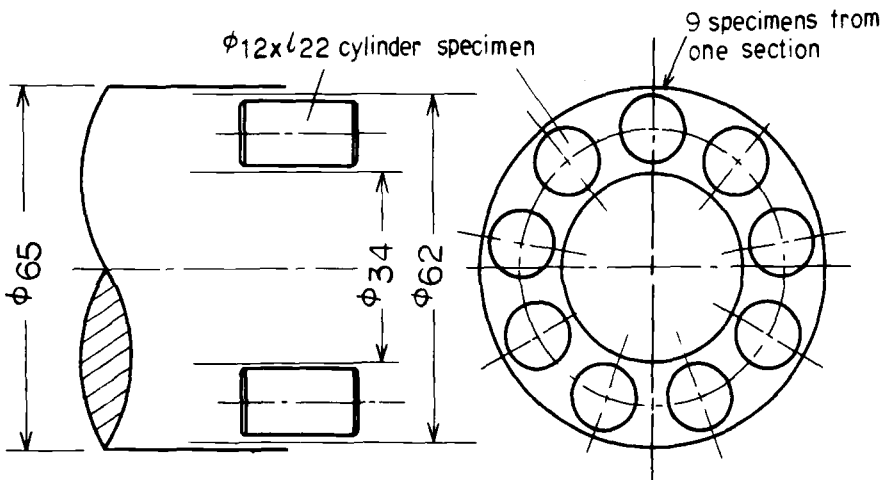
FIG. 3—*Specimens machined from a 65-mm diameter bar.*

[2]Fifty-six turbine oil is a mineral oil. The lubricant temperature during the test is 90°C. The viscosity at 90°C is 22 mPa·s and the pressure–viscosity coefficient at 90°C is 1.019×10^{-8} m·N.$^{-1}$
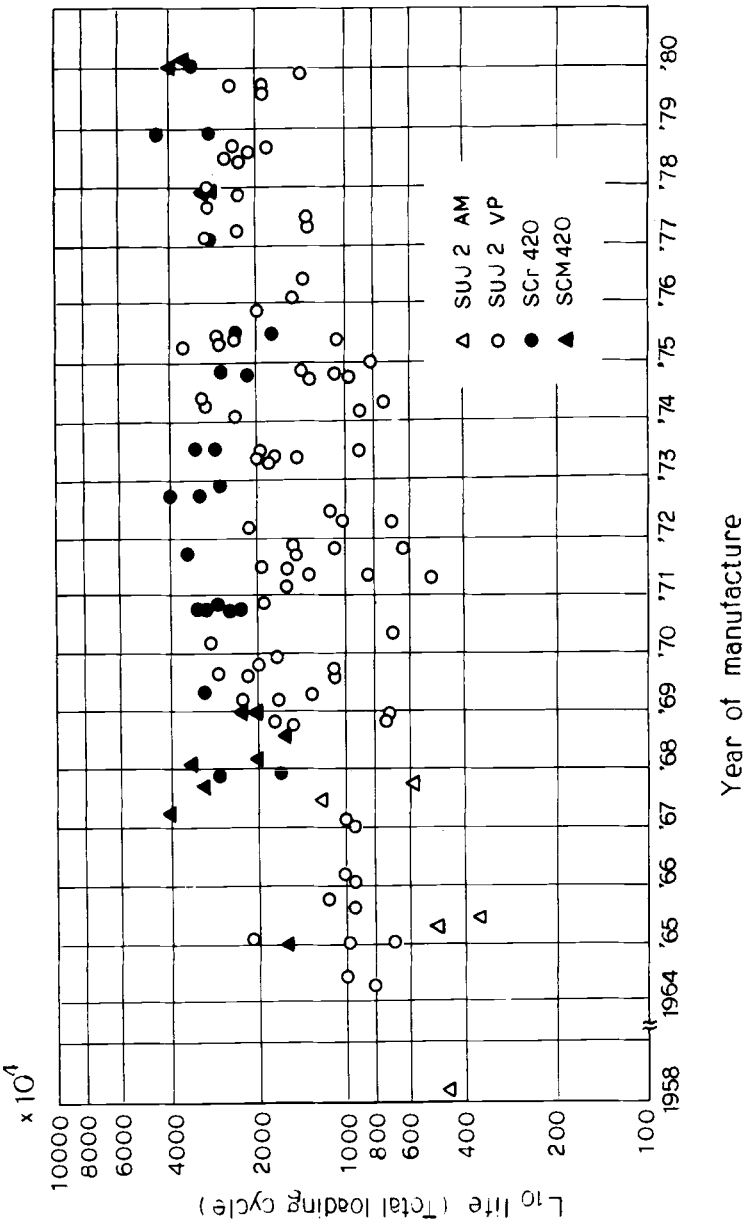
FIG. 4—*Improvement in the rolling contact fatigue life of ball bearing steel and carburizing steels in relation to the year of manufacture.*
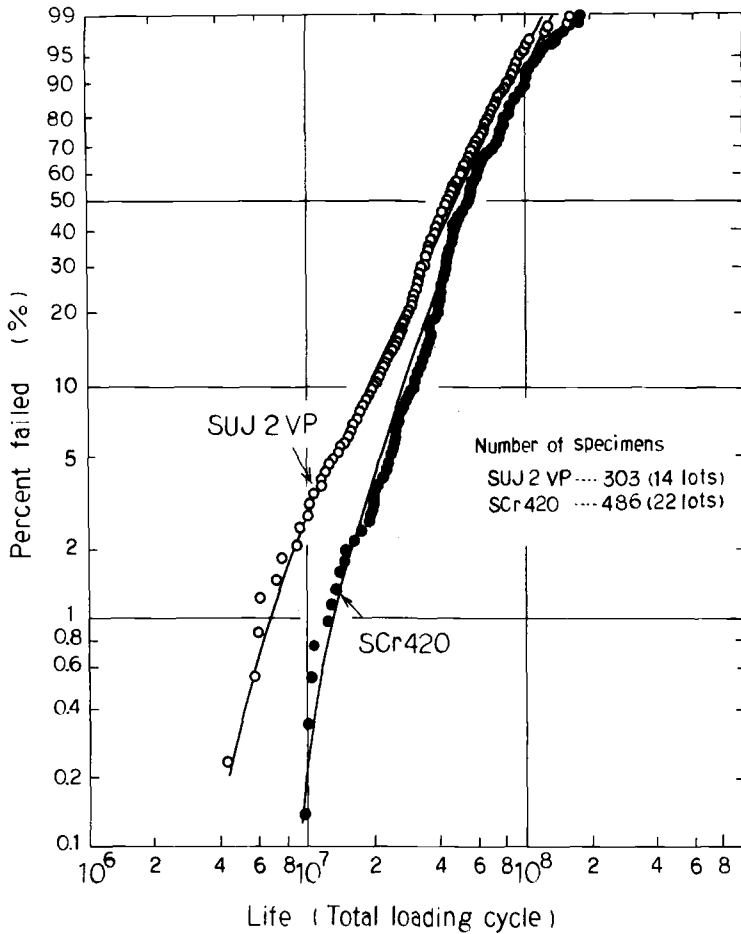
FIG. 5—*Weibull distribution of the lives of recent ball bearing steels and carburizing steels.*

specimens, respectively, of recent SUJ 2 (corresponding to AISI 52100) and carburized (SCr 420 in JIS) steels.[3] The scatter in life is relatively small for both materials; therefore, these are reliable materials in rolling contact fatigue life.

Correspondence to Full-Scale Size 6206 Ball Bearing Life Test

In order to accelerate the test, a 12-mm diameter specimen is subjected to a rolling contact fatigue test of high contact stress and high loading speed.

[3]SCr 420: 0.18 to 0.23 percent carbon, 0.15 to 0.35 percent silicon, 0.60 to 0.85 percent manganese, 0.90 to 1.20 percent chromium. SCM 420: 0.18 to 0.23 percent carbon, 0.15 to 0.35 percent silicon, 0.60 to 0.85 percent manganese, 0.90 to 1.20 percent chromium, 0.15 to 0.30 percent molybdenum.

Such a severe test condition produces severe microstructural changes and changes in microhardness and in the residual stress under the contact surface during the test [1].[4] It is feared that these changes affect rolling contact fatigue life in a way different from the conventional bearing life test. However, good correspondence between a 12-mm diameter cylinder specimen accelerated test and a size 6206 bearing life test has been confirmed as follows: a size 6206 ball bearing and 12-mm diameter cylinder specimen, both being made of the same charge material, were subjected to the respective life tests, and the results for various charge materials are shown in Fig. 6. The test conditions for the size 6206 bearing life test are a radial load of 6860 N ($C/P \cong 2.2$), an inner ring rotating speed of 2000 rpm, a splashing supply of 56 turbine oil, and 20 specimens. The rolling contact fatigue life obtained by the accelerated test with the specimen corresponds well with the size 6206 ball bearing life. Good correspondence between the 12-mm diameter specimen accelerated test and the 6206 ball bearing life test was also confirmed in research in which the variation in the rolling contact fatigue life with the hardness or the amount of retained austenite is similar in the acceleration test and the 6206 bearing test.

Life testing using a bearing requires a long testing time. For the 6206 ball bearing test, the average life of SUJ 2 VP steel is about 1000 h. For the 12-mm diameter specimen test, the average life of SUJ 2 VP material is about
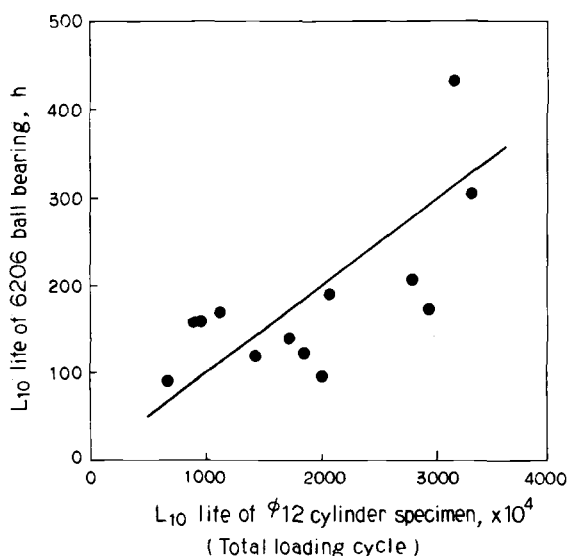
FIG. 6—*Relationship between L_{10} lives of a 12-mm diameter specimen and a size 6206 ball bearing made of the same charge SUJ 2 for each plot.*

[4]The italic numbers in brackets refer to the list of references appended to this paper.

5000×10^4 loading cycles, which corresponds to 18 h. Therefore about 50 times more life tests can be carried out in the accelerated test than in the 6206 bearing life test. The test rig shown in Fig. 1 requires about half a month for the life testing of 24 specimens in one lot.

Influence of Various Factors upon Rolling Contact Fatigue Life

The influences of oxygen content (nonmetallic inclusion rating), hardness, and retained austenite [2] upon rolling contact fatigue life have been reported but are not described in this paper.

Influence of Fiber Orientation—Specimens of 12-mm diameter cylinders with various fiber orientations were machined from a 65-mm diameter bar, as shown in Fig. 7. Ratios of L_{10} lives are shown in Fig. 7, where the ratio is 1.0 for the specimen with fiber orientation parallel to the axis ($\alpha = 0$ deg).

For SUJ 2 steel, the L_{10} life decreases to 60 percent at $\alpha = 30$ deg and to 17 percent at $\alpha = 90$ deg, which suggests that the influence of fiber orientation on the rolling contact fatigue life is great. The influence of fiber orientation for carburizing steel SCr 420 is smaller than that for SUJ 2. This may be due to the compressive residual stress or to the large amount of retained austenite.

FIG. 7—*Influence of the fiber flow angle on rolling contact fatigue life.*

FIG. 8—*Forging methods for the specimens in Table 1.*

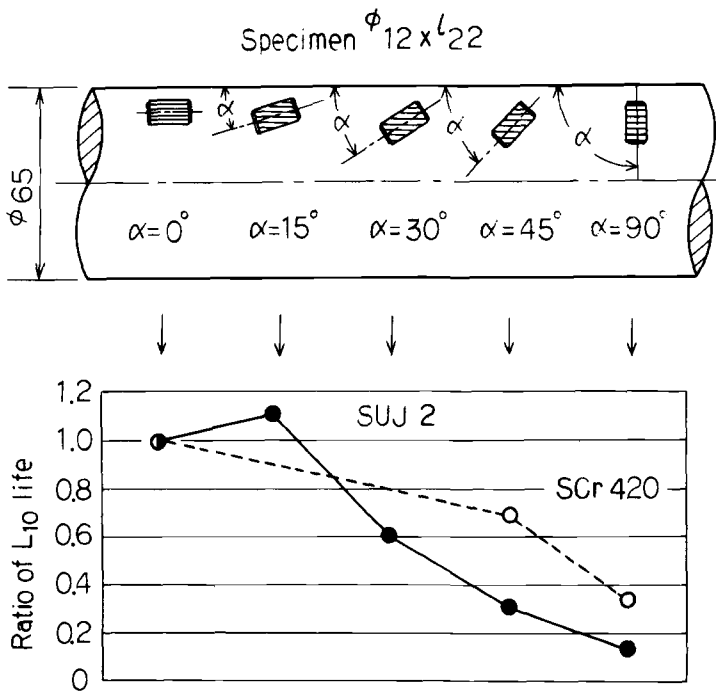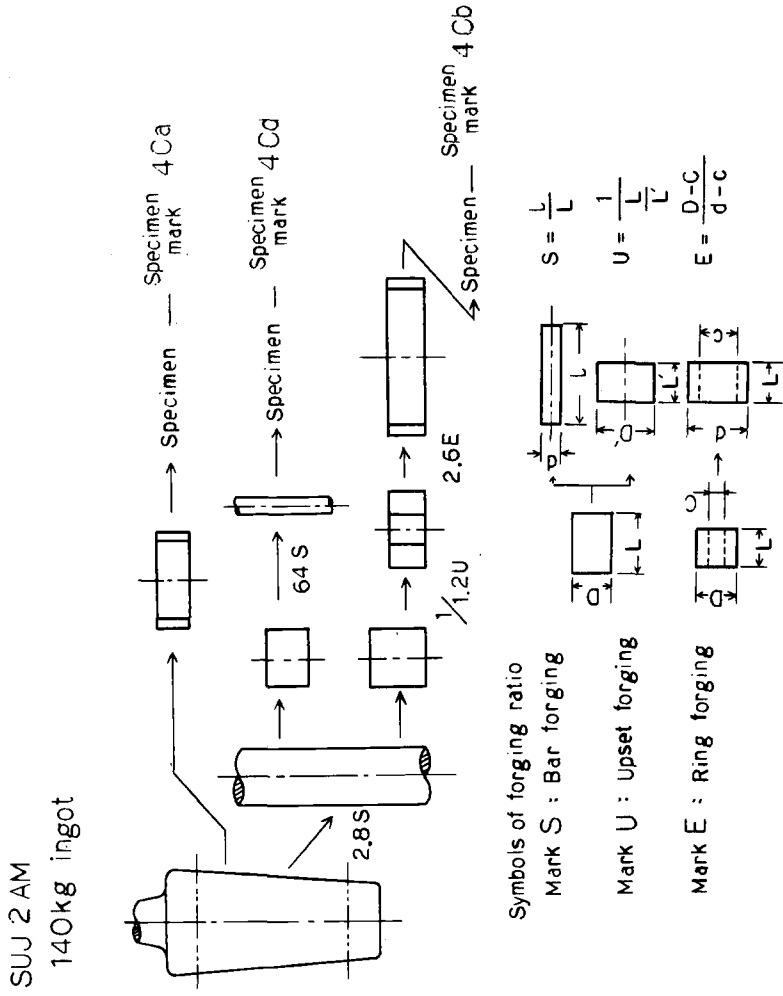TABLE 1—*Influence of various forging methods upon rolling contact fatigue life.*

Specimen Mark	Number of Specimens	L_{10} Life $\times 10^4$	L_{50} Life $\times 10^4$	Life Ratio	
				L_{10} Life	L_{50} Life
4Ca	24	37	106	0.040	0.041
4Cd	24	920	2600	1.0	1.0
4Cb	24	85	320	0.093	0.123

Influence of Forging—Bearing materials are usually rolled (forged) from ingot to bar, and then forged or machined, or both, to a bearing preform before they are heat treated. The influence of the forging method and forging ratio upon the rolling contact fatigue life was examined.

Figure 8 shows the method of forging used and the forging ratio, and Table 1 shows the results of the life test. Bar forging increases the rolling contact fatigue life greatly while upset forging followed by ring forging does not increase the rolling contact fatigue life. This may be due to the great influence of fiber orientation—namely, the orientation of nonmetallic inclusions—upon the rolling contact fatigue life.

Concluding Remarks

Life tests with the cylinder-to-ball rolling contact fatigue rig give results similar to the size 6206 ball bearing life test, therefore, they are very effective as accelerated tests.

The cylinder-to-ball test rig has many merits: the specimen is easy to manufacture and has high precision because of its simple shape; the ease of replacement of the specimen and high loading speed produce test results in a very short period of time. Therefore, this rig is the most suitable for the investigation of the influence of material and heat-treatment factors on rolling contact fatigue life.

At present, this type of rig is used in many companies in Japan, including Honda Motor Co., Ltd.; Nissan Motor Co., Ltd.; Yamaha Motor Co., Ltd.; Daido Steel Co., Ltd.; Sanyo Special Steel Co., Ltd.; Nippon Steel Corp.; Sumitomo Metal Industries, Ltd.; Kobe Steel, Ltd.; Kawasaki Steel Co., Ltd; and Nippon Koshuha Steel Co., Ltd.

It would be a great benefit to have a common test rig for rolling contact fatigue testing and would help in the improvement, new development, and increased reliability of bearing materials.

References

[1] Muro, H. and Tsushima, N., *Wear*, Vol. 15, 1970, p. 309.
[2] Muro, H., Sadaoka, Y., Ito, S., and Tsushima, N., *Proceedings of the 12th Japan Congress on Materials Research—Metallic Materials*, Kyoto, Japan, March 1969, p. 74.

I. Sugiura,[1] S. Ito,[1] N. Tsushima,[1] and H. Muro[1]

Investigation of Optimum Crowning in a Line Contact Cylinder-to-Cylinder Rolling Contact Fatigue Test Rig

ABSTRACT: The cylinder-to-cylinder rolling contact fatigue rig is a line contact type of accelerated test rig. As an example of the test results from this rig, an investigation of the influence of the full crowning value on the rolling contact fatigue life is described. In the contact stress distribution along the axis of the line contact, the contact stress at the crowning edge, P_{edge}, has a 1.4 times larger influence on the rolling contact fatigue life than the maximum contact stress, P_{max}, at the center of the contact area; the rolling fatigue life is therefore determined by P_{max} or 1.4 P_{edge}, whichever is larger. This result can also be interpreted by the contact stress at the edge, Q_{max}, calculated by Moyer's method. Then the rolling fatigue life is determined by P_{max} or Q_{max}, whichever is larger. The optimum crowning value is the value which gives $P_{max} = 1.4\,P_{edge}$ or $P_{max} = Q_{max}$.

KEY WORDS: rolling contact fatigue, line contact, crowning value, edge loading, bearing steels

Research on rolling contact fatigue has generally been conducted by point contact test rigs using ball bearings or disk-to-ball or cylinder-to-ball specimens; accelerated tests with line contact test rigs are very rare. This is because line contact requires a large test load for flaking to occur. For example, a cylindrical bearing requires twice as large a bearing load for the same rating life as a ball bearing of the same size. Application of a large load to the bearing results in problems, such as bending or fracture of the shaft or edge

---

[1]Research engineer, chief engineer, senior research scientist, and managing director, respectively, NTN Toyo Bearing Co. Ltd., Higashikata, (511) Kuwana, Japan.

loading between rolling contact elements, which complicate the test results and make the evaluation of these results difficult.

However, it is to much to say that point contact rolling fatigue tests are always comparable to line contact rolling fatigue tests for all factors influencing rolling fatigue. Moreover, there are some factors characteristic of line contact, for example, the influence of edge loading. These factors must be examined in a line contact rolling fatigue test.

The line contact rolling fatigue test rig described in this paper uses a 12-mm diameter specimen of simple shape which was rolling contact with a 20-mm diameter cylinder accurately guided to avoid inclined loading. In an accelerated test, the rig adopts a high loading speed (20 400 cpm) which permits a short testing time (about 8 h for 10^7 loading cycles). Specimens fail under relatively small contact stress (hertzian maximum contact stress, P_{max}, less than 4 410 MPa), possibly because of the wide contact track. Thus the formation of residual compressive stress and the microstructural change are slight, and since the influences of such material changes are insignificant, it is thought that a good correspondence between the test results and the life of the bearings actually used can be obtained. The test results obtained by this test rig in an investigation for the optimum crowning of rollers are described here.

Construction of the Rig

The rig is illustrated in Fig. 1, and the schematic construction of the essential part of the rig is shown in Fig. 2.

In this test rig, the cylinder specimen, with a 12-mm diameter and 12-mm length, rolls against two cylinders with 20-mm diameter and 20-mm length. The driving roll drives two 20-mm diameter cylinders, which rotate the 12-mm diameter specimen. The 12-mm diameter specimen is supported by the supporting roll, and the 20-mm diameter cylinders are supported by the upper or the lower rolls. The load is applied to the specimen through the upper roll, to which a lever is attached, thus magnifying the coil spring load. The 12-mm diameter specimen is subjected to high-stress rolling contact with 20-mm diameter cylinders twice per rotation of the specimen, and rolling contact between the 12-mm diameter specimen and the supporting roll involves so little contact stress that the rolling fatigue between them is negligible. When flaking occurs in the specimen or the 20-mm diameter cylinder, a sharp increase in the vibration level activates a switch to end the test.

Specimens

Five kinds of full crowning, namely, $R = 300, 480, 890, 1200$ mm, and ∞ (straight), as shown in Fig. 2b, were given to the 12-mm diameter specimens made of SUJ 2 steel (corresponding to AISI 52100) with hardnesses of 62.0 to 62.5 HRC. The 20-mm diameter specimen is a straight cylinder. The 12-mm
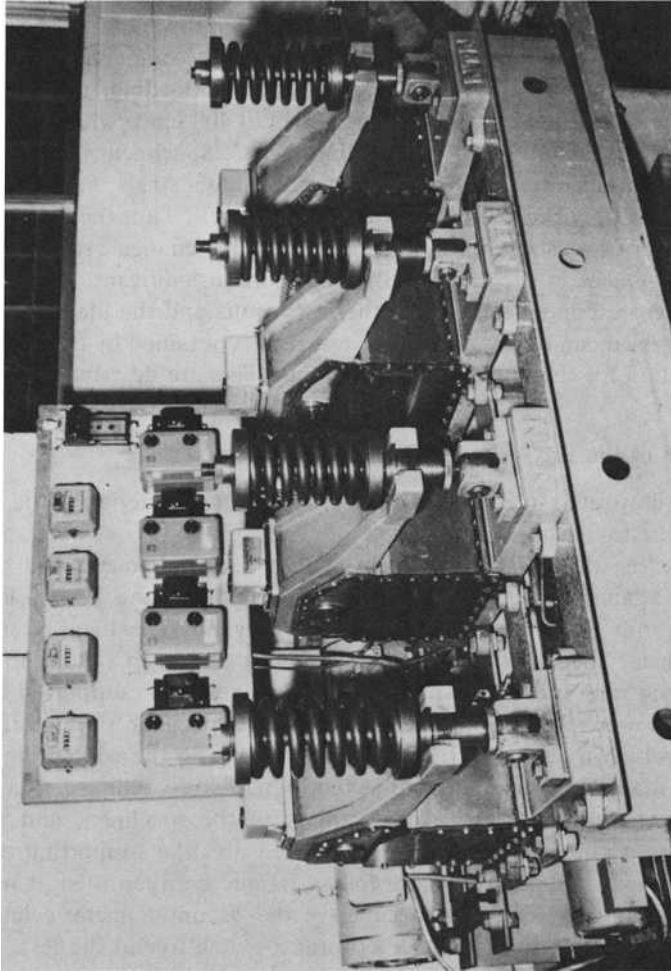
FIG. 1—A cylinder-to-cylinder type of test rig.
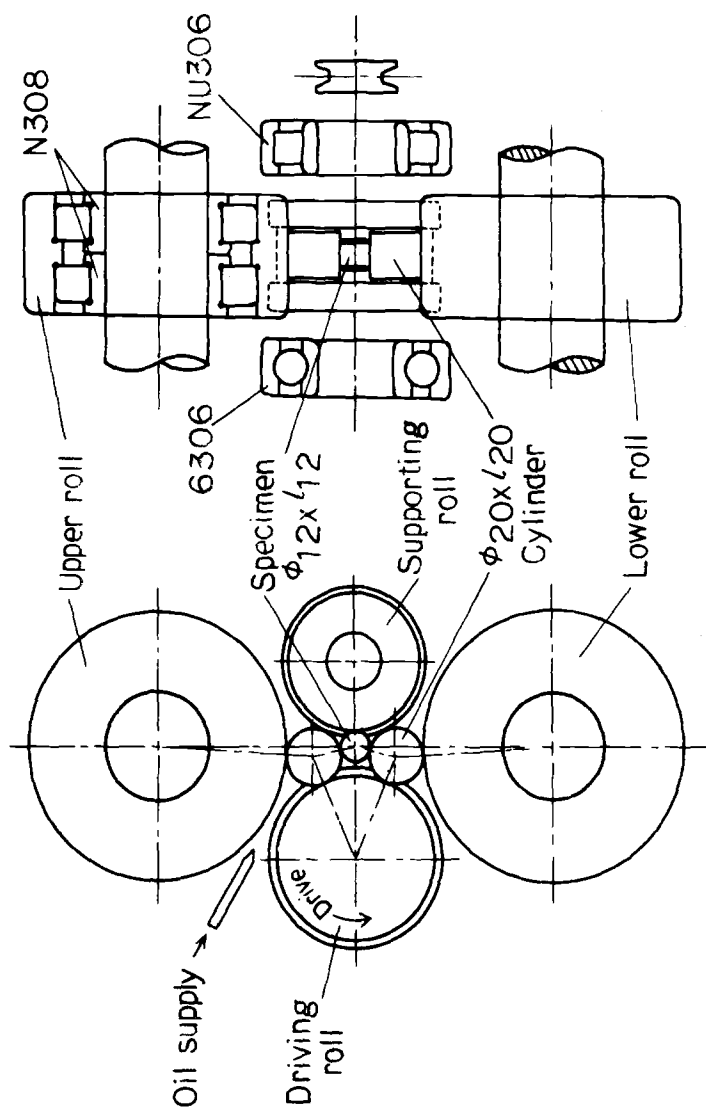
FIG. 2(a)—Schematic construction of the essential part of the test rig.
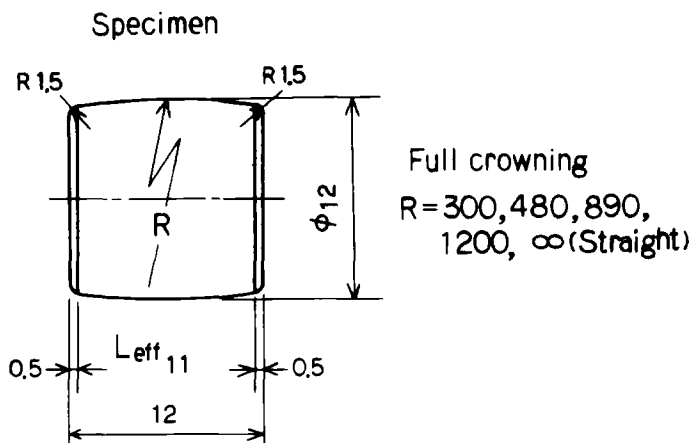
Specimen

FIG. 2(b)—*A 12-mm diameter by 12-mm long specimen and full crowning value.*

diameter specimens and the 20-mm diameter cylinders were superfinished to a surface roughness of a 0.04-μm center line average.

Test Conditions

The test conditions were as follows:

Load: 13.72 and 17.36 kN for $R = 480$, 11.76 kN for $R = 890$, 9.8 kN for $R = 1\ 200$
Loading speed: 20 400 cpm
Lubrication: 56 turbine oil[2] circulation
Life: total loading cycles till initiation of flaking on the raceway

Results

Results of rolling contact fatigue tests using specimens with five kinds of full crowning values under the loads of 13.72 kN and 9.8 to 17.36 kN are shown in Fig. 3a and b on Weibull papers, and the external appearances of flaking and the position of flaking in these specimens are shown in Fig. 4. The L_{10} and L_{50} lives obtained from Fig. 3 and the ratio of the number of specimens failed at the edge to the total number of specimens is shown in Table 1.

For the same test load of 13.72 kN, the L_{10} life is highest for the specimen with the full crowning value of $R = 480$ mm and lowest for the specimen with

[2]Fifty-six turbine oil is a mineral oil. The lubricant temperature during testing is 70°C. The viscosity at 70°C is 35 mPa·s, and the pressure–viscosity coefficient at 70°C is 1.183 $\times$ 10^{-8}m·N^{-1}.
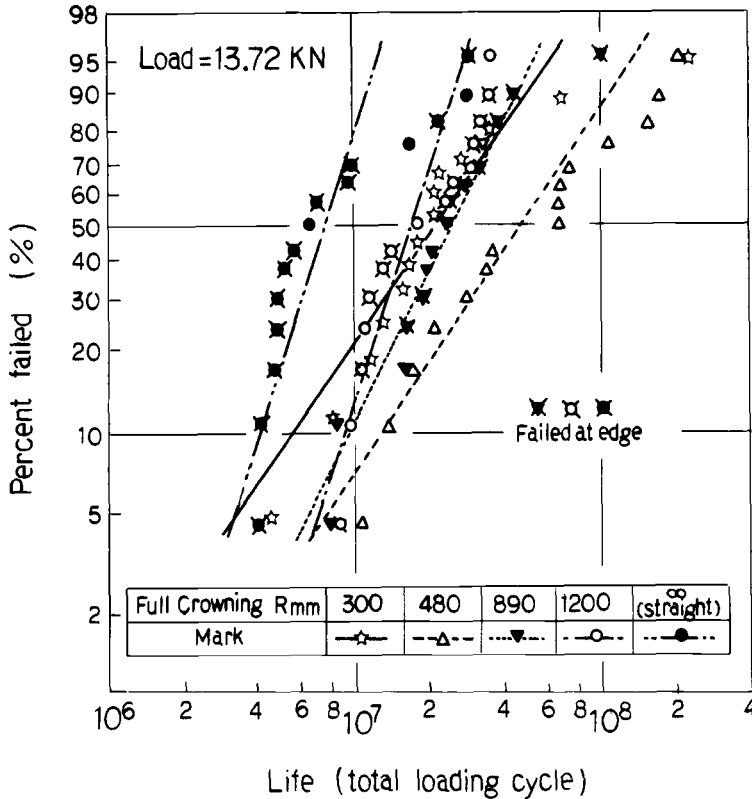
FIG. 3(a)—*Results of rolling fatigue tests under the same load of 13.72 kN.*

the straight cylinder ($R = \infty$). The number of specimens which failed at the edge increases with increasing R values.

Discussion

According to Palmgren, the index in the life formula, $L = (C/P)^p$, is $p = 3$ for point contact and $p = 10/3$ for line contact. Therefore, the relationship between rolling contact fatigue life and maximum contact stress, P_{max}, is expressed as $L \propto (1/P_{max})^p$, in which $p = 9$ for point contact and $p = 20/3$ for line contact are generally used.

In line contact, however, edge loading must sometimes be predominant in order for flaking to occur, which results in a short contact fatigue life. The objective of this paper is to assess the influence of edge contact stress on rolling contact fatigue.
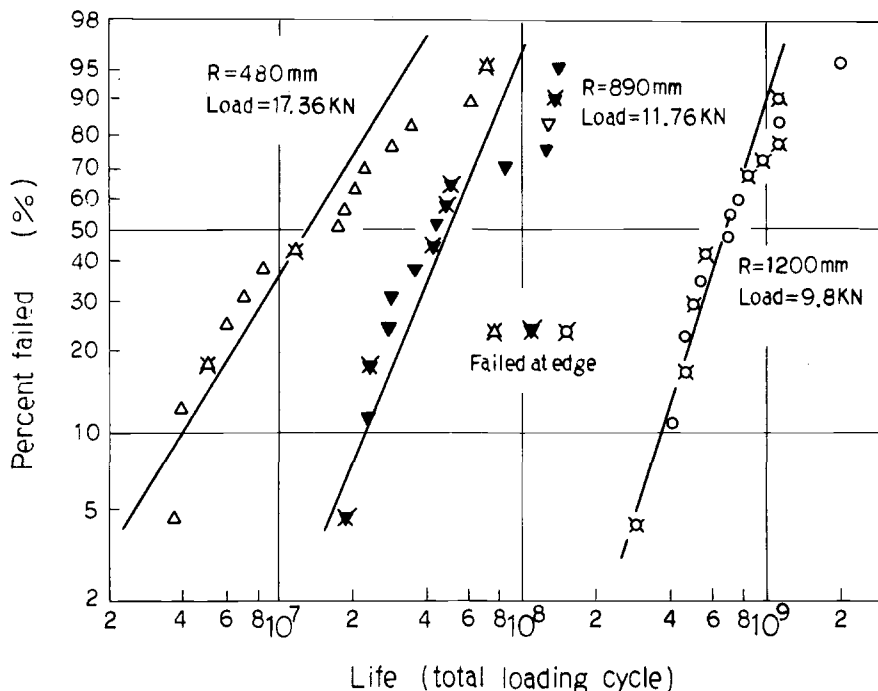
FIG. 3(b)—*Results of rolling fatigue tests using specimens with three kinds of full crowning values under the respective loads.*

Contact stress over the contact surface is calculated by Harris's method [1].[3] The calculations for the present specimens are shown in Fig. 5, and the contact stress at the center of the contact surface, P_{max}, and at the edge of the contact surface, P_{edge}, are added in Table 1.

For the specimens with full crowning, $R = 890$ mm and $R = 1200$ mm, tested under 13.72 and 9.8 kN, respectively, the ratio of the number of specimens flaked at the edge to the total number of specimens is about 0.5; the influence of P_{max} and P_{edge} on rolling contact fatigue is considered to be the same under these test conditions. In this case, $P_{max}:P_{edge} = 3920:2764 = 1.42:1$, or $P_{max}:P_{edge} = 3322:2332 = 1.42:1$. Therefore, the edge contact stress, P_{edge}, has a 1.42 times greater influence on rolling contact fatigue than P_{max} calculated by Harris's method.

For further detail, specimens in each lot were divided into two groups, one flaked at the edge and the other flaked at places other than the edge, and the rolling contact fatigue life of each group was obtained from each Weibull plot. The relationships between the L_{10} lives and P_{edge} for the groups flaked

---

[3]The italic numbers in brackets refer to the list of references appended to this paper.
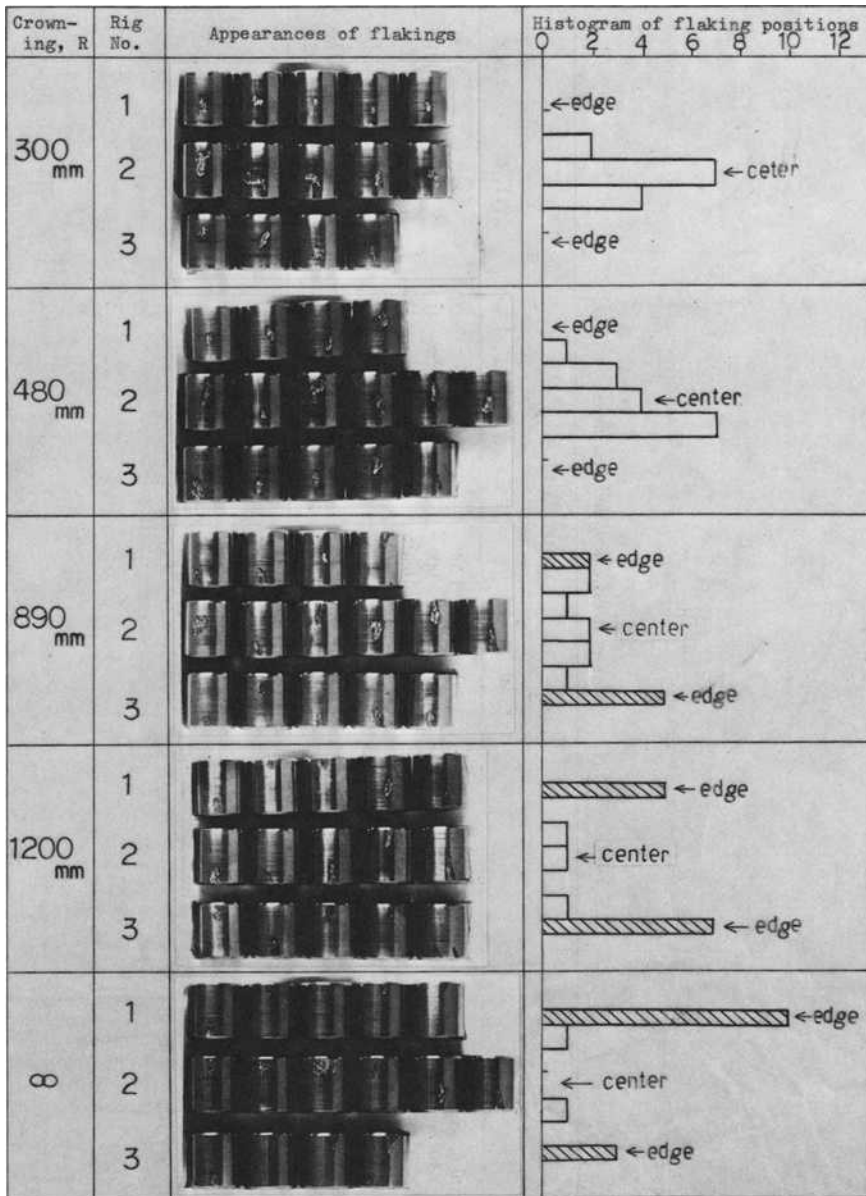
FIG. 4—*Appearance and positions of flakings from rolling contact fatigue tests.*

TABLE 1—*Test results and contact stress calculated by Harris's method.*

	Contact Load, kN							
	13.72					17.36	11.76	9.8
Full crowning, R, mm	300	480	890	1200	∞	480	890	1200
L_{10} life ($\times 10^4$)	560	1240	930	900	400	410	2200	4010
L_{50} life ($\times 10^4$)	2160	4640	2360	1640	745	1330	5100	7250
Ratio, failed at edge to total	0/14	0/15	7/15	12/15	13/15	3/15	6/15	8/15
P_{max}, MPa	4547	4204	3920	3832	3548	4616	3685	3322
P_{edge}, MPa	0	1862	2764	2989	3548	3568	2430	2332
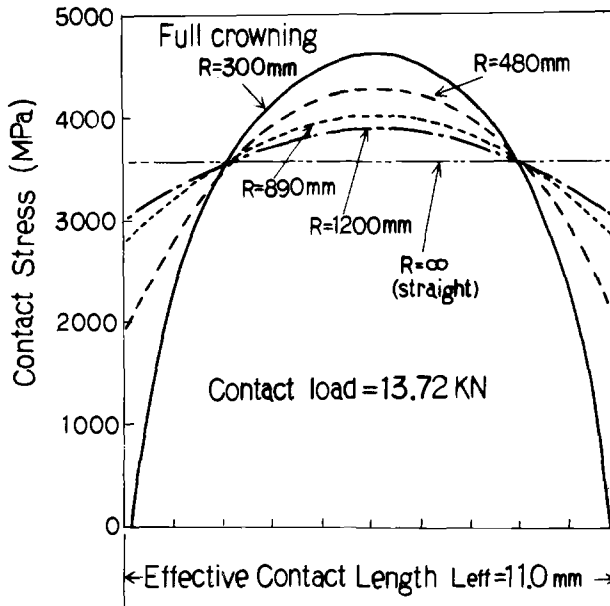
FIG. 5—*Contact stress distribution along the axis of the specimen calculated by Harris's method.*

at the edge and between the L_{10} lives and P_{max} for the groups flaked at other parts are plotted in Fig. 6. The relationships of the L_{10} to the P_{edge} and the L_{10} to the P_{max} are parallel, having the same index of $P = 7.0$ in $L \propto (1/P_{max})^P$, which is nearly the same as 20/3 for the line contact mentioned previously. Figure 6 suggests that the P_{edge} has 1.4 times more severe an influence on the rolling fatigue life than the P_{max} over the range of contact stresses. The rolling fatigue life is considered to be determined by P_{max} or 1.4 times the P_{edge}, whichever is larger.

Moyer [2] has proposed a calculation of edge contact stress. Figure 7 shows an example of an edge contact stress calculation by Moyer's method at the contact load of 13.72 kN and at other loads for various crowning values. On the assumption that rolling contact fatigue life is determined by the contact stress, P_{max}, at the center of the contact surface or the edge contact stress, Q_{max}, by Moyer's method, the L_{10} lives have been plotted in Fig. 8 in relation to the P_{max} or Q_{max}, whichever is larger, for all lots of test conditions. Life is related to the contact stress by the formula $L \propto (1/P_{max}$ or $1/Q_{max})^P$, where P is 6.7 or nearly equal to 20/3 obtained empirically. Therefore, Moyer's calculation is considered to be valid. The optimum crowning value is the one which makes $P_{max} = Q_{max}$ for a given contact load.

Since life is related to P_{max} or Q_{max} by the formula $L \propto (1/P_{max}$ or $1/Q_{max})^{20/3}$, the life ratio of the specimens failed at the edge to the specimens

Contact stress calculated by Harris' method
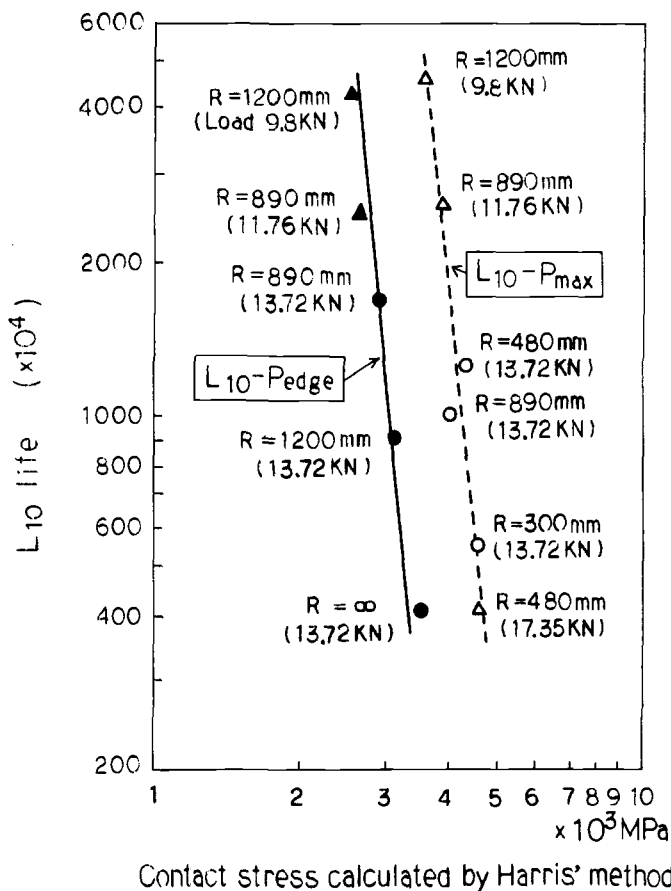
FIG 6—*Relationship between the L_{10} lives and P_{max} or P_{edge} calculated by Harris's method.*

failed at parts other than the edge is given by $1/(P_{max}/Q_{max})^{20/3}$. If we assume that the probability of flaking occurring at the edge is determined by $(Q_{max}/P_{max})^{20/3}$, the probability a is as follows

$$a/(1 - a) = (Q_{max}/P_{max})^{20/3}$$

$$a = \frac{(Q_{max}/P_{max})^{20/3}}{1 + (Q_{max}/P_{max})^{20/3}} \tag{1}$$

The probability of failure occurring at the edge was calculated by Eq 1 and given in Table 2 and are plotted in Fig. 9. Figure 9 shows that the probability of failure occurring at the edge under each test condition falls near the calculation curve.
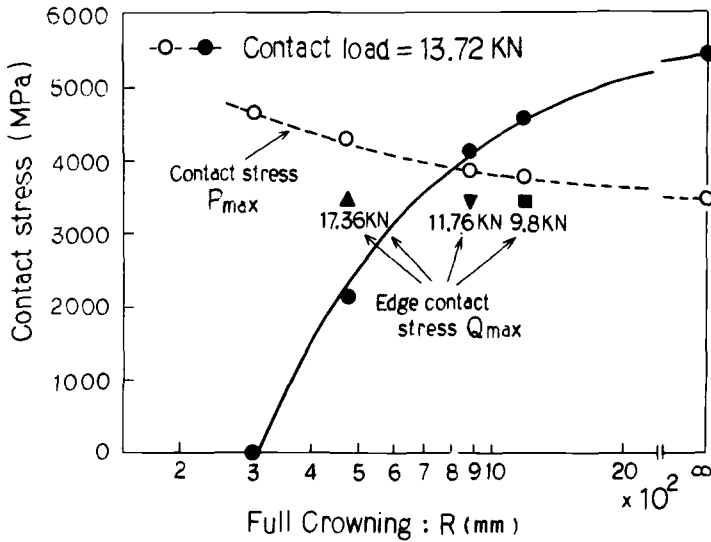
FIG. 7—*The edge contact stress, Q_{max}, calculated by Moyer's method and P_{max} in relation to the full crowning value.*
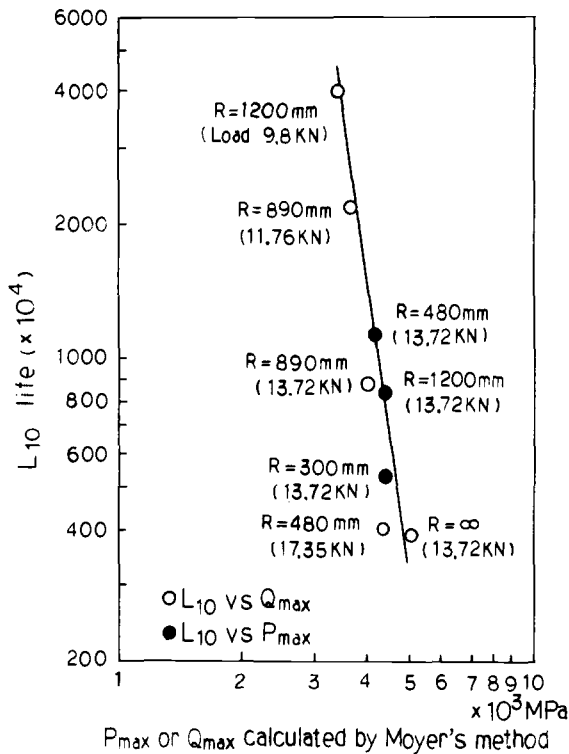
FIG. 8—*Relationship between the L_{10} lives and P_{max} or Q_{max}, whichever is larger.*

TABLE 2—*Calculation of the probability of failure from the edge.*

	Q_{max}/P_{max}											
	0.4	0.5	0.6	0.7	0.8	0.9	1.0	1.1	1.2	1.3	1.4	1.5
Life ratio, $1/(P_{edge}/P_{max})^{20/3}$	449.71	101.59	30.13	10.78	4.43	2.02	1.0	0.530	0.297	0.174	0.106	0.067
Probability	0.22	0.97	3.2	8.5	18.4	33.1	50.0	65.4	77.1	85.2	90.4	93.7
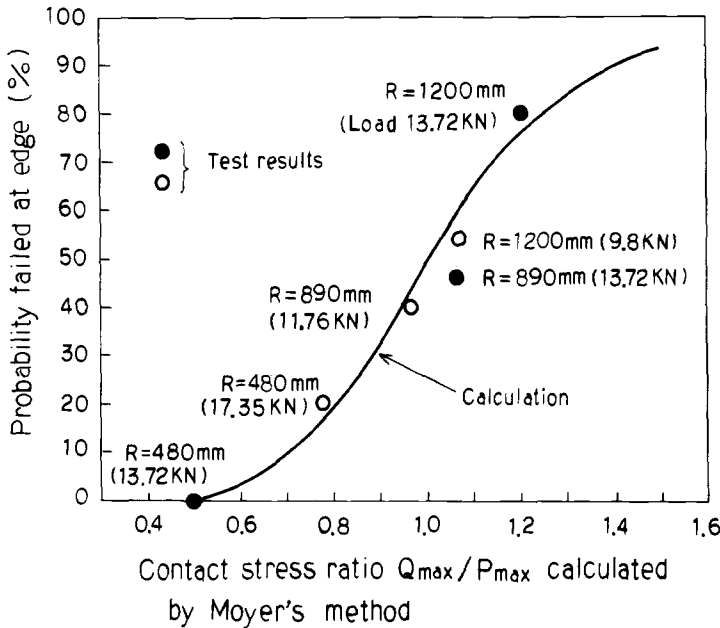
FIG. 9—*Probability of failure occurring at the edge in relation to the contact stress ratio,* Q_{max}/P_{max}.

Concluding Remarks

The line contact rolling fatigue test rig described in this paper conducts a high-speed and high-load rolling contact fatigue test with specimens of simple shape, which involves as little interaction as possible between the various factors that influence rolling contact fatigue. This rig can be used in an accelerated test, and a comparison of its test results with the results from tests using other types of rigs, such as point contact fatigue tests, makes the influences of various factors clearer.

The test results from an investigation of optimum crowning of rollers using this test rig have been described. The edge contact stress, P_{edge}, calculated by Harris's method has 1.4 times more severe an influence on rolling contact fatigue than the maximum contact stress, p_{max}, at the center of the contact area. The test results are also well interpreted by the contact stress, Q_{max}, at the edge, calculated by Moyer's method and the rolling contact fatigue life is determined by P_{max} or Q_{max}, whichever is larger. The optimum crowning value, then, is the value for which $P_{max} = 1.4$ times P_{edge} or $P_{max} = Q_{max}$.

References

[1] Harris, T. H., *Machine Design,* 29 Aug. 1968, p. 98.
[2] Moyer, C. A. and Neifert, H. R., *ASLE Transactions,* Vol. 6, 1963, p. 324.

M. Tokuda,[1] *M. Nagafuchi,*[1] *N. Tsushima,*[1] *and H. Muro*[1]

Observations of the Peeling Mode of Failure and Surface-Originated Flaking from a Ring-to-Ring Rolling Contact Fatigue Test Rig

ABSTRACT: The ring-to-ring rolling contact fatigue rig is a standard test rig for producing rolling contact fatigue. It is suitable for basic research on rolling contact phenomena. Observations of two types of surface cracks, peeling microcracks under moderate contact stress and surface cracks due to excessively high contact stress, are described in this paper. The peeling grade is related to the metallic contact ratio. The running-in property observed in metallic contact monitoring is an important factor in determining the relationship between the lubricant's characteristics and peeling failure. Rolling contact under high contact stress produces surface-originated flaking by a crack initiation mechanism, that is, crack initiation resulting from fatigue by repeated cycles of small tension and large compression.

KEY WORDS: rolling fatigue, peeling, surface-originated flaking, crack initiation mechanism, bearing steels

There are many types of rolling contact fatigue test rigs. Each has its merits and its disadvantages. For this reason, research on rolling contact fatigue cannot be thorough if only one type of rolling contact fatigue test is made. A ring-to-ring type of rolling contact fatigue test rig cannot perform an accelerated test because of its relatively low rotating speed, but this rig is considered to be a standard test rig for producing contact fatigue. It is suitable for basic research on rolling contact phenomena because the large area of contact of-

---

[1]Senior research scientist, staff engineer, senior research scientist, and managing director, respectively, NTN Toyo Bearing Co. Ltd., Higashikata, (511) Kuwana, Japan.

fered by the large dimensions of the specimen makes it easy, for example, to measure the metallic contact ratio (oil film thickness) or to observe crack initiation and propagation.

This paper describes observations of two types of surface crack initiation, namely, a peeling mode of failure under low contact stress [1][2] and a flaking process from surface-originated cracks under high contact stress [2].

Construction of Test Rigs

Two different test rigs were used, one capable of precise control of tangential force and measurement of the metallic contact ratio but unable to apply high contact stress, and the other capable of applying high contact stress.

Test Rig for Observation of Peeling Mode of Failure

An external view of the test rig used for observation of the peeling mode of failure is shown in Fig. 1a, and a schematic drawing of its construction is shown in Fig. 1b. Two specimens, whose dimensions are shown in Fig. 1b, are driven separately by two electric motors. The lower specimen has a constant rotational speed, for example, 2000 rpm, and the upper specimen rotates at variable speeds. When this rig is used for a smearing test, the rotational speed of the upper specimen is raised until seizure occurs on the rolling surfaces. In peeling tests, the rotational speed of the upper specimen is controlled so that the tangential force measured by the torque pickup is kept constant. In this experiment, the lower specimen always has a somewhat smaller rotational speed, within 0.5 percent of that of the upper one.

Electric resistance between the rolling bodies is measured by the circuit shown in Fig. 1c. Mercury contacts at the ends of the rotating shafts connect the specimens with the measuring circuit.

Test Rig for Observation of Flaking Process under High Contact Stress

An external view of the test rig for the observation of surface crack initiation and propagation under high contact stress is shown in Fig. 2a, and the essential part of the rig is diagrammed in Fig. 2b. Two specimens with different dimensions, as shown in Fig. 3, are rolling contacted. A motor drives the center shaft, which rotates the two sets of test shafts, located on opposite sides, by means of gears. No slip is given to the specimens when their diameters are exactly 53 and 50 mm, for upper and lower specimens respectively. By changing the diameters of each specimen, an arbitrary slip can be given, and by changing the radius of curvature of each specimen in the axial direction, various shapes of contact ellipses can be obtained.

---

[2]The italic numbers in brackets refer to the list of references appended to this paper.
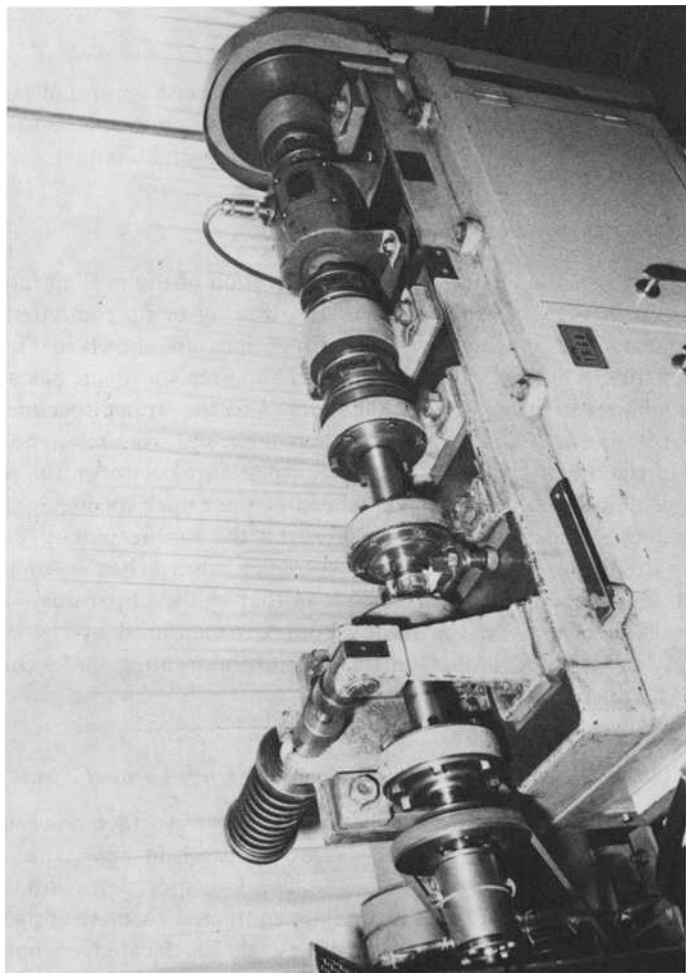
FIG. 1(a)—A ring-to-ring rolling contact fatigue test rig used for observation of the peeling mode of failure.
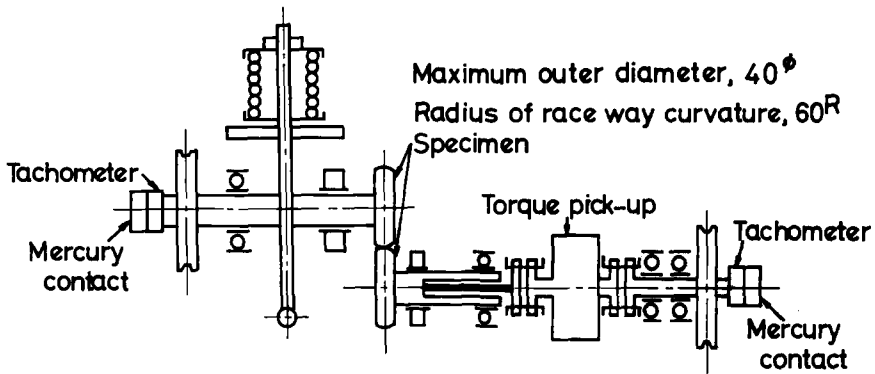
FIG. 1(b)—*Schematic construction of the ring-to-ring rig.*
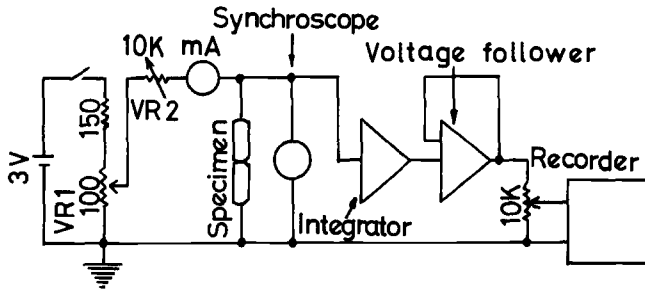
FIG. 1(c)—*Wiring for measuring the metallic contact ratio.*

Observation of Peeling

Definition of Peeling

When the hardness of one of the mating rolling elements is low, such as less than 58 HRC, or when the surface roughness of one of the mating rolling elements is rough, peeling occurs easily on the softer element, in the former case, or on the smoother element, in the latter case. Figure 4 is a surface view of a peeling, which looks like uniform wear over a relatively wide area. The magnified view in Fig. 5 shows a number of small flakings linked with micro-cracks, which is different from the usual wear. The sectional view in Fig. 6 shows very shallow flakings or pitlike dents, which are much shallower than those produced by maximum orthogonal shear stress or maximum shear stress due to rolling contact, by which general flaking is said to initiate. Figure 6 also shows that there is no thermally affected zone, such as a rehard-
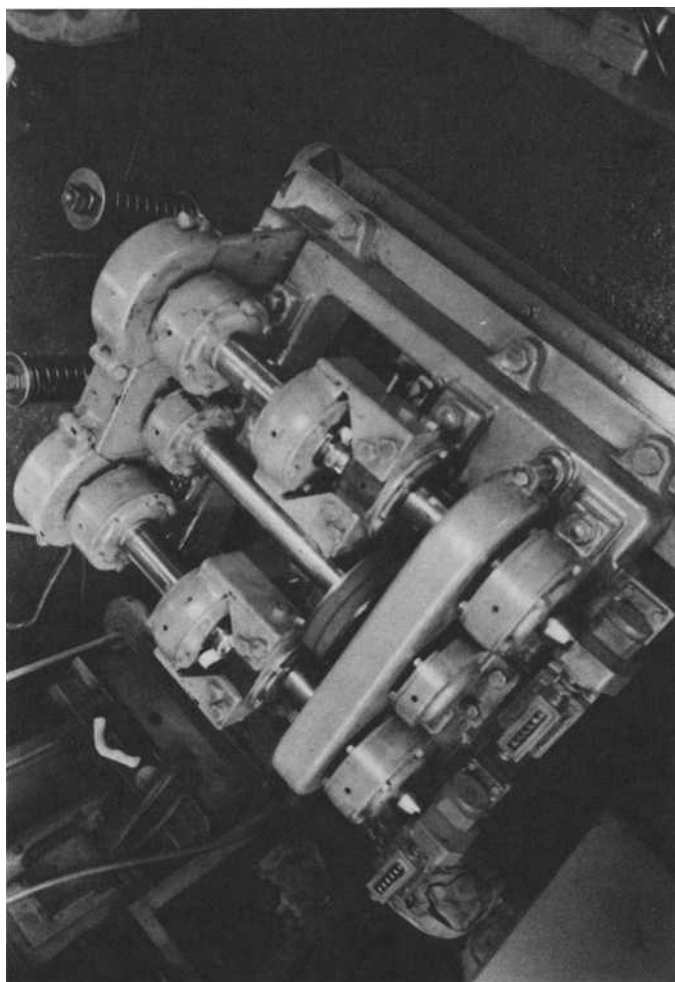
FIG. 2(a)—*The ring-to-ring rolling contact fatigue rig used for observation of the flaking process under high contact stress.*
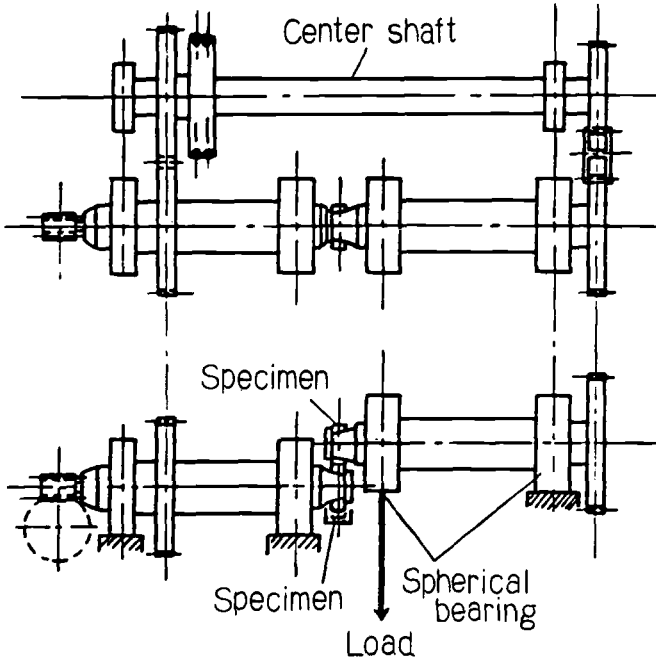
FIG. 2(b)—*Schematic construction of the essential part of the rig.*
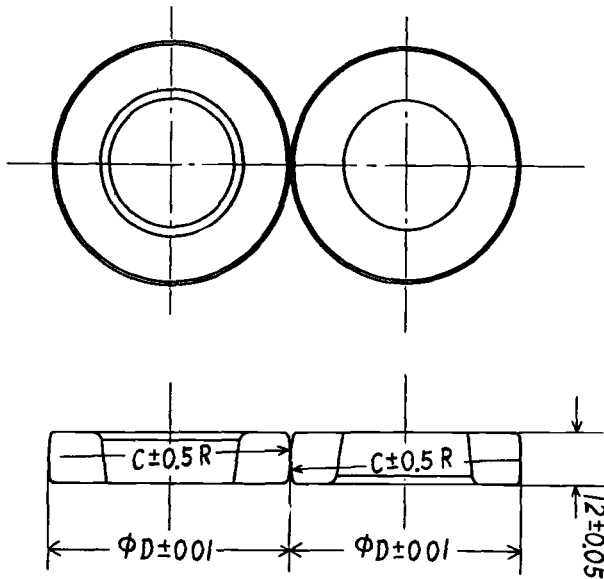
FIG. 3—*Dimensions of the specimen used in ring-to-ring testing.*
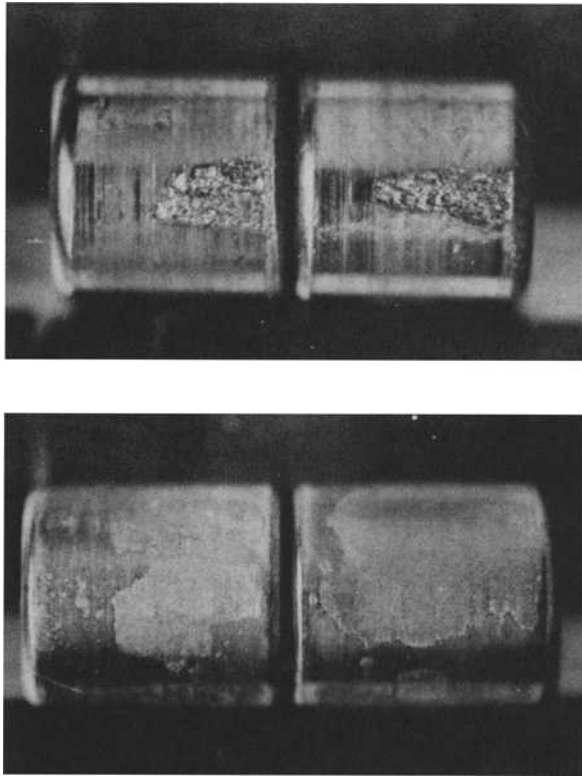
FIG. 4—*The appearances of flaking* (top) *and peeling* (bottom) *on cylindrical rollers.*

ened structure, which is common in smearing failure. Plastic deformation in the surface layer is sometimes observed in peeling failure; then it resembles pitting failure in soft materials.

In this experiment, the grade of peeling is evaluated by the percentage of pits and cracks found in a given area. The point counting method under the metallurgical microscope at ×400 magnification is used to determine this percentage.

Measurement of Metallic Contact Ratio

In order to monitor the condition of the oil film, the electric resistance is continually measured during the test. After preliminary experiments, the applied voltage was fixed at 60 mV, and the maximum current was 30 mA. Under these conditions electric erosion does not occur and the S–N ratio is hardly influenced by the noise. The applied voltage is set at 60 mV before the
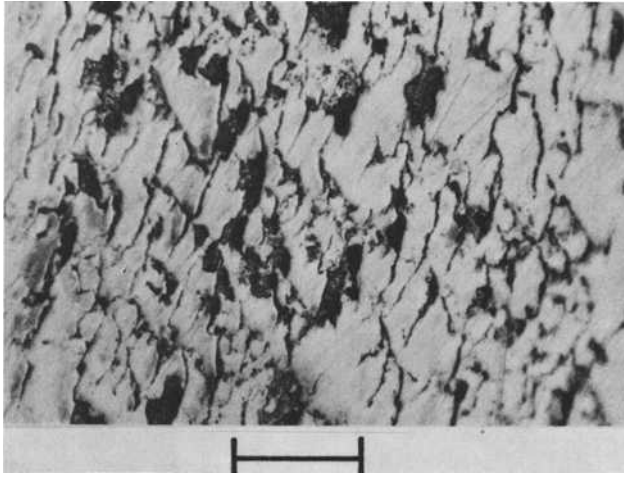
FIG. 5—*Magnified view of peeling. The marker is 0.1 mm; the rolling direction and tangential force are from bottom to top.*
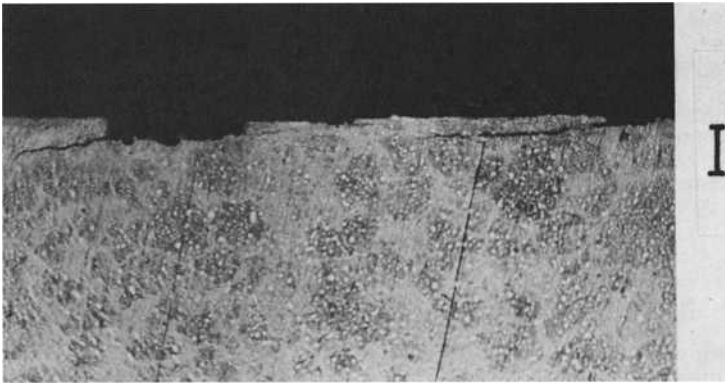
FIG. 6—*Sectional view of peeling. The marker is 10 μm; the rolling direction and tangential force are from left to right.*

two specimens come into contact. After the specimens are in contact and loaded, the current is regulated at 30 mA. In the running state, the potential drop between the specimens is observed by syncroscope, but in order to monitor the change of electric resistance throughout the test, it is convenient to integrate the potential drop with the time constant at 10 ms. The integrated voltage is recorded on a chart at intervals of 30 s. The integrated voltage indicates the time fraction in which metallic contact occurs.

Test Results

Using lubricants of various viscosities from spindle oil to gear oil, several synthetic oils, and typical greases, as shown in Table 1, the peeling test was made. To accelerate the initiation of peeling, the surface of the upper specimens in Fig. 1*b* was roughened by grinding to 0.6 μm center line average (CLA), while the lower specimens were ground and super finished to 0.04 μm CLA. The contact load was 1274 N, that is, the maximum hertzian contact stress was 2293 MPa.

The peeling grade after 4.8×10^5 revolutions is plotted in Fig. 7 against the viscosity at 37.8°C. The viscosity of base oil was used in the greases. The

TABLE 1—*Lubricants used in this test and their calculated film thickness.*

Lubricant	Viscosity, cSt		Film Thickness and Parameters[a]		
	37.8°C	98.9°C	h_0, μm, 40°C	Λ	D
Synthetic oils					
1 Diester oil					
2 Diester oil	11.1	3.0	0.142	0.26	22.5
3 Diester oil	12.5		0.142	0.26	22.5
4 Traction drive oil	33.6	5.6			
5 Polyester oil	35.2	6.0	0.283	0.515	11.3
6 Silicone oil	37.0	16.3	0.720	1.31	4.4
7 Polyester oil	66.1	9.4	0.439	0.80	7.3
8 Silicone oil	72.5	32.0	1.057	1.92	3.0
9 Silicone oil	350.0		3.490	6.40	0.9
Mineral oils					
10 Mineral terpen	0.5				
11 Spindle oil	10.5	2.1	0.197	0.36	16.2
12 Refrigerator oil	14.5	3.0			
13 Engine oil	45.0				
14 Refrigerator oil	48.0	5.8			
15 Turbine oil	59.5	7.6	0.712	1.29	4.5
16 Turbine oil	59.5	7.6			
17 Refrigerator oil	62.9	6.8			
18 Gear oil	183.6	15.5	1.625	2.96	2.0
19 Mist oil	510.0	31.0			
Greases, base oil					
A Li grease	13.0	3.4	0.134	0.24	23.9
B Li grease	52.0	6.8	0.539	0.98	5.9
C Ca, Li grease	99.4	10.3	1.212	2.20	2.6
D Na grease	103.8	10.6	1.310	2.38	2.4
E Li grease	138.0		1.352	2.46	2.4

[a]Key:
h_0 = minimum oil film thickness.
Λ = film parameter, $\Lambda = h_0/\sqrt{\sigma_1^2 + \sigma_2^2}$.
D = film parameter, $D = \Sigma R_{max}/h_0$.
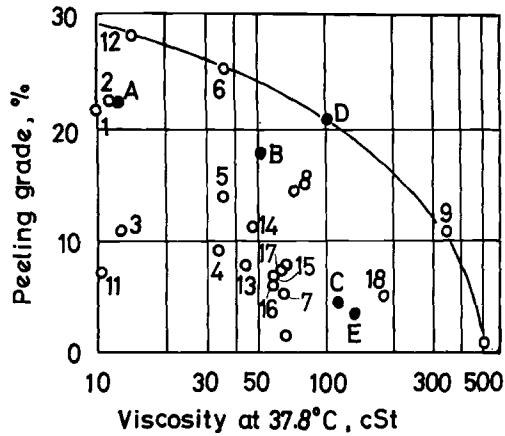
FIG. 7—*Peeling grade after 4.8 × 10⁵ revolutions against viscosity at 37.8° C for various lubricants.*

peeling grade tends to decrease with the increase in viscosity. However, in the range of 30 to 70 cSt, the peeling grade varies considerably depending on the kind of lubricant used. In this viscosity range, the peeling grade does not depend on the oil film thickness obtained from viscosity measurement; therefore, it cannot be predicted by elastohydrodynamic lubrication film calculation.

Figure 8 shows the monitoring chart of metallic contact ratios of various lubricants with nearly the same viscosity. The metallic contact ratio decreases gradually or abruptly within a half hour after the onset of the test. This decrease in metallic contact ratio depends on the kind of lubricant used rather than its viscosity and is called the "running-in" property. The relationship between the metallic contact ratio at 30 min after the onset of the test and the peeling grade after a 4-h run is plotted in Fig. 9, which shows that a good correlation exists.

The metallic contact ratio is also affected by the surface roughness of the specimen. Figure 10 shows a monitoring chart which was obtained from a test of various surface roughnesses of upper specimens against superfinished lower specimens under the same lubricant. Since the peeling grade depends on the metallic contact ratio, the peeling grade in this case is more severe for rolling contact with the rougher specimens.

Figure 11 shows the relationship between peeling grade and contact stress in rolling contact between specimens with a surface roughness of 1.0 μm CLA and 0.04 μm CLA under two kinds of lubricants. The peeling grade increases with increasing contact stress. No peeling was initiated after a long run under a contact stress of less than 980 MPa. Flaking was initiated from peeling after a 4-h run under a contact stress of 3920 MPa.
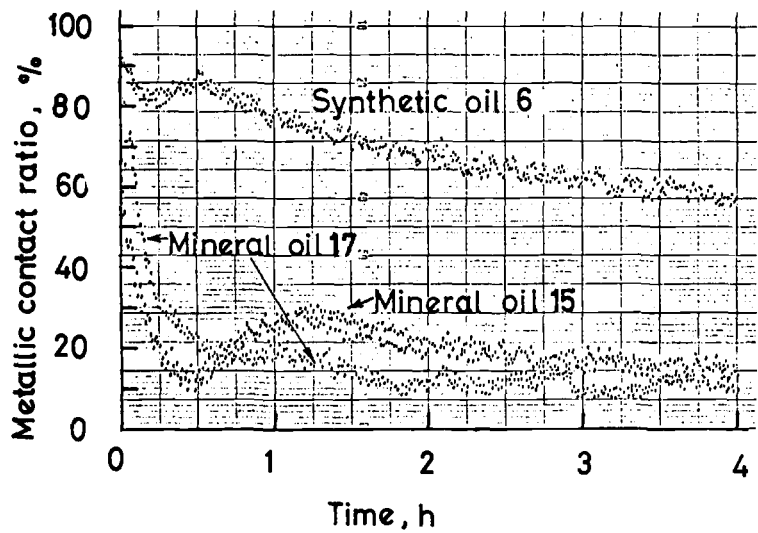
FIG. 8—*A monitoring chart of the metallic contact ratio of various lubricants.*
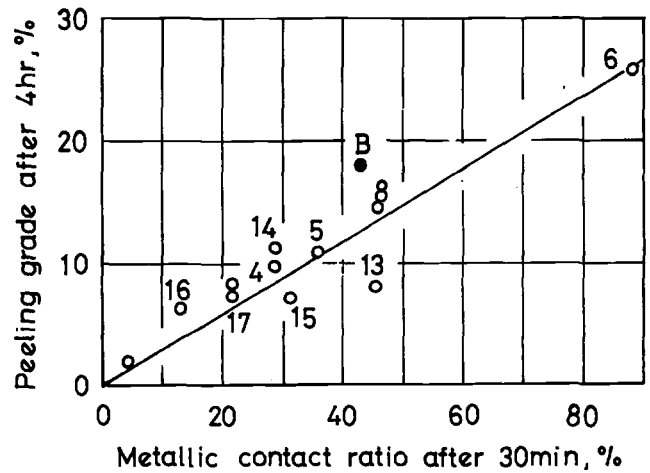
FIG. 9—*The relationship between the peeling grade after 4 h and the metallic contact ratio after 30 min.*
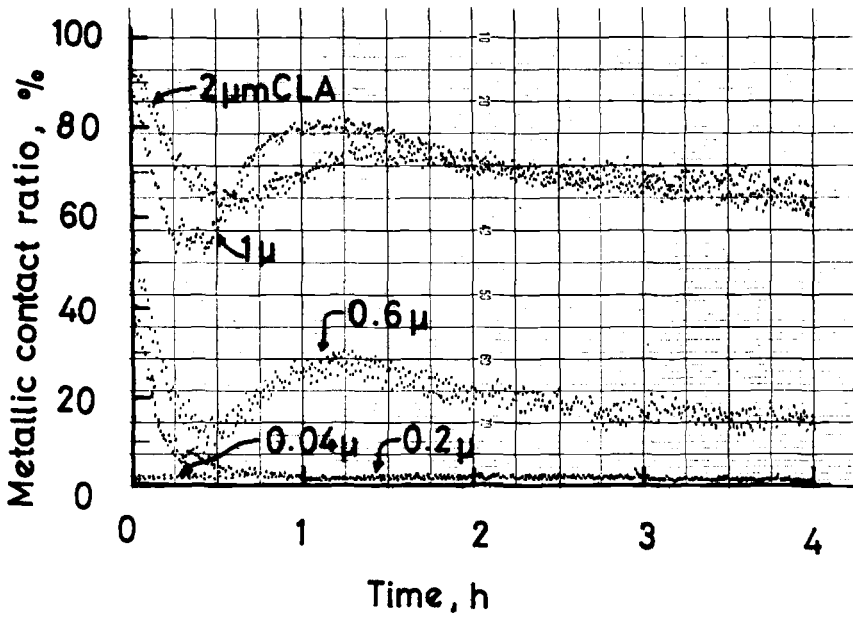
FIG. 10—*The metallic contact ratio with various surface roughnesses of the upper specimens.*
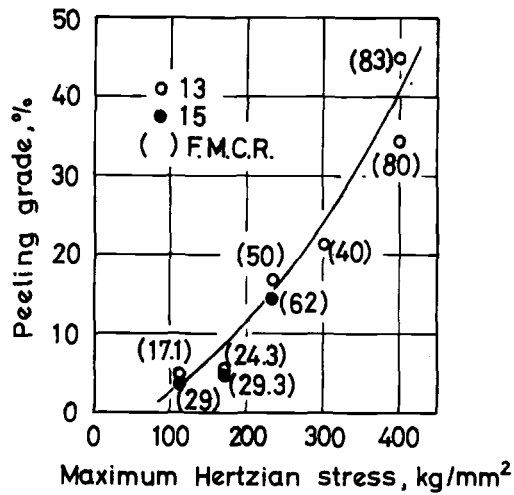
FIG. 11—*The influence of contact stress on peeling.*

Observation of Surface Crack Initiation and Its Propagation

Figure 12 shows the process of surface-originated crack propagation under typical rolling contact test conditions such as dimensions of $D = 53$ mm and $C = 26.5$ mm for the upper specimen and $D = 50$ mm and $C = 25.0$ mm for the lower specimen (See Fig. 3) and a maximum hertzian contact stress of 4900 MPa.

Cracks were initiated in the axial direction along a line of nonmetallic inclusions on or very near the surface. The position is not at the center of the raceway but $2/3 \cdot a$ ($2a$ = width of contact) from the center. The crack propagates gradually from both crack tips at an angle of 40° deg to the rolling direction. The crack which propagates toward the center of the raceway turns in a circumferential direction on reaching the center and subsequently leads to flaking. Generally, several cracks are observed on one raceway, and one of those cracks causes the final flaking.

The crack is propagated into the material almost at right angles to the surface, at first, but it then turns parallel to the surface at the upper side of the dark etching constituent (DEC). The section of surface-originated flaking is shown schematically in Fig. 13 to compare with the surface appearance. Area A is the first small piece flaked from the crack tip. It is shallower and smaller than the whole flake, and its base corresponds to the depth at which tensile residual stress turns to compressive stress. Area B is the broader of the flaked material, and its base corresponds to the center of the DEC.

Figure 14 shows an example of residual stress measurement on and under the contact surface. It shows a tensile residual stress peak larger than 300 MPa just below the surface. The tensile residual stress peak is always larger in the axial direction than in the circumferential direction. Residual stress turns to compressive stress, with the depth below the surface increasing. The compressive residual stress peak position corresponds to the depth of the maximum shear stress.

Residual tensile stress due to rolling contact is considered to be directly related to the initiation of a surface crack, and it is presumed that the surface crack initiates when there is residual tensile stress due to heat treatment. To verify this, the following experiment was carried out.

Specimens were quenched with various rates of cooling to obtain various tensile residual stress values. A maximum tensile stress of 150 MPa was obtained by this method. Using high-frequency induction heating for surface tempering, tensile residual stresses of 250 to 500 MPa were obtained. Residual stresses of specimens before testing, with the addition of a hoop tension of 50 MPa resulting from force-fitting the specimen to the shaft, are given in Table 2. The test conditions and the results are also given in this table. Cracks seem to initiate when the tensile stress is larger than 300 MPa.

During rolling contact, compressive stress occurs at the instant of contact, and tensile residual stress occurs between contacts, so that the specimen is
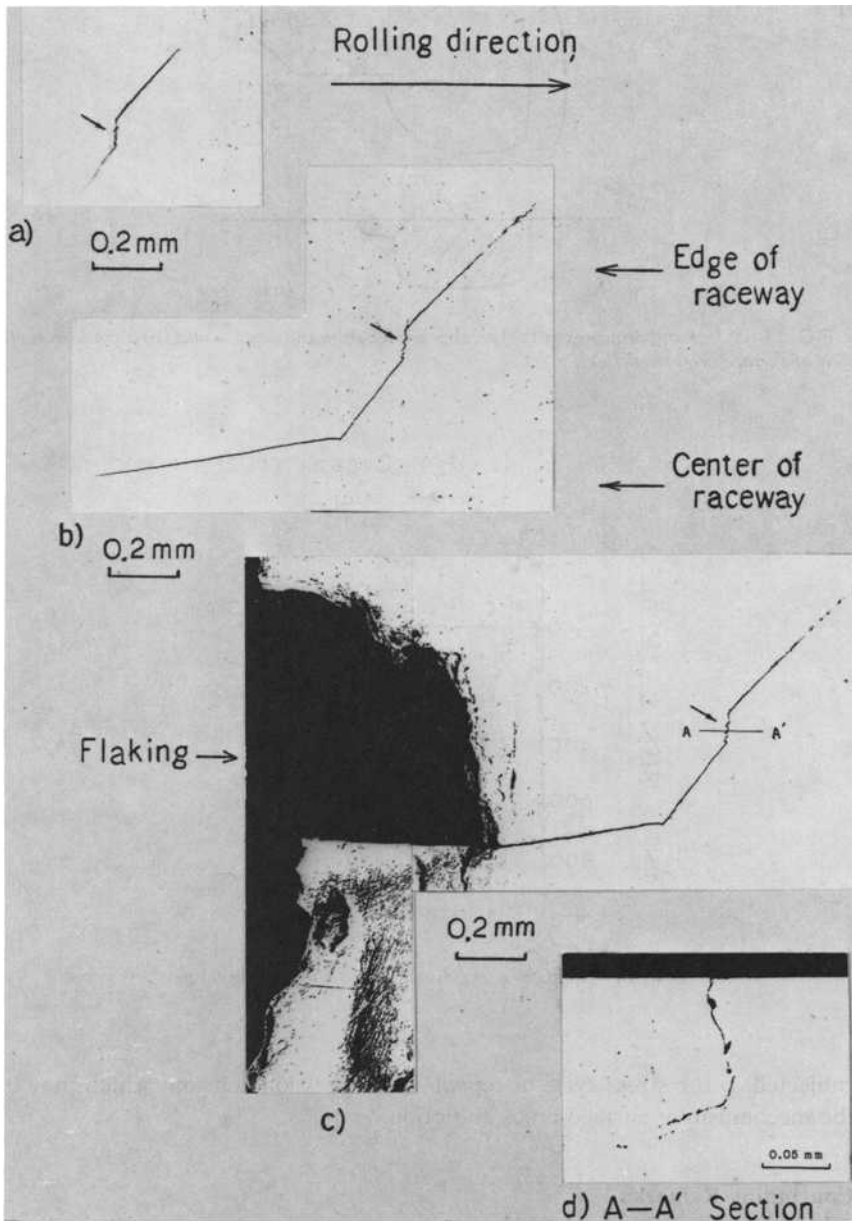
FIG. 12—*The process of surface-originated crack propagation. The arrows indicate the origin of cracking.* (a) *loading cycles* 91×10^4; (b) *loading cycles* 129×10^4; (c) *and* (d) *loading cycles* 150×10^4.
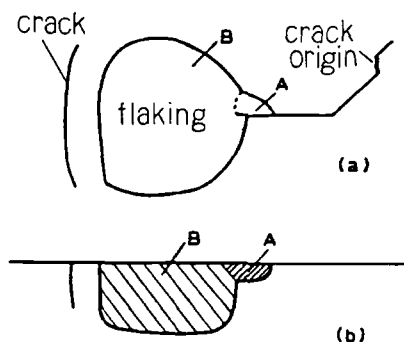
FIG. 13—*Schematic drawings of* (a) *the appearance from the surface and* (b) *a cross-sectional view of surface-originated flaking.*
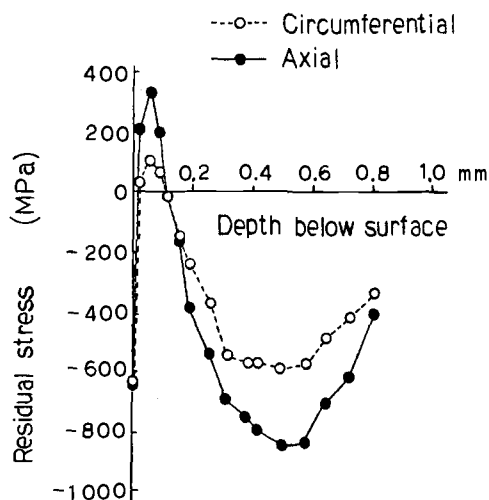
FIG. 14—*Residual stress distributions after rolling fatigue.*

subjected to the stress cycle of repeated compression–tension, which may be the mechanism of surface crack initiation.

Concluding Remarks

In this paper two types of surface cracks were discussed, namely, peeling microcracks and cracks initiated by repeated small tension–large compression cycles. These types of cracks are very important because they may be the cause of early failure in actual bearings. Bearings such as automobile trans-

TABLE 2—*Test results of rolling contact fatigue with specimens previously given tensile residual stress.*

Specimen Mark	Contact Stress P_{max}, MPa	Slip, %	Tensile Stress, MPa	Number of Cycles to Failure, $\times 10^4$	Failure Mode
B101	4508	0	411.6	9	surface crack → flaking
BB102	2940	0	529.2	210	surface crack → fracture
B103	2940	0	323.4	89	surface crack → fracture
DD101	2940	1.16	499.8	300	surface crack → fracture
DD102	2940	1.16	196.0	1790	no failure
D103	2940	1.16	98.0	3165	no failure
BB104	1960	0	509.6	1030	surface crack → fracture

mission bearings are used in lubricating oil, which is sometimes contaminated with fine particles such as wear chips from gears. In such cases, the bearings suffer from surface roughening of the raceway, which induces peeling and occasionally leads to flaking.

The crack initiation mechanism of repeated cycles of small tension and large compression also is not unusual. For example, a grinding burn of the raceway can have a tensile residual stress larger than 300 MPa, which is enough to produce a crack by the application of repeated contact stress. Hoop tension, tangential force due to slip, and residual tensile stress due to heat treatment are tensile stress components. Individually, these components are not great, but their combined action can produce stresses up to 300 MPa, which will produce surface cracks.

References

[1] Tokuda, M., Ito, S., Muro, H., and Oshima, T., *Proceedings of the Symposium of Rolling Contact Fatigue Performance Testing of Lubricants,* Institute of Petroleum, London, 1976.
[2] Muro, H., Tsushima, N., and Nagafuchi, M., *Wear,* Vol. 35, 1975, p. 261.

Rolling Contact Fatigue Testing in General: Comparison of Methods and Test Results

A. T. Galbato[1]

Methods of Testing for Rolling Contact Fatigue of Bearing Steels

ABSTRACT: Types of test equipment, apparatus, and the procedures employed in the evaluation of rolling contact fatigue are reviewed, covering both element and full-scale bearing tests and the significance of test results.

KEY WORDS: rolling contact bearings, bearing steels, rolling contact fatigue, test apparatus

Experience and history show us that less than 10 percent of all the bearing replacements in the field can be attributed to classic rolling contact fatigue. The remaining 90 percent are made for reasons and conditions not even closely related to pure bearing fatigue [1].[2] Because the number of classic fatigue failures is statistically insignificant to the final customer, the following important observations can be made.

1. The bearing industry has performed well in producing bearings of the necessary quality and design.
2. The bearing industry has and is continuing to pursue improvements in state-of-the-art bearing technology.
3. As design, installation, and lubrication systems are enhanced, rolling-element bearings will ultimately fail because of fatigue after extended service.

It is well known and well documented that the rolling contact fatigue life of bearings is dependent on many interacting factors, such as bearing materials, melting techniques, material processing variables, lubricant systems (for temperature control), elastohydrodynamic (EHD) film thickness, contact

---

[1]Manager, Product Research & Development, TRW Bearings Division, Jamestown, N.Y. 14701.
[2]The italic numbers in brackets refer to the list of references appended to this paper.

stress levels, and other environmental and operational effects (such as mis-alignment). The life adjustment design factors recommended by the American Society of Mechanical Engineers (ASME) Lubrication Division [2] provide a means of modifying the "engineering approximations" which are given in most bearing manufacturers' catalogs and thus permit better estimations of predicted bearing life under specific conditions.

Although ASME life adjustment factors can be applied to most ball and roller bearing applications, caution is recommended for cases of extreme environmental conditions. The combined influence of important environmental and operational factors requires that laboratory testing be conducted under conditions which simulate as closely as possible the expected service environment and that a sufficient number of tests be performed to evaluate the scatter of fatigue life as characterized by the Weibull distribution [3].

Paramount in laboratory testing, where development of bearing technology is pursued for optimum bearing performance, are adequate and proper test equipment, test procedures, and data analysis. Although the test equipment described in this paper is being used in the author's facility, the rig design concepts do not differ greatly among the various manufacturers' laboratories.

Design Concepts

Bearing Testers

Endurance test machines must be capable of subjecting test bearings to realistic operating conditions. Such operating conditions include the magnitude and type of load, the speed, the mode of lubrication, and the temperature. In conjunction with the test conditions, the type and size of bearing will determine the overall size of the test rig and drive system.

The basic arrangements employed in most standard bearing test rigs include a stationary frame, a movable housing frame, and a single test shaft on which test bearings are mounted. Figure 1 illustrates the various arrangements used for the different loading conditions as follows: (a) a four-bearing arrangement for radial loading only, (b) a three-bearing design for combined loading, and (c) a two-bearing setup for thrust loading only.

In Design a, the applied radial load (2 P) acts on the two inboard bearings of the bearing shaft system while reactionary forces (P) act on each of the two outboard bearings. This arrangement permits the simultaneous testing of four bearings.

In Design b, the applied radial load (2 P) acts on the center load bearing (B) and the thrust load (T) is applied axially on one outboard test bearing and opposed by the other. In this arrangement, the reactionary radial load (P), in combination with the applied and reactionary thrust load acting on

A = test bearing
B = load bearing
T = thrust load
P = radial load
D = drive
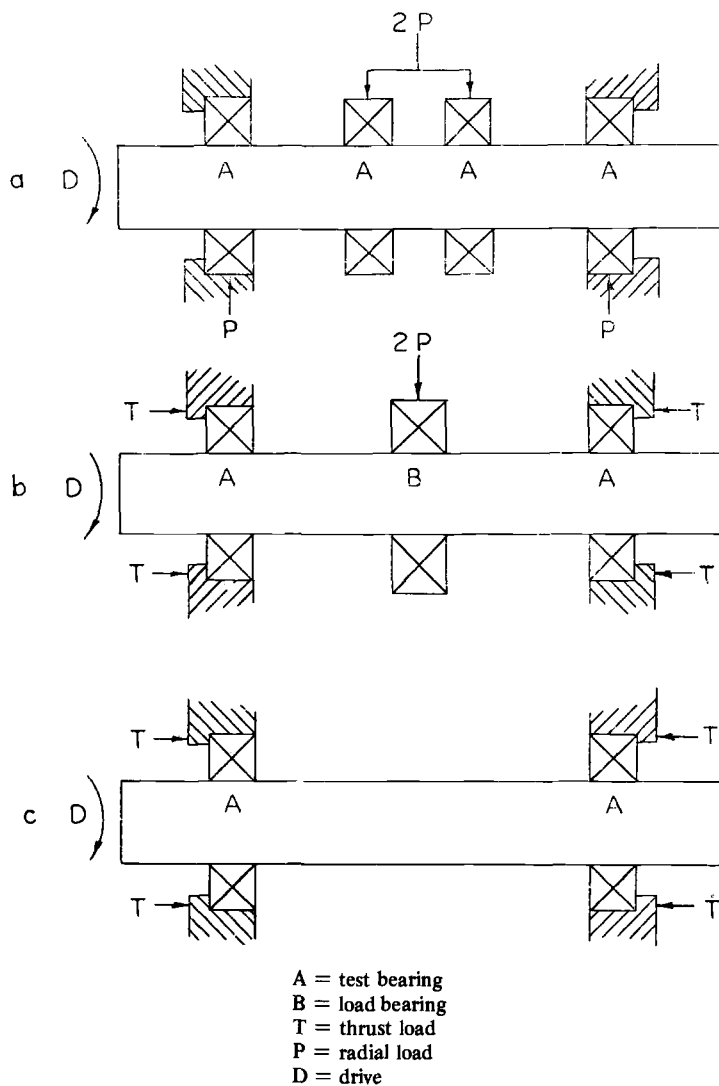
FIG. 1—*Basic test arrangements.*

the test bearings, provides a simultaneous combined loading test of two bearings.

In Design *c*, two test bearings are subjected to thrust loads where the thrust load (T) is applied on one bearing while the other bearing reacts with an equal amount of load.

Illustrated in Fig. 2 is a cross-sectional view of a test housing representing
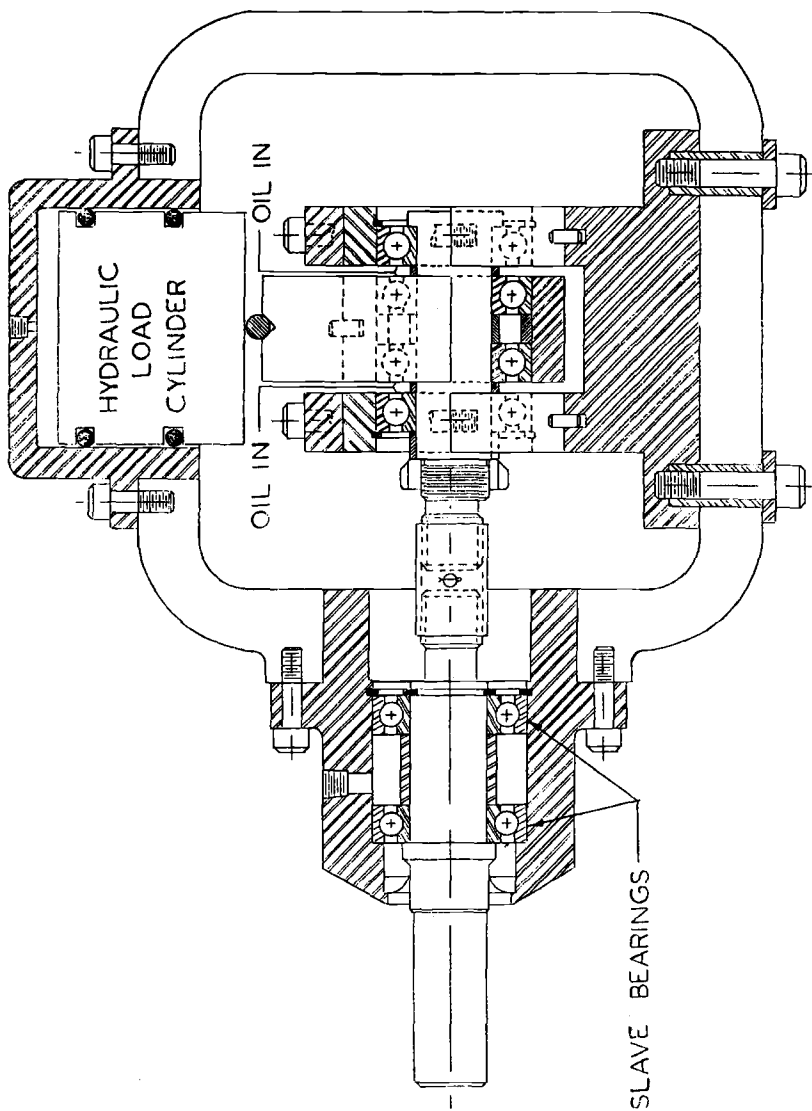
FIG. 2—*Four-bearing test unit.*

the four-bearing test concept given in Fig. 1a. The apparatus is belt driven by a 3-hp electric motor, and speeds from 1 000 to 10 000 rpm are possible; however, the normal test speed is 5 500 rpm. A flexible coupling connects the slave bearing spindle shaft to the test bearing shaft system.

Endurance testers of this kind normally test ball and roller bearings of 28-mm (1.1-in.) minimum bore and a maximum outside diameter (OD) of 85 mm (3.35 in.) under a maximum radial load per bearing of 9 kN (3000 lb). The radial load is applied through a hydraulic cylinder whose piston makes aligning contact with the center of the housing enclosing the middle two bearings of the test arrangement. Thus, the two middle bearings share equally the applied load. The two outboard bearings are mounted in housings fixed to the structure and react to the applied load equally. The loading cylinder is pressurized by a dynamic pumping system in which the applied load is controlled and maintained by a precision pressure regulator at the tester location.

The lubrication of bearings is by oil jet, with the oil free to escape on both sides of each bearing. The same oil is used for lubricating the test bearings and spindle slave bearings and for pressurizing the load cylinder. A central oil sump and pumping system provides for a group of such test machines, but each machine has its own controls in regulating oil-in flow rate for maintaining bearing operating temperature and controlling load pressure. When necessary, a heat exchanger is incorporated to control oil-in temperatures as required. The outer race temperatures are monitored and recorded.

A variety of automatic shutoffs are utilized at each test machine for detection of lubrication flow and load variations, motor overload, and fatigue spall. For the fatigue spall detector, a printed circuit board is located at the base of the housing. When a metallic chip of significant size emerges from a spall, it shorts out the circuit and automatically stops the operation of that particular machine. An elapsed-time meter records the operating test time at each test machine.

Figure 3 shows one bank of test machines such as those just described. Illustrated in Fig. 4 is a cross-sectional view of a test rig representing the three-bearing design concept illustrated in Fig. 1b, where two bearings are tested under combined radial and thrust loading. When the center load bearing and radial load system are removed, the two outboard bearings can be tested under pure thrust load. Belt-driven by a 5 or 10-hp electric motor, this test rig has speeds that can be varied from 500 to 7000 rpm. With a fixed frame on the drive end of the machine and a sliding frame at the opposite end, a variety of housing inserts are used to accommodate bearing sizes up to 190-mm (7.48-in.) OD.

Both radial and thrust loads are applied by separate mechanical leverage systems employing spring scales or dead weights that act on levers. Thrust loads up to 67 kN (15 000 lb) are applied at the sliding housing end, while the radial load, 67 kN (15 000 lb) maximum, is applied to the center or load
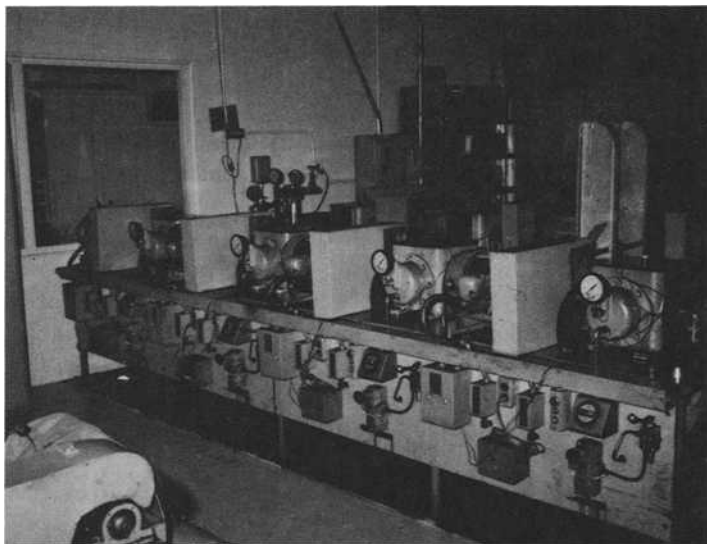
FIG. 3—*Four-bearing testers.*

bearing. The outboard test bearings share the applied radial load; each receives the full thrust load. The center bearing is not subjected to any thrust load.

This machine has its own independent circulating oil system—including reservoir, pump, filter—and capabilities for oil heating and cooling as required. Bearings are normally lubricated by jets with oil flow rates regulated for desired bearing operating temperatures. These machines also use the various detection and automatic shutoff systems discussed previously.

Figure 5 shows the same machine without the axial load system, which provides the flexibility of incorporating a four-bearing radial load test arrangement.

Figure 6 illustrates a bank of test machines where radial and thrust loads are applied as discussed earlier.

Bearing Element Testers

Whereas endurance testers are used to evaluate performance of full-scale bearings, as reviewed earlier, element testers employ rolling elements as their test specimens. Rolling elements are relatively inexpensive to produce and to test. The use of such bench-type testers provides for expedient evaluation and screening of materials and materials processing variables related to rolling contact fatigue prior to full-scale bearing testing. Sometimes element testers are also used for lubricant screening and oil film studies in rolling contact.
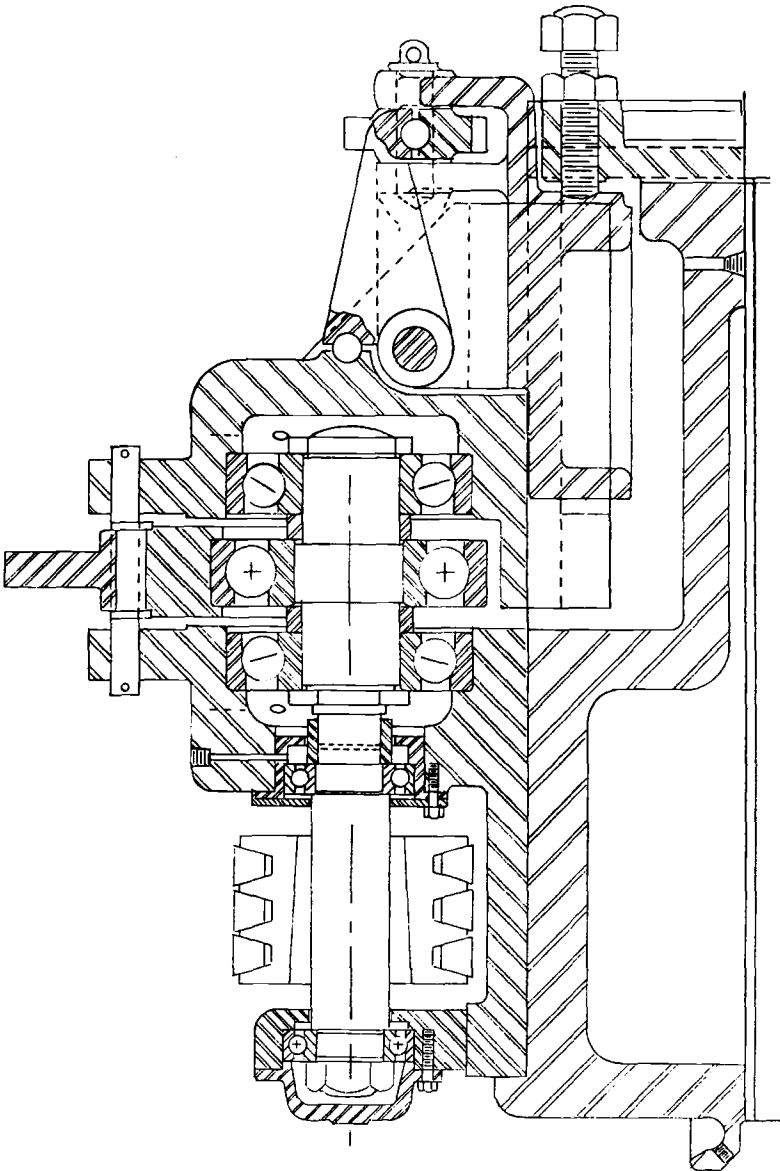
FIG. 4 — *Three-bearing test unit.*
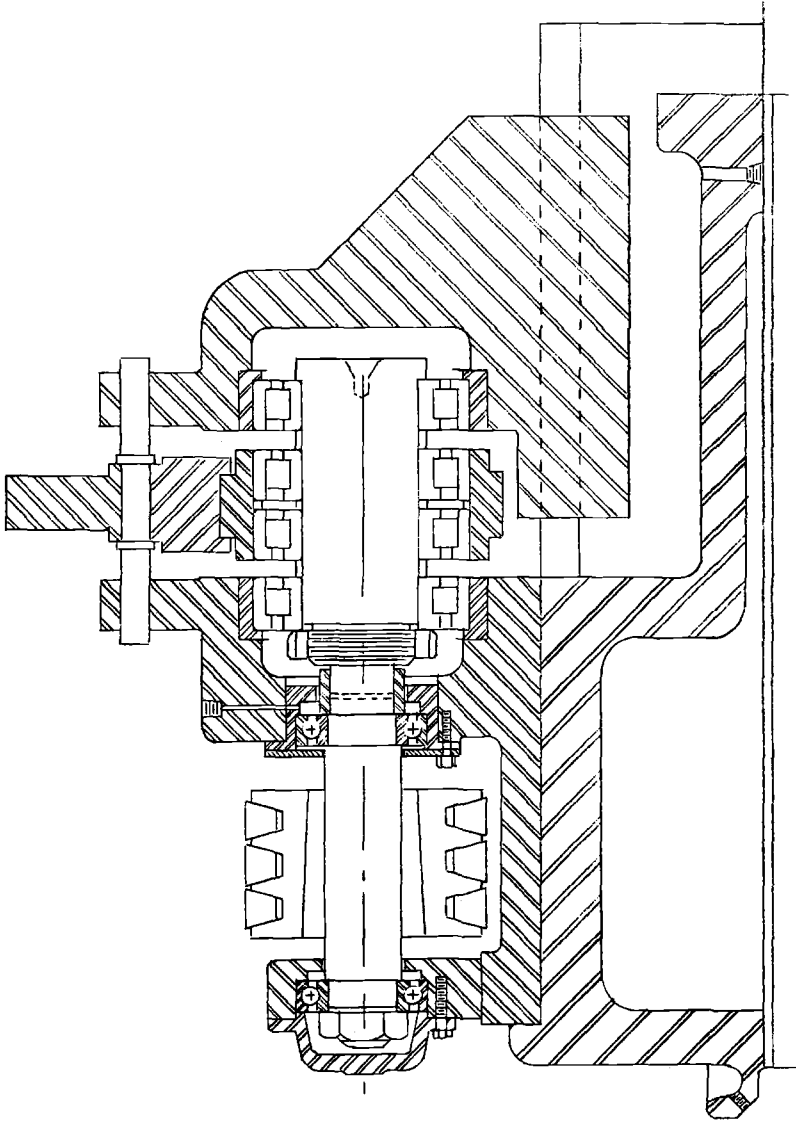
FIG. 5—*Four-bearing test unit.*
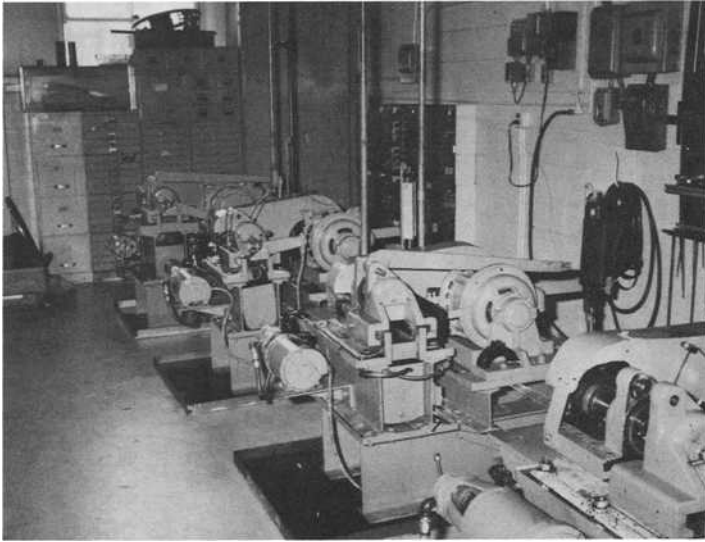
FIG. 6—*Three-bearing testers.*

Over a period of time, there have been at least 20 different rolling element fatigue testers on the market. Some of these designs are very similar to each other; some are no longer in use. Generally, these testers fall into one of the following three categories:

1. Two cylindrical surfaces roll against each other under load, or rollers or balls are run against a flat or cylindrical surface.

2. A ball or roller or a small-diameter cylinder specimen is loaded between two disks or rings of a much larger diameter. In some rigs the test cylinder is driven; in others one or both of the rings are driven.

3. A ball or conical specimen is rotated under angular contact against three or four support balls rolling in a race or track.

Element testing performed in our laboratories makes use of equipment which falls into the latter two categories. Specifically, Fig. 7 illustrates a single-ball fatigue tester (Category 2), which produces spalling-type failures. The rolling contact is designed to simulate the rolling and spinning conditions that exist in a high-speed ball bearing under thrust loading. These machines can be used to study spalling resistance of balls as affected by alloying elements, hardness, heat treatment, surface finish, out-of-roundness, operating temperature, loads, speeds, and lubricants.

The ball specimen is located between two 2.27-rad (130 deg) V-groove races and positioned horizontally by a silicon–iron bronze retainer. The lower
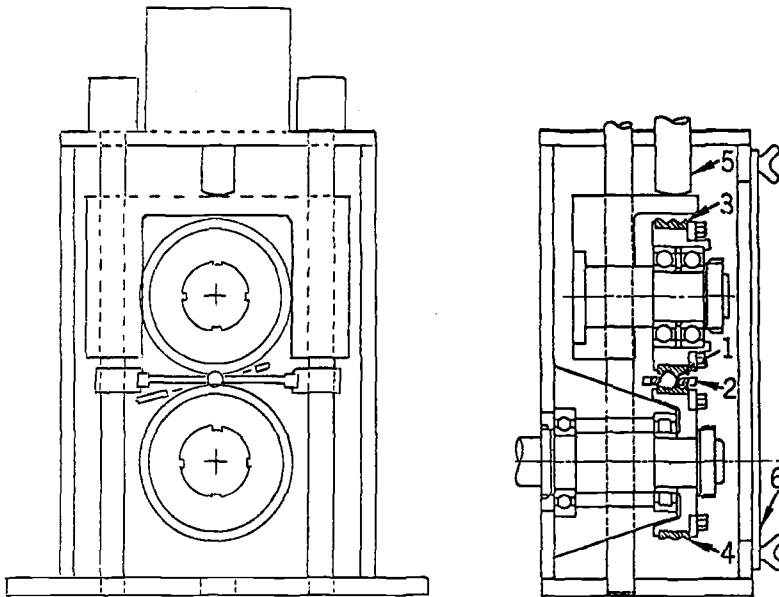
1 = test ball
2 = ball retainer
3 = upper race
4 = lower race
5 = load piston
6 = access panel

FIG. 7—*Single-ball tester* (left) *front view;* (right) *side view.*

race drives the ball as a compressive load is applied through a hydraulically loaded free-wheeling upper race by means of a load cylinder located on top of the machine.

The test ball cage may be adjusted to move the ball to two different tracks on the races to allow successive tests on an unused portion of the race. Removing the access panel exposes all test parts. The slave race is mounted on overhung bearings, which makes it readily accessible. Raising the upper shaft assembly allows the test parts to be replaced. The upper slave assembly can be positioned on its two vertical rods to accommodate balls of different diameter.

A failure is indicated by (*a*) excessive noise, (*b*) drive motor amperage excursion, or (*c*) an increased vibration level. In the event of a failure, the ball failure indicator lights a warning indicator and shuts off the circuit to the drive motor.

Typical test conditions are as follows:

Oil temperature:	328 K (130°F)
Oil flow rate:	0.9 kg/min (2 lb/min)
Speed:	7800 rpm
Hertz stress:	2.8 GN/m^2 (400 ksi)
Stress cycles per hour:	8.96 × 10^6
Ball size diameter:	12.7 mm (0.5 in.)
Races finish:	0.10 to 0.15-μm (4 to 6-μin.) rms

Another element tester in Category 2 is the rolling contact fatigue (RCF) machine. Figure 8 illustrates the overall view of the tester, which can be conveniently located in a 61 by 91-cm (2 by 3-ft) area. Figure 9 is a close-up view of the test specimen and loading disks arrangement. In contrast to the single-ball tester, the test specimen drives the two large hemispherically ground loading disks. The cylindrical rod test specimen, 9.53 mm (0.375 in.) or 12.7 mm (0.500 in.) in diameter by 76.2 mm (3 in.) long, is mounted in a precision chuck and rotated at 10 000 rpm. The loading disks are 190 mm (7.5 in.) in diameter, 12.7 mm (0.5 in.) in thickness, with a 6.35-mm (0.250-in.) transverse contact radius, and mounted in pendulum yokes. The rotating test rod is diametrically loaded (pinched) by the two large disks, which are mechanically brought together to bear against the test rod. The test load, capable of exerting maximum hertzian contact stress up to 5.85 GN/m^2 (850 ksi), is continuously monitored by a calibrated load cell.

The disks impinging upon the test bar produce a compressive stress pattern very similar to that seen on the inner race of a ball bearing. The resultant spalling fatigue failure is essentially identical to that observed on actual bearing races (see Fig. 10). Lubrication is by a drip feed system using a needle valve to control the flow rate at a constant 20 drops per minute. A velocity-type vibration transducer is mounted on one of the support yokes. This extremely sensitive instrument acts as a failure sensor and terminates the test immediately upon the occurrence of a spalling fatigue failure.

For Category 3 element testers, the five-ball planetary fatigue apparatus is a very popular design frequently used in the bearing industry, in governmental agencies, and by bearing users. As shown in Fig. 11, the upper test ball rotates with the drive spindle, through which the test load is applied by means of a dead-weight leverage system. The test specimen, supported by the four lower balls, is subjected to three stress cycles per revolution of the spindle, within a finite contact track of the test specimen. The lower test balls orbit within a supporting stationary raceway, with the contact angle fixed depending on internal geometry. A bronze cage is used to space the lower support balls. A ¾ hp electric motor drives the modified drill press spindle through a positive drive pulley and timing belt. The spindle is supported by two duplexed pairs of precision bearings, and speeds up to 10 000 rpm are achieved.
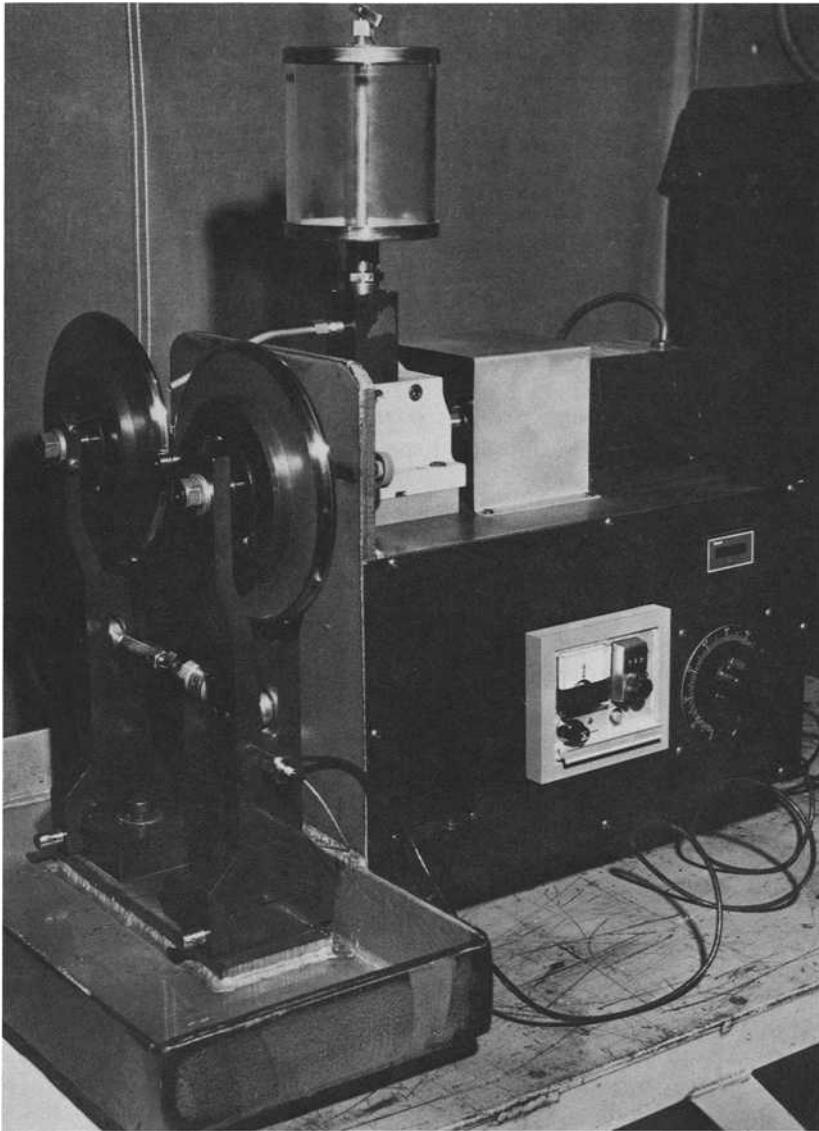
FIG. 8—*Rolling contact fatigue tester.*

Hertzian contact stress levels up to 5.5 GN/m^2 (800 ksi) max, on the test ball, are attainable. At a spindle speed of 10 000 rpm, the test specimen is subjected to 1.8 million stress cycles per hour. Fatigue failure of the test ball is detected by sensitive vibration transducers. Since the test ball is subjected to the higher stress frequencies and the axes of the support balls change
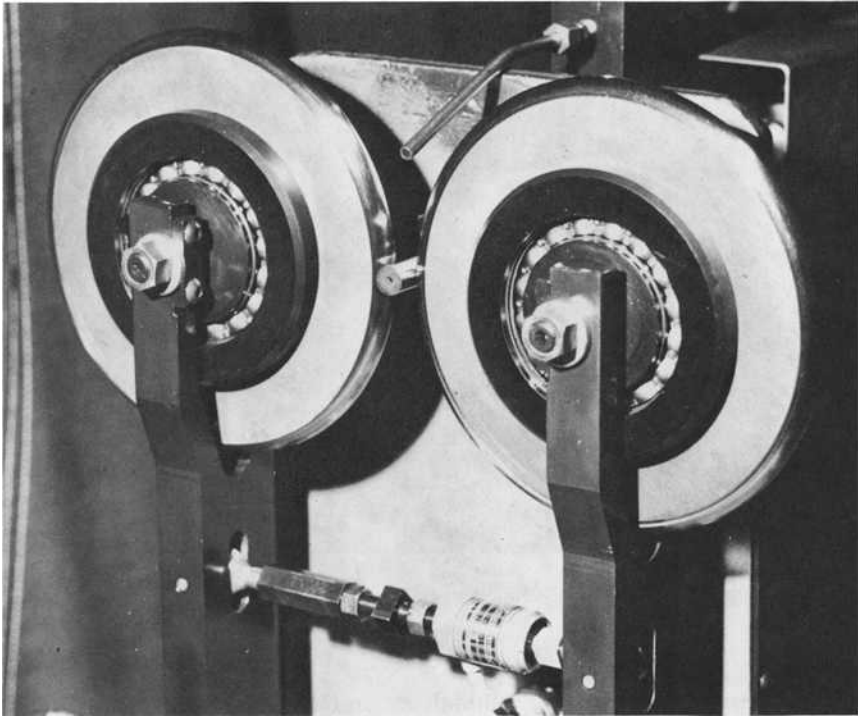
FIG. 9—*Close-up view of a rolling contact fatigue tester.*

orientation occasionally, thus spreading the stress more evenly over the support balls' surfaces, the vast majority of fatigue failures occur in the upper test ball. An automatic shutoff system is triggered by the vibration transducer when a fatigue spall is generated.

Lubrication of the test and support balls is provided by a once-through oil mist system. A flow rate of 6 to 10 g/h has proven to be quite satisfactory.

The temperature of the supporting raceway is continually monitored. For elevated temperature tests, heating elements are incorporated in the housing surrounding the raceway, with the temperature regulated by thermocouple control.

Figure 12 illustrates a bank of five-ball testers conveniently located on a laboratory bench. Because of the high stress cycle rate, significant fatigue data can be obtained in a relatively short period of time. Consequently, the five-ball test apparatus is used for several purposes, including wear testing, endurance testing, lubricant studies, material screening, and elastohydrodynamic film studies. Many of the research studies performed by the Na-
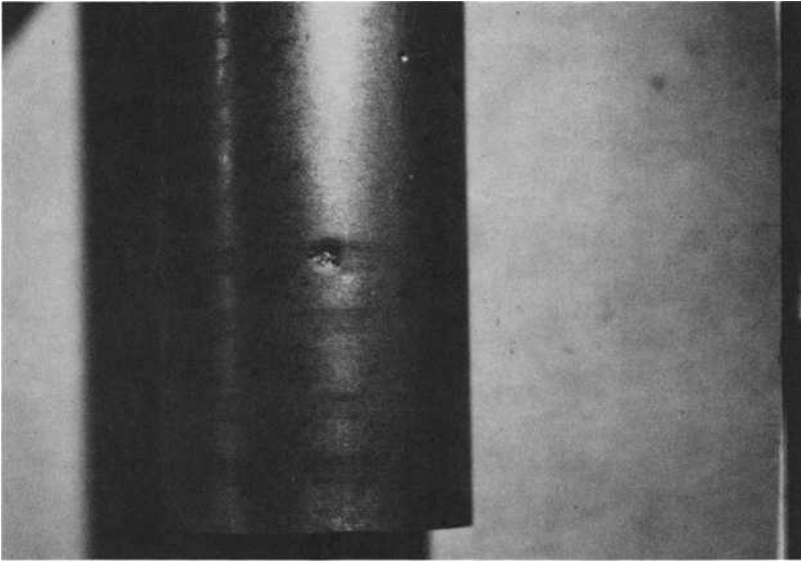
FIG. 10—*Fatigue spall from an RCF test bar.*

tional Aeronautics and Space Administration (NASA) (Ref. *4,* for example), employ this five-ball fatigue tester.

Data Reduction and Analysis

Whether evaluating bearings or bearing rolling elements, fatigue endurance testing in rolling contact is complicated by the statistical nature of the phenomenon. Failure inception and progression depend on a traveling, fluctuating stress peaking in a local volume of material which, by coincidence, is weaker or more brittle than its neighboring material.

Two identical ball bearings, subjected to operation under identical conditions, may achieve fatigue endurance lives which differ by an order of magnitude ($\times 10$). The testing of more bearings will produce individual lives which fall between the extremes, and probably some which will lie outside those extremes. To arrive at a statistically valid estimation of the fatigue endurance life of a group of specimens, a reasonable number of tests is necessary.

For the past 30 years, the statistical Weibull distribution [3] has been utilized to analyze fatigue endurance data and to permit comparison between sets of data from testing of different groups of specimens or bearings. It is understood, for purposes of this discussion, that each individual specimen in a particular group is "identical," that is, subjected to identical test condi-
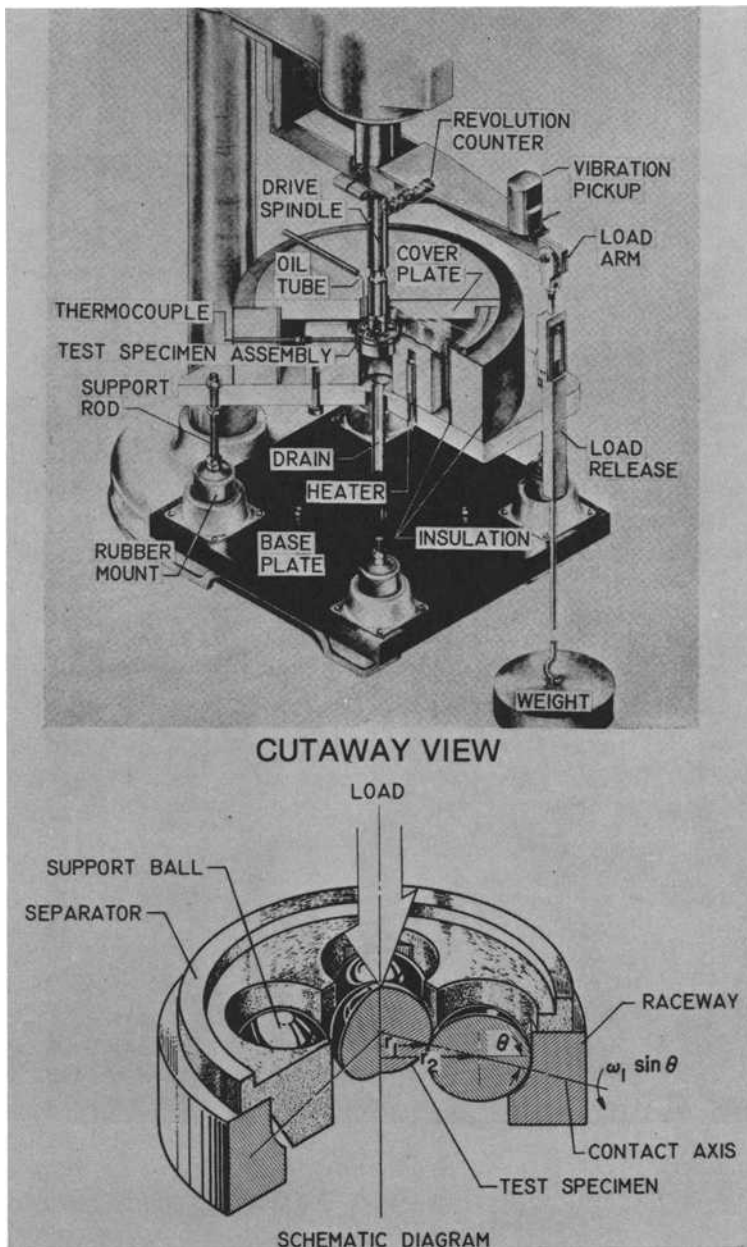
FIG. 11—*NASA five-ball fatigue tester.*
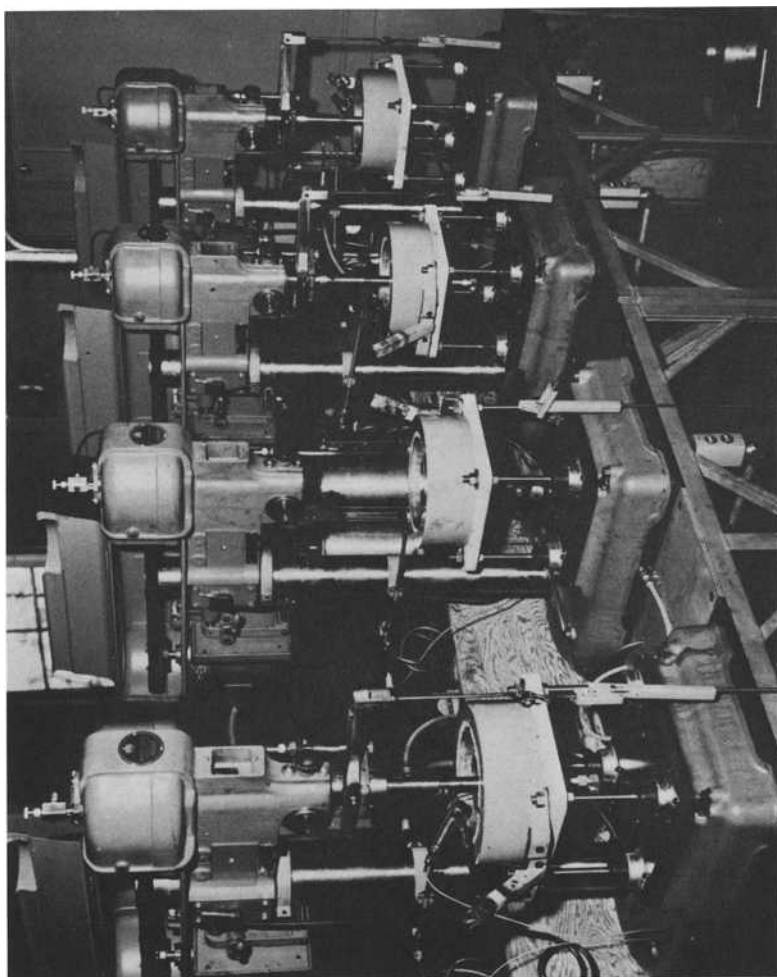
FIG. 12—*Five-ball fatigue testers.*

tions. Test groups should contain at least 10 units, with 20 or 30 units being preferable. Each specimen or bearing is tested to fatigue failure or until some high percentage has failed and all survivors have run longer than the failures.

The failures are then listed in ascending order of life, and a rank is assigned to each. The resulting data are then plotted on Weibull probability paper, as shown in Fig. 13, for example, which has life (in units of time or stress cycles) as the abscissa and sample percentage as the ordinate. Actually, the abscissa values are on a logarithmic scale, and the ordinate values are on a log–log scale. The best-fitting straight line is drawn through the points from which the slope and two lives of particular significance can be measured. The steeper the slope of the Weibull line, the less dispersion there is in the data. A slope of 1.0 to 1.5 is typical of rolling contact fatigue data. As a comparison, the slope of a line plotted from data which fit a normal (Gaussian) distribution is approximately 3.5. The points at which the Weibull line crosses the 10 and 50 percent ordinates, known as B_{10} and B_{50}, respectively, are used to compare endurance life data from different groups. Using textbook techniques [5], it is possible to arrive at confidence limits for the Weibull parameters. Basically, the steeper the Weibull slope and the more points involved in establishing the line, the greater confidence we have and the narrower the confidence band will be. Unless large amounts of data are available, an improvement of twofold is often required in order to be able to state with 90 percent confidence that any significant improvement exists between two population samples at the 50 percent life level.

As previously indicated, the rolling contact fatigue life of bearings is dependent on many interacting factors. Thus, when groups of bearings are to be tested and compared, it is important that the test groups be subjected to identical test conditions. Many times, testing of one single group (that is, new material) is performed, and the test results are compared with an established reference. When such evaluations are made, it is imperative to consider the effects of elastohydrodynamic lubrication and other operational factors so that a meaningful and genuine comparison can be executed.

To demonstrate the significance of environmental factors and their influence on bearing performance and test results, Fig. 14 illustrates the estimated life as a function of speed when ASME adjustment factors are employed. A standard 35-mm bore bearing, lubricated with SAE 20 oil at a temperature of 339 K (150°F) and radially loaded to 9 kN (2000 lb), is assumed. The L_{10} curve represents the calculated Anti-friction Bearings Manufacturers' Association (AFBMA) fatigue life which is a function of $(C/P)^3$, where C = basic load rating, and P = static equivalent radial load. Using the terminology of the ASME adjustment factor approach [2], the $D \cdot L_{10}$ and $D \cdot E \cdot L_{10}$ functions represent the estimated adjusted lives where the material factor, D, and processing factor, E, are selected as 2 and 3, respectively. As shown, the latter two functions are simply the displacement of the AFBMA life function to the right. The Z-type curve ($D \cdot E \cdot F \cdot L_{10}$)
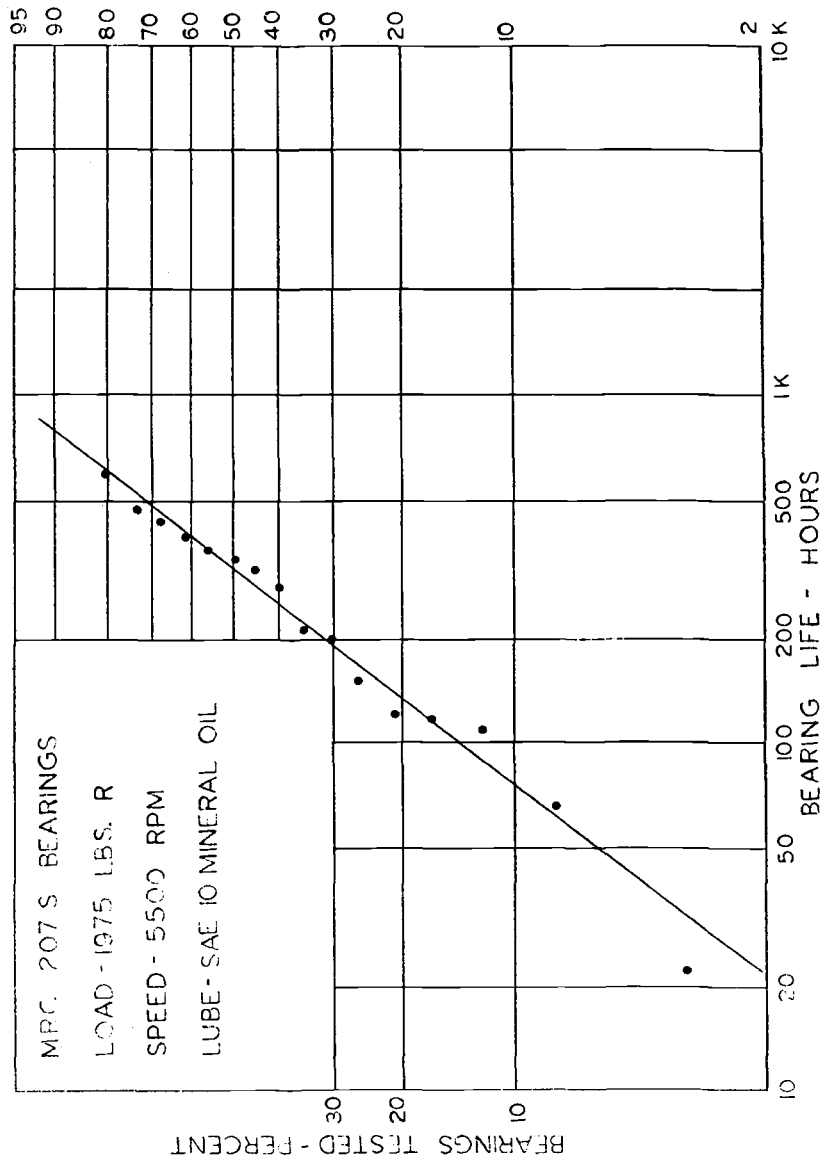
FIG. 13—*Weibull distribution of tested bearings.*
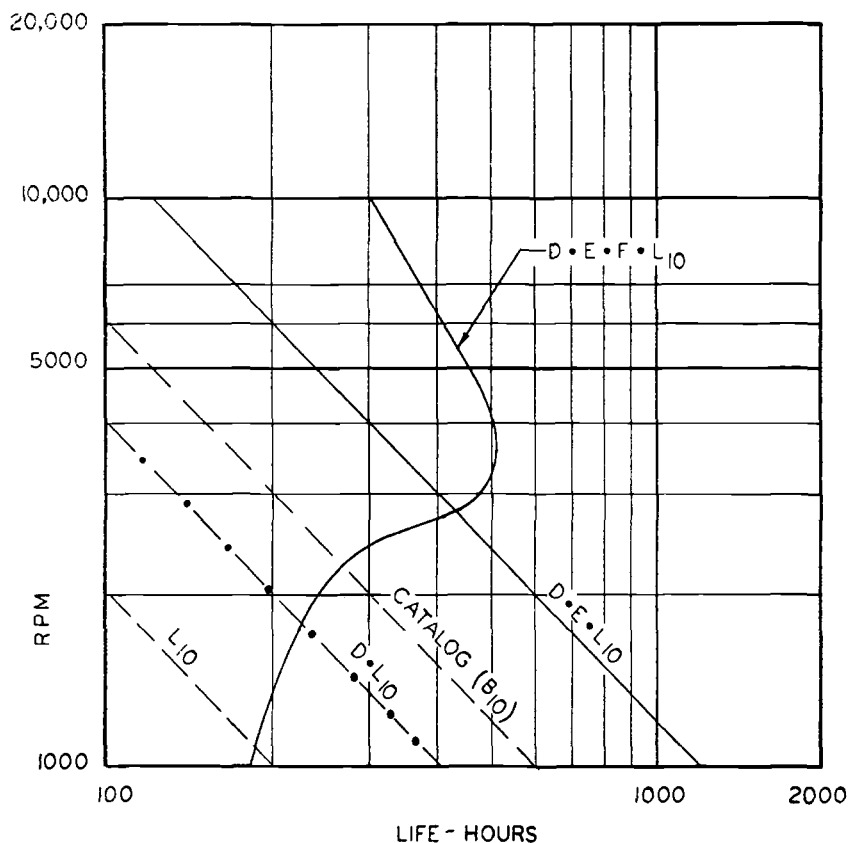
MRC 207S bearings
Load—9 kN (2000 lb) radial
Lubrication—SAE 20, each 339 K (150°F)
Factors:
    D = 2
    E = 3
    G = 1
    H = 1

FIG. 14—*Graph of the estimated life as a function of speed.*

represents further modification when considering the EHD or lubrication factor, *F*. As shown for this example, at speeds of above 2800 rpm, life improvement due to EHD effects is attained, whereas life reduction is realized at speeds below 2800 rpm because of a lack of adequate EHD lubrication. It becomes apparent from this illustration that when a bearing group, tested at an accelerated speed, is compared with some reference group, whose life basis reflects a lower speed condition or vise versa, there is a high probability

of erroneous comparison if one does not take into consideration the influence of EHD lubrication.

This deviation from linearity becomes most critical to programs intended to demonstrate required life and reliability in equipment in actual, practical use.

For example, we all have day-to-day contact with equipment which we expect to operate for at least 5 years, 24 h per day, 365 days per year, without failures. This represents a life of $365 \times 24 \times 5 = 43\ 800$ h.

If we accept 90 percent reliability, this means we must run a test group, such as 30 bearings, long enough to accumulate a statistically valid number of failures with which to plot the Weibull line. Experience dictates that we can expect enough such failures if we discontinue testing of individual bearings at something like four to five times the B_{10} life. For the example we have chosen, this means setting up each bearing to run $4 \times 43\ 800$ h, or 175 200—20 years!

If we build a battery of test machines to mount and run four bearings simultaneously, we will still need eight such machines to run 30 to 32 bearings in a 20-year time period. Faced with this impractical situation, it is natural to thrash around for a set of test conditions which will accelerate the testing.

We can increase speed, load, and, perhaps, temperature. To justify this approach, we had better have good data to prove we are not sliding into another failure mode, an operating mechanism, other than what the real-life application would invoke.

Conclusion

In an effort to achieve longer fatigue endurance lives, government agencies, steel companies, and bearing users and manufacturers continue to search for new materials, lubricants, and improved material and bearing processing variables. In pursuit of this goal, laboratory testing (and, ultimately, actual field testing) is required to investigate and evaluate life improvements.

For this evaluation to be effective the following three conditions are necessary:

1. Proper and adequate equipment must be employed.
2. Appropriate test procedures and conditions need to be implemented and controlled.
3. Test results need to be properly analyzed in order to realize significant and genuine evaluations.

References

[1] Anderson, W. J. and Zaretsky, E. V., "Rolling Element Bearings—A Review of the State-of-the-art," NASA TMX-71441, National Aeronautics and Space Administration, Cleveland, Ohio, 1973.

[2] Bamberger, E. N., Harris, T. A., Karmarsky, W. M., Moyer, C. A., Parker, R. J., Sherlock, J. J., and Zaretsky, E. V., *Life Adjustment Factors for Ball and Roller Bearings,* American Society of Mechanical Engineers, New York, 1971.
[3] Weibull, W., *Transactions of the American Society of Mechanical Engineers, Journal of Applied Machines,* Vol. 73, Sept. 1951, pp. 293-297.
[4] Parker, R. J. and Zaretsky, E. V., "Re-evaluation of the Stress-Life Relationship in Rolling-Element Bearings" NASA TND-6745, National Aeronautics and Space Administration, 1972.
[5] Lipson, C. and Sheth, N. J., *Statistical Design and Analysis of Engineering Experiments,* McGraw-Hill, New York, 1973.

G. B. Johnston,[1] T. Andersson,[1] E. v. Amerongen,[1]
and A. Voskamp[1]

Experience of Element and Full-Bearing Testing of Materials over Several Years

ABSTRACT: A review is made of several years' experience in determining quantitatively the influence of material and production processes on the fatigue performance of rolling element bearings. This experience covers bearing testing and two different "element" test methods—the radial ball bearing with cylindrical inner ring and the thrust ball bearing with flat washer methods.

So far, it has been difficult to correlate the results from those element tests with results obtained from full-bearing tests. This is due to the special features of the concentrated point contacts between the balls and nonconforming surfaces used in the element methods. These features are an apparently random groove formation and a material transformation and failure mode different from those of normal bearings.

KEY WORDS: fatigue tests, antifriction bearings, bearing steels, plastic deformation, statistical analysis.

Bearing manufacturers supply bearing users with quantitative information on the performance of their products in terms which are relevant to the products' performance in applications. Manufacturers must also have a knowledge of material influences on performance in order to select and recommend material. The classic failure mode of subsurface-originated rolling contact fatigue remains the basic factor determining the useful life of rolling bearings and is the main criterion for determining bearing size and permissible loads on bearings. Only under inferior conditions of lubrication and contamination do other failure modes come into play. Several purchasers of large quantities

[1] Manager of Mechanical Testing Department, statistician, research engineer, and researcher, respectively, SKF Engineering and Research Centre B. V., Nieuwegein, Netherlands.

of bearings also subject bearings to approval tests in which rolling contact fatigue endurance is evaluated.

These facts have to be borne in mind when judging the suitability of laboratory test methods for providing the performance data required and for selecting materials and processes. In the laboratory we must use accelerated tests either on full bearings or on simplified test elements to generate the required data in a reasonable time and at moderate cost.

This paper sums up the experience of several years using full-bearing tests and two "element" tests. Each method and our experience of it, viewed statistically, is discussed in turn, and a separate section deals with the function and fatigue mechanism of methods involving concentrated point contacts.

Full-Bearing Testing

Bearing testing has been carried out extensively over many years on various bearing types and under different conditions for monitoring the performance of our standard products, evaluating designs, and making specific material comparisons. For the purposes of this paper, we will consider only the testing of deep-groove ball bearings, (DGBBs), usually Type 6309, which is the method chosen when the determination of material factors is the object of the test program. Either the whole bearing, or the inner ring only, is made of the test material. The bearing is tested under pure radial load at $C/P = 2.16$ (where C is the bearing's dynamic load rating and P is the bearing load) and is run under conditions of full film lubrication with a very low level of contamination in the lubricating oil. The oil is free from additives except antifoam and antioxidant additives. The temperature is maintained within close limits. The condition of the bearings prior to the testing is closely controlled, and failure analysis is made after testing.

The DGBB is chosen since this bearing type is the least sensitive to minor geometrical deviations, and high-quality bearings can be made cheaply in volume production lines. To obtain a sufficiently narrow confidence interval on estimates of the L_{10} and Weibull slope, 60 bearings of any variant are tested, and the test is stopped, typically, when 10 bearings have spalled. The results are evaluated by an advanced computer program. Up to the late 1960s smaller numbers of bearings were tested per variant (for example, 30), which limited the discriminating power of the tests.

Due to improved quality of the inner ring the results of several series during the 1960s were much less precise owing to failure of the balls and outer rings. Today, these components have been improved, and inner ring failures are prevalent. The failure mode is subsurface-initiated spalling, and the raceways of unfailed bearings show virtually no signs of denting or distress. Normally, only one spall per ring is found, as shown in Fig. 1.

The results of DGBB tests can be related to the material's condition, and a statistical technique, described here, shows the discriminating power of the
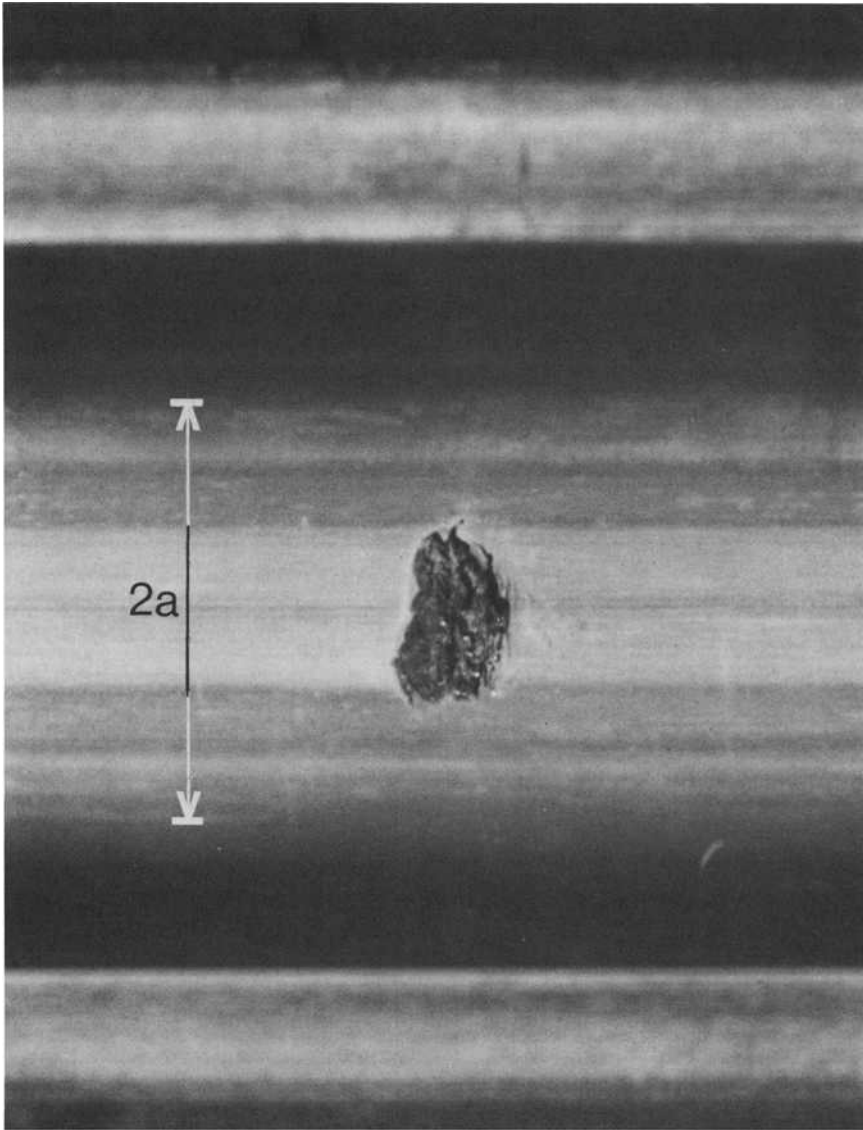
FIG. 1—*Typical spall in a DGBB inner ring.*

method, even with a sample size of 30 and a high proportion of failed bearings.

The results of all routine testing of standard steel quality over a given period have been pooled to provide a grand median L_{10} and Weibull slope. In Fig. 2 the results of each series are plotted in a Weibull diagram and com-
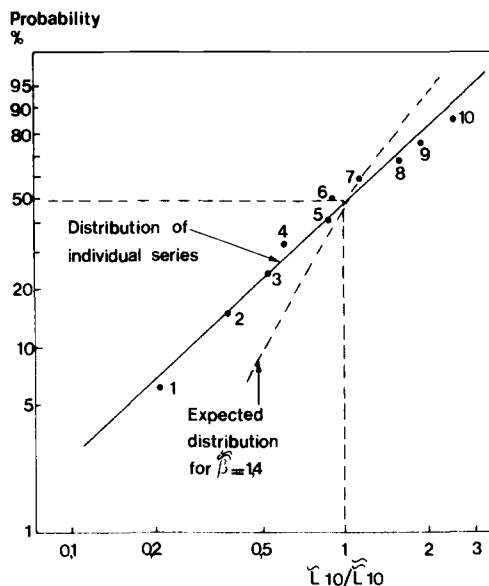
$\tilde{L}_{10}$ = estimated 10 percent life for individual series.

$\tilde{L}_{10}$ = median for all series.

$\tilde{\beta}$ = median Weibull slope for all series.

Strategy: Series size, 30; number of failures, 15.

FIG. 2—*Distribution of lives from 6309 full-bearing tests on ten different material batches.*

pared to with the theoretical distribution of L_{10} lives which would be observed by sampling from a population having an L_{10} and Weibull slope equal to the grand median values just mentioned and tested according to the same test strategy. The deviation in slope between the two curves shows the discriminating power.

Radial Ball Bearings with Cylindrical Inner Rings

As a consequence of the problems of ball and outer ring failures with DGBBs in the 1960s, an attempt was made to obtain results using a radial ball bearing with a cylindrical inner ring known as U6309. The bearing was run at a load giving $C/P = 2.16$, with full film lubrication and other conditions equivalent to those used in DGBB testing. Grooves formed on the inner ring and were considered acceptable up to a depth of 2 μm. Provision was made to locate the position of the housing in the axial direction. The initial results looked promising when care was taken to exclude rings with deep tracks, and only inner ring spalling occurred. In fact, a large proportion of rings had grooves deeper than 2 μm.

It was soon realized that contradictory results were being obtained and that, without further development, the method was unreliable. For example, Table 1 shows some inconsistencies.

By applying the same statistical technique of pooling results as was used for DGBBs, we can plot the graphs shown in Figs. 3 and 4. It can be seen that there is no difference between the distribution of the individual results and the distribution of the expected results. There is also less than a 10 percent difference between the grand medians for the two groups. We conclude that the method has no discriminating power and simply generates random numbers.

The failure mode differed from that normally found in DGBBs in that the spall extended beyond the contact width, and frequently several spalls or incipient spalls were found around the track. A typical spall is shown in Fig. 5.

Flat Washer Testing

For some years, flat washer testing was performed on the AO machine, which is equivalent to the well-known Unisteel machine. The latter has also been used when required by our steel customers. The AO method makes it possible to run a flat washer test on the side face of a 6309 inner ring.

Many contradictory results were obtained, and a last attempt was made in the early seventies to overcome all known disadvantages of the method. One of the main disadvantages was that the tracks showed many dents, which is not typical for DGBBs. The support spindle was changed to a high-speed, horizontal spindle on preloaded precision angular-contact ball bearings. A very clean lubricant supply was provided, and the grooved washer and balls were replaced after each spalling of the flat washer.

The improvements led to an absence of dents in the washer; but in a trial on two life series on 6309 inner rings, the lives obtained showed no significant differences, whereas those from the full-bearing tests on the same rings differed by a factor of 28.

It was common to find a surface crack extending over the full width of the

TABLE 1—*Comparison of the ranking of lives from full-bearing tests and U6309 tests.*[a]

Full-Bearing Test Results	Selected U6309 Test Results
$L_A < L_B$[b]	$L_B < L_A$ and $L_A < L_B$
$L_A < L_C$[b]	$L_C < L_A$
$L_A < L_D$[b]	$L_D < L_A$ and $L_A < L_D$
L (high residuals)	L (low residuals)
$<L$ (low residuals)	$<L$ (high residuals)
L (slack quenched)	L (correct structure)
$<L$ (correct structure)	$<L$ (slack quenched)

[a]Subscripts A through D refer to different steel-making processes.
[b]The rankings confirm expectations based on differences in inclusion ratings.
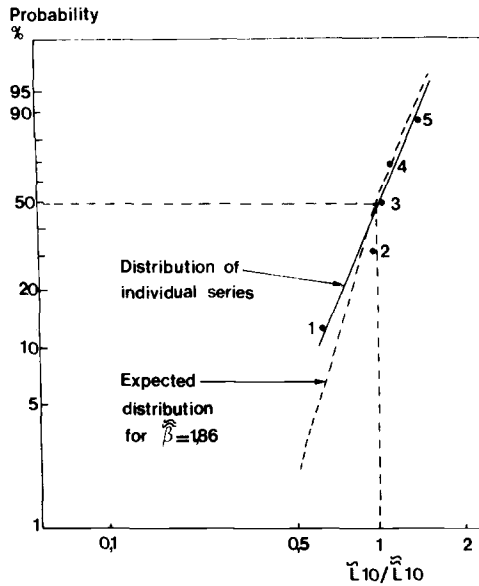
$\check{L}_{10}$ = estimated 10 percent life for individual series.

$\tilde{L}_{10}$ = median for all series.

$\tilde{\beta}$ = median Weibull slope for all series.

Strategy: Series size, 30; number of failures, 15.

FIG. 3—*Distribution of lives from U6309 test made in Laboratory A on five different material batches.*

contact area, which is not the case for DGBBs, where the whole spall only covers part of the contact width. Figure 6 shows a typical spall and one at an early stage. Scattered groove formation occurred as with the U6309 inner ring. Further, the Weibull distributions showed anomalies. Today flat washer testing is only performed on Unisteel at the request of specific steel customers.

Function and Fatigue Mechanism

To show how great the differences in contact conditions are between a 6309, a U6309, and a flat washer under life testing conditions, values for each are given in Fig. 7.

To investigate whether it was possible to improve the method using the U6309 test bearing, several aspects of the bearing were studied. The contact dimensions were checked using a footprint technique, which involved copper plating the ring with a layer about 0.1 μm thick. Footprints were taken on static bearings with a ball at the center of the loaded zone, on bearings in which the shaft was given a few degrees of rotation with a ball starting as before. Another group was run for 60 000 revolutions at speed. In the latter two
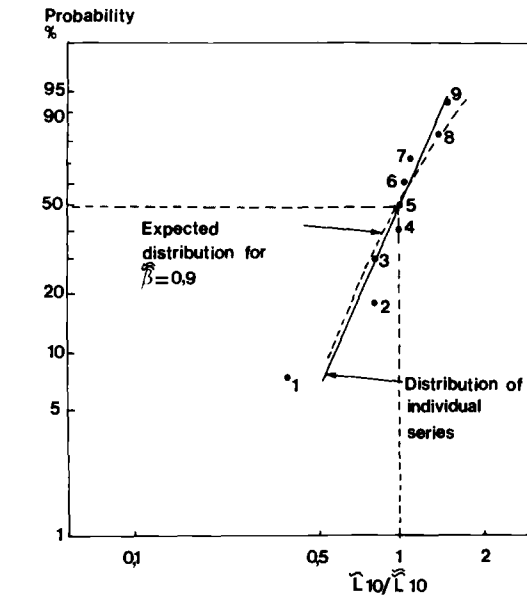
$\tilde{L}_{10}$ = estimated 10 percent life for individual series.

$\tilde{\tilde{L}}_{10}$ = median for all series.

$\tilde{\tilde{\beta}}$ = median Weibull slope for all series.

Strategy: Series size, 60; number of failures, 15.

FIG. 4—*Distribution of lives from U6309 tests made in Laboratory B on nine different material batches.*

cases, the groove profile was traced after loading. The results are shown in Fig. 8.

The profile shoulders correspond to the footprint width. This geometry has been investigated further by taking traces from many rings. Examples are shown in Fig. 9, and Figs. 10 and 11 show the dispersion. The groove width is greater than the calculated contact width, but is not as greatly dispersed as the depth. There is no correlation of groove depth with running time. To estimate whether these grooves would have a significant effect on bearing capacity, calculations were made of the radius at the bottom of the groove for each ring and are plotted against the groove depth in Fig. 12. The calculation was only made on "clean" traces and is estimated to be accurate within ±10 percent. It can be seen that even for shallow tracks a relatively small radius can be formed and that, for a given groove depth, a considerable variation in radius can occur. Figure 13 shows the influence of the radius on the basic rating life. It should be noted that many traces were not "clean," and in such cases the geometry is more complicated and much higher nominal stresses can occur.
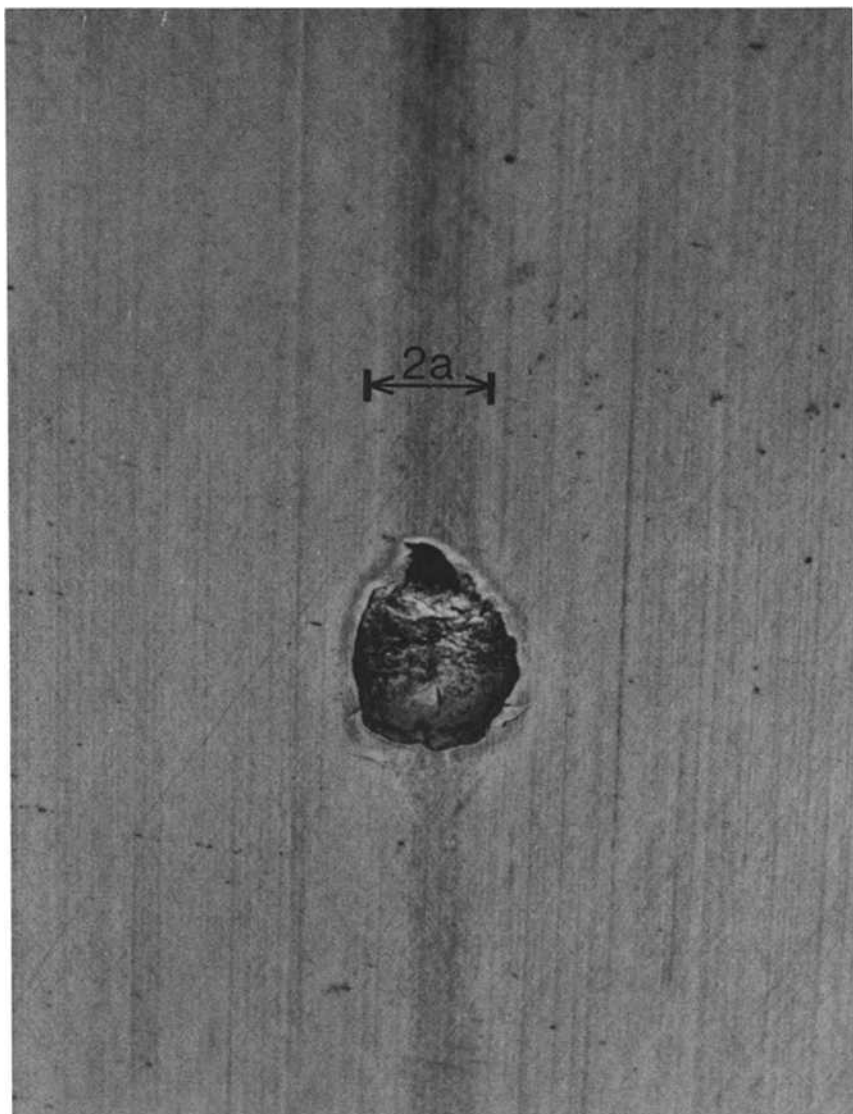
FIG. 5—*Typical spall in a U6309 inner ring.*
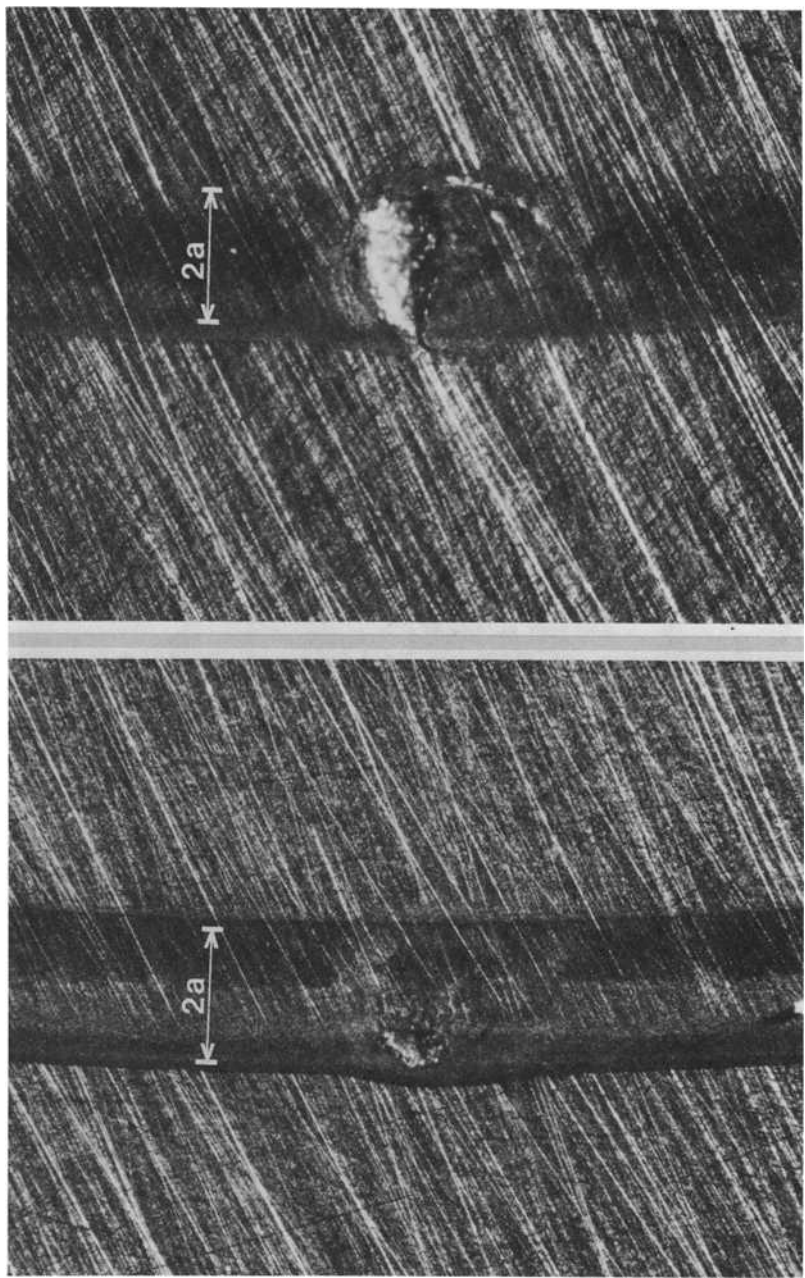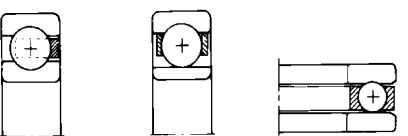
FIG. 6—*Spalls in an AO flat washer.*

Bearing type	6309	U6309	AO
Load (N)	18835	5390	$7500^{(1)}$
σ_0 (N/mm^2)$^{(2)}$	3275	5030	5000
$2\tau_0$ (mm)$^{(2)}$	1640	2230	2140
z_0 (mm)$^{(2)}$	0,188	0,181	0,12
a (mm)$^{(3)}$	4,0	0,58	0,34
b (mm)$^{(4)}$	0,38	0,48	0,34
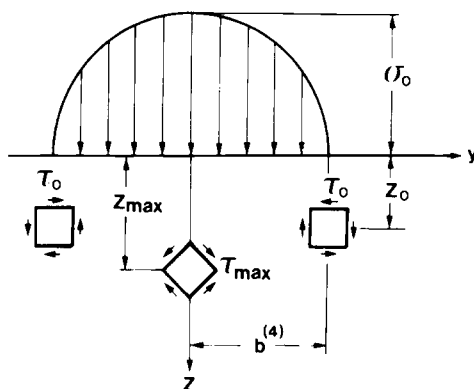
(1) on 6 balls
(2) see diagram
(3) major half-axis of contact ellipse
(4) minor half-axis of contact ellipse

FIG. 7—*Calculated contact conditions.*

This study of grooves shows that each individual ring creates its own geometry, which is far from the supposed simple geometry. Furthermore, the material in each ring is in a different state of plastic strain from that in other rings. The stress–strain condition depends on the yield properties rather than the fatigue properties of the material. Tests on material in a condition known to give inferior lives in DGBBs, such as a slack-quenched condition, gave superior lives in the U6309 bearings because of greater plastic deformation in spite of equivalent hardness. Yield properties at small amounts of plastic
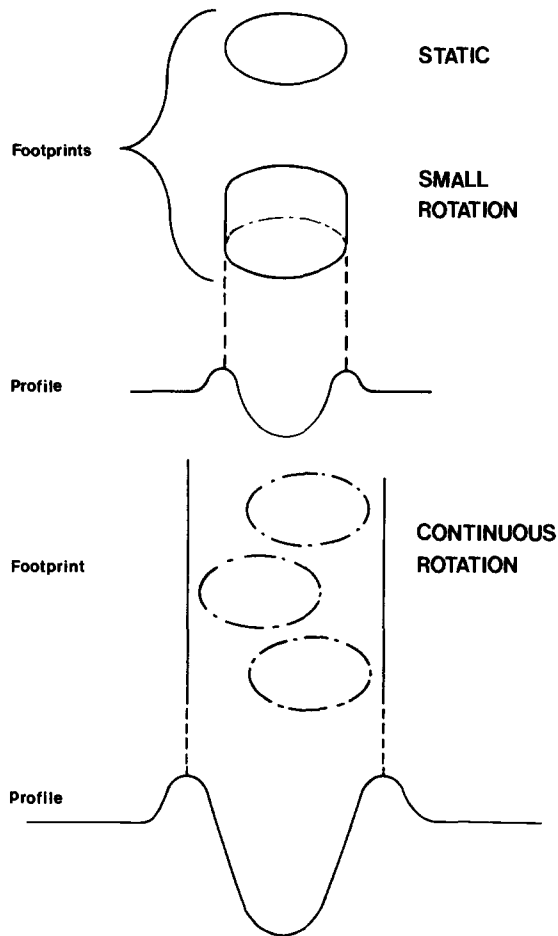
FIG. 8—*Footprints and profiles on a U6309 inner ring.*

strain seem to be more relevant in this context than hardness, which involves a very high degree of plastic strain under the indentor. The dispersion within a group indicates inhomogeneous yield properties.

A comparison has also been made between various aspects of the material condition in DGBBs and in the element methods. This covered development of the dark etching region (DER), retained austenite decay, and development of residual stresses. Results are shown in Table 2 and Figs. 14 and 15.

Part of this study, especially of groove formation, was also made on flat
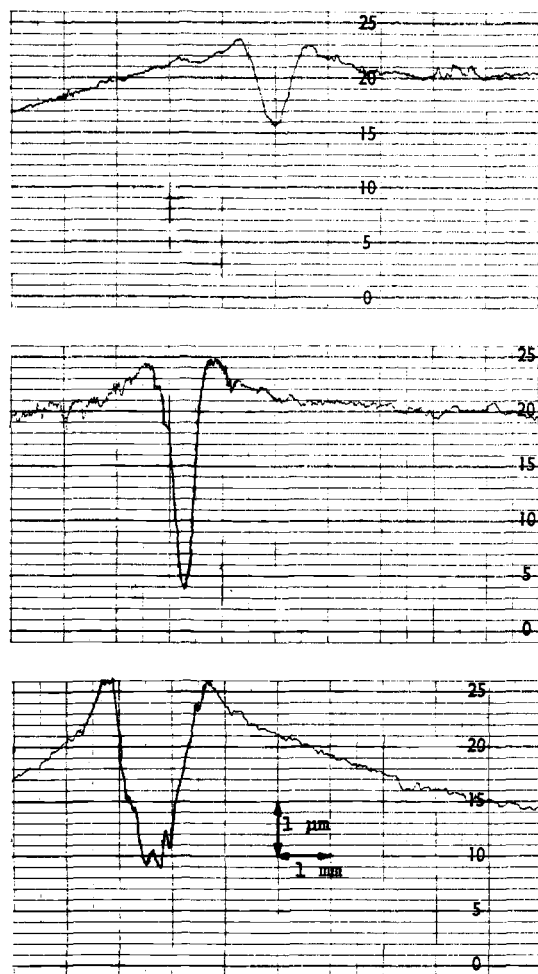
FIG. 9—*Examples of groove profile traces.*

washers, and the same features were found. It has been shown in another re-
search program that the looser the conformity for the same nominal stress,
the later the development of the material transformation will be. The less ex-
tensive material transformation in the U6309 is in line with this trend and
with the findings of Meredith and Sewell[2] who compared full bearings with
flat washers. We expect these findings to apply to all methods involving con-
centrated point contacts.

[2]Meredith, J. E. and Sewell, J. F. in *Bearing Steels: The Rating of Nonmetallic Inclusion,
ASTM STP 575,* American Society for Testing and Materials, Philadelphia, 1975, pp. 66-95.
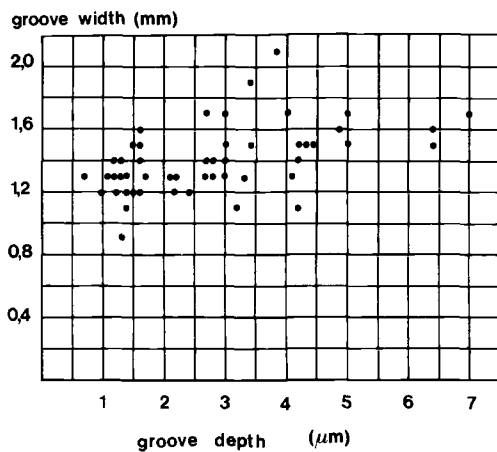
FIG. 10—*Scatter of the groove dimensions in U6309 inner rings*
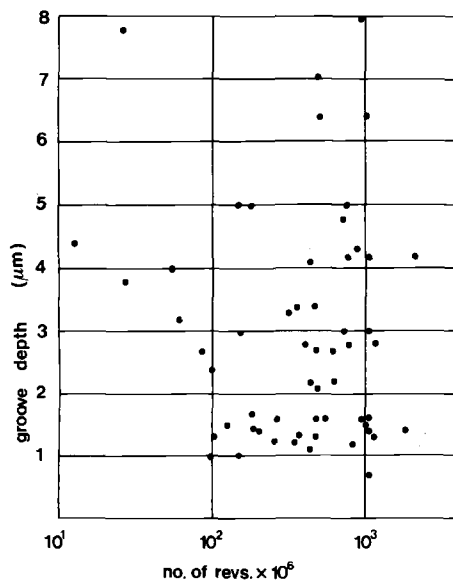
FIG. 11—*Scatter of the groove depths in U6309 inner rings.*
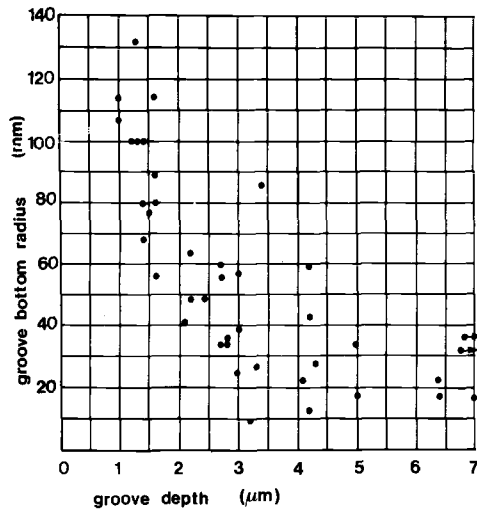
FIG. 12—*Groove bottom radius scatter in U6309 inner rings.*
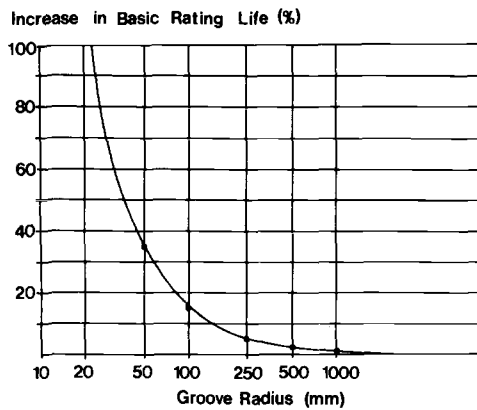
FIG. 13—*The calculated influence of the groove radius on the basic rating life for U6309 bearings.*

The authors conclude that the occurrence of material transformation is completely different from that occurring in DGBBs, and it is expected that this fact will influence the material fatigue properties and crack growth mechanism.

TABLE 2—*Occurrence of materials transformation.*

Feature	6309 Inner Ring	U6309 Inner Ring
Start of DER	after 50×10^6 revolutions; earlier the higher the load	much later (note: higher stress)
Frequency of DER observation	all life tests	not often seen; unpredictable
Phase changes[a]	always occur; can reach 100%; earlier at higher load	unpredictable never reaches 100%
Microplastic deformation[b]	develops faster the higher the load	less developed than 6309 inner rings for equivalent endurance

[a]Measured by quantitative austenite analysis.
[b]Measured by X-ray stress analysis.
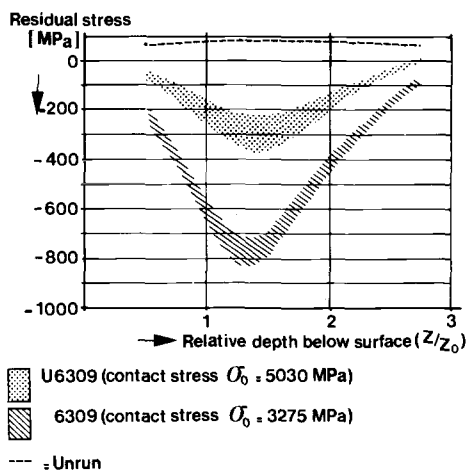
FIG. 14—*Residual stress changes in U6309 and 6309 bearings for the same endurance (10^9 revolutions at 55°C).*

Discussion

With, on the one hand, the confusing results from element testing and, on the other hand, the differences in function (especially groove formation), failure mode, and occurrence of material transformation between element tests and full-bearings tests, the authors had reason to doubt the value of element testing. In considering other element methods, we have not been able to find a test principle which appears to overcome the problems encountered. Several methods, such as rolling four-ball, three-ball/cone, and spin rigs (ball in cylinder), all involve concentrated point contacts. In addition to the prob-

Decomposition
of Retained Austenite (%)

Relative depth below surface (Z/Z_0)

U6309 (contact stress σ_0 = 5030 MPa)

6309 (contact stress σ_0 = 3275 MPa)
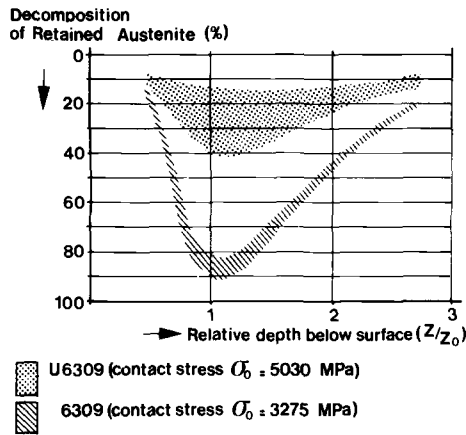
FIG. 15—*Retained austenite decay in U6309 and 6309 bearings for the same endurance (10^9 revolutions at 55°C).*

lems already mentioned, these methods also suffer the serious disadvantage of stressing only an extremely small volume of the material under evaluation.

As to the methods involving line contact, we do not consider these suitable since the actual stress situation is extremely sensitive to minute changes in the profiles of the surfaces in contact and the alignment of the rollers. The authors suggest that tests faster and cheaper than full-bearing tests may result from a more fundamental understanding of the various processes of crack initiation and propagation under conditions occurring in full bearings. Different processes will take place depending on the material used, design and the operating conditions.

Conclusions

In relation to the requirement of providing quantitative data on the influence of material on the rolling contact fatigue life of bearings in applications, we have concluded that:

1. The results from the two element test methods of which we have experience have not correlated well with full-bearing performance.

2. Tests on full bearings are currently required. Provided the failure mode is subsurface-initiated rolling contact fatigue and the test procedure is sound, the results will be valid.

3. If new, improved element test methods are considered for adoption, the results in terms of failure mode and life must agree with the results of tests on full bearings before extensive use is made of the methods.

4. New and valuable methods may arise from a better fundamental understanding of the process of crack initiation and propagation in rolling contact.

R. A. Hobbs[1]

A Four-Bearing Fatigue Life Test Rig

ABSTRACT: Specially developed machines for fatigue testing of rolling bearing steels frequently operate at stresses higher than the elastic limit, have contact conditions that differ widely from those in practice, or require special expensive test pieces. An alternative view is that standard bearings should be tested under conditions more closely simulating practice but at a stress level high enough to produce an acceptable test duration.

To this end, a rig containing four size 6208 bearings was developed and has been in use for many years. This paper describes the rig, which has recently been approved by the appropriate committee of the British Institute of Petroleum as a proposed test method for lubricating fluids and their effect on fatigue life. Normally, 32 bearings are tested to minimize the effects of scatter inherent in fatigue life testing, and since the rig is relatively inexpensive several may be run concurrently. When the sudden death technique is used, a test may be completed in less than 4 weeks.

The results from the rigs presented show the life improvement associated with vacuum-degassed steels manufactured by a basic electric arc process and the effects of oil film thickness on these lives. Other work exposes the severe life reduction caused by some fire-resistant fluids, and results from modified rigs at elevated temperatures are reported. The technique of sudden death testing is discussed, and results are presented which tend to confirm its validity.

KEY WORDS: rolling bearings, bearing test rig, sudden death tests, oil film thickness, fire-resistant fluids, fatigue life, bearing steels

From the bearing manufacturer's point of view, the object of fatigue testing rolling bearings is to improve the performance and cost-effectiveness of his products. Lubricant suppliers are concerned with the effect of lubricant formulations on fatigue life, and rigs may be used also for quality control or troubleshooting. For all of these purposes, the objective is to obtain an assessment of the fatigue life of a particular combination of material, lubricant, load, speed, and possibly temperature and generally to compare that life with those from other combinations.

Because of the wide scatter of life inherent in rolling contact fatigue, it is

---

[1]Principal applications engineer, RHP Industrial Bearings Ltd., Newark-on-Trent, Nottinghamshire, England.

essential to test a large number of samples, the required number depending on the ratio of lives from groups of samples being compared; for example, for an L_{10} life ratio of 2, 32 samples are required in each group to give about 90 percent confidence in the result at this level. Thus, in the interests of economy of time and money, the method of testing should use easily procured test samples, and the rig should be cheap to manufacture and maintain and should require a minimum of supervision during operation. The rig described in this paper fulfills these requirements by using a ball bearing in regular production and being of simple construction. However, even for a bearing manufacturer, the production of a small number of bearings in a special material can be expensive, so for material testing the rig tends to be regarded as a second line of testing following satisfactory development in screening tests on elemental rigs [1].[2] On the other hand, for lubricant testing for which standard bearings can be used, this rig may be considered as a first choice since manufacturers are able to supply large numbers of low-cost standard bearings and will probably agree to make them from one cast of material, thus ensuring a common basis of testing.

Design of Test Rig

A deep-groove ball bearing was chosen in preference to a roller bearing since it is less susceptible to the effects of misalignment, which are difficult to avoid in a heavily loaded rig. The basic design using four bearings was common to other bearing manufacturers [2]. It was decided to use only radial loading because combined axial and radial loading can cause tilting of the outer race since one housing has to float, and this seriously affects the load distribution among the balls. The rig was specifically designed for size 6208 C3 fit bearings, but it may also be used with NUP 208 ribbed cylindrical roller bearings. The present paper is concerned only with ball bearings.

A longitudinal section of the rig is shown in Fig. 1. The two inner bearings are fitted into a central housing into which is screwed the loading bolt, and the two outer bearings are located in the removable end housings. The bolt is loaded by two calibrated springs to 17 800 N (4 000 lb), that is, 8 900 N (2 000 lb) per bearing; springs were preferred to a dead-weight and lever system as they are not affected by local vibration, which may cause severe overloading with the latter system. The central housing is split on its horizontal center line to facilitate bearing removal. The calculated shaft slope at the outer bearings' seatings is 0.00026 rad. Each bearing is individually lubricated, and the drains are situated so that any debris from one bearing will not contaminate another. Lubrication is usually by drip or pump-metered feed, which is particularly useful when only limited quantities of a test fluid are available; however, a circulating oil feed may be used if preferred and has

---

[2]The italic numbers in brackets refer to the list of references appended to this paper.
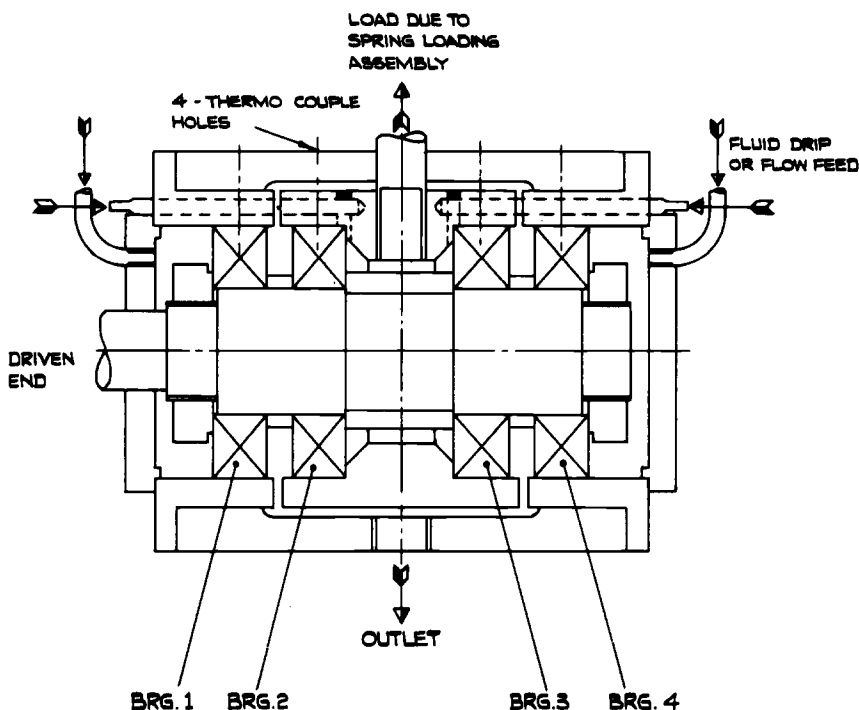
FIG. 1—A section of the four-bearing fatigue life test rig.

been used for some programs. The test speed is normally 3000 rpm, but with some fluids and greases the operating temperature has been found to be excessive (over 100°C), in which case the speed is reduced to 1000 rpm. The normal temperature, measured at the surface of the outer rings, is 60 to 80°C, depending on the oil flow rate, bath depth, and ambient temperature. Detection of failure is by accelerometers attached to the outer housings, which can be used for continuous monitoring and automatic shutdown if required. If this degree of sophistication is considered unnecessary, a hand-held vibration meter or audible detection may give satisfactory results. Normally the inner races have been the sites of pitting failures, which is consistent with the greater stress on this component.

The maximum hertz stress is 2 896 N/m² (420 000 psi), but because of plasticity the width of the track is increased by about 1.7 percent, which reduces it to 2 827 N/m² (410 000 psi) and the range of orthogonal shear stress to 1 427 N/m² (207 000 psi). Because these stresses are well within the shakedown limits, the test duration is minimized without causing serious plastic deformation, which may affect life since the process of fatigue failure is closely related to the mechanism of plastic deformation.

The author's laboratory has six rigs mounted on a single frame, and two similar assemblies have recently been installed at the Thornton Research Laboratories of the Royal Dutch Shell Group of Companies. A typical rig installation is shown in Fig. 2.

Test Technique

The usual practice is to test 32 bearings, as this gives a reasonable level of confidence: about 90 percent at the L_{10} level with a life ratio of 2:1, as previously mentioned. This number of bearings can also conveniently be tested by the sudden death technique using eight sets of four bearings and stopping each set after the first failure, the median value of the eight lowest lives being the $L_{15.9}$ value of the population [3]. Assuming the same Weibull slope for the population as for the eight lowest lives, an estimate of the population's L_{10} can be made. Alternatively, the unfailed bearings may be considered as suspensions and the results analyzed as a complete set of 32 bearings.

Results are analyzed using a PDP11 computer with the program printing out the L_{10} and L_{50} lives, Weibull slope, and also the 90 percent confidence limits on the lives. The basic Anti-Friction Bearings Manufacturers' Association (AFBMA) or International Organization for Standardization (ISO) L_{10} life of the size 6208 bearings at 3000 rpm is 125 h (equal to 22.5×10^6 revolutions), but assuming a high-quality steel with good elastohydrodynamic lubrication (EHL), an L_{10} life of up to 313 h (56.3×10^6 revolutions) may be expected. Based on this figure, the overall test duration for eight sets of four bearings is 500 to 700 h. This condition can be achieved by starting six rigs simultaneously and replacing two sets after the first two failures occur.

Results and Discussions

Validity of the Sudden Death Technique

One of the early investigations was to verify the sudden death (SD) testing technique. Twenty-four sets of four bearings were first tested by this method, and all four bearings were removed after the first failure; afterwards, they were all run to failure, as far as possible. The lives predicted by the SD test were $L_{10} = 52 \times 10^6$ revolutions and $L_{50} = 150 \times 10^6$ revolutions, which compared favorably with those from the complete runout of 48 and 170×10^6 revolutions, respectively. The Weibull plots are shown in Fig. 3.

The results from eight sets of four bearings were less accurate, but the SD L_{10} results were within 25 percent of the complete runout results, which was generally considered adequate in view of the savings. The time and cost of the sudden death tests were about one third of those of the runout.
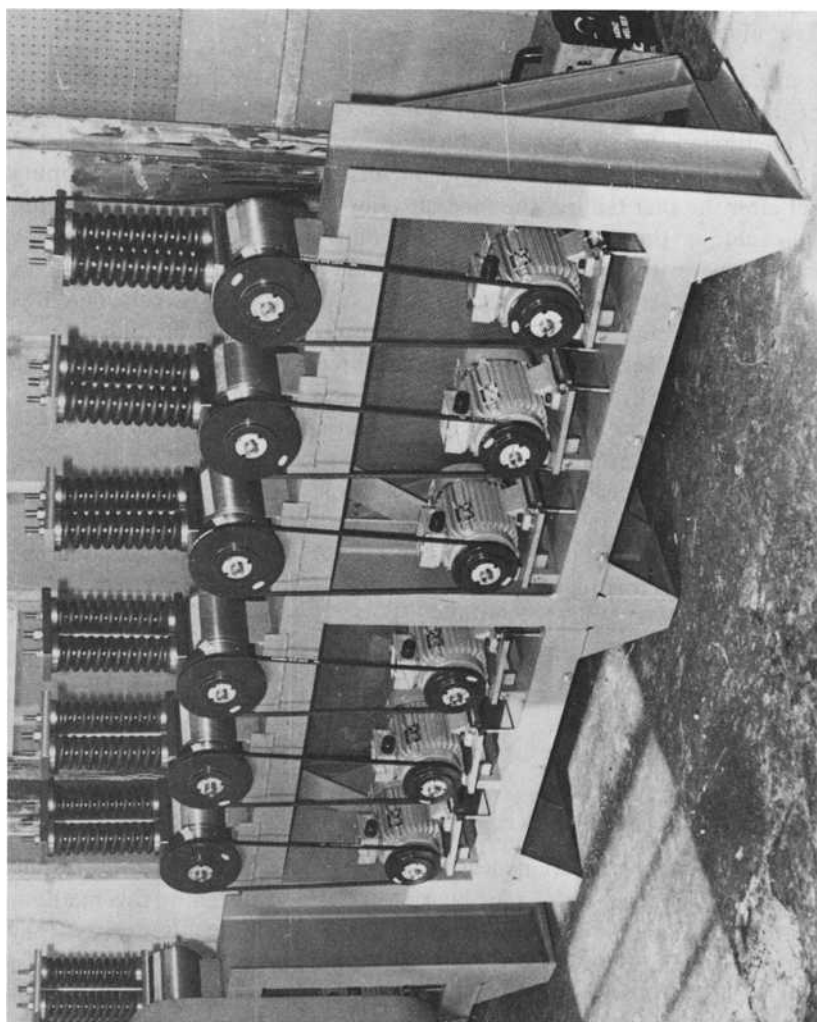
FIG. 2—A group of six test rigs.
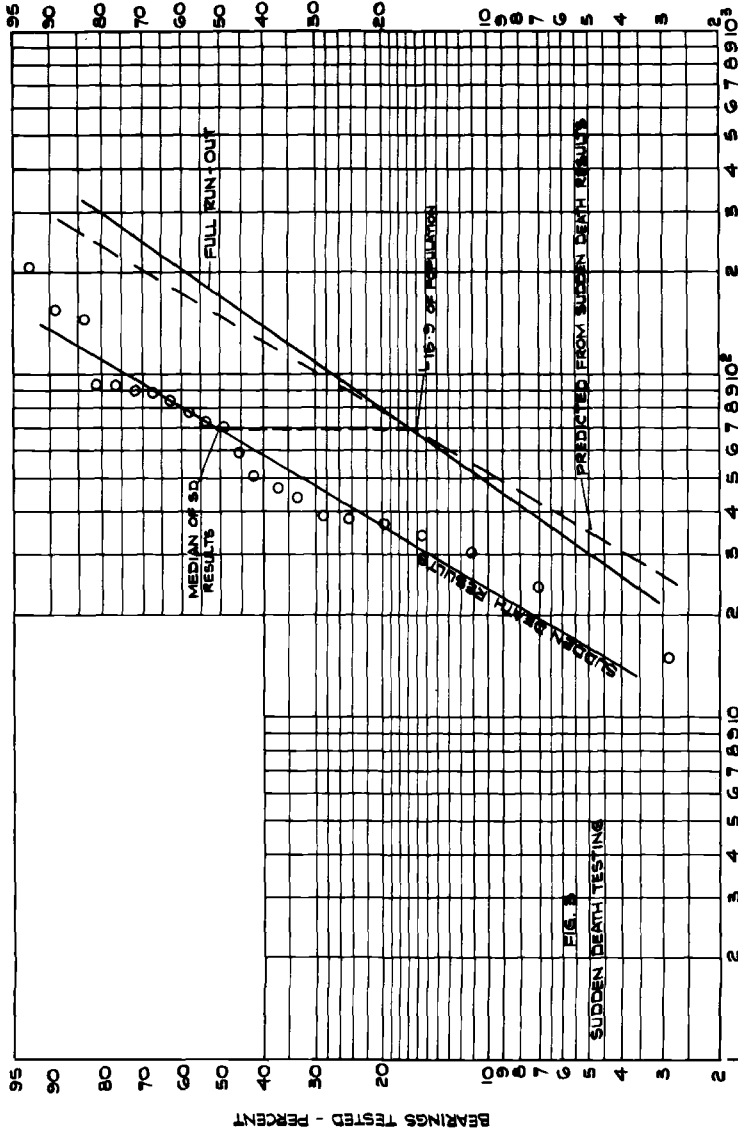
FIG. 3.—*Comparison of sudden death and complete runout tests.*

Repeatability

It was clearly necessary to establish that the lives produced by the six rigs in use were similar and that no systematic bias due to the rigs or their environment could be detected. Acknowledging the wide scatter of life inherent in rolling fatigue, it was not anticipated that the mean lives from each rig would be very close, and this proved to be the case. The first failures from each set of four bearings from a long series of tests on vacuum-degassed steels are given in Table 1 in ascending life order. The mean lives ranged from 74.4 to 122 $\times$ 10^6 revolutions, but statistical analysis showed that there was greater variance within rigs than between rigs and that the difference between the rigs did not indicate any significant effect due to the rigs.

The ability of the rigs to produce repeatable results, provided sufficient samples are tested, was thus demonstrated. However, care is necessary to ensure that they are properly maintained. In particular, it was found that bearing seatings became worn as a result of fretting. An ovality of up to 0.1 mm was usually acceptable as this maintained the shaft alignment within the permissible limits of bearing misalignment.

Material and Lubrication Factor (a_2a_3)

Vacuum Degassed and Nondegassed Steels—The rig was developed about 20 years ago, originally for the purpose of investigating the effects of various steel-making processes on fatigue life. At that time, the EHL theory had not been fully developed, but it was recognized that a high-viscosity oil improved life. For this reason a paraffinic high-viscosity mineral oil, DERD 2472B/O (MIL-L-6082D), was selected as the basic oil for comparative testing; it has a

TABLE 1—*Sudden death lives from six rigs.*

	Lives, millions of revolutions					
	Rig A	Rig B	Rig C	Rig D	Rig E	Rig F
	36.1	14.8	23.8	33.8	21.6	46.0
	50.3	21.6	26.6	48.1	26.3	51.1
	65.0	41.8	40.3	49.7	30.2	90.0
	122.0	66.5	50.7	68.0	46.8	107.0
	145.0	70.5	57.6	93.6	57.2	109.0
	158.0	80.0	75.0	111.0	167.0	172.0
		80.6	98.7	213.0	172.0	279.0
		112.0	108.0	222.0		
		118.0	123.0	230.0		
		133.0	170.0			
		148.0	208.0			
Means	96.1	80.6	89.2	118.8	74.4	122.0

viscosity of 68×10^{-3} N·s/m^2 (78 cSt) at 60°C and a minimum viscosity index of 95. The bearing material was through-hardened high-carbon–chromium steel (similar to the composition of SAE 52100) hardened to 62 to 64 HRC.

At a speed of 3000 rpm and a temperature of 60 to 80°C, the Λ value was between 3 and 4, thus ensuring subsurface-initiated failures and the maximum obtainable fatigue life ($\Lambda = h/R$, oil film thickness/surface roughness).

To establish a basis for future comparison, three groups of 32 bearings from each of two casts of nondegassed material were tested, running each group to failure as far as possible. Table 2 presents the results from these six groups.

The mean L_{10} life of the two casts was 17.65×10^6 revolutions, and the 90 percent confidence limits of the 192 samples were 14.2 and 22.1×10^6 revolutions. It will be noted that the lowest result falls just outside these limits. However, statistical tests showed that the difference between the combined L_{10} lives of each cast, 18.3 and 17.0×10^6 revolutions, was insignificant.

After examining many modifications to the steel-making practice, all with only marginal improvements of fatigue life, vacuum-degassed steel became available and tests immediately showed a very significant improvement. The results from groups of bearings made from six different casts are given in Table 3. They are estimated from eight or nine sets of four bearings in each group, tested by the sudden death method.

The six casts were from various sizes of melt produced by different makers. Group 1, showing the lowest lives, contained nondegassed steel balls, and the proportion of ball failures was abnormally high. Analysis of variance shows that the six groups can be considered homogeneous, and thus the figures for the combined results represent a range of steel suppliers' products. The improvement over nondegassed steel is by a factor of 3.5 at the L_{10} level, but only 2.0 at the L_{50} level because of the differences of slope. These values are in agreement with other published results [4-6], but for practical purposes, to take into

TABLE 2—*Fatigue lives from nondegassed steel bearings, 1960.*

		Lives, millions of revolutions			
Cast No.	Group No.	L_{10}	L_{50}	L_{10} 90% Confidence Limits	Slope
1	1	15.4	43.9	9.2 to 25.7	1.8
	2	18.7	77.1	9.3 to 37.4	1.33
	3	21.5	84.0	10.7 to 42.9	1.38
	combined	18.3	66.0	12.7 to 26.4	1.47
2	1	20.7	65.1	11.8 to 36.3	1.64
	2	13.5	79.1	5.7 to 32.1	1.07
	3	16.3	89.0	6.9 to 38.5	1.11
	combined	17.0	77.4	11.1 to 26.3	1.25

TABLE 3—*Fatigue lives from vacuum-degassed steel bearings, 1967.*

Group No.	L_{10}	L_{50}	L_{10} 90% Confidence Limits	Slope
1	41	132	23 to 72.6	1.60
2	68	225	41.5 to 110	1.56
3	70	280	35.7 to 136	1.35
4	77	350	40 to 149	1.24
5	60.2	188	34.5 to 105	1.65
6	63.6	185	35 to 115	1.76
Combined	62.0	227	40.3 to 95	1.44

account other types of bearings, a value of 2.5 is used for a_2a_3 in the modified AFBMA and ISO formula $L_{10a} = a_2a_3 (C/P)^3$ when full EHL is obtained.

Oil Film Thickness—It was stated in the last section that the value of a_2a_3 was taken as 2.5 for vacuum-degassed steel when full EHL was achieved (that is, when Λ exceeded 3). The effect of changing the value of Λ was examined in another series of tests on both vacuum-degassed and nondegassed steels. Film thickness was calculated by the method proposed by Archard and Cowking [7], which for 6208 bearings can be reduced to

$$h = 7.05 \times 10^{-3} (\alpha N \eta_0)^{0.74} \text{ m}$$

where

α = the pressure coefficient of viscosity in square metres per newton;
η_0 = the absolute lubricant viscosity in N·s/m^2; and
N = the rotational speed in revolutions per minute.

Combined surface roughness was measured as a center line average (CLA) value of 0.13 to 0.18 $\times$ 10^{-6} m and was the same for all tests.

The Λ value was varied by changing the values of η_0 and N, with slight changes of α, N being either 3000 or 1000 rpm.

The results are shown in Fig. 4 [8]. Oil A was the high-viscosity oil previously referred to, B was a medium-viscosity general purpose mineral oil containing antioxidation, antirust, and antifoaming additives, and C and D were lower-viscosity versions of B.

It is clear that the reduction of Λ produced a serious loss of fatigue life, particularly with vacuum-degassed steel when Λ was less than 2. Under these conditions a high proportion of ball pitting failures was produced, and ring spalls consisted of numerous surface cracks compared with the single deep subsurface-initiated cracks associated with higher values of Λ.

With vacuum-degassed steel and full EHL, $a_2a_3 = 2.5$, but under boundary lubrication conditions it was shown that its value could be as low as 0.6.
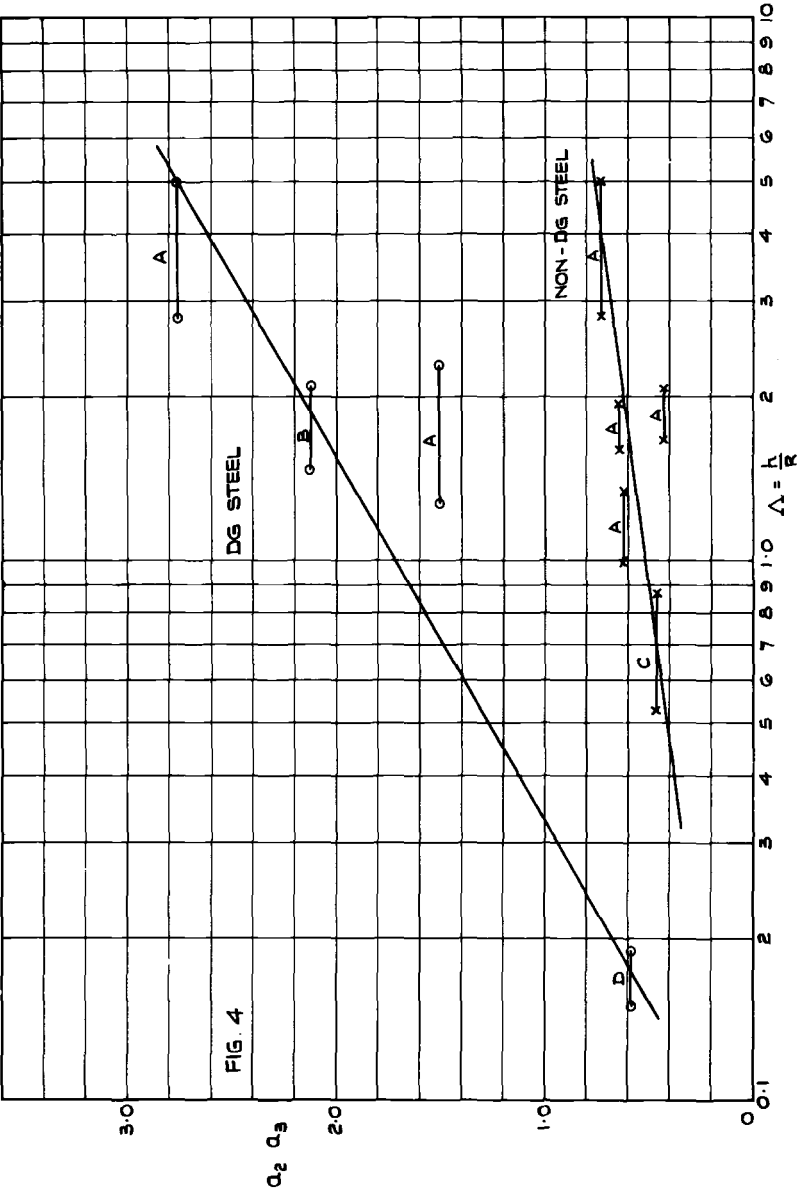
FIG 4—L_{10} lives of vacuum-degassed and nondegassed steels in mineral oil.

When this occurred, the fatigue life of vacuum-degassed steel was little better than that of nondegassed material, and its advantages could not be realized.

Similar findings have been reported by several other investigators [5,6,9,10], which eventually led to the inclusion of a_2 and a_3 factors in the 1977 revision of ISO 281/1, Rolling Bearings—Dynamic Load Ratings and Rating Life— Part 1.

Fire-Resistant Fluids. Further Life Factors—The effects of several fire-resistant fluids on bearing fatigue life have been reported in Ref 8 where results using this rig were presented. Since then other fluids have been tested, and the results are summarized in Table 4 for vacuum-degassed steel. These tests were performed at 1000 rpm to avoid high temperatures, which cause loss of some of the water-containing fluids by evaporation.

The water-containing fluids Types A, B, and C produced extremely low lives, and this pattern has been repeated in tests on flat washers. The cause of the early failures has been attributed to several mechanisms, such as surface corrosion, electrochemical corrosion, and hydrogen embrittlement. Hydrogen may be generated at the metal surfaces by the interaction of water and oxygen, and tests under controlled conditions in a four-ball machine have shown that these can have a very adverse effect on fatigue life [11]. Diffusion of the atomic hydrogen into high-stress areas may be reduced by additives to the lubricating fluids or by modification of the structure of the bearing steel. More recent work using a development Type A fluid with rings heat-treated to have a lower bainite microstructure has produced lives approaching those obtained with the high-viscosity oil [12].

These and other similar results have been used in the preparation of a method of estimating life in fire-resistant fluids [13,14]. In Refs 13 and 14 the basic life equation is modified to

$$L_{10} = \left(\frac{C}{KP} \right)^n$$

and values of K and n are presented for the four types of fire-resistant fluids.

TABLE 4—*Lives of vacuum-degassed steel bearings in fire-resistant fluids.*

| | Lives, millions of revolutions | | |
Lubricant	L_{10}	L_{50}	Slope
High-viscosity oil	34	167	1.19
Hydraulic mineral oil	13.9	63	1.26
5% oil in water (Type A)	5.6	12	2.48
40% water in oil (Type B)	7.1	24	1.54
40/60 water/glycol (Type C)	1.7	3.1	3.08
Phosphate ester (Type D)	20.2	121	1.06

Effect of Elevated Operating Temperature—Applications frequently arise in which bearings are required to operate at elevated temperatures. Standard practice at RHP Bearings Ltd. is to temper bearing rings at around 175°C and rolling elements at a slightly lower temperature. For stability, the upper operating temperature is usually restricted to 125°C to avoid dimensional changes which could occur after prolonged soaking at higher temperatures. For applications above 125°C, higher tempering temperatures are usually adopted.

To assess the effect of higher operating temperature on the fatigue life of standard tempered bearings, three rigs were electrically heated and tests were performed at 120 and 150°C. Eight sets of four bearings manufactured from vacuum-degassed steel were tested at each temperature, lubricated by an aviation gas turbine oil circulated through the rigs. The usual speed and load were used (3000 rpm and 8900 N). The results are shown in Table 5 together with lives at 60 to 80°C.

There is apparently a considerable loss of life at the higher temperatures. However, this can be attributed mostly to the reduced oil film thickness, the bulk oil temperatures giving Λ values of approximately 2 and 0.2 at 120 and 150°C operating temperatures, respectively. As shown in Fig. 4, these cause life reductions of a similar order as those in Table 5. For this reason, the a_2a_3 factor is maintained at a value of 2.5 up to 150°C, given full EHL.

Conclusion

It has been shown that the simple rig design is capable of producing fatigue life test results under a range of operating conditions. The contact parameters closely simulated normal practice, and the test duration is not excessive. The results obtained have been confirmed by other workers in the field, and by general practical experience in laboratory tests on full-scale machines and engineering applications. Life factors based on them are now in general use in manufacturers' catalogs and national and international standards.

For these reasons the rig was selected by the British Institute of Petroleum to be used in a proposed test method [15]. It is being given further considera-

TABLE 5—*Reduction of fatigue life at elevated temperatures.*

Operating Temperature, deg Celsius	Lives, millions of revolutions		
	L_{10}	L_{50}	Slope
60 to 80	62	227	1.44
120	49	210	1.28
150	16	60	1.40

tion for testing cylindrical roller bearings, and it is anticipated that the rig's use for testing lubricants, including greases, will be extended.

References

[1] Hollax, G. E., Hampshire, J. M., and Nash, J. V., this publication, pp. 46–66.
[2] Barish, T., *Fatigue Testing Machines for Ball and Roller Bearings, ASTM Proceedings,* Vol. 46, American Society for Testing and Materials, Philadelphia, 1946.
[3] Johnson, L. G., *The Statistical Treatment of Fatigue Experiments,* Elsevier, New York, 1964.
[4] Bamberger, E. N., Harris, T. A., Kacmarzky, W. M., Moyer, C. A., Parker, R. J., Sherlock, J. J., and Zaretsky, E. V., *Life Adjustment Factors for Ball and Roller Bearings. An Engineering Design Guide,* American Society of Mechanical Engineers, 1971.
[5] Vaessen, G. H. G. and De Gee, A. W. J., *Elastohydrodynamic Lubrication 1972 Symposium,* Paper No. C7/72, Institute of Mechanical Engineers, Leeds, 1972, pp. 40–44.
[6] Liu, J. Y., Tallian, T. E., and McCool, J. I., *A.S.L.E. Transactions,* Vol. 18, 1974, pp. 144–152.
[7] Archard, J. F. and Cowking, E. W., Elastohydrodynamic Lubrication Symposium, *Proceedings of the Institution of Mechanical Engineers,* Vol. 180, Part 3B, 1965, pp. 17–26.
[8] Hobbs, R. A. *Elastohydrodynamic Lubrication 1972 Symposium,* Paper No. C1/72, Institution of Mechanical Engineers, Leeds, 1972, pp. 1–4.
[9] Popinceanu, N. G., Grafitanu, M. D., Cretu, S. S., Diaconescu, E. N., and Hostiuc, L. T., *Wear,* Vol. 45, 1977, p. 17–32.
[10] Lorösch, H. K., *Ball and Roller Bearing Engineering,* 1976, p. 1.
[11] Ciruna, J. A. and Szieleit, H. J., *Wear,* Vol. 24, 1973, p. 107.
[12] Hollox, G. E., Hobbs, R. A., and Hampshire, J. M., *Wear,* Vol. 68, 1981, pp. 229–240.
[13] "Guidelines for Derating the Life of Ball Bearings when Used with Fire-Resistant Fluids," AHEM Publ. S5865, Association of Hydraulic Equipment Manufacturers Limited, London, 1977.
[14] Kenny, P., Smith, J. D., and March, C. N., *Performance Testing of Hydraulic Fluids,* Institute of Petroleum Symposium, 1978, Chapter 33.
[15] *IP Handbook 1981,* British Institute of Petroleum, London, 1981.

P. R. Eastaugh[1]

Use of Accelerated Tests to Establish the Lubricant–Steel Interaction on Bearing Fatigue Life

ABSTRACT: For several years the Royal Navy has used hydraulic fluids which differ significantly from the lubricants used by bearing manufacturers when establishing load to life characteristics. The performance of relevant fluids has been assessed in conjunction with standard EN31 (AISI 52100) steel test specimens using two standard test machines (the rolling four-ball and Unisteel) and a rolling contact fatigue rig designed and built in the author's department.

In addition, a high speed rolling four-ball machine is being commissioned. The test results show that wide variations in performance occur with different lubricant–material combinations, and it is necessary to run tests at several different levels of severity in order to predict service performance reliably. The standard rolling four-ball test did not give good correlation with other test data, and a metallurgical investigation of some failed specimens suggests that an abnormal failure mechanism could be operating.

KEY WORDS: antifriction bearings, fatigue life, lubricants, steels, accelerated tests, test equipment, bearing steels

Since the late 1960s the Chemistry and Petroleum Technology Department, National Gas Turbine Establishment (formerly the Admiralty Oil Laboratory), has been interested in evaluating the effects of different lubricant–material combinations on the fatigue life of rolling contact bearings. Since our prime function is to advise on suitable lubricants and fuels for use by the Royal Navy (RN), it is perhaps not surprising that we have concentrated on comparing the effect of different lubricants using a standard EN31 steel (equiva-

[1]Deputy head of Mechanical Evaluation Section, National Gas Turbine Establishment, Chemistry and Petroleum Technology Department, Pyestock, Farnborough, Hampshire, England GU14 0LS.

lent to AISI 52100). Although most of the test machines used were originally developed for steel tests rather than lubricant tests, the designs of the tests are obviously similar regardless of whether the primary interest is in steel or the lubricant.

Our initial work arose from the need to provide a lubricant for submarine hydraulic systems which would permit contamination with up to 10 percent seawater without disastrous consequences. A conventional mineral oil hydraulic fluid will not mix with seawater. As a result, the water is likely to cause corrosion of the pipes and other parts of the hydraulic system. Also, when a "slug" of water passes through a hydraulic pump or motor, it can cause rapid failure of the equipment. The emulsifying hydraulic fluid, designated OX-30, has additives to enhance the corrosion protection properties and also to form stable emulsions with up to 10 percent seawater. Since it is known that additives can have a detrimental effect on fatigue life, it was thought necessary to have tests which could evaluate this aspect of performance.

More recently we have been evaluating water-based fire-resistant hydraulic fluids for possible use by the RN. Because these are known to have detrimental effects on bearing fatigue life, a program of work was designed to show the magnitude of this effect for the fluids of interest. This paper discusses the results of tests on both mineral oil and fire-resistant fluids.[2]

Test Procedures

Four different types of test machine are used: a standard rolling four-ball machine, a Plint high-speed four-ball machine, the Admiralty Oil Laboratory (AOL) vertical rolling contact fatigue rig, and Unisteel machines. The Institute of Petroleum (IP) has published standard test methods[3] for the first and last of these machines: IP 300—Rolling Contact Fatigue Tests for Fluids in a Modified Four-Ball Machine and IP 305—The Assessment of Lubricants by Measurement of Their Effect on the Rolling Fatigue Resistance of Bearing Steel Using the Unisteel Machine. The test strategy is similar in both methods and is used for all four types of machine. The test bearing is run at constant load and speed and flooded with a supply of the test lubricant, which is changed continuously. When a failure occurs, the increase in vibration is detected by an accelerometer and used to activate a shutdown device which stops both the test machine and an elapsed time clock. A number of repeat runs (normally between 10 and 30) are carried out under identical conditions, and the results are processed using Weibull analysis to give estimates of the L_{10} and L_{50} lives and the Weibull slope.

---

[2]The views expressed in this paper are those of the author and do not necessarily represent those of the Ministry of Defense.

[3]*Institute of Petroleum Standards for Petroleum and Its Products: Part 1, Methods for Analysis and Testing,* Heyden and Son Ltd., London, published annually.

When running fatigue tests, we are, of course, faced with a classic dilemma: we can either choose a cheap, quick test which will inevitably operate under very high stress and so have a doubtful correlation with practice, or we can use a lower-stress, more realistic test which takes a lot longer and is more expensive. The four machines mentioned in the previous paragraph enable us to have a reasonable choice in deciding which of these conflicting requirements should have priority. The severity of operation can be indicated simply by the value of the factor C/P, where C is the dynamic capacity of the bearing and P the applied load. The range of C/P values over which each machine is normally operated is given in Table 1. The machines are described briefly in the following sections, and more detailed descriptions are available elsewhere.

Rolling Four-Ball Machine

This was the first rolling contact fatigue test machine used by us, and it is well established for use in testing both steels and lubricants [1,2].[4] The test specimen consists of four 12.7-mm (½-in.) diameter balls in a pyramidal configuration (Figs. 1 and 2). The upper ball is held in a collet and spun at a constant speed of 1500 rpm. The three lower balls are free to roll in an outer race and are driven by the top ball, the whole assembly being similar to an angular contact bearing. The assembly is flooded with oil which, in our tests, is recirculated. The assembly is subjected to a thrust load, normally 600 kg. The test bearing assembly is shown in Fig. 3 and the machine operating conditions in Table 1. The test is generally run in accordance with IP 300 except that bottom ball failures are included as valid, whereas IP 300 states that only top ball failures may be accepted. The restriction to top ball failures of IP 300 reflects the origins of the test, which tended to be for evaluating steels more

TABLE 1—*Operating conditions of test machines.*

Machine	Test Bearing Type	Speed, rpm	Range of C/P	Lubricant Supply
Rolling four-ball	simulated angular contact bearing	1 500	0.38 to 0.75	600 ml recirculated at 5 to 25 ml/min
Plint high-speed four-ball machine	simulated angular contact bearing	variable up to 20 000	0.38 to 2.3	4.5 litres recirculated at 250 ml/min (experimental)
AOL vertical rolling contact fatigue rig	17-mm bore thrust race	1 500	0.67 to 1.25	4.5 litres recirculated at 15 ml/h
Unisteel	flat washer on modified 50-mm bore thrust race	1 500	1.71 to 5.0	total loss drip feed c.7 ml/h

[4]The italic numbers in brackets refer to the list of references appended to this paper.
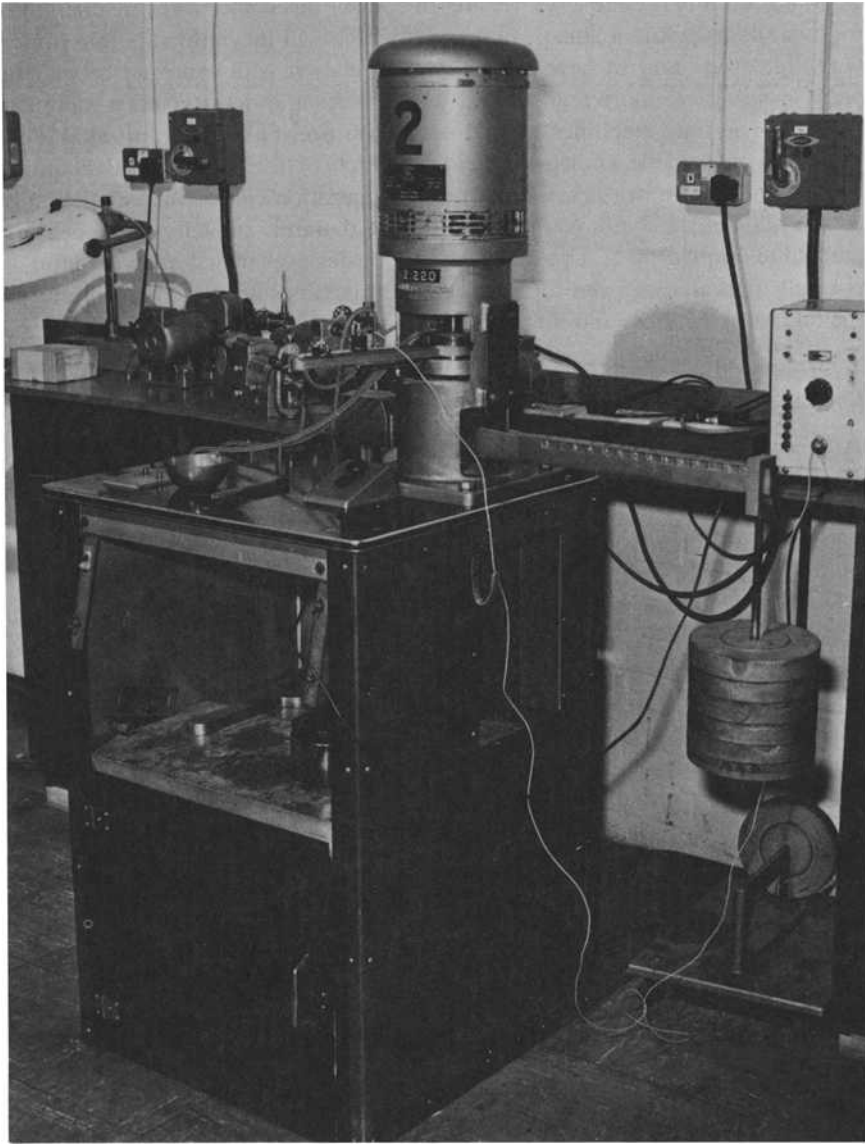
FIG. 1—*Rolling four-ball machine, general view.*

than lubricants; in these tests the top ball was made of the experimental steel while the lower balls were of a standard steel. Obviously, under these conditions a lower ball failure was not relevant. However, for lubricant testing this restriction is not really necessary. Our work with water-containing fluids has
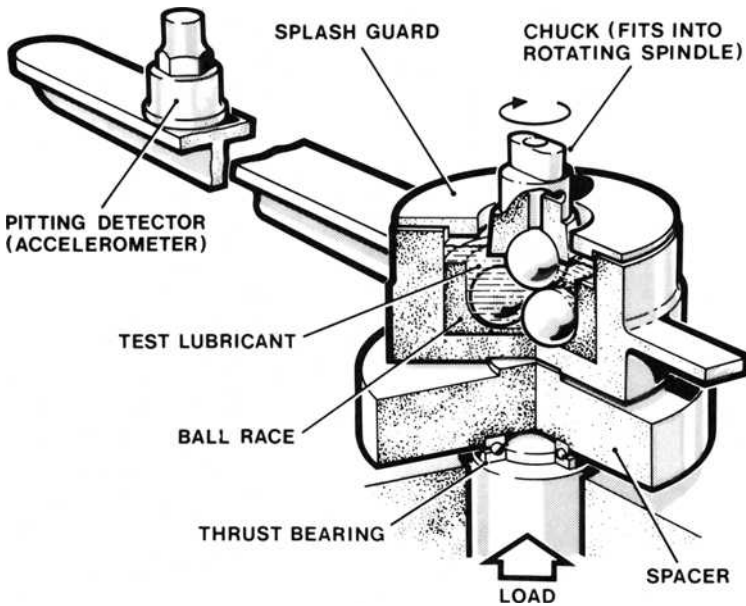
FIG. 2—*Rolling four-ball test layout.*

shown that these tend to generate a high proportion of bottom ball failures, and so we have decided to accept them as valid assembly failures.

Plint High-Speed Four-Ball Machine

The test specimen of the machine is identical to that of the standard rolling four-ball machine although, as Fig. 4 shows, there are major differences in general layout. The Plint machine is based on a high-speed four-ball machine developed at the National Engineering Laboratory [3]. Its most important advantage over the standard machine is that one can run tests on it at speeds up to 20 000 rpm. This enables tests to be run at lower stresses without extending the time and also allows more realistic film thicknesses to be generated. However, we have encountered a significant disadvantage, which is that equilibrium temperatures in excess of 100°C are generated at speeds of 15 000 to 20 000 rpm. While such temperatures are reasonable for certain applications (such as testing lubricants or materials for gas turbine engines), they are unacceptable for evaluating water-containing fluids. We are currently developing suitable cooling for the machine, but, as a result, no relevant test data are yet available.

Rolling 4 Ball   AOL Vertical Rolling
                         Contact fatigue Rig

Unisteel
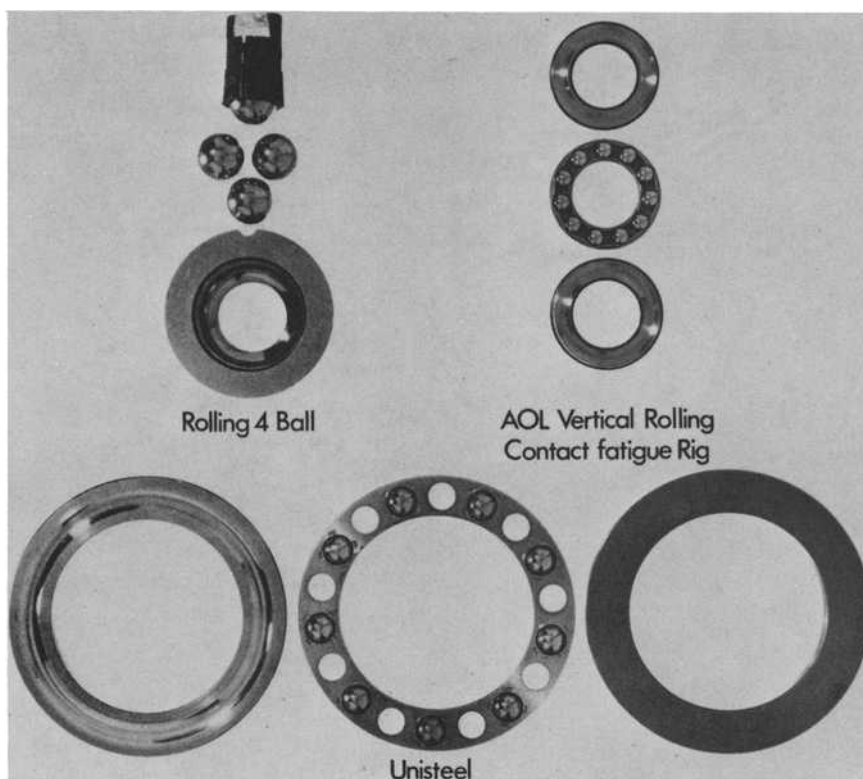
FIG. 3—*Comparison of test specimens.*

AOL Vertical Fatigue Rig

The AOL vertical fatigue rig was developed by the Admiralty Oil Laboratory to allow a more realistic test to supplement the standard rolling four-ball machine (Fig. 5). The rig is in many ways similar to a four-ball machine but uses a standard 17-mm bore thrust bearing as a test specimen to achieve greater realism. For the same reason the contact stress is reduced, but, as a result, average times to failure are increased by a factor of 20 to 30 times. To reduce the effect on the time taken to evaluate a product, six rigs were built and normally ran simultaneously on the same lubricant, recirculated from a central sump. Full details of the rig have been reported [4].

Unisteel Machine

The Unisteel machine has been available for steel–lubricant testing for a number of years. The machine has been described [5], and brief details are
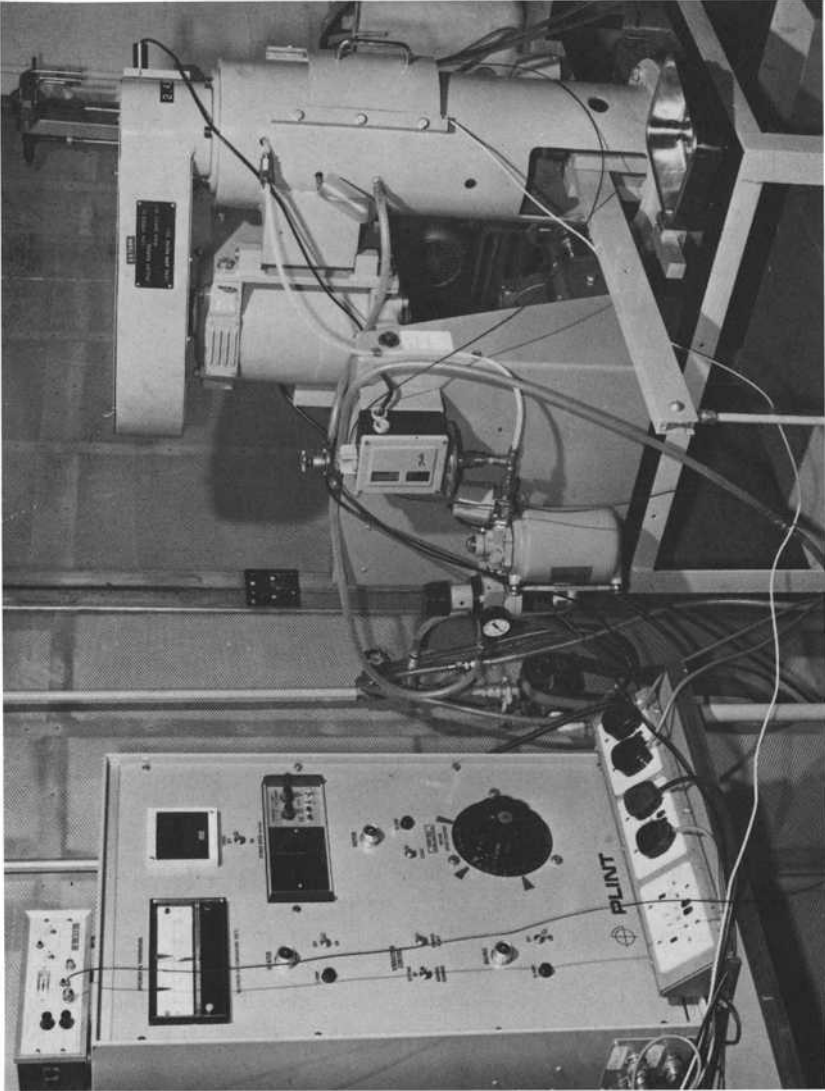
FIG. 4—*Plint high-speed four-ball machine.*

FIG. 5—*AOL vertical rolling contact fatigue rig.*

included in IP 305. The test bearing consists of a standard 50-mm (2-in.) bore thrust bearing and a flat washer. One track of the standard bearing is replaced by the flat washer, and alternate balls are removed (Fig. 3). When testing steels it is, of course, relatively easy to make the flat washer from the experimental steel, and the geometry ensures that fatigue pits normally occur on this component. The main disadvantage of the test is that, even at the maximum load, the average time of a test run is about 250 h with a mineral oil. For this reason many users tend to limit the number of repeat runs to ten, which obviously affects the accuracy of the results. However, the test becomes more useful when looking at water-based fluids with poor performance. The test data reported here were obtained under contract by the Leeds Industrial Unit of Tribology; however, we have recently installed four machines in our laboratories because of the encouraging results obtained with water-based fluids.

Test Results and Discussion

The rolling contact fatigue evaluation of the emulsifying hydraulic fluid and the fire-resistant hydraulic fluids was, of course, part of a comprehensive

test program covering a range of physical and chemical properties. The re-
sults of some of this work have been reported elsewhere [6-8]. Other workers
[9] have shown that the results of rolling contact fatigue tests at different
loads and on different machines can be presented on a single graph if the ratio
of bearing dynamic capacity to applied load, C/P, is used as the basis for
comparison. The technique is used in the presentation of these results. It has
been assumed from the beginning that data can be combined regardless of
the machine from which they were obtained, although results are tabulated
so that data can be linked to the relevant machine if desired. The aim of the
rolling contact fatigue evaluation was two-fold: first, to establish the maxi-
mum acceptable degree of severity (that is, the minimum C/P value) at which
results showed good correlation with practice and, second, to establish load–
life relationships for the fluids of interest. For the first series of tests, three
mineral oils were run at a range of C/P values between 0.38 and 1.71. Details
of the lubricants are given in Table 2 and test results in Table 3. The L_{50} lives
are also plotted against the C/P ratio in Fig. 6. This figure shows the fit of
the test data to the basic equation

$$L_{50} = 5(L_{10}) = 5(C/P)^3 \tag{1}$$

In general the results show reasonable agreement with this relationship.
There are indications that the rolling four-ball tests run at a C/P value of
1.38 are more severe than Eq 1 predicts. More important, it is difficult to see
a general trend in the order of ranking of the three mineral oils. Perhaps this
just reflects the fact that their performance is likely to be similar. However,
one might have expected the performance of OM-100 to be better at high
C/P values because of its higher viscosity. The data for OX-30 + 10 percent
seawater are, not surprisingly, significantly worse than those for the "dry"
oils. The test data for fire-resistant hydraulic fluids are given in Tables 4 and
5 and plotted in Figs. 7 and 8. These cover a wider range of C/P values (0.38
to 4.98) than was practicable for the mineral oils. In almost every case, the
results for the rolling four-ball test fall well below the best straight line in the
figures. This must cast further doubts on the validity of such high-stress
tests. In practice, the maximum acceptable test severity seems to be affected
by the quality of the lubricant being tested. In the AOL fatigue rig it was
noticeable that, while tests at a C/P of 0.67 were reasonable for mineral oils,
many early failures occurred with the fire-resistant fluids. This is not appar-
ent from the processed data because the method of maximum likelihood
which is used in the Weibull analysis procedure appears to be biased toward
longer lives.

---

[5]Plots of L_{10} lives against the C/P ratio have been omitted from this paper because of lack of
space. However, Tables 3 through 5 give the information necessary to construct these graphs if
desired.

TABLE 2—*Details of test lubricants.*

Designation	Type	Typical viscosity at 40°C, mm²/s	Typical viscosity at 21°C, mm²/s
OM-33	mineral oil hydraulic fluid with 0.5% triaryl phosphate	26	66
OM-100	mineral oil with rust and oxidation inhibitors for use in steam turbines, gearing, and some hydraulic systems	87	280
OX-30	emulsifiable hydraulic fluid for use in certain submarine hydraulic systems	26	70
HFB-1	water-in-oil emulsion containing about 40% water	46	87
HFC-1	mixture of water, glycols, and polyglycols containing about 36% water	38	82

The most important result of this test program can be seen in Fig. 9, which combines all the load–life plots (data points are omitted for clarity). From this it will be seen that the characteristic lines have different slopes (that is, the exponent in Eq 1 is not always 3). It is therefore impossible to evaluate a group of lubricants or materials, or both, by running tests at a single C/P value unless this is very close to the operating value in the equipment concerned.

Metallurgical Investigation

Even before the data presented here had been accumulated, there were doubts about the relevance of the standard rolling four-ball test, so we decided that it was worth examining the failed specimens in some detail to try to establish whether they differed fundamentally from other rolling fatigue failures. Examination of the balls from a standard rolling four-ball test to IP 300 shows that the top ball track had undergone plastic deformation as a result of the very high contact stresses. Two of the three lower balls each showed two running tracks (inner and outer race contacts) whereas the third tended to show a uniform darkening without any obvious tracks. The reason for this difference has not been established but is perhaps a result of top-ball eccentricity, combined with slight differences in diameter between the three lower balls. Theory predicts that the plastic deformation of the top ball which occurs at the standard load of 600 kg ($C/P = 0.38$) is inevitable at loads in excess of 300 kg. Rolling four-ball tests were run at 600, 500, 400, and 300 kg, and roundness measurements of the lower balls were made. These showed

TABLE 3—*Test data for mineral oils.*

| Fluid Type | Test Machine | No. of Runs | C/P | Weibull Analysis Data | | |
				L_{50}, million revolutions	L_{10}, million revolutions	Slope
OM-33	rolling four-ball	32	0.38	0.11	0.050	2.50
	AOL fatigue rig	27	0.67	3.24	0.35	0.85
		24	0.91	2.75	0.50	1.11
	Unisteel	10	1.71	18.9	3.3	1.1
OM-100	rolling four-ball	33	0.38	0.087	0.041	2.5
	AOL fatigue rig	24	0.67	1.45	0.42	1.52
		27	0.91	2.58	0.28	0.85
OX-30	rolling four-ball	40	0.38	0.065	0.031	2.50
	AOL fatigue rig	24	0.56	0.40	0.14	1.85
		22	0.67	1.62	0.49	1.56
		31	0.91	3.21	0.20	0.68
	Unisteel	24	0.91	4.48	1.1	1.35
		10	1.71	18.0	5.31	1.55
OX-30 + 10%	rolling four-ball	24	0.38	0.058	0.031	2.94
seawater		24	0.56	0.31	0.12	2.00
	AOL fatigue rig	24	0.67	0.64	0.18	1.52
		24	0.91	1.32	0.34	1.39
	Unisteel	10	1.71	4.59	2.25	2.7

FIG. 6—L_{50} *life versus the C/P ratio for mineral oils.*

that plastic deformation and wear were negligible at 300 kg, but increasingly severe deformation occurred at 400 kg and above. Next, the balls were etched for further examination. It was found that, around the running track of the top ball, a large number of fine cracks were apparent. Balls run in a variety of lubricants were examined, and it seems that the type of lubricant used does affect the severity of cracking (see Fig. 10, which was taken with a pe-

TABLE 4—*Test data for HFB-1 and HFB-1 + 10 percent seawater.*

Test Machine	No. of Runs	C/P	Weibull Analysis Data		Slope
			L_{50}, million revolutions	L_{10}, million revolutions	
		HFB-1			
Rolling four-ball	23	0.38	0.050	0.024	2.50
	24	0.38	0.055	0.025	2.38
	24	0.56	0.46	0.30	4.55
	24	0.56	0.65	0.33	2.78
	25	0.56	0.70	0.32	2.38
AOL fatigue rig	25	0.67	1.08	0.30	1.47
	25	0.72	1.33	0.31	1.28
	24	0.91	1.40	0.21	1.00
	28	1.25	2.02	0.61	1.56
	24	1.25	1.88	0.45	1.32
Unisteel	25	1.71	3.15	1.26	2.03
	10	2.49	9.81	4.23	2.23
	10	3.89	29.1	8.28	1.50
	10	4.98	98.3	19.9	1.18
		HFB-1 + 10% Seawater			
Rolling four-ball	24	0.38	0.038	0.011	1.56
	24	0.56	0.41	0.21	2.78
AOL fatigue rig	25	0.91	1.17	0.25	1.22
	26	1.25	2.10	0.54	1.39

TABLE 5—*Test data for HFC-1 and HFC-1 + 10 percent seawater.*

Test	No. of Runs	C/P	Weibull Analysis Data		Slope
			L_{50}, million revolutions	L_{10}, million revolutions	
		HFC-1			
Rolling four-ball	10	0.38	0.041	0.0099	1.28
	19	0.56	1.56	0.256	1.04
AOL fatigue rig	26	0.67	1.44	0.054	1.92
	25	0.91	1.05	0.26	1.35
	25	1.25	8.37	1.54	1.11
Unisteel	10	1.71	7.59	1.97	1.40
	10	2.49	14.4	7.74	3.06
	10	3.89	15.9	7.02	2.30
	10	4.98	32.0	19.4	3.76
		HFC-1 + 10% Seawater			
Rolling four-ball	24	0.38	0.076	0.022	1.52
	24	0.56	0.37	0.022	2.63
AOL fatigue rig	24	0.91	0.56	0.188	1.72
	25	1.25	0.95	0.264	1.47
Unisteel	10	2.49	2.22	1.42	4.23
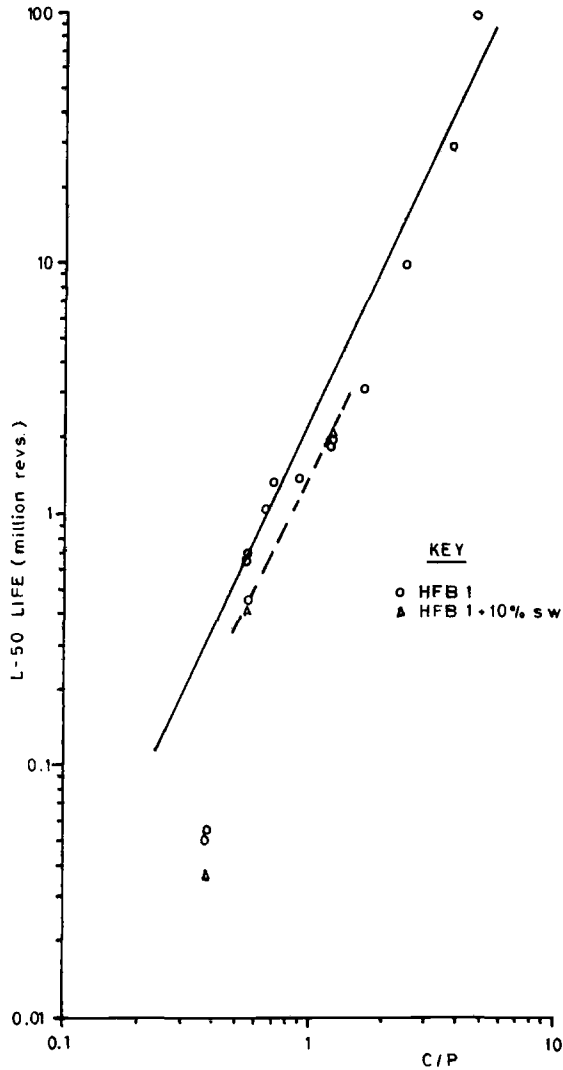
FIG. 7—L_{50} life versus the C/P ratio for HFB-1.

riphery camera). In some cases the cracks were visible before etching (this was particularly true of tests run with an extreme pressure gear oil, OEP-69). However, in most cases we assumed that the surface had been smeared and this masked the cracking. It is, of course, possible that the "cracks" are a result of selective acid attack during the etching. However, some of the balls from the low-load tests previously mentioned were also etched, and the results
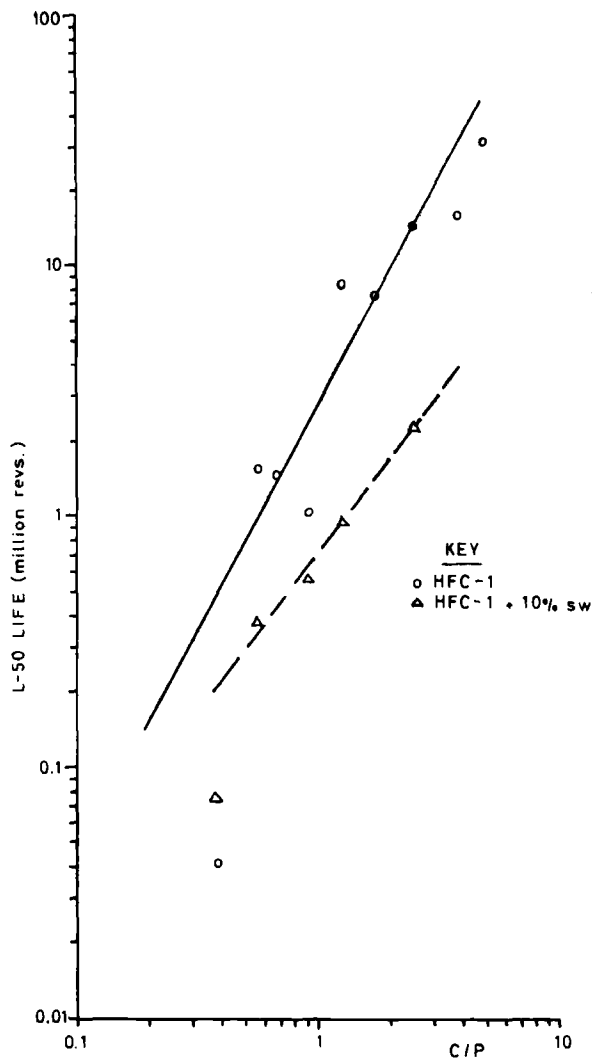
FIG. 8—L_{50} life verses the C/P ratio for HFC-1.

indicated that fewer cracks were likely at lower loads and shorter running times. We therefore concluded that the cracks were a genuine stress–lubricant effect.

Top and lower balls were sectioned through the running tracks, and in many cases a continuous subsurface crack was found at a depth of about 0.18 mm. This is approximately the distance at which the maximum hertzian
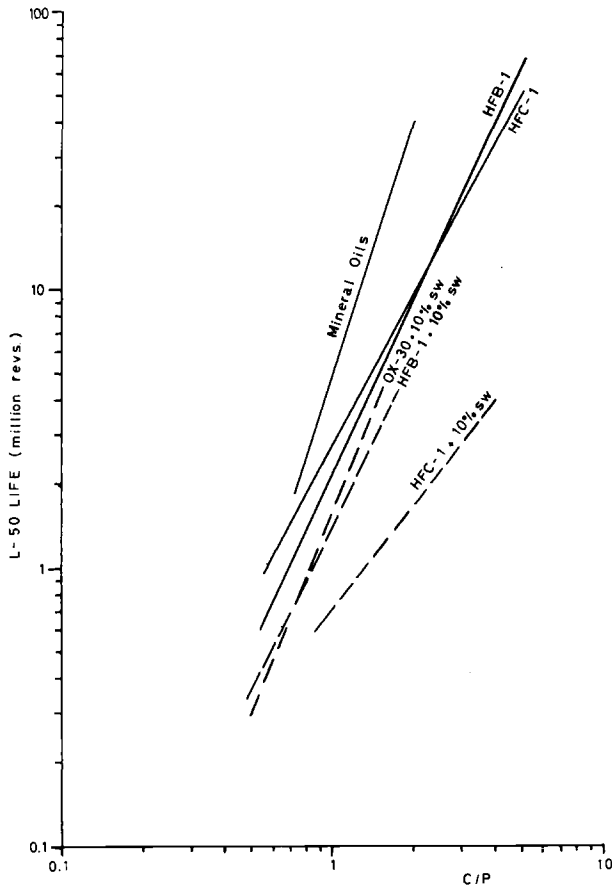
FIG. 9—*Comparison of load–life characteristics.*

shear stress might be expected to act. Again, these effects were most pronounced with the high-load tests, more limited at 400 kg, and not observed at all at 300 kg. Microhardness tests showed that work hardening took place in a band approximately 0.1 to 0.5 mm below the surface. A dark band was also observed in this region on nital-etched balls.

Thus it appears that the stresses under which the rolling four-ball test is normally run tend to induce plastic flow and cracking which is not representative of normal bearing operation. Conversely, it appears that the test when run at a load of 300 kg ($C/P = 0.75$) is much more likely to be a reasonable simulation test.
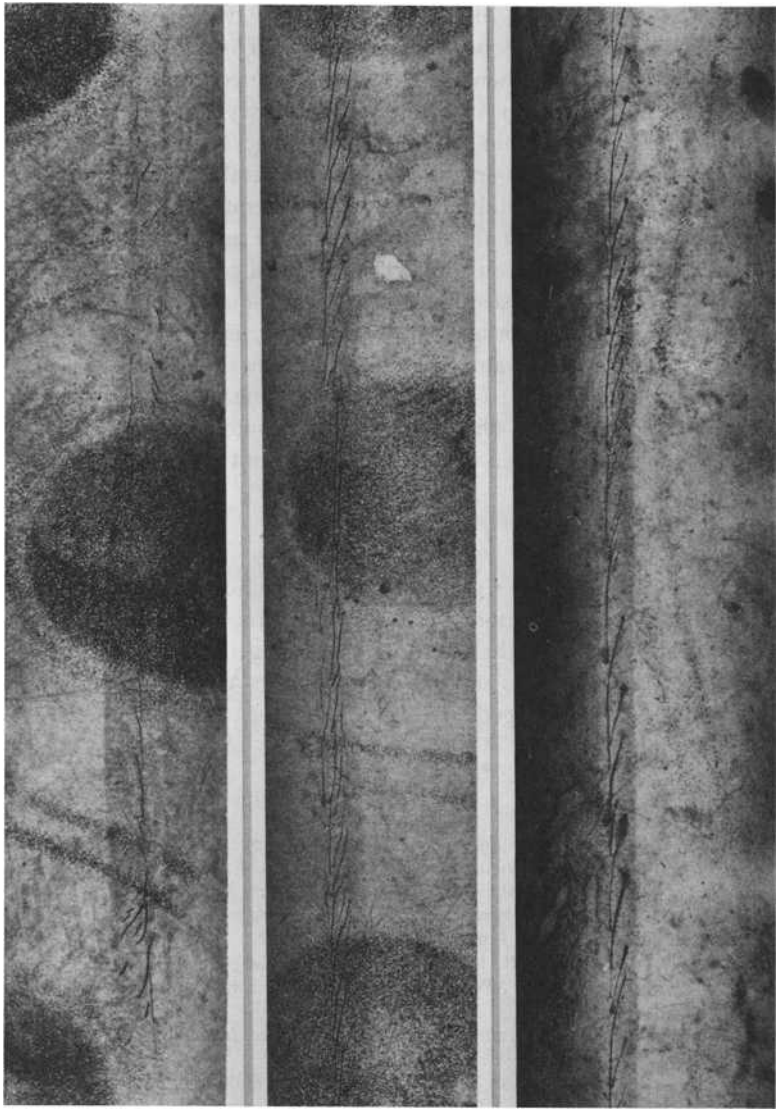
FIG. 10—*Typical top ball tracks: (top) OM-33; (middle) HFB-1; (bottom) OEP-69.*

Conclusions

Test data have been presented for three different designs of rolling contact fatigue test machine. These indicate that the standard rolling four-ball test is of dubious value in assessing the performance of lubricant–material combinations because of the very high stress (low *C/P* value) under which it operates. This conclusion has been supported by a metallurgical investigation of rolling four-ball specimens. If the load is reduced to give a more realistic *C/P* value, then the mean time to failure increases to such an extent that the machine is no longer a rapid screening test. However, the problem should be overcome by the Plint high-speed machine. It is unfortunate that difficulties in maintaining an acceptable lubricant temperature have delayed the program. The AOL fatigue rig and Unisteel machine are both capable of producing useful data, and tests on these machines will continue to be the tests on which we rely for final assessment of lubricant–material properties. The results demonstrate the importance of designing a test program to cover a range of *C/P* values when evaluating new materials or lubricants. Furthermore, the results for different lubricants indicate the vast spread of performance which can occur. The choice of an appropriate lubricant is therefore of the utmost importance when evaluating experimental steels.

References

[1] Barwell, F. T. and Scott, D., *Engineering,* Vol. 182, 1956, pp. 9–12.
[2] Scott, D. in *Rolling Contact Fatigue: Performance Testing of Lubricants,* R. Tourret and E. P. Wright, Eds., Heyden & Son, London, 1977, Chapter 1, pp. 3–15.
[3] Milne, A. A. and Nally, M. C., *Proceedings of the Conference on Lubrication and Wear,* Institute of Mechanical Engineers, London, 1958, pp. 459–462.
[4] Eastaugh, P. R. and Penfold, R. E. in *Rolling Contact Fatigue: Performance Testing of Lubricants,* R. Tourret and E. P. Wright, Eds., Heyden & Son, London, 1977, Chapter 7, pp. 97–105.
[5] Johnson, R. F. and Sewell, J. F., *Journal of the Iron and Steel Institute,* Vol. 196, 1960, pp. 414–444.
[6] Ritchie, J. and Thomson, J., "An Emulsifying Hydraulic Fluid for Submarine Systems," Second Fluid Power Symposium, British Hydromechanics Research Association, Bedford, England, 1971, pp. F1.1–F1.12.
[7] Eastaugh, P. R. and Ritchie, J., *Wear,* Vol. 34, No. 3, 1975, pp. 355–371.
[8] Onions, R. A. in *Performance Testing of Hydraulic Fluids,* R. Tourret and E. P. Wright, Eds., Heyden & Son, London, 1979, Chapter 30, pp. 439–458.
[9] Yardley, E. D., Kenny, P., and Sutcliffe, D. A., *Wear,* Vol. 28, No. 1, 1974, pp. 29–47.

Effects of Testing Conditions on Rolling Contact Fatigue and Evaluation of Test Results

F. R. Morrison,[1] *Thomas Yonushonis,*[1] *and James Zielinski*[2]

Rolling Bearing Life Tests and Scanning Electron Microscopy

ABSTRACT: Traditional techniques for the evaluation of a rolling bearing material or lubricant rely on the accelerated life testing of large lots of bearings. The rating of the bearing performance is then established on the basis of statistical estimates of the experimental Weibull parameters.

Optical evaluation of bearing surfaces has long been used to supplement life data. However, optical examination is limited to evaluating the validity of specific test points. Another surface analysis technique, scanning electron microscopy (SEM), can now be used to augment test data because of the high magnifications and depth of field available. SEM examination of tested surfaces at magnifications up to $\times 1000$ can define alterations in surface morphology produced by wear, fatigue, and corrosive failure modes long before signs would be detectable by optical means or failure would be precipitated. These characteristics can be qualitatively evaluated to supplement collected life data, and comparisons can yield relative evaluations of bearing performance. In this manner, meaningful long-range performance projections can be obtained using small test groups.

An example of the application of this technique for the evaluation of a series of synthetic lubricants and mineral oils is presented in this paper.

KEY WORDS: rolling contact fatigue, bearing life tests, failure analysis, lubricant evaluation, scanning electron microscopy, surface morphology, bearing steels

Rolling contact fatigue, like all fatigue processes, is a statistical phenomenon. The results of a bearing life test are thus expressed as the estimated parameters of a Weibull distribution [1].[3] The validity of these estimated values is directly related to the size of the test lot used and the number of failures produced during the test. Traditionally, the statistician emphasizes

---

the need for large test lots, 30 to 100 bearings, and a large failure rate. However, practical limitations of time and money force compromises to be made in both areas in experimental programs.

In recognition of these practical limitations, statisticians have developed improved estimation techniques. These techniques allow the treatment of small test lots which are terminated at a preset life, thus yielding a reduced failure rate [2-4]. In some instances, individual tests are suspended prior to the set time because of the existence of competing failure modes or extraneous factors in the test processes. Analytical techniques were developed to treat these intermediately censored data points [5-7]. Further reductions in group size were made possible by the evolution of hypothesis tests to check the statistical significance of differences between experimental lots [8] and by the development of techniques to handle the simultaneous analysis of parameters from multiple but related test lots [9]. Even with these advanced data analysis techniques, bearing endurance tests are expensive and time-consuming when a large number of variables must be evaluated.

During the same period of time, advances were being realized in the post-test evaluation of bearing contact surfaces. Examinations conducted using optical microscopy at magnifications up to $\times 30$ provided additional insight as to the interactions of the competing failure modes existent in rolling bearings. The subsequent application of established appearance definitions [10] allowed decisions to be made concerning the validity of individual test points. Generally, these examinations did not add to the accumulated data, since the tendency was only to reclassify apparent failures as suspended tests.

Scanning electron microscopy (SEM) has now considerably expanded surface evaluation capabilities. The depth of field available with a scanning electron microscope is significantly greater than that of an optical microscope. This additional capability allows meaningful surface examinations to be conducted at much higher magnifications. The SEM makes it possible to observe and document surface morphological features which were previously unknown. Over the last few years, a great deal of effort has been expended to identify and classify the types of surface alterations produced in rolling bearings and to define the origin of these alterations [11]. These definitions allow the direct application of SEM techniques to bearing test programs, and scanning electron micrographs can now be used to establish qualitative ratings of surface morphology. However, further experimentation was required to prove that SEM evaluations could be decisive in the establishment and comparison of extended bearing operating potential.

An experimental investigation was conducted to compare the properties of a number of lubricants. The test procedure developed for this purpose directly employed posttest SEM analysis to accumulate information on bearing surface alterations. This information was then extrapolated to long-term bearing performance. This effort verified the usefulness of scanning electron microscopy as a life test evaluation tool. This latter aspect of the investigation

is described in this paper while a portion of the specific data and their analysis have been previously published [12].

Experimental Approach

An experimental program was defined in conjunction with a major lubricant manufacturer to evaluate a number of natural and synthetic lubricating fluids in a rolling bearing environment. The objective of this investigation was to compare the lubricating characteristics of the fluids under operating conditions analogous to those seen in a typical petrochemical process pump.

These pumps normally have a single shaft supported by a double-row radial ball bearing near the overhung impeller and a pair of angular-contact ball thrust bearings, mounted back to back, near the driven end. Experience has established that the thrust bearings are more prone to failure in service, so this bearing was selected for the experimental vehicle. The majority of the pumps in service have shaft sizes ranging from 50 to 75 mm in diameter, whereas existing test machines were equipped to evaluate bearings having a 45-mm-diameter bore. It was concluded that the existing testing size would adequately reflect field performance if the operating d_mN value, the product of the bearing pitch diameter in millimetres and shaft speed in revolutions per minute, was scaled to agree with average field conditions. The normal field service speed is 377 rad/s (3600 rpm) with a d_mN range of 2.9 $\times$ 10^5 to 4.3 $\times$ 10^5. The test speed was established to be 576 rad/s (5500 rpm) equal to a 4.0 $\times$ 10^5 d_mN value.

An angular contact ball bearing of standard 7309 B design was utilized as the test element for this program. Test bearings were procured from open stock so that the results obtained would be typical of those expected from standard production bearings. The typical load seen by a thrust bearing in the application was scaled using the ratios of bearing capacities, producing a range from 8.9 to 13.3 kN (2000 to 3000 lb). These load levels were used for performance tests. The extended duration runs were completed under a heavier load, 26.7 kN (6000 lb), to accelerate the wear and fatigue processes in accordance with normal endurance testing considerations. Under the heavy load, the maximum hertz stress on the inner ring is 2.2 GPa (3.2 $\times$ 10^5 psi), and the theoretical bearing L_{10} life is 26 $\times$ 10^6 revolutions.

The test machines used were R2-type bearing endurance testers equipped for application of pure axial load. The test arrangement is illustrated schematically in Fig. 1 and the test machine is shown in Fig. 2. Basically, the tester consists of a horizontal belt-driven arbor supported on a solid base through two cylindrical roller bearings. The test bearings are located at either end of the arbor in independent housings to minimize interactions between the two. The alignment of the test bearing is maintained with a small cylindrical pilot bearing at the end of the shaft which controls the orientation of the floating housing without affecting the magnitude of the applied load.
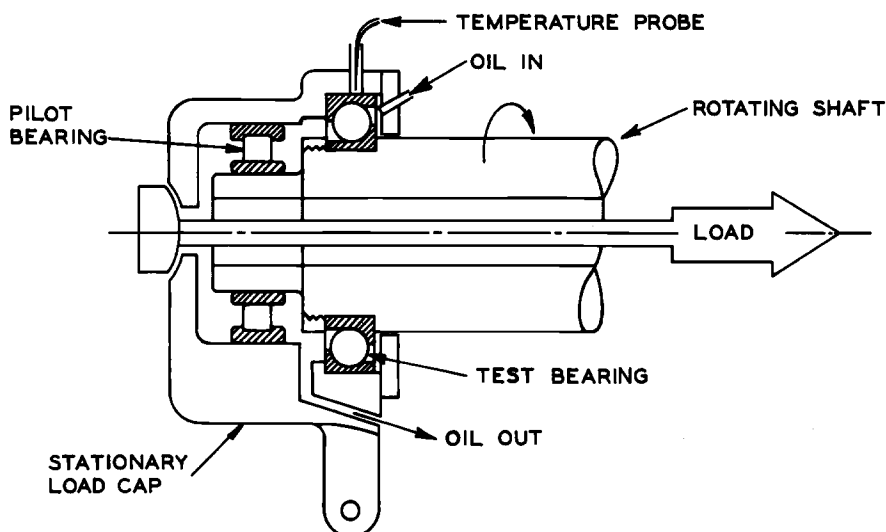
FIG. 1—*Schematic drawing of a bearing test rig.*

Thrust load is applied between the two test bearings by means of a rod passing through the center of the hollow arbor. A strain gage transducer at one end of the rod allows the applied force to be directly monitored throughout the test period. A thermocouple located on the bearing outer ring monitors the average operating temperature of each individual test bearing. The analog signals from the three transducers are monitored by a test control computer which constantly scans the data input points, maintains a historical test record, and alarms or terminates tests when parameters exceed preestablished control limits.

A relatively novel experimental approach was developed to evaluate the performance of the lubricants. First, small lots of bearings were run for extended periods of time in the test fluids. Subsequently, the contact surfaces of the tested bearings were examined in detail using SEM to compare the alterations produced in contact surface morphologies. This information was then extrapolated to estimate the extended duration wear–fatigue life effects of the test fluids. In this way, it was possible to establish the long-term performance of the lubricants in a significantly foreshortened test period.

The extended duration tests were conducted on lots of two to five bearings each. Individual bearings were run to failure or to a cutoff life of 82.5×10^6 revolutions. The test fluid was circulated to each specimen at a rate sufficient to control the bearing operating temperature at a preestablished level. The operating temperature levels were established for each lubricant during performance tests conducted with sump oil lubrication. This produced a slight variation in the elastohydrodynamic (EHD) film parameter, Λ, which affects
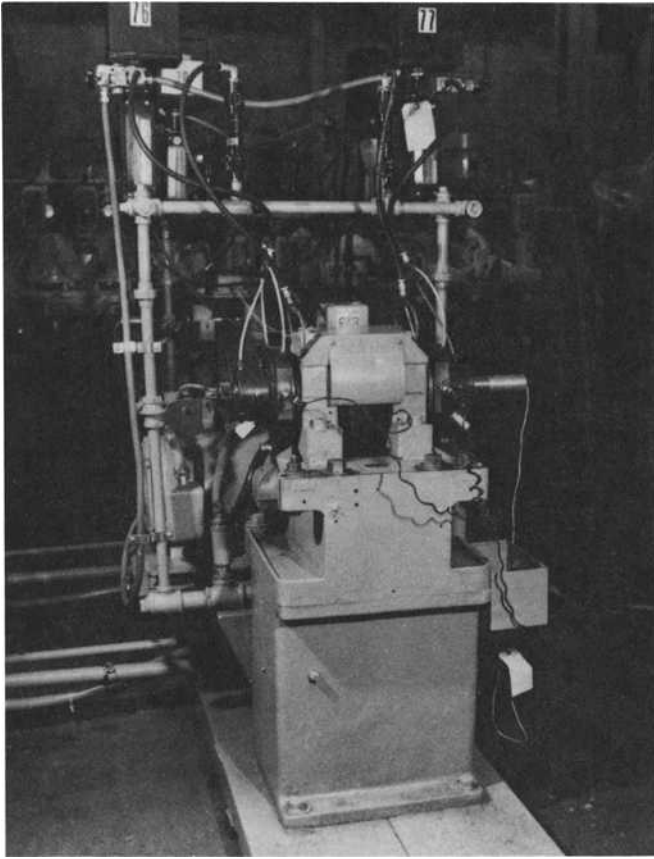
FIG. 2—*R2-type bearing endurance tester.*

the surface protection afforded by the lubricant. However, this was done to reflect conditions which would exist in the field.

Following the extended duration test runs, each bearing was visually examined at magnifications up to ×30. This investigation defined typical changes in the contact surface appearance for each lubricant and identified locations of abnormalities for further high-magnification study. Two inner rings, representative of the range of surface conditions noted, were selected from each lot and studied at high magnification on the SEM.

The specific scanning electron microscope used has a chamber large enough to accept an inner ring from this size bearing. The ring is mounted on a stage which can be translated, tilted, and rotated using externally mounted controls. In this manner, the entire contact surface of the tested inner rings can be studied directly.

First the ring was scanned circumferentially at approximately the center of the contact path at a magnification of ×50. This examination verified the observations of the visual examination and provided further definition of the abnormal-appearing areas. Also, this examination would identify other atypical areas not apparent under visual examination. The abnormal areas were then examined at magnifications ranging from ×250 to 1000 to identify their origin and establish their relationship to the lubricant used.

At a location judged to be typical, a cross-groove scan was made at a magnification of ×500 to define variations in the surface conditions produced by the distributions of hertzian loading and differential sliding existing across the contact. Documentation of these conditions was provided by a series of five photomicrographs taken at the approximate locations identified in Fig. 3. These photomicrographs were assembled into a linear series to provide a composite view of the overall groove conditions for comparative evaluations.
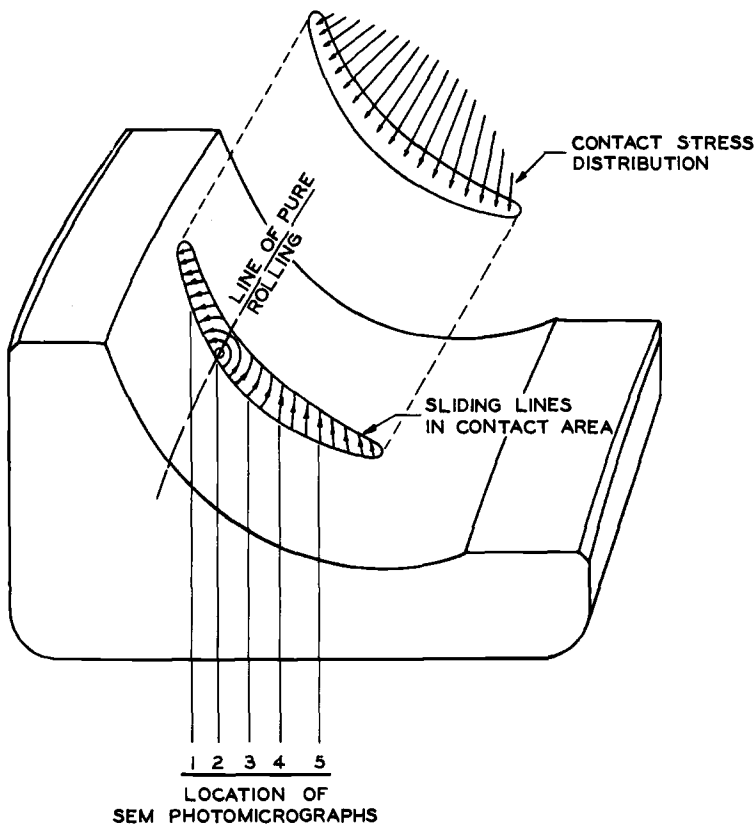
FIG. 3—*Inner ring contact detail in an angular contact ball bearing.*

The relative evaluation of the photomicrographs was accomplished using the following procedure:

1. The composite cross-groove views were grouped according to test fluids and arranged to facilitate the simultaneous viewing of all the photomicrographs.

2. The degree of microwear experienced in each bearing was qualitatively defined by the percentage of the finishing pattern still visible on the race surfaces at the most severely altered portion of the groove. Figure 4 illustrates the grinding lines that exist on a bearing surface before it is run, and the obliteration of the pattern as a result of running can be noted in Figs. 5 and 6. The degree of microwear was ranked using the ratings of trace, light, and moderate. A trace rating signifies minimal wear or a maximum number of visible grinding lines; light and moderate ratings denote progressively more severe microwear conditions. The rankings obtained from the individual bearings were then combined to achieve a ranking for the test fluids. It is important to note that even the most severe microwear would not be observed using high-magnification optical inspection techniques.

3. The bearing surface morphology was characterized by the examination of the composite photomicrographs and the individual photomicrographs
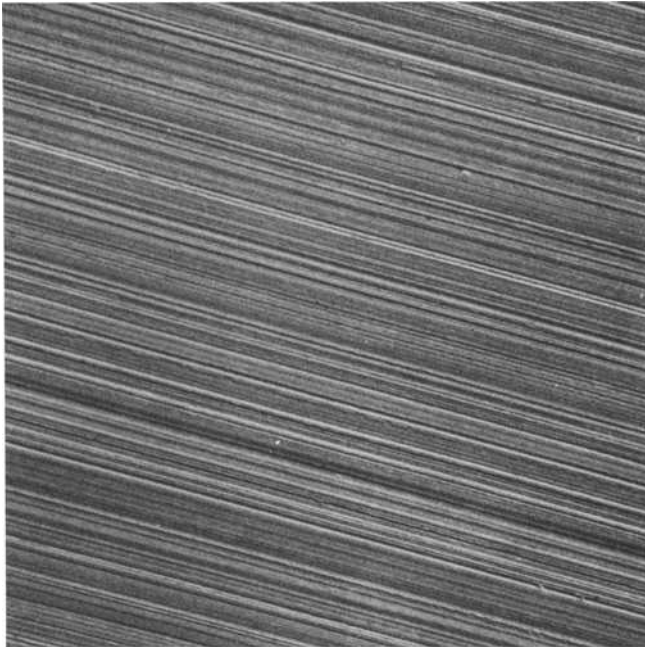
FIG. 4—*Surface morphology of a typical unrun bearing surface (magnification ×500).*
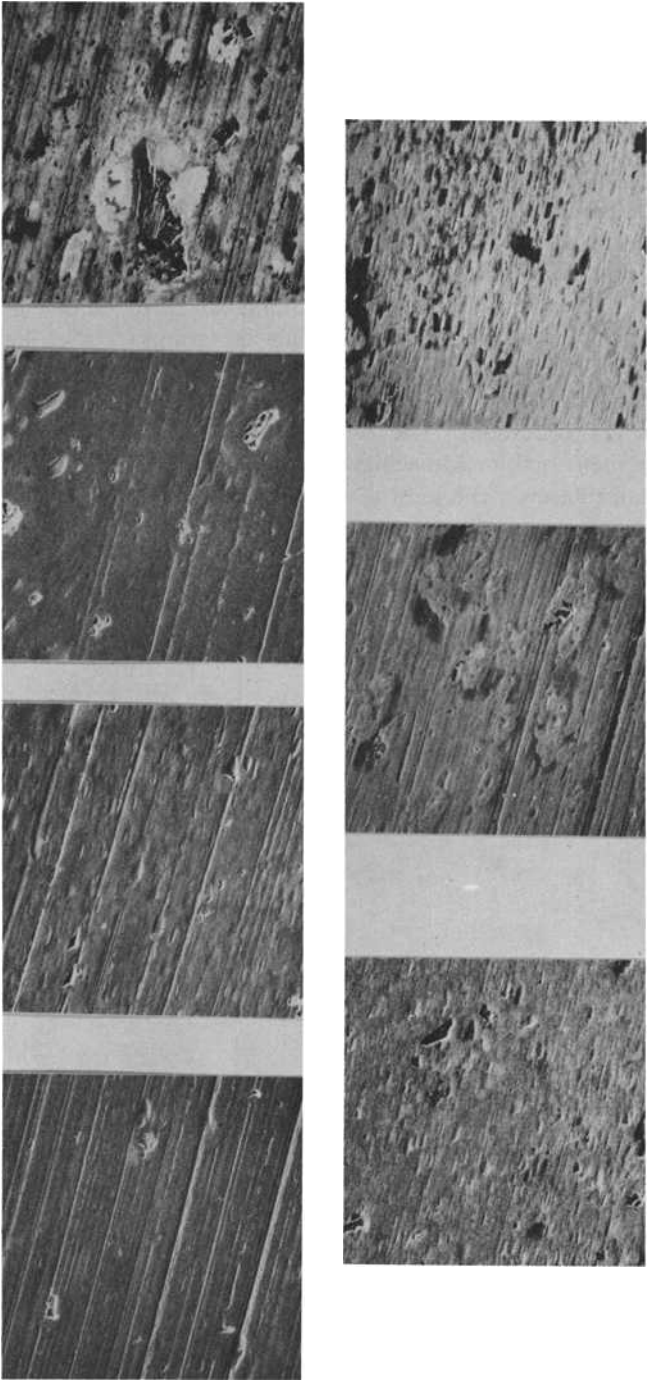
FIG. 5—Comparison of the surface morphology of run bearing contact surfaces with the seven test lubricants (top, left to right: Min A, Min B, Min C, Min D: bottom: Min E, Syn A, Syn B), the "best" surface at the center of the wear track (magnification ×400).
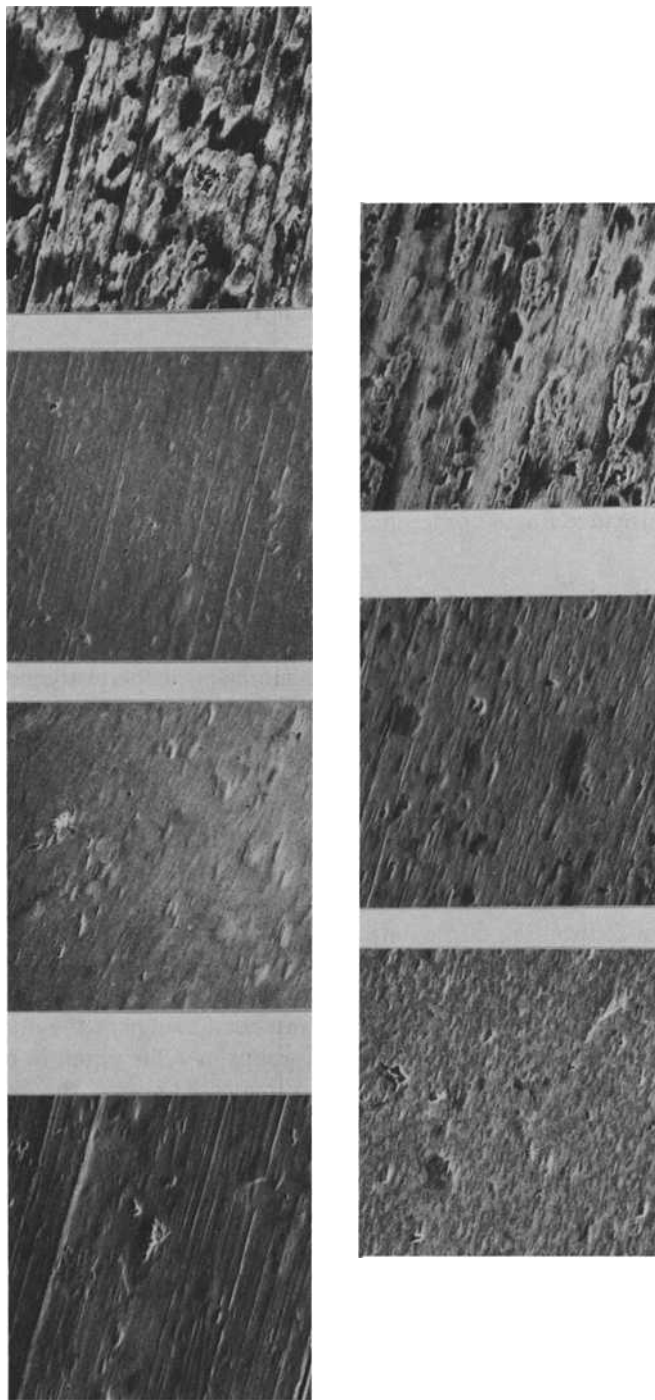
FIG. 6—Comparison of the surface morphology of run bearing contact surfaces with the seven test lubricants (shown in the same order as in Fig. 5), the "worst" surface at the center of the wear tract (magnification ×400).

taken from specific defect areas. In this test series, the morphologies were characterized as normal, microspalled, and micropitted. Microspalling refers to a distress of the surface composed of numerous small craters concentrated in the critical portion of the contact zone. These are thought to originate from a fatigue process. Micropitting is a similar-appearing distress which is generally observed over the entire surface and is most likely a corrosion phenomenon. Both microspalling and micropitting are undesirable conditions, since they can progress as a result of continued bearing operation to precipitate premature bearing failures. Once again, these morphological features are too small to be observed using optical inspection methods.

Seven test lubricants were evaluated in the experimental program: five paraffinic mineral oils and two synthetic diester lubricating fluids. These lubricants are described in detail in Table 1. The commercially available ISO VG-68 mineral oil, designated Min A, is the lubricant typically used in petrochemical process pumps. This fluid was thus used as the baseline of acceptable performance for the program.

Discussion of Results

The described test equipment and procedures were used to conduct life-microwear tests on seven lots of bearings. A summary of the test conditions and results for all seven groups is given in Table 2.

An attempt was made to calculate the experimental Weibull parameters for the test lots using a multigroup maximum likelihood procedure. This statistical method is normally quite effective for collections of small test lots since it used the total number of data points to estimate a common slope for the experimental series. This common slope is then used to calculate the life parameters for each individual group. In this case, the small number of failures and the distribution of the data did not allow the analysis to converge on a solution. The analysis was subsequently repeated using a slope value externally fixed at 1.3 to yield life estimates for the three groups, with failures as shown in Table 2. It had originally been intended to repeat the analysis, declaring a failure in each of the remaining groups at a life equal to one of the suspensions to achieve lower bound life estimates. However, the extreme range of the 90 percent confidence limits obtained in the first calculations, as large as 10^{45}, illustrated that these results could not reasonably be employed to differentiate the performance of the test lubricants.

The established surface ratings achieved through SEM examination of the contact surfaces are also shown in Table 2. The range of conditions typified by these ratings is illustrated in Figs. 5 and 6, which show the best and worst cases of surface alteration produced with each of the seven lubricants. In addition, Fig. 7 shows the cross-groove scans achieved with two test fluids, Min C and Syn A, and with the baseline fluid, Min A.

TABLE 1—*Identification of test lubricants.*

Designation	Type of Fluid	Base Stock	ISO Viscosity Grade	Kinematic Viscosity, m²/s	
				373 K (100°C)	313 K (40°C)
Min A	commercially available mineral oil	paraffinic	68	8.9	65.1
Min B	Min A plus experimental antifriction additive	paraffinic	68	8.9	65.1
Min C	commercially available mineral oil	paraffinic	32	5.5	30.1
Min D	Min C plus experimental antiwear additive No. 1	paraffinic	32	5.5	30.1
Min E	Min C plus experimental antiwear additive No. 2	paraffinic	32	5.5	30.1
Syn A	commercially available synthetic	ditridecyl adipate	32	5.6	30.1
Syn B	experimental synthetic	diisodecyl adipate	15	3.4	14.0

TABLE 2—Summary of test data.[a]

Lubricant	Operating Temperature, K	Film Parameter, Λ	No. of Bearings		Experimental L_{10}, millions of revolutions	SEM Observations	
			Tested	Failed		Microwear	Surface Morphology
Min A	348	4.3	2	0	...	trace	normal
Min B	343	4.6	4	0	...	light	microspalls
Min C	344	2.0	4	1	23	light	microspalls
Min D	352	1.6	4	0	...	trace	micropits
Min E	352	1.6	4	0	...	moderate	micropits; microspalls
Syn A	342	2.0	4	2	14	trace	normal
Syn B	338	1.2	5	1	32	moderate	microspalls

[a]Test bearing: 7309 B; axial load: 26.7 kN; test speed: 576 rad/s.
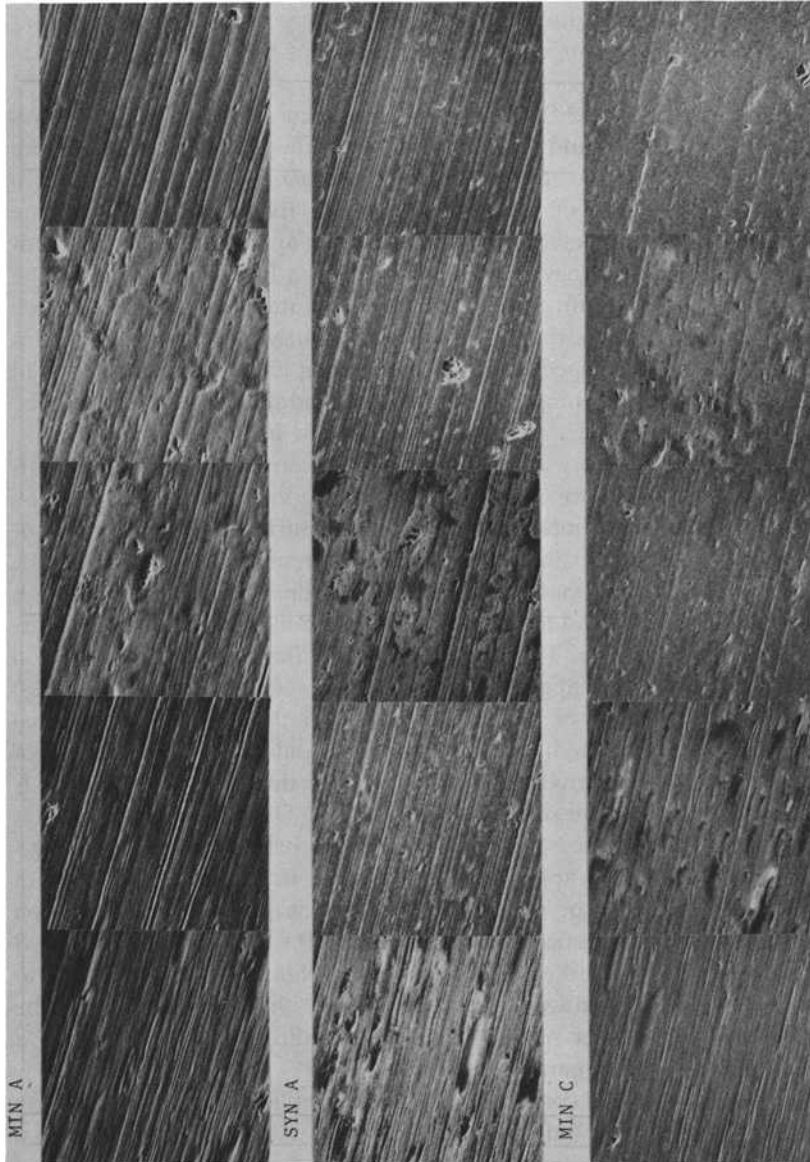
FIG. 7—*Cross-groove morphological scans with the three lubricants* (top: *Min A*; middle: *Syn A*; bottom: *Min C*).

Note that the SEM photomicrographs shown in Figs. 5, 6, and 7 are merely examples used to demonstrate the differences in surface morphology among bearings evaluated with different lubricants. In order to evaluate the surface conditions qualitatively, it is necessary to utilize a much larger number of photomicrographs. Unfortunately, it was not possible to present all of the SEM photomicrographs used to arrive at the lubricant ratings in this paper.

The comparisons of the SEM observations from the test lubricant with those from the baseline fluid proved to be much more decisive than the life test data. For example, the addition of the experimental additive packages to the commercial mineral oils failed to improve the performance of the lubricants. In fact, the presence of these additives appeared to be detrimental to the surface morphology of the contacts. From Figs. 5 and 6, it can be seen that the contacts run with these experimental fluids suffered both microspalling and micropitting. As stated previously, the presence of this microdamage would be expected to reduce bearing life. It can be concluded that the lubricants containing the experimental additive packages, that is, Min B, Min D, and Min E, are undesirable for use in the application.

The surfaces lubricated with the Syn B fluid were noted to have experienced significantly more wear than the remaining candidates. This can be seen by comparing the photomicrographs of the surfaces in Figs. 5 and 6. This result is, of course, explainable given the extremely thin lubricant film, $\Lambda = 1.2$, which is developed under these operating conditions. This high wear rate would be expected to produce a reduction in bearing life over an extended period of operation. The authors conclude that the Syn B fluid is also undesirable for use in the application.

Through SEM analysis of the bearing surfaces, the number of potential candidate lubricants was reduced to two, Min C and Syn A. Comparison of the surface protection offered by these fluids with that of the baseline oil is typified by the cross-groove scans shown in Fig. 7. Overall, it appeared that the conditions of the surfaces run with Syn A were better than those of bearings run with Min C and approached the conditions of the surfaces run in Min A. This result was not anticipated since it means that the lubrication performance of this synthetic fluid is superior to the performance projected on the basis of viscosity and calculated Λ values. Nonetheless, it was felt, on the basis of posttest surface appearances, that this lubricant could be substituted for the heavier mineral oil in the application without risk of a significant loss of bearing performance.

This result appeared to contradict the trends implied by the collected life data, since the group tested in Syn A was the only one to produce two failures. It was decided to run a verification life test on a 20-bearing test group using Syn A lubricant. The data from the two test lots were then combined for the calculation of the experimental Weibull parameters. The experimental L_{10} life was then compared with the basic theoretical rating life

and adjusted rating life values calculated considering life adjustment factors. These values are shown in Table 3. The resultant experimental value, $L_{10} = 29.3 \times 10^6$ revolutions, compares favorably with these calculated values. While this does not establish that Syn A provides lives comparable to those obtainable with Min A, it does show that the Syn A fluid could be substituted for Min A in the application with a minimum risk of an increase in the bearing failure rate.

On the basis of these experimental results, the Syn A fluid was released for extensive field evaluation. After approximately 3 years of service in petrochemical process pumps and compressors, this synthetic lubricant's field performance continues to support the validity of the conclusions reached during the laboratory investigation.

Conclusions

The experimental program and subsequent field trials described have demonstrated that bearing life testing conducted on small lots coupled with the posttest evaluation of surface morphologies by high-magnification scanning electron microscopy can be decisive in establishing the relative rankings of lubricants. The utilization of this technique in multivariable lubricant evaluation test programs can produce reliable results with a significant reduction of both time and cost expenditures from those required for the conduct of a traditional life test series. Furthermore, while it has not yet been attempted, it is probable that such techniques can also be employed in the comparative evaluation of the life potential of experimental bearing materials with a similar savings.

TABLE 3—*Comparison of calculated and experimental L_{10} values.*

Values	L_{10}, 10^6 revolutions
Calculated	
Basic Lundberg–Palmgren bearing rating life	26
Modified life for Syn A lubrication	20.8
Modified life for Min A lubrication	29.9
Experimental	
Estimated life with Syn A lubrication	29.3

References

[1] Weibull, W., *Journal of Applied Mechanics*, Vol. 18, 1951, pp. 293-297.
[2] Mann, N. R., Schafer, R. E., and Singpurwalla, N. D., *Methods for Statistical Analysis of Reliability and Life Data*, Wiley, New York, 1974.
[3] Gross, A. J. and Clark, V. A., *Survival Distributions: Reliability Applications in the Biomedical Sciences*, Wiley, New York, 1975.
[4] Nelson, W., *Life Data Analysis*, Wiley Interscience, New York, 1982.
[5] Birnbaum, Z. W., "On the Mathematics of Competing Risks," DHEW Pub. No. (PHS) 79-1351, U.S. Government Printing Office, Washington, D.C., 1979.
[6] Kaplan, E. L. and Meier, P., *Journal of the American Statistical Association*, Vol. 53, 1958, pp. 457-481.
[7] Moeschberger, M. L. and David, H. A., *Biometrics*, Vol. 27, 1971, pp. 909-933.
[8] McCool, J. I., *A.S.L.E. Transactions*, Vol. 21, No. 4, May 1974, pp. 271-284.
[9] McCool, J. I., *Journal of Statistical Planning and Inference*, Vol. 3, 1979, pp. 39-68.
[10] "Bearing Failures and Their Causes," SKF Industries, Inc., Philadelphia, Pa., 1980.
[11] Tallian, T. E., Baile, G. H., Dalal, H., and Gustafsson, O. G., "Rolling Bearing Damage Atlas, A Morphological Atlas," SKF Industries, Inc., Philadelphia, Pa., 1974.
[12] Morrison, F. R., Zielinski, J., and James, R., Jr., "Effects of Synthetic Industrial Fluids on Ball Bearing Performance," 80-PET-3, American Society of Mechanical Engineers, Energy Technology Conference, New Orleans, La., Feb. 1980.

R. S. Sayles[1] and P. B. Macpherson[2]

Influence of Wear Debris on Rolling Contact Fatigue

ABSTRACT: Results are presented on the influence of internally generated wear debris on the failure characteristics of rolling element bearings. The effects of lubricant filtration are studied, and by means of Weibull failure distributions the gains in fatigue life are shown to be as high as sevenfold if the filtration level is set correctly. Metallurgical results are presented which show that, when lubricant contamination is present, early failures, and particularly those which strongly influence L_{10} lives, are mostly surface initiated, and not subsurface in origin, as was previously believed to be the case with rolling contact.

KEY WORDS: filtration, rolling contact fatigue, Weibull distributions, reliability, bimodal distributions, surface-initiated failure, surface roughness, lubrication, bearing steels

Detailed studies of rolling element bearing failures will often reveal that spalls and cracks exist in and around indentations created by rolled-in debris. Such effects have been seriously considered by rolling element bearing manufacturers and users for some years, as evidence suggests that many of the early failures experienced have more than a random connection with this form of indentation history.

Over recent years, effective steps have been taken to improve the cleanliness of bearing steels, and this has resulted in greatly increased rolling contact fatigue lives. It seems reasonable to suppose that debris indentation could impair fatigue properties just as much as nonmetallic inclusion; yet, until recent years, such obviously damaging defects have been ignored.

Research into the effects of debris on fatigue life has not been given a great deal of attention, and this is not surprising in view of the many problems

[1]Lecturer, Imperial College of Science and Technology, Department of Mechanical Engineering, South Kensington, London, SW7, England.
[2]Head of Tribology, Westland Helicopters Ltd., Yeovil, Somerset, England.

which must be overcome to generate an unambiguous representation of a general principle. Fatigue is by nature a statistical process; combine this with the problems associated with generating, isolating, and quantifying populations of small particles, and a formidable problem emerges.

Work to date has tended to concentrate on standard fine dusts, where known particle distributions exist [1,2].[3] This research has emphasized the importance of filtration on fatigue life. The present authors considered the morphology of the indentation damage to be of such importance that they elected to study the effects of real wear debris rather than the artificial dusts used in earlier work.

The need for filtration in lubricant systems is a well-established principle, but at what level and by which means it should be accomplished are far from well defined. Current practice with, for example, helicopter gearboxes is to fit 25 or 40-μm cartridge filters. The present research shows that large increases in fatigue life can be obtained by reducing these to a 3-μm level. A relatively smaller improvement can be seen by further reducing the filter rating, but this has to be achieved by employing more complex techniques.

In view of the order of film thickness existing in hertzian contacts, improvements in life could be expected if filtration were achieved at a submicrometre level. To do this, the use of centrifugal and other mechanisms is necessary, and each mechanism has its own attendant problems, not the least of which is the possibility of damaging the long-chain molecules present in lubricating oils. However, centrifugal filters do offer the potential for removing air and water, the content of the latter being surprisingly high in some synthetic oils [3].

There are two main objectives to this paper. The first is to emphasize the increases in reliability, and therefore the times between overhaul (TBO), that can be achieved with well-designed filtration, and to identify the mechanisms and failure characteristics inherent in debris-induced failure. The second objective concerns the performance of rolling contacts in a real environment. An extract from the British Standard on load rating and life of rolling bearings [4] defines bearing life as:

> the period of unimpaired performance of a rolling bearing when the bearing is properly mounted, adequately lubricated, protected from foreign matter and not otherwise subjected to extreme operating conditions.

It would be difficult to find applications outside the laboratory where all these conditions are satisfied, and in the real world, failures are often the result of many conditions that are less than ideal. Attempts to include other effects have been proposed (for example, Ref 5) but only adopted in part by means of additional modifying factors to the basic life equation.

The possibility of more than one mode of failure influencing the same bearing population is often increased when the environment is outside the labora-

---

[3]The italic numbers in brackets refer to the list of references appended to this paper.

tory. Bompas–Smith [6] considers this situation of such importance that he includes a chapter on mixed distributions in his book on mechanical reliability. Evidence of multimode failure distributions with practical systems is widespread, and this is particularly the case with tribological systems where evidence of bimodal wear-out distributions abounds in the literature. Tourret and Wright [7] edited the proceedings of a recent rolling contact fatigue symposium in which about 30 percent of the Weibull distributions printed show the existence of a bimodal situation. One of the principal reasons for the occurrence of this form of distribution is discussed in this paper, and results are presented which indicates that early failures in rolling contacts, and therefore those which most influence L_{10} life and reliability estimates, are not caused by the accepted subsurface-initiated fatigue mechanism of failure but by wear debris or similar surface-initiated failure.

Test Equipment

The test equipment was designed to represent helicopter gearbox systems as closely as possible. A gear machine [8] based on the National Aeronautics and Space Administration (NASA) design was employed to generate wear debris quickly by running a gear pair in a helicopter-type oil specially formulated to have a low load-carrying capacity. The gears employed were of a helicopter form and manufactured from EN39B steel, carburized, and hardened to 750 VHN after grinding.

Because of continuous filtering and monitoring of the contaminated oil, known debris distributions could be fed into a parallel roller bearing fatigue machine. Bearing lives were to be measured in terms of absolute filter ratings and β values, which are more informative [9]. All other variables were maintained constant. A schematic diagram of the oil circuit is shown in Fig. 1, and the rate of particle generation as a function of the filter rating is demonstrated in Fig. 2. Figure 3a shows the general layout of equipment used to generate, filter, and monitor the lubricant supply. Contaminated oil is fed through a previously calibrated filter into the bearing machine. In-line particle counting is provided for continuous monitoring from positions downstream and upstream of the filter. Problems associated with air bubbles had been anticipated, but by using a funnel-shaped settling tank all air was liberated and no bubbles were, in fact, observed in the HIAC system. Provision was made for maintaining the oil at constant temperatures. The magnetic filter, seen to the left in Fig. 3, was used for submicrometre particle extraction and for the rapid polishing of the oil when required. The cartridge-type filters were of absolute ratings 40, 25, 8, 3, and 1 μm.

The bearing fatigue rig is shown in Fig. 3b, where an accelerometer, centrally located between the two test bearings, successfully registered the onset of spalling, and the machine was automatically shut down on reaching a predetermined vibration amplitude. The accelerometer had been positioned im-
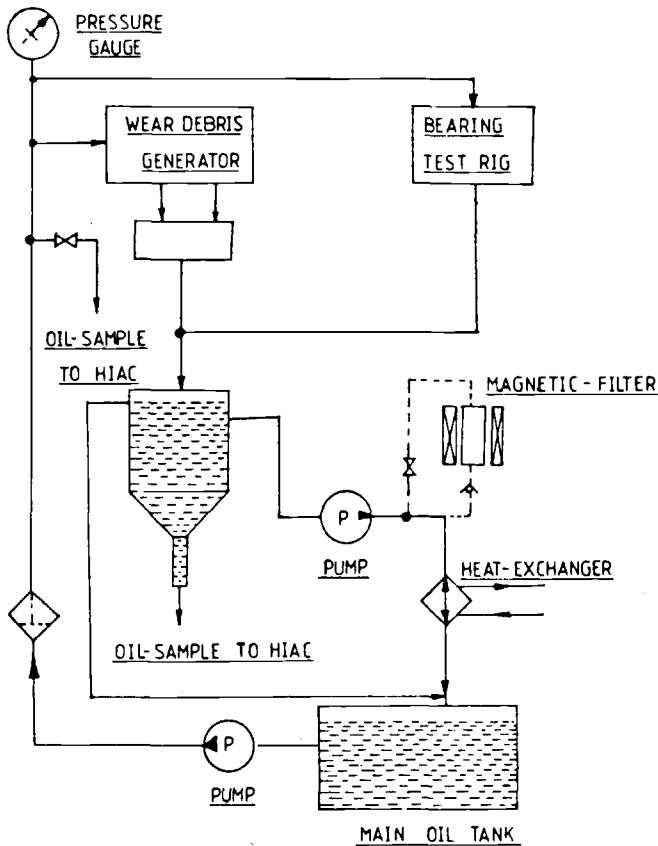
FIG. 1—*Test oil circuit.*

mediately over the loading bearing yoke, which, fortuitously, was acting as a mechanical amplifier. Repositioning the accelerometer rendered it useless, so throughout the testing both test bearings had to be removed and examined to determine which one had failed.

The test bearings employed were a standard 25-mm-bore extra-light series, single-row cylindrical-roller bearings with 14 inner located rollers in a brass cage. The radial internal clearance was specified as 25 to 35 μm prior to fitting. A list of bearing material properties appears in Appendix I.

Filter Characteristics

As with electric wave filters, the roll-off or cutoff characteristics of a filter are not abrupt. A filter rated at 40 μm will pass a proportion of particles both
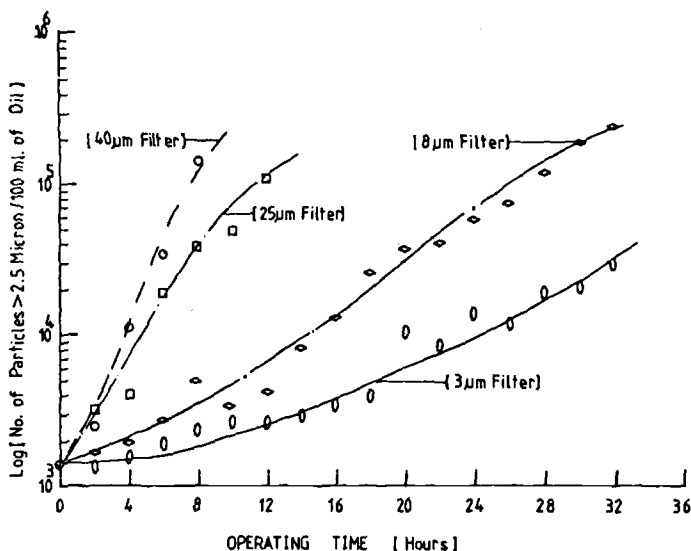
FIG. 2—*Rate of particle generation at various filtration levels.*

above and below the rated size. The present practice is to express a filter's performance in terms of β value [9], which is the ratio of the density of particles greater than a specified size which exist at the entrance and exit of the filter, respectively. Thus, by generating β values at various values of particle size, we can create the complement of the cumulative distribution function representing particles passing through the filter. Such curves are often called efficiency curves, and for the 25-μm nominal cartridge type used in this work, Fig. 4 shows the performance characteristics found to exist.

It is obviously convenient to use a single parameter to define performance, but the authors are by no means convinced that the β ratio, based on fine dust calibrations, fulfills this function any better than a root mean square (rms) or centerline average (Ra) value describes the topography of a surface. It seems clear that in both cases the single parameter is often useful when comparing like with like, but its usefulness is not so clear in other cases. Parameters such as collector size, porosity, material, flow rate, viscosity, length, and particle concentration must all influence filter performance. The authors have found discriminant functions [10] useful in determining the relative importance of groups of variables and are currently applying such techniques as part of a detailed theoretical study of many aspects relating to filtration and the damaging influence of debris.
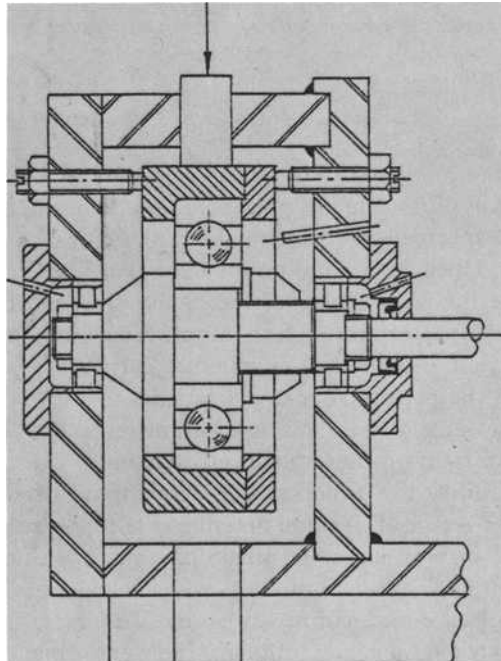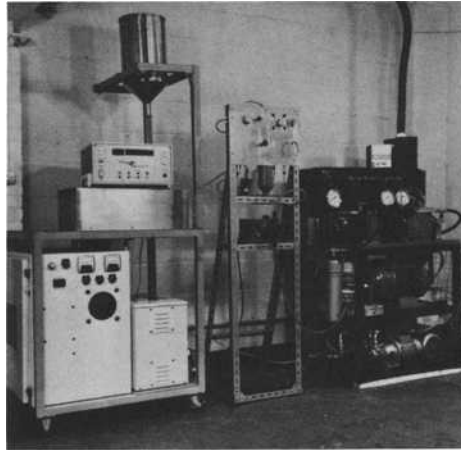
FIG. 3—(Top) *Layout of test equipment:* (bottom) *sectional view of the bearing test rig, showing the test bearings at each end of the main shaft.*
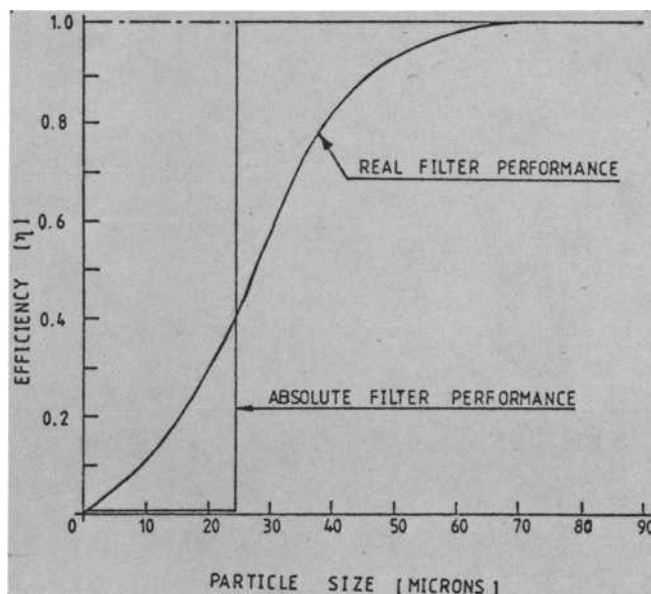
FIG. 4—*Filter transmission characteristic for the 25-μm filter.*

Results

Fatigue Tests

The bearing material properties and test conditions employed are given in Appendix I. Initial tests were carried out using 3-μm filtration to establish a rough *S–N* relationship [8], and this was used to specify test loads.

The principal tests were run under the conditions defined in Appendix I, and a sample of ten bearings was run to failure at each of the absolute filter ratings: 1, 3, 8, 25, and 40 μm. Each of the distributions, together with results obtained using magnetic filtration, are shown plotted on Weibull probability scales in Fig. 5. The best least-squares fit to the experimental points for each of the six Weibull plots is shown for comparison in Fig. 6. Tabulated results indicating the respective Weibull slopes and confidence limits associated with the 10 and 50 percent failure points are shown by entries 1 to 6 in Table 1. A consistent increase in fatigue life is obtained as the filter rating is reduced. This effect is also shown in the combined filter-size-V-life plot of Fig. 7.

Table 1 also shows the results of tests designed to examine the effects of film thickness and in what order filtration must be applied. Entries 7 and 8 show tests run at the lowest lubricant temperature of 30°C, which would theoretically increase the minimum film thickness from about 0.6 to 1 μm. The last entry (No. 9) shows the effect of running the test for an initial 30 min at
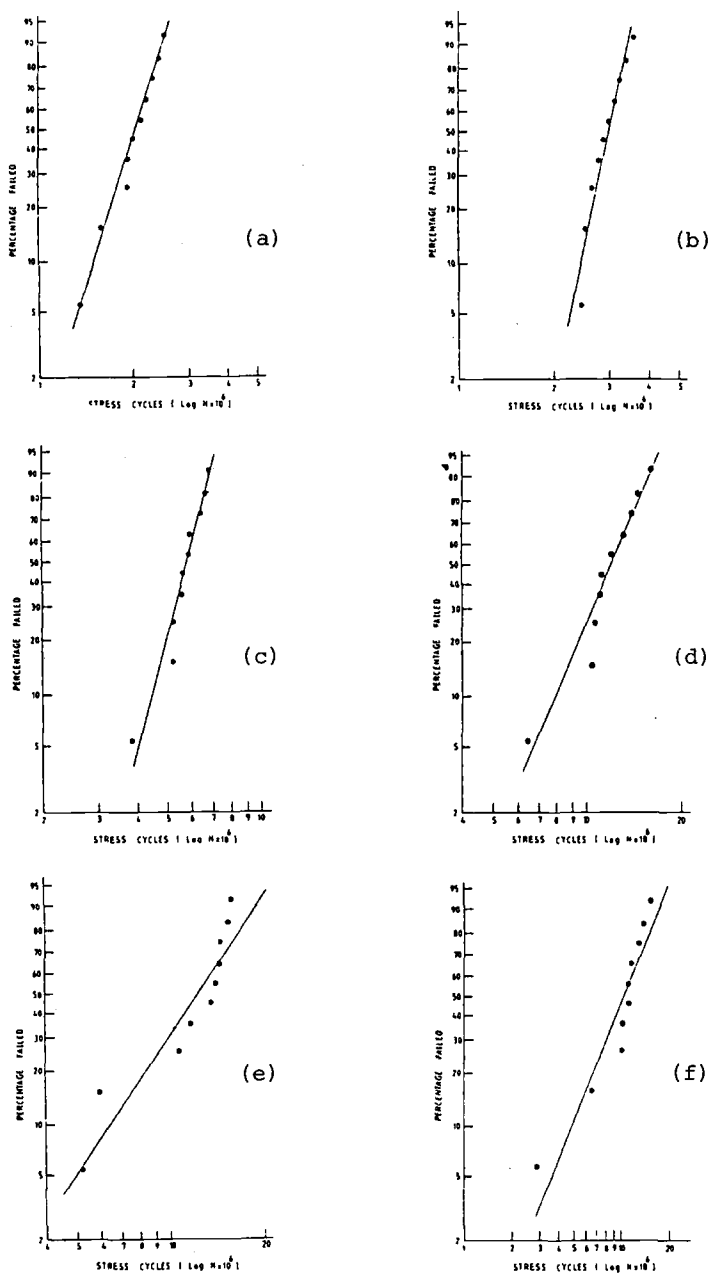
FIG. 5—*Weibull distributions of the bearing fatigue results under various levels of lubricant filtration: (a) 40 µm; (b) 25 µm; (c) 8 µm; (d) 3 µm; (e) 1 µm; (f) magnetic filter.*
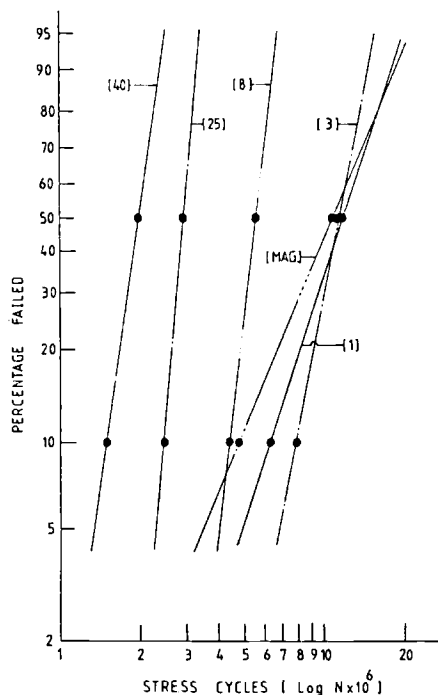
FIG. 6—*Weibull distributions of bearing failure under various levels of filtration. The best fit lines from Fig. 5 are shown together with the L_{10} and L_{50} lives at each filter rating.*

40-μm filtration and then running it to failure with only a 3-μm filter. It is apparent from these results that, although some improvement in life can be obtained by increased film thickness, this improvement is relatively small compared with that obtained by reduced levels of filtration.

The final entry in the table also shows that little improvement is obtained if the correct level of filtration is not applied from the outset. This result is extremely informative as to the mechanism of failure, as it suggests that the indentation damage caused by debris is what leads to failure and not the continued presence of that debris. The 10 and 50 percent failure times for this 40/3-μm test are not greatly removed from the result obtained by continuous 40-μm filtration, and the slight increase in life observed could be totally due to the increased film thickness. Thus it appears that the initial damage over 30 min of prerunning at 40-μm filtration set the future failure characteristics of the bearing.

Metallurgical Examination of Failures

Preliminary examination of the rolling surfaces was made under low magnification ($\times$25) where general features were noted and the nature of the fail-

TABLE 1—*Weibull failure parameters as a function of filter rating.*

Test No.	Test Filter Absolute Rating, μm	Experimental Life, millions of stress cycles				Weibull Slope
		B_{10} Life	90% Confidence Limits	B_{50} Life	90% Confidence Limits	
1[a]	40	1.497	1.00 to 2.02	2.076	1.89 to 2.29	5.76
2	25	2.457	2.04 to 2.95	3.002	2.91 to 3.09	9.40
3	8	4.470	3.44 to 5.81	5.849	5.44 to 6.33	7.00
4	3	8.036	5.54 to 11.64	12.022	10.70 to 13.46	4.68
5	1	6.535	3.60 to 11.77	12.427	9.94 to 15.54	2.93
6	magnetic	4.975	2.93 to 8.45	10.013	8.31 to 12.01	3.21
7	40	1.795	...	3.283	...	3.12
8	3	9.252	...	16.233	...	3.35
9	40/3	1.723	...	3.050	...	3.30

[a]Test results 1 through 6 relate to a calculated film thickness of 0.576 μm, and results 7 through 9 relate to 0.987-μm film thickness.
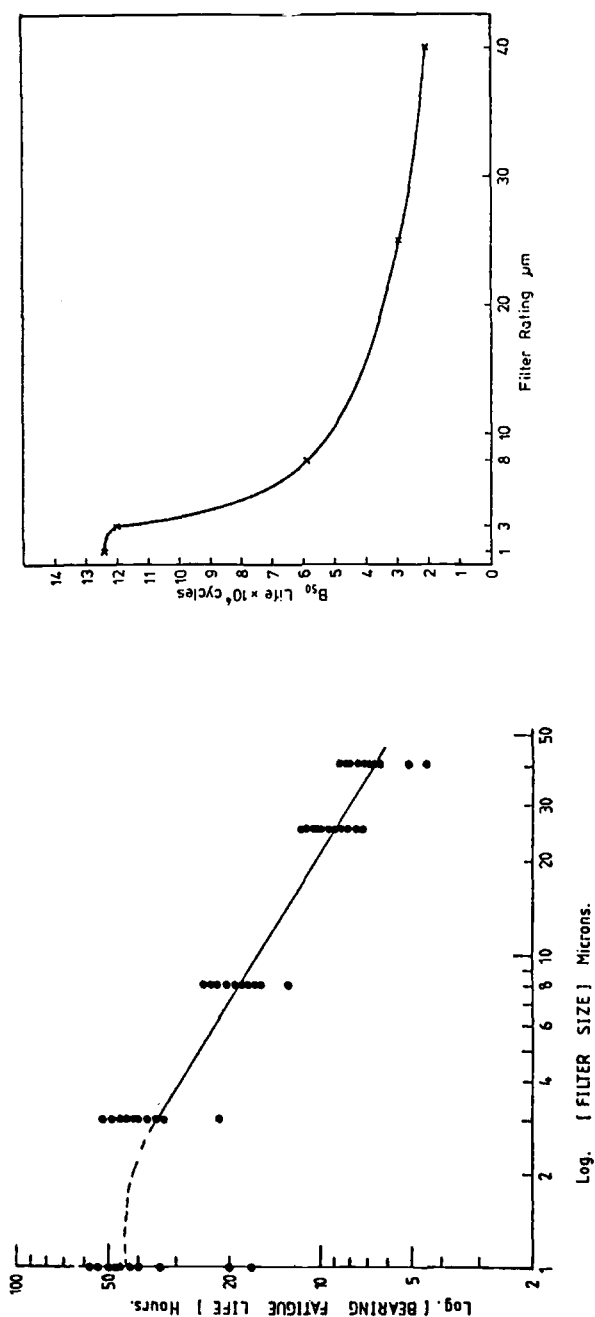
FIG. 7—Bearing life (L_{50}) as a function of filter size plotted on a log ordinate scale (left) and a linear ordinate scale (right). The continuous line of the graph at the left represents a 2/3 power law.

ures tentatively identified. Debris indentations were revealed over all the surfaces, along with occasional transverse cracks. Microhardness measurements were made across the rolling tracks, and nital-etch examination was made for possible grinding burns. The most interesting-looking failures were selected for detailed examination when metallographic sections were prepared through failure sites to study the microstructure and to obtain future information on the failure mechanism. Fatigue failure profiles were studied by progressively grinding back and polishing across the running path.

The failure modes were identified and classified as follows:

(a) transverse cracks across the running path,
(b) incipient failure at a transverse crack,
(c) straight-sided or circular pits at a transverse crack,
(d) incipient failure not associated with a transverse crack,
(e) fatigue pits not associated with a transverse crack,
(f) fatigue pits at an indentation, and
(g) extensive surface breakup near an indentation or crack.

The distribution of failure classification in terms of contamination level was studied, but no overall pattern was discernible. A summary of the main observations follows:

1. Generally, transverse cracks were found for all levels of filtration.
2. The presence of failures, whether associated with transverse cracks or not, under all levels of filtration suggested that the failure mechanism was independent of the filtration level.
3. Many of the failure pits were associated with debris indentations and surface scratches.
4. Metallographic examination in the rolling direction revealed that the transverse surface cracks penetrated perpendicularly to the surface to depths of between 0.20 and 0.75 mm.
5. Secondary cracking branching off the primary cracks was frequently observed at depths below the surface of 0.08 to 0.10 mm (Fig. 8, left).

A typical example of a crack initiated at a debris indentation site is shown to the right in Fig. 8. The average size of pit formed was between 0.4 and 0.6 mm in diameter and 0.05 to 0.10 mm deep.

Discussion

The results of the filtration level against the rolling contact life presented earlier are shown on a linear scale in Fig. 7b and indicate a well-defined improvement in life down to a filtration level of about 3 μm. A relationship of $L \propto \mu^{2/3}$ (where μ is the absolute filter rating) has been found to fit these results over the 3 to 40-μm range [8].
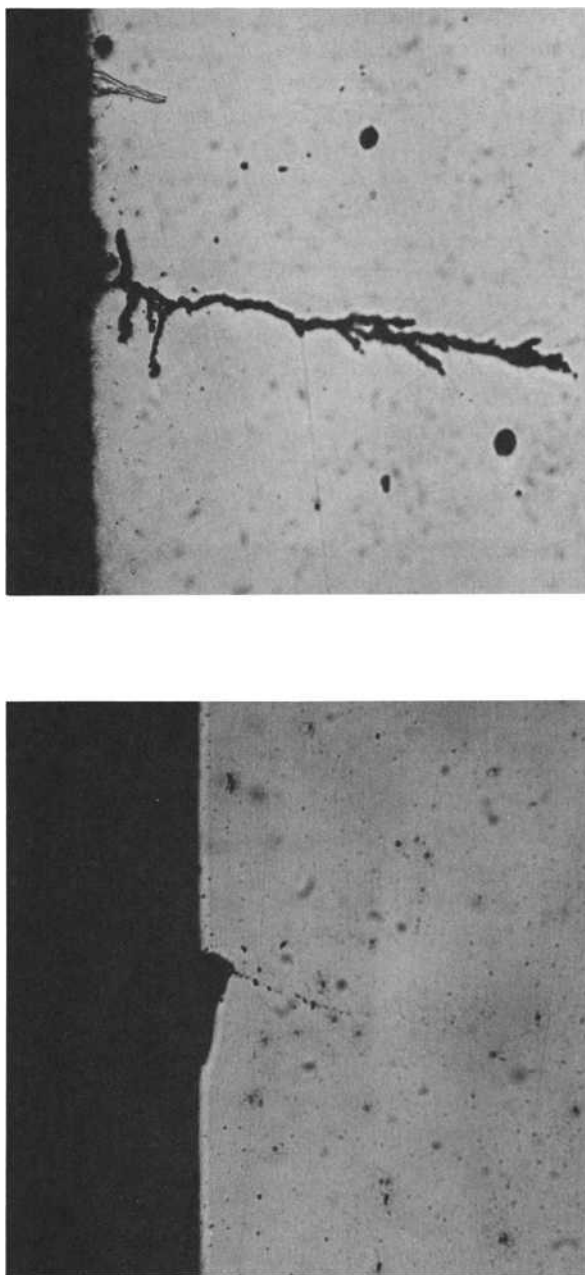
FIG. 8—Crack propagation from indentations created under (left) 40-µm and (right) 25-µm filtration (×400). The depth of the crack (right) is above 150 µm, almost twice the depth of the nominal maximum shear stress region.

Further results show that increasing the film thickness has the effect of increasing fatigue life. With approximately constant roughness, this increase is equivalent to an increase in the Λ ratio and is therefore not an unexpected result. However, the suggested reasons for failure are closely connected to the effects of surface roughness, and it seems that it might be appropriate to treat debris contamination effects in much the same way as we deal with the problems of roughness.

To incorporate a theory of debris influence on fatigue life without reference to surface roughness is as misguided as considering only that Λ ratio itself as important. One approach might be to consider the increase in roughness caused by debris indentation with rolling time and relate this to the gradual growth in the Λ ratio. A second approach might be to incorporate debris content or filtration rating in some dimensionless group with surface roughness as a conventional weighting parameter to use in the way environmental effects are incorporated at present.

The mechanism of fatigue initiation and subsequent failure is suggested by the results to be governed by the combined effects of film thickness, roughness, and debris size. It is tempting to state that a very narrow band of debris sizes around 3 μm influence fatigue life, and in fact the results obtained show that little advantage is obtained in going much below this figure. A very plausible theoretical explanation for this result can also be put forward, in that the maximum gap between surfaces within the contact will occur when deep valleys on each surface coincide. Assuming Gaussian topography, this would make the maximum local film about 6 standard deviations of the composite roughness plus the elastohydrodynamic (EHD) film thickness (in our case, around 2 to 4 μm). Thus debris of about 3 μm and less could find a path through the hertzian contact without causing a great deal of local damage. This appears to represent a reasonable explanation for the principal result of our work, that the optimal level of filtration is about 3 μm.

The preceding discussion portrays a minimum debris size of importance but says little about the range of sizes of the debris that is most influential in initiating fatigue failure. If filter cutoff characteristics were abrupt, then we would expect to see a marked change in fatigue life as we pass through the critical debris size range, in terms of filter ratings. This, unfortunately, is not the case, and by reducing filter ratings, we may be only seeing the effects of a gradual proportionate reduction in the content of the most damaging debris. This has the effect of masking the upper limit on debris size, which might be an important demarcation.

A study of the indentations present on the worn surfaces gives us some idea of the size of particles which enter the contact. Figure 9 shows such a surface from the 40-μm filter results. The majority of visible indentations are small, and the density appears to increase as a function of decreasing size. Intuitively, this is what would be expected with something like a log-normal distribution of indentation sizes existing. And based on the previous arguments and re-

FIG. 9—*Debris indentation damage created under 40-μm filtration conditions (×100).*

sults, the mode of this distribution would be expected to occur around or a little above the 3-μm level, which was found to be the particle size describing the lower limit of influential debris. The upper limit still cannot be defined by the indentation history; Fig. 9 shows damage up to sizes of about 60 μm, but all that can be said from this information is that particles in excess of 60 μm have entered the contact. An upper limit to the size of particles that can enter the contact must exist, but from these results it is impossible to define this limit accurately.

The final result in Table 1 indicates that the mechanism of failure is associated with a change in surface contact properties rather than the continued presence of a third body. A theory of the failure mechanism consistent with this result would be that over the initial 30-min running the larger debris causes a detrimental change in the topography of the contacting surfaces. The removal of this debris by subsequent continuous 3-μm filtration has little or no effect on the contact mechanics within the interface. Thus, the surfaces proceed to failure by contact stress cycling almost as if the lubricant were continuously filtered at a 40-μm level, the damage having already been done during the initial period.

The changes in topography required to generate failure as if 40-μm filtration were always present could vary considerably. One mechanism for which there is experimental evidence, in the way of photomicrographs of cracks ap-

pearing and pits beginning around the edges of indentations, is the associa-
tion of each pit with a considerable built-up edge, which represents a rela-
tively severe local asperity. A second mechanism could be thought of as the
effect of the indentations themselves acting as lubricant reservoirs, by one
means or another, and reducing the local film thickness within the contact
during running. In reality, a combination of these two effects is the most likely
cause of failure, creating increased local stresses around the shoulders of in-
dentations in a cyclic manner, which leads to crack initiation and propaga-
tion and subsequent pit formation.

The high values of Weibull slope shown by the results indicate a very rapid
degradation process operating over a relatively narrow band of failure times.
Loewenthal and Moyer [2] and also Tallian [11] have shown this to be the case
when debris is introduced into rolling contacts. Accelerated fatigue tests in-
variably produce higher Weibull slopes than those expected, and to some ex-
tent this is a direct result of the convergence often seen at high stress levels on
S-N relationships. In general, however, such effects produce slopes of around
1.0 to 1.5, much closer to those expected than to the higher values shown here.

An important implication of the results obtained is indicated by these high
slopes and their likely effects in real-life situations on early failures, and par-
ticularly on those failures affecting the definition of L_{10} lives. Many Weibull
plots show a bimodal form of failure with rolling contacts, and invariably the
early failures experienced show a tendency to possess a much higher slope
than later failures, which follow the life relationships expected and predicted
by bearing manufacturers. In a recent conference report on rolling contact
fatigue [7], about 30 percent of the Weibull distributions shown, taken from
a total of 18 papers, show the tendency described.

The Weibull distribution is a sensitive tool when used to disclose mecha-
nisms of failure [6], and the presence of the many bimodal distributions seen
in the literature points to the possibility of two different mechanisms of sur-
face fatigue failure. We believe the first is the well-established subsurface-
initiated failure mode, but a second, and in general much more important
mechanism as far as reliability prediction is concerned, is surface-initiated
failure. In the latter case, the presence of relatively high surface roughness,
or a third body in the form of debris suspended in the lubricant, acts to create
local stresses high enough to generate crack initiation at the surface. The ul-
timate result is that both mechanisms create much the same surface damage
in the form of spalling, but surface-initiated failure appears to be associated
with very early failures and also appears to be subject to much higher failure
rates.

To investigate bimodal failures in rolling contact fatigue, Harries et al [12]
first looked at the possibility of the effects of sampling from a larger popula-
tion. A total of 100 samples of 12 were randomly selected from a population
of 24 rolling contact four-ball tests carried out by Diaconescu [13]. The dis-
tributions were then considered to have slopes β_1 over the earliest 50 percent

of failures and β_2 over the later failures. A sample of the results for early failures is shown in Fig. 10 and serves to emphasize the inaccuracies in L_{10} life and Weibull slope which can arise from small-sample fatigue tests. The main conclusion drawn from these results, however, was that early failure results tend to show a slightly low rather than high value of slope. A further interesting result, which serves to emphasize this tendency, is shown in Fig. 11, where the distributions of L_{10} and L_{50} values are shown from the random sampling tests. Harries et al [12] went on to show that if early failure results from several published papers were interpreted as independent failure modes, then the Weibull slopes involved were much higher, and approached the tendency to high Weibull slopes seen from the debris-induced results. Thus, although this study did not prove that many of these early rolling contact failures are due to surface-initiated debris or roughness-induced fatigue, the possibility that random sampling is responsible for high initial Weibull slopes was dispelled. Thus further evidence is presented to support the body of opinion that reliability predictions based on L_{10} lives may be becoming much more sensitive to the cleanliness of our lubricants rather than to the material quality and manufacturing practices used in component production.

Conclusions

The effects of filtration on rolling contact fatigue life are examined in the light of test results obtained from roller bearing fatigue tests using lubricants contaminated with gear machine-generated debris, which was created as representative of that found in helicopter gearboxes. Results are presented
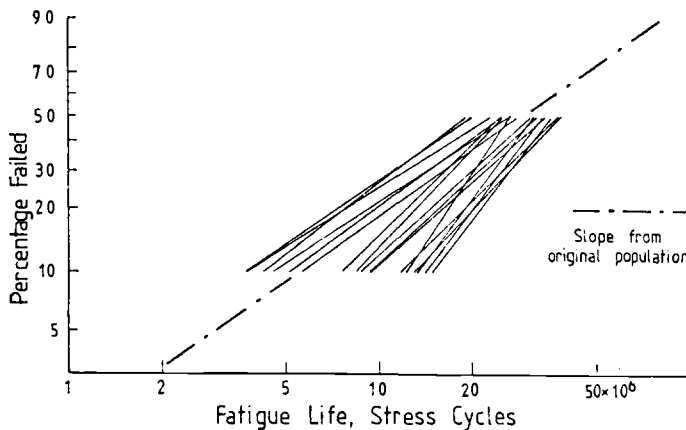
FIG. 10—*Best fit Weibull lines of some 16 randomly selected sets of 12 failures from an original population of 24. The data are plotted over the initial 50 percent lives to test the bimodal character of failure.*
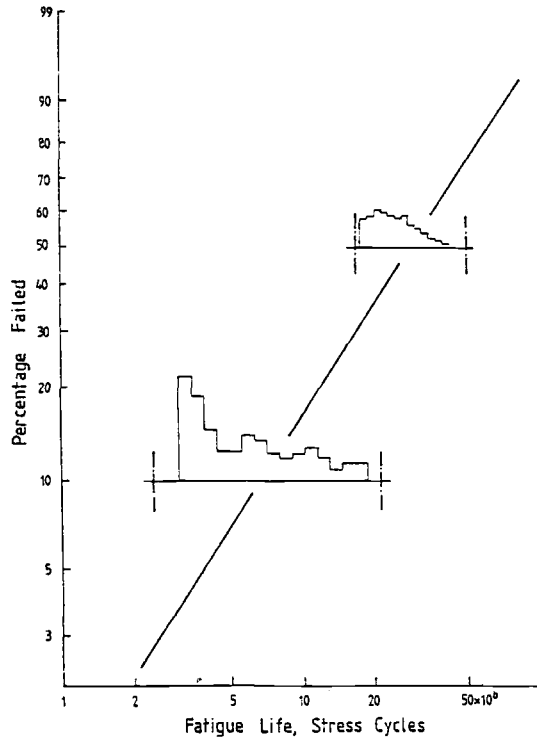
FIG. 11—*Histograms of* L_{50} *and* L_{10} *lives shown on a linear scale of 100 randomly selected sets of 12 failures from an original population of 24. The chain dotted line shows the 90 percent confidence limits.*

which show a well-defined sevenfold increase in L_{10} life as the filter size is reduced from 40 μm to an optimum of around 3 μm, the approximate maximum film thickness existing in test bearings.

The implications of this filter rating in terms of the mechanisms of fatigue initiation are discussed in detail, and evidence is presented which suggests that debris-initiated failure originates at the surface and not the subsurface. Results from tests using a 40-μm filter for a short period and then proceeding to failure with 3-μm filtration indicate that a change in surface contact mechanics takes place as a result of debris indentations on the contacting surfaces and that this new topography creates the conditions for fatigue failure, not the continuous presence of the debris itself, as might be expected. Such results indicate that correct filtration must be applied from the outset of running and not just over a limited period of operation.

The critical size range of debris is investigated and, although the existence of a possible upper limit of damaging particle sizes cannot be defined from these results, the all-important lower limit which can be used to define effec-

tive filtration is well established. Theoretical and experimental evidence is presented which sets this optimum filtration level at 3 μm.

Weibull analysis of fatigue results shows that the failure distributions possess relatively high slopes at all filter ratings. This relatively high negative skew has been shown by other research in this field [2] but has tended to reveal little change in the L_{10} values. The results presented here show that when real debris is employed, as opposed to the standard fine dusts used in previous work, the relative differences apparent around the mean and modal regions of the distributions are reproduced in the L_{10} regions, which therefore shows that definite differences in predictable reliability can be achieved by the specification of lubricant filter rating.

The presence of bimodal failure distributions in many reported fatigue results often reveals that early failures are represented by a high Weibull slope value. Random sampling tests are presented which show that this bimodal effect is unlikely to be the result of sampling, but is much more likely to be the effect of a different failure mechanism. In view of the high Weibull slopes apparent with debris-initiated failure, we tentatively suggest that many of the distributions presented in the published literature are showing two failure mechanisms: the first is surface initiated through the presence of lubricant contamination; the second is the classic subsurface-initiated mechanism. The importance of this hypothesis is not that these two mechanisms exist but that the early failures, and therefore those which most influence L_{10} lives and reliability predictions, are not totally dependent on loading conditions, contact geometry, and bearing design, but are most sensitive to lubricant cleanliness and surface roughness.

APPENDIX

Bearing Material Properties and Test Parameters

Material:	high carbon chromium EN31 steel (AISI 52100)
Compressive strength:	1.38 GPa (0.2×10^6 lb/in.^{2})
Elastic modulus:	207 GPa (30×10^6 lb/in.^{2})
Poisson's ratio:	0.3
Hardness:	750 VHN (min)
Surface roughness:	0.3 μm Ra (12 μin.) inner/outer race⎫ at 0.08-mm
	0.05 μm Ra (2 μin.) rollers ⎬ cutoff
Reduced elastic modulus:	357 GPa (51.8×10^6 lb/in.^{2})
Bore diameter:	25 mm (0.9843 in.)

Test speed: 5 000 rpm
Lubricant: modified Mobil Jet II
Operating temperatures: 70°C (158°F) and 30°C (86°F)
Radial load: 2957 N (665 lb)
Minimum lubricant film   0.5767 μm (22.70 μin.)
  thickness:
Maximum hertz contact stress: 2.82 GPa (408 900 psi)
Contact size: 0.293 × 3.708 mm (0.01152 × 0.146 in.)
Maximum depth to maximum   0.095 mm (0.00374 in.)
  shear stress:

References

[1] Dalal, H. and Senholzi, P., "Characteristics of Wear Particles Generated during Failure Progression in Rolling Bearings," *A.S.L.E. Transactions*, Vol. 20, No. 3, 1976.
[2] Loewenthal, S. H. and Moyer, D. W., "Filtration Effects on Ball Bearing Life and Conditions in a Contaminated Lubricant," *Transactions, ASME, Journal of Lubrication Technology*, Vol. 101, No. 2, 1979.
[3] Spikes, H. A. and Macpherson, P. B., "Water Content of Helicopter Gear Oils," Paper No. 80-C2/DET-12, International Power Transmissions and Gear Conference, San Francisco, Aug. 1980.
[4] "Rolling Bearings-Dynamic Load Rating and Rating Life," BS5512, Part 1, 1977.
[5] Jacobson, P. E., "Use of EHD Film Theory in Designing Practical Bearing/Lubricant Systems," International Ball-Bearing Symposium, Charles Stark Draper Laboratory Inc., Cambridge, Mass., 5-7 June 1973.
[6] Bompas-Smith, J. H., *Mechanical Survival*, McGraw-Hill, New York, 1973.
[7] Tourret, R. and Wright, E. P., *Rolling Contact Fatigue, Performance Testing of Lubricants*, Hayden & Son Ltd., London, 1977.
[8] Bhachu, R., Sayles, R. S., and Macpherson, P. B., "The Influence of Filtration on Rolling Element Bearing Life," presented at the meeting of the Mechanical Failure Prevention Group, National Bureau of Standards, Washington, D.C., at Gaithersburg, Md., 21 April 1981.
[9] Fitch, E. C., "Controlling Contaminant Wear Through Filtration," *Wear*, Vol. 34, No. 4, 1975.
[10] Sayles, R. S. "The Use of Discriminant Function Techniques in Reliability Assessment and Data Classification," Sixth Advances in Reliability Technology Symposium, University of Bradford, England, 9-11 April 1980.
[11] Tallian, T. E. "Prediction of Rolling Contact Fatigue in Contaminated Lubricants," *Transactions of the American Society of Mechanical Engineers*. Vol. 98, Paper No. 75-Lub-37 and 38, 1975 pp. 251-257 and 384-392.
[12] Harries, C. J., Webster, M., Sayles, R. S., and Macpherson, P. B., "Bi-modal Failure Mechanisms in Tribological Components," Third National Reliability Conference, Birmingham, England, 1981.
[13] Diaconescu, E. N., Kerrison, G. D., and Macpherson, P. B., "A New Machine for Studying the Effects of Sliding and Traction on the Fatigue Life of Point Contacts, with Initial Test Results," 74LC-5A-3, American Society of Mechanical Engineers and American Society of Lubrication Engineers Lubrication Conference, Montreal, Canada, 1974.

Hans-Karl Lorösch[1]

Influence of Load on the Magnitude of the Life Exponent for Rolling Bearings

ABSTRACT: Extensive realistic tests to determine rolling bearing life have previously indicated that the exponent p in the well-known formula $L_n = (C/P)^p$ is a constant, and various institutes of technology have agreed that for ball bearings in particular this constant $p = 3$. Acceptance of this constant means that even under low load conditions a finite life is always to be expected at rolling contact surfaces. However, the classic theory of the strength of materials states that metals, especially steel, have a virtually unlimited life under a cycling load below a defined level. Recent tests on rolling bearings confirmed that under low loads and with elastohydrodynamic lubrication there is no material fatigue, thus indicating that under such conditions bearing life is practically unlimited. The recent tests further indicate that surface damage caused by particles entering a rolling bearing is a much more important factor in limiting bearing life than had previously been believed.

KEY WORDS: rolling bearings, fatigue life, life exponent, contaminant-caused surface damage, bearing steels

The rolling bearing is a very reliable mechanical element with long endurance even under adverse operating conditions, and this, of course, is much appreciated by the user. In addition to the advantages offered by rolling bearings as standardized mechanical elements for design and maintenance, their long life and low-maintenance operation are essential preconditions for universal applicability. But it is just this long life which makes it hard for the researcher to analyze the correlation between the load-carrying capacity, the load, and the life and to establish generally applicable calculation methods.

[1]Manager, Research and Development, FAG Kugelfischer, Georg Schäfer & Co., Department M-PF, Georg-Schäfer-Strasse, Schweinfurt, West Germany.

It is of special interest, though only incompletely understood, to determine whether and how the results obtained from laboratory tests, performed at relatively high loading in order to reduce the testing times, can be applied to bearing performance under the lower loads that occur in field operation.

The life of a ball bearing in millions of inner-ring revolutions is determined by the formula

$$L_n = a_1 \cdot a_2 \cdot a_3 (C/P)^p$$

where

a_1 = factor for failure probability,
a_2 = factor for material,
a_3 = factor for application conditions,
C = dynamic load rating,
P = equivalent dynamic load, and
p = life exponent.

Tests to throw additional light on the influence of load on the life under actual field conditions have not been made beyond the investigations establishing the fundamentals for the exponent p of the life formula for Anti-friction Bearings Manufacturers' Association (AFBMA) and International Organization for Standardization (ISO) standards. A great variety of investigations into fatigue life carried out so far refer predominantly to the influence of new materials and production methods aimed at improving the bearing quality and reducing production costs to a minimum. The variables of such investigations are the design, material, heat treatment, and type of mechanical machining. Numerous investigations include the influence of lubrication on the life in order to determine the effect on rolling contact fatigue strength of a complete or faulty formation of the lubricating film between the active surfaces. The tests proved the cleaniness of the lubricant to be an important parameter.

At the FAG research center many questions concerning rolling bearing life are constantly being investigated. A comparison between old and recent test results shows that the applicability of laboratory test results to the field is questionable, particularly if the following two points are not considered:

1. The loads for life tests with rolling bearings must not be increased beyond reasonable limits. Hence, for over 10 years, long test runs have been accepted when decisions on general field applications have to be made.

The appropriate test conditions for such a case include, for example, a maximum contact pressure of well below 3000 N/mm² at point contact.

2. Test conditions must be defined as completely as possible. This was not done sufficiently in the past by FAG and other research institutes, as can be seen from the fact that rolling bearings in the field achieve longer running times than would be indicated by the commonly applied calculation meth-

ods. Full separation of the surfaces in rolling contact by the lubricating film and the cleanliness of the lubricant have proved to be important parameters influencing the life of rolling bearings. At the present state of technology, the effect of these two parameters on the life must be underlined. Therefore, recent investigations at FAG have included a more comprehensive definition of the test conditions, and thus a better reproducibility of the results.

All the tests described in this article are based on point contact between the surfaces.

Tests at High Loads

In order to get information on the high load range, older test results, some dating back many years, from fatigue life tests carried out at FAG and institutes of technology were sifted. Only results from comparable tests were considered: the specimens were made from vacuum-degassed rolling bearing steel SAE 52100, tested to FAG specifications, and accepted by FAG. The test specimens had to be machined to close tolerances and subjected to a special heat treatment.

Fatigue life tests were carried out on various test rigs for a contact pressure up to 5000 N/mm² (Fig. 1). With the loads chosen, results were produced after reasonable periods of time. As test specimens, complete bearings or bearing components were used, namely, rings, rolling elements, and also shafts. Some of the specimens varied greatly in size. [1,2].[2]

The information obtained from the results of the old tests is, of course, less accurate than that obtained from the new tests. According to the latest technological findings, the conditions of the tests were not sufficiently defined. Furthermore, too few accurate measuring results are available and, as a rule, only ten specimens per test variation were used. Nevertheless, a fairly reliable statement—particularly if these data were regarded as a tendency—could be made from the data gathered from the numerous tests.

Test Conditions

Table 1 lists the geometry of the test specimens and the contact pressures.

The specimens were austenitized at 840°C and, after hardening, tempered for 2 h at 180°C (balls at 150°C). Different surface qualities were obtained, depending on the specimen shape. The arithmetic average of the surface roughness finish of the balls was approximately 0.01 μm, and that of the other specimens was 0.08 and 0.2 μm.

The test specimens were cooled and lubricated with a machine oil of a viscosity of 46 cSt (cSt = mm²/S) at 40°C. The calculated lubricating film

---

[2]The italic numbers in brackets refer to the list of references appended to this paper.
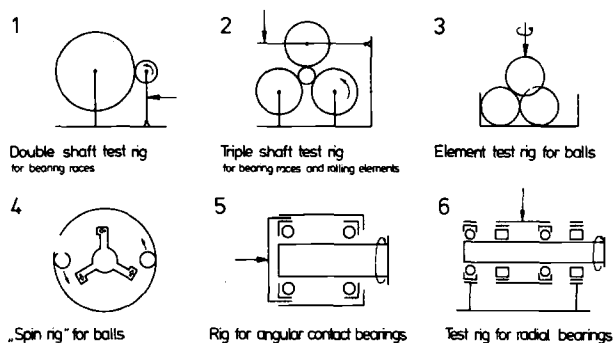
FIG. 1—*Fatigue test rigs.*

thicknesses, h_0, are indicated in Table 1. With some test variations the lubricating film thickness reached just the roughness value R.

$$R = \sqrt{R_{a_1}^2 + R_{a_2}^2}$$

R_{a_1} and R_{a_2} are the arithmetic average values of the surfaces in rolling contact. In favorable test cases almost a full separation of the surfaces was reached, with a ratio $h_0/R \approx 3$. Numerous in-house tests showed that for the investigated range with good cycling conditions, the influence of the lubricating film thickness on the life values can be expressed by a maximum factor of 2.5.

The lubricating oil was filtered. Particles larger than 25 μm were separated from the oil. Newer investigations with finer filters and extremely sensitive monitors, which discontinue the test run at the formation of the smallest pittings on the active surfaces, showed that the influence of contamination on the life had been underrated; the expected origin of damage below the raceway surface—in the area of peak stressing—was not the rule.

Results

The investigations conducted under the described conditions revealed two important results which furnish the key to an overall analysis.

1. Only in the tests with the lowest contact pressure of $p_0 = 2550$ N/mm² did measurable plastic deformations fail to occur. At higher stresses the plastic deformation of the running tracks grew. The typical plotter drawing across the raceway of a ball bearing ring is shown in Fig. 2. This figure shows the pattern of the theoretical pressure distribution (full line). This line is valid in the elastic range only. The broken line represents the pressure distribution assumed after plastic deformation has occurred. The actual maximum

TABLE 1—*Survey of specimen geometry, contact pressure, and load cycles for tests at high loads.*

Test Rig (Fig. 1)	Specimen	Stribeck Pressure, K, N/mm²	Maximum Hertz Pressure, p_0, N/mm²	Curvature Radii, mm[a]				h_0/R	B_{10} Load Cycles, $\times 10^6$	Expected Life Changes with Good EHD Lubrication and Specimen Bearing Type FAG 7205B[b]			
				Specimen 1	Specimen 1	Specimen 2	Specimen 2			Varying Plastic Deformation	Varying h_0/R	Varying Specimen Size	Expected Change
1	shaft	5.54	3800	46	21	∞	149	1.0	40	+	+	=	++
2	roller	4.08	3433	48	7	∞	29	1.0	45	=	+	−	=
2	roller	4.08	3433	48	7	48	29	1.0	150	=	+	−	=
2	ring	4.08	3433	48	29	48	7	1.0	130	=	+	=	+
2	roller	4.08	3433	78	24	∞	86	1.0	60	=	+	=	+
2	roller	4.08	3433	78	24	48	86	1.0	100	=	+	=	+
2	roller	4.08	3433	78	24	48	86	1.0	120	=	+	=	+
2	ring	4.08	3433	∞	86	78	24	1.0	35	=	+	+	++
3	ball	7.48	4200	6.35	6.35	6.35	6.35	3	17	+	=	−	=
3	ball	7.48	4200	6.35	6.35	6.35	6.35	3	50	+	=	−	=
3	ball	7.48	4200	12.7	12.7	12.7	12.7	3	23	+	=	−	=
3	ball	10.8	4750	6.35	6.35	6.35	6.35	3	9	+	=	−	=
3	ball	10.8	4750	6.35	6.35	6.35	6.35	3	12	+	=	−	=
3	ball	10.8	4750	6.35	6.35	6.35	6.35	3	15	+	=	−	=
4	ball	12.24	4950	6.35	6.35	∞	−42	2.7	19	+	=	−	=
5	JR7205B	2.83	3040	16.15	−4.13	3.97	3.97	1.1	45	=	+	=	+
5	JR7205B	2.83	3040	16.15	−4.13	3.97	3.97	1.1	60	=	+	=	+
5	JR7205B	1.67	2550	16.15	−4.13	3.97	3.97	1.1	210	=	+	=	+
5	JR7205B	1.67	2550	16.15	−4.13	3.97	3.97	1.1	250	=	+	=	+
5	JR7205B	1.67	2550	16.15	−4.13	3.97	3.97	1.1	300	=	+	=	+
5	JR7205B	1.67	2550	16.15	−4.13	3.97	3.97	1.1	410	=	+	=	+
5	JR7205B	1.67	2550	16.15	−4.13	3.97	3.97	1.1	600	=	+	=	+
6	JR6206	2.72	3000	18.25	−4.9	4.76	4.76	2	75	=	=	=	=
6	JR6206	2.72	3000	18.25	−4.9	4.76	4.76	2	87	=	=	=	=
6	JR6206	2.72	3000	18.25	−4.9	4.76	4.76	2	140	=	=	=	=
6	JR6206	2.72	3000	18.25	−4.9	4.76	4.76	2	200	=	=	=	=

[a] − means concave curvature.

[b] + is expected life increase, − is expected life decrease, and = is no change of life expected.
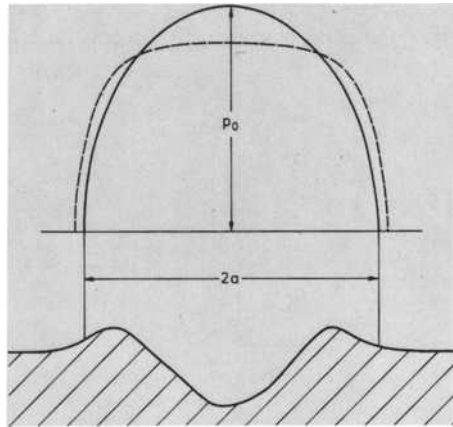
FIG. 2—*Change of pressure distribution by plastic deformation.*

contact pressure decreases with increasing plastic deformation and differs from the calculated contact pressure. At present, however, the preconditions are not given for the theoretical determination of the actual magnitude of stressing in the case of plastic deformation. The material properties are very important for the mechanism of plastic deformation. The influence of static load on the plastic deformation in the contact areas was described in the special literature [3]. With the ratio of the axes of the pressure areas approaching 1, minimum plastic deformations occur. This tendency certainly applies to bodies in rolling contact and should be considered for a dependable estimation of the influence of high loads on the life or of the life exponent. Most results from tests with high loads were obtained from ball-to-ball contact.

2. Contrary to the classic theory, the subsurface fatigue damage which is expected to develop in the area of peak stresses is not the most important damage.

Test specimens which were analyzed after very little damage had occurred generally exposed a V-shaped pitting with surface damage located in front of its point. This surface damage can only have been caused by the cycling of a larger, solid contaminant. A typical example of such damage is illustrated in Fig. 3. The particle indentation is located in front of the zone of material fatigue which increases in width in the cycling direction. Hence, it must be assumed that the lifetimes reached in the tests of Table 1 were generally determined by the influence of solid contaminants.

Figure 4 gives a survey of all the test results listed in Table 1. The total number of load cycles at a failure probability of 10 percent (hence, a "survivial probability" of 90 percent) is plotted versus K, the rolling contact pressure according to Stribeck. The pressure, K, was chosen because it is directly
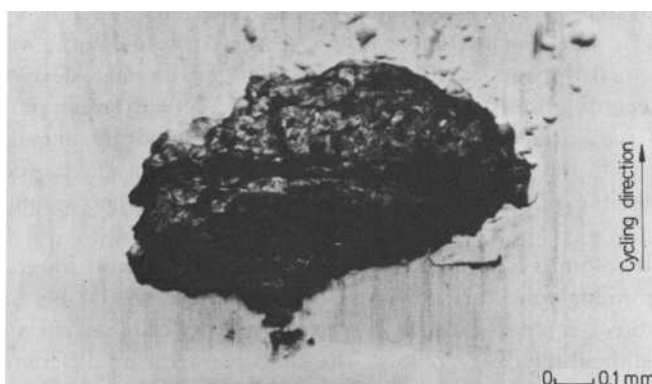
FIG. 3—*Typical pitting caused by a damaged surface area. The pitting enlarges in the cycling direction to form a V.*
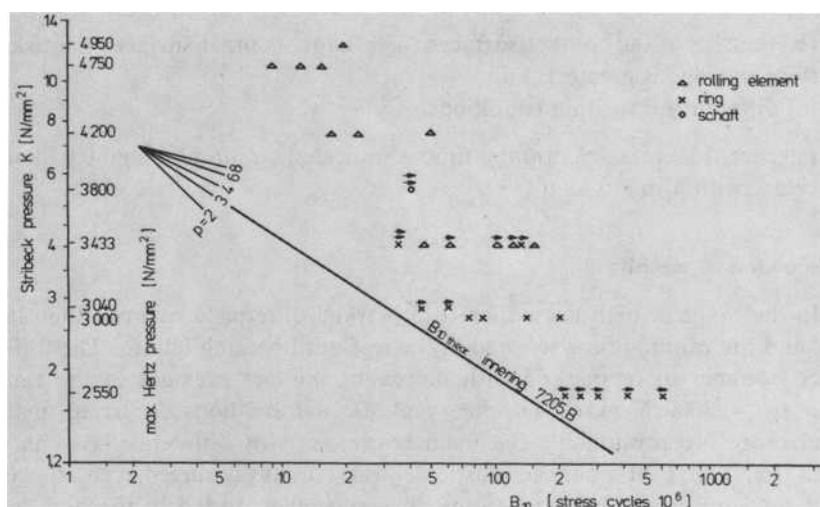
FIG. 4—*B_{10} life values versus the contact pressure for all the tests listed in Table 1.*

proportionate to the external loading. The following relationship between K and the contact pressure, p_0 applies to steel on steel in rolling contact

$$K = (p_0/2148)^3 \ [N/mm^2]$$

Figure 4 also shows the theoretical life of the FAG 7205B inner ring, expressed as the number of load cycles. The standard calculation of life consid-

ers the stressed volume. According to this criterion, larger test specimens have a shorter life. For the curve in Fig. 4, the stressed volume was not considered, which appears justifiable in view of the damage development recorded. According to this theory, the chance of a larger foreign particle penetrating to the surfaces in rolling contact and originating damage is more important than the volume stressed. This assumption is substantiated by the fact that the life values for the large test specimens are not beyond the ordinary range.

The four columns on the right side of Table 1 indicate, as rough estimates, how the running times of individual test specimens should be corrected to permit a direct comparison with the running times of inner rings of angular contact ball bearings FAG 7205B. The specimens having different sizes and shapes were tested under varying lubricating conditions; the inner rings of FAG 7205B bearings were tested with a separating elastohydrodynamic lubricating film. Three already mentioned parameters were considered:

(a) variable plastic deformation in relation to the shape of the contact surfaces,

(b) the size of the contact surfaces (with larger contact surfaces the risk of surface damage is greater), and

(c) different lubricating conditions.

An expected increase of running time is indicated with a plus sign ($+$) and a decrease with a minus sign ($-$).

Discussion of Results

In the range of high loads there is a marked difference between the rated life and the running time reached in the test until bearing failure. The difference becomes more marked with increasing contact pressure in the range over $p_0 = 3000$ N/mm^2. The heavy plastic deformations occurring in this load range are presumably the main reason for this difference. As can be seen from Fig. 2, pronounced plastic deformation has occurred even at a contact pressure of $p_0 = 2800$ N/mm^2. The specimens tested in the high load range were no longer available for a thorough inspection of the plastic deformations after completion of the tests.

The divergence between the actual life time and the rated life increases with the load. An exponent clearly below 3 can be seen for a high load range. The exact determination of the life exponent for the high load range requires further investigations.

In the range below a contact pressure of 3000 N/mm^2, the results obtained from these tests largely agree with the theory. This applies to the actual life time as well as to the exponent. This is surprising because, in the tests, the pittings generally developed from surface damage. The standardized life calculation is based on the assumption that the shear stress amplitude with its

peak value at a certain depth below the surface causes the material fatigue. The predominant agreement of test and calculation can only be explained by the empirically assessed factor contained in the load rating equation, which brings the theoretical formulation into correspondence with the test result. The tests for determining the empirical factor for the load rating equation must have been conducted under similar conditions.

Subsequent tests showed that fatigue below the surface occurs after much longer running times and follows other laws. Consequently, the validity of the standardized life calculation is restricted to those bearing sizes and operational conditions for which the empirical factor was assessed. Above all, the standardized life calculation must be supposed to allow for only an inaccurate determination of the actual life of larger bearings; to date, statistically confirmed life values for medium and large-sized bearings have not been established.

In view of this background, for many years only a relative importance has been attached to the rated life values by FAG. The bearings were instead dimensioned with the help of life coefficients which were obtained from identical or similar applications with satisfactorily and economically operating rolling bearings. Thus, dimensioning is constantly adapted to field experience.

The tests described in this article and many other tests, as well as the analysis of the operation data of bearings, which reached an actual running time far longer than expected from the theoretical life calculation, showed that, above all, the range of the low load must be more thoroughly investigated. Thus, the uncertainty connected with the extrapolation of test results over a wide scope of load ranges can be reduced. This, however, requires, more efficient test installations than those previously used.

The New Testing System

To eliminate surface contact between the test specimens during the test runs, the viscosity of the lubricant is increased by cooling. The surfaces in cycling contact and under load are completely separated by an elastohydrodynamic lubricating film. The increase of the rotary speed to 12 000 min^{-1} contributes to the separation of the surfaces. An efficient filter system prevents the penetration of contaminants larger than 5 μm to the active areas. With these provisions, fatigue damage can no longer originate at the damaged surface. Small foreign particles, which still pass through the lubricating gap, mark the running track on the specimen in the course of long testing (see Fig. 5). They do not, however, have a recognizable effect on the fatigue process.

Inner rings of angular contact FAG 7205B ball bearings with an increased raceway radius serve as test specimens. This increased radius ensures that the test specimens are the first to fail. The ratio of the raceway radius to the ball diameter is 0.55. The inner rings are assembled with 13 balls of
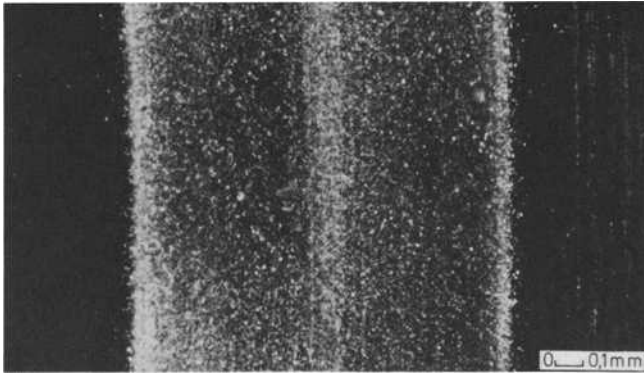
FIG. 5—*Running track after 2000 running hours with an efficient lubricant filter system.*

7.938-mm diameter and outer rings of standard bearings in such a way that, after mounting, the contact angles in the test bearings are identical. The ball riding solid cage is made of polyamide 66. Two bearings at a time are axially loaded in the test rig (Fig. 6) and driven at a rotary speed of 12 000 min^{-1} free from transverse forces (hence, without externally applied radial forces). Maintenance of the test rig is very easy, and the construction of the rig complies with high cleanliness requirements. For example, there are no pipes to be connected and removed. The oil is fed in through flow control valves in the housing. The load is applied by calibrated Belleville springs whose spring rates are frequently checked. A sensitive gage monitors the vibrations and discontinues the test run at the slightest sign of damage. By recooling in the oil reservoir, the oil flowing through the bearings is kept at a constant temperature of 45°C. The temperature variations of the test room amount to a maximum of 5°C over 1 year; temperatures between 70 and 80°C are measured at the outer rings.

To ensure the availability of a sufficient number of identical specimens for the tests with different loads and other test variations, a large number of inner rings from the same material heat were heat treated in one charge under these conditions:

> SAE 52100 steel, vacuum degassed
> austenitized at 840°C
> tempered at 180°C for 2 h

All test specimens were manufactured as one lot under defined conditions and to a high precision and surface quality. The quality corresponds to an machining accuracy of at least ABEC5 (P5).

Groups of 20 specimens were tested under the following thrust loads and resultant maximum contact pressures:

$$P_{ax} = 11\ 770\ N \qquad p_0 = 3\ 453\ N/mm^2$$
$$P_{ax} = \ \ 6\ 380\ N \qquad p_0 = 2\ 800\ N/mm^2$$
$$P_{ax} = \ \ 4\ 760\ N \qquad p_0 = 2\ 550\ N/mm^2$$

After the test runs, the raceway cross sections of the specimens were examined. Only at the lowest load had measurable deformations not occurred. In the two higher load ranges plastic deformations of different magnitudes were recorded. In order to assess the increase of the plastic deformation versus the time, the higher loaded test specimens were examined after approximately 20 h, after 200 h, and after failure. Figure 7 shows the deformations in the raceway versus the time. Within the investigated range, the plastic deformations head for a finite maximum value; that is, the increased rate of the deformation per time unit diminishes with increasing running time.

The running times reached by the higher loaded bearings are plotted in Figure 8 against the depth of the plastic deformation measured after the test run. Although the results were obtained under fixed testing conditions, it can clearly be seen that the life increases with growing plastic deformation. This confirms the statement made in connection with Fig. 2 that plastic deformation reduces the maximum contact pressure and thus increases the life.

For further evaluations, the test specimens of the two higher load ranges were divided into two identical groups according to the magnitude of the plastic deformations occurring in the tests. Group A included the test specimens with smaller deformations and Group B the specimens with larger deformations. Table 2 shows the results. In Fig. 9, the achieved B_{10} lives are
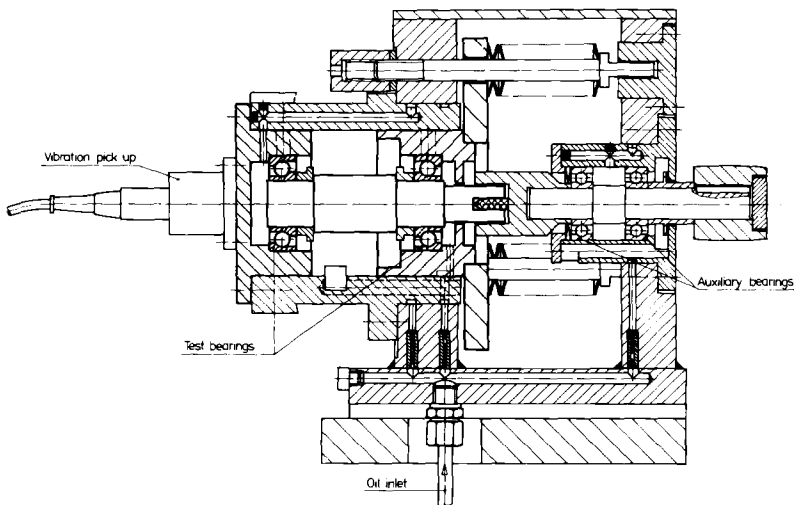
FIG. 6—*New FAG fatigue test rig for angular contact ball bearings.*
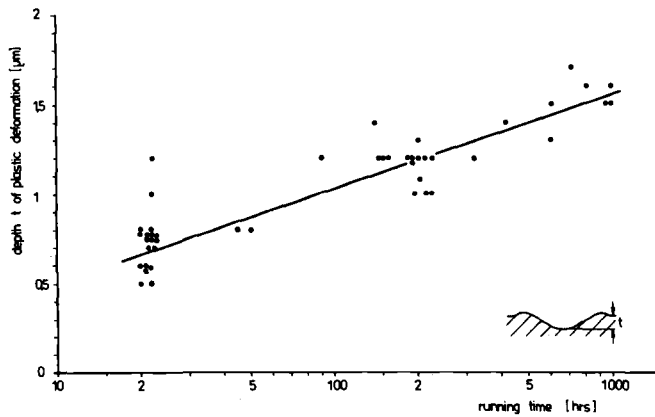
FIG. 7—*Plastic raceway deformation versus the running time,* $p_0 = 3453 \, N/mm^2$.
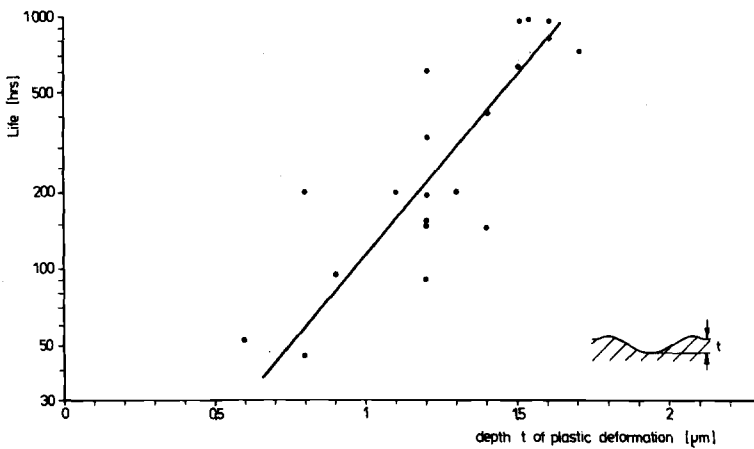
FIG. 8—*Life versus plastic raceway deformation,* $p_0 = 3453 \, N/mm^2$.

plotted versus the rolling contact pressure (according to Stribeck). The diagram also presents the calculated life, $L_n = a_1 \cdot a_2 \cdot a_3 \cdot (C/P)^p$ where $a_1 = a_2 = a_3 = 1$ and $p = 3$.

Discussion of Results

Earlier tests on test rig Type 5 (Fig. 1) were run with a constant load; the theoretical lubricating film thickness for the new testing system was increased by a factor of approximately 4. The surfaces are thus safely separated

TABLE 2—*Summary of all the tests with the new FAG testing system. All specimens are of the same heat.*

Group	Thrust Load, N	Contact Pressure Stribeck Pressure, N/mm²	Maximum Hertz Pressure, N/mm²	Number of Specimens	Life B_{10}, h	B_{50}, h	Weibull Scattering, k	Mean Depth of Plastic Deformation, t, μm	$B_{10\,test}/B_{10\,nominal}$	p
A	11 770	4.15	3 453	10	42	163	1.38	1.04	12	4.16
A	6 380	2.21	2 800	10	540	1 800	1.54	0.08	23.5	
B	11 770	4.15	3 453	10	180	660	1.44	1.5	51	3.8
B	6 380	2.21	2 800	10	1 850	5 900	1.6	0.56	81	
A	6 380	2.21	2 550	20	540	1 800	1.54	0.08	23.5	8.7
B	4 760	1.67	2 800	10	6 900	22 000[b]	1.6[b]	0	128	
B	6 380	2.21	2 550	20	1 850	5 900	1.6[b]	0.56	80	4.49
C[a]	4 760	1.67	2 550	10	6 900	22 000[b]	1.6[b]	0	128	
C	6 380	2.21	2 800	10	99	750	0.91	0	4.78	3.02
C	4 760	1.67	2 550	10	240	1 600	0.98	0	4.4	

[a]With indentations of a 0.1-mm diameter in the raceway.
[b]Estimated.
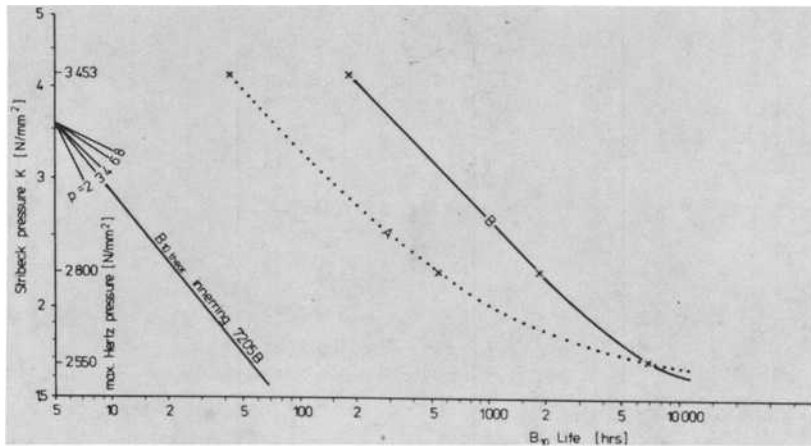
FIG. 9—B_{10} life versus the Stribeck pressure for the undamaged specimens of Table 2.

by the lubricating film. According to all known special literature and in-house test results obtained for point contact, the safe surface separation could be expected to increase the life by, at most, a factor of 4. Previously, the rated life was just safely reached; now it is exceeded 128-fold.

This extraordinary increase of the life is primarily due to the influence of the cleaner lubricant, so that fatigue—in accordance with the theory—originates below the surfaces. The following points favor this assumption:

1. In no case could damages be found on the raceway surface ahead of the pittings.

2. The material inspections after the test runs revealed "white bands" (WBs) (Fig. 10) below the surface in the area of highest stress. The WBs indicate that structural changes have occurred to such an extent that they have led to material fatigue. Early signs of white bands were found even in the first failed specimens with the lowest load.

Both observations suggest that fatigue damage developed in this way represents the classic case of material fatigue, which starts below the surface. Hence, the material properties alone are the decisive factor in achieving the running times. A further increase of the life at identical loads could only be achieved by improved material properties.

The Exponent p

The exponent p of the life equation is not constant at contact pressures below $p_0 = 3000$ N/mm². The exponent increases with decreasing load. At a contact pressure of $p_0 = 2550$ N/mm², plastic deformations of the surfaces
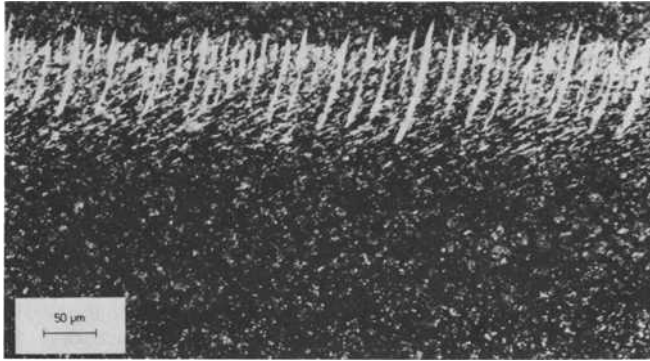
FIG. 10—*Typical material changes (*white bands*) of fatigued specimens.*

are not perceivable on the plotter diagrams. Material changes take place only in the microstructural range.

Between Group A, with the smallest plastic deformation at $p_0 = 2800$ N/mm^2, and the group which was tested at $p_0 = 2550$ N/mm^2, a life exponent of $p = 8.7$ was assessed. To the author's knowledge, this is the largest exponent so far found between two test groups.

In the range between $p_0 = 2550$ N/mm^2 and $p_0 = 3453$ N/mm^2, the exponent decreases more quickly as the plastic deformation grows larger. With the material tested, the smallest exponent assessed between the middle and the highest values of the contact pressure is $p = 3.8$.

From these findings and the results of previous tests which furnished an exponent p far below 3 for the pressure range above 3500 N/mm^2, it must be concluded that the exponent increases with decreasing contact pressure. At the lowest investigated pressure of $p_0 = 2550$ N/mm^2, the value p assessed as tangent to the dotted curve in Fig. 9 has far exceeded the value 8.7. It can be assumed that with only slightly lower contact pressure, the endurance strength, analogous to the S–N curve, is reached. Since major changes of the exponent are connected with changes of the plastic deformation and since the results of Groups A and B, which vary in their plastic deformation behavior, coincide at $p_0 = 2550$ N/mm^2, it can be assumed that there is little difference between the subsequent curve patterns for the two groups.

It would be very interesting to get more information from tests. This possibility is frustrated, however, by the prospective running times. With 6900 h the B_{10} life at the lowest load was almost 1 year. After two failures the test was discontinued because of the very long testing time required, although the remaining specimens had not yet become fatigued.

Under ideal operating conditions, the range of the endurance strength is assumed to be clearly above the range where the majority of bearings are applied in the field.

Influence of Defined Surface Damage on the Life and the Life Exponent

Since surface damage from foreign particle indentations was found to be the predominant cause of failure, the investigation of the effect of predetermined indentations in a preliminary test under identical conditions appeared to be of interest.

The specimens for these tests were taken from the same lot as the specimens tested earlier. Four indentations were evenly spaced over the circumference in the middle of the intended running tracks of every specimen by means of a Rockwell hardness tester. The diameter of the indentations was 0.1 mm. The point radius of the diamond spheroconical penetrator was 0.2 mm. The indentation has such a small diameter because only the sphered point of the penetrator took effect. Figure 11 shows an indentation and the emanating fatigue damage. The test loads were of the low range.

The results are shown in Table 2. Figure 12 shows all the test results as relative life values plotted versus the Stribeck contact pressure, K. The rating life values, L_n, of the test inner rings at the lowest contact pressure serve as reference values.

The B_{10} lives of the two specimen groups with indentations in the running tracks are also shown in Fig. 12. The life values are greatly reduced by the indentations. The ratio of the actual B_{10} lives to the calculated life values is similar to that obtained by the previous tests.

Further tests would be necessary to find out whether the exponent p is reduced to values in the order of 3 with surface damage of a different kind. At low loads and, consequently, high life values, the exponent p is likely to drop to low values when there is surface damage due to contamination.

Rolling contact stress, which, in relation to failure originating below the surface, is in the range of the endurance strength, can deteriorate into the finite life range because of surface damage.

Summary of Results and Conclusions

Investigations into the life of rolling bearings with point contact between the cycling surfaces have been described. The test results allow various important conclusions to be drawn.

Under ideal conditions, rolling bearings last essentially longer than expected from the standard calculation methods. Ideal conditions prevail at full separation of the surfaces by a "clean" lubricant. Thus, surface damage does not occur and the material becomes fatigued below the surface in the area of the highest stress. In this case the material properties are fully utilized.

Under ideal conditions the life exponent, p, is not constant. It increases with decreasing load. In the tests, p values below 3 were assessed for high loads and above 8 for low loads.
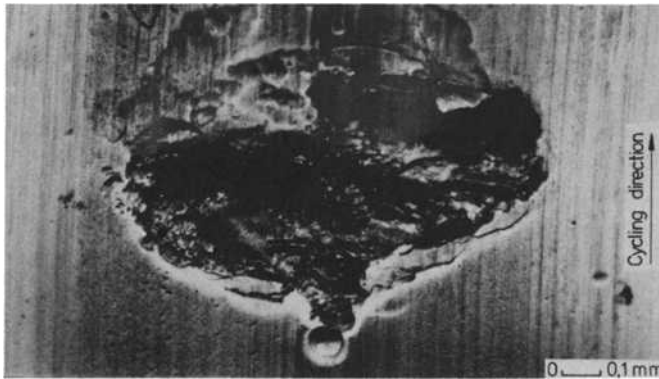
FIG. 11—*Pitting with indentation in front caused by the diamond spheroconical hardness tester.*
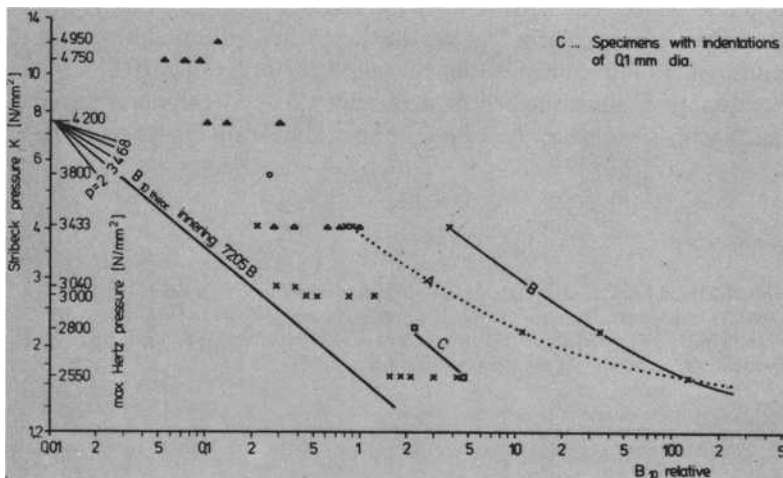
FIG. 12—*Summary of all the test results.*

The rapid increase of the exponent in the low load range, at about $p_0 = 2500$ N/mm², and the inspection of the material of cycled specimens described in the special literature [4] suggest that the endurance strength is reached by a further reduction of the load.

The degree of plastic deformability of the material is the decisive factor in the reduction of the life exponent. The influence of plastic deformation on fatigue life is not yet sufficiently established, thus the extrapolation of test results under high loads is not dependable.

The results obtained in the tests are reached in the field only in exceptional

cases because of the deviation from ideal operating conditions. In particular, solid contaminants which are present in a machine or which enter by means of the filter system cause surface damages. These lead to early fatigue damage.

The standard calculation of fatigue life furnishes realistic life values for current field conditions and, as generally indicated in the literature, also for most test conditions. This is due to the empirically assessed factor in the load rating equation which adjusts the theory to test results. The validity of the standardized calculation is ensured in the field only for bearings of a size corresponding to the size of the test bearings.

The value of $p = 3$ is not unrealistic for general field applications. The test results with predetermined damage of the raceway surfaces show that low-loaded, long-lived test rings undergo greater life reductions than higher-loaded ones. The operating conditions dictate whether the exponent is reduced to 3 at a contact pressure below 3000 N/mm^2.

Depending on the load and conditions prevailing in the tests, specimens of comparable quality reached, at identical contact pressure, widely varying life values. This is particularly true of the range near the endurance strength. The differences found in this range were on the order of 1:100.

The quality of a bearing can be determined only by comparative tests. It is not sufficient to compare the running time till bearing failure with the rating life.

References

[1] Lorösch, Hans-Karl, *Ball and Roller Bearing Engineering*, Vol. 2, 1966, pp. 26–31.
[2] Lorösch, Hans-Karl, *Ball and Roller Bearing Engineering*, Vol. 1, 1976, pp. 7–10.
[3] Brändlein, J. and Zwirlein, O., *Antriebstechnik*, Vol. 19, Nos. 7–8, 1980, pp. 316–322.
[4] Zwirlein, O. and Schlicht H., this publication, pp. 358–379.

J. I. McCool[1]

Analysis of Sets of Two-Parameter Weibull Data Arising in Rolling Contact Endurance Testing

ABSTRACT: Frequently in conducting rolling contact endurance tests, several small samples are subjected to some kind of "treatment." It is shown herein that if the treatment affects the rating life but not the Weibull shape parameter the data can be analyzed as a set rather than as individual samples, with considerable improvement in the precision with which the rating lives can be estimated.

Methods and supporting tables are given for the detailed analysis of sets of such data under the assumption that they represent censored data samples drawn from two-parameter Weibull populations.

The complete analysis consists of the following:

(a) a test for the equality of shape parameters among the populations, and, when a common shape parameter is found to be plausible,

(b) two tests for the equality of scale parameters or any fixed percentile,

(c) an interval and bias-corrected point estimation of the common shape parameter and the tenth percentiles of the individual groups, and

(d) a procedure for assessing which of the populations differ in their scale parameter and, hence, any percentile values.

The numerical values of key percentage points of the relevant distributions required for carrying out the analyses cover the range from $k = 2$ samples of size $n = 5$, censored at the third ($r = 3$) failure, to $k = 5$ and $n = r = 30$. As an illustration, the analyses are applied to two sets of rolling contact endurance data obtained with various steel materials fabricated into cylindrical rod and ball test specimens.

Two procedures for the selection of sample size are discussed, and illustrative examples are given of their use.

KEY WORDS: one-way classification, maximum likelihood estimation, likelihood ratio, multiple comparisons, rolling contact fatigue, bearing steels

[1]Research scientist, SKF Industries, Inc., King of Prussia, Pa. 19406.

The purpose of this paper is to present, in the context of rolling contact endurance testing, techniques recently developed under the sponsorship of the U.S. Air Force Office of Scientific Research [1][2] for a comprehensive analysis of a set of samples drawn from each of k possibly different two-parameter Weibull distributions.

Such sets of data arise in rolling contact endurance testing when the effect of a single factor such as material analysis, material processing, or the lubricant is under investigation, and life tests are performed at each of several levels of that factor. Single-factor experiments such as this are often described in the literature on design of experiments as one-way classification experiments.

It is assumed in the analysis that the k Weibull distributions from which the samples are drawn have a common though unknown shape parameter and differ, if at all, only in their scale parameter values. This is a commonly made, but seldom exploited, assumption in rolling contact endurance testing. Its validity may be tested by comparing the k individual sample shape parameter estimates [2,3].

Subject to acceptance of the common shape parameter assumption, we present (1) two statistical hypothesis tests for evaluating the equality of the k estimates of any fixed percentile, (2) methods for setting confidence limits on the common shape parameter and any fixed percentile of the individual populations, and (3) a multiple comparison procedure for dividing the populations into subsets within which there are no demonstrable differences but between which there are differences.

In addition, procedures are given for selecting the sample size for single-factor experiments to meet various criteria of precision or discrimination.

The common shape parameter assumption is shown to permit a great reduction in the sample size required to attain a given level of precision in estimating the rating life of bearings.

Tabular data required for implementing the procedures described in this paper are herein extended from the maximum sample size of 10 given in Ref *1* to a maximum sample size of 30.

The Two-Parameter Weibull Distribution

The statement that the endurance life of an item follows a two-parameter Weibull distribution implies that the probability that the life of a randomly selected item is less than some value "x" is given by an equation of the form

$$\text{Prob [life} < x] = F(x) = 1 - \exp\left[-\left(\frac{x}{\eta}\right)^{\beta}\right] \qquad (1)$$

---

[2]The italic numbers in brackets refer to the list of references appended to this paper.

The positive constants, η and β, are known as parameters; η is called the scale parameter and β the shape parameter. $F(x)$ is said to be the cumulative distribution function for the two-parameter Weibull model.

The median life is that life, designated $x_{0.50}$, prior to which an item has a 50 percent chance of failing. The median life is alternatively called the 50th percentile. Correspondingly, the tenth percentile or 90 percent reliable life, $x_{0.10}$, is the life prior to which the chance of failing is 10 percent; $x_{0.10}$ is the standardized life used for rating bearing performance in fatigue and is designated L_{10} in the standards of the Anti-friction Bearings Manufacturers Association and, frequently in practice, as B_{10}. In general the $100\,p^{th}$ percentile, x_p, may be expressed in terms of the shape and scale parameters using $F(x_p) = p$ in Eq 1

$$x_p = \eta k_p^{1/\beta} \tag{2}$$

where

$$k_p = -\ln(1 - p) \tag{3}$$

Maximum Likelihood Estimation in Single Samples

The method of maximum likelihood (ML) is an efficient way of estimating the Weibull parameters from the lives observed in a fatigue test (see Ref 4).

It is assumed that n items are tested until the rth item has failed ($r \le n$). The ordered lives of the failed items are denoted as $x_{(1)} < x_{(2)} < \ldots x_{(r)}$.

The unfailed items are said to be censored observations. When testing is suspended at a specific time, the mode of censoring is said to be "Type I." We consider only "Type II" censoring, under which testing terminates at the occurrence of a fixed ordered failure number; that is, the life at test suspension for all unfailed items is x_r.

The ML estimate of the shape parameter, β, is denoted $\hat{\beta}$ and may be calculated by solving the equation

$$1/\hat{\beta} + \left(\sum_{i=1}^{r} \ln x_i \right) \Big/ r - \left(\sum_{i=1}^{n} x_i^{\hat{\beta}} \ln x_i \right) \Big/ \left(\sum_{i=1}^{n} x_i^{\hat{\beta}} \right) = 0 \tag{4}$$

Having thus determined $\hat{\beta}$, the ML estimate of η may be calculated as

$$\hat{\eta} = \left\{ \sum_{i=1}^{n} x_i^{\hat{\beta}} / r \right\}^{1/\hat{\beta}} \tag{5}$$

The ML estimate of a general percentile is then

$$\hat{x}_p = \hat{\eta}(k_p)^{1/\hat{\beta}} \tag{6}$$

ML Estimation in Multiple Samples Having a Common β Value

We consider that k levels of some "treatment" (such as loads, lubricants, or coatings) are under investigation and that items to which the ith level of the treatment is applied ($i = 1, \ldots k$) will fail in accordance with a two-parameter Weibull distribution with (1) a scale parameter, η_i, that depends on the treatment level and (2) a shape parameter, β, that does not depend upon the treatment level. The cumulative distribution function for items receiving the ith treatment level is therefore

$$F_i(x) = 1 - \exp[-(x/\eta_i)^\beta] \tag{7}$$

If n items are tested at each treatment level until the first r fail, the ML estimate of β is the solution $\hat{\beta}_1$ of the equation

$$1/\hat{\beta}_1 + \sum_{i=1}^{k} \sum_{j=1}^{r} \ln x_{i(j)}/rk - \sum_{i=1}^{k} \left[\sum_{j=1}^{n} x_{i(j)}^{\hat{\beta}_1} \ln x_{i(j)}/k \sum_{j=1}^{n} x_{i(j)}^{\hat{\beta}_1} \right] \tag{8}$$

where $x_{i(j)}$ denotes the jth ordered failure or suspension time among the items to which the ith treatment level was applied.

$$(x_{i(1)} < x_{i(2)} < \ldots x_{i(r)} = x_{i(r+1)} \ldots x_{i(n)})$$

After this equation is numerically solved for $\hat{\beta}_1$, the ML estimate of η_i is calculated as

$$\hat{\eta}_i = \{(\sum x_{i(j)}^{\hat{\beta}_1}/r)\}^{1/\hat{\beta}_1} \tag{9}$$

The ML estimate of x_{pi} is

$$\hat{x}_{pi} = [k_p]^{1/\hat{\beta}_1} \cdot \hat{\eta}_i \tag{10}$$

As shown in Ref 5, the estimate $\hat{\beta}_1$ is invariant with respect to scale differences among the k groups; that is, multiplying the data in each sample by different arbitrary constants will not affect the value of $\hat{\beta}_1$ calculated from Eq 8.

Testing the Common β Assumption

A simple test of the common shape parameter assumption may, as shown in Refs 2 and 3, be based on the ratio of the largest to the smallest of the k individual β estimates obtained by solving Eq 4 for each sample. When the k populations have different shape parameters, the ratio of the largest to smallest of the individual maximum likelihood shape parameter estimates will tend to be larger than when all of the k population shape parameters are equal.

Define the random variable

$$w(r, n, k) \equiv \hat{\beta}_{max}/\hat{\beta}_{min} \tag{11}$$

as the ratio of the extremal ML shape parameter estimates among k samples each of size n, each censored at the rth failure time, and drawn from Weibull distributions which *do* have the same shape parameter. Percentiles of the distribution of $w(r, n, k)$ may be determined by Monte Carlo sampling.

In practice, values of $\hat{\beta}_{max}/\hat{\beta}_{min}$ higher than the 90th percentile $w_{0.90}(r, n, k)$ will, by definition, occur due to chance with only a 10 percent probability.

If one adopts the rule of declaring the shape parameters different when the observed ratio exceeds $w_{0.90}(r, n, k)$, that is, whenever

$$\hat{\beta}_{max}/\hat{\beta}_{min} > w_{0.90}(r, n, k) \tag{12}$$

one will erroneously declare the shape parameters different when they are actually equal, 10 percent of the time. When inequality (Eq 12) holds, the shape parameters are said to differ at the 10 percent significance level; that is, the risk is 10 percent that the shape parameters will be declared different when, in fact, they are not. Risk levels smaller or higher than 10 percent may, of course, also be used. Twenty-one percentage points of $w(r, n, k)$ for 17 selected pairs of n and r values are listed in a table in Ref 6 for $k = 2, 3, \ldots 10$. Table 1 gives $w_{0.90}$ values for $k = 2, 3, 4, 5$, and 10. This test and subsequent tests and analyses will be illustrated with data from two one-way classification experi-

TABLE 1—*Critical values* $w_{0.90}(r, n, k)$ *for testing homogeneity of* k *Weibull shape parameter estimates.*

n	r	$k = 2$	$k = 3$	$k = 4$	$k = 5$	$k = 10$
5	3	5.45	8.73	11.0	13.4	22.2
5	5	2.77	3.59	4.23	4.69	6.56
10	3	6.04	9.93	12.5	15.4	26.8
10	5	3.21	4.35	5.16	5.69	7.98
10	10	1.87	2.23	2.47	2.61	3.16
15	5	3.20	4.48	5.28	5.90	8.39
15	10	2.02	2.44	2.69	2.90	3.56
15	15	1.65	1.87	2.05	2.16	2.45
20	5	3.31	4.54	5.28	6.24	9.05
20	10	2.11	2.50	2.80	3.00	3.69
20	15	1.72	1.96	2.15	2.30	2.70
20	20	1.52	1.70	1.80	1.90	2.14
30	5	3.28	4.47	5.38	6.11	8.95
30	10	2.11	2.54	2.90	3.10	3.88
30	15	1.78	2.05	2.27	2.40	2.82
30	20	1.61	1.82	1.95	2.06	2.40
30	30	1.41	1.53	1.61	1.67	1.84

ments reported in Ref 7. The purpose of both the experiments was to evaluate the comparative performance in rolling contact fatigue of several material and processing method combinations of interest for high-speed turbine engine bearing applications.

One set of tests was conducted at Wright-Patterson Air Force Base on the following material types:

(a) consumable electrode vacuum-melted AISI M-50 tool steel,

(b) vacuum induction melted and vacuum arc remelted (VIMVAR) AISI M-50 tool steel,

(c) powder metal (P/M) processed AISI M-50,

(d) P/M processed AISI T-15, a cobalt–tungsten tool steel, and

(e) CRB-7, a high-chrome stainless steel alloy. In development this steel had the temporary designation EX00007 and is thus referred to in Ref 7.

In these tests ten cylindrical specimens 76.2 mm (3 in.) in length and 9.53 mm (0.375 in.) in diameter were prepared from each material and rolled at 10 000 rpm between opposed 191-mm (7.5-in.)-diameter disks loaded so as to produce a maximum contact stress of 4 826 MPa (700 000 psi) on the test specimens. The recorded times to failure are given in Table 2 in units of test specimen stress cycles. (The individual failure times are not given in Ref 7).

Also shown in Table 2 are the individual raw maximum likelihood estimates of the tenth percentile and the Weibull shape parameter calculated from Eqs 8 and 10.

In the second set of experiments, conducted by the Air Force contractor, the test specimen was a ball, 23.8 mm ($^{15}/_{16}$ in.) in diameter, loaded between opposed V-groove disks to produce a maximum contact stress of 4 136 MPa (600 000 psi) and rotated at 41 000 rpm.

TABLE 2—*Fatigue lives (10^6 cycles) and ML estimates of $x_{0.10}$ and β [4 826 MPa (700 000 psi) maximum contact pressure, 10 000 rpm rotational speed].*

Powder-Processed M-50	CEVM M-50	Powder-Processed AISI T-15	VIMVAR M-50	Powder-Processed CRB-7
3.03	3.19	3.46	5.88	6.43
5.53	4.26	5.22	6.74	9.97
5.60	4.47	5.69	6.90	10.39
9.30	4.53	6.54	6.98	13.55
9.92	4.67	9.16	7.21	14.45
12.95	5.78	10.19	8.59	16.81
15.21	6.79	10.71	9.80	18.39
16.04	9.37	12.58	12.28	20.84
16.84	12.75	13.41	25.46	21.51
$\hat{x}_{0.10}$ 5.06	2.60	4.72	3.49	8.83
$\hat{\beta}$ 2.59	2.32	3.13	1.94	3.65

In these tests the sample size ranged from 15 to 34. The CEVM M-50 material was omitted in these tests, giving $k = 4$. The sample sizes and individual maximum likelihood shape parameter and $x_{0.10}$ estimates (in millions of revolutions) are shown in Table 3. The individual failure times may be found in Ref 7. To test the hypothesis that the shape parameters are equal, one uses the ratio $w = \hat{\beta}_{max}/\hat{\beta}_{min}$ of the maximum and minimum shape parameter estimates.

For the cylindrical specimen tests this gives

$$w = \frac{\hat{\beta}_{max}}{\hat{\beta}_{min}} = \frac{3.65}{1.94} = 1.88$$

From Table 1, with $k = 5$ and $n = r = 10$, one finds $w = 1.88 < w_{0.90} = 2.61$. There is, thus, no evidence that the shape parameters are systematically different. In fact, the observed ratio is quite close to the median $w_{0.50} = 1.84$ (not listed in Table 1), thus indicating that the observed scatter in shape parameter estimates is quite typical.

For the single-ball tests, the ratio is

$$w = 1.99/0.786 = 2.53$$

Using (conservatively) $k = 4$, $n = 30$, and $r = 15$, one finds from Table 1 that $w = 2.53 > w_{0.90} = 2.27$, so that for this experiment there is evidence that the common shape parameter assumption does not hold. Excluding the T-15 test and recalculating gives

$$w = 1.99/1.66 = 1.20$$

From Table 1, now using $k = 3$, one has

$$w = 1.20 < w_{0.90} = 2.05$$

TABLE 3—Sample sizes and ML estimates for single-ball tests.

Values	VIMVAR M-50	P/M M-50	P/M T-15	CRB-7
		Material		
n	15	30	34	30
r	15	30	26	24
$\hat{x}_{0.10}$	23.7	15.4	6.54	38.0
$\hat{\beta}$	1.99	1.80	0.786	1.66

It is, therefore, reasonable to assume that the three steels, VIMVAR M-50, P/M M-50, and CRB-7, have a common shape parameter. The low shape parameter estimate for T-15 is not expressly discussed in Ref 7.

The low shape parameter value observed could be a property of this material or the result of a problem in fabrication or testing. Inasmuch as the shape parameter estimate for T-15 in the cylindrical specimen tests was in the same range as the other materials, it would seem not to be an inherent material problem.

The maximum likelihood estimates of the common shape parameter calculated from Eq 8 are

$$\hat{\beta}_1 = 2.480 \text{ cylindrical specimen tests}$$

and

$$\hat{\beta}_1 = 1.792 \text{ ball specimen tests (excluding T-15)}$$

The ML estimates of the tenth percentile computed from Eq 10 are given in Table 4 in ascending numerical order. It should be noted that the ranking of the materials by the cylindrical specimen tests has changed from that based on the individual $x_{0.10}$ estimates listed in Table 2. The ranking now agrees with the ranking given by the larger ball test sample sizes. It should be further noted that the ball test ranking has not been changed by the common shape parameter assumption, and only small numerical changes have occurred in the $x_{0.10}$ estimates.

Testing the Equality of Scale Parameters (or x_p Values)—Shape Parameter Ratio Test

If, in addition to a common shape parameter, there is no difference among the k groups in the scale parameters, that is, each group has the same scale parameter, η_0, the k data samples may be regarded as a single sample of size kn having kr failures. This combined sample is *not* Type II censored because of the different censoring times $x_{1(r)}$, $x_{2(r)} \ldots x_{k(r)}$ for each of the k groups.

TABLE 4—*Material rankings by cylindrical and ball specimen test results.*

| Material | $\hat{x}_{0.10}$, 10^6 revolutions | | Order in Table 2 |
	Cylindrical	Ball	
CEVM M-50	2.811	. . .	1
P/M T-15	3.798	. . .	3
P/M M-50	4.838	15.24	4
VIMVAR M-50	4.873	20.53	2
P/M CRB-7	6.342	42.19	5

The ML estimator of the shape parameter calculated from this combined sample is denoted $\hat{\beta}_0$ and is given as the solution of

$$1/\hat{\beta}_0 + \sum_{i=1}^{n} \sum_{j=1}^{r} \ln x_{i(j)}/rk - \sum_{i=1}^{k} \sum_{j=1}^{n} x_{i(j)}^{\hat{\beta}_0} \ln x_{i(j)} / \sum_{i=1}^{k} \sum_{j=1}^{n} x_{i(j)}^{\hat{\beta}_0} = 0 \quad (13)$$

The ML estimate of η_0 from the combined sample is denoted $\hat{\eta}_0$ and is given by

$$\hat{\eta}_0 = \left\{ \sum_{i=1}^{k} \sum_{j=1}^{n} x_{i(j)}^{\hat{\beta}_0}/rk \right\}^{1/\hat{\beta}_0} \quad (14)$$

Unlike $\hat{\beta}_1$, the estimate $\hat{\beta}_0$ is only valid if the η_i values are equal. When the η_i values differ, $\hat{\beta}_0$ tends to decrease or, more properly, becomes stochastically smaller. This is readily seen intuitively in the context of graphical estimation. Figure 1 shows plots on a Weibull probability grid of the results of three life tests of five samples which clearly have different scale parameters. The slope of the line fitted to the points on this grid is a graphical estimate of the Weibull shape parameter. The small differences in slope among the three groups are due to chance. When the groups are combined and replotted as a single group of 15 samples, the scale differences cause the data to span a much wider range than any of the individual groups, and an estimate of the shape parameter obtained graphically as the slope of the combined group will be smaller than the mean slope of the three individual samples.

Inasmuch as the common shape parameter estimator, $\hat{\beta}_1$, is invariant with respect to scale parameter differences, while the estimator, $\hat{\beta}_0$ tends to underestimate β when the scale parameters differ, the ratio $\hat{\beta}_1/\hat{\beta}_0$ is a plausible statistic to use to test for the equality of the scale parameters. (Since we have assumed a common shape parameter to begin with, testing the equality of scale parameters is equivalent to testing the equality of any percentile that may be of concern). As shown in Ref 5, this shape parameter ratio (SPR) test statistic follows a distribution that depends only on sample size parameters (that is, n, r, and k) when the scale parameters are truly equal. When the scale parameters differ, the distribution of $\hat{\beta}_1/\hat{\beta}_0$ becomes stochastically larger.

Table 5 lists the values of the 90th and 95th percentiles of $\hat{\beta}_1/\hat{\beta}_0$ determined by Monte Carlo sampling for various n, r, and k values ranging from $n = 5$, $r = 3$, and $k = 2$ to $n = 30$, $r = 30$, and $k = 5$.

To illustrate the conduct of an SPR test, we return to the cylindrical and ball fatigue test data.

The combined group shape parameter estimates were calculated to be

$$\hat{\beta}_0 = 2.089 \text{ for cylindrical specimen tests}$$

$$\hat{\beta}_0 = 1.372 \text{ for ball specimen tests (excluding T-15)}$$
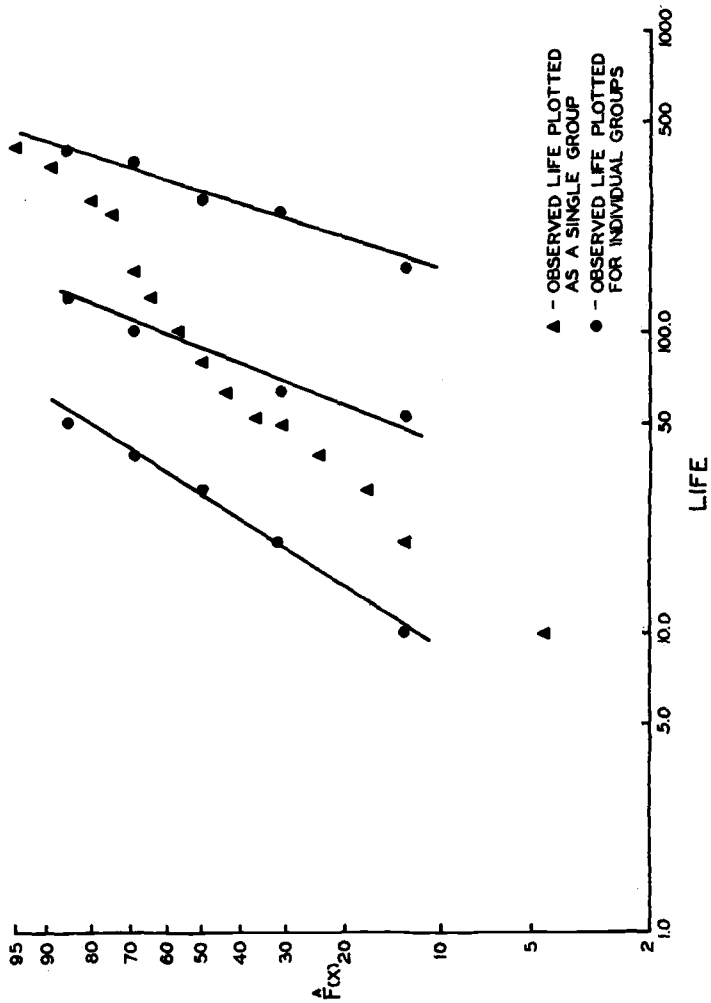
FIG. 1—*Probability plots for three data samples.*

TABLE 5—Selected percentage points as a function of sample size.

n	r	k	$\hat{\beta}_1/\hat{\beta}_0$ 0.90	$\hat{\beta}_1/\hat{\beta}_0$ 0.95	$-2\ln\lambda$ 0.90	$-2\ln\lambda$ 0.95	v_1 0.05	v_1 0.50	v_1 0.95	u_1 0.05	u_1 0.50	u_1 0.95	t_1 0.90	t_1 0.95	c	$-2c\ln\lambda$ 0.95	$\chi^2(k-1)$ 0.95
5	3	2	1.799	2.144	5.357	7.235	0.7618	1.505	3.833	-1.175	0.6861	5.325	2.833	3.752	0.514	3.717	3.81
5	3	3	1.788	2.078	7.913	10.24	0.8431	1.471	3.022	-1.135	0.6111	3.864	3.294	4.192	0.574	5.878	5.99
5	3	4	1.769	2.009	10.29	12.80	0.8915	1.462	2.673	-1.131	0.6124	3.417	3.605	4.342	0.596	7.673	7.81
5	3	5	1.744	1.925	12.34	15.07	0.9331	1.446	2.485	-1.112	0.6216	3.073	3.733	4.512	0.623	9.384	9.49
5	3	10	1.644	1.747	21.78	24.88	1.038	1.430	2.030	-1.084	0.5889	2.439	4.158	4.707	0.667	16.59	16.9
5	5	2	1.259	1.366	3.794	5.290	0.7773	1.195	2.056	-0.9715	0.3875	2.750	1.441	1.802	0.715	3.785	3.81
5	5	3	1.273	1.361	5.984	7.804	0.8265	1.184	1.816	-0.8715	0.3473	2.255	1.742	2.111	0.758	5.914	5.99
5	5	4	1.275	1.353	8.076	10.08	0.8609	1.178	1.703	-0.8321	0.3410	1.980	1.950	2.285	0.776	7.819	7.81
5	5	5	1.267	1.339	9.843	12.10	0.8888	1.177	1.621	-0.7907	0.3470	1.810	2.082	2.392	0.788	9.538	9.49
5	5	10	1.246	1.284	17.94	20.72	0.9545	1.167	1.453	-0.7314	0.3336	1.471	2.409	2.702	0.818	16.95	16.9
10	5	2	1.363	1.508	4.142	5.782	0.7677	1.256	2.326	-0.8691	0.2856	2.424	1.576	1.999	0.662	3.826	3.81
10	5	3	1.372	1.491	6.443	8.372	0.8281	1.242	2.039	-0.8526	0.2727	1.959	1.900	2.296	0.708	5.930	5.99
10	5	4	1.367	1.463	8.467	10.51	0.8679	1.234	1.877	-0.8303	0.2761	1.729	2.084	2.426	0.739	7.765	7.81
10	5	5	1.365	1.438	10.39	12.45	0.8904	1.230	1.768	-0.7987	0.2794	1.587	2.209	2.547	0.757	9.420	9.49
10	5	10	1.328	1.378	18.84	21.58	0.9669	1.219	1.575	-0.7994	0.2733	1.361	2.549	2.823	0.782	16.88	16.9
10	10	2	1.105	1.150	3.165	4.472	0.8130	1.087	1.516	-0.7161	0.1587	1.444	0.8509	1.040	0.855	3.822	3.81
10	10	3	1.116	1.149	5.317	6.834	0.8508	1.082	1.414	-0.6590	0.1460	1.204	1.062	1.231	0.872	5.962	5.99
10	10	4	1.115	1.142	6.981	8.706	0.8794	1.077	1.355	-0.6117	0.1448	1.066	1.171	1.330	0.893	7.772	7.81
10	10	5	1.114	1.139	8.755	10.55	0.8939	1.076	1.319	-0.5883	0.1519	0.9899	1.256	1.406	0.895	9.442	9.49
10	10	10	1.105	1.121	16.16	18.61	0.9405	1.073	1.235	-0.5766	0.1450	0.8384	1.468	1.598	0.905	16.84	16.9
15	5	2	1.374	1.535	4.090	5.770	0.768	1.269	2.414	-0.879	0.203	1.976	1.569	2.02	0.656	3.788	3.81
15	5	3	1.392	1.522	6.393	8.428	0.822	1.256	2.080	-0.876	0.190	1.645	1.899	2.308	0.710	5.987	5.99
15	5	4	1.392	1.491	8.579	10.626	0.857	1.246	1.927	-0.848	0.193	1.474	2.110	2.475	0.736	7.819	7.81
15	5	5	1.377	1.462	10.238	14.443	0.891	1.239	1.815	-0.864	0.189	1.377	2.206	2.548	0.753	10.889	9.49
15	10	2	1.131	1.190	3.260	4.653	0.799	1.106	1.611	-0.668	0.157	1.352	0.873	1.080	0.816	3.797	3.81
15	10	3	1.144	1.185	5.370	6.846	0.845	1.100	1.489	-0.613	0.145	1.152	1.080	1.254	0.858	5.873	5.99
15	10	4	1.145	1.181	7.224	8.962	0.866	1.097	1.412	-0.586	0.143	1.033	1.200	1.381	0.869	7.790	7.81
15	10	5	1.143	1.176	8.881	10.873	0.888	1.094	1.375	-0.573	0.138	0.987	1.289	1.457	0.877	9.531	9.49
15	15	2	1.066	1.096	3.101	4.436	0.836	1.056	1.369	-0.615	0.108	...	0.671	0.817	0.876	3.885	3.81
15	15	3	1.072	1.095	5.071	6.562	0.871	1.052	1.302	-0.559	0.098	0.904	0.827	0.949	0.909	5.964	5.99
15	15	4	1.074	1.091	6.843	8.497	0.890	1.049	1.258	-0.515	0.097	0.805	0.920	1.036	0.912	7.749	7.81
15	15	5	1.074	1.090	8.477	10.378	0.902	1.048	1.230	-0.497	0.095	0.772	0.987	1.101	0.917	9.514	9.49

TABLE 5—*Continued.*

n	r	k	$\hat{\beta}_1/\hat{\beta}_0$ 0.90	$\hat{\beta}_1/\hat{\beta}_0$ 0.95	$-2\ln\lambda$ 0.90	$-2\ln\lambda$ 0.95	v_1 0.05	v_1 0.50	v_1 0.95	u_1 0.05	u_1 0.50	u_1 0.95	t_1 0.90	t_1 0.95	c	$-2c\ln\lambda$ 0.95	$\chi^2(k-1)$ 0.95
20	5	2	1.382	1.546	4.110	5.749	0.761	1.278	2.428	−0.937	0.119	1.660	1.575	2.020	0.664	3.821	3.81
20	5	3	1.408	1.542	6.455	8.469	0.818	1.267	2.078	−0.912	0.127	1.403	1.922	2.348	0.708	5.996	5.99
20	5	4	1.398	1.495	8.487	10.505	0.864	1.251	1.916	−0.918	0.118	1.299	2.121	2.486	0.732	7.685	7.81
20	5	5	1.389	1.478	10.339	12.412	0.892	1.246	1.836	−0.937	0.119	1.226	2.223	2.580	0.745	9.251	9.49
20	10	2	1.139	1.197	3.220	4.587	0.796	1.109	1.650	−0.621	0.125	1.231	0.871	1.072	0.829	3.801	3.81
20	10	3	1.155	1.202	5.453	7.004	0.836	1.104	1.507	−0.587	0.125	1.035	1.098	1.282	0.852	5.968	5.99
20	10	4	1.155	1.195	7.233	9.120	0.866	1.100	1.446	−0.573	0.115	0.953	1.213	1.384	0.862	7.867	7.81
20	10	5	1.155	1.190	9.068	11.008	0.885	1.099	1.402	−0.550	0.117	0.915	1.304	1.475	0.865	9.520	9.49
20	15	2	1.079	1.112	3.088	4.297	0.826	1.064	1.425	−0.569	0.0982	1.013	0.672	0.809	0.887	3.813	3.81
20	15	3	1.088	1.114	5.102	6.583	0.857	1.062	1.337	−0.531	0.0988	0.874	0.830	0.964	0.899	5.920	5.99
20	15	4	1.088	1.111	6.862	8.591	0.882	1.058	1.289	−0.497	0.0914	0.800	0.922	1.057	0.907	7.789	7.81
20	15	5	1.089	1.108	8.603	10.560	0.896	1.059	1.263	−0.472	0.0955	0.743	0.999	1.120	0.907	9.583	9.49
20	20	2	1.048	1.068	3.012	4.194	0.855	1.040	1.300	−0.531	0.0723	0.874	0.566	0.678	0.917	3.848	3.81
20	20	3	1.054	1.069	4.986	6.456	0.881	1.037	1.242	−0.486	0.0746	0.7422	0.702	0.803	0.918	5.926	5.99
20	20	4	1.054	1.068	6.740	8.460	0.898	1.037	1.208	−0.461	0.0715	0.665	0.785	0.883	0.924	7.821	7.81
20	20	5	1.053	1.065	8.428	10.231	0.911	1.036	1.187	−0.433	0.0714	0.623	0.836	0.941	0.927	9.491	9.49
25	5	2	1.383	1.545	4.003	5.634	0.764	1.287	2.427	−1.002	0.0776	1.407	1.560	1.200	0.662	3.729	3.81
25	5	3	1.400	1.522	6.365	8.142	0.822	1.264	2.102	−0.996	0.0786	1.246	1.910	2.308	0.707	5.754	5.99
25	5	4	1.402	1.498	8.518	10.401	0.866	1.256	1.952	−0.977	0.0740	1.144	2.114	2.469	0.730	7.596	7.81
25	5	5	1.390	1.481	10.287	12.419	0.894	1.251	1.846	−0.986	0.0719	1.098	2.231	2.562	0.749	9.306	9.49
25	10	2	1.143	1.199	3.211	4.485	0.791	1.117	1.652	−0.605	0.107	1.099	0.871	1.061	0.831	3.728	3.81
25	10	3	1.160	1.208	5.403	7.038	0.832	1.107	1.527	−0.586	0.0957	0.979	1.091	1.278	0.851	5.992	5.99
25	10	4	1.161	1.202	7.274	9.074	0.864	1.103	1.456	−0.575	0.0987	0.887	1.219	1.387	0.863	7.831	7.81
25	10	5	1.158	1.191	8.872	10.828	0.885	1.100	1.401	−0.557	0.0946	0.838	1.289	1.466	0.878	9.502	9.49
25	15	2	1.084	1.122	3.079	4.465	0.817	1.069	1.447	−0.551	0.0969	0.974	0.673	0.827	0.877	3.917	3.81
25	15	3	1.094	1.123	5.116	6.633	0.855	1.063	1.358	−0.501	0.0830	0.849	0.835	0.972	0.894	5.933	5.99
25	15	4	1.096	1.123	6.993	8.885	0.878	1.061	1.308	−0.477	0.0847	0.753	0.932	1.072	0.902	8.017	7.81

25	15	5	1.095	1.116	8.544	10.520	0.893	1.061	1.277	−0.458	0.0843	0.710	0.996	1.118	0.912	9.594	9.49
25	20	2	1.056	1.078	2.994	4.250	0.841	1.045	1.336	−0.519	0.0762	0.857	0.567	0.682	0.911	3.871	3.81
25	20	3	1.063	1.081	4.988	6.453	0.874	1.043	1.268	−0.469	0.0710	0.745	0.701	0.811	0.922	5.952	5.99
25	20	4	1.167	1.080	6.783	8.448	0.892	1.041	1.236	−0.435	0.0692	0.661	0.785	0.882	0.929	7.846	7.81
25	20	5	1.165	1.077	8.212	10.154	0.905	1.041	1.208	−0.426	0.0681	0.618	0.836	0.931	0.936	9.505	9.49
25	25	2	1.037	1.054	2.945	4.210	0.864	1.032	1.255	−0.494	0.0629	0.752	0.497	0.601	0.925	3.895	3.81
25	25	3	1.042	1.054	4.894	6.450	0.890	1.030	1.204	−0.445	0.0607	0.655	0.615	0.710	0.935	6.030	5.99
25	25	4	1.042	1.053	6.616	8.330	0.905	1.030	1.178	−0.409	0.0541	0.581	0.686	0.779	0.941	7.836	7.81
25	25	5	1.041	1.051	8.122	9.919	0.916	1.028	1.051	−0.387	0.0570	0.539	0.736	0.814	0.949	9.409	9.49
30	5	2	1.394	1.571	4.111	5.852	0.761	1.285	2.436	−1.066	0.0177	1.289	1.591	2.060	0.656	3.840	3.81
30	5	3	1.414	1.544	6.489	8.396	0.827	1.267	2.120	−1.070	0.0342	1.151	1.938	2.367	0.698	5.863	5.99
30	5	4	1.411	1.529	8.601	10.827	0.871	1.256	1.963	−1.065	0.0331	1.049	2.148	2.515	0.723	7.831	7.81
30	5	5	1.399	1.492	10.373	12.674	0.895	1.256	1.838	−1.062	0.0275	1.019	2.256	2.607	0.739	9.367	9.49
30	10	2	1.148	1.212	3.259	4.704	0.789	1.117	1.674	−0.587	0.0874	1.020	0.880	1.095	0.821	3.862	3.81
30	10	3	1.165	1.215	5.452	7.200	0.831	1.109	1.528	−0.576	0.0804	0.896	1.099	1.303	0.845	6.086	5.99
30	10	4	1.167	1.206	7.402	9.171	0.861	1.108	1.454	−0.570	0.0819	0.828	1.228	1.407	0.854	7.832	7.81
30	10	5	1.165	1.199	9.071	11.028	0.883	1.104	1.410	−0.570	0.0795	0.787	1.313	1.492	0.863	9.517	9.49
30	15	2	1.087	1.124	3.033	4.312	0.813	1.071	1.458	−0.513	0.0823	0.886	0.669	0.813	0.884	3.817	3.81
30	15	3	1.096	1.125	5.046	6.549	0.815	1.068	1.365	−0.583	0.0767	0.776	0.832	0.965	0.908	5.945	5.99
30	15	4	1.099	1.125	6.967	8.663	0.875	1.065	1.319	−0.470	0.0734	0.721	0.940	1.067	0.907	7.857	7.81
30	15	5	1.098	1.121	8.588	10.513	0.893	1.066	1.288	−0.460	0.0768	0.692	1.004	1.136	0.908	9.546	9.49
30	20	2	1.059	1.083	2.921	4.167	0.833	1.049	1.349	−0.490	0.0737	1.083	0.560	0.679	0.920	3.834	3.81
30	20	3	1.065	1.084	4.844	6.256	0.871	1.045	1.280	−0.442	0.0680	0.704	0.698	0.796	0.935	5.849	5.99
30	20	4	1.067	1.084	6.687	8.405	0.889	1.045	1.243	−0.430	0.0664	0.629	0.781	0.884	0.934	7.848	7.81
30	20	5	1.067	1.082	8.361	10.167	0.903	1.045	1.219	−0.410	0.0701	0.621	0.842	0.942	0.934	9.493	9.49
30	25	2	1.044	1.061	2.956	4.116	0.853	1.037	1.280	−0.481	0.0572	0.882	0.500	0.595	0.921	3.790	3.81
30	25	3	1.047	1.061	4.753	6.168	0.882	1.035	1.226	−0.425	0.0593	0.627	0.609	0.699	0.956	5.894	5.99
30	25	4	1.048	1.060	6.562	8.082	0.899	1.033	1.195	−0.396	0.0575	0.583	0.683	0.771	0.949	7.670	7.81
30	25	5	1.048	1.058	8.129	9.886	0.913	1.033	1.175	−0.380	0.0599	0.549	0.736	0.816	0.950	9.388	9.49
30	30	2	1.031	1.044	2.890	4.025	0.873	1.026	1.224	−0.458	0.0530	0.668	0.448	0.534	0.930	3.744	3.81
30	30	3	1.035	1.044	4.765	6.192	0.895	1.025	1.184	−0.406	0.0513	0.574	0.552	0.635	0.954	5.906	5.99
30	30	4	1.035	1.044	6.511	8.123	0.911	1.024	1.156	−0.387	0.0467	0.529	0.618	0.698	0.950	7.717	7.81
30	30	5	1.035	1.042	8.121	9.938	0.921	1.024	1.142	−0.368	0.0493	0.496	0.665	0.740	0.956	9.938	9.49

For the cylindrical specimens the shape parameter ratio test statistic is

$$\hat{\beta}_1/\hat{\beta}_0 = 2.480/2.089 = 1.19$$

From Table 5, for $n = r = 10$, $k = 5$, the critical value of $\hat{\beta}_1/\hat{\beta}_0$ for a 5 percent level significance test is 1.139. We thus reject the hypothesis that the $x_{0.10}$ values for the five materials are equal.

For the single-ball tests, the shape parameter ratio is

$$\hat{\beta}_1/\hat{\beta}_0 = 1.792/1.372 = 1.306$$

From Table 5, using $n = 30$, $r = 15$, and $k = 3$, the critical ratio for a 5 percent significance level test is 1.125. Thus the differences among the single-ball estimates of $x_{0.10}$ are significant.

As noted, the shape parameter test has a graphical interpretation, and graphical estimates could be substituted for the ML estimates as a convenient approximation to the SPR test. If this were done, the average of the individual group slopes should be used in lieu of $\hat{\beta}_1$.

Testing the Equality of Scale Parameters (or x_p Values)—Likelihood Ratio Test

The likelihood ratio test [8] is a classic method for testing statistical hypotheses. The test statistic is the ratio λ of (1) the likelihood function maximized under the constraint imposed by the hypothesis to (2) the likelihood function maximized without this constraint.

In the present context

$$\lambda = L(x_{i(j)}, \hat{\eta}_0, \hat{\beta}_0)/L(x_{i(j)}, \hat{\eta}_1, \hat{\beta}_1) \tag{15}$$

where $L(x_{i(j)}, \eta_i, \beta)$ denotes the likelihood function in terms of the sample data, the scale parameters of each group, and the common shape parameter. It is shown in Ref 1 that the natural logarithm of λ may be expressed as

$$\ln \lambda = -rk \ln(\hat{\beta}_1/\hat{\beta}_0) + \sum_{i=1}^{k} \sum_{j=1}^{r} \ln(x_{i(j)}/\hat{\eta}_0)\hat{\beta}_0 - \sum_{i-1}^{k} \sum_{j=1}^{r} \ln(x_{i(j)}/\hat{\eta}_i)^{\hat{\beta}_1} \tag{16}$$

When the η_i values are all equal, the distribution of λ, and hence any monotonic function of λ, may be shown to depend only on sample size parameters and not on the underlying Weibull parameters.

The leading term in Eq 16 is seen to be just a monotonic transformation of the shape parameter ratio statistic discussed in the previous section.

A discussion of the comparative performance of the likelihood ratio and

shape parameter ratio tests is given in a later section. Since a computer is necessary for either test, it is recommended that both $\hat{\beta}_1/\hat{\beta}_0$ and $-2 \ln \lambda$ be routinely calculated. They will rarely lead to different conclusions.

Asymptotically, that is, for a sufficiently large r value, the distribution of $-2 \ln \lambda$ tends toward a chi-square distribution with $k - 1$ degrees of freedom. The 90th and 95th percentage points of $-2 \ln \lambda$ determined by Monte Carlo sampling are listed in Table 5 for various n, r, and k values. Also shown for comparison are the 95th percentiles of χ^2 $(k - 1)$, with $k - 1$ degrees of freedom. It is apparent that the asymptotic convergence of $-2 \ln \lambda$ is slow. Moreover, since the calculated percentiles of $-2 \ln \lambda$ substantially exceed the asymptotic values, use of the asymptotic critical values would result in an appreciable number of false rejections. That is, the probability that $-2 \ln \lambda$ exceeds $\chi^2_{0.95}$ $(k - 1)$ is considerably in excess of 0.05. By determining a constant, c, so that the mean of $-2c \ln \lambda$ and χ^2 $(k - 1)$ coincide, one finds that the 95th percentiles of $-2c \ln \lambda$ and χ^2 $(k - 1)$ are in good agreement, particularly for $r > 3$.

One may take advantage of this fact to approximate critical values of $-2 \ln \lambda$ for sample sizes other than those listed in Table 5 by dividing the appropriate χ^2 critical value by the value of c, interpolated or extrapolated on sample size.

For the data of Table 2, the calculated value of $-2 \ln \lambda$ is

$$-2 \ln \lambda = 17.96$$

From Table 5, with $n = r = 10$ and $k = 5$, the critical value for a 5 percent level test is 10.55.

Since

$$17.96 > (-2 \ln \lambda)_{0.95} = 10.55$$

the likelihood ratio test rejects the equality of $x_{0.10}$ values just as the shape parameter ratio test did.

Similarly, for the single-ball tests the calculated value of $-2 \ln \lambda$ is

$$-2 \ln \lambda = 37.5$$

From Table 5, with $k = 3$, $n = 30$, and $r = 15$, $(-2 \ln \lambda)_{0.95} = 6.549$, and thus the $x_{0.10}$ values of the three single-ball tests are significantly different.

Confidence Limits for Common Shape Parameter

The random variable

$$v_1(r, n, k) = \hat{\beta}_1/\beta \tag{17}$$

follows a distribution over repeated random sets of k samples of size n censored at the rth failure, which does not depend on any of the Weibull parameters, that is, on the η_i $(i = 1, \ldots k)$ or β values. Functions having this property are known as pivotal functions; they facilitate the calculation of exact confidence limits.

Table 5 contains values of the 5th, 50th, and 95th percentiles of the distribution of v_1 determined by Monte Carlo sampling for various n, r, and k values.

A 90 percent confidence interval for the common β may be set as

$$\hat{\beta}_1/(v_1)_{0.95} < \beta < \hat{\beta}_1/(v_1)_{0.05} \tag{18}$$

For the data of Table 2, with $n = r = 10$ and $k = 5$, the calculated value of $\hat{\beta}_1$ was 2.48, so that, using Table 5, a 90 percent interval is calculated as

$$1.88 = 2.48/1.319 < \beta < 2.48/0.894 = 2.77$$

A median unbiased point estimate of the common shape parameter, that is, an estimate which is as likely to be smaller or larger than the true but unknown value, is calculated as

$$\hat{\beta}' = \hat{\beta}_1/(v_1)_{0.50} \tag{19}$$

For the data of Table 2 this gives

$$\hat{\beta}' = 2.48/1.076 = 2.30$$

Inasmuch as it is based on all nk tests, a confidence interval calculated from Eq 18 will be tighter than would be calculated using the method in Ref 4 and just the data in a single one of the k samples.

For the single-ball tests using $k = 3$, $n = 30$, and $r = 15$, a 90 percent interval for the shape parameter is

$$1.31 = 1.792/1.365 < \beta < 1.792/0.815 = 2.20$$

The median unbiased estimate is

$$\hat{\beta}' = 1.792/1.068 = 1.68$$

Ratios of the two shape parameter estimates could be used to test whether the cylindrical and single-ball shape parameters differ.

Tables of critical values are not available, however, except for comparisons of shape parameter estimates obtained from single samples of the same size. From Table 1, the ratio of largest to smallest shape parameter estimates in

pairs of samples of size $n = 30$ with $r = 30$ failures will not exceed 1.41 more than 10 percent of the time due to chance alone.

For the cylindrical and ball specimens, the ML shape parameter ratio is $2.480/1.792 = 1.38$. Considering that the cylindrical specimen tests have a combined sample size of $n = 50$ with $r = 50$ failures, while the three single-ball tests being considered have a total sample size of $n = 75$ with $r = 69$ failures, the shape parameter difference between the two types of tests is likely to be real.

Confidence Limits for $x_{0.10}$

The function

$$u_1(r, n, k, 0.10) = \hat{\beta}_1 \ln (\hat{x}_{0.10}/x_{0.10}) \tag{20}$$

where $\hat{x}_{0.10}$ is calculated from Eq 10, is shown in Ref 1 to be a pivotal function. A 90 percent interval for $x_{0.10}$ is computed as

$$\hat{x}_{0.10} \cdot \exp [-(u_1)_{0.95}/\hat{\beta}_1] < x_{0.10} < \hat{x}_{0.10} \cdot \exp [-(u_1)_{0.05}/\hat{\beta}_1] \tag{21}$$

Similarly, a median unbiased estimate of $x_{0.10}$ may be calculated as

$$\hat{x}'_{0.10} = \hat{x}_{0.10} \cdot \exp [-(u_1)_{0.50}/\hat{\beta}_1] \tag{22}$$

These percentiles of u_1 are listed in Table 5 as functions of n, r, and k.

Using Eqs 21 and 22 and the point estimates of $x_{0.10}$ calculated from Eq 10 for each of the data groups, the values of the median unbiased point estimates and 90 percent confidence intervals for $x_{0.10}$ shown in Table 6 are calculated.

For the single-ball tests we have used $r = 15$, $n = 30$, and $k = 3$. If the values of u_1 for the actual, unequal group sample sizes were available, the calculated confidence limits for the ball tests would be tighter than those shown in Table 6.

Multiple Comparisons

When it is determined by the shape parameter ratio test or by the likelihood ratio test that there is a difference among the k groups, it is then important to determine which among them differ and which do not.

Such comparisons may be made by means of the distribution of the random variable

$$t_1(r, n, k) = \hat{\beta}_1 \ln [(\hat{x}_p)_{max}/(\hat{x}_p)_{min}] \tag{23}$$

TABLE 6—*Median unbiased and 90 percent confidence interval estimates for* $x_{0.10}$.

Material	$\hat{x}_{0.10}$	90% Interval for $x_{0.10}$
Cylindrical Specimen Tests		
CEVM M-50	2.645	1.89 to 3.56
P/M T-15	3.574	2.55 to 4.82
P/M M-50	4.553	3.25 to 6.13
VIMVAR M-50	4.576	3.27 to 6.18
P/M CRB-7	5.968	4.25 to 8.04
Single-Ball Tests		
P/M M-50	14.6	9.90 to 21.1
VIMVAR M-50	19.7	13.3 to 28.4
P/M CRB-7	40.4	27.4 to 58.4

computed for the case that there are no true differences in scale parameter (or any percentile) among groups. The distribution of $t_1(r, n, k)$ does not depend on the percentile under discussion, that is, $\hat{x}_{0.10}$, $\hat{x}_{0.50}$, or the scale parameter estimates $\hat{\eta}$ could be used.

An upper percentile of the distribution of t_1 may be used to judge whether the ratio of two $\hat{x}_p$ values is unusually large. For example, using a 10 percent significance level, the ratio of any two $x_{0.10}$ estimates, say $(\hat{x}_{0.10})_i$ and $(\hat{x}_{0.10})_j$, is considered significantly large if

$$\hat{\beta}_1 \ln [(\hat{x}_{0.10})_i / (\hat{x}_{0.10})_j] < (t_1)_{0.90} \qquad (24)$$

The smallest significant ratio (SSR) occurs when equality holds in Eq 24. Solving for the SSR gives

$$SSR = \exp [(t_1)_{0.90} / \hat{\beta}_1] \qquad (25)$$

Values of $(t_1)_{0.90}$ and $(t_1)_{0.95}$ are given in Table 5 for various n, r, and k values. For the cylindrical specimen test data, $\hat{\beta}_1 = 2.48$. With $n = r = 10$ and $k = 5$, one finds from Table 5

$$(t_1)_{0.90} = 1.26$$

Thus from Eq 25

$$SSR = \exp [1.26/2.48] = 1.66$$

Any groups for which the ratio of $x_{0.10}$ estimates exceeds 1.66 differ significantly from each other.

The following data display the five ordered $x_{0.10}$ estimates of the example with a common line underscoring those which do *not* differ significantly.

Material:	CEVM M-50	P/M T-15	P/M M-50	VIMVAR M-50	P/M CRB-7
$\hat{x}_{0.10}$:	2.811	3.798	4.838	4.873	6.342

This is a convenient way to summarize the results of the test, showing at a glance which differences can be explained by chance and which cannot.

For the ball tests, using $(t_1)_{0.90}$ corresponding to $n = 30, r = 15$, and $k = 3$, the SSR is

$$SSR = \exp [0.832/1.792] = 1.59$$

The three groups, therefore, cluster as follows:

P/M M-50	VIMVAR M-50	P/M CRB-7
15.25	20.53	42.19

The single-ball tests are thus conclusive regarding the superiority of P/M CRB-7 over P/M M-50 and VIMVAR M-50 while, with the smaller sample sizes of the cylindrical tests, P/M CRB-7 was clearly superior only to CEVM M-50 and P/M T-15. For both sets of tests, the apparent difference between P/M M-50 and VIMVAR M-50 could easily have been due to chance.

It is worth noticing that the multiple comparison procedure has shown that P/M CRB-7 is different from VIMVAR M-50 even though the confidence limits for $x_{0.10}$ shown in Table 6 overlap. Failure of confidence limits to overlap is an overly conservative but widely practiced means for testing for differences among data groups.

Discriminating Power of Scale Parameter Tests and Sample Size Selection

We have considered two tests for the equality of Weibull scale parameters (or x_p values) applicable under the common shape parameter assumption and have shown how to construct these tests so that when the scale parameters *are* equal, they will be correctly accepted as such, with a specified high probability.

An associated issue is the behavior of the tests in correctly detecting differences among the scale parameters when such differences exist. The power, or probability of correctly detecting differences among k scale parameters, naturally depends on how large those differences are. It has been found [1] that for given n, r, and k values the probability of detection for the shape pa-

rameter ratio test depends on the actual scale parameter values through the function

$$\phi_1 = \sum_{i=1}^{k} \ln{(\eta_i^\beta)} \left[\left(\eta_i^\beta \Big/ \sum_{i=1}^{k} \eta_i^\beta \right) - 1/k \right] \tag{26}$$

This function has the following properties:

1. It is a symmetric function in η_i^β, and therefore the value of ϕ_1 does not depend on the arbitrary numbering of the populations.
2. It is nonnegative and reduces to zero when the η_i values are equal.
3. It is scale invariant, that is, its value is the same irrespective of the units in which the η_i^β values are expressed. In particular, in view of Eq 2, any fixed percentile $(x_p)_i$ could be used in lieu of η_i.

The power of the likelihood ratio test depends not only on ϕ_1 but also upon the additional symmetric function ϕ_2 defined as

$$\phi_2 = \sum_{i=1}^{k} \ln{\left[\sum_{i=1}^{k} \eta_i^\beta / k \eta_i^\beta \right]} \tag{27}$$

For a given ϕ_1 value, the likelihood ratio test may be more or less powerful than the shape parameter test, depending on the value of ϕ_2. In general, the shape parameter test was observed to be the more powerful when all but one of the scale parameters were equal and $k > 2$. The likelihood ratio test appears more powerful against more "diffuse" alternatives. In any case the differences as ϕ_2 varies are small, and it suffices from a practical point of view to design tests, that is, select sample sizes, based on ϕ_1 alone.

Table 7 lists for various n and r values, with $k = 2$ and $k = 10$, the probability, P_a, of accepting the scale parameters as equal in 10 percent significance level likelihood ratio (LR) and shape parameter ratio (SPR) tests as a function of η_1^β for $\eta_i^\beta = 1.0$ $(i > 1)$. The values of ϕ_1 and ϕ_2 are also shown for reference.

It is noted that for the same value of η_1^β the acceptance probability, P_a, for $k = 2$ is only slightly greater than the acceptance probability for $k = 10$. This suggests that the $k = 2$ results can be used for all $2 \leq k \leq 10$ in selecting sample sizes for experiments.

Figure 2 is a plot of the acceptance probability, P_a, as a function of ϕ_1, for $k = 2$ and the various n and r values listed in Table 7. The curves depend primarily on r and only slightly on n. Because the curves for the same r are so close, only one has been plotted.

As an example of the design of a series of life tests that have the required discriminating power, consider a case where three new materials are to be investigated. It is considered desirable to have the sample size large enough so that, should one of the materials yield an $x_{0.10}$ life larger than the others by a

TABLE 7—*Acceptance probabilities for LR and SPR tests as a function of ϕ_1 and ϕ_2*
($\alpha = 0.10$).

n	r	k	$\eta_1{}^\beta$	P_a LR	P_a SPR	ϕ_1	ϕ_2
5	3	2	1.0	0.900	0.900	0	0
			2.0	0.841	0.840	0.11552	0.11778
			5.0	0.602	0.605	0.53648	0.58779
			7.0	0.495	0.496	0.72972	0.82668
			10.0	0.379	0.383	0.94197	1.10691
5	3	10	1.0	0.900	0.900	0	0
			2.0	0.851	0.844	0.05671	0.85779
			5.0	0.564	0.511	0.41386	1.7553
			7.0	0.416	0.357	0.65674	2.7541
			10.0	0.271	0.216	0.98163	4.1160
5	5	2	1.0	0.900	0.900	0	0
			2.0	0.755	0.764	0.11552	0.11778
			5.0	0.296	0.311	0.53648	0.58779
			7.0	0.163	0.176	0.72972	0.82668
			10.0	0.077	0.082	0.94197	1.10691
5	5	10	1.0	0.900	0.900	0	0
			2.0	0.785	0.774	0.05671	0.85779
			5.0	0.272	0.250	0.41386	1.7553
			7.0	0.128	0.110	0.65674	2.7541
			10.0	0.047	0.040	0.98163	4.1160
10	5	2	1.0	0.900	0.900	0	0
			2.0	0.780	0.782	0.11552	0.11778
			5.0	0.340	0.349	0.53648	0.58779
			7.0	0.199	0.202	0.72972	0.82668
			10.0	0.099	0.103	0.94197	1.10691
10	5	10	1.0	0.900	0.900	0	0
			2.0	0.798	0.784	0.05671	0.85779
			5.0	0.296	0.254	0.41386	1.7553
			7.0	0.149	0.120	0.65674	2.7541
			10.0	0.060	0.043	0.98163	4.1160
10	10	2	1.0	0.900	0.900	0	0
			2.0	0.586	0.604	0.11552	0.11778
			5.0	0.064	0.050	0.53648	0.58779
			7.0	<0.01	<0.01	0.72972	0.82668
			10.0	≪0.01	≪0.01	0.94197	1.10691
10	10	10	1.0	0.900	0.900	0	0
			2.0	0.625	0.614	0.05671	0.85779
			5.0	0.034	0.030	0.41386	1.7553
			7.0	<0.01	<0.01	0.65674	2.7541
			10.0	≪0.01	≪0.01	0.98163	4.1160
30	5	2	1.0	0.900	0.900	0	0
			2.0	0.763	0.764	0.11552	0.11778
			3.0	0.585	0.586	0.27465	0.28768
			7.0	0.196	0.196	0.72972	0.82668
			10.0	0.102	0.103	0.94197	1.10691
30	10	2	1.0	0.900	0.900	0	0
			1.5	0.784	0.787	0.04055	0.04082
			2.0	0.581	0.584	0.11552	0.11778
			3.0	0.267	0.269	0.27465	0.28768

TABLE 7—*Continued.*

| n | r | k | $\eta_1{}^\beta$ | P_a | | ϕ_1 | ϕ_2 |
				LR	SPR		
			4.0	0.118	0.119	0.41589	0.44629
			8.0	<0.01	<0.01	0.80867	0.79191
30	15	2	1.0	0.900	0.900	0	0
			1.5	0.714	0.716	0.04055	0.04082
			2.0	0.432	0.433	0.11552	0.11778
			2.5	0.228	0.231	0.19635	0.20294
			3.0	0.114	0.116	0.27465	0.28768
			6.5	≪0.01	≪0.01	0.68633	0.77171
30	20	2	1.0	0.900	0.900	0	0
			1.3	0.788	0.788	0.01711	0.01716
			1.5	0.650	0.651	0.04055	0.04082
			1.8	0.438	0.442	0.08397	0.08516
			2.2	0.225	0.228	0.14784	0.15155
			5.5	≪0.01	≪0.01	0.59011	0.65256
30	25	2	1.0	0.900	0.900	0	0
			1.3	0.766	0.772	0.01711	0.01716
			1.8	0.331	0.336	0.08397	0.08516
			2.0	0.243	0.254	0.11552	0.11778
			2.2	0.154	0.164	0.14784	0.15155
			4.5	≪0.01	≪0.01	0.47857	0.51912
30	30	2	1.0	0.900	0.900	0	0
			1.3	0.731	0.741	0.01711	0.01716
			1.5	0.544	0.567	0.04055	0.04082
			1.8	0.287	0.312	0.08397	0.08516
			2.0	0.168	0.192	0.11552	0.11778
			2.2	0.0961	0.113	0.14784	0.15155
			3.5	≪0.01	≪0.01	0.34799	0.36910

factor 3.0, this difference would be detected with 90 percent probability. In addition, the significance level of the test is to be 10 percent.

The test sample sizes must, therefore, be sufficiently large that the acceptance probability of a 10 percent level test is $P_a = 0.10$, when

$$(x_{0.10})_1{}^\beta = (3.0)^\beta$$

$$(x_{0.10})_2{}^\beta = (1.0)^\beta$$

$$(x_{0.10})_3{}^\beta = (1.0)^\beta$$

Using a value of $\beta = 1.3$ for planning purposes, the ϕ_1 value appropriate for using the $k = 2$ curves is calculated as

$$\phi_1 = \ln(4.17)[4.17/6.17 - 1/2] = 0.251$$
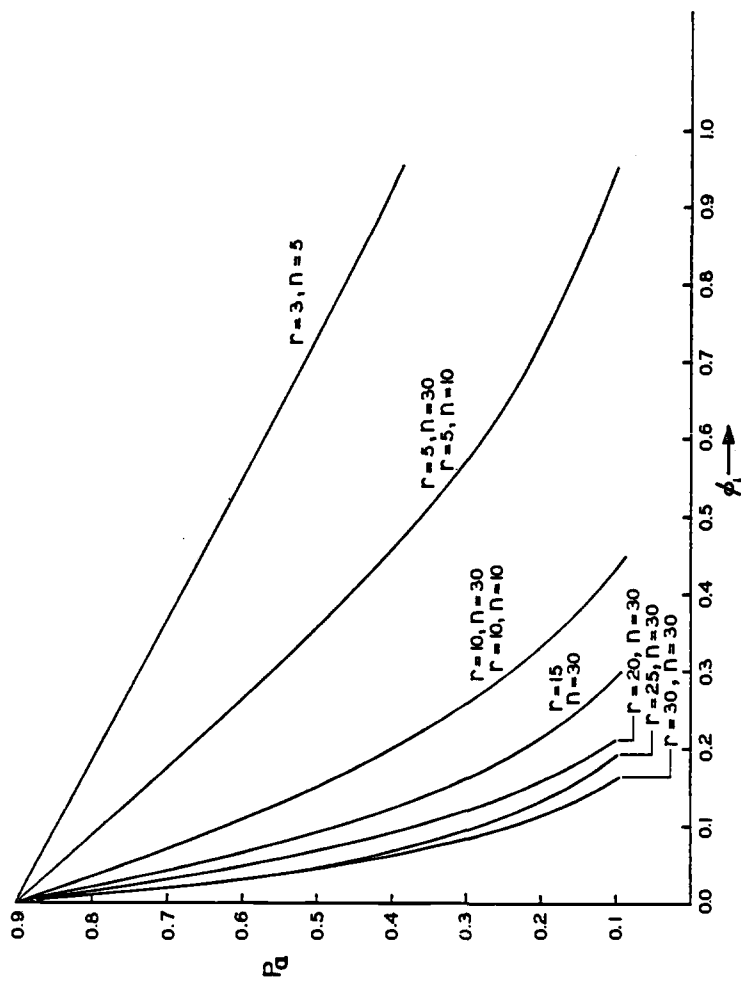
FIG. 2—*Plot of acceptance probability curves as a function* ϕ_1; *for* $K = 2$ *and various n and r values listed in Table 7.*

Using $P_a = 0.10$ in Fig. 2, it is seen that the required r value is somewhere between 15 and 20. An acceptable experiment could thus be to test a group of 30 samples until 18 to 20 failures occur for each of the three materials.

Sample Size Selection for Specified Precision

Selecting the sample size to give a prescribed power to discriminate between groups was discussed in the previous section.

Frequently testing is performed, not so much to find differences but primarily to determine the values of the shape parameter or $x_{0.10}$ for reference purposes.

The sample sizes for tests having this purpose should be selected so that the estimated parameters are sufficiently well determined.

A reasonable measure, R, of the precision with which β is determined by a set of k tests is the ratio, R, of the upper to lower ends of a 90 percent confidence interval, for example. From Eq 20 this ratio is [1,9]

$$R = (v_1)_{0.95}/(v_1)_{0.05}$$

The ratio of the upper to the lower end of a confidence interval for $x_{0.10}$ contains the random variable $\hat{\beta}_1$ and so cannot serve as a sample size–dependent precision measure. The median value $R_{0.50}$ of this ratio can be so used, however, and may be computed as

$$R_{0.50}^{\beta} = \exp \{[(u_1)_{0.95} - (u_1)_{0.05}]/(v_1)_{0.50}]\} \tag{29}$$

Table 8 lists values of R and $R_{0.50}^{\beta}$ for various n, r, and k values. Interesting tradeoffs are possible using this table. For example, consider the effect on R of the following three ways in which one may test 30 items until all fail:

k	n	r	R
3	10	10	1.66
2	15	15	1.64
1	30	30	1.62

If our objective is to estimate the shape parameter, naturally, the best way is to use a single group of 30 samples. However, if some other variable is present in the testing that might influence life, such as, different test machines, days of the week, or other factors, this effect will tend to bias the shape parameter estimate downward. It is preferable in this situation to divide the testing into groups according to the extraneous variable, since the estimate, $\hat{\beta}_1$, is invariant with between-group differences. In the case shown here, the precision loss in estimation for dividing the test items into two or three groups is quite small.

TABLE 8—*Precision index for shape parameter and $x_{0.10}$ estimation for various sample sizes, amounts of censoring, and numbers of samples.*

k	n	r	R	$R_{0.50}^\beta$
1	5	3	10.7	898
2	5	3	5.03	75.1
3	5	3	3.58	29.9
4	5	3	3.00	22.4
5	5	3	2.66	18.1
10	5	3	1.96	11.7
1	5	5	4.14	92.4
2	5	5	2.65	22.5
3	5	5	2.20	14.0
4	5	5	1.98	10.9
5	5	5	1.82	9.11
10	5	5	1.52	6.60
1	10	5	5.06	36.7
2	10	5	3.03	13.8
3	10	5	2.46	9.62
4	10	5	2.16	7.96
5	10	5	1.99	6.96
10	10	5	1.63	5.88
1	10	10	2.49	15.3
2	10	10	1.86	7.30
3	10	10	1.66	5.59
4	10	10	1.54	4.75
5	10	10	1.48	4.34
10	10	10	1.31	3.57
1	15	5	5.78	18.2
2	15	5	3.14	9.49
3	15	5	2.53	7.44
4	15	5	2.25	6.45
5	15	5	2.04	6.10
1	15	10	2.72	11.4
2	15	10	2.02	6.21
3	20	20	1.41	3.26
4	20	20	1.35	2.96
5	20	20	1.30	2.77
2	25	5	3.18	6.50
3	25	5	2.56	5.89
4	25	5	2.25	5.41
5	25	5	2.06	5.29
2	25	10	2.09	4.60
3	25	10	1.84	4.11
4	25	10	1.69	3.76
5	25	10	1.58	3.55
2	25	15	1.77	4.16
3	25	15	1.59	3.56
4	25	15	1.49	3.19
5	25	15	1.43	3.01
2	25	20	1.59	3.73
3	25	20	1.45	3.20
4	25	20	1.39	2.87
5	25	20	1.33	2.73
2	25	25	1.45	3.34
3	25	25	1.35	2.91
4	25	25	1.30	2.61
5	25	25	1.15	2.46

TABLE 8—*Continued.*

k	n	r	R	$R_{0.50}^{\beta}$
1	30	5	5.36	8.12
2	30	5	3.20	6.25
3	15	10	1.76	4.98
4	15	10	1.63	4.37
5	15	10	1.55	4.16
1	15	15	2.03	8.41
2	15	15	1.64	4.88
3	15	15	1.49	4.02
4	15	15	1.41	3.52
5	15	15	1.36	3.36
1	20	5	5.45	13.8
2	20	5	3.19	7.63
3	20	5	2.54	6.22
4	20	5	2.22	5.88
5	20	5	2.06	5.67
1	20	10	2.83	8.89
2	20	10	2.07	5.31
3	20	10	1.80	4.35
4	20	10	1.67	4.00
5	20	10	1.58	3.79
1	20	15	2.19	7.37
2	20	15	1.73	4.42
3	20	15	1.56	3.75
4	20	15	1.46	3.41
5	20	15	1.41	3.15
1	20	20	1.82	6.13
2	20	20	1.52	3.06
3	30	5	2.56	5.77
4	30	5	2.25	5.38
5	30	5	2.05	5.24
1	30	10	2.89	5.99
2	30	10	2.12	4.22
3	30	10	1.82	3.77
4	30	10	1.69	3.53
5	30	10	1.60	3.42
1	30	15	2.26	5.37
2	30	15	1.79	3.69
3	30	15	1.67	3.57
4	30	15	1.51	3.06
5	30	15	1.44	2.95
1	30	20	1.981	5.04
2	30	20	1.62	4.48
3	30	20	1.47	2.99
4	30	20	1.40	2.75
5	30	20	1.35	2.68
2	30	25	1.50	3.72
3	30	25	1.39	2.76
4	30	25	1.33	2.58
5	30	25	1.29	2.46
1	30	30	1.62	4.22
2	30	30	1.40	3.00
3	30	30	1.32	2.60
4	30	30	1.27	2.45
5	30	30	1.24	2.33

Table 8 illustrates the great improvement in precision for $x_{0.10}$ that can be achieved by shape parameter pooling. For example, suppose one tests single groups of size $n = 10$ until all fail ($r = 10$). Using Table 8, $R_{0.50}^{\beta} = 15.3$. If two such tests are conducted under different conditions which do not affect the shape parameter, then the pooled shape parameter estimate may be used for estimating $x_{0.10}$, and $R_{0.50}^{\beta}$ will be reduced to 7.30. In Table 8 this value of $R_{0.50}^{\beta}$ is seen to be equivalent to a single ($k = 1$) uncensored sample of a size somewhere between $n = 15$ and $n = 20$.

Finally, consider selecting the sample size needed for testing $k = 3$ materials to ensure that the median ratio of the upper to the lower end of a 90 percent confidence interval for the $x_{0.10}$ of each group is no larger than 2.5. Assuming a shape parameter value of 1.3 for planning purposes gives

$$R_{0.50}^{\beta} = (2.5)^{1.3} = 3.29$$

Scanning the $k = 3$ entries in Table 8, it is apparent that $r = 20$ with $n = 20$, 25, or 30 will be adequate.

Acknowledgment

References

[1] McCool, J. I., *Journal of Statistical Planning and Inference*, Vol. 3, 1979, pp. 39–68.
[2] McCool, J. I., *I.E.E.E. Transactions on Reliability and Quality Control*, Vol. R-24, No. 3, 1975, pp. 186–192.
[3] McCool, J. I., *American Society of Lubrication Engineers Transactions*, Vol. 21, No. 4, 1978, pp. 271–284.
[4] McCool, J. I., *American Society of Lubrication Engineers Transactions*, Vol. 13, 1970, pp. 189–202.
[5] McCool, J. I., in *Theory and Applications of Reliability*, C. Tsokos and I. Shimi, Eds., Academic Press, New York, 1977, pp. 335–379.
[6] McCool, J. I., "Inferential Techniques for Weibull Populations," Interim Technical Report ARL TR 74-0180, AD A 009 645, Aerospace Research Laboratory, Wright–Patterson Air Force Base, Ohio, Dec. 1974.
[7] Brown, P. F. and Potts, J. R., "Evaluation of Powder Processed Turbine Engine Ball Bearings," Technical Report No. AFAPL-TR-77-26, Air Force Aero-Propulsion Laboratory, Wright–Patterson Air Force Base, Ohio, 1977.
[8] Kendall, M. G. and Stuart, A., *The Advanced Theory of Statistics*, Vol. 2, Griffin and Co. Ltd., London, England, 1961.
[9] McCool, J. I., "Censored Sample Size Selection for Life Tests," in *Proceedings, 1973 Annual Reliability and Maintainability Symposium*, IEEE Catalog No. 73CH0714-64, Institute of Electrical & Electronics Engineers, New York, 1973.

Effects of Material and Structural Variations on Rolling Contact Fatigue

P. F. Brown, Jr.,[1] *G. A. Bogardus,*[1] *R. D. Dayton,*[2]
and D. R. Schulze[2]

Evaluation of Powder-Processed Metals for Turbine Engine Ball Bearings

ABSTRACT: Two different types of rolling element fatigue testers and a full-scale bear-
ing tester were used in a program aimed at developing a highly fatigue-resistant powder-
processed material (P/M) for use in turbine engine bearings. The testers were the single-
ball machine evaluating 0.0238-m ($^{15}/_{16}$-in.)-diameter balls, a rolling contact fatigue
machine evaluating 0.00953-m ($^3/_8$ in.) rods, and a full-scale bearing rig evaluating
140-mm-bore, 0.0238-m ($^{15}/_{16}$ in.)-diameter ball, angular contact thrust bearings.
  The two-element testers, used to screen three different P/M alloys and the baseline
vacuum induction melted–vacuum arc remelted (VIMVAR) M-50 alloy, each produced
essentially the same ranking for these materials. The best results, about twice the life of
the baseline VIMVAR M-50, were achieved with P/M CRB-7, a 14 percent chrome
corrosion-resistant alloy. P/M M-50 produced lives equivalent to VIMVAR M-50. P/M
T-15, a 4 percent chrome alloy, exhibited lives ranging from that realized with the
baseline material down to one third of that level. Based on these tests, CRB-7 was
selected as the material out of which the balls and races for 20 full-scale 140-mm bearings
were subsequently fabricated and tested. The tests were conducted at a thrust load of
34 872 N (7 840 lb) and at a speed of 12 500 rpm. A wear problem encountered in these
tests was circumvented by nickel plating the cage guiding surfaces of the inner ring lands.
The B_{10} rolling contact fatigue life realized with these bearings was equivalent to that ex-
pected for these same bearings had they been made of conventional VIMVAR M-50
material. These results were quite encouraging considering the fact that this was the first
attempt at applying powder processing to the manufacture of aircraft-quality rolling ele-
ment bearings.

[1]Head and senior test engineer, respectively, Mechanical Technology section, United
Technologies Corp., Pratt & Whitney Aircraft Group, Commercial Products Div., East Hart-
ford, Conn. 06108.
  [2]Group leader and mechanical engineer, respectively, Lubrication Branch, Air Force Wright
Aeronautical Laboratories, Aero-Propulsion Laboratory, Wright–Patterson Air Force Base,
Ohio 45433.

A review of service experience for existing aircraft turbine engines indicates a continuing need for bearing material improvement. Advanced engines require bearing designs capable of operating at higher speeds, loads, and temperatures. New materials or processes which would extend bearing life by improving both rolling contact fatigue performance and corrosion resistance would benefit the industry economically. Corrosion can occur in service due to the presence of ingested windblown seawater or water condensate from temporary on-the-wing storage in a humid atmosphere or acidic lubricant resulting from thermal degradation of the oil. If a bearing with such corrosion on the load-carrying surfaces is not removed from service it will experience extensive surface-originated spalling leading to complete bearing failure and engine damage. Powder metal technology provides an extremely attractive and promising approach for satisfying these requirements and has the further merit of its cost-reduction potential. A principal source of rolling contact fatigue failure in present high-quality M-50 bearings for aircraft engines is the occurrence of undesirably large carbide formations in the metal matrix. These act as points of weakness under the highly cyclic loading experienced in bearing operation and are suspected of being the source of fine cracks which lead to spalling and bearing failure. The use of powder metal processing promises to produce alloys with uniform carbide distribution and to minimize carbide size. Carbide size would be limited to the dimensions of the powder particles and would not change in size as a result of subsequent processing. Although the potential of powder metal for rolling contact bearings has been recognized for several years, it has only been within the relatively recent past that the necessary purity of the powder product could be ensured.

A program plan was developed for screening and testing various powder-processed alloy candidates. The first step involved a review of past test experience with the single-ball fatigue machine to identify the three best-performing alloys, as reported in Ref 1.[3] These would then be powder processed and evaluated in single-ball and rod element testers, and the best performer would be fabricated and tested in full-scale bearings.

Alloy Selection

Review of past rolling contact fatigue data from single-ball tests disclosed that, of the many materials evaluated, only two alloys had exhibited fatigue

---

[3]The italic numbers in brackets refer to the list of references appended to this paper.

lives that equalled or surpassed that of M-50 alloy, the current standard for aircraft gas turbine use. These alloys are T-15, a high tungsten–cobalt tool steel with 4 percent chromium by weight, and CRB-7, a stainless steel alloy which has 14 percent chromium. There is a certain difficulty in assessing the relative performance of materials when the data being compared have been acquired at different times over a period of years. The performance of the M-50 baseline material has changed over the years because of improvements in processing, manufacturing, and quality control. For this reason the B_{10} life data presented are identified with the calender year of the test and on a relative or normalized scale to minimize confusion.

Balls manufactured from T-15 alloy were tested in 1965 in the single-ball rolling contact fatigue test facility, and the observed life of 15.57 million stress cycles was 1.77 times that of the M-50 steel tested up to that time, as shown in Fig. 1. At the time these data were obtained this life difference, although indicating a gain, was not considered high enough to warrant further evaluation of the material until now.

Single-ball rolling contact fatigue tests are normally conducted with either of the two most widely used aircraft gas turbine engine oils, namely, MIL-L-7808 or MIL-L-23699. Typical test results of these two oils in 1965 indicated there is no statistically significant difference in their performance, as shown in Fig. 1, when used to evaluate M-50 alloy.

Many other candidate alloys were evaluated in the late 1960s, and none of these has exhibited fatigue life values that equalled the performance of M-50 or T-15. Notable among the many were WB-49, BG-42, and WADC-65 alloys, whose lives are compared with M-50 alloy B_{10} life in Fig. 2. WB-49
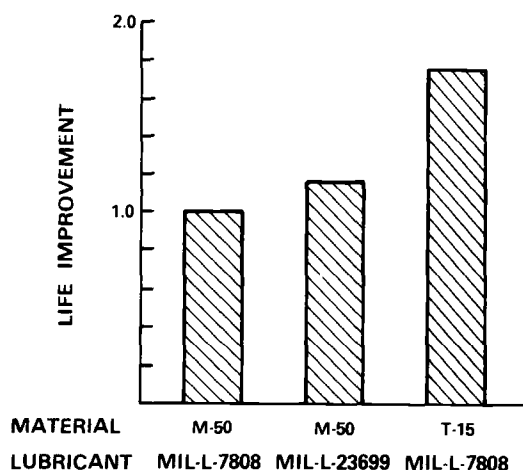
FIG. 1—*The single-ball tester results from 1965, revealing life improvement for the T-15 alloy.*
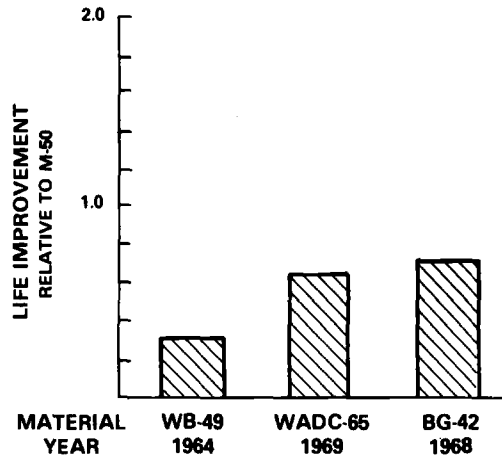
FIG. 2—*The single-ball tester results from 1964 to 1969, showing no life improvement for three candidate materials.*

alloy was tested in 1964, and its performance was 32 percent of the B_{10} life of M-50; BG-42 alloy tested in 1968 had a B_{10} life of only 71 percent of that of M-50; and WADC-65 tested in 1969 exhibited a fatigue life which was 64 percent of that of the baseline M-50 alloy.

An experimental alloy designated CRB-7, a recently introduced material which is basically a stainless steel, produced significant life improvement results when tested in the single-ball rigs. As shown in Fig. 3, this is the only material provided from a laboratory heat to equal or surpass the current
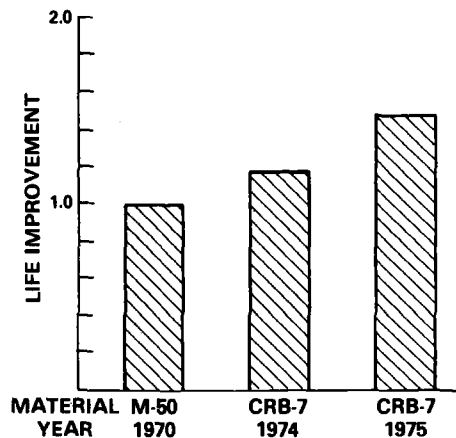
FIG. 3—*Single-ball tester results showing that the CRB-7 alloy has the greatest life improvement.*

M-50 alloy performance, and it produced the highest B_{10} life in the history of single-ball testing. This alloy was retested in 1975 with a batch of balls processed from a production-quality ingot and indicated a ball life which eclipsed even the performance obtained from the laboratory heat ball lot.

The three bearing alloys, M-50, T-15, and CRB-7, were thus selected for further evaluation in this powder metal development program on the basis of their single-ball rolling contact fatigue test results and other considerations. M-50 was chosen as the baseline material because of its widespread current use in service engines. In addition to their demonstrated fatigue life improvement, T-15 and CRB-7 also exhibited improved hot hardness and corrosion resistance beyond the levels available from AISI M-50 alloy steels. Available data on the hot hardness retention of these alloys are presented in Fig. 4 and show that T-15 and CRB-7 alloys are superior to M-50 and other stainless steels such as Types 14-4 and 440C.

There is no common base of information available on the corrosion resistance of various alloys, thus it is difficult to form an absolute judgment in this regard. However, it is the opinion of many metallurgists that an alloy's chromium content governs the material's corrosion resistance. Thus CRB-7, which has 14 percent chromium, would have superior corrosion resistance to M-50 and T-15, which both contain only 4 percent chromium. The three alloys, M-50, T-15, and CRB-7, have significantly different chemical compositions, as noted in Table 1. As a result, they produce microstructures with marked differences not only in the number of carbides but in their distribution and morphology as well.

Production of Powder-Processed Material (P/M) for Element Tests

The starting materials for this program were conventionally processed ingots prepared either by vacuum induction melting (VIM) or vacuum induction
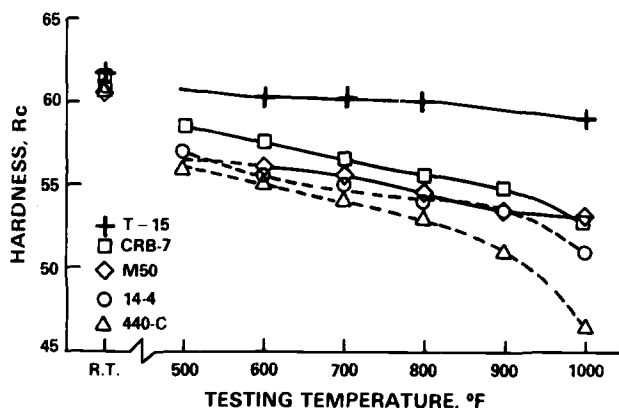
FIG. 4—*Superior hot hardness demonstrated by candidate alloys T-15 and CRB-7.*

TABLE 1—*Alloy chemical composition, weight percent.*

Alloy	C	Cr	Mo	V	W	Co	Cb	Si	Mn
CRB-7	1.1	14.0	2.0	1.0	...	...	0.3	0.3	0.4
T-15	1.6	4.0	...	5.0	12.0	5.0	...	0.3	0.3
M-50	0.8	4.0	4.2	1.0	...	...	...	0.2	0.2

melting–vacuum arc remelting (VIMVAR) techniques. Conversion of the ingots into powder was accomplished with equipment which is schematically shown in Fig. 5. The atomizing system is enclosed and is evacuated to a pressure level which removes all traces of atmospheric contamination before the ingot is remelted. Melting is accomplished by induction heating techniques in a crucible in the upper section of the unit. After the metal becomes molten, it is poured through an atomizing nozzle into another vacuum chamber located below the remelt chamber. The molten metal is discharged as refined droplets from the nozzle. Vacuum pumping acts continuously to maintain the chamber pressure well below atmospheric pressure. The cooled droplets solidify and drop to the bottom of the lower chamber. This powder now contains carbides that are many times smaller than those that were present in the original, large ingot. The powders were reconsolidated into new ingots at temperatures well below the alloy melt temperature in order to ensure that no coalescence of growth of the alloy carbides occurred. By means of this process it is ensured that the final product will exhibit refined carbides.

For this program, powder separation was accomplished by sieving under an inert gas to prevent oxygen and nitrogen contamination of the powders. After the rough sieving, the various batches of powder were blended to pro-
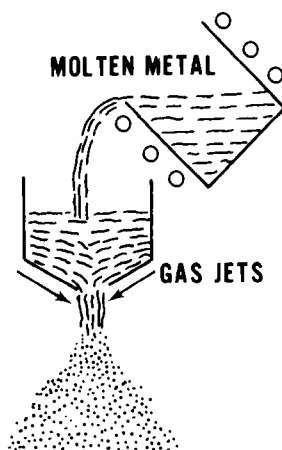
FIG. 5—*Gas atomization of molten alloy, producing powdered metal.*

vide a homogeneous mixture. Particle size distribution of the powders, shown in Table 2, indicated that the bulk of the powders were smaller than 86.4 μm (0.0034 in.).

Powder Consolidation and Micrographic Results

Consolidation of the blended powders was accomplished by hot isostatic pressing (HIP) by heating the containers of powders to 1177°C (2150°F) under a gas pressure of 103.4 MPa (15 000 psi) for 4 h. The resulting billet size was 0.1727 m (6.8 in.) in diameter by 1.27 m (50 in.) in length. A micrographic study of the CRB-7 alloy after HIP and annealing operations revealed an ideal microstructure, as seen in Fig. 6, which was homogeneous with refined carbides uniformly dispersed. The maximum carbide size was estimated to be 2.54 μm (0.0001 in.).

Fabrication of Ball Test Hardware

The test balls used in both the single-ball test and the full-scale bearing endurance programs were fabricated from HIP billets, which were then forged and rolled into 0.019-m (¾-in.) diameter bars. Rough-shaped balls were then produced by upset forging of short lengths of these bars. Test balls of nominal 0.0238-m (¹⁵⁄₁₆-in.) diameter were finished to Grade 10 of the Anti-Friction Bearing Manufacturers' Association (AFBMA) ball standard.

The powder metals apparently responded to the finishing operations in a manner that differed somewhat from that normally achieved with the conventional ball material as a 0.05 to 0.076-μm (2 to 3-μin.) arithmetic average (AA) finish was achieved instead of the desired 0.025-μm (1-μin.) AA finish. The balls were accepted with this variation for subsequent fatigue testing as further lapping might have negated the existing good ball sphericity.

The test balls were then machined to provide parallel flats. This configuration, when run in the single-ball test rigs, causes the balls to track because of

TABLE 2—*Blended powders particle size distribution, weight percent.*

Mesh Size, Wires per in.[a]	Average Size, μm (in.)	Alloys		
		M-50	T-15	CRB-7
−80, +100	162.6 (0.0064)	1.0	1.0	3.0
−100, +140	127.0 (0.0050)	9.1	10.2	15.2
−140, +200	86.4 (0.0034)	16.8	17.6	21.1
−200, +325	58.4 (0.0023)	32.7	30.5	28.3
−325	43.1 (0.0017)	40.4	40.7	32.4
Total percent		100.0	100.0	100.0

[a]1 in. = 25.4 mm.
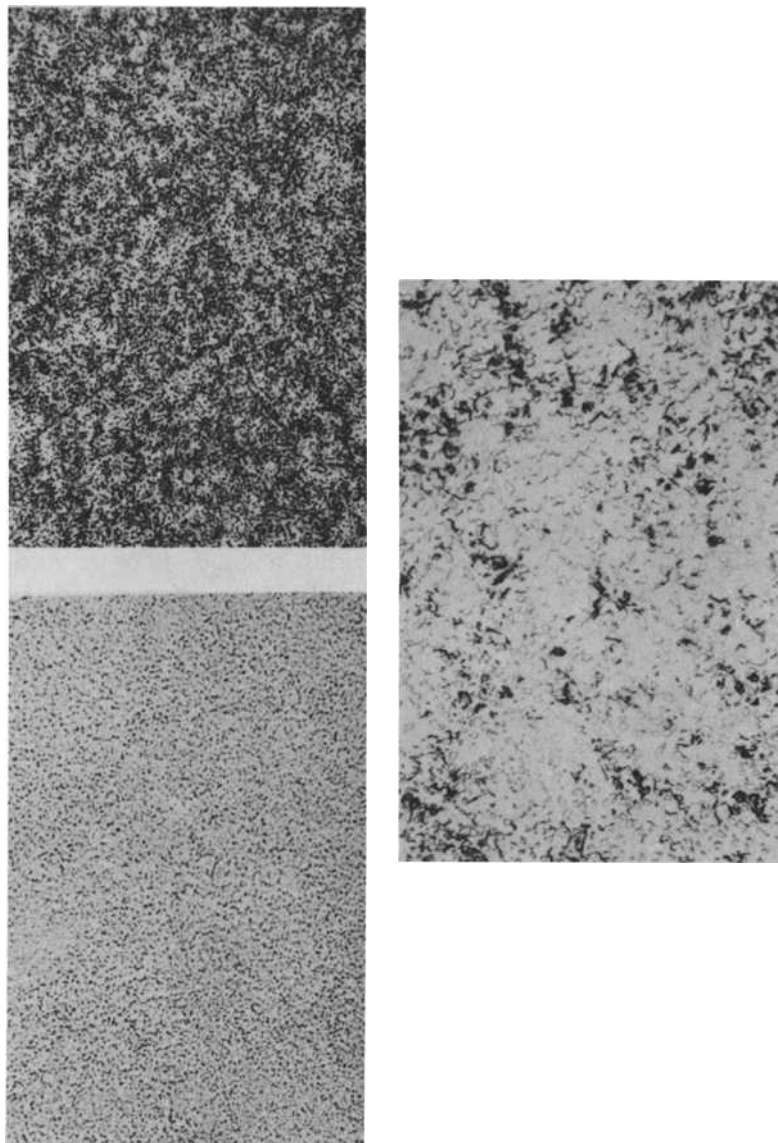
FIG. 6—Photomicrographs of the CRB-7 alloy after the HIP operation, which reveals a homogeneous microstructure; (top left) magnification ×90, unetched; (top right) magnification ×90, picral and hydrochloric etchant; (bottom) magnification ×450, picral and hydrochloric etchant.

gyroscopic action. This tracking action forces stress cycling to occur in two very narrow bands, thus accelerating the testing and markedly reducing the test time required. Normally, spherical balls are reoriented periodically during the test, and the stress is distributed randomly over the entire ball surface. The machined flats also provide a convenient ball surface for determining ball hardness. In this regard, the desired hardness range of 63 ± 1 HRC was achieved for all three of the P/M alloys tested.

Ball Fatigue Testing

To achieve rolling contact fatigue failures, dynamic ball testing was accomplished by loading individual balls in compression between two rotating 130-deg V-grooved rings in test rigs, as illustrated in Fig. 7. The test ball, held in position by a stationary retainer with the ball flats aligned so that rolling contact was limited to the spherical surface only, was driven by the lower hub. The upper hub acted as an idler through which the loading was accomplished by means of a hydraulic cylinder. Oil jets above and below the ball provided flood lubrication.
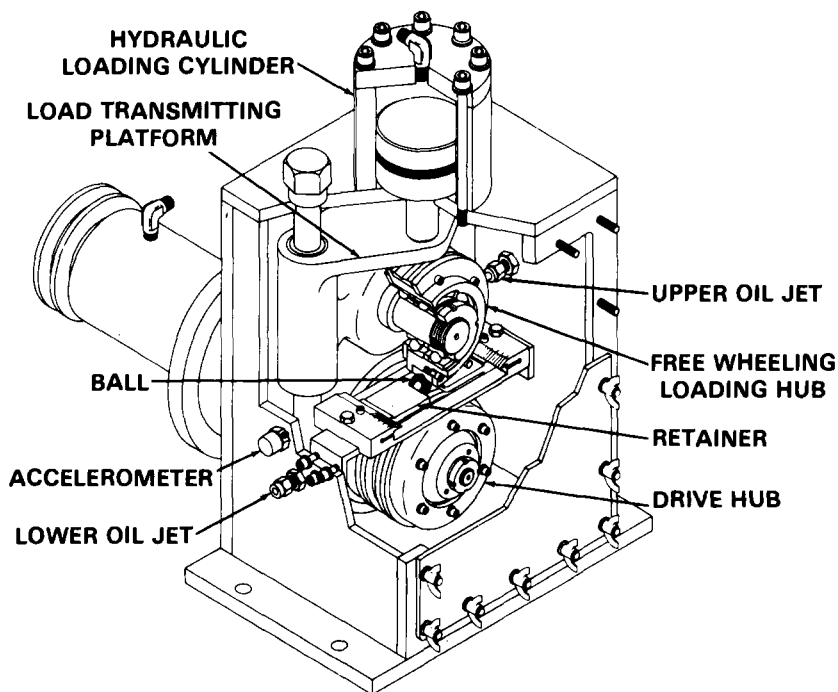
FIG. 7—*The single-ball fatigue test rig, which simulates the contact conditions in jet engine mainshaft ball thrust bearings.*

Single-ball test rigs have proven to be highly consistent in their ability to properly rank materials, processes, and lubricants as to their influence on bearing fatigue life. This ability of the single-ball tester was considered to be a direct result of careful attention to the development of ball–ring contact conditions that simulated the application. The V-groove geometry of the matching rings on which the ball rides imparted a spin–roll ratio action tailored to match average conditions encountered in main shaft, jet engine, ball thrust bearings. Also, the lubrication and the surface topography of the V-rings were carefully controlled to simulate those encountered in the bearing application. A specific example of how the single-ball tester can relate to real bearings has been well illustrated in work reported by the Coordination Research Council [2].

The 0.0238-m ($^{15}\!/_{16}$-in.)-diameter test balls were individually tested at a load of 6 005 N (1 350 lb) to develop a maximum hertz stress of 4 140 MPa (600 000 psi) at the ball race contact area. This stress level was sufficient to cause spall failure within a few hours but was below the threshold of plastic deformation. The lubricant, MIL-L-7808G, was heated to 149°C (300°F) and was supplied to the ball–race contact area by means of a pair of oil jets. The V test rings spun the test balls at 41 050 rpm. The V-ring race surfaces were honed to a nominal 0.127 μm (5 μin.) AA finish. Ball failure by spalling of the ball surface or operation without failure for the predetermined runout time of 40 h constituted completion of a test.

A summary of the B_{10} life test results is provided in Table 3 for the program baseline material, VIMVAR M-50, and the three powder-processed alloys. The B_{10} life value of the CRB-7 material exceeded that for the VIMVAR M-50 by a factor of 1.83. Utilizing Johnson's method [3] for assigning a confidence level to this life difference, it was determined that there was an 85 percent confidence that the observed life difference was real. Based upon this performance, it is apparent that the CRB-7 alloy has considerable potential for providing improved B_{10} life performance in full-scale bearings as compared to today's production bearings.

Metallurgical Examination of Test Balls

Five short-lived and five long-lived balls from each alloy test lot were examined in an attempt to discern if there were obvious and distinct differences between the two groups. A scanning electron microscope, equipped with electron source X-ray detection equipment (KEVEX) was employed and allowed study of ball surfaces and the subsequent supplemental X-ray analysis of suspect areas within the matrix. It appears that it is virtually impossible, even with today's methods, to differentiate between groups of short-lived and long-lived specimens since failure in both groups apparently result from the same cause.

TABLE 3—*Bearing steel fatigue life results, Air Force Powder Metal Program.*

Alloy	No. of Tests	$B_{10} \times 10^{-6}$ Stress Cycles	$B_{50} \times 10^{-6}$ Stress Cycles	Weibull Slope
Program baseline				
VIMVAR M-50	15	20.56	60.78	1.74
P/M M-50	30	16.99	44.05	1.98
P/M T-15	34	6.67	67.65	0.81
P/M CRB-7	30	37.61	116.57	1.67

Nonmetallic contamination appeared to be as prevalent in the VIMVAR M-50 test balls as in the P/M T-15, P/M CRB-7, and P/M M-50 alloy balls. Examination of typical incipient spall regions revealed aluminum enrichment, attributed to traces of alumina thought to be eroded from the ceramic vessels used in both the melting process and the atomization of the ingot into powder. The observed inclusions were judged to be indicative of a Jern-koneret (J-K) rating of ½, which is representative of the best steel quality that vacuum-melting technology can provide. It appears that these nonmetallic inclusions, despite their smallness, were the primary cause of spalling in the balls tested in this program.

Evaluation of the P/M Alloys in the Rolling Contact Tester

Concurrent with the single-ball tests, a rolling contact (RC) disk machine (Fig. 8) was used to generate fatigue life estimates of the same three powder-processed materials: T-15, CRB-7, and M-50. The test specimens, which were fabricated from the same HIP billets used for ball manufacture, were cylindrical bars having a diameter of 9.525 mm (0.375 in.) and a finish of 0.15 to 0.20 μm (6 to 8 μin.) rms.

Each bar was individually mounted in a precision chuck. The bar was driven by an electric motor and in turn drove two 0.1905-m (7.5-in.)- diameter disks which were hemispherically ground with a 0.00635-m (0.25-in.) radius and a surface finish of 0.20 to 0.30 μm (8 to 12 μin.) rms. These disks (or rollers) were each mounted on a ball bearing on a shaft supported by a massive pendulum yoke. The test load was applied by tightening a strain-gaged turnbuckle which closed the rollers against the test bar. The aligned rollers produced two elliptical contacts on a single track of the test rod with a maximum hertz stress of 4 830 MPa (700 000 psi) on each contact. Test rotational speed of the bar was 10 000 rpm. The number of stress cycles accumulated during a test was monitored with a mechanical counter driven through a worm gear reducer by the motor. An accelerometer mounted on one of the roller support yokes automatically initiated test shutdown when a spall developed on the test bar.
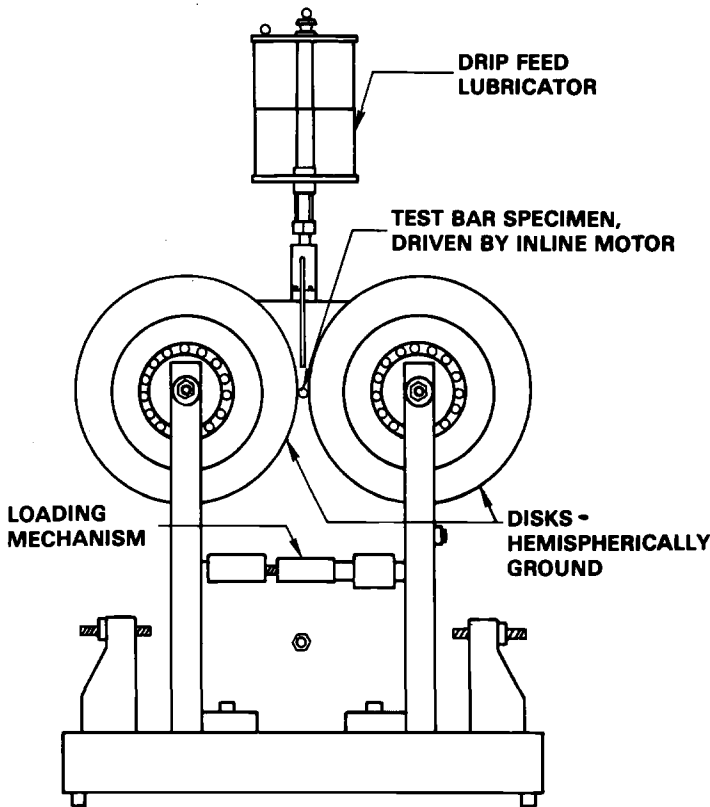
FIG. 8—*The rolling contact disk machine, which provides economical B$_{10}$ life data.*

Before each test, the rollers and test bar were thoroughly cleaned. The test bar was inserted in the chuck and checked for alignment to within 0.025 mm (0.001 in.). Next, the rollers were loaded onto the test bar using the output from the strain gages on the turnbuckle and a previously obtained calibration. A lubricant that met MIL-L-7808 specifications was dripped onto the test bar at a rate of 20 drops per minute. The test bar was then brought up to the proper speed, and the final alignment of the rollers was performed by adjusting the screws loaded against the roller axles until the proper oil spray pattern was obtained.

Ten tests were conducted with each material, and all the tests terminated because of rolling contact fatigue spalling. In addition to the three powder-processed materials, specimens of CEVM and VIMVAR M-50 materials were tested to provide a baseline of comparison. The results of these tests are shown in Table 4. Powder-processed CRB-7 again provided the longest life of all the materials, generally corroborating the results observed in the single-ball test program.

TABLE 4—*Fatigue test life results.*

Alloy	Rockwell Hardness, C scale	B_{10} Life, $\times 10^{-6}$ Cycles	B_{50} Life, $\times 10^{-6}$ Cycles	Weibull Slope
CEVM M-50	62	2.72	5.93	2.42
VIMVAR M-50	62	3.89	9.54	2.10
P/M M-50	62	3.87	10.26	1.93
P/M T-15	64	4.05	8.50	2.54
P/M CRB-7	63	7.73	14.64	2.95

Material for Full-Scale Ball Bearings

Based on the results of the single-ball and RC rig testing of the P/M processed alloys, the material chosen for further evaluation in full-scale bearings was the CRB-7 alloy. Applying the same processing techniques previously used to provide ball material, Carpenter Technology produced sieved powder in a quantity sufficient to make 20 sets of 140-mm-bore ball bearing inner and outer races. Samples of the sieved powder were measured for particle size distribution, and the results (Table 5) showed some variation from that achieved with the powder used to make the balls (Table 2). Approximately 7.2 percent of this quantity of powder was larger in size than $+80$ mesh, compared with essentially 0 percent in this category for the powder used to make the test balls. The decision was made to accept this powder with its small portion of large particles because of the experimental nature of this program and related cost considerations.

Further metallurgical examination of the raw material was conducted on specimens taken from the bar form after the powder had been subjected to the HIP process. A cleanliness check per the ASTM Recommended Practice for Determining the Inclusion Content of Steel (E 45-76) revealed that the nonmetallic inclusion content was low. A Jernkontoret rating of ½ was

TABLE 5—*CRB-7 blended powder size distribution.*

Mesh Size, Wires per in.[a]	Average Size		Weight %
	μm	in.	
$+60$	246.4	0.0097	0.1
$-60, +80$	210.8	0.0083	7.1
$-80, +100$	162.6	0.0064	6.0
$-100, +140$	127.0	0.0050	14.7
$-140, +200$	86.4	0.0034	19.4
$-200, +325$	58.4	0.0023	23.2
-325	43.1	0.0017	29.5
Total percent			100.0

[a]1 in. = 25.4 mm.

assigned, a rating which typifies the quality achieved with the cleanest of vacuum-melted bearing steel alloys. Micrographs of the etched samples showed that the microstructure of the CRB-7 alloy samples was homogeneous, with refined carbides uniformly dispersed. Maximum carbide size was estimated to be 2.54 μm (0.0001 in.).

Endurance Bearing Design and Procurement

The bearing design selected in this program was a 140-mm-bore angular contact ball thrust bearing for which extensive rig and service engine experience exists. This bearing, described in detail in Ref 4, had a split inner ring with a silver-plated AMS 6415 steel cage that was one piece, fully machined, and inner-ring guided. This bearing design had a complement of 20 balls 23.8125 mm (0.9375 in.) in diameter, which was the same size as those tested earlier in the single-ball rig screening program. Twenty of these bearings were manufactured from CRB-7 powder-processed metal bar stock. The bearings were inspected on receipt and found to be acceptable for testing in this program.

Full-Scale Bearing Endurance Test Facility

Endurance evaluation of the CRB-7 powder metal alloy test bearings was conducted using the bearing test rig shown in Fig. 9. It consisted of a cylindrical housing with an annular thrust loading system on one end. In opera-
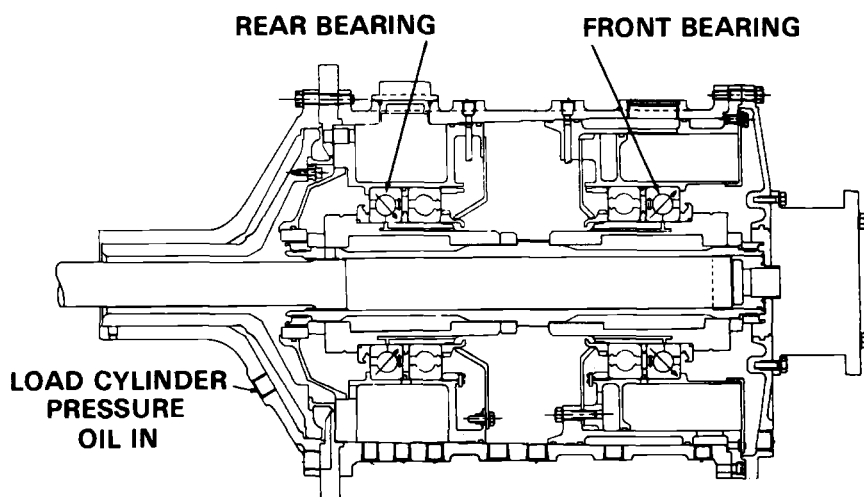
FIG. 9—The thrust bearing test rig, which permits the simultaneous testing of two bearings under identical conditions.

tion, the hydraulic loading piston applied an axial load to the rear test bearing outer ring housing. The load path was through the rear bearing to the common shaft, to the front bearing, and thence to the rig case. Thus two bearings were operated simultaneously under identical test conditions. A multiheaded speed increaser was driven by a transmission gearbox which in turn was driven by an electric motor. This system provided the capability to operate four rigs simultaneously. Instrumentation to measure operating temperatures and vibration levels was installed to permit continuous monitoring of the test rigs during the endurance tests. Controls were installed in the various rig support systems which permitted unattended operation of the rigs. A self-contained microprocessor controlled the data acquisition and recording of critical bearing and oil system parameters.

Endurance Test Bearing Program

An endurance test program to evaluate eight bearings simultaneously utilizing the sudden-death approach was designed. The sudden-death test approach yields life estimates at a specific percentage of failure level which are at least as accurate as estimates provided by the standard approach but with approximately half the number of test hours. The operating test conditions for the 140-mm-bore CRB-7 powder metal endurance bearing were established on the assumption that the test condition thrust load would produce the same theoretical B_{10} life, 308 h, that would be expected for the same geometry bearing made from VIMVAR M-50 material. Test conditions employed in this test were as follows: thrust load, 34 872 N (7 840 lb); oil flow, 9.07 kg (20 lb) per minute with MIL-L-7808G lubricant at 121°C (250°F); and a bearing speed of 12 500 rpm or $1.75 \times 10^6 \, DN$, where DN is a product of the bearing bore in millimetres and shaft speed in revolutions per minute. The inner race and outer race mean contact hertz stresses under these conditions were 1 270 MPa (184 000 psi) and 1 255 MPa (182 000 psi), respectively.

Bearing Endurance Tests

After the installation of eight bearings in the test rigs, the stand lubrication system was activated and the oil was circulated through the rigs and gearbox. The start-up conditions were normal, the bearing instrumentation was acceptable, and the endurance conditions were set. After approximately 2 h, an automatic shutdown of the test facility initiated by a rise in rig vibration occurred. Disassembly of all the rigs revealed various degrees of inner ring land wear and cage bore distress on all of the test bearings. An attempt to eliminate this problem by improving the surface texture of the inner ring lands was not successful. This wear problem was eventually circumvented by

coating the bearing inner ring lands with a thickness of hard electroplated nickel. For detailed discussion of this wear phenomenon and subsequent analysis of it, see Ref 4. Subsequent testing of these bearings revealed a much reduced rate of wear on the lands to a level that permitted the planned fatigue testing to be accomplished.

Due to the extent of the wear damage that had occurred on some of the bearings, however, the number of bearings available to the endurance test program had been reduced to twelve. Because of this reduced number it was no longer possible to produce viable endurance test data by means of the sudden-death technique. The program plan was then altered to employ the standard endurance test procedure of running each bearing to failure or to a predetermined runout time—1000 h in this instance.

The twelve bearings were run, under the endurance program load and speed conditions, for a cumulative total of 7491 h. The maximum time run on any one bearing was 942h. It was deemed cost-effective to discontinue the program at that time, and not run it out to 1000 h, because any further rolling contact fatigue failures that may have occurred would not have altered the B_{10} life already established. A total of four of the twelve bearings were identified as having failed in rolling contact fatigue.

Posttest Analysis

A visual examination with binocular assistance was conducted on the twelve bearings. Rolling contact fatigue failures or spalls were observed on balls from three bearings which had accumulated 157.4, 500.0, and 942.0 test h, and one bearing which had an outer race spall at 942 test h. Two bearings that were removed after 2.6 h were examined, and it was observed that each had experienced an apparent loss of axial thrust test load as evidenced by the presence of ball tracking on both inner race grooves. The inner rings of four bearings had experienced land wear distress, up to a radial depth of 0.178 mm (0.007 in.). Only one of these four failed due to spalling, and it was removed after 500 h. The other three bearings had 917, 942, and 942 h, respectively. The remaining bearings had either no wear or varying degrees of wear up to 0.102 mm (0.004 in.) in depth. Cage bore pitting was observed on most of the tested bearings and varied in extent from a 40 deg circumferential arc to as much as a 150 deg arc.

Results and Discussion

Utilizing existing Weibull analysis computer program procedures and using the test times of 157.4, 500.0, 942.0, and 942.0 h associated with the four rolling contact fatigue failures, a B_{10} life of 249 h and a slope of 1.23 was calculated. This compared favorably with the calculated or theoretical B_{10}

life of 308 h, with an ideal slope of 2.0 for an equivalent VIMVAR M-50 alloy bearing. The results of the two Weibull analyses, shown in Fig. 10, indicate that as the 90 percent confidence bands overlap there is no significant dif⁴ ference between the B_{10} life of the powder metal CRB-7 alloy and the theoretical B_{10} life of the M-50 bearing.

The fact that the P/M CRB-7 ball bearings tested in this program produced a B_{10} life equivalent to the industry standard VIMVAR M-50 is highly encouraging considering the pioneering nature of this effort. The significance of this result can perhaps be best appreciated by looking back in time to that point when the Type 52100 alloy was the standard production bearing material for aircraft gas turbine use. In the mid to late 1950s the tool steel M-50 was first introduced experimentally for such applications, and its B_{10} life was found to be generally in the range of 10 to 50 percent of that for Type 52100 material of that day. Improvements in M-50 resulting from heat treatment and quality control changes, and the introduction of vacuum melting
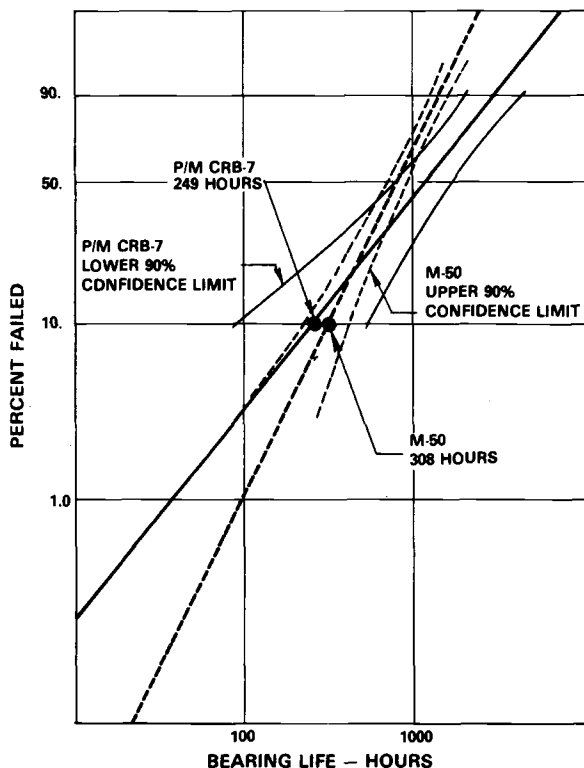
FIG. 10—*The Weibull plot of bearing results, showing no significant difference between the test B_{10} life of P/M CRB-7 and the theoretical B_{10} life of VIMVAR M-50 alloy.*

processes paid off with a material that, today, provides a life more than 2 orders of magnitude better than what was initially available with that alloy. Although it is not reasonable to expect the same levels of improvement with P/M CRB-7 alloy in the next decade or two, a considerable measure of improvement can be expected since a solid foundation has obviously been laid, as evidenced by the work presented herein.

The subject program, because of its limited scope, permitted evaluation of only three powder-processed alloys in the element test phase and the best of these in the full-scale bearing test phase. Other alloys surveyed but not selected for this program include WADC-65, BG-42, and WB-49. In all fairness it must be acknowledged that any one of these alloys or others not mentioned here might respond well to powder processing and produce a product with superior resistance to rolling contact fatigue. The fact that this possibility exists is testimony to the current lack of in-depth understanding of the interactions between bearing steel chemistry and powder processing and how those interactions affect fatigue life. Further gains in rolling contact fatigue performance will undoubtedly be realized through an expansion of the work already accomplished by evaluating other alloys and exploring the optimization of powder processing parameters, including particle size.

Some note should be made of the consistency of the ranking achieved by the two-element testers used in this program. The single-ball testers and the RCF machines both ranked P/M CRB-7 as the best and P/M M50 and VIM-VAR M-50 as equivalent and in second place. The only notable difference occurred with the P/M T-15 material, the single-ball tester ranking it a poor third and the RCF tester showing it equivalent to the M-50 materials. It is beyond the scope of this paper to speculate in detail as to the reason for this difference in the results obtained on the two machines. Suffice it to state that care in preparing the specimens, resulting in good homogeneity, contributed much to obtaining consistent results from the two testers.

The encouraging results with the element testers were somewhat offset by the unanticipated wear problem experienced with the 140-mm P/M CRB-7 ball bearings. The nickel plating of the inner rings allowed the continuation of the rolling contact fatigue endurance program but did not entirely eliminate the wear problem. It was speculated that the nickel plate and the P/M CRB-7 material wore due to a lack of proper lubrication at the bearing test speeds combined with a possible cage resonance condition. This combination of factors may have produced local cage pitting damage similar to damage caused by the collapse of cavitation bubbles. The bubbles possibly were created by large local pressure fluctuations in the lubricating film. These hydrodynamically erosive pressures may have then released material from both surfaces, the harder ring particles released becoming embedded in the soft silver plate on the cage bore and thus removing more material from the inner-ring land surface by an abrasive machining action.

Conclusions

This powder-processed bearing technology program, coupled with development of a new bearing steel, has led to the following conclusions:

1. Metallurgical studies demonstrated that powder processing can provide steels with cleanliness levels that are equal to or exceed those already established for double vacuum melted steels.

2. Single-ball tests of powder-processed CRB-7 alloy yielded a B_{10} life of 1.83 times that observed for VIMVAR M-50 and 2.21 times better than that obtained on tests of powder-processed M-50 material.

3. Rolling contact fatigue machine testing substantiated these single-ball fatigue rig results.

4. The B_{10} fatigue life of powder-processed CRB-7 bearings was equal to that calculated for the same bearings fabricated from VIMVAR M-50 alloy. Weibull analysis indicated that there was a 90 percent confidence that there was no significant difference between the two materials.

References

[1] Brown, P. F. and Potts, J. R., "Evaluation of Powder Processed Turbine Engine Ball Bearings," Air Force Aero-Propulsion Laboratory Interim Report AFAPL-TR-77-26, Pratt & Whitney Aircraft Group, Government Products Division, West Palm Beach, Fla., 30 June 1977.
[2] "Development of Equipment and Techniques for Evaluating Effects of Oil in Bearing Fatigue Life," Coordinating Research Council Bearing Fatigue Panel, CRC Report No. 413, CRC Inc., New York, June 1968.
[3] Johnson, L. G., *The Statistical Treatment of Fatigue Experiments*, Elsevier, Amsterdam, London, New York, 1964.
[4] Brown, P. F., Bogardus, G. A., and Miner, J. R., "Evaluation of Powder Processed Turbine Engine Ball Bearings," Air Force Aero-Propulsion Laboratory Final Report AFAPL-TR-81, Pratt & Whitney Aircraft Group, Government Products Division, West Palm Beach, Fla., June 1981.

D. Popgoshev[1] and R. Valori[1]

Rolling Contact Fatigue Evaluation of Advanced Bearing Steels

ABSTRACT: A series of rolling contact fatigue tests were performed on nine advanced rolling element bearing materials and processes in combination with three lubricants (an unformulated ester base stock, a qualified MIL-L-23699, and an advanced MIL-L-23699-type lubricant) in order to determine their rolling contact fatigue performance. The performance of each material was compared with the performance of a baseline AMS-6490 (AISI M-50) steel. The results indicate that (1) all of the test materials and processes perform at least as well as AMS-6490, (2) the best performing materials were a powder-processed CRB-7 and an AMS-5749, and (3) the performance of one material (CBS-1000M) improved with the use of fully formulated lubricants.

KEY WORDS: bearing steels, rolling contact fatigue, lubricants

The trend in turbine engine technology toward decreased specific weights over the past two decades has required that main-shaft engine bearings operate reliably at ever increasing levels of load, speed, and temperature. This trend is expected to accelerate over the next decade with the development of variable cycle engines for the improved engine efficiencies required of future multimission aircraft. These engines are projected to operate at such high rotational speeds that the resulting large centrifugal forces on the bearing's rolling elements against the outer race dramatically reduce the rolling contact fatigue life of the bearing below that of current design practice. Moreover, the variable cyclic nature of these engines impose such large variations in bearing thrust loads that bearing contact fatigue reliability is further compromised. Improvements in bearing materials or designs, or both, are required for bearing reliability for future engines to be at levels consistent with

---

[1]Project engineer and program manager, respectively, Naval Air Propulsion Center, Trenton, N.J. 08628.

current aircraft requirements. In addition, the currently used main-shaft engine bearing steel, that is, AMS-6490 and 6491, commonly known as M-50 steel, has two major shortcomings:

1. It is highly susceptible to corrosion. Data received from Naval Air Rework Facilities [1][2,3] indicate that approximately 35 percent of all main-shaft bearing rejections are due to corrosion.

2. Its fracture toughness is not adequate at high DN (bearing bore in millimetres times revolutions per minute) levels, that is, above $2.5 \times 10^6 DN$. Ball and roller bearing tests run at this level have suffered from catastrophic ring fractures subsequent to inner race spalling [2,3].

This program was initiated to investigate the rolling contact fatigue properties of various candidate AMS-6490 replacement steels for application to advanced propulsion systems. These included two carburizing steels, three powder-processed steels, and two corrosion-resistant steels.

Three different lubricants were used in this evaluation to determine their interactive effect with these steels. All three are in the 5 cSt [372 K (210°F)] range which is typical of MIL-L-23699 gas turbine engine lubricants. Specifically, they were an unformulated base-stock ester lubricant, a qualified MIL-L-23699 lubricant, and an XAS-2354-type lubricant.

The work reported herein presents the results of rolling contact fatigue element tests conducted on nine materials and processes in combination with three types of lubricants. The results of AMS-6490 steel tested with each lubricant were used as a baseline for comparing improvements in the rolling contact fatigue life of the various candidate steels.

The Rolling Contact Fatigue Tester

The rolling contact fatigue (RCF) tester is a simple machine used to generate fatigue spalls similar to those found in rolling element bearings [4]. An overall view of the RCF machine is shown in Fig. 1. A close-up view of the test section is shown in Fig. 2. A cylindrical test rod 0.1524 m (6.0 in.) long by 0.0095 m (0.375 in.) in diameter is mounted in a precision collet. Two hemispherically ground AMS-6490 steel disks are loaded against the rod by means of a calibrated load cell and micrometer-threaded turnbuckle arrangement. The disks are between 0.1778 m (7.0 in.) and 0.2032 m (8.0 in.) in diameter and have a crown radius of 6.35 mm (0.25 in.). The test rod is driven by a small electric motor, and the rod in turn drives the two load disks. This arrangement is such that there is essentially no gross slip between the test rod and the load disks. Lubrication is achieved by means of a drip

---

[2]The italic numbers in brackets refer to the list of references appended to this paper.

[3]G. Kuhlman, Naval Air Rework Facility, North Island, Calif., personal communication, 1978.
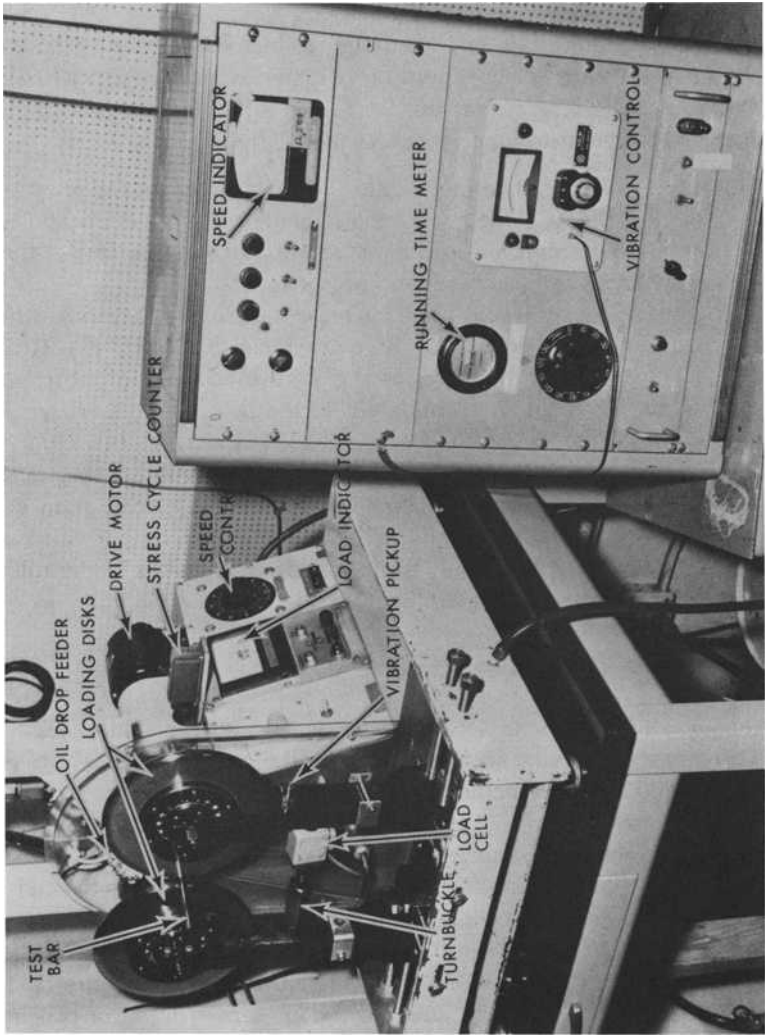
FIG. 1—*Rolling contact fatigue test machine.*
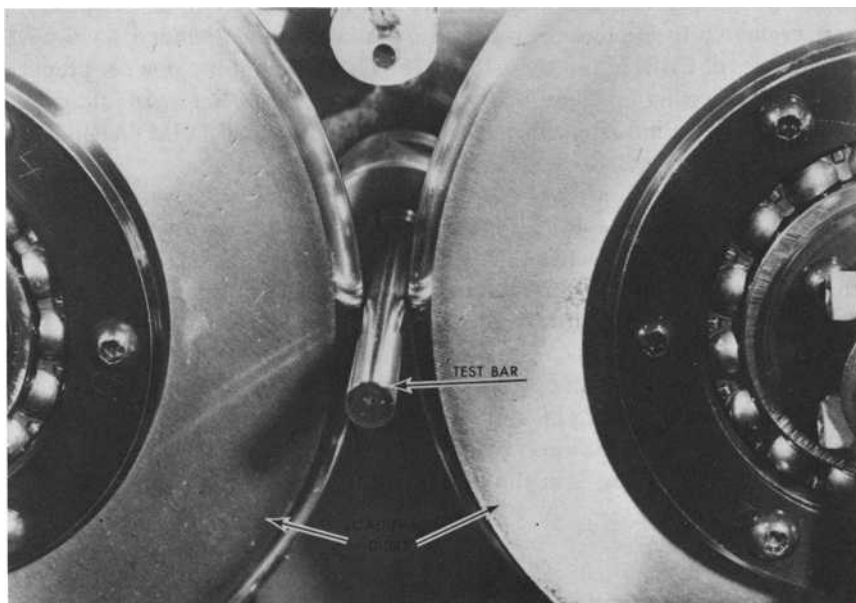
FIG. 2—*Close-up of the test section of the rolling contact fatigue tester.*

feed system. The lubricant flow is controlled to a constant rate by a needle valve assembly. The test lubricant may be heated before it enters the contact area. The lubricant supply drip tube is wrapped with resistance heating wire, and the temperature is measured and controlled at the exit of the drip tube. A simple "on–off" type of temperature controller is connected to the resistance coil to achieve control.

An accelerometer mounted on the load wheel yokes is used to sense a failure and subsequently to stop the drive system.

Test Materials

Rolling contact fatigue test rods were made of the following materials:

(*a*) AMS-6490 (AISI M-50 CEVM),
(*b*) AMS-6491 (AISI M-50 VIMVAR),
(*c*) AMS-5749 (BG-42 VIMVAR),
(*d*) CBS-1000M (Timken designation),
(*e*) CBS-600 (Timken designation),
(*f*) CRB-7 (formerly EX00007), and
(*g*) AISI T-15.

The processing was also considered a variable in that three of the steels were evaluated from powder-processed materials. These included AMS-6491, two batches of CRB-7, and the AISI T-15. The details of the powder preparation and processing for these materials are presented in Ref 5. In addition, a wrought vacuum induction melted–vacuum arc remelted (VIMVAR) CRB-7 material was also evaluated.

A typical chemical analysis of each of the test materials evaluated in this program is shown in Table 1. Typical heat-treatment procedures used on the test materials are shown in Table 2. Table 3 contains the hardness characteristics of each of the materials and processes evaluated. The surface roughness of the active surface of each of the test specimens was measured and is presented in Table 4, along with the ratio of elastohydrodynamic, (EHD) film thickness to the composite surface roughness of the contact zone. This ratio is considered to be an index of the severity of the contact. For this particular test series, the ratio for all of the test specimens is essentially the same, that is, operation is in the mixed film lubrication regimen.

Test Lubricants

The following three different lubricants were used in conjunction with the material evaluations of this program:

1. Hercolube A base-stock lubricant—This is a standard unformulated mixed acid (C_5 average) pentaerythritol ester base-stock lubricant manufactured by Hercules, Inc. It is a commonly used base-stock for formulating lubricants conforming to the MIL-L-23699 lubricant specification.

2. A qualified MIL-L-23699 lubricant—One qualified lubricant was selected based on a survey of the currently available lubricants in the U.S. Navy inventory (PVO, Incorp. STO-6530). This particular lubricant was determined to be in plentiful supply, and its formulation is representative of other MIL-L-23699 lubricants.

3. An XAS-2354-type lubricant—This is an advanced high-temperature–high-gear-load lubricant developed for aircraft propulsion and drive systems. The particular lubricant used in this program is the Shell Oil Co. Aero Shell Turbine Oil 555.

The physical properties of each of these lubricants are listed in Table 5.

Method of Test

The RCF tests conducted in this evaluation were performed under the following conditions:

(*a*) oil temperature—299.8 K (80°F);
(*b*) test rod temperature—ambient;

TABLE 1—Typical elemental analysis of advanced bearing alloys, percent by weight.

Element	AMS-6490, AMS-6491	AMS-5749	CBS-1000M	CBS-600	CRB-7	AISI T-15
Carbon	0.85	1.15	0.14	0.19	1.05	1.50
Manganese	0.25	0.50	0.50	0.55	0.30	...
Silicon	0.20	0.30	0.50	1.10	0.35	...
Phosphorus	0.015[a]	0.015[a]	0.025[a]	0.025[a]	0.015[a]	...
Sulfur	0.010[a]	0.015[a]	0.025[a]	0.025[a]	0.015[a]	...
Chromium	4.00	14.5	1.05	1.40	14.1	4.00
Molybdenum	4.25	4.00	5.00	1.00	2.05	...
Nickel	0.15[a]	...	3.00	...	0.075	...
Vanadium	1.00	1.20	0.325	...	1.05	5.00
Copper	0.10[a]	...	...	...	...	...
Tungsten	0.25[a]	...	...	...	...	12.00
Cobalt	...	...	...	...	...	5.00

[a]Maximum allowable.

TABLE 2—Typical heat-treatment process for advanced bearing steels.

Treatment	AMS-6490, AMS-6491	AMS-5749	CBS-1000M	CBS-600	CRB-7	CRB-7 PWD	AISI T-15 PWD	AMS-6491 PWD
Preoxidize								
Temperature, K (°F)			1228 (1750)					
Time, h			1					
Carburize								
Temperature, K (°F)			1228 (1750)	1228 (1750)				
Time, h			2 + 11	2 + 11				
Preheat								
Temperature, K (°F)	1117 (1550)	1117 (1550)	1117 (1550)	867 (1100)	1089 (1500)	1117 (1550)	1117 (1550)	1117 (1550)
Time, h			0.25	4				
Austenitize								
Temperature, K (°F)	1394 (2050)	1381 (2025)	1367 (2000)	1108 (1535)	1422 (2100)	1422 (2100)	(2250)	1394 (2050)
Time, h	0.05	0.50	0.10	0.50	0.12	0.12	0.12	0.12
Quench, temperature, K (°F)	811 (1000)	839 (1050)			811 (1000)	867 (1100)	867 (1100)	867 (1100)
Stress relief								
Temperature, K (°F)		422 (300)			422 (300)	422 (300)	422 (300)	422 (300)
Time, h		1			1	1	1	1
Deep freeze								
Temperature, K (°F)		200 (−100)			197 (−105)	189 (−120)	189 (−120)	189 (−120)
Time, h		0.25			0.5	2	2	2
Temper								
Temperature, K (°F)	811 (1000)		700 (800)			783 (950)	839 (1050)	811 (1000)
Time, h	2		2			3	3	3
Deep freeze								
Temperature, K (°F)	183 (−130)		189 (−120)			189 (−120)	189 (−120)	189 (−120)
Time, h	1.5		4			2	2	2
Temper								
Temperature, K (°F)	811 (1000)	797 (975)	811 (1000)	589 (600)	797 (975)	783 (950)	839 (1050)	811 (1000)
Time, h	2	2	2	2	2	3	3	3
Temper								
Temperature, K (°F)	811 (1000)	797 (975)	811 (1000)	589 (600)	797 (975)	783 (950)	839 (1050)	811 (1000)
Time, h	2	2	2	2	2	3	3	3
Temper								
Temperature, K (°F)			811 (1000)					
Time, h			2					

(c) test rod rotating speed—208 rps (12 500 rpm);

(d) applied load—1467.84 N (330 lb.);

(e) maximum hertz stress—4.826 GPa (700 ksi); and

(f) lubricant flow rate—20 drops/min.

A test track separation of 0.0032 m (0.125 in.) was maintained so that interaction effects between tracks could be avoided. This separation accounts for the contact width [approximately 0.00081 m (0.032 in.)] and any wear

TABLE 3—*Hardness values for the test materials.*

	AMS-6490	AMS-6491	AMS-5741	CRB-7	AISI T-15	CBS-600	CBS-1000M
Hardness, HRC	59.5	60	61.5	60	60	62(case) 34.5(core)	65(case) 42.5(core)

TABLE 4—*Surface roughness and EHD film parameters for the test materials.*[a]

Material	σ μm (μin.)	λ
AMS-6490	0.330 (13.0)	1.11
AMS-6491	0.114 (4.5)	1.84
AMS-5749	0.114 (4.5)	1.84
CBS-1000M	0.089 (3.5)	1.94
CBS-600	0.191 (7.5)	1.54
AISI T-15 PWD[b]	0.305 (12.0)	1.17
CRB-7	0.076 (3.0)	1.98
CRB-7 PWD1	0.165 (6.5)	1.64
CRB-7 PWD2	0.076 (3.0)	1.98
AMS-6491 PWD	0.152 (6.0)	1.69

[a]$\sigma_c = \sqrt{\sigma^2_{rod} + \sigma^2_{rollers}} \equiv$ composite surface roughness.

$\sigma_{rollers} = 0.203$ μm (8 μin.) arithmetic average.

h at 80°F; 12 500 = 0.429 μm (16.9 μin.) = EHD film thickness.

$\lambda \equiv h/\sigma_c$.

[b]PWD = powder processed.

TABLE 5—*Properties of the lubricants used in the materials evaluation.*

Property	Base Stock	MIL-L-23699	XAS-2354
Kinematic viscosity, cSt			
311 K (100°F)	21.40	26.50	28.0
372 K (210°F)	4.50	5.10	5.30
Flash point, K (°F)	517 (470)	531 (495)	533 (500)
Pour point, K (°F)	211 (−80)	211 (−80)	217 (−70)
Specific gravity,			
289 K (60°F)	0.998	0.997	0.994

which may occur. A track location on a test specimen was run until one of the following occurred:

(*a*) failure of the test rod by fatigue spalling, or
(*b*) failure of the load disks by fatigue spalling.

The number of stress cycles was recorded as a data point for each test. In order to ensure that each of the test materials was affected in essentially the same manner by the rig and that any extraneous variables affected each material in the same manner, each material was tested in a random order. In addition, a test was conducted on a baseline AMS-6490 rod after every two tests of the candidate materials. With this method it may be assumed that all extraneous time-dependent variables affected both the baseline and the candidate test rods in the same way: therefore, any comparisons performed would be a reflection only of the materials or processing variation being evaluated.

Data Analysis

The rolling contact fatigue data generated during this program were assumed to be distributed as a Weibull function. This type of probability distribution fits rolling contact fatigue data very closely [6]. A computer program utilizing the methods of Ref 7 and a least squares regression analysis was used to obtain the best fit of the data generated to a Weibull distribution. The most important parameters calculated by the program and used in the current analysis are L_m life = the mean life of the population, and $\hat{\beta}$ = the Weibull slope (the slope of the probability versus the life line) of the Weibull distribution. This parameter is indicative of the scatter in the data. The scatter decreases with increasing slope.

Each of the materials described in Table 1 was tested with each of the lubricants listed in Table 5. A minimum of six RCF tests were conducted with each lubricant-material combination. Each bar was therefore utilized for a minimum of 18 RCF tests (6 test/rod × 3 lubricants). A total of 191 RCF tests were performed on the materials being evaluated. In order to make valid comparisons with this group of data, the following method of data analysis was utilized. A control AMS-6490 rod had been run after every two failures of the test materials. In this manner a large group of data points were made available from the baseline steel from which a comparison of the RCF lives could be made. Once a major component of the rig (load rollers, motor, and so on) or a lubricant was changed, it was assumed that the RCF tests conducted on the baseline (AMS-6490) steel were a single group. (Experience with the RCF machine indicates that a major component change may cause a shift in population parameters.) A Weibull analysis was then performed on each group of baseline data. Each of these analyses corresponds to a set of

RCF tests on the candidate AMS-6490 replacement materials. Each data point of these candidate materials is divided by the mean life of the corresponding AMS-6490 group with which it was obtained. All of the data points for each material are then combined. A Weibull analysis is then performed on the resulting group of data points, the mean life of which is the mean life ratio compared to AMS-6490. This method of analysis allows the combination of all data by compensating for variations due to changes in major machine components.

Throughout this paper the mean life is used as a basis for any comparisons. It is considered to be a better index for comparison than the L_{10} life since it is less sensitive to variation and is generally representative of the life of the population. The L_{10} life, on the other hand, is generally representative of material flaws, subsurface damage, or low cycle fatigue (extreme values). In addition, the L_{10} is very sensitive to spurious failures which may originate from rig variations and are not representative of the failed population.

Discussion

The results of the Weibull analysis for the mean life ratio for each lubricant–material combination are listed in Table 6 and are presented in Fig. 3 for each of the three lubricants used in this evaluation. Each lubricant–material group is compared independently. For the test series with the base-stock lubricant, the best performing material is the powder-processed CRB-7; the powder-processed AMS-6491 is second and the AMS-5749 third. The analyses for the test series with the MIL-L-23699 lubricant indicate that the best-performing material is the powder-processed CRB-7; the AMS-5749 is second, and the CBS-1000M is third. The results of the test series with the XAS-2354 lubricant show that the best-performing material was again the powder-processed CRB-7, the AMS-5749 was second,

TABLE 6—*Mean life ratios of the advanced materials.*

Material	Base Stock		MIL-L-23699		XAS-2354	
	L_m^R	β	L_m^R	β	L_m^R	β
AMS-6490	1		1		1	
AMS-6491	2.65	0.86	1.27	4.97	1.68	3.02
AMS-5749	5.25	0.57	4.77	2.90	8.76	0.70
CBS-1000M	1.10	1.39	4.56	1.65	4.96	1.47
CBS-600	2.20	1.57	2.03	3.18	2.27	1.36
AISI T-15 PWD	4.56	1.13	1.49	3.10	1.42	2.82
CRB-7	1.75	1.97	1.46	1.54	2.99	0.89
CRB-7 PWD1	6.81	0.54	5.38	1.21	14.98	0.77
CRB-7 PWD2	3.17	1.15	1.95	1.74	1.85	1.66
AMS-6491 PWD	5.44	1.17	2.19	2.17	3.61	0.86
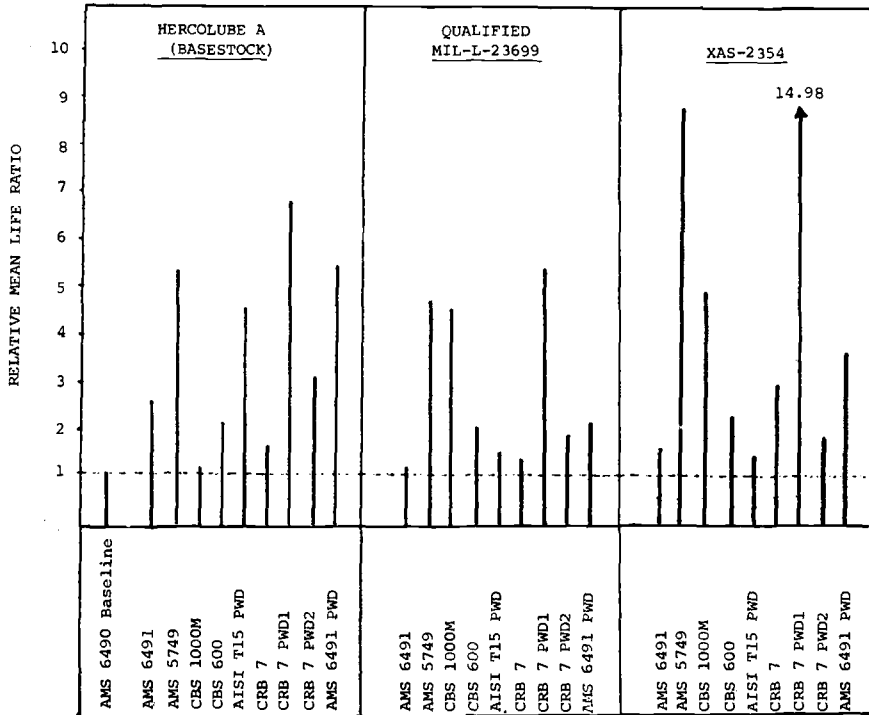
FIG. 3—*Relative mean life for the material-lubricant combinations.*

and the CBS-1000M was third. All of the materials tested have mean fatigue lives equivalent to or greater than the mean life of the AMS-6490 material. A comparison of the mean fatigue lives of each of the test materials to AMS-6491 is presented in Table 7 since AMS-6491 is currently being used

TABLE 7—*Mean life ratios of the advanced materials compared to AMS-6491.*

Material	Base Stock, L_m^R	MIL-L-23699, L_m^R	XAS-2354, L_m^R
AMS-6491	1	1	1
AMS-5749	1.98	3.76	5.21
CBS-1000M	0.42	3.59	2.95
CBS-600	0.83	1.60	1.35
AISI T-15 PWD[a]	1.72	1.17	0.85
CRB-7	0.66	1.15	1.78
CRB-7 PWD1	2.57	4.24	8.92
CRB-7 PWD2	1.20	1.54	1.10
AMS-6491 PWD	2.05	1.72	2.15

[a]PWD = powder processed material.

for all bearings previously using AMS-6490. This comparison may therefore be considered more appropriate in judging any improvements realized with advanced materials, since they are not as great with this baseline.

Figures 4, 5, and 6 are photomicrographs of the microstructures of all the test materials. Note that the microstructure of one of the powder-processed
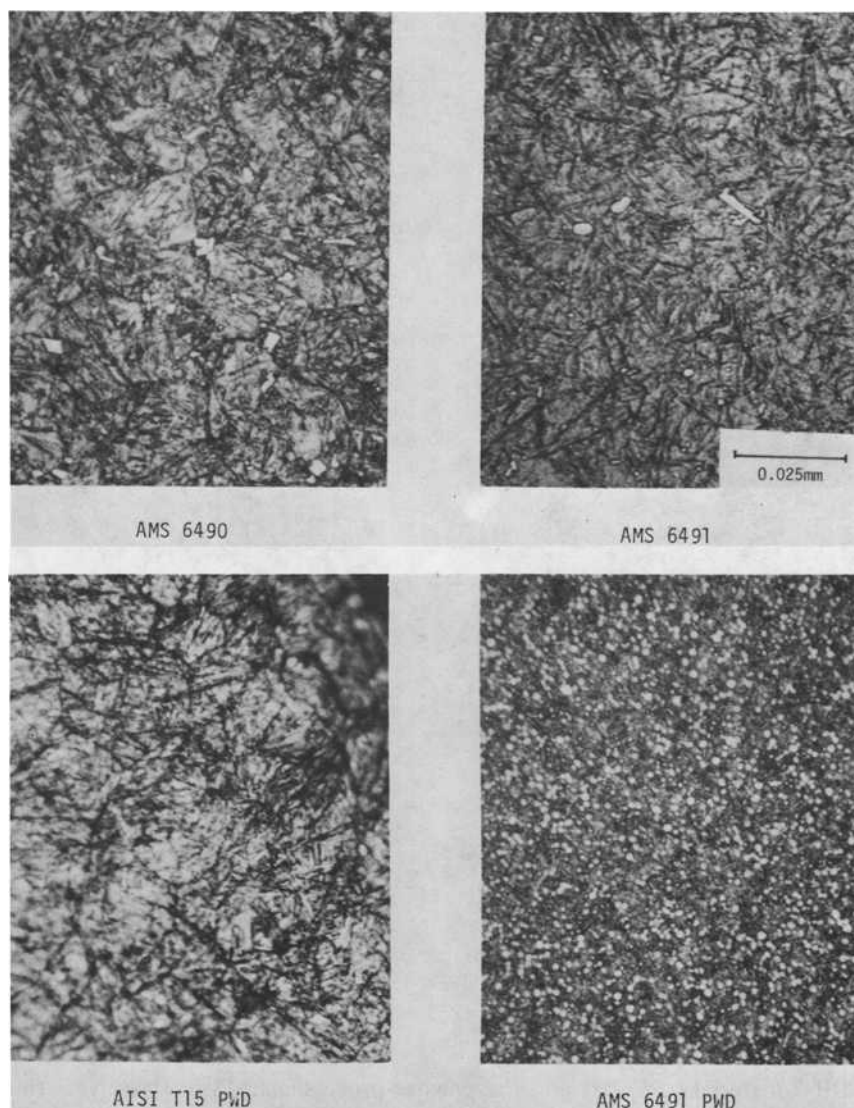
FIG. 4—*Typical microstructures of four bearing steels and processes: AMS-6490* (top left); *AMS-6491* (top right); *AISI T-15 PWD* (bottom left); *AMS-6491 PWD* (bottom right).
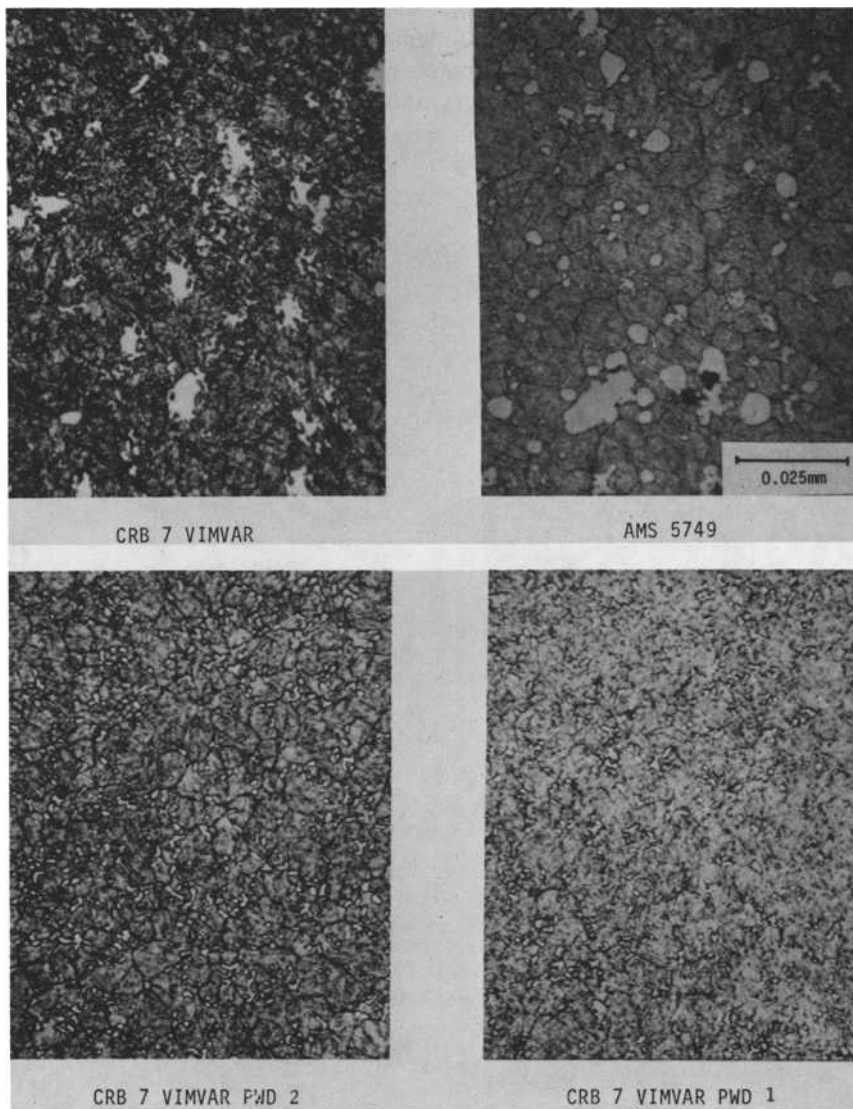
FIG. 5—*Typical microstructures of four corrosion-resistant bearing steels and processes: CRB-7 VIMVAR (top left); AMS-5749 (top right); CRB-7 VIMVAR PWD 2 (bottom left); CRB-7 VIMVAR PWD 1 (bottom right).*

CRB-7 materials (PWD1) and the powder-processed AMS-6491 are very fine and the grain boundaries are not clearly resolvable when etched, which indicates superior material cleanliness (Figs. 4 and 5). It is not surprising, therefore, that these two steels performed best in contact fatigue life. The
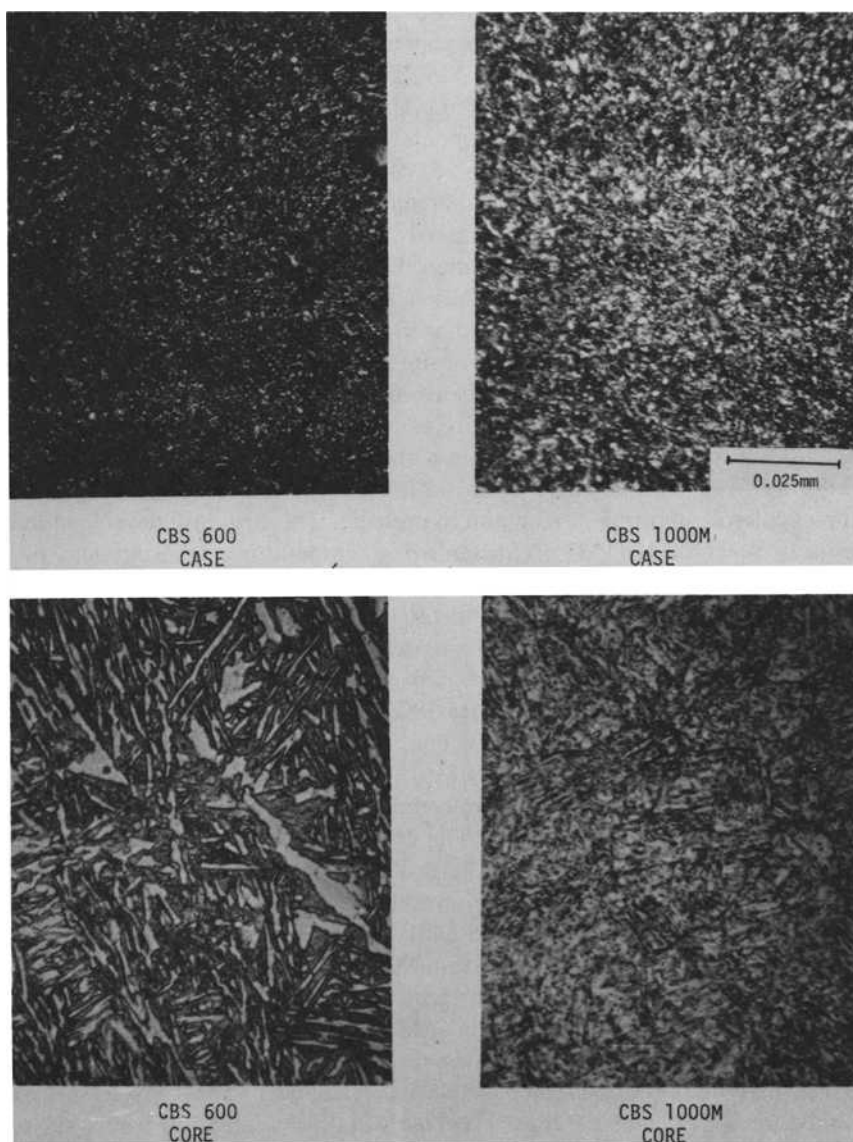
FIG. 6—*Typical microstructures of two carburized bearing steels: CBS-600 case (top left); CBS-1000M case (top right); CBS-600 core (bottom left); CBS-1000M core (bottom right).*

other batch of powder-processed CRB-7 material also contained a very fine grain structure, but the grain outlines etched through very easily. Both batches of the powder-processed CRB-7 material in Fig. 5 were etched for the same length of time (10 s) with a Vilellas reagent. The greater definition of the

grains of one batch of powder-processed CRB-7 compared to the other batch indicates that the bonding may be poorer and therefore detrimental to the fatigue life. The powder-processed AISI T-15 (Fig. 5) etched readily and did not exhibit this "adhesiveness" of the grains, and the RCF results do not indicate any significant life improvements compared to the AMS-6490. The microstructure of the AMS-5749 (Fig. 5) contained a significant quantity of retained austenite (approximately 20 percent) compared to less than 3 percent for the other through-hardened materials. The 20 percent retained austenite is not consistent with the heat treatment listed in Table 2 and suggests a procedural error. An investigation by Parker and Hodder [8] on the RCF performance of AMS-5749 has indicated that increasing levels of retained austenite may be detrimental to the RCF life of the material. It may therefore be possible to realize even greater improvements in the RCF life than those generated in this evaluation. The case structure of both the CBS-600 and CBS-1000M (Fig. 6) is a fine-tempered martensite with high carbon content and excellent uniformity (no carbide segregation). The core of the CBS-600 contains a duplex microstructure of ferrite and martensite. The structure developed as a result of the 1108 K (1535°F) austenitizing temperature. Investigations performed subsequent to the heat treatment of the test rods[4,5] indicate that austenitizing temperatures of 1158 to 1164 K (1625 to 1635°F) would achieve the desired core microstructures. A martensitic structure is considered to be the desirable core microstructure, based on experience with other materials. The core microstructure of the CBS-1000M is a martensitic structure with prior austenite grain boundaries. The effective case depth on the test specimens was 1.78 mm (0.070 in.) with a minimum hardness of HRC 58 at 0.64 mm (0.025 in.). The maximum orthogonal shear stress depth at the test conditions is 0.25 mm (0.010 in.). The core microstructures would therefore have no effect on the RCF life of the test specimens.

The data indicate that there are several materials available which perform better than AMS-6490 and AMS-6491. As previously stated, all of the materials perform better than AMS-6490 with all three lubricants, and a considerable number of them perform better than the AMS-6491. The powder-processed CRB-7 and the AMS-5749 perform better than the AMS-6490 and AMS-6491 regardless of the lubricant used. This performance may be a result of their similarity in analysis. The CBS-1000M exhibited the only detectable interaction with the formulated lubricants in that its performance was significantly better with the formulated lubricants. This material has exhibited a similar behavior in scuffing and scoring evaluations [9]. The only other possible lubricant effect is the degradation of performance of the PWD AISI T-15 material with the fully formulated lubricants.

[4]P. Fopiano, U.S. Army Materials and Mechanics Research Center, Watertown, Mass., personal communication, 1979.
[5]A. R. Swirno, American Lohmann Corp., Hillside, N.J., personal communication, 1979.

The other materials showed variations, but these were not considered to be statistically significant.

References

[1] Cunningham, J. S. and Morgan, M. A., *Lubrication Engineering*, Vol. 35, 8 Aug. 1979, pp. 435–441.

[2] Bamberger, E. N., Zaretsky, E. V., and Signer, H., "Endurance and Failure Characteristics of Mainshaft Jet Engine Bearing at 3×10^6 DN," ASME Paper 76-Lub-16, American Society of Mechanical Engineers.

[3] Brown, P. F., Dobek, L. J., Hsing, F. C., and Miner, J. R., "Mainshaft High-Speed Cylindrical Roller Bearings for Gas Turbine Engines," Pratt and Whitney Aircraft Interim Report FR011453, Pratt and Whitney Aircraft, Oct. 1978 for NAPC Contract N00140-76-C-0383 and AFAPL MIPR No. FY 14557600623.

[4] Valori, R., "Development of Rolling Contact Fatigue Machine for the Evaluation of Fatigue Characteristics as Related to Rolling Element Bearings," NAPTC-AED-1949, Naval Air Propulsion Test Center, June 1971.

[5] Brown, P. F. and Potts, J. R., "Evaluation of Powder Processed Turbine Engine Ball Bearings," Technical Report AFAPL-TR-77-26, U.S. Air Force, June 1977.

[6] Harris, T. A., *Rolling Bearing Analysis*, Wiley, New York, 1966.

[7] Johnson, L. G., *The Statistical Treatment of Fatigue Experiments*, Elsevier, Amsterdam, London, New York, 1964.

[8] Parker, R. J. and Hodder, R. S., "Rolling Element Fatigue Life of AMS-5749 Corrosion Resistant, High Temperature Bearing Steel," ASME Paper 77-Lub-30, American Society of Mechanical Engineers,

[9] Popgoshev, D., and Valori, R., "Scuffing Resistance of Advanced Gear Material/Lubricant Combinations," ASME, Paper 79-Lub-29, American Society of Mechanical Engineers.

O. Zwirlein[1] and H. Schlicht[1]

Rolling Contact Fatigue Mechanisms—Accelerated Testing Versus Field Performance

ABSTRACT: Cycling tests in the laboratory serve to assess the qualitative and quantitative influences of specific parameters on the service life of rolling bearings by systematically varying these parameters in the tests. The applicability of the test results to the field is a precondition for the optimization of material and design.

Material stress is analyzed and described by various alterations in the material caused by cyclic stressing. The conditions under which cyclic stressing generates structural alterations are demonstrated. This paper refers especially to the influence of different contact pressures and residual stresses on material stress and the failure mechanism at cyclic stressing.

KEY WORDS: rolling contact, materials fatigue, bearings, structural alterations, dark etching areas, white bands, residual stress, material stress, contact pressure, *S-N* curve, hardness, toughness, bearing steels

Cycling tests in the laboratory serve to determine the stress-carrying capacity of elements in rolling contact in order to select a bearing of the appropriate design and size for a specific application. The results from these investigations should be applicable in practice. Since generally very long running times are required to test a group of specimens, the test conditions were, and still are, intensified by increasing the contact pressure. In many cases, loads were selected which result in hertzian pressures (p_0) in the rolling elements of far above 3000 N/mm^2 [1-10].[2] The pressures reached in actual field conditions are clearly below these values. The current contact pressures

---

[1] Manager and vice president, material science, respectively, FAG Kugelfischer Georg Schäfer & Co., Georg-Schäfer-Strasse, Schweinfurt, West Germany.
[2] The italic numbers in brackets refer to the list of references appended to this paper.

at point contact are about $p_0 = 2000$ to 2500 N/mm^2 and in highly loaded ball bearings up to 2800 N/mm^2. At line contact, the current p_0 values are between 1400 and 1800 N/mm^2.

Contact pressures of $p_0 \gtrapprox 3000$ N/mm^2 (depending on the material and heat treatment) cause macroscopic plastic deformations. The deformations change the geometry of the contact zone, which leads to reductions of the contact pressure and modifications of the relative motions in the contact zone. Plastic deformations also effect considerable alterations in the material (material properties and residual stress condition); the material is stressed in a different way than material in an undeformed condition. Hence, the question arises whether test loads much greater than the actual loads supply results that are acceptable for actual field conditions.

In the following paragraphs the stress to which the material is subjected in rolling contact is described first. The stress hypothesis that best describes material stress is illustrated by means of various characteristics identifying material alterations due to cyclic stressing. Second, the dependence of the material alterations on the load and the running time are described, and resulting correlations are indicated. From the findings are deduced the properties that the material should have to ensure optimum performance of the rolling bearing.

Stressing of the Material in Rolling Contact

Structural Alterations of the Material due to Cyclic Stressing

With rolling elements cycling on one another, the force is transmitted through the surfaces, which are more or less separated by the lubricant. In a very complex way the material stress of the individual elements is dependent on the size and shape of the element, the curvature ratio, the contact pressure (normal forces), the elastohydrodynamic (EHD) conditions (and thus the tangential forces transmitted in the surface due to friction), the tribomechanical properties of the lubricant, the operating temperature, and other factors.

The formation of pitting in the classic way (with fatigue starting below the surface, the development of microcracks, crack growth, and spalling of material particles) is known to occur only rarely in the field. For the sake of clarity, however, it appears reasonable to start with the description of material stress under ideal cycling conditions.

What stress is the material subjected to from externally applied stress? There are very many signs which allow conclusions to be drawn about external stresses. The material becomes fatigued only if the stress provokes slip motions in the lattice, that is, if plastic deformations occur. This is possible

only with loads above a certain threshold [11–13]. A well-known sign of the irreversible structural changes due to cyclic stressing are the dark etching areas (DEAs); in these areas, which appear dark after etching, slip motions in the lattice have occurred [8–11,14–21]. Figure 1 shows a DEA in an axial and a parallel section of a ring. It can be seen that, with the exception of two locations marked by arrows, the dark zone extends to the surface. Presumably the two marked areas were subjected to a lower stress level than the neighboring areas. The cause of the difference in material stress can be seen in Fig. 2. As the ball cycles in the groove, pure rolling takes place only at two points. In the center of the contact face, backward sliding occurs, and forward sliding occurs at the ends. The additional stress due to this forced sliding leads to the formation of the DEA [22].

When a different etching method is used, light zones appear instead of the dark areas. The parallel section (Fig. 3) shows that these zones are white layers or white bands (WBs) which extend at a certain angle to the tangent of the raceway. The left part of Fig. 3 shows WBs which form an angle of 30 to 35 deg with the tangent, in the right part the WBs extend across one another. The dominant, steep WBs form an angle with the surface of about 75 to 80 deg. The steep and the flat WBs also differ in their positions: the WBs are not congruent, but the steep bands are located closer to the surface in the area of the greatest density of the flat bands.

The reason for the different formation of the white bands is the running time. The ring whose structural changes are shown in the left part of Fig. 3 was cycled for 2000 h, and that on the right for 2500 h (in both cases $p_0 = 3000$ N/mm^2).

The decisive parameters for the formation of DEAs [8,11,14,17,20,21] and WBs [8,20–25] are the contact pressure and the cycling time. The structural changes become more marked with increasing running time and contact pressure. The hardness pattern is also indicative of this development (Fig. 4). The hardness values measured below the raceways of rings with different running times show that as the number of load cycles increases the hardness drops in the areas of structural changes. In a ring which was cycled for 3000 h at a contact pressure of $p_0 = 3000$ N/mm^2, the decrease in hardness is approximately 140 VHN 0.1 kg test load. The diagram in Fig. 4 further shows that the hardness minima are displaced toward the surface as running time increases.

The structure's changed reaction to etching, the decrease in hardness, and the drop of the half-value breadth assessed by X-ray (Fig. 5) are indicative of the more or less pronounced decay of the martensite. According to the investigations described in the literature [20,21,24,26], the white bands found consist of ferrite particles which are surrounded by carbon-rich, carbidelike zones and residual martensite.
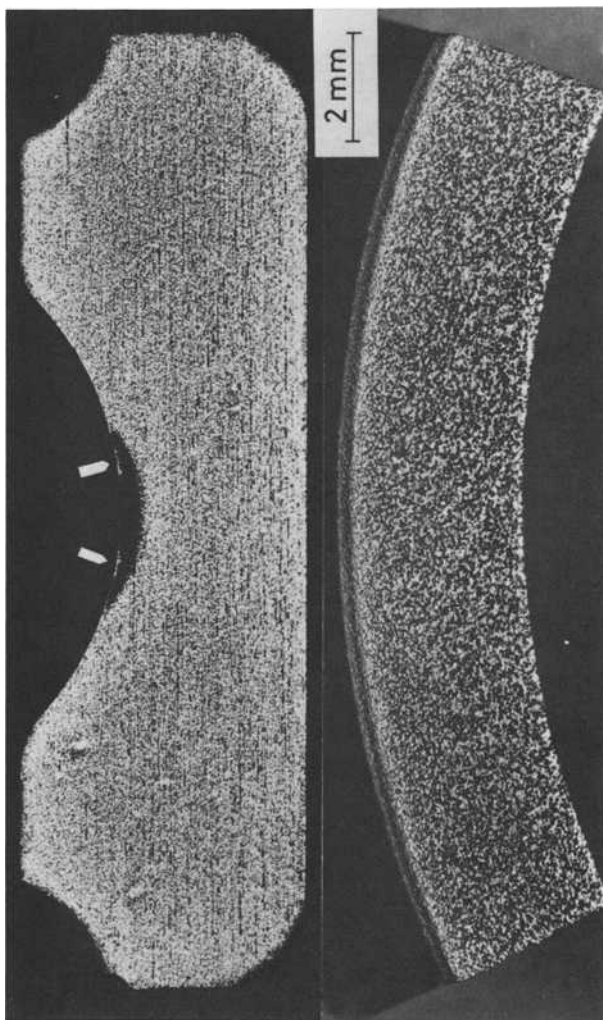
FIG. 1—*Dark etching area in axial and parallel sections of a deep-groove ball bearing inner ring.*
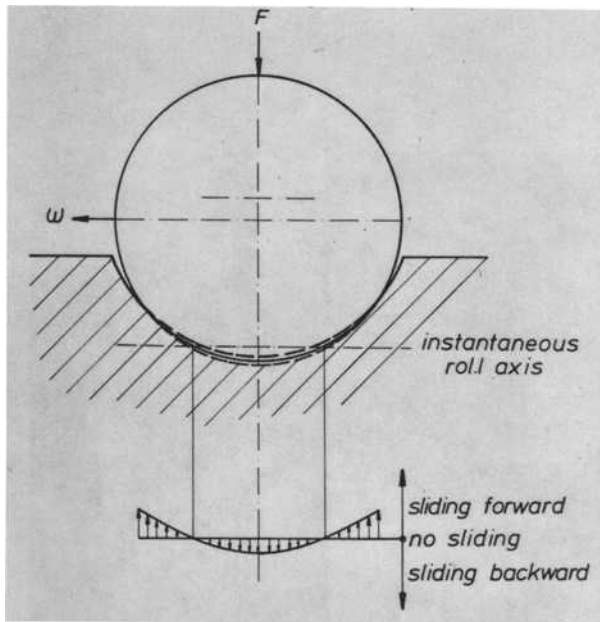
FIG. 2—*Sliding motions, provoked by the curvature of the area under pressure.*

Interpretation of the Development of White Bands

According to the literature [8,20,21,24], the decay of the martensite is assumed to be caused by high alternating shear stresses because the zone of WB formation and the zone of the maximum alternating shear stresses coincide. The following arguments, however, are against this hypothesis:

1. In any multiaxial state of stress in polycrystalline materials, the distortion energy hypothesis describes best the material stress under which plastic deformation starts. This also applies to stress of rolling bearings [27]. Fatigue does not occur, however, without slip motions in the material.

2. Residual stresses can influence the permissible magnitude of the external load [27–29]. Residual stresses superimposed on external load stresses do not change the alternating shear stresses.

3. Structural alterations which are frequently found in bodies in rolling contact and are a sign of material fatigue never extend parallel or perpendicular to the surface but at angles of 40 to 45 deg (butterflies) and approximately 20 to 40 deg or 70 to 80 deg (white bands).

It should be possible from the position, the density, and the direction of the white bands to draw conclusions about the stress condition that was effective at the time of the formation of the WBs. A comparison of the various
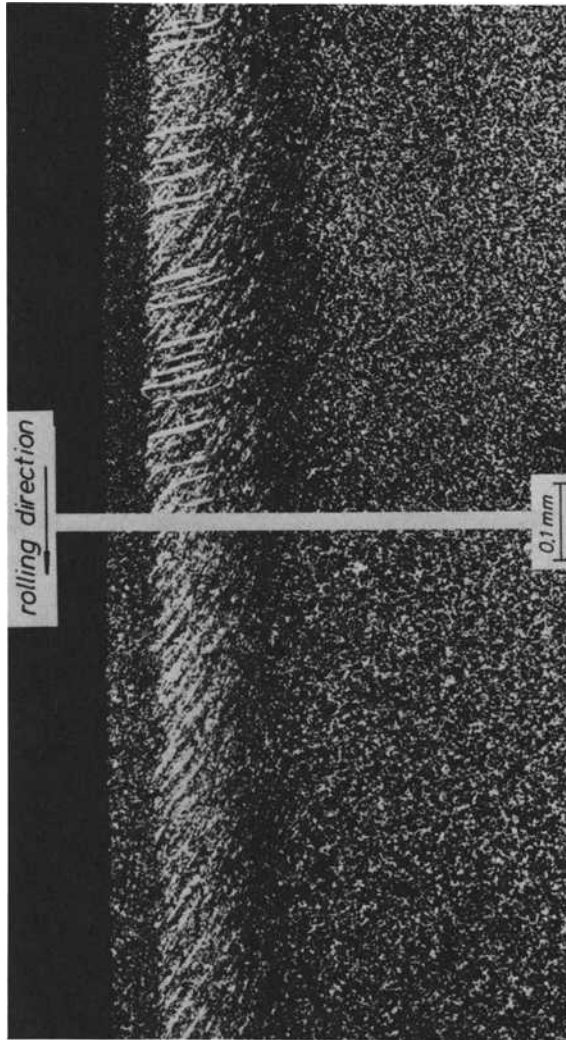
FIG. 3—White bands in cycled deep-groove ball bearing inner rings (parallel sections in the groove bottom); (left) flat white bands; (right) flat and steep white bands.
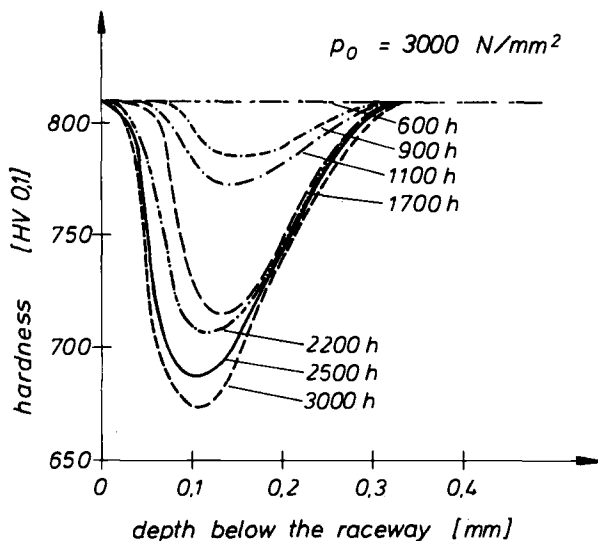
FIG. 4—*Hardness patterns in deep-groove ball bearing inner rings which were cycled for different periods of time.*

stress hypotheses shows that the distortion energy hypothesis can best describe material stress with reference to the formation of DEAs inclusive of the minimum load at which slip motions in the material can occur. The position and direction of the WBs cannot be explained by use of the various hypotheses. Taking into account one of the most important changes caused by cyclic stressing, namely, residual stress (see Fig. 5), the phenomenon of the WBs can be explained. At a sufficiently high load, cyclic stress generates compressive residual stresses which must be considered for the description of material stress. It is not sufficient to superimpose residual stresses on the load stresses in the area of maximum stressing without residual stresses. This is exemplified in Fig. 6. For the depth $z = 0.5 \cdot b$ ($b = \frac{1}{2}$ the width of the pressure area), the ratio of the equivalent stress to the contact pressure (σ_v/p_0) is plotted versus x/b (σ_v calculated from the distortion energy hypotheses). For the case of line contact described here, constant residual stress values were superimposed on the cycling stress in the x (circumferential) and y (axial) directions. It is known that in the load case, $K = 0$ (no residual stresses), the maximum material stress is located in the middle of the pressure area, hence at $x/b = 0$. At a superimposed residual stress of $K = -0.06$, σ_v/p_0 has clearly dropped; the material stress, however, is constant up to $x/b \approx 0.5$. At higher compressive residual stresses, the equivalent stress keeps decreasing in the middle of the pressure area ($x = 0$); at the margin of the pressure area a new maximum builds up. Figure 6 shows
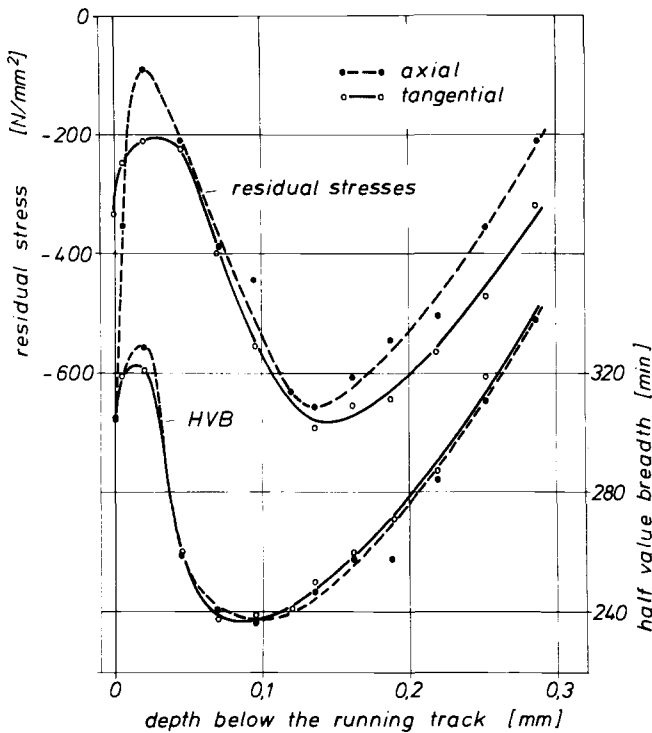
FIG. 5—*Residual stresses and half-value breadths in the cycled deep-groove ball bearing inner ring whose structural changes are shown in Figs. 1 and 3 (right).*

that with increasing compressive residual stresses, material stress does not constantly decrease but may again increase.

The pertinent variations are obtained for different depths, including the surface. By plotting the maximum stresses effective at varying depths, stress patterns result, as shown in Fig. 7. Different residual stresses are superimposed on the load stresses. A tensile residual stress increases the level of stress, and the location of the maximum stress is practically maintained. At a compressive residual stress of $K = -0.1$, the location of the maximum stress is more or less maintained, too; the stress, however, is lower than is the case without residual stresses. With $K = -0.2$, σ_v/p_0 drops only at greater depths; for $0.04 < z/b < 0.44$, the stress increases, as compared with $K = -0.1$. The maximum stress displaces closer to the surface. This becomes more pronounced with still higher residual stresses. With $K = -0.3$, σ_v/p_0 increases noticeably, as compared with $K = -0.2$, and the maximum of σ_v/p_0 is even closer to the surface.

The example described was based on residual stresses of identical mag-
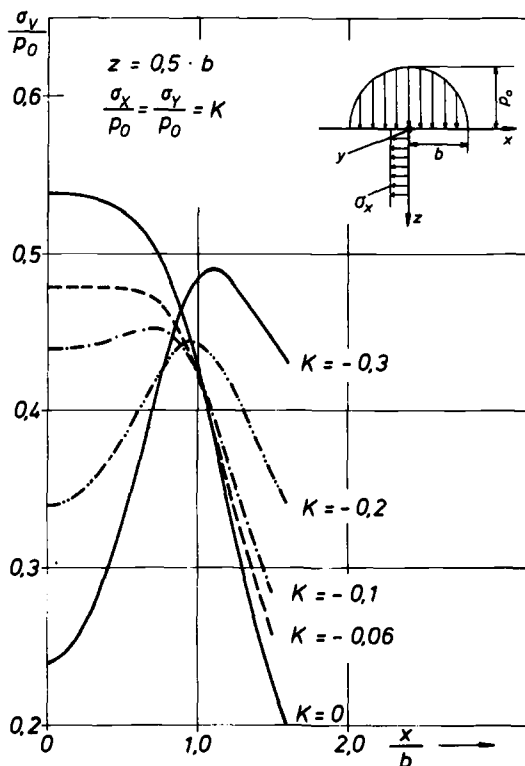
FIG. 6—*Equivalent stress, σ_v/p_0 versus x/b for the depth z/b = 0.5. Parameter: residual stresses superimposed in x and y directions.*

nitude in x and y directions and independent of the depth, z. In reality, changes in the residual stresses are restricted to the areas where plastic deformation of the structure due to cyclic stressing has occurred. The effects of the residual stresses, which differ depending on the location and direction, are shown in Fig. 8 for the case described in Fig. 5. Figure 8 is divided into three parts: in the middle is the structure; below are the residual stresses assessed by X-ray; and above is the calculated stress with and without residual stresses. The comparison shows that the compressive residual stress pattern practically corresponds to the pattern of σ_v without residual stresses. Also the coincidence of the position of the maxima of compressive residual stresses and σ_v without residual stresses is fairly good. The comparison between the location of the flat and steep WBs with the pattern of σ_v superimposed with residual stresses demonstrates a very good correspondence: the maximum stress occurs at a depth of approximately 0.1 mm in the area of greatest structural changes. At this depth the lowest values for half-value breadths (see Fig. 5) and hardness (see Fig. 4) are found.
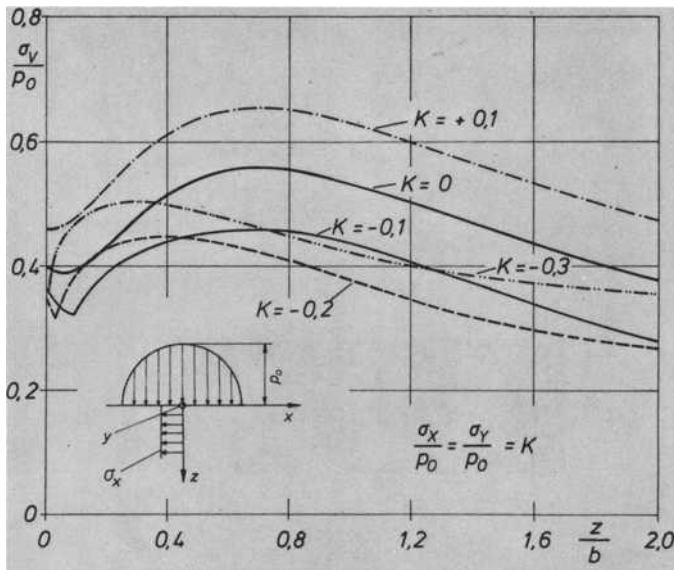
FIG. 7—*Equivalent stress σ_y/p_0 versus the depth for various residual stresses superimposed on rolling contact stress.*

In addition to the alteration of the magnitude and position of the stress, residual stresses effect a change of direction of the maximum stress in the multiaxial state of stress. It can be demonstrated [22] that the flat WBs (see Fig. 9) are perpendicular to the greatest normal stress; in other words, the flat WBs grow perpendicular to the direction of the greatest "relative tensile stress"[3] (like a crack perpendicular to the direction of tension). This means that the decay of the martensite is oriented. The direction of the steep WBs coincides with the direction of the maximum shear stress. Hence, it can be concluded that steep WBs are generated by the action of the maximum shear stress as a consequence of the breakdown of the structure built by the flat WBs.

It can be observed through microscopy that, after nucleation, the steep WBs (Fig. 3) grow primarily in the direction of the maximum shear stresses (75 to 80 deg to the surface). This oriented growth is assumed to result from the interfacing areas, which are clearly less supported in this direction than before the breakdown of the bands (effect of the residual stresses of Type II).

---

[3]By subtracting the mean stress [$\sigma_m = (\sigma_1 + \sigma_2 + \sigma_3)/3$, the first invariant of the tensor of stress] from the greatest normal stress (σ_1 = greatest principal stress), a positive stress in the direction of σ_1 results, designated as the "relative tensile stress." The "relative compressive stress," $\sigma_3 - \sigma_m$, acts to offset about an angle of 90 deg [22].
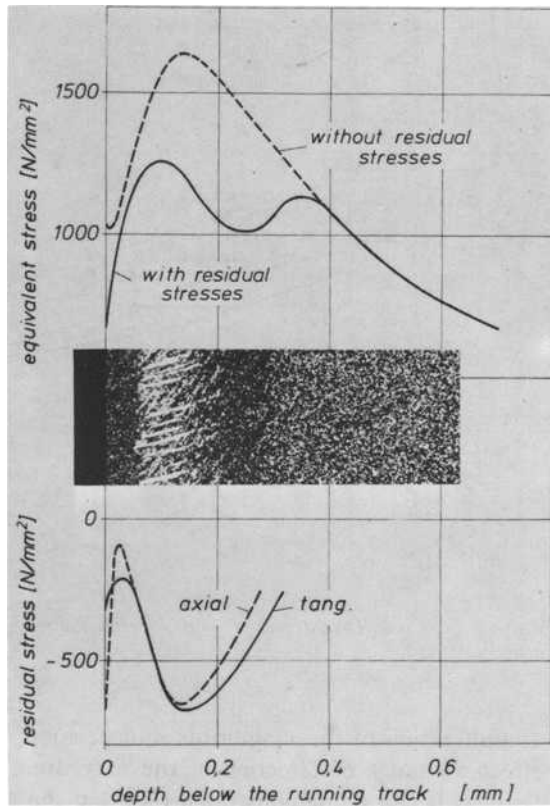
FIG. 8—*Comparison of material stress with and without the effect of residual stresses, the measured residual stresses, and the structural alterations.*
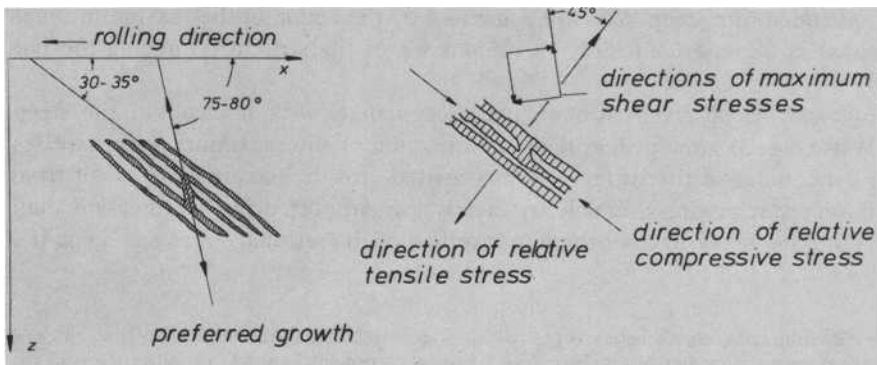
FIG. 9—*Directions of white bands and effective stresses (diagrammatic).*

This is also demonstrated by the fast growth of WBs into areas that are less weakened or not weakened at all (Fig. 10).

The residual stresses of Types I and II generated with the WBs and the structural changes are favorable conditions for the formation of pittings. If microcracks have occurred, the hertz's calculation does not apply any more, even for the present load case. At the margin of the pressure area, tensile stresses may act perpendicular to the raceway, thus leading to flaking of the material.

The mechanism of fatigue described here shows that the distortion energy hypothesis is best suited for determining the material stress of bodies in rolling contact. Of course, all influences (friction, residual stresses, and others) must be considered.

Influence of the Contact Pressure and the Number of Load Cycles on the Generation of DEAs and WBs

As already indicated, the formation of DEAs and WBs depends on the magnitude of the contact pressure and the running time. This relationship is shown in the diagram of Fig. 11 for SAE 52100 steel (standard heat treated). The curves are based on our own investigations and those of others [14,17,20]. Figure 11 shows that below a specific limiting load, structural changes, as determined by any known method, do not occur. The origins of WBs that depend on p_0 and number of load cycles scatter only slightly. The curves for the flat and the steep WBs converge with the increasing number of load cycles. The load limit for the development of WBs is at $p_0 \approx 2500$ N/mm^2.

Figure 12 shows the WBs originating in this limiting area. The photomicrograph was taken from the parallel section of a ring which was subjected to over 3×10^{10} load cycles at $p_0 = 2550$ N/mm^2. At a depth of 0.15 mm below the raceway is an inclusion (Fig. 12, right). Originating from this material flaw, the WBs grow at an angle of approximately 30 deg to the raceway just as with higher loads. Another photomicrograph taken at another location on the same ring, shows the WBs on the left side of Fig. 12. A special material flaw cannot be detected but is assumed to exist. The photomicrograph also shows that after extremely high numbers of load cycles and the slow procedure of growth of the WBs, steep WBs have formed although the flat WBs have not yet fully developed.

X-ray microstructure investigations proved that, as expected, in the area of maximum stress below the raceway of this ring compressive residual stresses had occurred due to cyclic stress. The stresses, however, are only low. It can be assumed that in the area of the flaw the stress was somewhat higher because the angle between the flat WBs and the surface is 30 deg, as under the influence of higher contact pressures. Rings which were cycled under the same
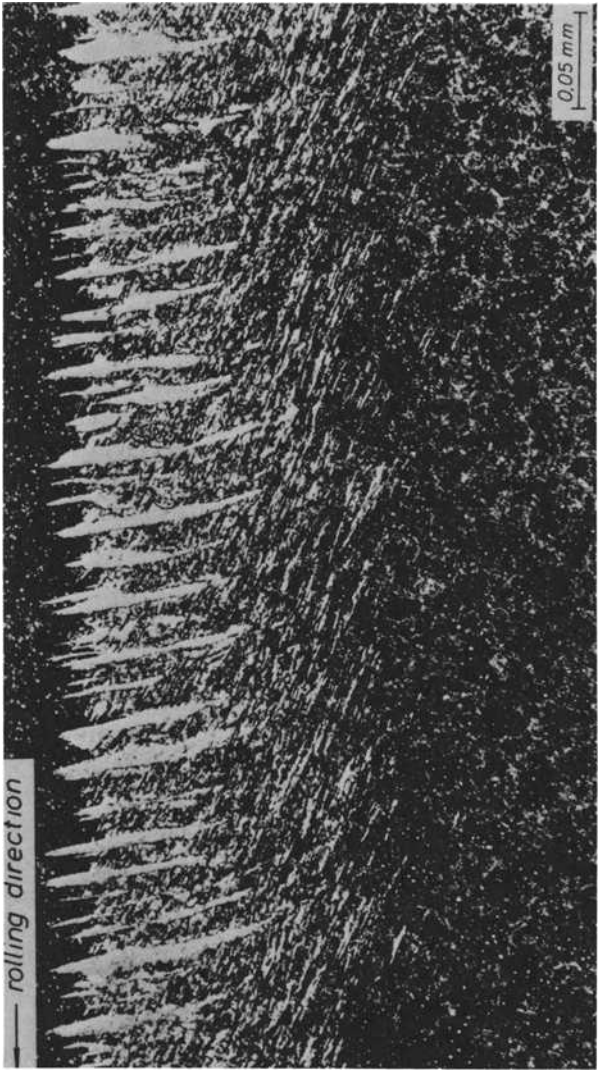
FIG. 10—Flat and steep white bands in a cycled angular contact bearing inner ring.
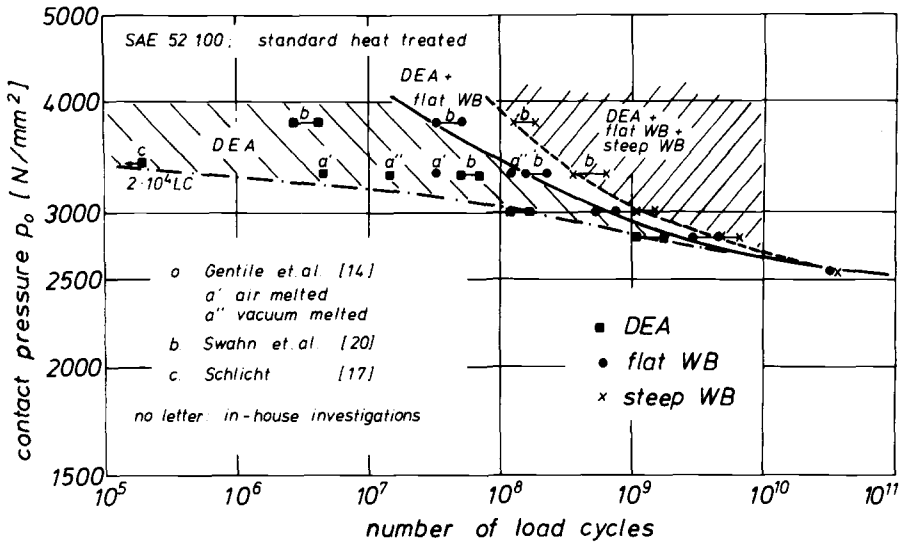
FIG. 11—*Correlation between the contact pressure, the number of load cycles, and the development of structural changes.*

load but for shorter periods did not expose structural changes, nor could alterations of the residual stress and the half-value breadth be measured.

The dependence of DEAs on the p_0 and the number of load cycles is not so obvious as that of WBs (Fig. 11). This is presumably primarily due to the preparation technique. The same material, same material properties, and same state of fatigue (p_0 and number of load cycles) should lead to the same degree of blackening of the DEAs. Whereas WBs can be made visible by any method of etching (nitric acid, picric acid, or others), different etching methods for detecting DEAs yield different results. The presence of DEA, however, is a sign of a high level of material stress. No DEAs were exposed on the inner ring, which was subjected to 3.3×10^{10} load cycles at a pressure of $p_0 = 2550$ N/mm² (see the WBs in Fig. 12), even after several etching procedures.

In addition to the level of stress and the number of load cycles, the formation of DEAs and WBs depends on the material used (composition, degree of cleanliness) and its treatment. With identical material and heat treatment, structural changes occur after fewer load cycles when there are many inclusions than when the material is very clean.

Because structural changes can be well correlated with p_0 and the number of load cycles and p_0 can be assessed from the position of the compressive residual stresses (see Refs 22 and 30, and Fig. 8), it is possible to draw conclusions on the level of stress and the number of load cycles of a used bearing (for example, at an inspection of damage).
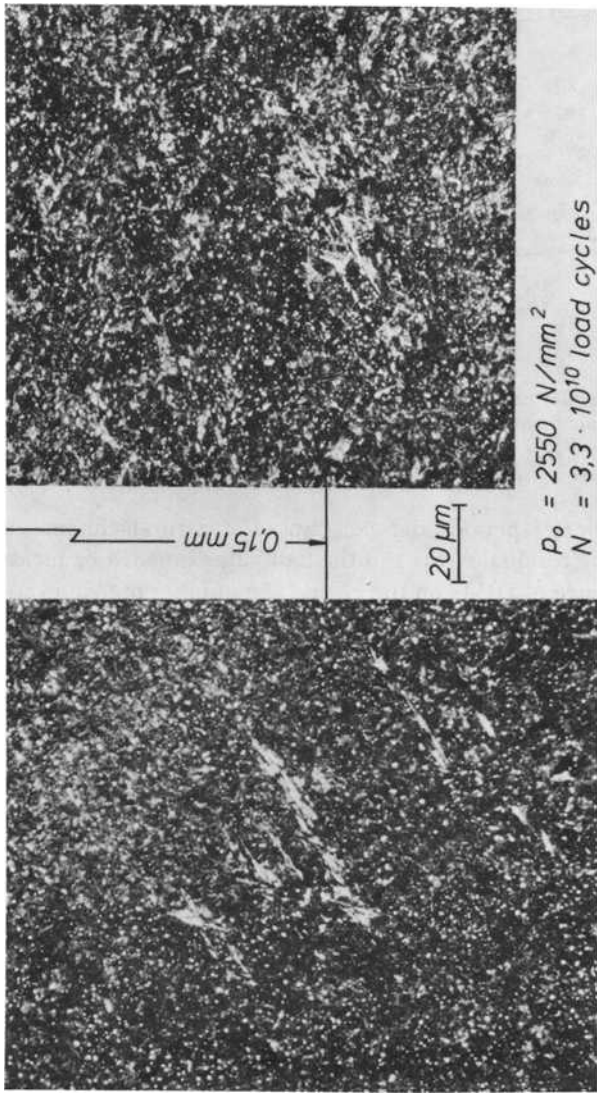
FIG. 12—*Development of the white bands in the range of "true endurance strength."*

Dependence of Rolling Contact Fatigue on Contact Pressure

The plastic deformation of the structure is a precondition of material fatigue. This means, according to the laws of materials mechanics, that at loads provoking material stress below the cyclic yield strength, fatigue of the material cannot occur (with hardened steels the static yield strength corresponds approximately to the cyclic yield strength). Hence, an endurance strength exists in the case of cyclic stressing as with other types of stress. At loads above this threshold value, material fatigue is principally unavoidable; the process of fatigue depends primarily on the deformation behavior of the material and also on the limiting value of deformability in the microstructure—that is, quite simply, on the material's toughness.

Yield strength, hardness, and toughness are properties determined by the material (its composition, degree of cleanliness, and so on) and its treatment. Consequently, it must be possible to draw conclusions about rolling contact fatigue strength from the properties which were determined by static tests. The mechanical properties of SAE 52100 steel after various heat treatments are well known [31]. With a supportable stress at rolling contact calculated from the yield strength determined in the tension test—for instance, for standard heat-treated SAE 52100 steel—material subjected to a contact pressure of $p_0 \leq 2300$ N/mm^2 in the cycling test should not be expected to fail from fatigue. Figure 13 shows that this assumption is correct. Investigations at contact pressures of $p_0 = 2550$ N/mm^2 resulted in a B_{10} life of 3.23×10^{10} load cycles.[4] This number of load cycles corresponds to a running time of
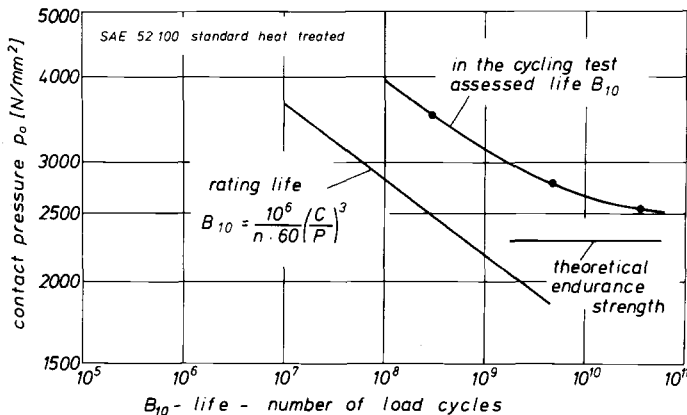
FIG. 13—*Influence of contact pressure on the fatigue life* B_{10} *(S-N curve) (angular contact ball bearing 7205 B; n = 12 000 min^{-1}).*

[4]Test bearings: angular contact ball bearings 7205 B; test conditions: $n = 12\ 000$ min^{-1}; $h_0/R_a = 3 \ldots 4$ [32].

almost 1 year. Contact pressures of $p_0 < 2550$ N/mm² do not lead to the formation of pitting within a foreseeable period. This corresponds to "true endurance strength", which can be defined as a load parameter at which fatigue processes start in the material but are stopped by a change in stress due to residual stresses. The true endurance strength presumably is not much above the theoretical endurance strength.

The results obtained from numerous previous cycling tests with very high contact pressures lead to the exponent 3 in the life formula. Converted to contact pressure, this is $B_1/B_2 = (p_{02}/p_{01})^9$. For contact pressures of $p_0 > 3500$ N/mm² this assumption is nearly correct, with some reservations, such as the plastic deformation and consequently the curvature ratio change and load reduction. At low loads the life curve deviates from the calculated life (Fig. 13). Since the life calculation for the dimensions of a rolling bearing is based on the standardized life formula, the rolling bearings have a very high safety factor against classic fatigue within the load range to which they are commonly applied. It can even be stated that for line contact of cylindrical roller bearings and tapered roller bearings, which usually operate at a contact pressure of $p_0 < 2000$ N/mm², classic fatigue of the through-hardened components of a rolling bearing steel corresponding to the manufacturers' specifications is not possible. In these cases, failures are due to additional stresses such as micro sliding motions and skidding, breakdown of the lubricating film (due to increased temperatures, for instance), and contamination of the lubricant [32]; hence, the crack always originates on the surface.

The comparison of Figs. 11 and 13 shows a surprisingly good correspondence of the life curve with the appearance of steep white bands. The two diagrams were purposely not drawn as one. It can be deduced, however, that under ideal conditions rolling contact fatigue strength depends on material decay, as shown by the structural changes visible as white bands. The weakening of the material has proceeded to such an extent, and the level of stress has increased so greatly (including the residual stresses of Types I and II) that even without the presence of a greater material flaw a crack can develop and propagate below the surface and lead to pitting.

The Influence of Heat Treatment on the S–N Curve

In Fig. 13 the hertzian pressure, p_0, is plotted as a function of the number of load cycles (B_{10}). The curve applies to rings which were made from one heat of SAE 52100 steel and heat treated together. All influences from machining (grinding and so on) were kept constant for all rings. Investigations showed that under ideal cycling conditions at a contact pressure of $p_0 = 2800$ N/mm², rings of SAE 52100 steel of the same heat but with different heat treatment within a hardness range of 58 to 64 HRC have the same life.

As can be seen from Fig. 14, differences in life depending on the heat-treatment methods cannot be found, particularly when considering the confidence ranges (20 specimens per variant) of the Weibull failure distributions. This contradicts the values indicated in the special literature [1-4], where the life is generally said to increase with increasing hardness. The divergence between these statements is based on the different magnitudes of contact pressure. It is obvious that at high contact pressures the correlation $B_{10} \sim$ hardness is correct, because during each load cycle the material is subject to heavy plastic deformations, and the resistance to plastic deformation increases with the hardness (principle of the hardness measurement). Material fatigue is not determined by the limits of deformability of the microstructure so much as by the load cycles; this fatigue is in proportion to the plastic deformation per load cycle and thus in inverse proportion to the hardness. This relationship is valid as long as a certain minimum deformability exists in the material (no coarse material flaws). Under such test con-

FIG. 14—*Running times of angular contact ball bearings of different heat treatments.*
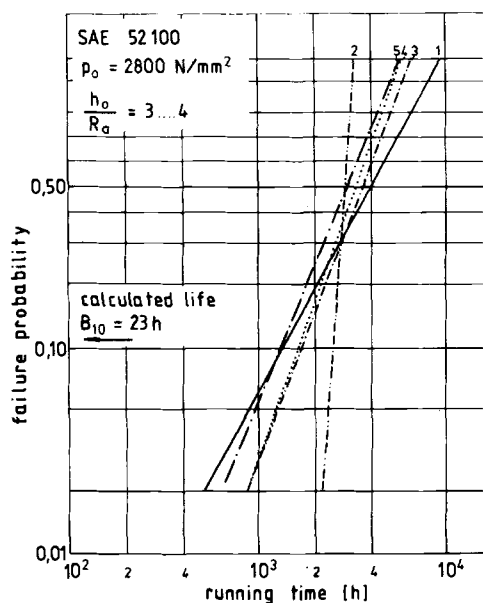
variant:	tempering temp. (°C):	hardness (HRC)		
		before cycling:	after cycling:	
1	. . .	65	62	
2	150	64	62	austenitizing
3	200	61	61	temp.: 840°C
4	240	60	60	
5	270	58	58	

ditions, varying material properties, at identical composition and hardness, also lead to different results. At identical hardness, for instance, a higher toughness reached by ausforming or the use of a cleaner steel prolongs the life. An optimum heat treatment, however, cannot be determined because at the lower contact pressures prevailing in the field, other failure mechanisms apply. This is indicated in the diagram of Fig. 15. While, at high contact pressures, life depends on hardness, this dependence does not exist for hardness values greater than 58 HRC within the loading range usual in the field ($p_0 < 3000$ N/mm^2). The optimum hardness of SAE 52100 steel can be assumed to be below 60 HRC in the range of the endurance strength.

As already described, the failure at contact pressures between the endurance strength and $p_0 \approx 3000$ N/mm^2 is essentially due to the martensite decay. This long-term process is predominantly influenced by the cyclic yield strength. Tests showed that between 10^9 and 10^{10} load cycles the formation of WBs is identical at different states of heat treatment (58 to 64 HRC). Also, the same hardness decrease was measured in the structure zones with martensite decay. This means that the cyclic yield strength of SAE 52100 steel is about the same at these high numbers of load cycles for hardness values from 58 to 64 HRC.

Failure at Cyclic Stressing under Imperfect Conditions

The preceding paragraphs referred to material fatigue at EHD contact. Less perfect conditions prevail in the field: metal-to-metal contact due to poor lubrication and cycled contaminants in the lubricant cause indentations in the raceway which disturb the formation of a lubricating film and weaken the material. Furthermore, it must be taken into account that the material is not perfect, either. Not only nonmetallic inclusions and other inhomogeneities but also the fiber orientation and the state of the material in the surface layer must be considered. Any additional stress and reduction of
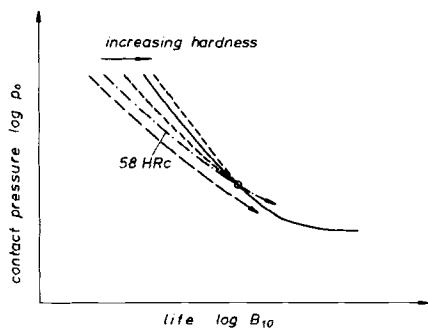
FIG. 15—*Influence of the hardness on the S-N curve (diagrammatic).*

strength lead to a displacement of the S–N curve (see Figs. 13 and 15) toward shorter running times and lower contact pressures.

A basic statement can be made concerning material stress during rolling contact: in addition to a satisfactory hardness, the material should have a high cyclic yield strength and the highest possible toughness. In such a case the effect of a disturbance, caused, for instance, by inclusions (nonmetallic inclusions as well as carbides) or a foreign particle indentation, is minimized by local plastification.

This statement was confirmed by laboratory tests and in the field. Investigations with rings of different degrees of austenitizing at $p_0 = 2550$ N/mm^2 under imperfect conditions (mixed friction plus foreign particle indentations) showed that the maxima of life and hardness occur at different austenitizing temperatures (Fig. 16). This is further confirmed by field experience. The performance of rolling bearings with a hardness between 58 and 60 HRC is as good or even better than that of bearings with a higher hardness. The findings from cycling tests at contact pressures of $p_0 > 3500$ N/mm^2, according to which the performance of SAE 52100 steel is better with martensitic structure (hardness $\sim$ 62 HRC) than with bainite (hardness $\sim$ 59 HRC), are contradicted by the results obtained from the field. Rolling bearings with bainitic-hardened rings as a rule prove to be more successful in the field than those with martensitic-hardened rings. This is essentially due to the higher toughness of the bainitic structure of the material.
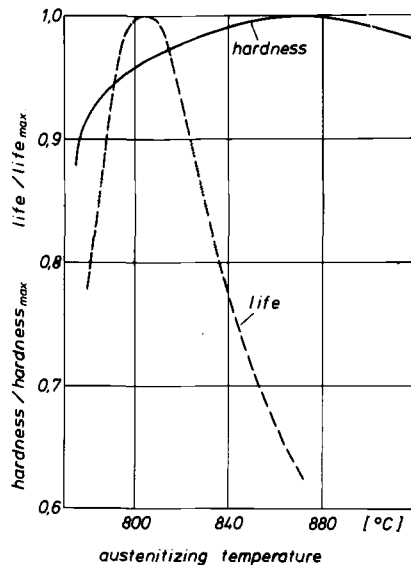
FIG. 16—*Life* (B_{10}) *and Vickers hardness number versus the austenitizing temperature (angular contact ball bearing 7205 B;* $n = 3000\ min^{-1}$; $h_0/R_a = 1 \ldots 2$; $B_{50,max} = 1500\ h$).

The question of the damage propagation after the formation of pitting should not be neglected. Also in this case greater toughness has a favorable effect. The greater the toughness, the slower is the speed of growth of pitting.

Summary

After the description of the various types of stress during rolling contact, the method which best describes material stress was indicated. Rolling contact fatigue strength as a function of contact pressure was discussed. The heat treatment of elements in rolling contact and imperfect operating conditions were considered. The results are summarized as follows:

1. Deformation processes in the material alter the residual stresses, half-value breadths, and structure. At very long running times complete martensite decay is possible.

2. The formation of white bands and their orientation to the raceway can be interpreted by laws of material mechanics.

3. The distortion energy hypothesis has proved to best describe material stress at rolling contact.

4. An *S-N* curve exists for rolling contact stress as for normal cyclic stress.

5. Cycling tests at high p_0 values allow conclusions to be drawn on the effect of material flaws (for example, nonmetallic inclusions) on the life; they are not suitable, however, for determining an optimum heat treatment. The assumption that the life increases with the hardness of the elements could not be confirmed by tests under realistic load conditions. In cycling tests under ideal conditions and $p_0 = 2800$ N/mm^2, rolling elements with hardness values from 58 to 64 HRC have proved to be of identical quality.

6. Imperfect cycling conditions, such as mixed friction, foreign particle indentations, and so on, displace the *S-N* curve toward shorter running times and lower pressures. Under such stress conditions, a high toughness of material at satisfactory hardness is an advantage.

Results obtained by cycling tests and field experiences confirm the favorable influence of toughness on the formation of pitting as well as on the propagation of pitting (service behavior) in rolling bearings.

References

[1] Bamberger, E., Harris, T. A., Kacmarsky, W. M., Moyer, C. A., Parker, R. J., Sherlock, J. J., and Zaretsky, E. V., *Life Adjustment Factors for Ball and Roller Bearings*. American Society of Mechanical Engineers, New York, 1971.

[2] Jackson, E. R., *American Society of Lubrication Engineers Transactions*, Vol. 2, 1959, pp. 121-128.

[3] Baughman, R. A., *Journal of Basic Engineering*, Vol. 82, 1960, pp. 287-294.

[4] Carter, T. J., Zaretsky, E. V., and Anderson, W. J., "Effect of Hardness and Other Mechanical Properties on Rolling-Contact Fatigue Life of Four High-Temperature Bearing

Steels," NASA TN D-270, National Aeronautics and Space Administration, Lewis Research Center, Cleveland, Ohio, 1960.

[5] Yajima, E., Miyazaki, T., Sugiyama, T., and Terajima, H., *Transactions of the Japan Institute of Metals,* Vol. 15, 1974, pp. 173–179.

[6] Kinoshi, M. and Koyanagi, A. in *Bearing Steels: The Rating of Nonmetallic Inclusions, ASTM STP 575,* American Society for Testing and Materials, Philadelphia, 1975, pp. 138–149.

[7] Johnson, R. F., Sewell, J. F., and Robinson, J. L. in *Bearing Steels: The Rating of Nonmetallic Inclusions, ASTM STP 575,* American Society for Testing and Materials, Philadelphia, 1975, pp. 114–137.

[8] Voskamp, A. P., Österlund, R., Becker, P. C., and Vingsbo, O., *Metals Technology,* Jan. 1980, pp. 14–21.

[9] Bear, H. R. and Butler, R. H., "Preliminary Metallographic Studies of Ball Fatigue under Rolling-Contact Conditions," NACA TN 3925, National Advisory Committee for Aeronautics, Washington, D.C., 1957.

[10] Styri, H., *A.S.T.M. Proceedings,* Vol. 51, 1951, pp. 682–700.

[11] Bush, J. J., Grube, W. L., and Robinson, G. H., *Microstructural and Residual Stress Changes in Hardened Steel due to Rolling Contact. Rolling Contact Phenomena,* Elsevier, New York, 1962, pp. 365–399.

[12] Littman, W. E. in "Interdisciplinary Approach to the Lubrication of Concentrated Contacts," NASA SP-237, National Aeronautics and Space Administration, Washington, D.C., 1970, pp. 309–377.

[13] Johnson, R. F. and Blank, J. F., *Symposium: Fatigue in Rolling Contact,* Institution of Mechanical Engineers, London, 1963, pp. 95–102.

[14] Gentile, A. J., Jordan, E. F., and Martin, A. D., *Transactions of the Metallurgical Society of AIME,* Vol. 233, June 1965, pp. 1085–1093.

[15] Muro, H. and Tsushima, N., *Wear,* Vol. 15, 1970, pp. 309–330.

[16] Jones, A. B., *A.S.T.M. Proceedings,* Vol. 46, 1946, pp. 1–26.

[17] Schlicht, H., *Wear,* Vol. 12, 1968, pp. 149–163.

[18] King, A. H. and O'Brian, J. L., *Advances in Electron Metallography, Vol. 6, ASTM STP 396,* American Society for Testing and Materials, Philadelphia, 1966, pp. 74–88.

[19] Vasilca, G. H. and Raszillier, V., *Wear,* Vol. 19, 1972, pp. 1–15.

[20] Swahn, H., Becker, P. C., and Vingsbo, O., *Metallurgical Transactions A,* Vol. 7A, 1976, pp. 1099–1110.

[21] Becker, P. C., Swahn, H., and Vingsbo, O., *Mécanique Matériaux Electricité,* Nos. 320–321, 1976, pp. 8–14.

[22] Zwirlein, O. and Schlicht, H., *Zeitschrift für Werkstofftechnik,* Vol. 11, 1980, pp. 1–14.

[23] Amerongen, E. V., *Eurotrib '77, 2.* Europäischer Tribologie-Kongress, Düsseldorf, Vol. 1, 1977.

[24] Swahn, H., Becker, P. C., and Vingsbo, O., *Metals Science,* Metals Society, Jan. 1976, pp. 35–39.

[25] Lund, T., *Jernkontoret Annaler,* Vol. 153, 1969, pp. 337–343.

[26] Österlund, R. and Vingsbo, O., *Metallurgical Transactions A,* Vol. 11A, 1980, pp. 701–707.

[27] Zwirlein, O., Eberhard, R., and Schlicht, H., *Härterei-Technische Mitteilungen,* Vol. 30, 1975, pp. 338–345.

[28] Kepple, R. K. and Mattson, R. L., *Transactions of the American Society of Mechanical Engineers F,* Vol. 92, 1970, pp. 76–82.

[29] Kloos, K. H. and Broszeit, E., *VDI-Berichte,* No. 243, 1975, pp. 189–204.

[30] Ilg, U., dissertation, University of Karlsruhe, Karlsruhe, Germany, 1980.

[31] Zwirlein, O., Mützel, R., and Schlicht, H., *Härterei-Technische Mitteilungen,* Vol. 31, 1976, pp. 277–286.

[32] Lorösch, H. K., in this publication, pp. 275–292.

K. Tsubota[1] and A. Koyanagi[1]

Effect of Platelike Carbides Below the Rolling Surface in a Ball-Washer Thrust Rolling Contact Fatigue Tester

ABSTRACT: It has been observed that platelike carbides form immediately underneath the rolling track of a specimen subjected to rolling contact fatigue tests on the ball-washer thrust type of tester. These carbides are less likely to form when the carbon concentration of the martensite matrix is low and more likely to present themselves when the carbon content is high.

Carbon is diffused in the matrix by repeated stresses in the specimen during rolling contacts. This carbon is caught by dislocations between oxide inclusions in fields right beneath the rolling track, where the density of such dislocations is high, and it precipitates as carbide.

We have assumed that flakings of the specimen from rolling contact fatigue are attributable to the development and propagation of cracks which originate at the site of the platelike carbides under the rolling track. In order to improve the rolling contact fatigue strength of bearing steel, it is necessary to lower the carbon concentration of the matrix while maintaining the hardness required for the rolling element, and also to reduce and finely disperse oxide inclusions.

KEY WORDS: ball-washer thrust-type rolling contact fatigue tester, microstructural alteration, platelike carbide, rolling contact fatigue mechanism, bearing steels

It is well known that shearing stress induced by rolling contact immediately below the contact surface causes a variety of microstructural alterations in bearing steel. Typical of such changes are dark etching constituents (DECs) [1,2],[2] white etching constituents (WECs) [3,4], and lenticular carbide (LC) [4,5].

These microstructural alterations are found with bearings in actual use and with specimens loaded in various types of accelerated rolling contact

---

[1] Manager, Research Section II, Technological Research Laboratory, and managing director and general manager, Technical Administration Headquarters, respectively, Sanyo Special Steel Co., Ltd., Himeji 672, Japan.

[2] The italic numbers in brackets refer to the list of references appended to this paper.

380

fatigue testers. The ball–washer thrust type of rolling contact fatigue tester, however, produces platelike carbides in major microstructural change rather than the aforementioned ordinary constituents [6, 7]. Although on specimens tested on the thrust type of rolling contact tester DECs and WECs are observed on rare occasions, they are randomly present immediately beneath the rolling track but not in the neighborhood of or next to the flaking. Furthermore, LC is not found at all.

The rolling surface of a specimen for the thrust type of tester is usually a cross-sectional plane perpendicular to the rolling direction in steel making. Therefore, the fibrous structure and nonmetallic inclusions as well are at right angles to the rolling contact surface.

The presence of different microstructural constituents in the specimen of the thrust type of tester is probably due to the fact that the rolling surface in industrial bearings and the roller or needle in accelerated rolling contact testers are parallel to the rolling direction in steel manufacturing, while in the thrust tester the rolling surface is perpendicular to the rolling direction in steel manufacturing.

The platelike carbides have hardnesses of approximately 1300 VHN [7], and a majority of them are accompanied by cracks. Many platelike carbides are found in the vicinity of the flaking, and this fact indicates that the flaking is caused by this type of carbide.

Carbon must diffuse in the martensite matrix to form the platelike carbides, and differences in the diffusion rate are assumed to control the rate of formation of these carbides in the area surrounding the flaking.

Accordingly, the authors conducted a series of tests in which the carbon concentration in the martensite matrix was varied by tempering temperatures to study its influence on the formation of such carbides as well as to clarify the mode of the formation and effect of nonmetallic inclusions on carbon concentration. At the same time, the characteristics of life testing by means of the thrust type of tester and the mechanism of rolling contact fatigue were explored.

Procedures

In the thrust-type tester [8, 9] three 9.525-mm (3/8-in.) steel balls retained in a separator roll along the 38.1-mm (1½-in.) diameter track on a lap-finished disk specimen 60 mm in diameter and 5 to 10 mm thick. The No. 51305 thrust bearing race driven with a motor revolves the steel balls from above while they are loaded from below by a lever which pushes up the frame supporting the specimen.

The occurrence of the flaking was detected by a vibration monitoring device attached to the loading lever, and the tester automatically stopped when acceleration of around 0.2 to 0.25 cm/s^2 was sensed when the flaking had taken place.

The test conditions were as follows:

Maximum nominal hertzian stress: $P_{max} = 4903$ N/mm^2
Lubricant and its temperature: No. 60 spindle oil at 30 to 31°C
Stress repetition rate: 1800 cpm
Surface finish of the specimen: 0.35 μm (H_{max})
Oil film parameter: 0.7 [elastohydrodynamic lubrication (EHL) theory]

The flakings themselves and cracks on the track were examined by microscope after the specimen was cut by an arbitrary combination of the three following methods:

1. Grinding down in the direction of the thickness of the disk specimen, parallel to the rolling contact surface.
2. Cutting down the middle of the rolling track tangentially to the track and perpendicular to the rolling surface.
3. Cutting the specimen perpendicular to both the rolling track and the rolling surface.

The rolling contact surface of the specimen used in this experiment was perpendicular to the rolling direction of the steel. The 9.525-mm (⅜) balls and upper race were also examined microscopically after they were cut using Method 3. All the microscopic specimens were etched by picral.

Results

Formation Mode of Platelike Carbides

Most of the platelike carbides observed immediately under the flaking on the specimen surface perpendicular to the rolling direction in steelmaking, are, as has often been confirmed by the authors, classified into two types: (1) those perpendicular to the rolling surface and at right angles to the rolling direction and (2) those parallel to the rolling surface.

Most of the platelike carbides occasionally observed to form along the flakings of 9.525-mm (⅜-in.) balls lay parallel to the ball surface, wherever the flakings occurred at the poles or equator.

Right below the flaking, even in the upper race in the thrust-type tester, some platelike carbides formed almost along equally stressed lines under a maximum hertzian surface stress of approximately 2118 N/mm^2.

Under a maximum hertzian stress of 4903 N/mm^2, the depth of the platelike carbides is, according to past experiments, 0.01 to 0.56 mm below the rolling surface. For 0.01 and 0.56 mm, the hertzian shearing stress is approximately 588 N/mm^2 under $P_{max} = 4903$ N/mm^2, which in turn represents the critical shearing stress for forming platelike carbides. This value is converted to a maximum hertzian surface stress of 1863 N/mm^2 for contacts between the disk and balls.

Figure 1 shows the platelike carbides along the bottom of the flaking in the
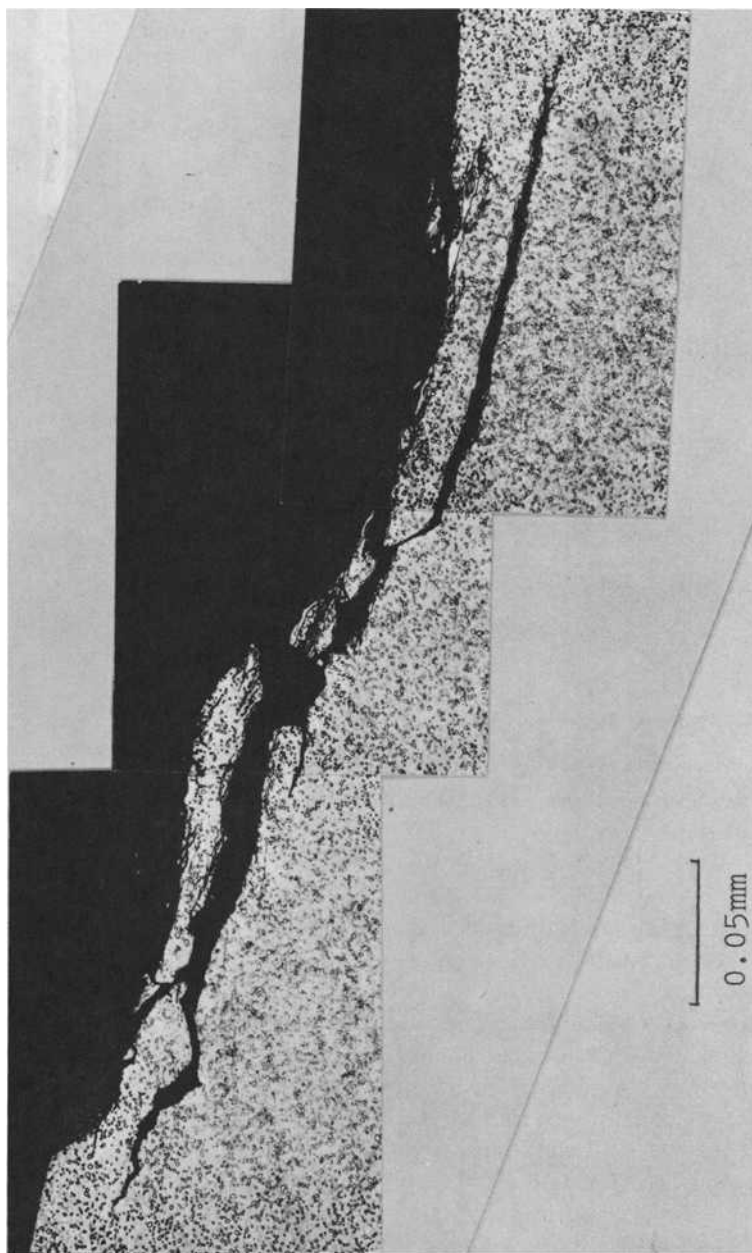
FIG. 1—Platelike carbides (white constituents) below 9.525-mm (3/8-in.) steel ball flaking.
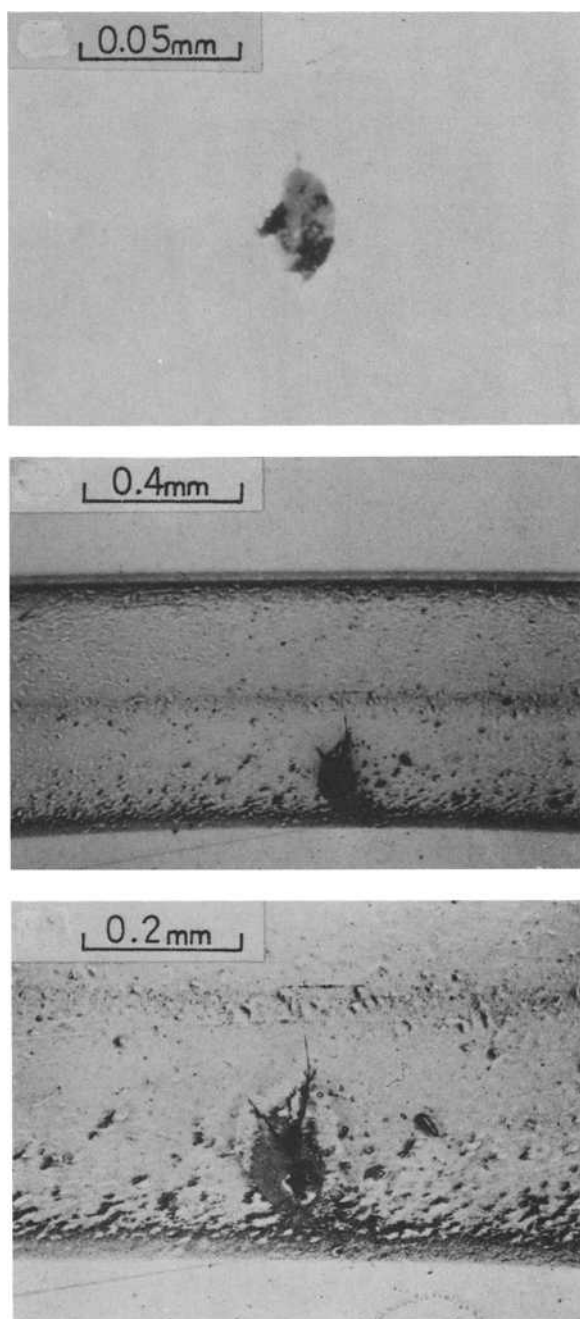
FIG. 2—*Platelike carbides directly under flaking on the rolling track:* (top) *oxide inclusion on the rolling track;* (middle and bottom) *cracks on the track.*
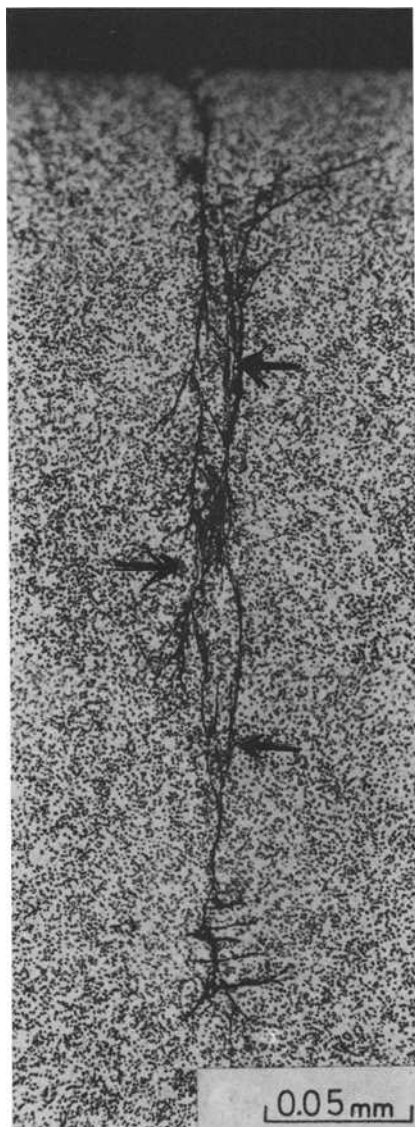
FIG. 2—*Continued: the white constituents indicated by the arrow are platelike carbides.*

9.525-mm (⅜-in.) ball. The typical platelike carbides observed just below an oxide inclusion in the disk specimen are shown in Figs. 2 and 3.

Relationship Between Formation of Platelike Carbides and Oxide Inclusions

The known fact that oxide inclusions adversely affect the rolling strength of steel has been attributed to a notch effect of these inclusions. Close study of flakings in the disk specimen from various angles reveals that they originate at the platelike carbides produced during rolling contact tests, because many platelike carbides are recognized around these flakings. It is, then, logical to assume that the flaking develops and propagates from the incipient cracks thus originated rather than from a notch effect of inclusions.

The frequent observation that the platelike carbides are accompanied by oxide inclusions prompted us to investigate the relationship between the two.

In the present experiment, the microstructure just below the flaking on the inclusions that developed cracks was examined after reciprocal rolling contact stresses were applied to the previously recognized inclusions on the rolling track.

The following facts have been discovered from specimens of 1C–0.5Si–1Mn–1.5Cr alloy with a hardness of 62 HRC and an L_{10} life of 5.7×10^6.

1. The minimum number of stress cycles for formation of platelike carbides was 1.0×10^6. This corresponds to about one third of the L_{10} life.

2. All the platelike carbides formed immediately under the oxide inclusions found on the rolling track.

3. Not all the oxide inclusions on the rolling track formed platelike carbides.

It will be explained later under the Discussion section that platelike carbides form between inclusions on the rolling track and those immediately beneath the track. Examples of the oxides on the rolling track and platelike carbides are shown in Fig. 2.

Relationship Between Carbon Concentration in the Martensite Matrix and the Formation of Platelike Carbides

Diffusion of carbon is required for the formation of platelike carbides during rolling contact stress. More carbon will diffuse when the carbon content is high in the matrix and less when it is low.

The rate of formation of platelike carbides was examined in the martensitic matrix which had various carbon concentrations caused by different tempering temperatures.

The chemical composition of the specimen was 0.96 percent carbon, 0.23 percent silicon, 0.40 percent manganese, 0.009 percent phosphorus, 0.012 percent sulfur, 1.42 percent chromium, and 0.001 percent oxygen. Heat treat-
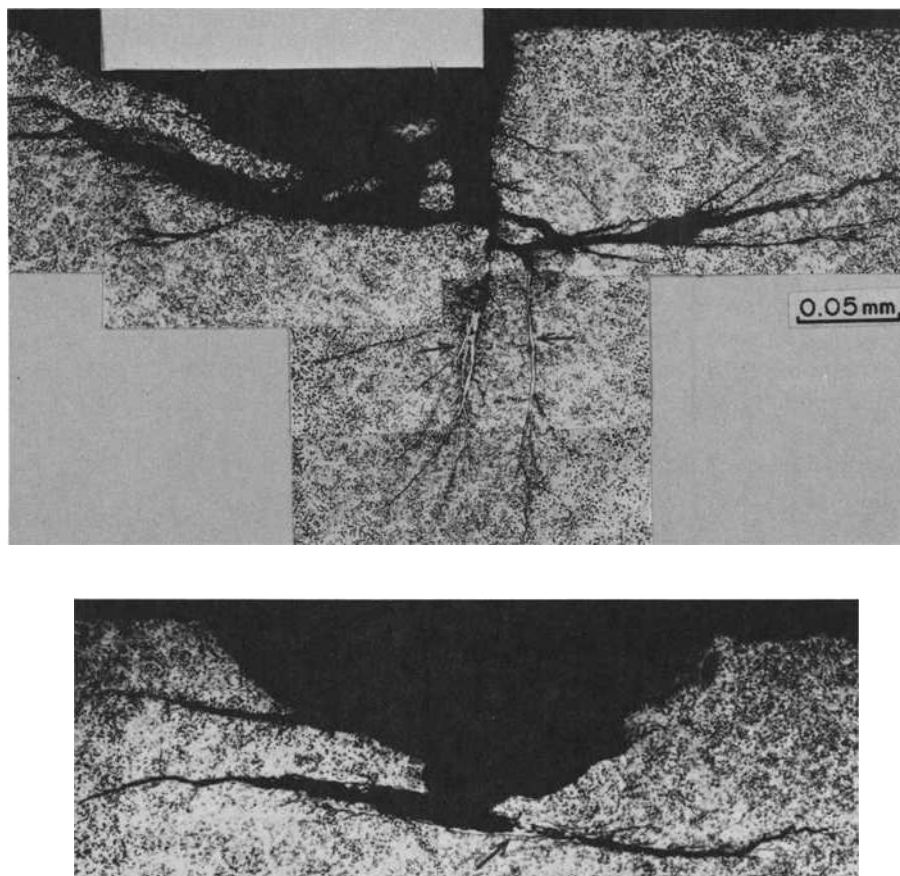
FIG. 3—*Platelike carbides directly under flaking on the rolling track:* (top) *in the specimen of 62.5 HRC;* (bottom) *in the specimen of 56.0 HRC. The white constituents indicated by the arrow are platelike carbides.*

ment, the hardness of the specimens, and the carbon concentration in the matrix are shown in Table 1. An increase in tempering temperature reduces hardness as well as carbon concentration.

Table 1 also shows the rolling contact fatigue life and the corrected calculation values of test surface pressure under nominal P_{max} = 4903 N/mm^2.

In microscopic examination made under a magnification of 400×, flaking was recognized after the specimen was cut according to the methods mentioned earlier. The rate of formation of platelike carbides under flaking, the carbon concentration in the matrix, the hardness of the specimen, and the L_{10} life for various tempering temperatures are shown in Table 1.

TABLE 1—*Formation rate of platelike carbides at various tempering temperatures.*

Heat Treatment	Hardness of Specimen, $H_R C$	Carbon Concentration in Matrix,[a] %	Corrected Hertzian Stress, N/mm^2	L_{10} life,[b] $\times 10^6$	Formation Rate of Platelike Carbides, %
830°C × 20 min OQ[c] → −60°C × 60 min → 160°C × 60 min AC[d]	64.2	0.57	4722	2.14	71.4
830°C × 20 min OQ → 180°C × 60 min AC	62.5	0.53	4643	7.35	78.6
830°C × 20 min OQ → 210°C × 60 min AC	60.8	0.46	4450	4.05	63.6
830°C × 20 min OQ → 300°C × 60 min AC	56.0	0.29	3872	2.51	50.0
830°C × 20 min OQ → 400°C × 60 min AC	50.9	0.18	3613	0.08	0

[a]The analysis method is shown in Ref *10*.
[b]Corrected L_{10} life by the ninth power law for a hertzian stress of 4903 N/mm^2.
[c]OQ = oil quenched.
[d]AC = air cooled.

The rate of formation of platelike carbides decreases with decreasing carbon concentration in the matrix, notwithstanding the fact that the corrected surface pressure is considerably higher than the critical stress (1863 N/mm^2) required for platelike carbide formation. This reveals that the formation of platelike carbides depends to a large extent on the carbon concentration in the matrix.

Figure 3 shows examples of platelike carbides under flaking in specimens of HRC 62.5 and 56.0 among others.

Discussion

Platelike carbides appear 0.01 to 0.56 mm below the rolling track under a maximum hertzian surface pressure of 4903 N/mm^2. The hertzian shearing stress is more or less the same (588 N/mm^2) for the distances 0.01 and 0.56 mm below the rolling track, and a maximum shearing stress in the contacts between the balls and disk reaches 588 N/mm^2 when $P_{max} = 1863$ N/mm^2. Platelike carbides also form in the upper race of the thrust tester under a surface pressure of 2118 N/mm^2. This fact substantiates the previous results.

Platelike carbides generally formed right under oxide inclusions on the rolling track, however, they are not found under all oxide inclusions. The ratio of the number of platelike carbides observed to the number of oxide inclusions is rather low. Other oxide inclusions are often found below the platelike carbides when the specimen is further ground to reduce its thickness. These results lead the authors to believe that platelike carbides form only in locations specifically between the inclusions.

Because the formation of platelike carbides, as explained by the foregoing results, is substantially influenced by carbon concentration in the matrix, and since the carbides are confirmed by our investigations as cementite (Fe$_3$C), a considerable amount of diffused carbon is required for such formation. Microscopic observation reveals that there is no tendency for the number of spheroidized cementites to decrease. Carbon required for formation of platelike carbides must, accordingly, be diffused from the neighborhood by rolling stress. Platelike carbides are more likely to form with higher carbon levels in the matrix, as more carbon would naturally be expected to diffuse more easily.

It is assumed from all the results that platelike carbides are Fe$_3$C [7] precipitates formed by carbon diffusion started by rolling stress and stopped by dislocations in an area of stress concentration between nonmetallic inclusions under the rolling track.

Rolling contact fatigue life is considered to be adversely affected by platelike carbides since they possess a hardness of approximately 1300 VHN [7].

That platelike carbides form under a maximum hertzian surface pressure of 1863 N/mm^2 indicates that a considerable amount of carbon may diffuse under a pressure produced in industrial bearings.

In industrial ball bearings in which the rolling track runs parallel to the direction of steel rolling, the cause of the cracks frequently found parallel to and under the track can be explained in the following way. Carbon diffused by rolling stress is caught in an area where nonmetallic inclusions are located parallel to the rolling surface, and the microcracks initiated there develop into large cracks.

An effective way to improve rolling contact fatigue life is to decrease the carbon levels in the matrix while maintaining an acceptable hardness and to reduce the nonmetallic inclusions, particularly the oxide inclusions where stress concentrates. It is also thought that an effective method of improving rolling contact fatigue life is to add an alloying element such as silicon to restrain carbon diffusion.

Many reports have been published on the deteriorating effect of oxide nonmetallic inclusions on rolling contact fatigue life, and the same conclusion can be deduced from the mechanism of platelike carbide formation in thrust tests.

The thrust type of tester may be considered especially suitable for observing how nonmetallic inclusions in general, and oxides in particular, influence rolling contact fatigue life, as oxide inclusions are closely tied to the formation of platelike carbides which cause the flaking. Also, there have been no reports of finding platelike carbides with other types of accelerated life testers.

Conclusions

The following conclusions have been made from the experimental results.

1. Platelike carbides precipitate as cementites where carbon diffused by rolling contact stress is stopped by dislocations in an area of stress concentration between oxide nonmetallic inclusions immediately under the rolling track. They are more likely to form where more carbon is available to be diffused by stress in matrixes with higher carbon concentrations.

2. The hardness of platelike carbides is approximately 1300 VHN, and these carbides can be the initiating points of cracks which cause flaking.

3. Improved rolling contact life can be attained by a decrease in oxide inclusions, a drop in carbon concentration while the required hardness is maintained, and, possibly by restraint of the diffusion of carbon.

4. The thrust type of rolling contact life tester is suited for evaluating the effect of oxide inclusions on rolling contact life.

Reference

[1] Jones, A. B., *Steel*, Vol. 30, Sept. 1946, pp. 68-70, 97-100.
[2] Valisca, G. and Raszillier, V., *Wear*, Vol. 19, 1972, pp. 1-15.
[3] O'Brien, J. L. and King, A. H., *Transactions of the American Society of Mechanical Engineers*, Vol. 59, 1966, pp. 568-572.

[4] Martin, J. A., Borgese, S. F., and Eberhardt, A. D., *Transactions of the American Society of Mechanical Engineers,* Vol. 59, 1966, pp. 555-567.

[5] Buchwald, J. and Heckel, R. W., *Transactions of the American Society for Metals,* Vol. 61, 1968, pp. 750-756.

[6] Tsubota, K., *Tetsu to Hagane,* Vol. 57, 1971, S.206.

[7] Tsubota, K., *Tetsu to Hagane,* Vol. 65, 1979, S.1068.

[8] Ueno, M., Nakajima, H., and Ikeda, S., *Tetsu to Hagane,* Vol. 47, 1961, pp. 124-129.

[9] Kinoshi, M. and Koyanagi, A. in *Bearing Steels: The Rating of Nonmetallic Inclusion, STP 575,* American Society for Testing and Materials, Philadelphia, 1975, pp. 138-149.

[10] Takimoto, K., Taguchi, I., and Matsumoto, R., *Journal of the Japan Institute of Metals,* Vol. 40, 1976, pp. 834-838.

R. M. Lamothe,[1] T. F. Zagaeski,[1] Ray Cellitti,[2] and Clarence Carter[2]

Effect of Test Variables on the Rolling Contact Fatigue of AISI 9310 and VASCO X-2 Steels

ABSTRACT: An investigation of two gear steels, AISI 9310 and VASCO X-2, carburized to a depth of 1.524 mm, was conducted to evaluate the effect of materials processing parameters on the fatigue lives of these materials in rolling contact fatigue, in single-tooth bending fatigue, and, finally, in a four-square dynamometer gear testing fixture. The study was carried on simultaneously at the International Harvester Co. (IH) and the Army Materials and Mechanics Research Center (AMMRC).

Rolling contact fatigue (RCF) was performed on two types of RCF machines which yielded different mean lives for each material. The RCF testing at IH was done on a machine designed to produce a 30 percent negative slippage at a contact stress magnitude of 3102 MPa (1 MPa = 145 psi). The AMMRC RCF tests, on the other hand, were conducted on a machine designed primarily for evaluating the fatigue life of ball bearings and had no provisions for including slippage. The magnitude of the contact stress obtained in the AMMRC tests was adjusted to 5171 MPa.

The mean fatigue life of VASCO X-2 in comparison to AISI 9310, was approximately five times greater at the B_{50} mean life on data generated with the IH machine. The higher fatigue life of VASCO X-2 was attributed to surface carbides and retained austenite. However, data generated on the AMMRC apparatus indicated the reverse, that is, the mean life of AISI 9310 steel was greater than that of VASCO X-2. Rationales for the observed differences in mean lives between the different materials and between the results of the two testing apparatuses are presented.

KEY WORDS: rolling contact fatigue, steel, AISI 9310 steel, VASCO X-2 steel, bearing steels

[1]Supervisory materials engineer and electronics engineer, respectively, Army Materials and Mechanics Research Center, Watertown, Mass. 02172.
[2]Managers, Metallurgical Process Research, International Harvester Co., Hinsdale, Ill. 60521.

The desire to achieve ever-increasing payloads, speed, and range in heli-copters is requiring the gear designer to become more selective in the choice of materials [1].[3] Although analyses are available, the ability of the selected material to perform satisfactorily under higher load requirements is generally determined from a number of selected tests.

One particular test procedure, rolling contact fatigue (RCF) testing, has been devised to obtain the pitting life of materials. The RCF test is well documented in the literature and may take on several specimen configura-tions, such as the rod/roller or ball/disk configuration. Regardless of speci-men configuration, the failure mode (pitting) is caused by a detrimental shear stress (hertzian) occurring below the contact surfaces.

The objective of this study was to test and compare statistically (Weibull plot) the rolling contact fatigue responses of AISI 9310 and VASCO X-2 steels on two RCF machines, the Polymet and the Caterpillar. These two machines differed in that the Caterpillar machine produced 30 percent slip-page into the test specimen and the Polymet produced 0 percent.

Material

The initial materials were obtained in the form of 76.2-mm[4] diameter rounds of AISI 9310 and VASCO X-2 steels and were produced by the con-sumable vacuum melt (CVM) process. The rounds were further reduced to 31.75-mm diameters to produce the 25.4-mm stepped and 9.525-mm-diam-eter roller specimens. The load roller (127-mm diameter for the Caterpillar machine) was machined from type 52100 steel bar stock and heat treated to obtain a surface hardness of 60 to 61 HRC. The chemistries of the AISI 9310 and VASCO X-2 steels are shown in Table 1.

Heat Treatment

One-inch stepped and 9.525-mm-diameter test specimens (0.25-mm over-size) of AISI 9310 and VASCO X-2 steels were machined and heat treated in accordance with two heat treatment processes. The specifics of the AISI 9310 heat treatment are listed in Table 2. The heat treatment of VASCO X-2 is proprietary to Boeing Vertol and was conducted by a qualified U.S. govern-ment–approved aircraft-gear manufacturing facility licensed to perform the Boeing Vertol heat treatment process.

Hardness traverses were conducted on pins that accompanied the batch loads throughout the complete hardening and tempering cycles. The hard-ness values obtained are displayed in Table 3.

---

[3]The italic numbers in brackets refer to the list of references appended to this paper.
[4]25.4mm = 1 in.

TABLE 1—*Chemical analysis of AISI 9310 and VASCO X-2 steels.*

Material	C	Si	Mn	Ni	Cr	Mo	Co	V	W	Cu
9310	0.1	0.27	0.55	3.25	1.22	0.12	...	...	...	...
VASCO X-2	0.15	0.94	0.26	0.06	4.85	1.35	0.07	0.44	0.32	0.09

TABLE 2—*Specifications for heat treatment of AISI 9310 steel.*

Step	Temperature
Carburized	913 to 941°C
Austenitized	821 to 843°C
Quenched (0.1 s)	60 to 71°C
Preliminary Temper (1 h)	121 to 157°C
Subcooled	−73°C
Tempered (2 h)	141 to 157°C
Subcooled	−73°C
Air cooled	

TABLE 3—*Hardness gradient of AISI 9310 and VASCO X-2 steels.*

Distance[a]	AISI 9310, HRC	VASCO X-2, HRC
0.125	63	67
0.250	63	65
0.375	63	65
0.500	63	64
0.625	63	64
0.750	62	63
0.875	62	62
1.000	62	61
1.125	61	60
1.250	60	58
1.500	56	54
1.750	52	51
2.000	48	49
2.250	44	47
2.500	44	45

[a]In millimeters from the surface.

Microstructure

Microspecimens were sectioned, prepared, and examined for each alloy in the heat-treated condition. Examination of AISI 9310 at ×500 magnification revealed a case structure of fine, tempered martensite with 8 to 9 percent retained austenite. Discontinuous intergranular carbides (approximately 1 percent) were present to a depth of 0.25 mm. Intergranular oxidation at the surface was absent. Microexamination of VASCO X-2 steel indicated numerous scattered carbides and discontinuous intergranular carbides (approximately 4 percent) to a depth of 0.625 mm. A structure of fine, lightly tempered martensite was also visible with retained austenite (3 percent). Intergranular oxide was present to a depth of 0.15 mm.

Test Apparatus

Rolling contact fatigue tests were conducted at both the International Harvester Co. (IH) and the Army Materials and Mechanics Research Center (AMMRC) using two different types of machines. The IH RCF data were obtained on a Caterpillar model [2], whereas AMMRC's data were generated on a Polymet machine. A description of each machine is given in the following sections.

Caterpillar RCF Test Machine

In the Caterpillar RCF machine, the test roller or specimen (Fig. 1) is mounted on the lower shaft that is driven through belts and pulleys by an electric motor. The load roller (Fig. 2) is mounted above the test specimen on a parallel shaft attached to a pivot frame. The upper and lower shafts are connected at one end by phasing gears which control roller surface speeds and the degree of sliding. The specimen load is applied to the free end of the upper pivot frame (lever arm) by an air cylinder. In order to monitor the load, a loading rod instrumented with strain gages is connected in series between the pivot arm and cylinder. Calibration of the strain-gaged rod in terms of
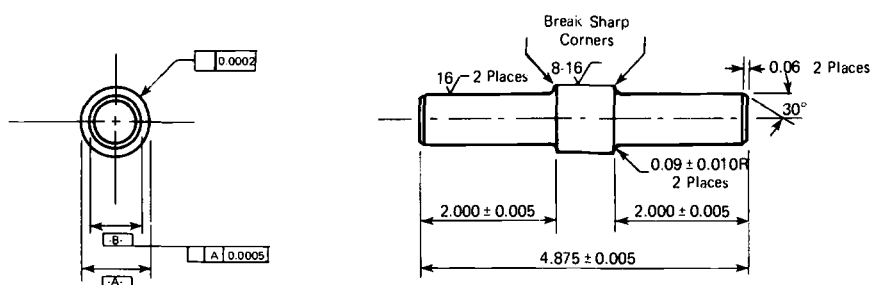
Routing Methods

A.

1. Turn and grind Diameter A to 1.000 to 1.002 in., observing surface finish. Note B, turn Diameter B to 0.765 to 0.767 in.
2. Heat treat.
3. Recenter concentric to Diameter A within 0.0005 in.; finish grind Diameter B to 0.7554 to 0.7556 in.

B.)

1. Turn Diameter A to 1.000 to 1.002 in. plus two times grinding allowance specified; turn Diameter B to 0.765 to 0.767 in.
2. Heat treat.
3. Recenter concentric to Diameter A within 0.001 in.
4. Finish grind Diameter A to 1.000 to 1.002 in. and Diameter B to 0.7554 to 0.7556 in. per surface finish and concentricity requirements.

FIG. 1—*Test specimen roller of the Caterpillar RCF Machine. The dimensions are in inches; 1 in. = 25.4 mm.*
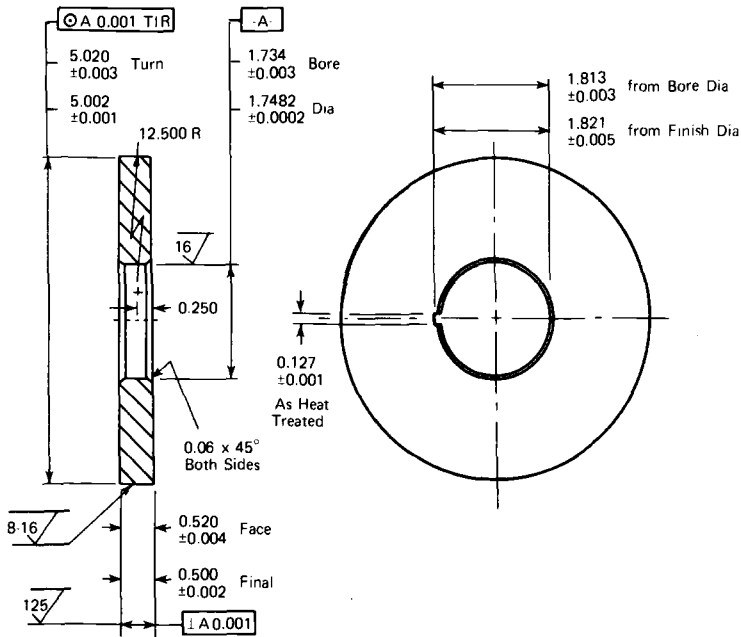
FIG. 2—*Load roller of the Caterpillar RCF machine. The dimensions are in inches; 1 in. = 25.4 mm.*

load is achieved by means of a standard proving ring in series with the load rod. The contact position of the rollers (specimen and load) is midway between the pivot point and the load application. The entire roller assembly is enclosed to contain oil which is filtered and pumped to both the test specimen and the machine bearings. An oil immersion heater controlled by a Fenwal switch maintains the oil temperature within ±2°C. Finally, the surface finish on the specimens of both materials was 16 rms.

Polymet RCF Test Machine

The Polymet machine (Fig. 3) differs significantly from the Caterpillar machine in that there are two load rollers positioned 180 deg apart which are driven by the test specimen rod (9.525 mm in diameter). The load is applied by drawing the two rollers together by means of a turnbuckle arrangement. Load monitoring is achieved by a load cell in series with the turnbuckle. Periodic calibration of the load cell is obtained external of the RCF machine by comparing its output with that of a standard proving ring. The surface finish for both the AISI 9310 and VASCO X-2 specimens was 8 to 12 rms.
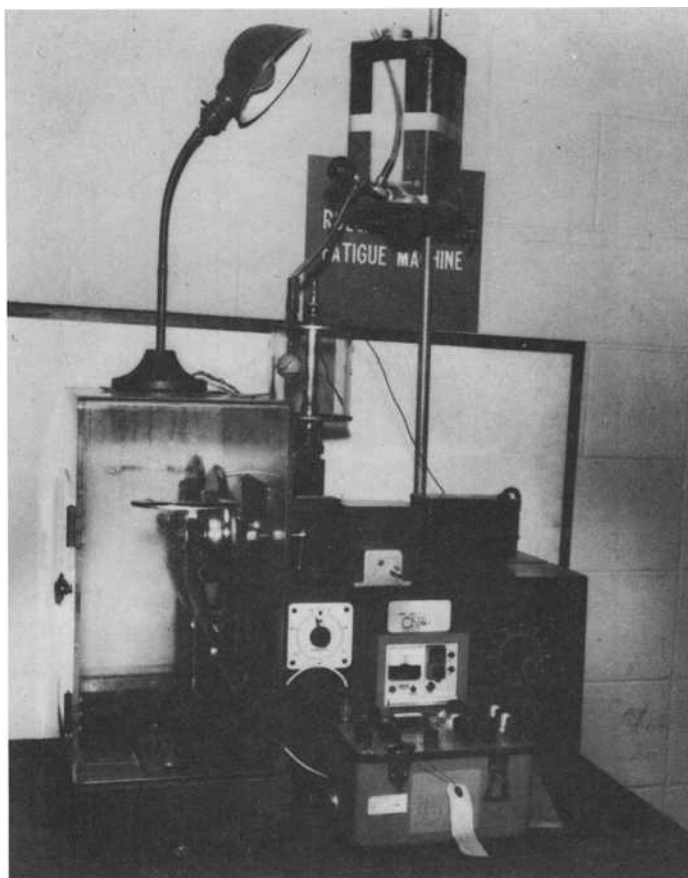
FIG. 3—*Polymet RCF machine.*

Experimental Test and Results

The rolling contact fatigue test was designed to produce pitting failures within approximately 20 million cycles. From previous RCF experiences (Fig. 4) on AISI 9310 steel (carburized to 0.90 percent carbon) utilizing the Caterpillar machine, it was established that a contact stress of 2758 MPa or less would cause pitting fatigue failure in approximately 2.5 million cycles with unrefrigerated, ground specimens. To ensure failures in the finite life region for both AISI 9310 and VASCO X-2 specimens, the contact stress level was adjusted upwards to a magnitude of 3102 MPa in those tests conducted on the Caterpillar RCF machine.

However, with the Polymet RCF machine, the load was set to produce a contact stress of 5171 MPa. The discrepancy in stress levels obtained with the
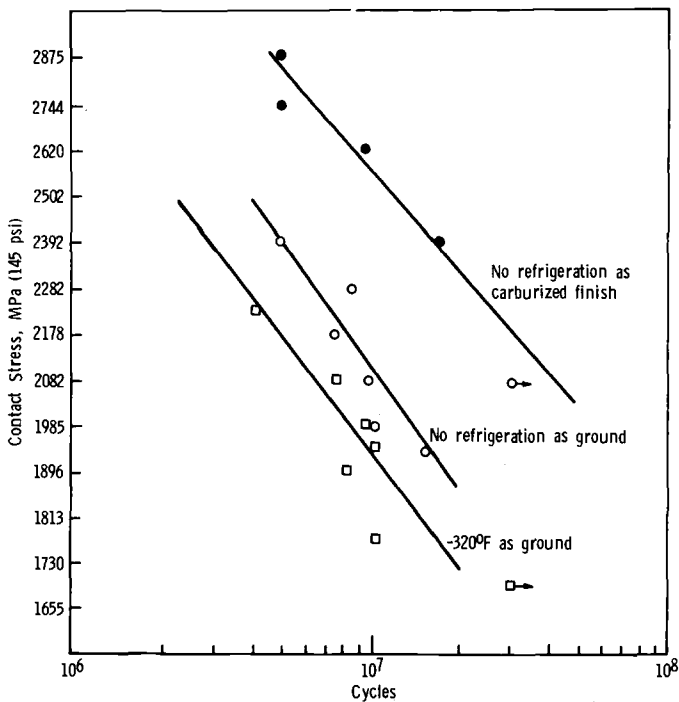
FIG. 4—*Pitting fatigue for AISI 9310 steel carburized to 0.90 percent carbon.*

two machines is due in part to the operational requirements of the Polymet machine [3]. The test conditions for both systems are shown in Table 4.

The magnitude of loads needed to produce the required maximum compressive contact stresses are calculated from the following reduced and simplified expression

$$\sigma_{max} = KP^{1/3}$$

where

P = applied load and
K = 27 322 (Caterpillar) or
K = 101 443 (Polymet).

The total number of tests conducted was 31; 20 were obtained on the Polymet and 11 on the Caterpillar machine. To preclude wear debris from biasing the data, the oil was replaced and the roller or rollers inspected after each test. The results are presented in Table 5 and graphically represented in Figs. 5 though 8. The regression line through the data points was obtained by the method of least squares fitting. Weibull parameters resulting from the plot are listed in Table 6.

TABLE 4—*Rolling contact fatigue test conditions for the Caterpillar and Polymet machines.*

Conditions	Caterpillar	Polymet
Contact stress	3 102 MPa	5 171 MPa
Oil lubricant	American multipurpose gear lubricant	Hytran SAE 80
Oil temperature	82°C	40°C
Phasing gear ratio	3.5 to 1	
Test roller speed	1 330 rmp	
Load roller speed	380 rmp	
Test specimen diameter		9.525 mm
Specimen speed		10 000 rpm

TABLE 5—*RCF test results, cycles to failure.*

AISI 9310		VASCO X-2	
Caterpillar	Polymet	Caterpillar	Polymet
966 000	1 948 940	2 434 000	1 066 800
997 000	3 338 900	2 737 000	2 317 020
1 301 000	4 927 020	4 596 000	4 005 500
1 827 000	13 036 780	8 411 000	4 725 060
2 083 000	14 721 940	9 847 000	5 548 500
4 349 000	17 417 060	. . .	5 961 220
. . .	17 851 220	. . .	5 967 960
. . .	24 555 520	. . .	6 456 040
. . .	31 557 620	. . .	8 135 820
. . .	31 819 900	. . .	10 968 340

Discussion of Results

Analysis of the data presented in Tables 5 and 6 indicate some unusual trends. This revelation is not too startling since the two RCF tests used are not identical. Because of this fact, the results on each machine will be discussed separately.

Caterpillar RCF

Referring to Table 6, the slope of the VASCO X-2 data is approximately 25 percent less than the slope of the AISI 9310 data. This decrease indicates that the VASCO X-2 steel exhibits a lower failure rate. Further evidence of the VASCO X-2 pitting fatigue life is substantiated by comparing the mean, median, and characteristic life ratios. The life of VASCO X-2, when compared in this manner, is approximately five times greater than that of the 9310 steel.
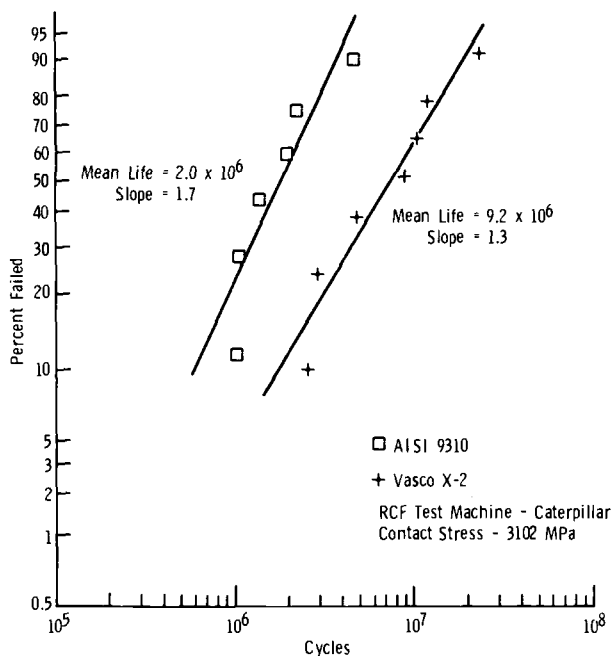
FIG. 5—*Pitting fatigue life of AISI 9310 and VASCO X-2 steels.*
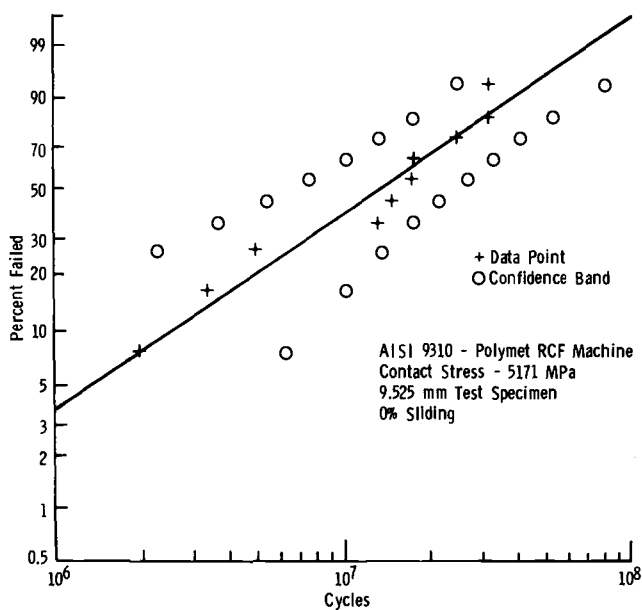
FIG. 6—*Pitting fatigue life of AISI 9310 steel.*
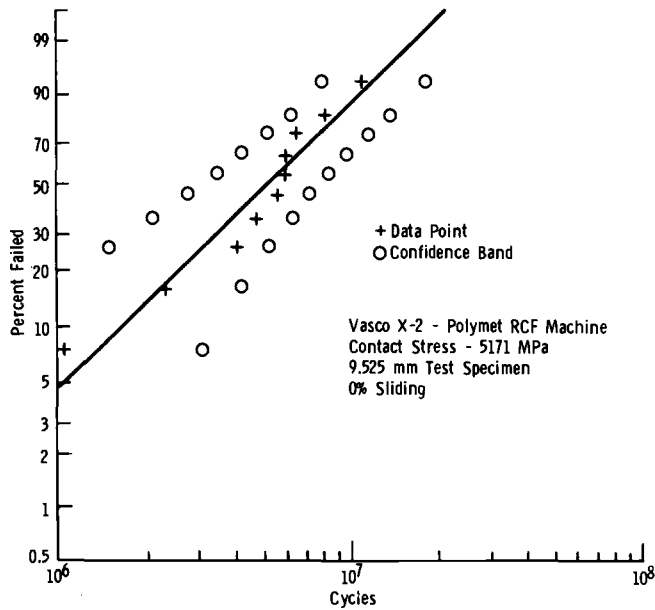
FIG. 7—*Pitting fatigue life of VASCO X-2 steel.*
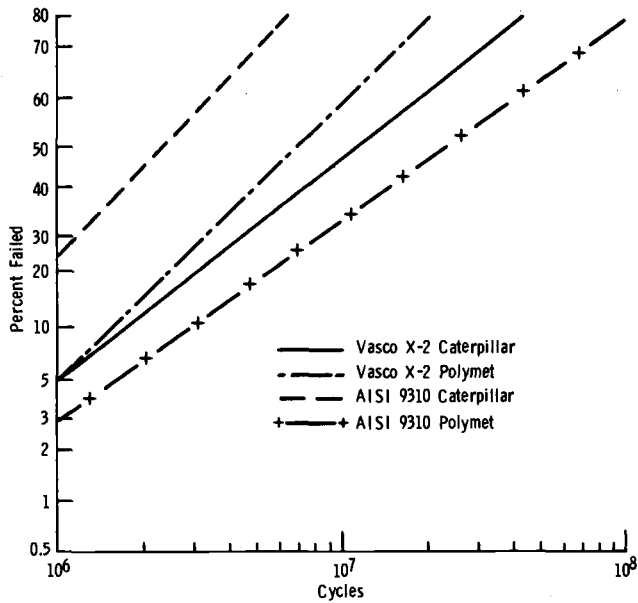
FIG. 8—*Comparison of data on AISI 9310 and VASCO X-2 steels from tests on two different RCF machines.*

TABLE 6—*Weibull parameters determined from Table 5.*

Parameter	AISI 9310		VASCO X-2	
	Caterpillar	Polymet	Caterpillar	Polymet
Slope	1.70	1.28	1.30	1.86
Mean life	1.98×10^6	16.17×10^6	9.17×10^6	5.51×10^6
Median life	1.79×10^6	16.07×10^6	7.50×10^6	5.76×10^6
Characteristic life	2.22×10^6	19.06×10^6	9.94×10^6	6.21×10^6
Standard deviation	1.20×10^6	13.59×10^6	7.12×10^6	3.5×10^6
Reliability, 10^6 cycles	77.4%		95.1%	

The improved performance of VASCO X-2 in pitting fatigue with 30 percent sliding can possibly be attributed to a beneficial microstructure of carbides and retained austenite. Scattered massive carbides in the presence of retained austenite have been observed to improve pitting fatigue in previous RCF tests. The beneficial influence of this type of microstructure (retained austenite) has been reported by other investigators [4,5]. Substantiation of this trend was further verified by Binder and Mack [5] when they reported an increased B_{50} level at a contact stress magnitude of 3102 MPa. The improved pitting resistance of VASCO X-2 is believed by the current authors to be due to (a) better surface quality caused by the uniform distribution and (b) higher hardness and material shear strength.

Polymet RCF

Again referring to Tables 5 and 6, the RCF data on AISI 9310 and VASCO X-2 obtained with the Polymet machine are in direct contrast to data obtained on the Caterpillar. On this particular RCF machine, the pitting fatigue life of AISI 9310 was found to be superior to that of VASCO X-2 steel. This discrepancy is further noted in Fig. 8, where data on both machines and materials are plotted on a Weibull probability chart format. This type of trend behavior with the Polymet and these particular materials has been observed by other investigators. Several possible explanations of this anomaly have been proposed. One is that insufficient data points were obtained to analyze the data statistically. In a two-parameter Weibull function, statisticians generally require a minimum of 30 data samplings to ensure reasonable confidence (90 percent). Perhaps the most rational explanation rests with the design of the machine. It might be argued that a contact stress level of 5171 MPa is much too severe and that the stress distribution [6] directly under the contact point is markedly different from that of specimens tested in the Caterpillar machine. The validity of the Caterpillar RCF data is qualified to some extent in Fig. 9, where the pitting life fatigue of six-pitch
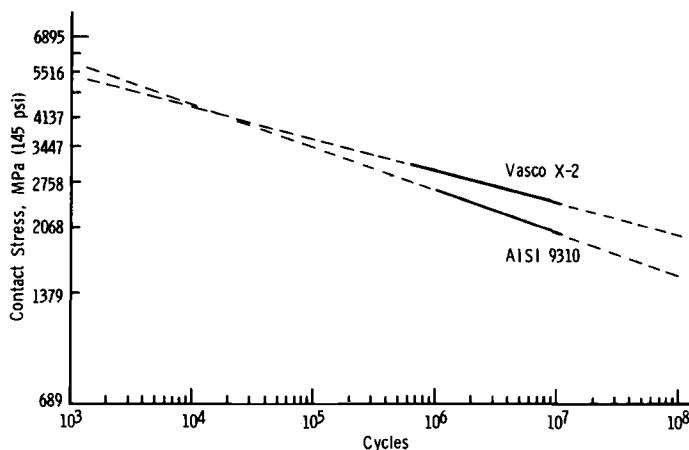
FIG. 9—*Pitting fatigue life on a six-pitch ground test pinion in a four-square gear tester.*

AISI 9310 and VASCO X-2 gears were observed. In a number of tests, the VASCO X-2 steel exhibited the higher fatigue life.

Comparison of Fatigue Lives in RCF and Four-Square Gear Testing

An important phase of the overall assessment of AISI 9310 and VASCO X-2 steels emphasized the four-square gear testing of six-pitch gears at various contact stress levels. The *S–N* (stress cycles) results are shown in Fig. 9. It is significant to note that the VASCO X-2 gear life at a contact stress of approximately 2758 MPa is approximately five times greater than that of the AISI 9310, which parallels the results obtained in RCF with the Caterpillar machine. In Fig. 10 a comparison is made between four-square and RCF pitting lives for AISI 9310 at different contact stress magnitudes. The RCF data were obtained in a Caterpillar-type RCF machine on unrefrigerated and ground specimens (Fig. 4). Although a limited amount of data are presented, there appears to be a quantifiable relationship. This fact supports the view that the Caterpillar-type RCF machine, with 30 percent sliding, simulates the average slide/roll conditions prevalent with actual gear testing.

Conclusions

1. VASCO X-2 steel exhibits a higher rolling contact fatigue life than AISI 9310 steel when tested on a Caterpillar RCF machine at a contact stress magnitude of 3102 MPa.

2. However, when these materials are tested in a Polymet RCF machine, the reverse is observed; that is, AISI 9310 steel appears to have a better fatigue life.
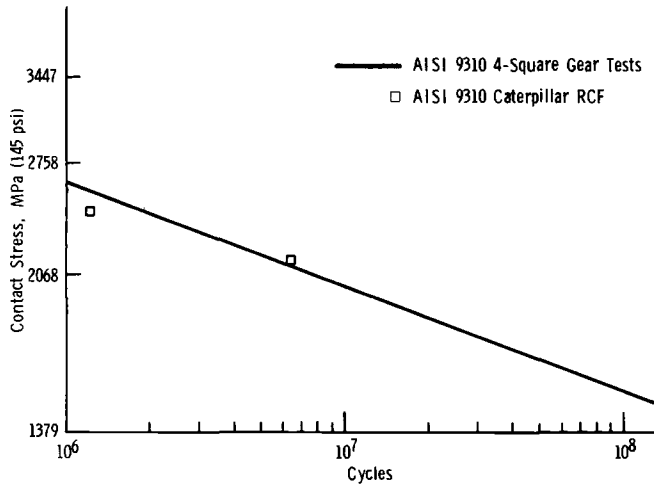
FIG. 10—*Contact stress versus the life cycles for six-pitch gears and roller contact fatigue tests. Note: the dimensions are in incles; 1 in. = 25.4 mm.*

3. Although based on limited data, the pitting life obtained in four-square gear testing parallels the results obtained with the Caterpillar RCF machine.

Recommendations

1. Additional RCF test results are needed to complement the data obtained with the Polymet RCF machine.

2. Additional test data at preselected contact stress magnitudes are needed to establish whether the correlation of the gear test to the RCF test data is meaningful.

References

[1] Spangenberg, R. L., *ManTech Journal,* Vol. 2, No. 2, 1975, p. 35.
[2] Cunningham, R. J., "VASCO X-2, Test Results and Final Report," Contract DAAJ501-71-C-0840 (P6A), Boeing Co., Vertol Division, Philadelphia, Pa., 1974.
[3] "Operational Procedures for the Polymet Rolling Contact Fatigue Machine," Polymet Corp., Cincinnati, Ohio, 1975.
[4] Winter, H. and Weiss, T., "Some Factors Influencing the Pitting, Micro-pitting and Slow Speed Wear of Surface Hardened Gears," ASME Publication 80-C2/DET-89, American Society of Mechanical Engineers, Technological University of Munich, Germany, 1980.
[5] Binder, S. and Mack, J. C., "Experience with Advanced High Performance Gear Steel," ASME Publication 80-C2/DET-77, Amercian Society of Mechanical Engineers, Boeing Vertol, Philadelphia, Pa., 1977.
[6] Seely, F. B. and Smith, J. O. in *Advanced Mechanics of Materials,* Wiley, New York, 1952, pp. 342-378.

Summary

Summary

The papers in this volume are divided into four sections. The first section deals with element testing machines of a given design with collaborative testing results. The second section deals with rolling contact fatigue (RCF) testing in general and presents a comparison of methods and test results. The third section deals with effects of test conditions on rolling contact fatigue and the evaluation of test results. The fourth section deals with the effects of material and structural variations on rolling contact fatigue.

The National Aeronautics and Space Administration (NASA) has in the past 20 years conducted extensive RCF testing in its Lewis Research Center in Cleveland, Ohio. As a single institution, it has, perhaps, enriched the knowledge of RCF in engineering communities more than any other in the world. A NASA five-ball fatigue tester was developed in late 1958, and since then a total of approximately 500 000 h of testing has been accumulated. Zaretsky et al present a paper in this volume which reviews from both a technical and historical perspective the research conducted at NASA's Lewis Research Center. Studies have been conducted on the effect of the contact angle, hardness, material chemistry, lubricant type and chemistry, heat treatment, elastodynamic film thickness, deformation and wear, vacuum, temperature, and hertzian and residual stresses on rolling element fatigue life. A correlation between the five-ball test results and those obtained with full-scale rolling element bearings has been established.

The paper by Hampshire et al deals with the testing of flat washer samples under accelerated conditions of high thrust load. This is probably the most popular method of RCF testing adopted outside the United States. The greatest advantage of this method is that test specimens are very easy to make, a fact most welcomed by manufacturers that don't make bearings. In the paper a review is presented of this method of testing, and its relationship to other methods of testing is discussed. The use of this method is illustrated by comparing the relative lives of case-hardened and through-hardened steels of standard commercial quality. The authors believe that this test has been an invaluable tool in the development of new materials and heat treatments subsequently used for commercial production of rolling bearing components.

Day's paper covers the same thrust washer tester as the paper by Hampshire et al, but his basic objective was to screen aircraft bearing materials and their heat treatment prior to or as an alternative to full-scale testing. His aim was to obtain a statistically significant quantity of data relatively quickly and

relatively cheaply in comparison with data obtained from full-scale rig or engine testing. The rig and its operating techniques are described with their known virtues and shortcomings as well as a description of the typical results analysis technique used. Typical comparative results obtained from a range of through-hardened and case-hardened materials are included, illustrating the variations obtained from different melting sources, heat treatments, and so on. These are supplemented with subsequent detailed metallographic investigation and examples.

The paper by Bamberger and Clark discusses the development of the rolling contact (RC) rig and its correlation with full-scale bearing tests. Further, it details some of the major investigatory programs that have been performed with this apparatus in the authors' laboratory at the General Electric Co., Cincinatti, Ohio. These programs include the evaluation of metallic and nonmetallic materials for bearing operation at temperatures ranging from room temperature to 489°C (1200°F), evaluation of effects of different metallurgical structures (and anomalies) on rolling contact fatigue, and the investigation of unique processes such as ausforming and hollow rolling elements.

Also reviewed is the initial work performed on the second generation RC rig, a high-speed version capable of surface speeds up to 25 m/s (82 ft/s), which thus permits operation well into the elastohydrodynamic regime.

Glover's paper describes the development of an accelerated rolling contact fatigue tester that attempts to minimize the testing and specimen variables. The important design features of the tester and the specimen–rolling element finishing technique are described.

Test results of typical bearing steels are presented in graphic form. Ito et al have developed a cylinder-to-ball type of rig independently. After the authors describe the test conditions they discuss the influence of material and heat treatment factors—such as various kinds of steels (through-hardened steels and carburized steels), nonmetallic inclusions, oxygen content, forging ratio, fiber orientation, hardness, quenching speed, and the amount of retained austenite—upon rolling contact fatigue life. The testing was conducted at an extremely high load and high loading speeds so that a specimen made of AISI E 52100 steel could fail in 18 h. The authors feel, however, that results obtained by this test rig are similar to those obtained by the conventional bearing life test in the relationship between rolling fatigue life and such factors as hardness, oxygen content, and the amount of retained austenite.

Sugiura et al used a line contact cylinder-to-cylinder RCF test rig and found it useful in investigating the optimum crowning of roller bearings.

Tokuda et al used a ring-to-ring RCF tester and in their paper discuss their observation of the peeling mode of failure and the flaking process from surface-originated cracks of quench-hardened ball bearing steel. In the test to develop the peeling mode of failure, the metallic contact ratio was continuously monitored by measuring the electric resistance, and the relation-

ship between the metallic contact ratio and factors such as the lubricant, surface roughness, contact stress, and slip ratio were examined. The initiation of peeling was found to be greatly affected by the running-in properties of lubricants. The running-in property is the one which cannot be predicted from oil film calculation by electrohydrodynamic (EHD) theory with viscosity and pressure viscosity coefficient. Therefore, an accelerated test to develop peeling is more important for the evaluation of lubricants than the conventional smearing test.

The second section begins with a paper by Galbato describing and comparing several RCF testers. The types of test equipment and apparatus and the procedures employed in the evaluation of rolling contact fatigue are reviewed, covering both element and full-scale bearing testing, their advantages and disadvantages, and the significance of the test results.

Johnston et al review several years experience in relation to determining quantitatively the influence of the material and the production process on the fatigue performance of rolling element bearings. The authors' experience includes bearing testing and several different "element" test methods. The latter have not delivered reliable results and are no longer in general use, leaving full-bearing testing as the only means of testing. The authors believed that the shortcomings of groove formation, the failure mode, and the occurrence of material transformation found in element testing apply to all element methods involving concentrated point contacts of high "stresses."

Hobbs takes into consideration that specially developed machines for fatigue testing bearing steels frequently operate at stresses higher than the elastic limit, have contact conditions widely different from those in practice, or require special expensive test pieces. An alternative view is that standard bearings should be used at a stress level within the elastic limit but high enough to give an acceptable test duration. To this end, a rig using four size 6208 bearings was developed and has been in use for many years. To minimize the effects of scatter inherent in fatigue life testing, a large number of bearings (normally 32) can be tested. Results from the rigs are presented which show the life improvement associated with vacuum degassed steels manufactured by the basic electric arc process and the effects of oil film thickness on these lives. The effects of tempering temperature are also illustrated, and a correlation between size 6208 bearing testing and Unisteel rig testing is demonstrated. The technique of sudden death testing is discussed, and results are presented which confirm its validity.

Eastaugh has investigated accelerated tests which can be used to evaluate the lubricant–steel interaction. Although the primary intention of the work was to evaluate the effect of different lubricants on the life of standard bearing steel (equivalent to AISI 52100), the program demonstrates equally well the applicability of the tests concerned for evaluating bearing steels.

Tests have been run on the AOL vertical rolling contact fatigue rig, which was designed and built in-house. In addition, tests have been run using two

machines (the rolling four ball and the Unisteel) for which the Institute of Petroleum in the United Kingdom has standard tests methods. Eastaugh's paper discusses the results of tests on a variety of lubricants, and their implications on the suitability of the machines involved. The results of a metallurgical investigation into the effects of the very severe operating conditions of the rolling four-ball machine are included.

Section 3 includes a paper by Morrison et al, who feel that optical evaluation of posttest conditions of the contact surface has long been used to supplement the life data. However, the effectiveness of optical examination is often limited to evaluation of the validity of specific test points. Normally it provides little enhancement of the overall discriminatory power of the test.

The advent of scanning electron microscopy (SEM) has significantly altered this situation. SEM examination of tested surfaces conducted at magnifications up to $\times 500$ can define alterations in surface morphology produced by wear, fatigue, or corrosive failure modes, long before signs would be detectable by optical means. These characteristics, which could have a sizable impact on the long-term operating capabilities of the bearing, can be qualitatively evaluated to supplement the collected life data. Resulting comparisons of posttest surface microgeometrics can be utilized to differentiate further the endurance capabilities of test bearing lots in cases where the life statistics are inconclusive. Examples of the application of this combined technique are presented in the paper by Morrison et al.

The paper by Sayles and Macpherson presents results on the influence of internally generated wear debris on the failure characteristics of rolling element bearings. The effects of lubricant filtration are studied, and by means of Wiebull failure distributions the gains in fatigue life are shown to be as high as sevenfold if the filtration level is set correctly. Metallurgical results are presented which show that, when lubricant contamination is present, the early failures, and particularly those which strongly influence L_{10} lives, are mostly surface initiated, and not subsurface in origin as was previously believed for rolling contacts.

Lorösch presents results of tests over many years, conducted under sufficiently realistic load conditions. The results show, among other things, that the exponent p in the life equation

$$L_n = a_1 \cdot a_2 \cdot a_3 \cdot (C/P)^p$$

is not constant. It depends on the material properties as well as on the test conditions and varies with point contact in the tested range between values clearly below 3 and values of about 8.

The author makes important statements on the validity of commonly applied life rating methods, shows the restrictions which have to be taken into account when test results are applied to practice, and derives guidelines for adequate interpretation of expressive fatigue life tests.

McCool notes that frequently in conducting rolling contact endurance tests, several small samples are subjected to some kind of "treatment." He shows that if the treatment affects the rating life but not the Weibull shape parameter the data can be analyzed as a set rather than as individual samples, which considerably improves the precision with which the rating lives can be estimated. Two procedures for the selection of sample size are discussed, and illustrative examples are given of their use.

The fourth section contains six interesting papers. The paper by Brown et al describes work done primarily with a powder-processed material (P/M) called CRB 7 which is a 14-Cr (percent by weight) steel. Although the objective of the study was to develop a highly fatigue-resistant, powder-processed material for use in turbine engine bearings, a potential payoff of high corrosion resistance was recognized. Balls and races of 20 angular-contact, 140-mm-bore diameter bearings were manufactured from P/M CRB 7 and rig-tested at 3628.7 kg (8 000 lb) thrust and 12 500 rpm. Tests showed the bearings to have reasonable rolling contact fatigue endurance.

The paper by Popgoshev and Valori describes the use of the rolling contact fatigue tester to evaluate advanced bearing steels, namely, CBS 600, CBS 1000M, AMS 5749, CRB 7, M-50 vacuum induction melt–vacuum arc remelt (VIMVAR) and powder-processed M-50, CRB 7, and T-15 steels. CEVM M-50 bearing steel was used as a baseline for comparison. Results indicate that improvements in rolling contact fatigue life superior to those of both CEVM and VIMVAR M-50 steels are achievable.

Zwirlein and Schlicht present a most interesting paper on rolling contact fatigue mechanism. We have learned in the past that for the phenomenon of rolling contact fatigue, pure "rolling" exists only in rare and limited cases. Metal-to-metal contact is nonexistent under conditions of elastohydrodynamic lubrication. Fatigue limits also did not exist because, under the conventional life formula

$$L_n = (C/P)^\epsilon$$

life, Ln, always has a finite value, even under extremely light dynamic load rating, C, and equivalent dynamic load, P, when ϵ is a constant. Zwirlein and Schlicht establish that there is a fatigue limit, as defined by the conventional S/N curve, for RCF similar to that of normal cyclic stress. This new RCF mechanism is indeed revolutionary.

Tsubota and Koyanagi have observed that when a rolling contact fatigue test of SAE 52100 steel is conducted using the thrust-type rolling contact fatigue tester, platelike carbides are often discovered directly beneath the flaking that occurs in the rolling track of the specimen. Therefore, these authors studied the conditions under which carbides develop and tried to clarify the mechanism of rolling fatigue. Observation of many areas beneath the flaking has proved that there is a close relationship between the development of platelike carbides and the occurrence of flaking.

Lamothe et al investigated two gear steels, AISI 9310 and VASCO X-2, carburized to a depth of 1.524 mm (0.060 in.), to evaluate the effect of materials processing parameters on the fatigue lives of the materials in rolling contact fatigue, in single-tooth bending fatigue, and finally in a four-square dynamometer gear testing fixture.

The mean fatigue life of VASCO X-2, in comparison with AISI 9310, was approximately five times greater at G 50 percent mean life on data generated with the IH machine. The higher fatigue life of VASCO X-2 was attributed to surface carbides and retained austenite. However, data generated on the AMMRC apparatus indicated the reverse, that is, the mean life of AISI 9310 steel is greater than that of VASCO X-2. Rationales for the observed difference in mean life within the materials and the test apparatus are presented.

The number and quality of papers accepted for this symposium far exceeded our original expectation. The editor hopes that continued efforts in the coming years by ASTM Subcommittee A01.28 on Bearing Steels and ASTM Committee A-1 on Steel, Stainless Steel, and Related Alloys will present further research results to the general engineering and scientific communities.

J. J. C. Hoo

Acciaierie e Ferriere Lombarde Falck, S.p.A. of Milano, Italy; Acciaierie di Bolzano, S.p.A. of Bolzano, Italy; symposium chairman and editor.

Index